Order Number 9230623

Performance prediction of gas/steam cycles for power generation. (Volumes I and II)

Consonni, Stefano, Ph.D.

Princeton University, 1992

U·M·I
300 N. Zeeb Rd.
Ann Arbor, MI 48106

PERFORMANCE PREDICTION OF GAS/STEAM CYCLES FOR POWER GENERATION

by

Stefano Consonni

VOLUME 1

A Dissertation

Presented to the Faculty

of Princeton University

in Candidacy for the Degree

of Doctor of Philosophy

Recommended for Acceptance

by the Department of

Mechanical and Aerospace Engineering

June, 1992

PERFORMANCE PREDICTION OF GAS/STEAM CYCLES FOR POWER GENERATION

Prepared by

Stefano Consonni

Approved by

Professor Robert H. Socolow
Dissertation Advisor

Professor Ennio Macchi
Dissertation Reader

Professor Paul Ronney
Dissertation Reader

Dr. Robert H. Williams
Dissertation Reader

ABSTRACT

This Thesis develops an algorithm for the calculation of the thermodynamic performance of Gas/Steam Cycles for power production, where the term "Gas/Steam Cycle" indicates all cycles where there is some combination between a gas turbine and a steam cycle.

Most of the modelling effort has been devoted to the gas turbine, in an attempt to find the best compromise between accuracy and complexity. The pressure-temperature history is portrayed by a sequence of expansion and mixing processes without referencing to the specifics of turbomachinery design. The model can handle both convection and film cooling, as well as thermal barrier coatings; specific applications of impingement cooling are also considered. Agreement with the performance of actual turbines is obtained by calibrating key model parameters according to the performance of commercial engines.

Gas/steam systems are calculated by a modular scheme whereby the cycle configuration is built by assembling a number of elementary components. The flexibility of this modular structure allows analyzing essentially all cycle configurations of interest. Judgements on thermodynamic characteristics are made easier by the inclusion of a detailed 2nd-law analysis, which devotes particular attention to mixing between perfect gases and condensible vapors.

After comparing performance estimates with the performance of actual systems (whenever possible), or with those calculated by other authors, the Thesis closes with a systematic parametric analysis showing the merits and the potential of both mixed and unmixed cycles.

Aside from these results, the importance of the present model lies primarily in its capability to: (i) calculate the performance of a vast class of power systems; (ii) help determine future research directions; (iii) predict the impact of technological improvements.

ACKNOWLEDGEMENTS

The author gratefully acknowledges the help and the assistance of the many people at Princeton University's Center for Energy and Environmental Studies and at the Dept. of Energetics of Politecnico di Milano who have contributed to this work.

Besides my advisor - Prof. R.H. Socolow - and Dr. R.H. Williams - who has followed the work at Princeton most closely - special thanks go to Prof. E. Macchi, whose help, encouragement and constant guidance have played a crucial role in the preparation of this dissertation. Grateful acknowledgements also go to Dr. G. Lozza, for his constructive assistance in writing the computer program and critically analyzing the results; to A. Lloyd, for his careful review of the code and the draft; to P. Chiesa, for his valuable contribution to the enhancement of the computer program; to R. Biscuola and G. Zucchetti, for their accurate preparation of many of the drawings and to Mrs. Jean Wiggs, for her kind assistance in maintaining close contacts with Princeton during my trips to Milano.

One final, devoted acknowledgement goes to the Faculty, staff and students of Princeton University, for the unique climate of cultural enrichment which has significantly contributed to motivate and gratify my work.

This dissertation carries the identification number 1893-T in the records of the Department of Mechanical and Aerospace Engineering.

TABLE OF CONTENTS

VOLUME 1

(.. cont. table of contents Vol.1)

(.. cont. table of contents Vol.1)

(.. cont. table of contents Vol.1)

VOLUME 2

(.. cont. table of contents Vol.2)

(.. cont. table of contents Vol.2)

(.. cont. table of contents Vol.2)

ACRONYMS

AD	Aero-derivative	
CC	Combined Cycle	
CCGT	Closed Cycle Gas Turbine	
COT	Compressor outlet temperature	[C]
EPRI	Electric Power Research Institute	
GSC	Gas-Steam Cycle	
HD	Heavy-duty	
HHV	Higher Heating Value	[J/kg]
HP	High Pressure	
IGSC	Integrated Gas/Steam Cycle	
IEA	International Energy Agency	
ISO	International Standard Organization	
ISTIG	Intercooled Steam injected gas turbine cycle	
IP	Intermediate pressure	
LHV	Lower Heating Value	[J/kg]
LP	Low Pressure	
NTU	Number of thermal units	
RPM	Revolutions per minute	
STIG	Steam injected gas turbine cycle	
SC	Simple cycle gas turbine	
TBC	Thermal Barrier Coating	
TIT	Turbine inlet temperature	[C]
TOT	Turbine outlet temperature	[C]

1. MOTIVATION: THE SCENARIO FACED BY THE POWER INDUSTRY

This chapter describes the motivations behind this work. Although the analyses presented further incorporate specialized details of gas turbine design, their motivation involves considerations on a planetary scale. The purpose of this chapter is to provide some broader context to permit the reader to better grasp the significance of the results presented in this Thesis.

The presentation focuses on the circumstances which are forcing the power generation sector toward a radical reorganization, whereby the steam turbine – for more than 80 years the indisputable leader of power generation – gives way to the gas turbine both in utility and cogeneration applications. Major causes of this shift are the impressive advancements of gas turbine technology, the abundance of low-cost natural gas, the tightening of environmental regulations and the crisis of the nuclear industry.

1.1 The new scenario for power generation

The basic thrust behind the development of this Thesis has been a number of fundamental changes in the scenario faced by the power generation industry in the second half of the Eighties. These fundamental changes are largely the result of four factors:

1. Rapid progress in power generation technology.
2. Abundant supply of natural gas at relatively low cost.
3. Severe tightening of environmental regulations.
4. Crisis of the nuclear industry

While technological advancements and environmental awareness can be considered irreversible, cheap natural gas will ultimately vanish, while the nuclear industry might one day rise again. However, the current situation is very likely to last for several generations of power plants, thereby justifying substantial shifts in the long term strategies of the power industry.

The economic implications of this strategy shift are staggering, as can be grasped by few elementary considerations:

- In 1988 net world installed capacity of thermal electric plants was about 1700 GW (Fig. 1.1), rising at a rate between 1 and 2% per year. For an average plant life of 30 years, the capacity to be installed due to replacement and capacity augmentation sums up to about 80 GW per year; at the very conservative average cost of 1000$/kW$_e$ this gives a market of $ 80 billion per year.

- In 1986, fossil fuels (coal, oil, natural gas) accounted for ≈85% of total OECD primary energy consumption and for ≈59% of the input into electricity generation (Tab. 1.1). A 25% increase in the average conversion efficiency of OECD fossil fuel plants – say, from 34 to 42% – could save about 160 Mtoe per year, more than 4% of total 1986 OECD primary energy consumption or – "charging" all savings to oil only – 14% of 1989 OPEC production*. At a conservative average price

* In 1989, the average production of OPEC countries was 23.2 Million barrels/day (Unione Petrolifera Italiana, 1991). Since one metric ton equals 7.33 barrels, this corresponds to a yearly production of 1150 Mtoe.

of \$ 15 per barrel of oil equivalent, OECD economies would save about \$ 18 billion per year*. Given that the average electric conversion efficiency of non-OECD countries is much lower, on a global scale the gain could be much larger.

- Given all things equal, any increase of electric conversion efficiency contributes to cut CO_2 emissions. If concerns for global warming are confirmed, the reduction of CO_2 emissions will presumably become the driving force of a dramatic shift in power generation technology.

This Chapter briefly reviews the four issues listed above and illustrates why there is a need for further, detailed study of the thermodynamics of Gas/Steam Cycles — which I henceforth indicate with the acronym GSC.

	Fuel input into electricity generation		Total primary energy consumption			
	OECD 1973	OECD 1986	OECD 1973	OECD 1986	WORLD 1986	WORLD 1989
Solid fuels, %	38.4	42.2	20.2	23.9	28.4	27.8
Oil, %	24.6	8.4	53.3	43.0	38.6	38.7
Nat. gas, %	12.1	8.7	19.6	18.4	20.9	21.4
Nuclear, %	4.3	21.8	1.2	7.8	5.1	5.6
Hydro and other, %	20.6	18.9	5.7	6.8	7.0	6.5
TOTAL, Mtoe	**977**	**1362**	**3535**	**3786**	**7380**	**8050**

Tab. 1.1 Energy consumption by primary fuels. OECD countries account for about 50% of total world energy consumption; the fraction of total primary energy used for electricity generation is now around 36%, rapidly rising over time. 1 Mtoe (Million metric tons of oil equivalent) corresponds to 41.86 10^6 MJ, or 11.63 TWh. OECD data from IEA (1988a); World data from Unione Petrolifera Italiana (1991).

* This estimate is purely theoretical. Higher conversion efficiency and lower fuel consumption would presumably force down the price of fuels and shift the economies toward higher energy intensities. In addition, since part of the \$ 18 billion worth of fuel saved is produced by OECD countries themselves, there will be transfer of economic surplus from primary energy producers to energy consumers. The micro- and macro-economic implications of these changes are beyond the scope of this work.

1.2 Progress in power generation technology

Electric power can be produced by an array of diverse technologies: gas, hydraulic, steam and wind turbines; reciprocating engines; Stirling engines; fuel cells; photovoltaic cells, Magneto-Hydro-Dynamic (MHD) generators, etc.; however, for the past one hundred years the steam turbine has been by far the most commonly used technology. Although the potential of other systems may be relevant (e.g. Ogden and Williams, 1989), at the moment the only technology apparently capable of challenging the steam turbine's leadership is the gas turbine. Thus, while acknowledging the importance of research into other technologies, I will limit this outline to the competition between steam and gas turbines.

1.2.1 Steam turbines

The success of the steam turbine stems from the combination of its superior characteristics and the excellent qualities of the Rankine cycle. Among the former, the following deserve special consideration:

- High fluidynamic efficiencies (can be above 90%)
- Continuous (well above 8000 hrs/year), very reliable operation
- Very long life (over 200,000 hrs)
- Very high unit power (in excess of 1000 MW)
- Moderate unit cost (compared to competing power generation technologies), low maintenance cost and low vibration.

As for the Rankine cycle:

- Being a closed cycle, it can be used for a wide spectrum of primary energy sources: any type of fossil fuel, nuclear, solar, geothermal, biomass.
- It exhibits best thermodynamic performance in the medium-low temper-

ature range (up to 600-650°C), i.e. up to approximately the same maximum temperature tolerable by steel.

- It "forgives" poor component efficiencies, always allowing the production of net power*; the turbomachinery efficiency threshold below which there is no net power production is very low – less than 10%!

It can be seen that the supremacy enjoyed by the steam turbine has been based on sound thermodynamic and technical reasons. On the other hand, given its long history the steam turbine can definitely be considered a "mature" technology, and little improvement can be expected in the future. In fact, since the early 60s there has been no increase in the efficiency of fossil fuel steam turbine plants (Fig. 1.2); on the contrary, because of increasing environmental constraints there are actually indications of decreasing efficiencies and strong increases in unit capital costs (Fig. 1.3).

1.2.2 Gas turbines

Even more than steam turbines, gas turbines are characterized by superior mechanical and fluidynamic characteristics. In particular, given their widespread use for aircraft propulsion reliability has been of vital importance and reaches values unparalleled by any other power generation device.

Despite these excellent qualities, until the mid-80s gas turbines played only a marginal role within the power generation industry due to a number of "flaws" of the Brayton cycle:

* This is due to the very high ratio between turbine and pump specific power which, in the ideal case with $\eta_t = \eta_{pump} = 1$, is typically in the range 50≈150. As a consequence, even if turbomachinery efficiencies are very poor the difference between turbine and pump power – i.e. net power – is still positive. This is the reason why the practical applications of the steam cycle were realized long before the gas cycle.

- Due to introduction and rejection of heat at variable temperature (isobaric processes), the ideal efficiency of a Brayton cycle operating over a given temperature range is lower than that of a Carnot cycle*.

- The achievement of high conversion efficiencies calls for high maximum cycle temperatures and high component efficiencies, two requirements that delayed the succesful utilization of gas turbines until the late 40s**.

- The high temperatures necessary to obtain good efficiencies can be reached only by internal combustion, thus preventing the use of lower cost, "dirty" fuels like coal or heavy oil.***

Although these drawbacks have not prevented the "explosion" of gas turbine use for aircraft propulsion, they have dramatically hampered its use for power generation. In fact, until the mid-80s stationary gas turbines were used only as peaking units - where the major factor is capital, rather than fuel cost - or in niche markets - e.g. pipeline compressor drive. However, unlike the steam turbine the gas turbine is

---

* With ideal components it is possible to achieve the Carnot efficiency by going to the maximum pressure ratio compatible with the given temperature range; however, this would result in zero specific work. The thermodynamics of Brayton cycles is dealt with in many textbooks, e.g. El-Wakil (1984).

** Unlike the Rankine cycle, in an ideal gas turbine cycle the ratio between expansion and compression work is very low, typically 1.5≈2. Consequently, unless turbomachinery efficiencies are very high - at least 75≈80% - it is not possible to generate net power. There are four ways to get around this limitation: (i) increase maximum cycle temperature; (ii) "adulterate" the cycle by injecting steam into the turbine, thus increasing expansion work; (iii) reduce compression work by intercooling; (iv) increase expansion work by reheat. Gas turbine pioneers used the first two methods: in 1905-06 a Company started by Charles Lemale and René Armengaud assembled a 3.5% efficient gas turbine with a carborundum-lined combustor directing gases at the astonishingly high temperature of 1800°C to a two-stage, water-cooled Curtiss turbine. The steam raised in the cooling circuit was led to nozzles and passed through the same turbine wheel (Armengaud, 1907). However, the extreme operating conditions prevented use in any practical application; yet, as reported in the insightful narration of Constant (1980, p. 93), "... The Armengaud-Lemale turbine was a rarity in that it worked at all ...".

*** Low quality fuels can be used in external combustion, Close Cycle Gas Turbines (CCGT), which however are very severely limited by heat exchanger temperature capability (Fig. 1.4).

a technology ongoing major improvements and, after "conquering" the aircraft propulsion market, in the last decade it has reached a point where there are virtually no handicaps as compared to steam turbines. This success is basically due a dramatic increase of Turbine Inlet Temperature (Fig. 1.4), which has been realized mainly by means of sophisticated blade cooling technology (see Ch. 5). State-of-the-art turbines now operate 400-500°C above the maximum temperature tolerable by materials.

1.2.2.1 Efficiency

The higher TITs brought about by technological improvements are responsible for two major occurrences:

- The efficiency of simple cycle machines has reached those achievable by large steam cycle power stations. In fact, the General Electric aero-derivative LM6000 – to be introduced in 1992 – has a net electric efficiency* in excess of 40% (Oganowski, 1990).
- The efficiency of state-of-the-art Combined Cycles (CC) is now around 52%, about 30% higher than conventional steam plants. For CCs, higher TITs "pay twice": besides higher gas turbine efficiencies, there is also an increase of the bottoming steam cycle efficiency brought about by higher gas turbine outlet temperatures.

The dramatic improvement of gas turbine-based power plant efficiency experienced in the last few years can be seen in Figs. 1.5 and 1.6. It needs to be emphasized that the transition documented by the figures has taken place in less than five years, indicating an efficiency improvement of about 1 percentage point per year. A similar rate of improvement was previously reached by steam turbines only in their

* Unless specified otherwise, all efficiencies are referred to fuel lower heating value (LHV).

golden age – the 20s and the 50s, see Fig.1.2*.

1.2.2.2 Technological aspects

Although its importance cannot be overemphasized, efficiency is only one of the factors sustaining the escalation of gas turbine technology. Two other elements are of the utmost importance:

- Capital cost
- Environmental impact

With respect to capital costs, a comparison between Figs. 1.3 and 1.7 shows that for large systems (over 300-400 MW_e) the cost of conventional steam plants is almost double the cost of a CC – approximately 1300 $/$kW_e$ vs. 700 $/$kW_e$**. At smaller scales (10-100 MW_e) the relative cost of conventional plants is even higher because, while the unit cost of steam turbine systems escalates rapidly with decreasing power outputs, GSC systems are much less sensitive to scale: at 50 MW_e the cost of STIG systems is about 700 $/kW (Kolp and Moeller, 1989), while the 50 MW_e Combined Cycle based on the LM6000 should cost around 800 $/kW (Bressan, 1991)***.

The environmental benefits of CCs vs. conventional coal-fired plants are evidenced in Fig. 1.8. Advocates of coal-fired steam systems might

* The comparison is somewhat inaccurate because Fig. 1.2 reports <u>average</u> efficiencies, while Figs 1.5 and 1.6 report <u>state-of-the-art</u> efficiencies. Considering that the 20's and the 50's were periods of strong economic expansion – and thus high rate of substitution of old, inefficient plants – in those years the rate of improvement of state-of-the-art steam turbine technology was presumably lower than shown in Fig. 1.2.

** Unless specified otherwise, all costs are in 1990 US dollars.

*** Based on these data, the slope of the three upper bands in Fig. 1.7 (Cogen systems) appears a bit conservative. Anyhow, more data are needed to justify a different trend.

object that the comparison in the figure is not "fair", because much of the reduced environmental impact of CCs is due to the use of natural gas, rather than to the gas turbine itself. This is true; however, if a comparison has to be made, it must be between CCs and coal-fired (or oil-fired) systems, which can benefit from lower fuel costs. Considering gas-fired conventional steam plants doesn't make much sense because – aside from existing plants – gas-fired capacity additions will, in most cases, be CCs. Moreover, Tab. 1.2 illustrates that by integrating the CC with a coal gasification system (IGCC-Integrated Gasification Combined Cycle) it is possible to achieve emission levels close to those from a gas-fired CC*.

For certain types of GSC systems emissions are even lower than depicted in Fig. 1.8. For example, due to the decrease in peak flame temperature provided by steam injection, steam injected gas turbines can reach NO_x emissions levels – without Selective Catalytic Reduction (SCR) – as low as 200-250 mg/kWh_e**. Even lower NO_x emissions are expected from chemically recuperated systems (Lloyd, 1991), which however have not yet been commercially developed.

---

* Except for ash and CO_2, which are inherently related to coal composition and can be reduced only by increasing plant efficiency.

** Unfortunately, the units used to evaluate emission levels are not yet standardized, and in order to perform comparisons it is often necessary to perform tedious conversions. The unit typically used for gas turbines NO_x emissions is ppmv (part per million, volume) referenced to 15% O_2 in the exhaust gases. A gas-fired steam-injected turbine can reach emissions in the range 12–15 $ppmv_{15\%O2}$ which – assuming that all NO_x is in the form of NO_2 (molecular weight 46 kg/kmol) and that the exhaust gas molecular weight is 29 kg/kmol – corresponds to an NO_2 mass fraction of 19–24 mg/kg_{gas}; for a specific work of 350 kJ_e/kg_{gas}, this translates to 195-250 mg/kWh_e.

Efficiency and Emissions	IGCC Cool Water plant, by type of coal					coal-fired steam plant	gas fired CC
	SUFCO Main	SUFCO Quench	Illinois no.6	Pittsburg no.8	Lamington		
η_{LHV}, %	33	23.5	31.3	31.3	33.6	42	52
CO, mg/kWh$_e$	7.5	17	20	< 9.5	4.5	75	34
NO_x, mg/kWh$_e$	362	411	488	337	282	600	350
SO_2, mg/kWh$_e$	95	118	350	612	137	600	0
Particulate mg/kWh$_e$	55	76	45	48	58	440	0
Ash, g/kWh$_e$	35	48	45	27	61	34	0
CO_2, g/kWh$_e$	1048	1456	1065	1043	1011	830	380

Tab. 1.2 Lower heating value efficiency (η_{LHV}) and emissions of the Cool Water demonstration IGCC plant vs. conventional coal-fired plants and gas-fired CCs. Cool Water emissions have been calculated from the average measured emissions in lbs/hr given by Clark and Holt (1990, p. 4-99), assuming an average power output of 90 MW$_e$ (65 MW$_e$ for SUFCO Quench); "Main" and "Quench" refer to the two gasifiers tested at Cool Water. Figures for conventional and CC plants are representative of state-of-the-art emission control technology (see also Fig. 1.8). Notice that estimates for coal steam plants are somewhat optimistic because in order to realize η_{LHV}=42% it is necessary to adopt a double-reheat, supercritical cycle, a configuration disliked by most utilities due to poor reliability history.
NO_x emission can be cut by a factor of 5-6 by means of selective catalytic reduction while further, dramatic reductions in SO_2 emissions of IGCC systems could be achieved with only a modest increase in capital cost (EPRI, 1982).

1.3 Natural gas supply

As indicated in Fig. 1.9, up to now natural gas has never played a prominent role in electricity generation. On the contrary, due to its superior qualities natural gas has often been regarded as a resource to be spared for future use. This attitude led to a number of restrictions on utilities both in the US (1978 Fuel Act) and in Europe (1975 EEC directive), with consequent substantial reductions of its use for electricity generation (Tab. 1.1). The large increase in natural gas reserves experienced in the 70s and 80s (Fig. 1.10) and a reserves/production ratio more favourable than for oil (Tab. 1.3) have reduced most of these concerns, leading to the repeal of limitations on gas use.

	COAL		OIL		NAT. GAS	
	Reserves	Prod.	Reserves	Prod.	Reserves	Prod.
North America	215,000	572	4,365	457*	6,700	527
Western Europe	63,000	193	2,568	n.a.	4,900	157
USSR/Eastrn Europe	264,000	573	8,199	642	39,000	683
Middle East	160	1	90,075	625**	31,200	88
Africa	50,000	102	8,027	n.a.	6,750	56
Latin America	15,000	25	17,057	n.a.	6,000	80
Asia and Oceania	261,000	768	6,349	n.a.	7,200	131
TOTAL	**868,160**	**2,234**	**136,640**	**3,165**	**101,750**	**1,722**
RESERVES/PROD, yrs	**389**		**43**		**59**	

Tab. 1.3 Reserves and production of fossil fuels as of 1989 (from Unione Petrolifera Italiana, 1991). Except for the reserves/production ratio, all data are in Mtoe. North America includes only Canada and the United States.

* Only United States

** Only Saudi Arabia, Iran, Iraq and Kuwait

Until technologies like coal or biomass gasification become economically viable and widely used, the diffusion of gas turbines for power generation will rely on the availability of natural gas at a price which – for current capital costs – should not be higher than about twice the price of coal*. The basic determinant of the gas supply cost curve is transportation. Based on current proven reserves and on estimated costs of projects under study, A.D. Little has projected the gas supply cost curve for Western Europe depicted in Fig. 1.11. Based on this curve and considering that:

(i) even at the trough of the 1986-87 oil price slump, the price of heavy fuel oil remained above 2 \$/MMBtu (Fig. 1.12);
(ii) in the last decade steam coal never went below 1.8 \$/MMBtu

in Europe gas could well be competitive even at consumption levels of 180 billion m^3/year (price $\leq$ 3 \$/MMBtu), about seven times the 1989 Western Europe consumption for electricity generation of 25 bm^3 (Fig. 1.13).

Expectations of strong gas consumption growth are shared by major forecasting agencies and authoritative scientists:

- As shown in Fig. 1.13, expected gas consumption in Western Europe for the year 2000 has been revised upward several times.
- According to the logistic substitution model developed by Marchetti and Nakicenovic at IIASA since the late 70s, in the first half of the next century world primary energy consumption will be clearly dominated by natural gas (Fig. 1.14).
- Williams and Larson (1989) argue that even if from 1995 to 2010 all new capacity additions in Europe were gas-based there should be no upward pressure on gas price; the introduction of IGCC technology would cause a major change in gas pricing policy, whereby gas would

* The evaluation of this price ratio is very involved because, besides fuel costs, it depends on: (i) capital costs; (ii) assumed interest rate and plant life; (iii) differences in maintenance and operational costs; (iv) utilization factor; (v) geographic location (which determines fuel transportation costs); (vi) fiscal legislation; (vii) emission regulation. The value of 2 given above is based on figures presented by Macchi (1990).

be linked to coal rather than to oil. Some evidence of this tendency has already appeared in Britain and Denmark (COMETEC, 1989, p. 17).

Discussing the reliability of these predictions is not the purpose of this work. However, the consensus built around them is a good indication of the important role that is expected to be played by natural gas.

1.4 Environmental regulations

The 80s have witnessed a strong worldwide escalation in the environmental awareness of public opinion. In addition to "routine" problems which had been calling for urgent, decisive action for many years, this shift is due to a series of particularly critical episodes – mostly energy-related – which have marked the decade: the Three Mile Island and Chernobyl accidents, the Exxon Valdez oil spill, the destruction of Kuwaiti oil wells during the Gulf war, alarm over the ozone hole, expectations of global warming due to anthropogenic CO_2 emissions, indiscriminate deforestation of large tropical areas, increasing acid rain, etc. Without entering the details of these episodes, it is important to stress that – particularly in industrialized countries – they have substantially modified the attitude of both public opinion and legislators in that:

- Environmental issues are felt much more on a global scale. People are forced to realize that the "not in my backyard" and "dilution is the solution to pollution" policies do not work. This has encouraged international cooperation and agreements on regulations to be applied worldwide.
- Environmental concerns are perceived to be a major driving force behind technological development.

The first point indicates that the power industry will be faced with a permanent, worldwide change of "boundary conditions"; the second introduces a new rationale for technological competition which – for power generation – decisively favours gas turbines.

Most industrialized countries have reacted by intensifying legislative action (Fig. 1.15) and tightening existing regulation (Tab. 1.4); everywhere gas turbines have emerged as the leading technology for power generation because:

- Both with natural gas and coal it allows the lowest production of all major pollutants – except possibly NO_x.
- It is a proven, reliable technology still undergoing major improvements to reduce its environmental impact*.
- In many instances it produces environmental benefits at the lowest cost.

Beside cost and efficiency considerations, the choice of gas turbines may be a must. For example, for conventional steam systems with Flue Gas Desulfurization (FGD) sulphur removal rates beyond 90-95% appear economically and technically doubtful; in contrast, IGCC systems can go above 99% (EPRI, 1982), which means reducing SO_2 emissions by a factor of ten. A similar situation exists for NO_x. Gas turbine manufacturers are now targeting dry (i.e. no steam injection) emissions of 10 ppmv which, for a 50% efficient Combined Cycle with specific work of

Pollutant	Pre-NSPS	NSPS 1971	NSPS 1979	Cool Water 1984
NO_x	None	1083	774–929	201
SO_2	None	1857	155–1393	46.5–248
Particulate	≈310	155	46.5	15.5

Tab. 1.4 Trend in air pollution standards – in mg/kWh_{fuel} – for new coal-fired power plants in the US (converted from data in $lbs/MMBtu_{fuel}$ quoted by Rubin, 1989). NSPS–New Source Performance Standard. "Cool Water" refers to the permit limits for the IGCC demonstration plant realized in California. For SO_2, the regulation requires 70% to 90% sulphur removal, with a ceiling of 1857 mg/kWh_{fuel}; thus, emissions vary with the type of coal. Since emission limits are specific to the fuel heat content, the maximum allowed emissions per unit of electricity (mg/kWh_e) vary with the net plant electric efficiency η_e (must divide the figures in the table by η_e); notice that this rationale gives no advantage to technologies with high efficiency.

---

* Research is concentrated on NO_x, which is the only pollutant of interest. All major manufacturers are working toward reducing NO_x emissions without resorting to water or steam injection which, aside from requiring substantial amounts of make-up water, may induce high CO emissions.

500 kJ/kg_{gas}, translates into ≈115 mg/kWh_e, or ≈58 mg/kWh_{fuel}. For steam cycles such low emission levels are possible only with atmospheric circulating fluidized bed boilers with staged combustion (IEA, 1988a, pp. 72-75), which however require very high capital and waste disposal costs.

1.5 The crisis of the nuclear industry

Although this Thesis focuses on systems fired with fossil fuels, it seems appropriate to close this brief overview with few considerations on nuclear power*.

The debate on the prospects of the nuclear industry is still open and several authoritative scientist hold that in the near future its contribution to energy production will continue to increase (e.g. Fig. 1.14). Nonetheless, it is hard to dispute that, after the number of inauspicious events occured in the 80's, the current prospects of nuclear power appear rather grim. In particular, it is worth recalling that:

- The Chernobyl accident has produced an enormous impact on public opinion, strongly supporting the many doubts on the safety of nuclear plants. Aside from few exceptions (e.g. France), the public opinion of all industrialized countries now tremendously hampers the construction of any new plant.
- Several European countries have banned the operation of any nuclear plant (Austria, Italy), or the construction of any new plant (Switzerland), or decided to phase out all existing plants (Sweden).
- More and more stringent safety regulations have produced a rapid, sharp escalation of capital costs, posing serious doubts on the economic viability of these plants. In particular, decomissioning costs are very uncertain, a consideration which has discouraged all investors involved in the privatization of the English National Electricty Board**.

The outcome of this situation is documented in Fig. 1.16, which clearly shows that by the early 90's the industry has come to an almost complete halt. Global warming caused by energy-related emissions $-CO_2$,

---

* The discussion is limited to fission reactors. Commercial operation of fusion reactors is at the moment too remote to affect the strategies of the power industry.

** As a result, all English nuclear plants have remained under the control of the State, while most other plants have been sold to private investors.

N_2O and O_3 emissions from fossil-fuel-fired power plants, CH_4 from pipeline leakages – may revive the interest for nuclear power. However, in addition to operational safety and economic consideration, further expansion of the nuclear industry will depend on its capability to address two crucial issues:

- The problem of nuclear waste disposal. Despite vigorous efforts and more than ten years of study the US Environmental Protection Agency has yet to find an appropriate disposal site. In most cases, nuclear waste is now disposed at fuel processing plant sites, a "temporary" solution which lasts since the early days of commercial nuclear power.
- Safety of plutonium handling. Given that with thermal reactors Uranium reserves can cover energy primary demand for a rather limited period – for the US El-Wakil (1984, p. 454) quotes 50 years – the long term prospects of nuclear power rely on breeder reactors. However, breeder reactors produce large quantities of plutonium, the basic ingredient for the constructions of nuclear bombs. The risks connected to the disposal of the large quantities of plutonium generated by widespread utilization of breeder reactors have been pointed out by Williams and Feiveson (1990). The unstable and uncertain political situation created by the collapse of the Soviet Union has further increased these concerns.

To summarize, there are good indications that in the short and medium term nuclear power will not contrast significantly the expanding role of fossil-fuel-fired, gas-turbine-based systems. It must also be noticed that – although the vast majority of existing nuclear plants is now based on steam turbines – nuclear power is not necessarily antagonistic to gas turbines. On the contrary, High Temperature Gas Reactors (HTGR) are promising candidates for the next generation of nuclear plants (McDonald, 1990): in such system the heat produced by nuclear fission is transferred to a closed-cycle gas turbine which – similarly to a CC – may be bottomed by a steam cycle.

1.6 Why this Thesis

The previous paragraphs have shown why in the next decades gas-turbine-based power plants are very likely to be at the forefront of power generation technology. The need for research on the thermodynamics of GSCs stems from three considerations:

1. Since gas cycles have been developed for mobile applications, little attention has been devoted to options relevant only to stationary applications (intercooling, regeneration, steam cooling, etc.)
2. Gas and steam cycles – taken separately – have been studied quite extensively. However, the same is not true for the opportunities created by their integration: steam/water injection, steam cooling, evaporative regeneration, etc.
3. Due to the strong influence of blade cooling on cycle thermodynamics, any attempt to produce reliable predictions of GSC performance requires accurate modeling of the gas turbine expansion. Except for proprietary codes developed by manufacturers for specific engines, such models are not available.

The importance of assessing the potential of new cycle configurations is amplified by the circumstance pointed out by Williams and Larson (1989): " *....a paradoxical aspect of the development of the stationary gas turbine is that most of the well-known "low-technology" cycle modifications available for improving performance ... remain largely unexploited, even though enormous "high-technology" advances have been made in turbine blade materials, design, fabrication ... The situation presents an enormous opportunity because it means that major improvements can be made in the performance of gas turbines for stationary power applications with modest R&D efforts*". This Thesis aims at filling the gaps left open by this situation by:

- Developing a tool to predict the perfomance of possibly all GSC systems of interest (Chs. 3-6, 8-9).
- Calibrating the prediction model in accordance to state-of-the-art gas turbine technology (Ch.7).
- Verifying the potential of the most promising options (Ch. 10).

1.7 Anticipation of basic findings

The objectives of this work have been accomplished almost entirely, and are briefly summarized below:

GSC modeling. Except for closed-circuit steam cooling – which requires further integration between the calculation of the gas turbine and the steam section – the computer program described in Ch. 9 can handle practically all GSC systems proposed in the literature.

Calibration against available commercial engines. The results of Ch. 7 show that the gas turbine model predicts efficiency, specific work and turbine outlet temperature of commercial engines within a few percent, an accuracy close to typical tolerances quoted in manufacturers' guarantees. Regarding the whole GSC system, the validations of Ch. 10 show that: (i) the agreement with measured perfomance data of actual plants is similar to the one achieved for commercial simple cycle engines; (ii) for systems not yet realized, there are in some case substantial discrepancies with the predictions of other authors.

Investigation of innovative configurations. The results reported in Ch. 10 shed light on the competition between "conventional", unmixed schemes – commonly referred to as Combined Cycles – and mixed schemes (steam or water injection). Due to the absence of mixing losses, the former systematically achieve higher efficiencies; on the other hand, the latter exhibit higher specific work and – presumably – lower investment costs. Thus, the competition between unmixed and mixed solutions is likely to be centered around the trade-off between the higher efficiency afforded by the former and the presumable lower costs of the latter, with additional considerations to be made about water consumption.

REFERENCES

Armengaud R. (1907), "The Gas Turbine: Practical Results with Actual Operative Machines in France", Cassiers Magazine, Vol. XXXI, no. 3, pp. 187-198.

Bressan L. (1991), FIATAVIO, Turin, Italy, Personal Communication.

Clark E.V. and Holt N.A. editors (1990), "Cool Water Coal Gasification Program: Final Report", EPRI report GS-6806 (Research Project 1459), Palo Alto, California.

COMETEC* (1989), "Natural Gas for Electricity Generation", Preliminary report 1989-09-26, Sept. 1989, Bruxelles.

Constant E.W. (1980), The Origins of the Turbojet Revolution, John Hopkins University Press, Baltimore, Maryland.

EL-Wakil M.M. (1984), Power Plant Technology, McGraw-Hill, New York.

ENEL** (1990), "ENEL Historical Data (1963-1989)", Internal Report, Rome, Italy.

EPRI*** (1982), "Economics of the Texaco Gasification Process for Fuel Gas Production", EPRI report AP-2488, Palo Alto, California.

EPRI (1986), "TAG - Technical Assessment Guide, Vol I: Energy Supply", EPRI Report P-4463-SR, pp. 6.3-6.5, Palo Alto, California.

Garribba S. (1991), Director, Energy Technology, Research and Development, IEA, Paris, Personal Communication.

Gas Turbine World (1986), *Gas Turbine World Handbook 1985-86*, Pequot Publishing, Southport, Connecticut.

Gas Turbine World (1990a), "New Productions Models and Design Uprates", in *The 1990 Gas Turbine World Handbook*, Pequot Publishing, Southport, Connecticut.

Gas Turbine World (1990b), "Budget Pricing for Gas Turbine Packages", in *The 1990 Gas Turbine World Handbook*, Pequot Publishing, Southport, Connecticut.

Haupt G. (1990), "Combined Cycles Permit the Most Environmentally Benign Conversion of Fossil Fuels to Electricity", ASME Paper 90-GT-367.

* Comitè puor l'Etudes Economic dell'industria del gas .., Bruxelles (now named EUROGAS).

** Italian National Agency for Electricity.

*** Electric Power Research Institute.

IEA* (1988a) "Emission Controls in Electricity Generation and Industry", OECD/IEA report, Paris.

IEA (1988b), "Use of Natural Gas in Power Generation in IEA Countries", IEA/SLT(88)59 report, Paris.

IEA (1989), "Projected Costs of Generating Electricity from Power Stations for Commissioning in the Period 1995-2000", OECD NEA/IEA Report, Paris.

Jones H. (1990), "Power Sector Sees Major Surge in Demand for Gas", Gas World International, June 1990, pp. 30-31.

Kolp D.A. and Moeller D.J. (1989), "Wolrd's First Full STIG LM5000 Installed at Simpson Paper Company", J. of Eng. For Gas Turbines and Power, Vol. 111, pp. 200-210.

Lloyd A. (1991), "Thermodynamics of Chemically Recuperated Gas Turbines", CEES/Princeton University report no. 256, Princeton, NJ.

Macchi E. (1990), "Power Generation (Including Cogeneration)", invited lecture given at the IEA Conference on *Emerging Gas Technologies - Implications and Applications*, Oct. 8-11, 1990, Lisbon, Portugal.

Marchetti C. (1988), "How to Solve the CO_2 Problem Without Tears", Plenary Speaker, *7th World Hydrogen Conference "Hydrogen Today"*, Moscow Sept. 25-29, 1988.

Marchetti C. and Nakicenovic N. (1979), "The Dynamics of Energy Systems and the Logistic Substitution Model", Research Report RR-79-13, International Institute for Applied System Analysis, Laxenburg, Austria.

McDonald C.F. (1990), "Gas Turbine Power Plant Possibilities with a Nuclear Heat Source - Closed and Open Cycles", ASME Paper 90-GT-69.

Oganowski G. (1990), "GE LM6000 Development of the first 40% Thermal Efficiency Gas Turbine", presented at the 1990 ASME Gas Turbine Congress and Exhibition (Brussels), GE Marine & Industrial Engine & Service Division, Evendale, Ohio.

Ogden J. and Williams R.H. (1989), Solar Hydrogen: Moving Beyond Fossil Fuels, World Resources Institute, Washington DC.

Rubin E.S. (1989), "Implications of future environmental regulation of coal-based electric power", Ann. Rev. Energy, 1989, pp.19-45.

Unione Petrolifera Italiana** (1991), *Energia e Petrolio. Data Book 1991*, Milan, Italy.

United Nations (1990), "1988 Energy Statistics Yearbook", New York.

* International Energy Agency.

** Italian Oil Association.

Williams R.H. and Larson E.D. (1989), "Expanding Roles for Gas Turbines in Power Generation", in Electricity, Johansson T.B., Bodlund B. and Williams R.H. eds., pp. 503-553, Lund University Press, Lund, Sweden.

Williams R.H. and Feiveson H.A. (1990), "Diversion-resistance criteria for future nuclear power", Energy Policy, July/August 1990, p. 543.

FIGURES

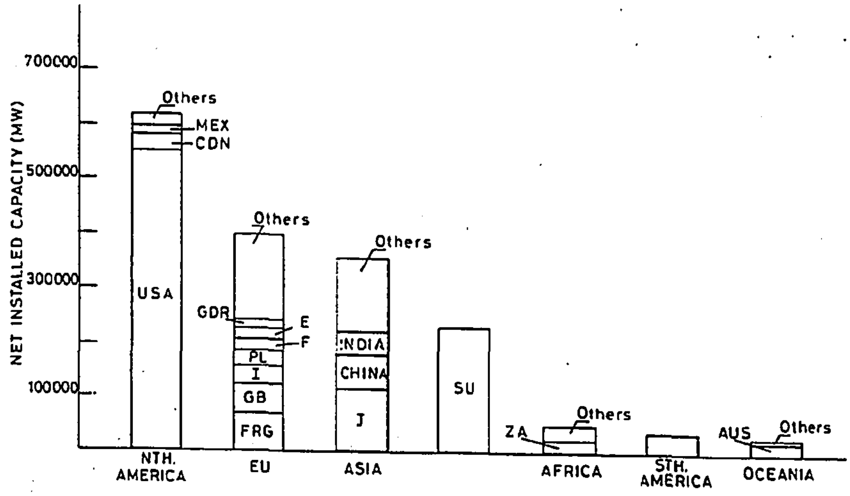

1:1 Net installed thermal electric capacity in major industrialized countries in 1988 (United Nations, 1990). SU=Soviet Union. Total world capacity was about 1700 GW.

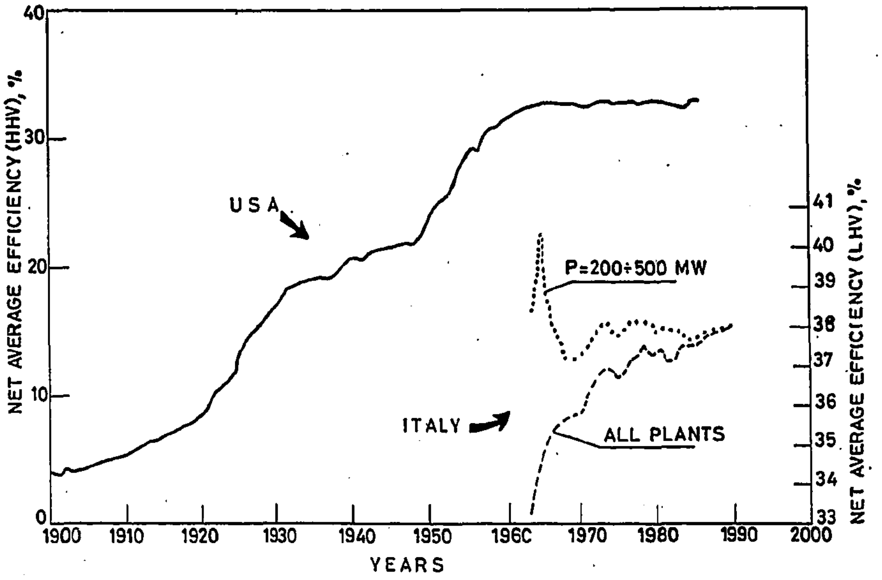

1.2 Net average efficiencies of US (left scale, HHV, from Williams and Larson, 1989) and Italian (right scale, LHV, from ENEL, 1990) steam Power Stations. The two curves cannot be referred to, the same scale because the average HHV/LHV ratio is not known. The curve for large Italian power stations shows that since the early 60s there has been no increase in the efficiency of large, new plants, and that the increase of the Italian average plant efficiency has been due to the substitution of obsolete, low-efficient plants. The spike at the year 1964 corresponds to the completion of the supercritical, double-reheat plant of La Spezia, with net efficiency in excess of 40%. Despite this remarkable performance, this plant scheme was abandoned due to high capital costs and low reliability, a pattern followed by all major world utilities.

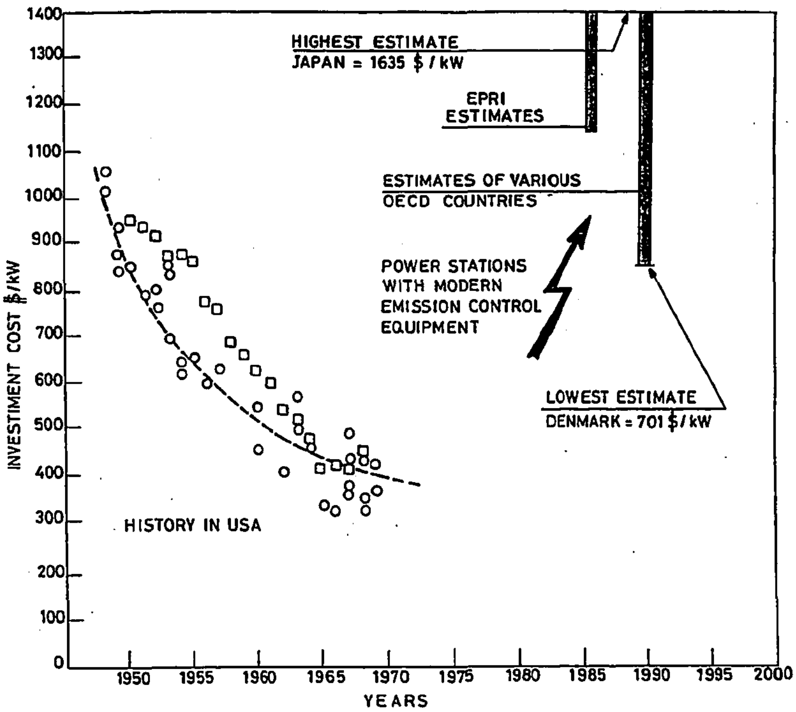

1.3 Investment costs for large (over 200-300 MW) steam power stations as reported by Williams and Larson (1989, USA history), EPRI (1986) and the International Energy Agency (1989, OECD countries).

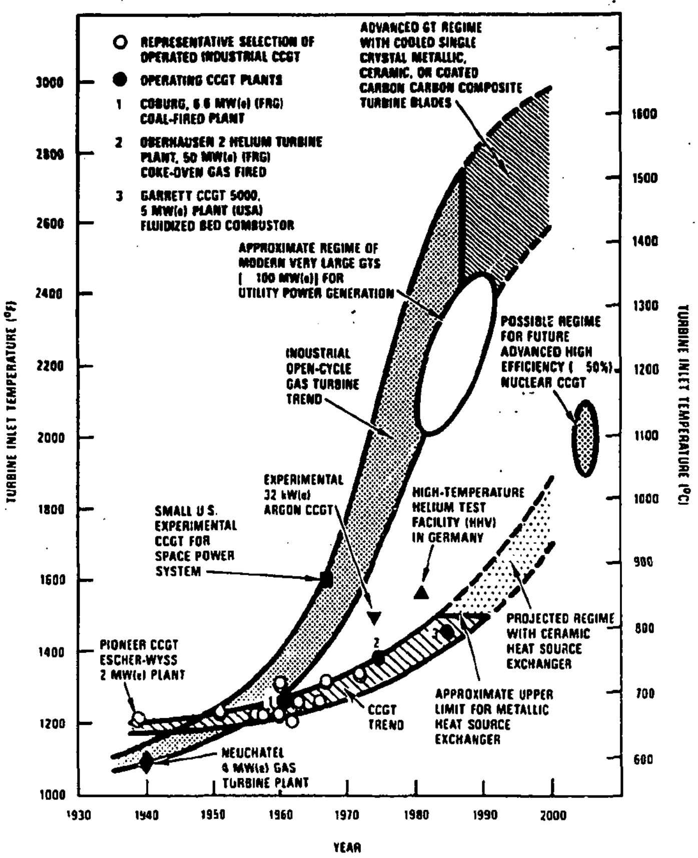

1.4 Gas turbine temperature trends as given by McDonald (1990). Closed Cycle Gas Turbines (CCGT) are limited by heat exchanger technology, which currently allows operation up to about 800°C. On the contrary, open-cycle, internal combustion engines can now operate well above 1200°C.

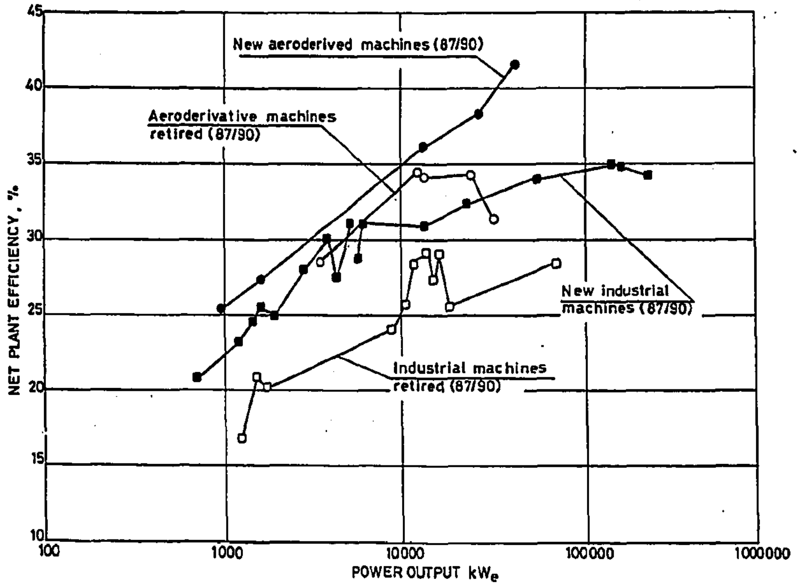

1.5 Simple cycle efficiency of commercial stationary gas turbines vs. size for units retired from and introduced into the market in the period 1987-90 (from Macchi, 1990, based on data from Gas Turbine World, 1990a). The obsolete models had been introduced into the market approximately 20 years before. The new generation of turbines has brought about an efficiency improvement of about 5 percentage points.

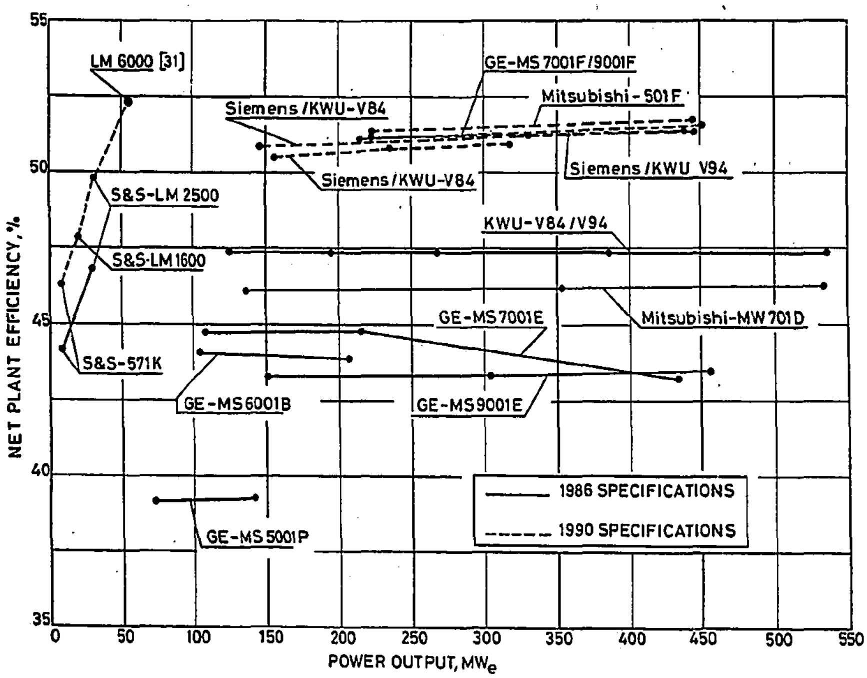

1.6 Advertised efficiencies of Combined Cycles offered by major world manufacturers as resulting from 1986 and 1990 catalogs (from Macchi, 1990, based on data from Gas Turbine World, 1986 and 1990a). In some case (e.g. GE systems) the efficiency improvement has been as large as 7-8 percentage points.

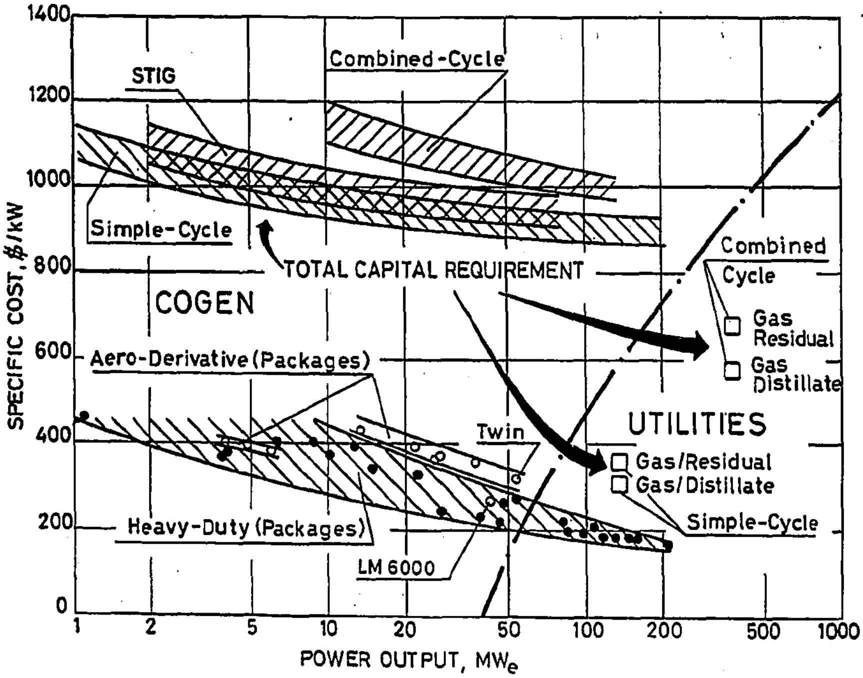

1.7 Specific costs of gas turbines and Combined Cycles (from Macchi, 1990). Circles refer to quoted 1990 FOB prices for gas turbine packages (Gas Turbine World, 1990b) inclusive of: gas turbine, electric generator, skid, enclosure, inlet and exhaust ducts, silencer and standard control system. Squares are 1987 EPRI estimates of total capital requirements inclusive of: engineering and construction firm fees, field construction, fuel tanks, control rooms, system interfaces, building enclosures, concrete pads and interest during construction.

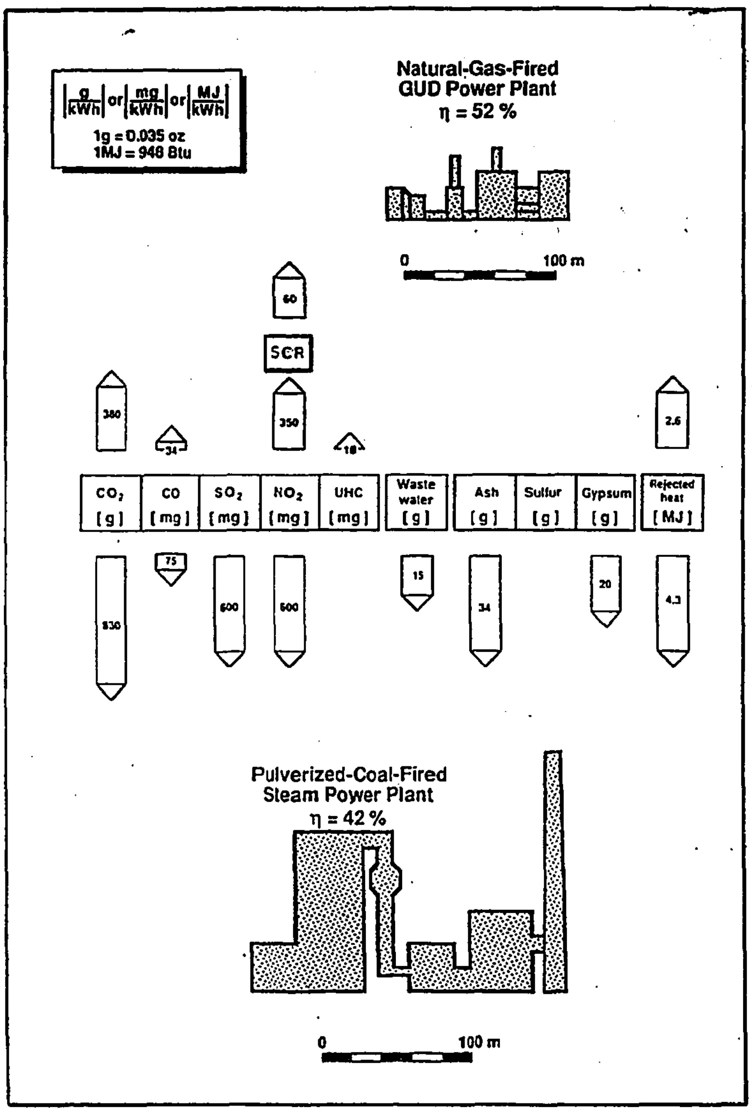

1.8 Comparison between the emissions of a 42% efficient coal-fired steam plant and a 52% efficient gas-fired Combined Cycle (from Haupt, 1990). Both plants represent state-of-the-art technology: notice that to reach 42% efficiency the coal plant requires a supercritical, double-reheat cycle. All data are specific to 1 kWh of electric energy. "GUD" stands for Combined Cycle (Gas und Dampf); SCR stands for Selective Catalytic Reduction.

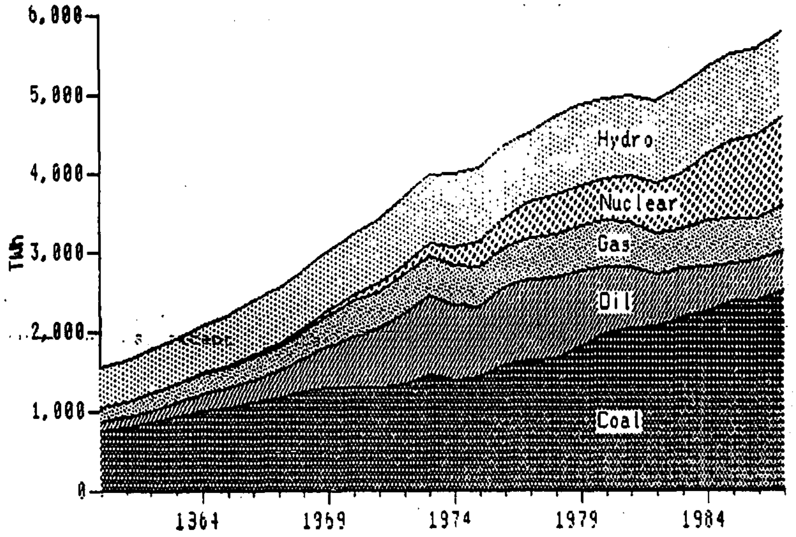

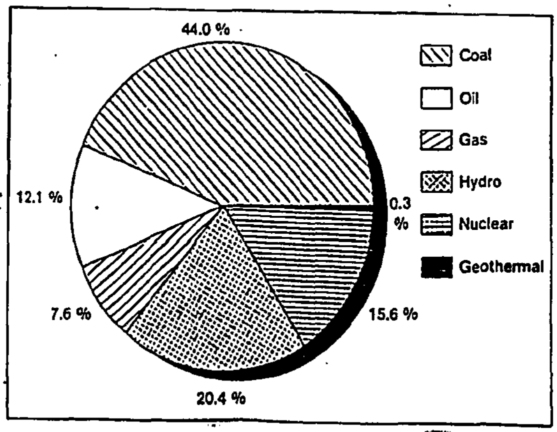

1.9 Evolution of electricity generation by primary fuel in OECD countries (IEA, 1988b). The pie represents the situation in 1986. Notice that – unlike Tab. 1.1 – this figure shows net electricity production rather than fuel input.

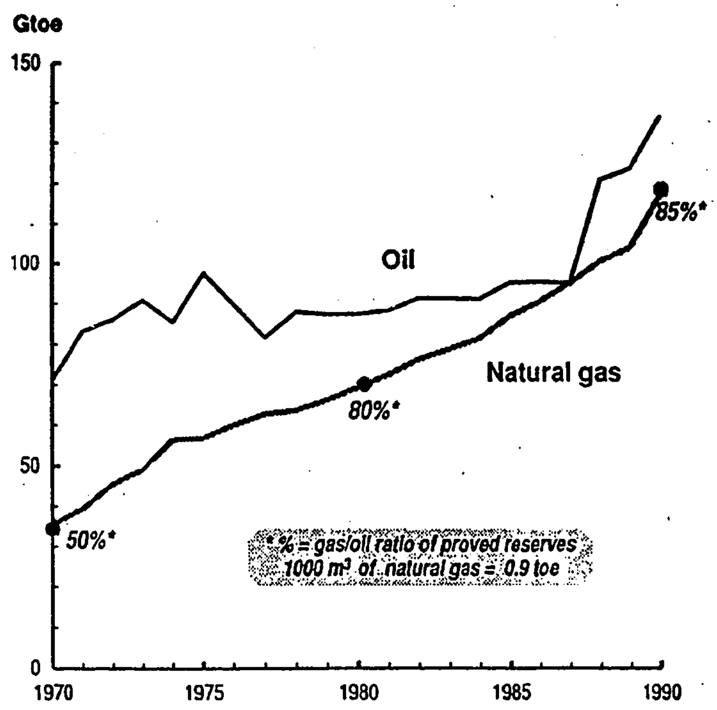

1.10 Evolution of proven reserves of oil and natural gas in the world (Garribba, 1991).

Gas supply cost curves

Arthur D. Little has projected a European gas supply cost curve for 1990-2010

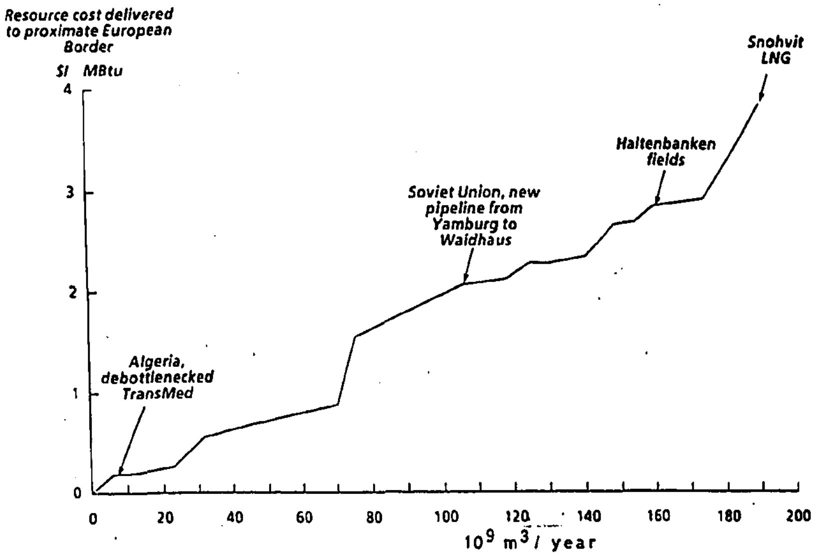

1.11 European gas supply cost curve as predicted by the forecasting consulting agency A.D. Little (from Garribba, 1991). 1 $/MMBtu (0.95 $/GJ) corresponds to about 40 $/ton of oil and to 25 $/ton of coal.

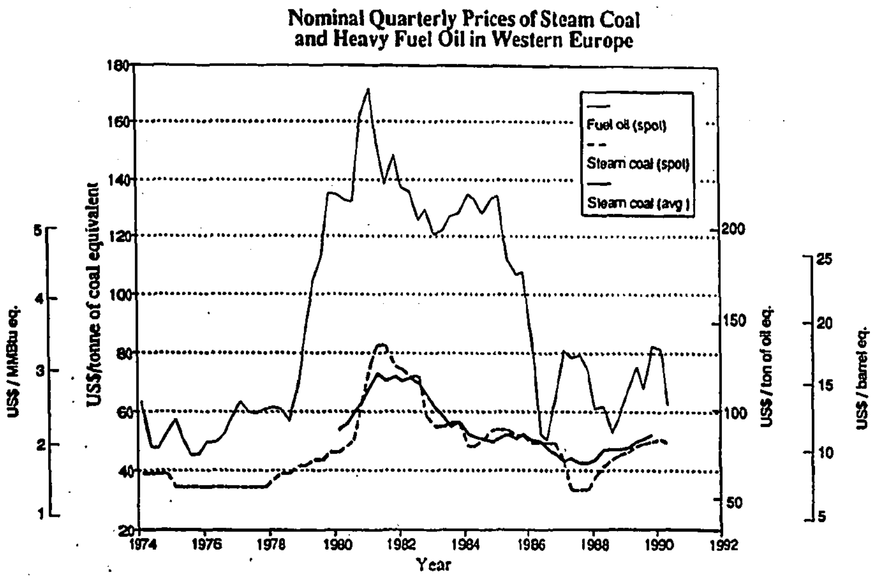

1.12 Nominal quarterly prices of steam coal and heavy fuel oil in Western Europe (Garribba, 1991). 1 metric ton of coal equivalent = 0.62 metric tons of oil equivalent = 25.953 GJ = 24.6 MMBtu.

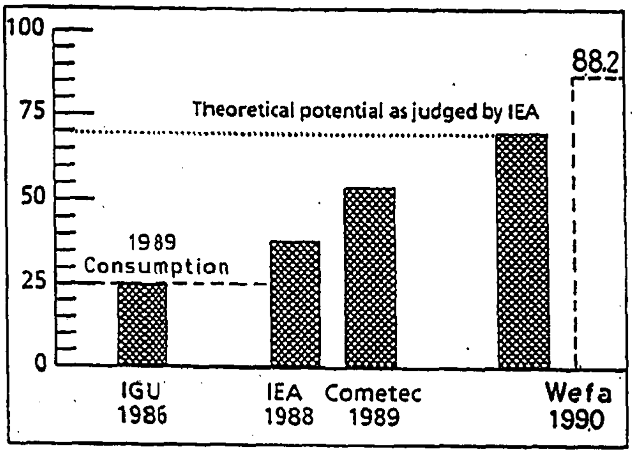

1.13 Natural gas consumption for electricity generation in Western Europe in the year 2000 as estimated at various times by the International Gas Union (IGU), the International Energy Agency (IEA) and COMETEC (1989). Ordinate axis reports billion Normal-m^3/year. The figure is taken from COMETEC (1989), with the addition of the 1990 prediction of WEFA, a London-based forecasting consulting agency (Jones, 1990). Actual 1988 consumption was 25 billion Nm^3.

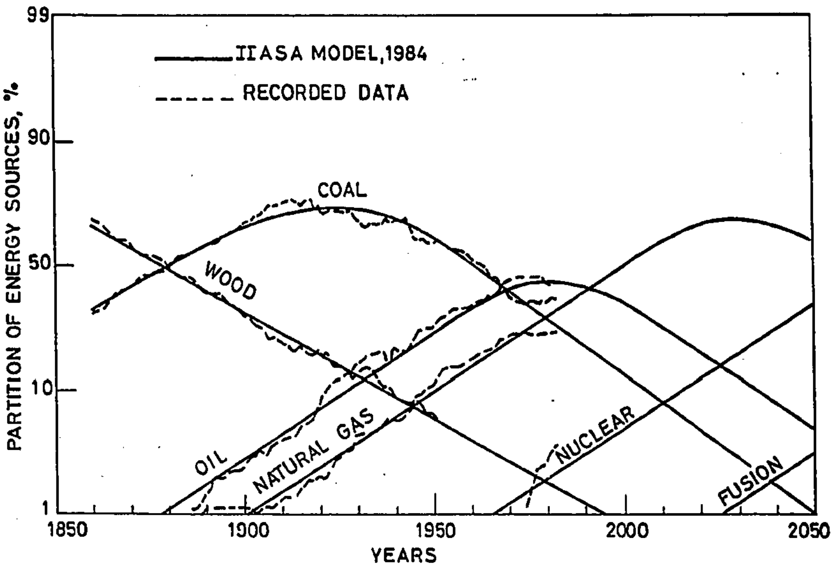

1.14 Historic evolution of the global market shares of primary energy sources as reconstructed and forecasted by Marchetti and Nakicenovic (1979; update to 1984 in Marchetti, 1988). The ordinate axis reports market shares on a logarithmic scale.

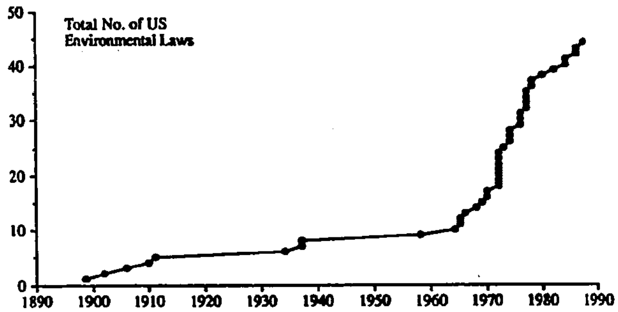

1.15 Evolution of the number of environmental laws enacted in the United States (Rubin, 1989). The increase experienced in the past two decades highlights the rapidly growing importance of environmental concerns.

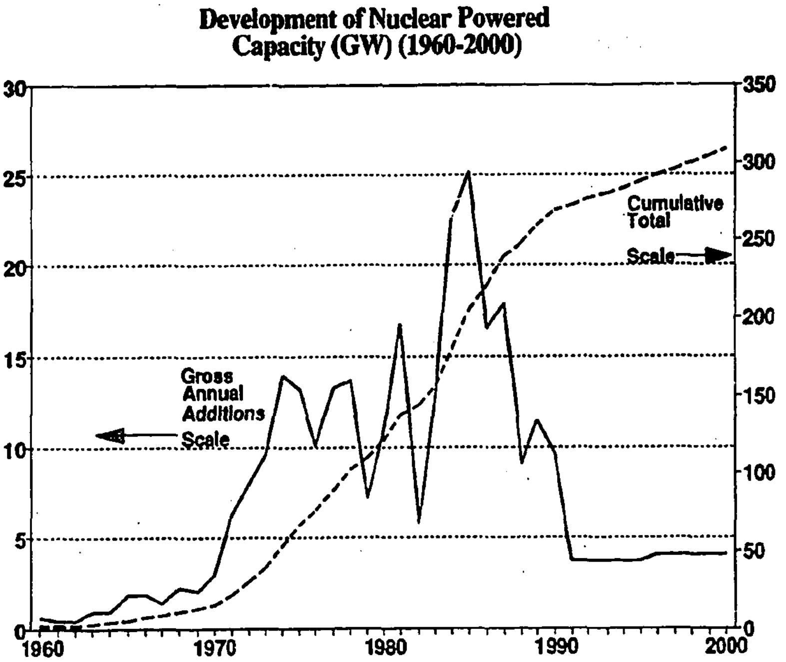

1.16 Worldwide additions of nuclear power capacity in the last 30 years and expected for this decade (Garribba, 1991). The increase of nuclear capacity of the last ten years is the outcome of projects started or approved in the 70's. Very few additions are expected for the next decade.

2. REVIEW OF MAJOR ISSUES AND RELEVANT CONCEPTS

This Chapter aims at acquainting the reader with issues and fundamental concepts related to GSC performance prediction. Many of the issues introduced here will be analyzed extensively in further Chapters; others are presented as a quick reference to the reader not familiar with gas turbine practice.

In order to limit the extent of the presentation I will discuss in some detail only the most relevant concepts, and assume that the reader is familiar with the basic concepts of fluid dynamics and of power system thermodynamics.

2.1 Gas/Steam Cycles

In this Thesis the term "Gas/Steam Cycle" is used to indicate all cycles – both mixed and unmixed – where there is some combination between a gas turbine and a steam cycle*.

Due to the multiplicity of the interconnections which can be established between the gas and steam section – and to the array of different arrangements available for the gas and steam section themselves – the variety of plant configurations resulting from their combination is rather large.

Most of these configurations can be exemplified by referring to the gas and steam cycles represented in Fig.2.1a which, for the sake of simplicity, shows only two injection locations along the gas cycle (points 6 and 7), only two outputs from the heat recovery section (points D and E) and does not show gas turbine cooling flows nor steam reheat. The dashed circles around the compressor and the gas turbine indicate that they can be substituted by several components connected in series, thus realizing intercooled and/or reheat gas cycles. A generic GSC configuration can be obtained by properly connecting one (or more) points designated by numbers with points designated by letters and, if necessary, eliminating some of the points and of the components. Three examples are illustrated in Figs. 2.1b to 2.1d where – again for the sake of simplicity – intercooling and reheat have not been considered. The cycles in the figures have been composed by:

- Connecting points 5 and A and suppressing points 6, 7, F, I (Fig. 2.1b), thus obtaining a dual-pressure Combined Cycle.

---

* Following a convention widely used in the field, the term "Combined Cycle" is reserved for the class of GSC where steam and gas do not mix, and the steam section is essentially a closed Rankine cycle which uses gas turbine exhaust gases as the heat source.

- Connecting points 5–A, F–6, D–7 and suppressing points G, H (Fig. 2.1c), thus obtaining a dual-pressure steam injected cycle with topping steam turbine.

- Connecting points 5–A, 2–H, E–3 and suppressing points 6, 7, D, F, G (Fig. 2.1d), thus obtaining a water injected regenerative cycle. Notice that in this case heat recovery takes place between gas turbine exhaust and a mixture of water and compressed air.

Other, more complex configurations can be generated by considering the following cycle options:

- Intercooling and/or reheat of the gas turbine. The heat rejected by intercooling can be utilized for feedwater heating or for producing low pressure steam.

- Higher number of: (i) evaporation pressure levels; (ii) injections into the gas turbine; (iii) bleeds from the steam turbine.

- Single and double steam reheat.

- Gas turbine cooling with steam, water or with low-temperature compressed air*. In particular, steam and water cooling can be "open" – i.e. steam or water are eventually discharged into the mainstream gas – or "closed" – i.e. steam used for cooling returns to the steam cycle to be expanded into a steam turbine.

- Supplementary firing of gas turbine exhaust.

This list of possible cycle options clearly indicates the complexity of the problem. Even if the analysis of one single configuration might result relatively simple, the comparison among many cycle options requires a very flexible computational tool, capable of warranting the same accuracy for all configurations.

* This can be realized by passing the air to be used for gas turbine cooling through a heat exchanger placed downstream the bleed from the compressor.

2.1.1 Classification

The three examples of Figs. 2.1b to 2.1d are particularly relevant because they are the "prototypes" of the three classes of cycles which comprise the majority of GSCs:

Combined Cycles (Fig. 2.1b), where gas and steam are secluded from each other all along the cycle.

Steam-injected cycles (Fig. 2.1c), where steam produced in the Heat Recovery Steam Generator (HRSG) is expanded directly into the gas turbine together with combustion gases.

Water-injected, regenerative cycles (Fig. 2.1d), where heat recovery from gas turbine exhaust is accomplished by heating a mixture of air and water to be fed to the combustor.

Due to the strict separation between gas and steam, Combined Cycles will also be referred to as unmixed cycles, while steam injected and water injected cycles will often be grouped under the name of mixed cycles. Although the vast majority of GSC can be assigned only to one of the three classes above, there are few configurations which fall somewhere in between, e.g. Combined Cycles with open circuit steam cooling: in this case part of the steam produced in the HRSG is used for gas turbine cooling and then mixes with the combustion gases, thus realizing an hybrid situation (Chiesa, Consonni and Lozza (1992).

In Combined Cycles the connection between the gas and the steam cycle is established only through the gas turbine outlet temperature and, in some configuration, heat recovery from intercoolers or from cooling air heat exchangers*; consequently, performance calculations require little interaction between the gas turbine and steam turbine sections. On the contrary, steam injected and water injected cycles are

* The heat rejected by the air to be used for gas turbine cooling may be used for feedwater heating or to produce low-pressure steam.

characterized by a much tighter connection between the gas and the steam cycle which: (i) requires the simultaneous calculation of the whole system and (ii) "propagates" throughout the whole cycle the consequences of variations in component characteristics.

2.2 Turbomachinery

In a GSC system turbomachines play the crucial role of converting the energy-producing potential of the working fluid into mechanical energy (or viceversa). Although the aim of this Thesis is the study of GSC thermodynamics, some understanding of turbomachine operation is necessary because:

- The "shape" – and thus the performance – of the gas cycle crucially depends on turbomachinery efficiency (Fig. 2.2). On the other hand, estimating turbomachinery efficiency requires the specification of the thermodynamic cycle, i.e. pressure ratios, temperatures, enthalpy drops. As a result, there is a strict and very important connection between the evaluation of thermodynamic and turbomachinery characteristics.
- Beside turbomachinery efficiency, the gas cycle also depends on how much flow is required to cool the turbine (Fig. 2.3). Accurate evaluation of gas turbine cooling flows requires the detailed knowledge of turbine geometry and flow conditions, thus establishing one more strict connection between thermodynamics and turbomachinery.
- The configuration of the bottoming steam cycle depends on the gas turbine outlet temperature (Fig. 2.4), which in turn depends on gas turbine efficiency and cooling flows.

The strongest interaction between thermodynamics and turbomachinery characteristics occurs in mixed cycles, where the gas and steam sections interact not only through the gas turbine outlet temperature, but also by sharing the gas turbine as the only producer of net work; consequently, any variation of turbine work is totally "transferred" to variations of net work and overall cycle efficiency.

Coming to the steam cycle, the connection between steam turbine performance and cycle thermodynamics is looser than for the gas turbine (Fig. 2.5), because compression is performed in the liquid phase and heat rejection takes place at constant temperature; nonetheless, accurate evaluation of steam turbine efficiency is crucial to the estimation of work output.

To summarize, turbomachinery characteristics seriously affect GSC thermodynamics through:

- turbomachine efficiencies
- gas turbine cooling flows

Due to cooling and to the influence of its outlet temperature on the bottoming steam cycle, the gas turbine is the turbomachine which affects performance predictions most crucially. Thus, any thermodynamic analysis of GSCs must include an appropriate model of at least the gas turbine.

2.2.1 Basic features and design methods

The three turbomachines of a GSC – gas turbine compressor, gas turbine, steam turbine (if present) – share the following traits:

- Axial flow, i.e. the working fluid proceeds along the axis of the rotating shaft. The reason is twofold: (i) axial machines allow "swallowing" high volumetric flows; (ii) for the operating parameters typical of GSCs, they yield the highest efficiencies. The only exceptions are compressors for low-power-output gas turbines (below 1 MW_e), which are generally radial.

- Multistage, because the enthalpy drop made available from (or to) the working fluid cannot be handled by a single stage with acceptable efficiency. The limit on the maximum enthalpy drop per stage is much tighter for compressors, where the adverse pressure gradients create a much higher risk of boundary layer separation.

- Rotational speed of the gas turbine compressor and the gas turbine are the same, because they are mounted on the same shaft. In multi-spool gas turbines there is a shaft for the HP compressor and HP turbine and another – coaxial to the first – for the LP compressor, LP turbine and generator (possibly with a reduction gear).

The first, fundamental step in evaluating turbomachinery performance is what is called "1–D" design. Also termed "mean-line" design, because the flow is analyzed along the mean diameter, it is used to lay out a first approximation of the engine: thermodynamic conditions, mean velocities and angles at inlet and outlet of each cascade, mean diameters, blade height and chord, solidities*, etc. Despite their relative simplicity, proper mean line methods can predict the efficiency of an axial turbine within 1-2% (Macchi, 1985). Subsequent refinements involve 2-D and quasi-3-D analyses: "through-flow" calculations (Hirsch and Denton, 1981) – whereby the radial equilibrium equations are solved in the plane containing the axis – and "blade-to-blade" analyses – whereby the flow is solved on an axisymmetric surface concentric with the axis (Fig. 2.6). The speed and the large memory capacity of modern computers have recently made possible full 3-D viscous flow analyses. At present these computations are used to verify the flow field corresponding to given inlet and outlet conditions for a single cascade or – in some case – for a whole stage**. Although the continuous, spectacular increase of computer speed may soon make possible the use of 3-D viscous calculations as a design tool for

* Solidity – generally denoted by σ – is the ratio between blade chord and blade spacing along the tangential direction. Given all things equal, the higher σ the higher the number of blades and the more the cascade is "filled" with blades, which justifies the name given to σ.

** The simulataneous calculation of the flow through stationary and rotating cascades poses formidable problems because the relative motion of the two cascades – whereby the blade of one cascade "sees" the periodic passage of the blades of the other cascade – requires: (i) to assume that the flow is "truly" unsteady, thus preventing from using many computational algorithms developed to accelerate the convergence of steady flow solutions; (ii) to interface properly the computational grids of the stationary and the rotating cascade, which inevitably leads to very large memory requirements.

single stages, the design of a whole multistage machine will presumably rely on 1-D and 2-D analysis for quite a long time.

Even if it involves only the solution of algebraic equations, the 1-D design of a multistage turbomachine can be very demanding (Lozza, Macchi and Perdichizzi, 1982) and goes beyond the scope of a thermodynamic analysis which, as emphasized in the previous paragraph, requires to determine only efficiency and cooling flows. All other quantities (see next paragraph) are relevant to the design of the turbomachine, but don't directly affect cycle thermodynamics.

2.2.2 Relevant concepts and parameters

This paragraph introduces fundamental turbomachinery concepts and parameters mentioned in later chapters.

2.2.2.1 Similarity Theory

Similarity theory comes from applying dimensional analysis to the laws defining the behaviour of a turbomachine (Csanady, 1964; Balje, 1981). Basically, it states that if two turbomachines are *geometrically similar* (ratio between the dimensions of all components is constant) and operate with the same dimensionless groups (specific speed, specific diameter, etc., see further), then they have the same efficiency. Departures from this theoretical behaviour may be due to: (i) compressibility (differences in Mach numbers); (ii) viscosity (differences in Reynolds numbers); (iii) scale (preventing the realizing of perfect geometrical similarity); (iv) fluid properties (different variations of specific heat, real gas effects); (iv) cavitation (hydraulic machines only).

2.2.2.2 Specific speed

Specific speed is the most important dimensionless group appearing in similarity theory:

$$n_s = \omega \cdot V_{in}^{0.5}/\Delta h_{is}^{0.75} \quad \text{for compressor stages}$$
$$n_s = \omega \cdot V_{out}^{0.5}/\Delta h_{is}^{0.75} \quad \text{for turbine stages} \qquad (2.1)$$

where ω is the rotational speed [rad/s], V_{in} and V_{out} are the volumetric flows at the stage inlet and outlet [m³/s], Δh_{is} is the stage isentropic enthalpy drop (or rise). In order to remove the dependence on stage efficiency, V_{out} is always referred to isentropic outlet conditions (also for D_s and SP, see below). For compressors, the definition is in terms of V_{in} because the architecture of a turbomachine stage is always determined by the largest volumetric flow.

Each class of turbomachines attains optimum efficiencies within a rather narrow range of n_s (Fig. 2.7). In particular (Csanady, 1964):

$$n_{s,opt} = 1.5-5 \quad \text{for axial compressors}$$
$$n_{s,opt} = 0.3-2 \quad \text{for axial gas and steam turbines}$$

The important implication is that the rotational speed, the volumetric flow and the specific work (Δh) of a turbomachine stage cannot be assigned arbitrarily: to obtain good efficiencies they must give a value of n_s within the range typical of the turbomachine class considered.

2.2.2.3 Specific Diameter

Specific diameter is another dimensionless group appearing in similarity theory:

$$D_s = D_m \cdot \Delta h_{is}^{0.25}/V_{in}^{0.5} \quad \text{for compressor stages}$$
$$D_s = D_m \cdot \Delta h_{is}^{0.25}/V_{out}^{0.5} \quad \text{for turbine stages} \qquad (2.2)$$

where D_m is the mean stage diameter. If "pure" similarity were to hold – i.e. no compressibility, viscous, scale and fluid property effects – then the efficiency of a class of turbomachines would be a function of only n_s and D_s, with a maximum for one peculiar combination $(n_s,D_s)_{opt}$ (Fig. 2.8). A popular, empirical diagram due to Cordier (Fig. 2.9) depicts the locus of all such $(n_s,D_s)_{opt}$.

2.2.2.4 Size Parameter

The size parameter is the ratio between D_m and D_s:

$$\begin{aligned} SP &= D_m/D_s = V_{in}^{0.5}/\Delta h_{is}^{0.25} && \text{for compressor stages} \\ SP &= D_m/D_s = V_{out}^{0.5}/\Delta h_{is}^{0.25} && \text{for turbine stages} \end{aligned} \tag{2.3}$$

Since for each class of turbomachines D_s falls in a narrow range, SP is proportional to the actual stage size, and can be used as an indicator of scale effects.

The definitions of Eq.(2.3) apply to one stage, i.e. to a situation where V is clearly defined by the conditions at the stage outlet (or inlet). In order to use SP in the continuous expansion model of Ch. 3 – where stage outlet conditions are not known – it is necessary to the extend its definition by referring to the local volumetric flow (see Par. 4.6.1):

$$SP_{local} = V_{local}^{0.5}/\Delta h_{is}^{0.25}$$

2.2.2.5 Load factor

The load factor establishes a link between stage specific work and kinematic quantities:

$$k_{is} = \Delta h_{is}/(u^2/2) \tag{2.4}$$

where u is the blade peripheral speed ($\omega \cdot D/2$); alternative definitions resulting in values proportional to k_{is} are called "head coefficient" or "head number". As for all other dimensionless groups, to obtain good efficiencies the value of k_{is} must fall within a well defined range:

k_{is} = 0.1–0.25 for axial compressor stages

k_{is} = 1–3 for high-reaction, axial turbine stages

k_{is} = 2–6 for low-reaction, axial turbine stages

With low-density fluids like gas or steam, material stresses are dominated by the centrifugal force field, i.e. by u (for state-of-the-art gas turbines u=400–450 m/s). Thus, since u is limited by material strength, k_{is} indicates the maximum work which can be obtained by one stage. The first, heavily-cooled stages of gas turbines are designed with high k_{is} in order to "bring down" the gas temperature as quickly as possible*.

2.2.2.6 Degree of reaction

The degree of reaction is the ratio between the enthalpy drop (or rise) in the rotor and the total change of enthalpy in the stage. There can be several definitions depending on the expansion (or compression) path considered; referring to the isentropic process:

$$r_{is} = \Delta h_{is,r}/\Delta h_{is} \qquad (2.5)$$

* There are actually two schools of thought regarding this point (Benvenuti, 1990). The first – followed by General Electric – favours zero-degree of reaction, high-k_{is} designs with the aim of reducing the number of stages (and thus heat transfer areas and costs) despite some efficiency penalty. The second – followed by ABB, Siemens and others – adopts non-zero degree of reaction, lower-k_{is} designs, thus obtaining higher fluidynamic efficiencies but also larger surfaces to be cooled and more stages.

Typically, low-degree of reaction stages produce more work (higher k_{is}) but yield lower efficiencies. Zero-degree of reaction stages are also called impulse stages.

In axial turbines designed for optimum efficiency there is a strict correlation between $k_{is,opt}$ and $r_{is,opt}$, a correspondence which is rather indipendent of scale (Macchi and Perdichizzi, 1981). In particular, for low r_{is} the optimum k_{is} is high, i.e. impulse stages are optimized when they produce much work.

2.2.2.7 Flow factor

The flow factor φ is a measure of the "swallowing" capacity of a turbomachine. For an axial stage:

$$\varphi = v_{a,out}/u \quad \text{for turbines}$$
$$\varphi = v_{a,in}/u \quad \text{for compressors} \qquad (2.6)$$

where v_a is the axial component of the absolute flow velocity, i.e. the component responsible for the transport of volumetric flow. Under the assumptions of perfect similarity all stages which are geometrically similar are characterized by a unique relationship – called characteristic line – betweeen the flow and the load factor.

2.2.2.8 Velocity triangles

Velocity triangles are formed by the absolute, peripheral and relative velocities at inlet and outlet of a turbomachine rotor (Fig. 2.10a and 2.10b). "Absolute" refers to a stationary reference system; "relative" to a system rotating with the rotor. Notice that v and w represent average velocities; in reality, in the channel between blades there are dramatic variations of velocity. If the ratio H/D_m between blade height and mean diameter is small – 5–10% – the velocity triangle at the mean diameter can be considered representative of the whole flow. For higher H/D_m, radial variations cannot be neglected. Fig. 2.11 reports the velocity triangles of the last stage of a steam turbine with H/D_m=0.3.

Defining the velocity triangles of a stage essentially coincides with defining its operating characteristics because Δh_{is}, k_{is}, r_{is}, φ and – indirectly – n_s and D_s all depend on the velocity triangles.

2.2.2.9 Scale effects

Departures from similarity depend on the size of the turbomachine. They are caused by: (i) lack of geometric similarity due to manufacturing constraints; (ii) differences in Reynolds numbers which – all other things equal – are proportional to the reference characteristic dimension. The former is generally more important and is due to the inability to manufacture machines with clearances, surface roughness, trailing edge thickness, etc. below certain limits; thus, when going from "large" to "small" engines, it is impossible to maintain the same ratio between the dimension of all components (see Par. 4.4 for details).

Macchi and Perdichizzi (1981), have shown that scale effects can dramatically reduce the efficiency to be expected by an axial turbine stage and that the maximum efficiency achievable by optimizing a stage depends on the size parameter SP (see also Par. 4.4.1).

2.2.2.10 Compressibility effects

Compressibility effects consist of departures from similarity due to variations of volumetric flow between stage inlet and outlet. Large flow variations require strong variations – between inlet and outlet – of cross sectional areas and axial velocities; moreover, in a multi-stage engine subsequent stages cannot be identical because, all other things equal, variations of V cause variations of n_s. Notice that, besides the Mach number, a very important indicator of compressibility is the volumetric ratio V_{out}/V_{in}: a supersonic stage with $V_{out}/V_{in} \leq 2-3$ still behaves very similarly to a stage handling incompressible flow (i.e. $V_{out}/V_{in}=1$, see Fig. 2.12).

2.2.3 Definitions of efficiency

The quality of the thermodynamic process taking place within a turbomachine is expressed by its "efficiency". This statement qualitatively defines "efficiency" as an indicator of turbomachine performance but, due to the diverse definitions of efficiency used in practice, it is so undefined as to be almost useless; Wilson (1984, p.83) appropriately points out that "... *competition in machine efficiencies is marked by charlatanism principally because of intentional or unintentional failure to define which of many efficiency is being used*".

2.2.3.1 Isentropic and politropic efficiency

The two definitions most commonly used for cycle thermodynamic analyses are the *isentropic (or adiabatic) efficiency* η_{is} and the *politropic efficiency* η_p:

$$\begin{aligned} \eta_{is} &= \Delta h_{is}/\Delta h && \text{for compressors} \\ \eta_{is} &= \Delta h/\Delta h_{is} && \text{for turbines} \end{aligned} \tag{2.7}$$

$$\begin{aligned} \eta_p &= dh_{is}/dh = [v\cdot dP]/[v\cdot dP+\delta W_l] && \text{for compressors (dP>0)} \\ \eta_p &= dh/dh_{is} = [v\cdot dP+\delta W_l]/[v\cdot dP] && \text{for turbines (dP<0)} \end{aligned} \tag{2.8}$$

where the definitions refer to <u>adiabatic</u> processes (not necessarily coinciding with one stage) and δW_l is the work lost (or required) by irreversibilities. These two efficiencies coincide only for infinitesimal processes; for finite ΔP they differ because — since in the h-s diagram the vertical distance between two isobars increases as s increases (Fig.2.13) — $\int dh_{is}$ along the actual transformation is different from Δh_{is}.

While η_p depends only on the ratio $[\delta W_1/v\cdot dP]$ — i.e. which fraction of ideal work is lost by irreversibilities — η_{is} depends both on $[v\cdot dP/\delta W_1]$ and the expansion (or pressure) ratio; for this reason η_p is a much more appropriate indicator of the quality of an adiabatic process. The term "politropic" comes from the fact that a process at constant η_p is a politropic transformation described by the equation $P\cdot v^m$=constant, where:

$$\eta_p = [(\gamma-1)/\gamma]/[(m-1)/m] \quad \text{for compressors}$$
$$\eta_p = [(m-1)/m]/[(\gamma-1)/\gamma] \quad \text{for turbines} \qquad (2.9)$$

2.2.3.2 Inclusion of kinetic terms

For transformations like the ones occuring in a turbomachine stage where the variation of kinetic energy is of the same order of Δh the definitions of Eqs.(2.7) and (2.8) become ambiguous, because they don't include the flow velocity. In this case it is necessary to distinguish between *static* and *total* conditions, where the latter are defined by $h_{tot}=h_{st}+v^2/2$ and $s_{tot}=s_{st}$ (Fig. 2.14). This distinction produces three different definitions:

- Total-to-total efficiency η_{tt}, which compares actual and ideal variations of total enthalpy. This definition assumes that the flow is properly defined by its total conditions, i.e. either kinetic energy is negligible, or it can always, totally be converted into pressure rise ($P_{tot}-P_{st}$).
- Static-to-static efficiency η_{ts}, which refers only to static enthalpies and disregards any variation of kinetic energy.

- <u>Total-to-static</u> efficiency η_{ts}, which compares the actual stage work – always given by Δh_{tot} – to the variation between total inlet conditions and static outlet conditions. This definition assumes as potentially recoverable the kinetic energy at inlet but not the one at outlet.

It must be emphasized that these definitions are relevant only for the description of what takes place "inside" the turbomachine, i.e. to analyze single stages or single cascades; for a whole turbomachine the difference between inlet and outlet kinetic energy is generally negligible, and therefore $\eta_{tt}=\eta_{ss}=\eta_{ts}$.

Specific expressions and discussions on the significance of each definition can be found in textbooks (e.g. Vavra, 1960, pp.422-423, or Wilson, 1984, pp.83-97). For the sake of simplicity I'll give here only the formulation for expansion processes. Referring to Fig. 2.14, isentropic efficiencies are defined by:

$$\eta_{is,tt} = \Delta h_{tot}/\Delta h_{is,tot} = [(h_1-h_2)+(v_1^2-v_2^2)/2]/[(h_1-h_{2'})+(v_1^2-v_2^2)/2]$$

$$\eta_{is,ss} = \Delta h_{st}/\Delta h_{is,st} = (h_1-h_2)/(h_1-h_{2'})$$

$$\eta_{is,ts} = (h_{1,tot}-h_{2,tot})/(h_{1,tot}-h_{2',st}) = [(h_1-h_2)+(v_1^2-v_2^2)/2]/[(h_1-h_{2'})+v_1^2/2]$$

The definition of politropic efficiency for an elementary, infinitesimal process is problematic, because in a turbomachine rotor the absolute kinetic energy changes discontinuosly from inlet to outlet according to the velocity triangles. Nonetheless, the definitions of η_{tt} and η_{ss} can be extended to an infinitesimal process as follows:

$$\begin{aligned} \eta_{p,tt} &= dh_{tot}/dh_{is,tot} = [dh+d(v^2/2)]/[dh_{is}+d(v^2/2)] \\ \eta_{p,ss} &= dh_{st}/dh_{is,st} \end{aligned} \qquad (2.10)$$

<u>2.2.3.3</u> <u>Reheat factor</u>

The reheat factor r_h accounts for the difference between the value of $\int dh_{is}$ calculated along an isentropic line and the value calculated along a politropic. Using the same symbols of Fig. 2.13, the definition of r_h for a turbine is (for details see Wilson, 1984, p. 95):

$$r_h = \Sigma\Delta h_{is,i}/\Sigma\Delta h^*_{is,i} = [\int dh_{is}]_{politropic}/[\int dh_{is}]_{isentropic} > 1$$

It is easy to show that $r_h = \eta_{is}/\eta_p$, where η_{is} and η_p are overall efficiencies based on inlet and outlet conditions. For cooled turbines the definition above becomes ambiguous, because $\Delta h^*_{is,i}$ is "artificially" augmented by the temperature decrease due to cooling. If the coolant flow is very high, η_{is} and η_p may even be larger than one, and consequently $r_h<1$.

2.3 Simple cycle gas turbines

Predicting the performances of modern gas turbines is quite difficult for a number of reasons. Among the most important:

- Air bled from several points of the compressor is reinjected into the hot gases after cooling turbine nozzles and blades, discs, bearings, etc.
- Compression and expansion occur neither adiabatically nor with constant polytropic efficiency.
- Turbomachinery efficiency depends on size, pressure ratio, number of stages and number of shafts.
- Leakage, pressure drops and heat losses take place in many parts of the engine.
- The flow is highly turbulent, unsteady, often with marked 3-D behaviour.

Accurate evaluation of these complex phenomena can be performed only by manufacturers, who can resort to exhaustive experimentation to calibrate computer programs specifically developed for a single engine ("cycle decks"). Besides being proprietary, such codes are geared toward the detailed simulation of the turbomachinery and are not suitable for thermodynamic analyses of a wide range of cycle parameters and configurations.

Given that adequate programs were not available (see Par. 3.2.2), the parametric analyses envisioned for this Thesis could be realized only by developing a new calculation model, for which there were two basic and antagonistic requirements:

1. Be simple enough for use on a wide array of configurations.
2. Be accurate enough to capture all major physical phenomena.

2.3.1 Definition of Turbine Inlet Temperature

Given the crucial role it plays in gas cycle analyses, the turbine inlet temperature (TIT) must be defined unequivocally. Following a convention widely used among manufacturers and in the technical literature, TIT is defined as the total temperature at the first rotor inlet (see Fig. 2.15). For an uncooled machine this is equal to the combustor outlet temperature; when the first nozzle is cooled the two temperatures differ due to injection of cooling air, and TIT is a weighted average of the combustor outlet and cooling air temperature. Since only the rotor inlet total temperature determines the work that can be produced in the turbine, the TIT defined above is approximately equivalent to the one of an engine where the first nozzle is uncooled, and the combustor outlet temperature equals the given TIT*: for this reason, the nozzle cooling flow is often referred to as "non-chargeable". If nozzle total pressure losses are incorporated into combustor losses, all machines with no cooling downstream of the first nozzle can be considered uncooled.

2.3.2 ISO ambient conditions

Unlike steam plants, the performance of gas turbine systems varies strongly with ambient conditions because:

- The mass flow entering the compressor – which determines power output – is proportional to P_{amb}/T_{amb}; depending on location and the period of the year, the variation of such ratio can be as large as 20%.

---

* The equivalence is not rigorous because the cooling flow in the nozzle follows an expansion path different from the mainstream flow and causes additional total pressure losses (see Par. 4.2.1).

- Variations of T_{amb} induce variations of compressor work, compressor outlet temperature, fuel flow rate and, ultimately, cycle efficiency.

For these reasons, the definition of ambient conditions is particularly important. All calculation of Chs. 7 and 10 are referred to standard ISO conditions:

- T_{amb}=15°C, P_{amb}=101.325 kPa, absolute humidity 0.0065 (i.e. relative humidity φ=60%).

- Molal composition of dry air 78.09% N_2, 20.95% O_2, 0.93% Ar, 0.03% CO_2.

2.4 Steam cycle

Even if the steam section does not exhibit many high-tech features, it has very important impacts on the overall performances of a GSC. An improper design of the steam section may well result in efficiency penalties of 2-3 percentage points, thus erasing the benefits brought about by advancements in gas turbines technology.

The steam cycle introduces two major complications: (i) optimization of the Heat Recovery Steam Generator (HRSG) temperature profile; (ii) estimation of steam turbine efficiency. The former aims at minimizing the losses due to irreversible heat transfer (see Par. 8.1) and requires:

- Adopting several evaporation pressures
- Properly arranging the sequence of economizers, boilers and superheaters (Fig. 2.16)

As for the steam turbine, there are a number of issues which substantially differentiate it from the gas turbine:

- There is no blade cooling.
- The volumetric expansion ratio V_{out}/V_{in} is much higher than that of gas turbines (1000 against 10–15). Consequently, the estimation of steam turbine efficiency cannot neglect the variation of n_s between turbine inlet and outlet*.
- In order to limit the specific speed of the last stages, the low pressure section is often split in two, or possibly four cyclinders.
- The expansion ends within the two-phase region; liquid droplets cause additional fluidynamic losses, which must be accounted for by penalizing the efficiency of the last part of the expansion.

---

* At constant ω and Δh_{is}, n_s can vary by a factor larger than 30. In practice, the higher D_m of LP stages allows increasing u and thus Δh_{is}, limiting the variation of n_s (without flow splitting) to a factor of 20–25. For comparison, the variation of n_s experienced in a gas turbine is rarely larger than 5.

2.5 Integrating the gas and steam sections

The integration of the gas turbine and the steam section poses further challenges because:

- For most mixed cycles, the calculation of the gas turbine requires the knowledge of steam/water conditions and flow rate. In turn, such information is available only after knowing the gas turbine outlet conditions.

- The gas and steam section of "conventional" Combined Cycles can be calculated sequentially. However, alternative configurations may require iterations similar to mixed cycles: heat recovery from gas turbine intercooler, steam cooling, water pre-heating with heat discharged by gas turbine cooling flows, etc.

These circumstances call for the simultaneous calculation of all cycle components. However, the relationships modeling each component are mostly non-linear, and often require internal iterations to account for working fluid property variations and/or step-wise calculation schemes (e.g. the gas turbine). Thus, an analytical solution is completely impractical; the only option is an iteration scheme whereby cycle components are calculated sequentially until convergence. The iteration scheme poses serious numerical challenges because:

- The system to be solved is highly non-linear.

- The choice of the convergence criterion is critical because there are variables which converge more slowly than others*. Requiring convergence on *all* variables at *all* points may be useless because, as long as temperature, pressure and mass flow at key points do no longer change from one iteration to the other it is irrelevant if, say, the gas turbine exit Mach number has not yet converged.

- Commercial routines for the solution of non-linear algebraic systems cannot be used due to constraints on computational time. In fact, such routines necessitate at least tens (often hundreds) of iterations for each convergence variable and their use would require computer speeds 2–3 orders of magnitudes higher than that of present, 486 desktop computers.

* In some case there are variables experiencing "micro-oscillations" which retard convergence, a phenomenon which might indicate the possibility of numerical instabilities.

2.6 Implementation on existing engines and off-design issues

One further issue arises when considering the implementation of mixed cycles to gas turbines designed for simple cycle operation. While in a Combined Cycle the gas turbine is not affected by the presence of the bottoming steam cycle – except for the higher discharge pressure losses caused by the HRSG – in a steam injected cycle the mass flow and the enthalpy drop across the gas turbine are substantially modified. The larger mass flow can be accommodated only by increasing the expansion ratio, which in turn calls for a higher compression ratio. This problem is specifically addressed in a paper by Consonni, Lozza and Macchi (1988) and therefore will not be covered in this Thesis.

Aside from the peculiarities of steam injection, the issue of off-design operation is important both to the designer and the user because:

- Unlike steam cycles, gas turbine power output varies strongly with ambient temperature. Thus, in order to estimate the economic rate of return it is necessary to account for the cyclic variation of ambient conditions.
- To maintain good off-design heat recovery from the gas turbine exhaust evaporation pressures should "slide" with load. This complicates substantially the calculation of off-design performances: Gyarmathy and Ortmann (1991), have analyzed CCs with up to two pressure levels.
- The higher the system complexity (e.g. intercooling, regeneration, reheat, steam cooling, etc.), the more demanding (and important) the estimation of off-design performance.

Although off-design performances constitute an important aspect for the evaluation of GSCs, their inclusion into the present work would make the analysis and the calculation model too involved to be included in this Thesis. Therefore, off-design issues have not been considered here; the calculation model exclusively evaluates design performance.

2.7 Approach adopted in this work

A detailed treatment of all the issues mentioned in this Chapter is much beyond the scope of this Thesis. Since the objective was the estimation of overall thermodynamic characteristics I have proceeded as follows:

- Many turbomachinery issues have been left aside, addressing only the ones strictly necessary to estimate efficiency and cooling flows.
- The analysis is limited to <u>on-design</u> conditions, always assuming that each component is specifically designed to operate under the conditions being calculated.
- Rather than focusing on the characteristics of each component (e.g. turbomachinery 1-D design), I have given priority to thermodynamic judgment (e.g. entropy analysis of Ch. 8) and the capability to handle system complexity (e.g. full integration between gas and steam sections).
- Convergence of the calculation scheme is sought by a heuristic method which, although it doesn't guarantee a solution, has always worked successfully within very few iterations.

REFERENCES

Balje O.E. (1981), Turbomachines, A Guide to Design, Selection and Theory, John Wiley, New York.

Benvenuti E. (1990), Head of Research and Development, Nuovo Pignone, Florence, Italy, Personal Communication.

Chiesa P., Consonni S. and Lozza G. (1992), "Gas/Steam Cycles with Open Circuit Steam Cooling of Gas Turbine Blades", to be presented at the 2nd Florence World Symposium on Energy Research, Florence, Italy, May 1992. Proceedings published by Nova Science, New York.

Consonni S, Lozza G. and Macchi E. (1988) "Turbomachinery and Off-Design Aspects in Steam-Injected Gas Cycles", Proc. of the *23rd IECEC (Denver, Aug. 1988)*, pp. 99-108.

Csanady G.T. (1964), Theory of Turbomachines, McGraw-Hill, New York.

Gyarmathy G. and Ortmann P. (1991), "The Off-Design of Single and Dual Pressure Steam Cycles in Combined Cycle Plants", Proc. of the *V ASME COGEN-TURBO (Budapest)*.

Hirsch Ch. and Denton J.D. editors (1981), "Through Flow Calculations in Axial Turbomachines", *AGARD AR-175*, Neuilly sur Seine, France.

Lozza G., Macchi E. and Perdichizzi A. (1982), "On the Influence of the Number of Stages on the Efficiency of Axial-Flow Turbines", ASME Paper 82-GT-43.

Macchi E. (1985), "Design Limits, Basic Parameter Selection and Optimization Methods in Turbomachinery Design", in *Thermodynamics and Fluid Mechanics of Turbomachinery*, Ücer A.S., Stow P. and Hirsch Ch. editors, Vol. II, pp. 805-828, Martinus Nijhoff Publishers, Dordrecht, The Netherlands.

Macchi E. and Perdichizzi A. (1981), "Efficiency Prediction for Axial-Flow Turbines Operating with Nonconventional Fluids", J. of Eng. for Power, Vol. 103, pp.718-724.

Serovy G. (1981), "Axial-Flow Turbomachine Through-Flow Calculation Methods", in *AGARD AR-175*, pp. 285-305, Neuilly sur Seine, France.

Vavra M.H. (1960), Aero-Thermodynamics and Flow in Turbomachines, John Wiley, New York.

Wilson, D.G. (1984), The Design of High-Efficiency Turbomachinery and Gas Turbines, The MIT Press, Cambridge, Massachusetts.

NOMENCLATURE

c	Blade chord (Fig.2.10a)	[m]
D_m	Stage mean diameter	[m]
D_s	Stage specific diameter (Eq.2.2)	
h	Specific enthalpy	[J/kg]
H	Blade height	[m]
k_{is}	Stage load factor (Eq.2.4)	
m	Politropic index (Eq.2.9)	
n_s	Stage specific speed (Eq.2.1)	
P	Pressure	[Pa]
r_h	Reheat factor (Par.2.2.3.3)	
r_{is}	Degree of reaction referred to the isentropic path	
s	Blade spacing (see Fig.2.10a) or	[m]
	specific entropy	[J/kg-K]
SP	Stage Size parameter (Eq.2.3)	[m]
u	Peripheral velocity, $\omega \cdot D/2$	[m/s]
v	Absolute velocity, or specific volume	[m/s, or m^3/kg]
V	Volumetric flow	[m^3/s]
w	Relative velocity	[m/s]
α	Angle of cascade discharge velocity (Fig.2.10a)	
Δh	Actual enthalpy drop (or rise)	[J/kg]
Δh_{is}	Isentropic stage enthalpy drop (or rise)	[J/kg]
ΔT_{ap}	Approach ΔT (Fig.2.16)	[°C]
ΔT_{pp}	Pinch point ΔT (Fig.2.16)	[°C]
ΔT_{sc}	Subcooling ΔT (Fig.2.16)	[°C]
φ	Relative humidity	
η	Efficiency	
σ	Solidity, c/s	
ω	Rotational speed	[rad/s]

Subscripts

a	Axial or Absolute system
amb	Ambient
ct	Cooled turbine
g	Gas
in	Stage inlet
is	Isentropic
opt	Optimum
out	Stage outlet
p	Politropic
r	Rotor or Relative system
ss	Static-to-static
st	Static conditions
tot	Total conditions
ts	Total-to-static
tt	Total-to-total
1	Rotor inlet
1n	Outlet of first stage nozzle
2	Rotor outlet

FIGURES

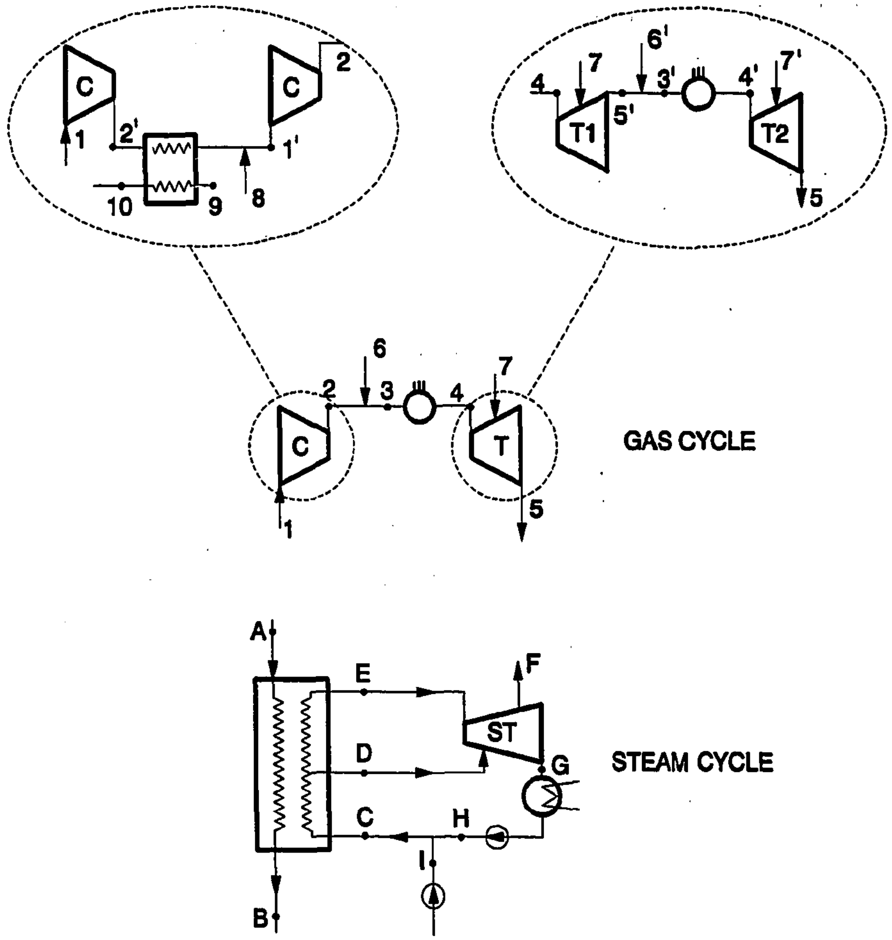

2.1a Schematic of gas turbine and steam cycles. The schemes within the dashed circles indicate that the base gas turbine cycle can be modified by adding intercooling and reheat.

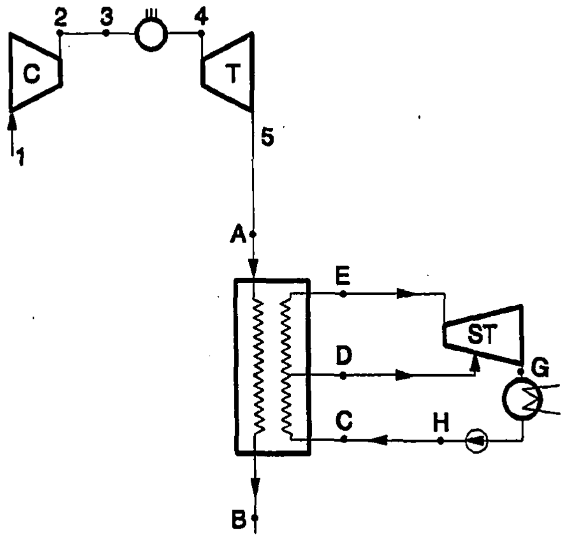

2.1b Schematic of dual-pressure Combined Cycle as obtained by connecting points 5 and A and suppressing points 6, 7, F, I of Fig. 2.1a.

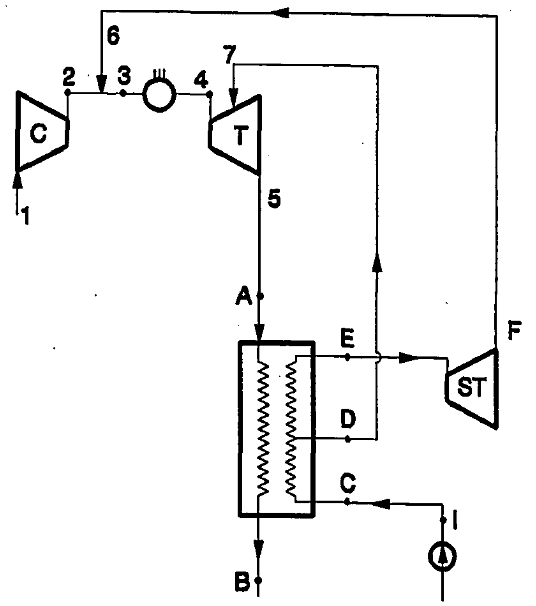

2.1c Schematic of dual-pressure steam injected cycle as obtained by connecting points 5–A, F–6, D–7 and suppressing points G, H of Fig. 2.1a.

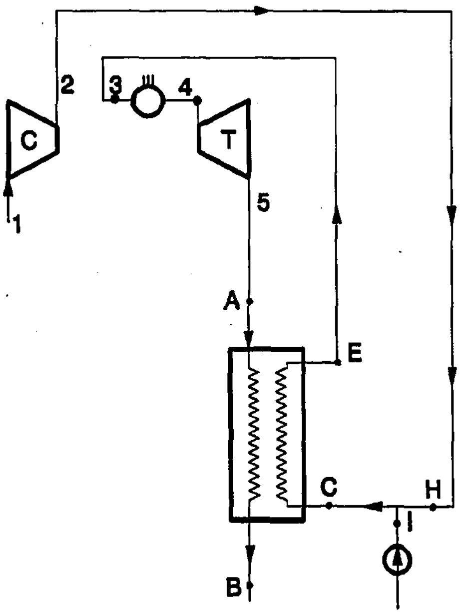

2.1d Schematic of water injected regenerative cycle as obtained by connecting points 5-A, 2-H, E-3 and suppressing points 6, 7, D, F, G of Fig. 2.1a.

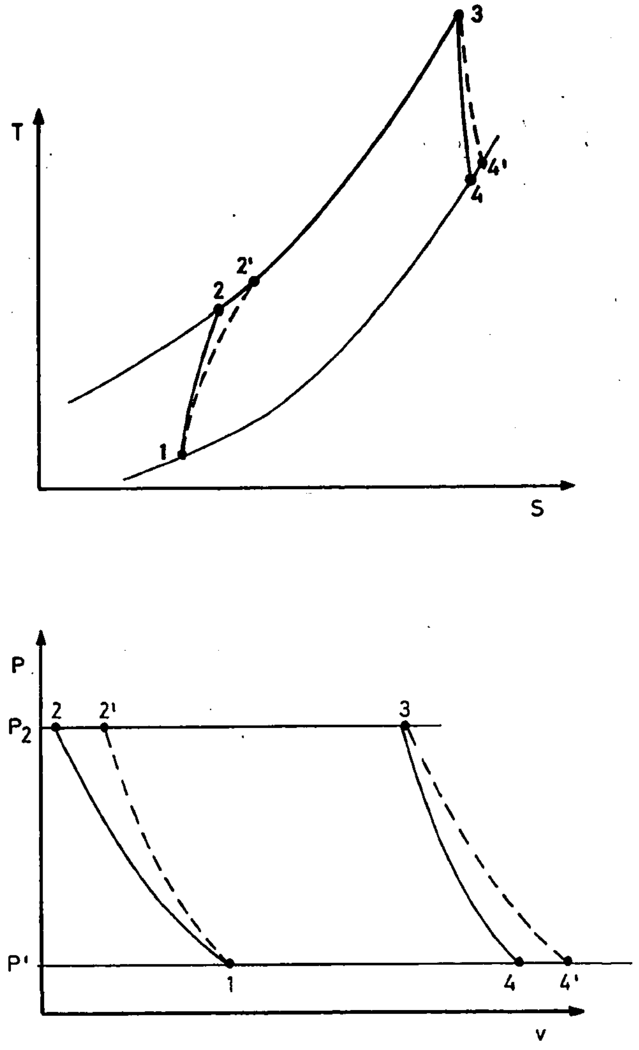

2.2 Influence of turbomachinery efficiency on gas turbine cycle thermodynamics. Dashed lines show the consequence of lower turbomachinery efficiency on a cycle with given pressure ratio and turbine inlet temperature.

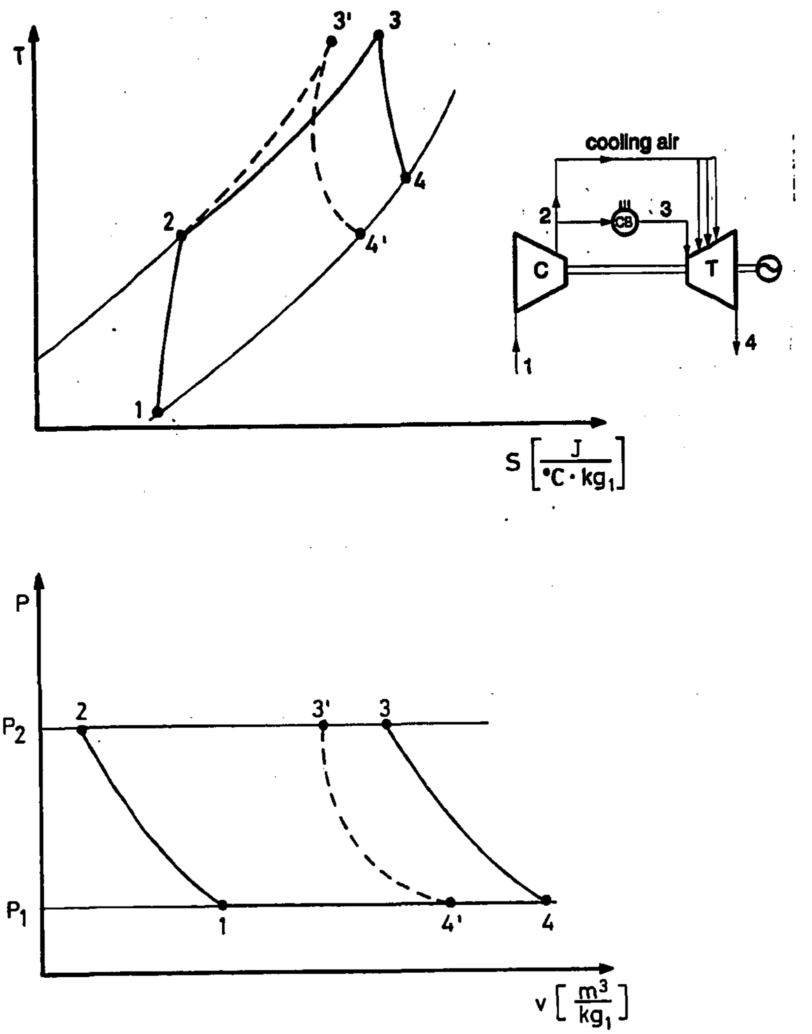

2.3 Influence of turbine cooling on gas turbine cycle thermodynamics. Solid lines indicate an uncooled cycle; dashed lines refer to a cycle where cooling air bled at point 2 (compressor exit) is injected along the first, high temperature section of the gas turbine. Notice that dashed lines 2–3' and 3'–4' refer to a mass flow different from the one at point 1. Since cooling air by-passes the combustor, the heat input per kilogram of air entering the compressor – indicated by kg_1 – is reduced, thus reducing entropy and volume (specific to kg_1) at point 3.

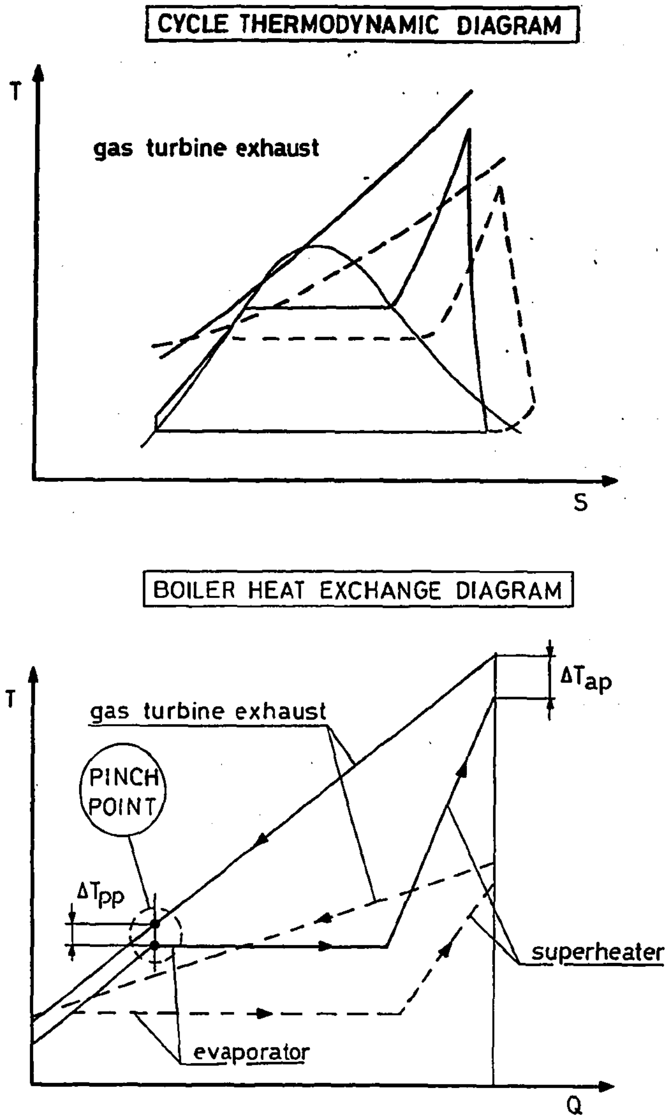

2.4 Influence of gas turbine outlet temperature (TOT) on the thermodynamics of a single-evaporation pressure bottoming steam cycle. Dashed lines show the consequence of lower TOT on a cycle with given condensation pressure. The heat recoverable in the evaporator and the superheater is approximately proportional to $TOT-T_{ev}-\Delta T_{pp}$(in the temperature range of interest the variations of gas specific heat are negligible); thus, in order to maintain acceptable heat recovery from the gas turbine exhaust when TOT decreases also T_{ev} must decrease.

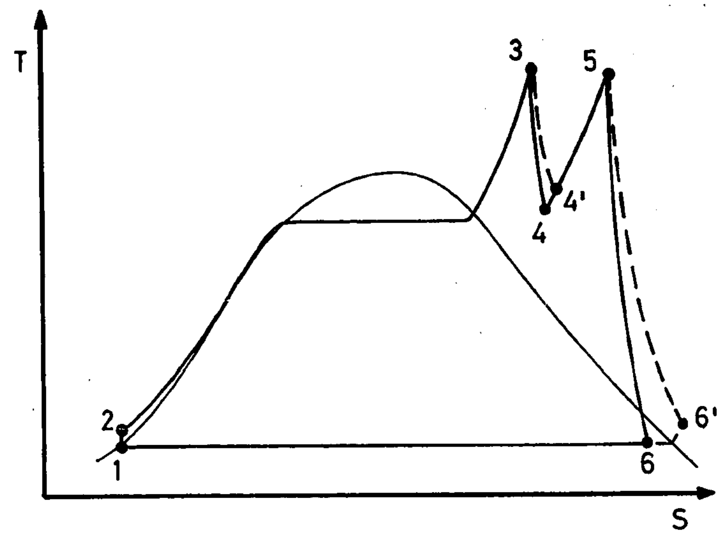

2.5 Influence of steam turbine efficiency on the thermodynamics of a single-evaporation pressure, single-reheat steam cycle. Dashed lines show the consequence of lower turbine efficiency on a cycle with given condensation, evaporation and reheat pressures and given maximum steam temeprature.

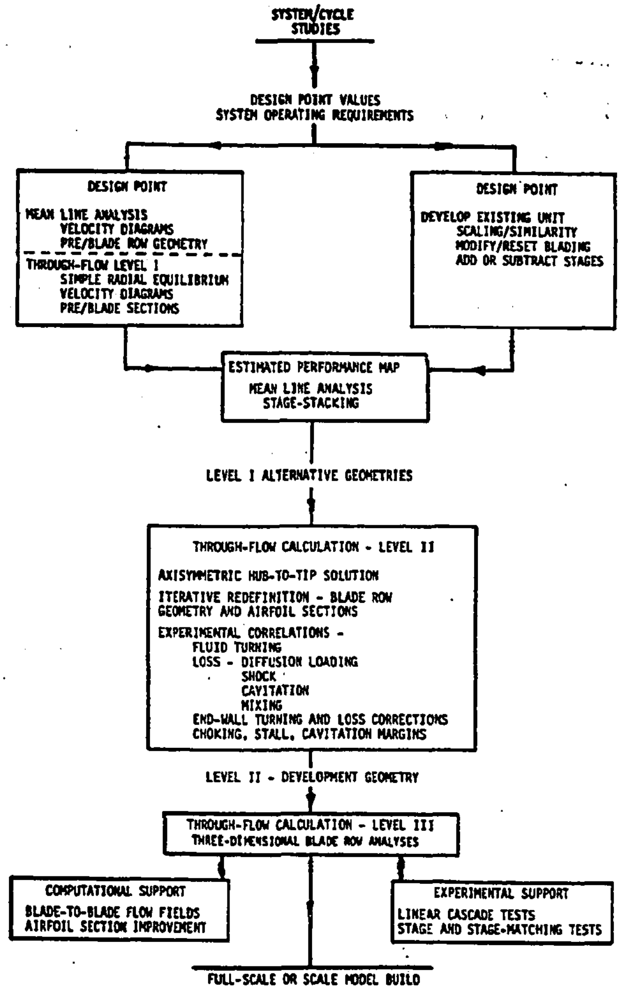

2.6 Scheme of the typical procedure followed for the design of an axial turbomachine (after Serovy, 1981).

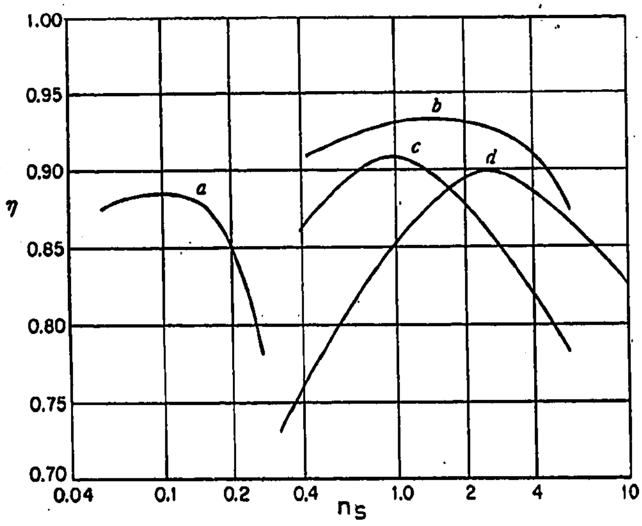

2.7 Attainable efficiencies of various turbomachines as function of specific speed (from Csanady, 1964): (a) Pelton wheels; (b) Francis and fixed blade propeller turbines; (c) large, single-stage centrifugal pumps; (d) compressors (polytropic).
"Attainable" means that it is possible to design a machine with efficiency as indicated in the figure. Due to constraints unrelated to efficiency – capital cost, noise, size, weight, etc – the efficiency of actual turbomachines may be lower.
Notice that outside the optimum range η collapses very quickly to unacceptably low values. Technological development acts by shifting the curves upward; however, the optimum range of n_s of each class of engines remains approximately the same.

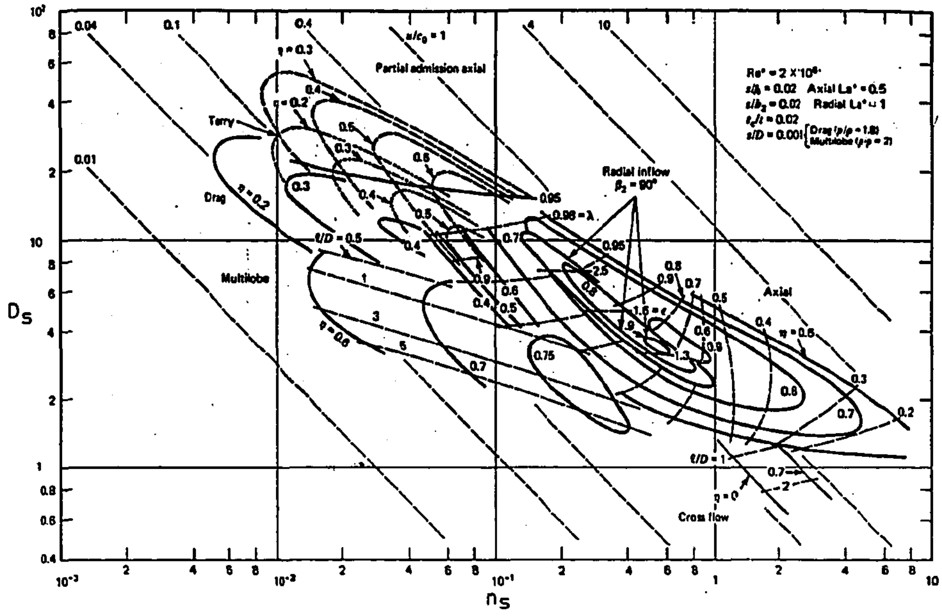

2.8 Efficiency contours of single-stage turbines operating with compressible fluids as function of n_s and D_s (from Balje, 1981). For each class of turbines there is a combination $(n_s, D_s)_{opt}$ giving maximum efficiency.

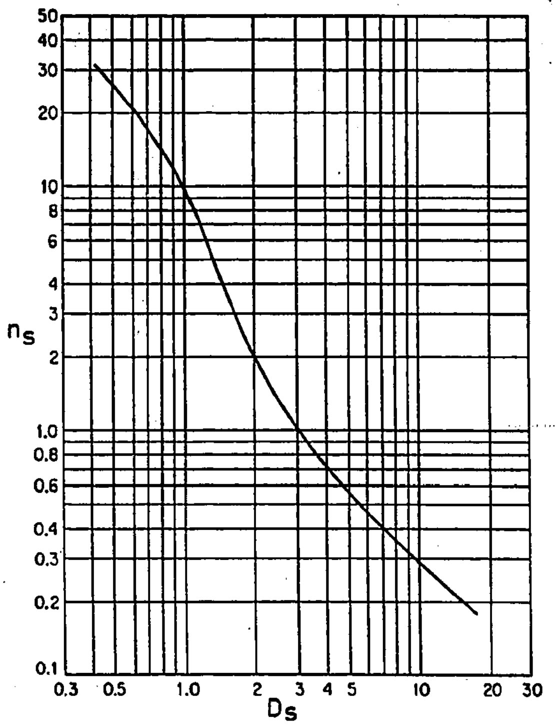

2.9 Cordier diagram showing the empirical relationship between n_s and D_s giving optimum efficiency (from Csanady, 1964). Each class of turbomachines – e.g. axial turbines, centrifugal pumps, cross-flow blowers, etc. – should be represented by one single point.

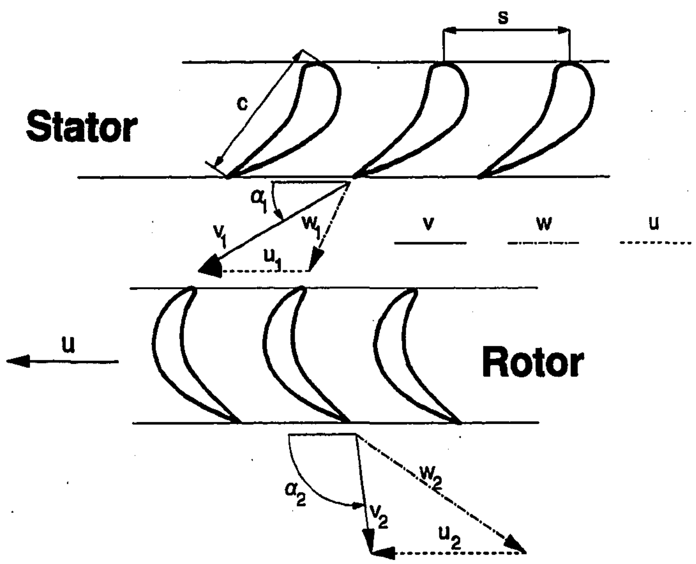

2.10a Velocity triangles of an axial turbine. u, v, w indicate peripheral, absolute and relative velocity, respectively; subscript "1" refers to rotor inlet, "2" to rotor outlet. The figure represents the generic situation with $u_1 \neq u_2$, i.e. $D_{m,1} \neq D_{m,2}$; this implies that the rotor blade cross-sections above lie on an axisymmetric surface with D variable along the axis. The blade chord c and the spacing s along the tangential direction – represented only for the stator – vary for each cascade.

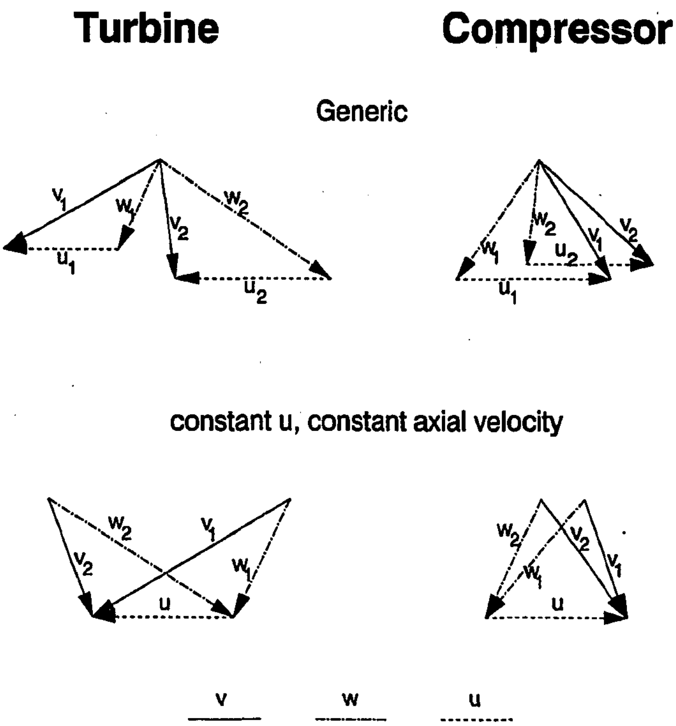

2.10b Velocity triangles of an axial turbomachine. For the vast majority of actual machines $D_{m,1}=D_{m,2}=D_m$, so that $u_1=u_2=u$; if the axial velocity is also constant (a very common design option) the triangles look like the ones on the bottom.

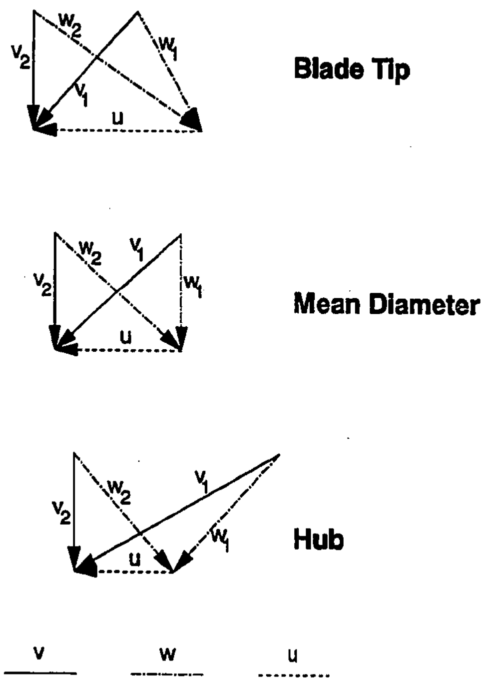

2.11 Variation of velocity triangles along the radial direction for an LP steam turbine stage with $H/D_m=0.3$. The triangles correspond to the conventional free-vortex design, whereby specific work and discharge velocity are constant along the radius.

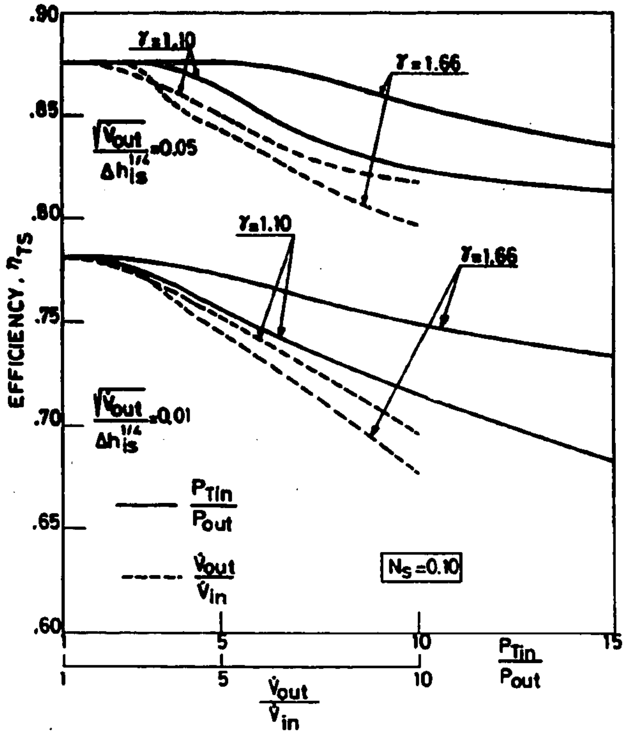

2.12 Influence of volumetric flow rate variations on the efficiency of an axial turbine stage with $N_s = n_s/2\pi = 0.10$, for two values of γ and two values of $SP = V_{out}^{0.5}/\Delta h_{is}^{0.25}$ (after Macchi and Perdichizzi, 1981).

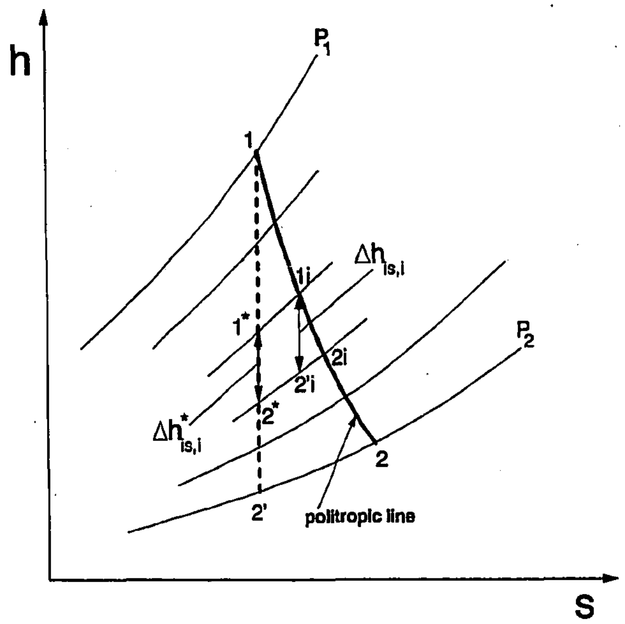

2.13 "Reheat effect" of turbines. Due to the divergence of isobaric lines $\Delta h^*_{is,i} < \Delta h_{is,i}$, and therefore $\int dh_{is}$ is larger when evaluated on the actual, politropic expansion line.

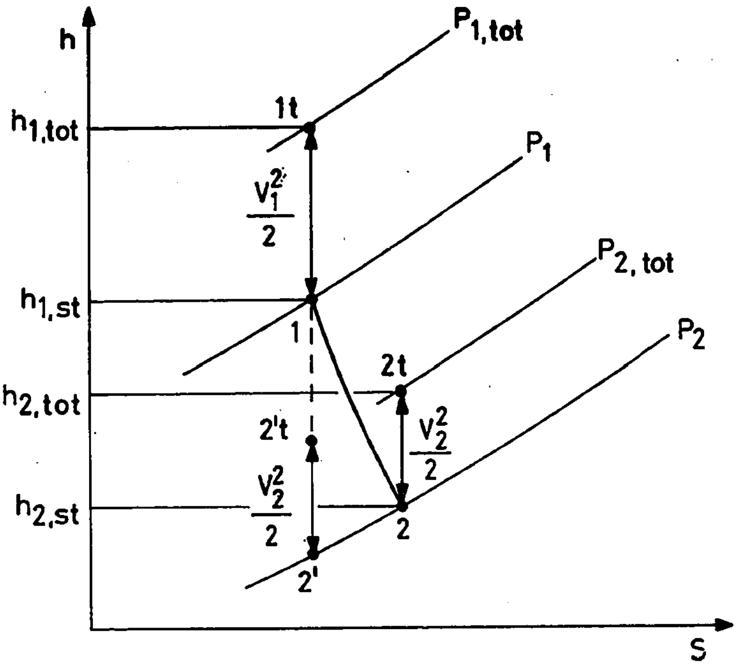

2.14 Thermodynamic diagram of the transformation taking place in a turbine rotor. Points 1 and 2 indicate conditions at rotor inlet and rotor outlet, respectively; point 2' indicates the conditions after an isentropic expansion.

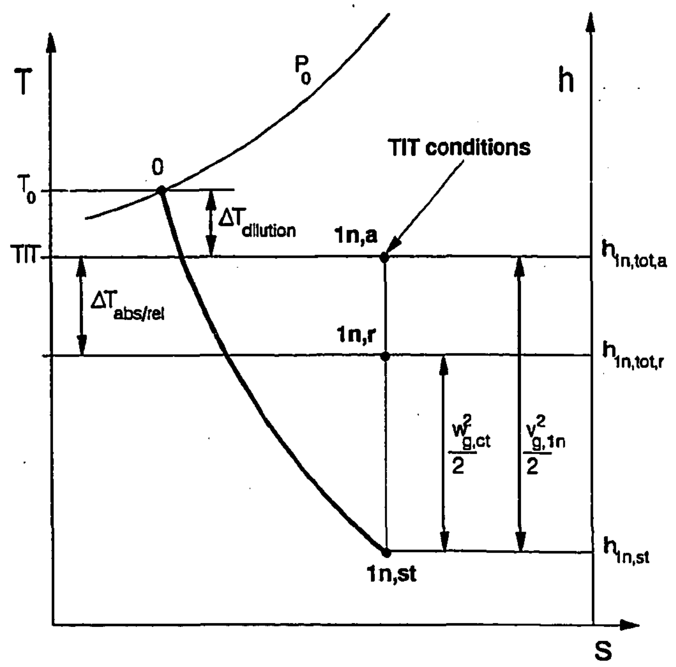

2.15 Definition of Turbine Inlet Temperature. Point 1n,st represents the static conditions at nozzle exit; 1n,a and 1n,r refer to the total conditions in the absolute and relative system, respectively. The difference T_0-TIT is due to dilution of the nozzle cooling flow; ΔT_{tot} is due to the difference between v and w and depends on the velocity triangles.

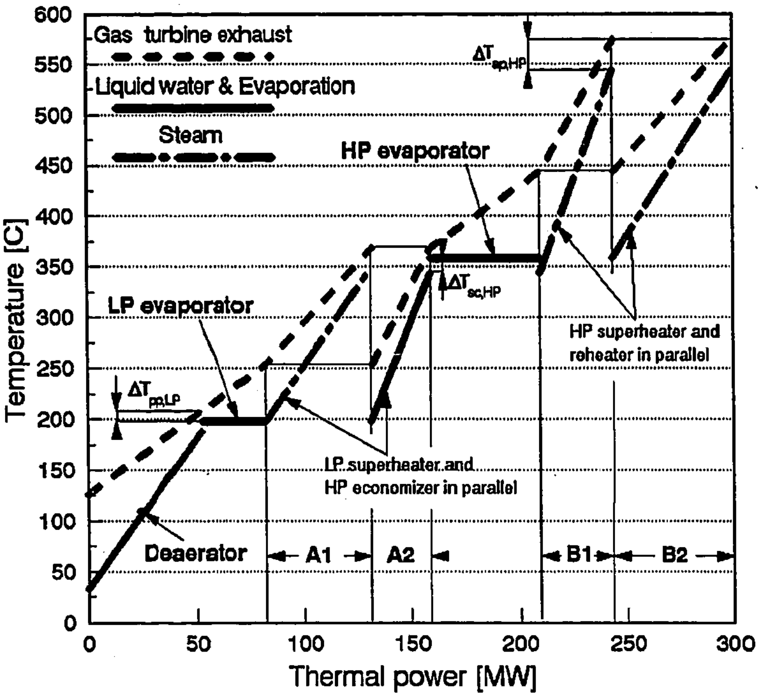

2.16 HRSG temperature profile of a two-pressure level, reheat Combined Cycle with tube banks "A" (LP superheater/HP economizer) and "B" (HP superheater/reheater) in parallel. The thin horizontal lines connecting the the gas flows at the beginning and at the end of the sections in parallel signify that at those location the gas flow(s) is split or merged. This arrangement allows keeping the gas and steam temperature very close together, thus reducing losses due to irreversible heat transfer. The figure also indicates the relevant temperature differences defining the HRSG profile: pinch point (ΔT_{pp}), subcooling (ΔT_{sc}) and approach (ΔT_{ap}).

3. COOLED TURBINE MODEL

This Chapter illustrates the model developed to compute the expansion taking place in cooled gas turbines. Here I deal only with the general scheme. The details regarding turbomachinery efficiency and cooling flows will be covered in Chs. 4 and 5.

The description is preceded by an overview of the methods developed by other authors and by a summary of the reasons which have motivated the current model. Given the target – thermodynamic analyses of complex GSCs – the calculation of many turbomachinery details is unnecessary. Thus, the philosophy underlying the model is to describe the pressure-temperature history of the gas turbine without entering the specifics of its design.

Since no reference is made to the thermo-physical properties of a specific coolant and/or hot gas composition, the model can be used to evaluate cycles with working fluids other than combustion gases and air, notably steam.

3.1 Relevance of cooling flow

The calculation of systems involving radical modifications of the simple gas turbine cycle requires physical insight into the determinants of turbine cooling flow, in particular the following aspects:

1) The mass flow of the cooled section varies along the expansion.
2) Expansion is not adiabatic. The heat extracted from the hot gases reduces the energy available for producing work.
3) Turbine outlet temperature depends on cooling flow conditions.
4) Bleeding coolant before the compressor exit reduces compression work.
5) Spent coolant acceleration to the velocity of the mainstream flow causes total pressure losses.
6) The rotor centrifugal field compresses the rotor coolant, an effect referred to as "pumping loss".
7) Injecting spent coolant into the mainstream flow may create fluid dynamic disturbances and penalize the expansion efficiency.

The model proposed accounts for all these effects. The modeling effort involves only the turbine because, due to the absence of cooling flows – and as long as interest is limited to on-design conditions – the compressor can be effectively modelled as a "black box" completely determined by its efficiency.

3.2 Previous models

The development of a model for predicting the performances of a cooled turbine has been pursued since the early 50s (Hawthorne, 1956). Due to its complexity, the problem cannot be solved analytically without resorting to simplifying assumptions which seriously compromise accuracy. All models aiming at predicting the performances of actual engines require the development of a computer program which can be very complex. The models which have appeared so far can be divided into two classes:

Purely thermodynamic, 0-D models, whereby cooling flows are calculated by referring only to the temperature-pressure history along the turbine. Since they do not require a description of the geometry and the flow field, these models require a minimum of computational time. If fluid properties and component performances are assumed constant (c_p, coolant conditions, heat transfer effectiveness, expansion efficiency, etc.), it is possible to determine closed analytic expressions for P, T, h and s (El-Masri, 1986). Due to their simplicity, they are particulary suited to systematic parametric analyses.

1-D models, whereby the cooling flows are calculated on the basis of the flow field and the geometry resulting from a "mean-line" design of the turbine. These models require a much more complex calculation procedure and exhaustive input data but (i) are more accurate and (ii) produce detailed information on the engine design. Their major drawback is the need for input data which are difficult to produce: turbine geometry, cooling effectiveness curves, details of blade cooling technology, compressor and turbine maps, etc. Many of these data must be determined experimentally and manufacturers regard them as strictly proprietary. Due to their complexity, these models may require long computing times and thus are not suited for parametric analyses of complex cycles. Despite their higher accuracy, also 1-D models require some form of calibration to reproduce the performances of actual engines. The two most popular codes now on the market, GATE/CYCLE and GT-PRO (see 3.2.2), are provided with input data sets specifically calibrated to reproduce the behaviour of a number of commercial engines. This further illustrates the difficulty of modelling actual gas turbines.

3.2.1 Thermodynamic, 0-D models

The philosophy of these models is to describe the thermodynamic history of the expansion without requiring a description of turbine geometry and velocity triangles, nor cooling effectiveness correlations. Since no reference is made to kinetic terms, the turbine is characterized only by the variations of total quantities (all expansion efficiencies are total-to-total).

3.2.1.1 Traupel

The scheme proposed by Traupel (1977) is illustrated in Fig. 3.1. The calculation is based on three assumptions:

- Total cooling flow is a function of TIT, i.e. $m_{cl}=f(TIT)$
- The distribution of m_{cl} along the expansion is linear with pressure, i.e.

  $$dm_{cl}/m_{cl} = dP_g/(P_0-P_{endcool})$$

  where P_0 and $P_{endcool}$ are the pressures at the nozzle inlet and at the end of the cooled section, respectively.
- The local expansion efficiency is penalized proportionally to dm_{cl}, i.e.

  $$\eta_{p,ct} = \eta_{p,ut} - \kappa \cdot dm_{cl}/dP_g$$

The function f(TIT) and the proportionality constant κ, to be determined empirically, summarize the heat transfer and fluid dynamic characteristics of the cooling technology. If they are known, the expansion can be calculated step-by-step as a sequence of infinitesimal expansions followed by mixing at constant pressure. The end of the cooled section is set at the point where $T_g = T_{bmx}$: since the corresponding pressure is unknown, it is necessary to perform an iteration over the pressure $P_{endcool}$. The model has been utilized by Rufli (1987) to perform a systematic analysis of Combined Cycles. Its major drawback is that, rather than being constants, f(TIT) and κ vary in reality with the cooling method and the coolant conditions.

3.2.1.2 El-Masri

In the model developed by El-Masri (1986) the turbine is still represented as a sequence of infinitesimal expansions each followed by mixing. However:

- The cooling flow of each step is given by:

  $$dm_{cl} = h_g \cdot dS \cdot (T_g - T_{bmx}) / [\varepsilon_1 \cdot c_{p,cl} \cdot (T_{bmx} - T_{cl,in})]$$

  where dS is the heat transfer area, ε_1 is the effectiveness defined by Eq.(5.26) and h_g is calculated by assuming constant $St_g = 0.005$.

- Thermodynamic history and heat transfer areas are linked by stipulating that (supercript "stg" refers to the whole stage):

  $$dw/w^{stg} = dS/S^{stg}$$

- Effectiveness ε_1 and expansion polytropic efficiency are constant.

- Coolant acceleration losses (Par. 3.8) are explicitly accounted for.

The representation of the pressure-temperature history is similar to that of Fig. 3.1, with the difference that the variation of m_{cl} is no longer linear with $P - P_{endcool}$.

By assuming that $c_{p,g}$, $\bar{c}_{p,cl}$, S^{stg}/A_g and $w^{stg} \cdot m_g/u^2$ are constant ($w^{stg} \cdot m_g$ is the work specific to one kg of gas), the equations for m_{cl}, P_g, T_g and s_g can be integrated to give a closed analytic description of the expansion. The use of such analytic expressions is very convenient, although the many simplifying assumptions – c_p, $\eta_{p,t}$ and ε_1 all constant – may produce significant inaccuracies. The model has the merits of properly breaking down the factors affecting blade heat transfer and of utilizing constants of clear physical meaning, which can be estimated reasonably well.

3.2.1.3 Stecco and Facchini

Stecco and Facchini (1988) have presented a simplified scheme where the total cooling flow is proportional to (TIT$-T_{bmx}$) and, rather than calculating the expansion step-by-step, one single gas-coolant mix is performed at a temperature between TIT and T_{bmx} (upper diagram of Fig. 3.2). Before mixing, work is produced only by ($m_a+m_f-m_{cl}$); after mixing, work is produced by the whole (m_a+m_f). Due to its simplicity, the model is convenient for parametric analyses of complex cycles. However, it is also very approximate because: (i) in reality, total cooling flow increases faster than (TIT$-T_{bmx}$); (ii) the proportionality constant between m_{cl} and (TIT$-T_{bmx}$) must be determined empirically, it is subject to major uncertainties and, as in the Traupel model, it depends on the cooling technology; (iii) only part of the cooled expansion is affected by coolant conditions.

3.2.1.4 Consonni and Macchi

Finally, Consonni and Macchi (1988) have proposed another simple model whereby the whole cooling flow, which varies with TIT according to a non-linear function, is mixed with the gas at the turbine inlet (lower diagram of Fig. 3.2). To account for all other losses (mixing, acceleration, pumping, variable mass flow), turbine efficiency is penalized by a factor depending on TIT. Both m_{c1}(TIT) and the turbine efficiency correction factor are derived from performance data supplied by gas turbine manufacturers (the same given in App. C).

Due to the more correct, non-linear relationship between m_{c1} and TIT, the provision for losses due to cooling, and the reference to the performances of actual engines this model can give reasonably accurate (within 5÷8%) performance predictions of simple cycle turbines. However, since it does not model the details of turbine cooling its extension to cycles different from the simple cycle is highly questionable.

3.2.2 1-D models and available computer codes

In 1-D models the problem of determining a relationship between thermodynamic history and heat transfer areas is solved by performing a tentative design of the turbine. Since such 1-D design is essentially a means to determine the cooling flows, it is not particularly sophisticated nor subject to optimization. Except for the GASCAN code developed by El-Masri (1988a), spanwise (hub-to-tip) variations (see Fig. 2.7) are always neglected.

The 1-D approach has been used by Louis, Hiraoka and El-Masri (1983), in the GATE program developed by the Electric Power Research Institute (Cohn and Waters, 1982; Cohn, 1983), and in the GASCAN code written by El-Masri (1988a). GATE* (GAs Turbine Evaluation) and GASCAN** (GAS Cycles ANalysis) are interactive commercial programs running on Personal Computers designed to analyze complex multi-spool engines. The gas cycle can include regeneration, reheat, steam injection, pre-cooling of the air used for blade cooling and pre-cooling of the air entering the compressor. The main features of these 1-D models are briefly summarized below.

Cooling flow. Louis, Hiraoka and El-Masri calculate the cooling flow for blades and shrouds*** ($\tilde{m}_{clb}$) on the basis of a constant value for the effectiveness ε_1 (see Eq. 5.26) and, for film cooled blades, on a correlation for the isothermal effectiveness determined experimentally by Louis (1977). In GASCAN and GATE, the cooling flow is based on semi-empirical correlations for the cooling effectiveness φ:

$$\varphi = (T_g - T_{bg})/(T_g - T_{cl,in}) = f(\tilde{m}_{clb}/m_g) \qquad (3.1)$$

where $\tilde{m}_{clb}$ is the blade cooling flow for the row being considered. The gas and blade temperatures to be used may vary: in GATE, T_g and T_{bg} are the peak values for blades, the bulk averages for shrouds and endwalls

* The original program developed by EPRI has been subsequently upgraded and integrated with a model for the calculation of steam cycles by Enter Software Inc., which now commercializes it under the name GATE/CYCLE (see also Par. 9.1). Program development has been carried out under the supervision of Dr. M. Erbes, whose helpful comments on this Thesis are gratefully acknowledged.

** Although many aspects of the methodology are the same, GASCAN does not constitute the implementation of the thermodynamic model discussed in Par. 3.2.1.2. In his 1986 paper, El-Masri calculates the turbine by integrating the equations governing the cooled expansion. Instead, in GASCAN the turbine is calculated stage by stage, and the cooling flows are based on semi-empirical cooling effectiveness relations.

*** In general, $\tilde{m}_{clb}$ does not coincide with total cooling flow due to the non-negligible, additional flow required for disc cooling (see Par. 3.9 and Eq.3.20).

(Cohn, 1983). Although very convenient, this procedure "hides" the physics of the gas-coolant heat transfer in the coefficients of the correlation φ vs. $\tilde{m}_{cl}/m_g$ and requires a different function for each cooling configuration. This is accomplished by adopting the functional relationship:

$$\tilde{m}_{cl}/m_g = C\cdot[\varphi/(\varphi_{mx}-\varphi)]^E$$

where the coefficients C and E vary with the component (stator, rotor, endwall, etc.), the cooling technology (convection, advanced convection, impingement, film cooling, transpiration etc.) and the cooling medium (air or steam). φ_{mx}, the value corresponding to infinite coolant flow, equals $1/(1+Bi_{bw})$. In order to include the effect of increasing heat transfer areas along the expansion, in GATE $\tilde{m}_{cl}$ is multiplied by the ratio S/S_0, where S and S_0 are the heat transfer areas of the current cascade and the one at the turbine inlet, respectively. In all models gas-coolant mixing is always performed at the exit of each cascade.

<u>Gas-side heat transfer coefficient</u>. Always assumed constant for each cascade, it is based either on the hypothesis of constant St_g (Louis, Hiraoka and El-Masri) or on correlations developed for flat plates (GATE). In GATE, h_g is used only to evaluate $Bi_{bw}=t_w\cdot h_g/k_b$, with $\tilde{m}_{clb}$ subsequently calculated by Eq.(3.1). In GASCAN, Bi_{bw} is one of the inputs and there is no need to calculate h_g.

<u>Expansion efficiency</u>. Louis et al. and GASCAN assume constant total-to-total stage isentropic efficiency, but allow for losses due to mixing and coolant acceleration at the inlet and outlet of each cascade. Since such losses are a strong function of Ma_g, Louis et al. account for

intra-cascade variations of Ma_g by assuming that $\tilde{m}_{cl}$ is injected in three equal amounts in zones with Ma_g=0.3, 0.5 and 0.8 and angles of injection (measured from the mainstream direction) of 180°, 30° and 30°, respectively; in GASCAN, acceleration losses are corrected by a factor accounting for the non-zero streamwise velocity of the injected coolant. Rather than calculating mixing losses, in GATE the stage isentropic efficiency is penalized according to:

$$\eta_{is} = \eta_{is,ut} \cdot \left[1 - C_{stator} \cdot (\dot{m}_{cl}/\dot{m}_g)_{stator} - C_{rotor} \cdot (\dot{m}_{cl}/\dot{m}_g)_{rotor}\right]$$

where the coefficients C_{stator} and C_{rotor} vary with the cooling technology. The rotor expansion is divided into a number of small steps (typically 25) to account for changes in thermodynamic gas properties. Although the GASCAN and GATE approaches are essentially equivalent, the former better represents the fundamental fluid dynamics of mixing.

3.3 Rationale of model proposed

The model proposed is essentially thermodynamic and 0-D, although it includes some features of 1-D schemes. It falls somewhere in between the 0-D scheme of El-Masri (1986) and the 1-D model of Louis, Hiraoka and El-Masri (1983), with three major differences:

1) The sequence of gas expansion, coolant acceleration, gas-coolant mixing is performed for a number of "small" expansion steps rather than for each cascade (Fig. 3.3). This allows eliminating the distinction between stators and rotors and the need to perform a 1-D design of the turbine.

2) The heat transfer effectiveness ε_1 is a result of the calculation and changes along the expansion. ε_1 is evaluated by extending a model first proposed by Ainley (1957).

3) The expansion efficiency is a function of the local size parameter SP and changes along the expansion.

The underlying philosophy is to describe the expansion without referring to the specifics of the turbine geometry but, at the same time, to account for kinetic terms (difference between static and total quantities, coolant acceleration). This approach has been chosen because:

- The focus of this work is on the thermodynamics of complex gas/steam cycles. Given the already high number of cycle parameters and configurations to be investigated, a turbine model requiring many additional parameters would make the analysis very impractical. For this same reason the commercial codes for the calculation of complex cycles use simplified turbine models.

- The turbine model is just one part of a much larger scheme. The benefits of a more sophisticated 1-D model on the accuracy of the overall cycle calculation are dubious because – as extensively discussed in Par. 2.2 – cycle thermodynamics is affected only by efficiency and cooling flows. As long as the model predicts these quantities correctly, there is no need for further, detailed treatment of the turbine*.

---

* Notice that this consideration does not mean that 1-D model are worthless! This Thesis clearly shows that predicting efficiency and cooling flows without the turbine design poses serious problems.

- The detailed information produced by a 1-D design of the turbine might be interesting for the final solution, but are clearly irrelevant for all the iterations performed to achieve convergence.

- 1-D designs are based on a number of assumptions which are reasonable for the current ranges of cycle parameters. When exploring conditions very far from the ones now adopted – as done in the present work – the same assumptions might yield unrealistic designs.

- Since a thermodynamic, 0-D model requires only few parameters, its calibration with data publicly available is relatively simple. It must be remembered that manufacturers generally provide only (i) efficiency, (ii) specific power, (iii) turbine inlet temperature and pressure ratio, (iv) turbine outlet temperature. This information is definitely inadequate to calibrate a detailed model like GATE, which requires massive amounts of experimental data*.

3.3.1 Limits, expected accuracy, applications

Circumventing the turbine design has of course its drawbacks, because it becomes problemmatic to account for the effects of parameters such as the number of shafts, speed of revolution, degree of reaction, stage loading etc.

It is also important to emphasize – as already stated in Par. 2.5 – that the model is limited to the calculations of on-design conditions. Thus, there is no connection between flow handled and expansion ratio.

The accuracy to be expected by the model depends strictly on the data used used for its calibration. Due to the inconsistencies of the data available (see Par. 7.1), the calibrated predictions of commercial engines are not dramatically better than that produced by the much simpler, 0-D model developed earlier by Consonni and Macchi (1988). However, while the extension of the simple model to cycles other than

* As properly pointed out by Erbes (1991) – the supervisor of GATE/CYCLE development – commercial packages are constantly changing, so that their drawbacks are progressively eliminated or bypassed. For example, new correlations are under development for GATE which relieve the user of the need to specify much of the data currently required.

the simple cycle would be highly questionable*, the model presented here embodies enough physical insight to justify its extension to cycles very different from those used for calibration.

* The 0-D model cannot account for variations of coolant conditions and/or composition, material temperature, film cooling, number of stages, etc.

3.4 Schematic of turbine expansion

Proceeding from inlet to outlet, the turbine expansion is divided into four parts:

1) First nozzle. Flow is accelerated at constant efficiency $\eta_{p,nz}$ to a Mach number Ma_{nz} to be specified in input (Fig. 3.4a), giving an outlet velocity $v_{g,in}$. $T_{g,tot}$ changes due to gas-coolant mixing.

2) Cooled turbine. Flow expands with η_p as given in Fig. 4.5. The average velocity $v_{g,ct}$ relative to the blade is constant, while $T_{g,tot}$ changes due both to work extraction and to gas-coolant mixing (Fig. 3.4b). At the interface with the first nozzle the kinetic energy difference $(v^2_{g,in}-v^2_{g,ct})/2$ is recovered with the efficiency $\eta^1_{p,ct}$ of the first cooled turbine step.

3) Uncooled turbine. Flow expands with efficiency $\eta_{p,ut}$. The same efficiency is also used to convert to work the kinetic energy $(v^2_{g,ct}-v^2_{g,dif})/2$ (Fig. 3.4c). $T_{g,tot}$ changes only due to work extraction.

4) Diffuser. Kinetic energy $v^2_{g,dif}/2$ is recovered with efficiency η_{dif}; what is left is totally dissipated (Fig. 3.4d). $T_{g,tot}$ is constant.

The cooled turbine ends when the "effective" gas temperature T^*_{gr} used to evaluate the cooling flow (see Par. 5.2.2) drops below the maximum temperature tolerated by the blade (T_{bmx}). Important points to be mentioned are:

- The enthalpy drop used to calculate $SP=V^{0.5}/\Delta h_{is}^{0.25}$ is the one of the current stage. The distribution of expansion ratios and Δh_{is} among stages is performed at the beginning of the calculation as described in Par. 3.6.

- The velocity $v_{g,ct}$ relative to the blade is different from the mass velocity $U_g=m_g/(\rho_g \cdot A_g)$ – corresponding to the average axial velocity – used in the definition of $St_g=h_g/(\rho_g \cdot U_g \cdot c_{p,g})$.

- While the first nozzle and the diffuser are always present, one of the turbine sections may not be: section 3) is missing if the turbine is completely cooled; section 2) is missing if cooling ends within the first nozzle.

- The nozzle inlet velocity $v_0=m_g/(\rho_g \cdot A_g)$, i.e. no tangential component.

- Cooled turbine gas velocity $v_{g,ct}$ and diffuser inlet velocity $v_{g,dif}$ are determined by specifying the corresponding inlet Mach numbers Ma_{ct} and Ma_{dif}. Notice that Ma_{ct} is not the first rotor inlet Mach: it just defines the velocity $v_{g,ct}$ used to calculate acceleration losses and to distinguish among T_{gr}, $T_{g,st}$ and $T_{g,tot}$.

- All efficiencies are static-to-static; in particular, $\eta_{p,nz}$ and η_{dif} are constant input values.
- In the cooled turbine, the Mach number increases due to reductions of T_g.

Except for the first nozzle, no reference is made to stators or rotors. The rationale is to describe an expansion where the flow and the geometrical parameters vary continuously, thus smoothing the discontinuities of total temperature, pressure and relative velocity existing at the cascade interfaces. The gas average velocity and the geometrical parameters discussed in Appendix A must be considered as averages between typical values for stators and rotors.

3.4.1 Cooled sections

As shown in Fig. 3.3, the cooled sections are divided into "small" steps – each composed of an expansion followed by mixing – calculated sequentially starting from the turbine inlet. The calculation of each step assumes finite variations of the flow variables, so that it is not necessary to approach an infinitesimal treatment by adopting a high number of steps. However, in order to legitimize the "continuous" expansion model, it is appropriate to adopt at least 3-4 steps for each cooled row. The sensitivity to the choice of n_{step} is discussed further at Par. 7.4.3.

The maximum, total number of steps $n_{step,mx}$ is assigned in input; however, the total number $n_{step,nz}+n_{step,ct}$ of actual steps may be lower because when $T^*_{gr}=T_{bmx}$ the step-wise procedure is truncated. An iteration whereby all P_{2i} would be adjusted until $n_{step,nz}+n_{step,ct}=n_{step,mx}$ would be useless.

The initial conditions of each step (mainstream gas and coolant composition, P, T, h, s, u, v, etc..) are completely known because they are the ones at the end of the previous step or, for the very first step, the turbine inlet conditions. With the exceptions illustrated at Par. 6.2.1, the expansion ratio of each step is set by (refer to symbols in Fig. 3.3):

$$(P_{2i}-P_{1i})/P_{1i} = \ln(\beta_{nz+ct})/n_{step,mx} \tag{3.2}$$

where $\beta_{nz+ct}=P_{ut,in,st}/P_{0,tot}$ is the expansion ratio of the whole cooled section obtained at the previous iteration*. Since the ensuing $(P_{2i}-P_{3i})$ depends on the amount of coolant injected, the overall ΔP per step is variable, and cannot be set in advance. Expansion and mixing are evaluated as follows:

a) In the nozzle, expansion is performed at constant $h_{g,tot}$ (gas acceleration) and efficiency $\eta_{p,nz}$. In the cooled turbine, it is performed at constant $v_{g,ct}$ and static-to-static efficiency $\eta^{i}_{p,ct}=f(SP)$ (see Par. 4.6).

b) Coolant acceleration and mixing are performed at constant $v_{g,ct}$, charging all variations to P_g and T_g (see Par. 3.8)**.

Gas and coolant flow, temperature, pressure, heat transfer and cooling effectiveness all change continuously from one step to another.

The cooling flow Δm_{clt} – calculated immediately before mixing – is the sum of the flow required to cool blades and shrouds (Δm_{clb}, see

---

* This expression comes from approximating $(1+\Delta P_g/P_g)^{n_{step,mx}}=\beta_{nz+ct}$. In order to maintain approximately the same $\Delta c/c$, the computer program actually differentiates between the nozzle and cooled turbine $\Delta P_g/P_g$ (see Pars. 3.5 and 6.2.1).

Notice that by "expansion ratio" I indicate quantities always smaller than one; the opposite holds for "compression ratio".

** Although they are calculated altogether, acceleration and mixing constitute two distinct thermodynamic processes: at constant $v_{g,ct}$, the former is mainly responsible for variations of pressure, the latter for variations of temperature.

Ch. 5) and a term accounting for disks, casings, struts etc. (Δm_{dsk}, see Par. 3.9).

3.4.2 Uncooled sections

The uncooled turbine and the diffuser are calculated in one single step. $\eta_{p,ut}$ is determined from the mean value theorem applied to the function in Fig. 4.5:

$$\eta_{p,ut}=\int_{in}^{out}\eta_{p,t}(SP)\cdot dSP/(SP_{ut,in}-SP_{ut,out}) \tag{3.3}$$

The stage enthalpy drop used to evaluate $SP_{ut,in}$ and $SP_{ut,out}$ is different from the one used for the cooled turbine (see Par. 3.6), reflecting the widespread practice of designing uncooled stages with lower load factors and – in multi-shaft engines – lower peripheral speeds.

The efficiency given by Eq.(3.3) is also used to convert to work the difference between inlet and outlet kinetic energy (Fig. 3.4c):

$$W_{ut} = m_g\cdot[(h_{in,st}-h_{out,st})+\eta_{p,ut}\cdot(v^2_{g,ct}-v^2_{g,dif})/2] \tag{3.4}$$

where $(h_{st,in}-h_{st,out})$ is the gas enthalpy drop calculated from $\eta_{p,ut}$. For turbines which are completely cooled, it is assumed that the diffuser requires no cooling flow besides the one already included in m_{dsk}; notice that in this case it is still necessary to account for the term $\eta_p\cdot(v^2_{g,ct}-v^2_{g,dif})/2$, where η_p is the efficiency of the last expansion step.

3.5 Heat transfer areas

The calculation of cooling flows calls for a link between heat transfer areas and pressure-temperature history. This is realized by assuming that the blade portion $\Delta c/c$ spanned at each step (Fig. 3.5) is constant. For the nozzle, $\Delta c/c$ is simply given by $(1/n_{step,nz})$, where $n_{step,nz}$ is the number of steps performed to reach Ma_{nz}. For the cooled turbine:

$$(\Delta c/c)_{ct} = (2 \cdot n^{cs} - 1)/n_{step,ct} \qquad (3.5)$$

where n^{cs}, the number of cooled stages, is treated as a real number and is evaluated as illustrated in Par. 3.6.1; $(2 \cdot n^{cs} - 1)$ is the number of cooled turbine rows; $n_{step,ct}$ is the total number of steps performed to calculate the cooled turbine (see Par. 3.4.1).

Since the variations of the total step $\Delta P_g/P_g$ are small (they are due to variations of mixing ΔP, see Fig. 3.3), Eq.(3.5) implies that the variation of P_g along the turbine axis is roughly logarithmic (constant dP/P), a good approximation of the low-reaction stages typical of heavily cooled turbines.

Besides $\Delta c/c$, the other geometrical parameters necessary to evaluate cooling flows are:

a) Ratios defining stage geometry: H/c, H/D_m, Φ, σ, etc. (App. A)
b) Gas cross-sectional area A_g
c) Ratio a_t between blade+shroud surface and blade surface
d) A parameter summarizing the characteristics of the cooling channels

The calculation of a), b) and c) is based primarily on similarity rules and is illustrated in Appendix A. The influence of cooling channels geometry is discussed in Par. 5.2.

3.6 Number of stages

Within the cooled turbine there is no distinction between stators and rotors; nonetheless, the knowledge of the current stage number is required for two reasons: (i) to update the enthalpy drop defining SP and (ii) to update the number of cooled stages, which determines the total area to be cooled (Eq. 3.5). The computer program allows estimating the distribution of Δh_{is} and pressures among stages according to four design options:

1) Constant β^{stg} and given number of stages
2) Constant β^{stg} and given* $\Delta h^{stg}_{is,mx}$
3) Constant Δh^{stg}_{is} and given number of stages
4) Constant Δh^{stg}_{is} and given $\Delta h^{stg}_{is,mx}$

With options 3) and 4) the reheat factor (Par. 2.2.3.3) used to estimate the constant stage Δh_{is} is based on the overall η_p and η_{is} of the previous iteration. Once the expansion ratio and thus the exit pressure of each stage are known, the current stage number is determined according to the current step static pressure.

At the end of the cooled expansion n^{cs} is updated by adding to the current stage number (which is an integer) a fraction calculated accordingly to the hypothesis of $\Delta P_g/P_g \approx$constant. Letting β^{stg}, P^{stg}_{in} be the current stage expansion ratio and inlet pressure, and $P_{ut,in,st}$ the pressure at the end of the cooled section (Fig. 3.4b), the portion of the last stage which requires cooling is:

$$\ln(P_{ut,in,st}/P^{stg}_{in})/\ln(\beta^{stg}) \tag{3.6}$$

---

* If n^{stg} is integer, the input value of Δh_{is} cannot exactly correspond to Δh^{stg}_{is}: in this case the input value is used as an upper bound.

For any actual turbine n^{stg} will obviously be an integer. However, when considering a wide range of β and/or TIT, imposing an integer n^{stg} introduces discontinuities: for this reason the computer code can also treat n^{stg} as a real number.

Due to the relevance of heat transfer areas in determining the cooling flow, the choice of the design option (constant β^{sts} or constant Δh_{is}^{sts}) and the number of stages are factors of crucial importance. Constant-β^{sts} designs are superior because they yield higher gas temperature drops in the first stages. Within the framework of the model, increasing Δh_{is}^{sts} is almost always beneficial because n^{cs} and thus the cooling flow are reduced, while $\eta_{p,ct}$ suffers only modest penalties due to reductions of SP. In practice, adopting very high Δh_{is}^{sts} without increasing peripheral velocity (which is limited by material capabilities) gives efficiency penalties due to stage overloading, an effect not accounted for by the model. For this reason, and given state-of-the-art peripheral velocities around 400 m/sec, the efficiency prediction given by the curve in Fig. 4.5 is plausible as long as Δh_{is}^{sts} < 350–400 kJ/kg.

3.6.1 Distribution of enthalpy drops

The calibration discussed in Ch. 7 and the test cases presented in Ch. 10 have been performed assuming that:

- All cooled stages have the same β^{sts}; its value is set to give the input $\Delta h_{is,mx}^{sts}$ for the first stage.
- All uncooled stages have the same Δh_{is}^{sts}.

Since the turbine inlet conditions and β_t are almost always fixed input parameters, the distribution of β^{sts} and Δh_{is} is generally calculated only at the first iteration.

It is important to emphasize that – since the design option affects the number of cooled stages and thus cooling flows – it has significant effects on performance predictions. The choice adopted here is closest to the design of actual commercial engines.

3.7 Coolant conditions

Fig. 3.6 depicts the path followed by the rotor coolant (compression 0–1 is meaningful only for air cooling). In stationary cascades there is no pumping, i.e. points 2 and 3 coincide. Transformation 3–4 represents the expansion taking place within the coolant ejection holes, with $v_{cl,is}$ denoting the ideal outlet velocity. Point 3 represents the conditions used to evaluate the cooling flow; point 4 the one used to evaluate acceleration losses. The figure is based on the assumption that the coolant is always bled at stationary points. If not, there should be an expansion immediately following point 1, to represent the process between the bleed at the compressor shroud and the engine axis. Notice that the expansion work corresponding to this process is very likely to be lost anyway.

The pressure drop (P_1-P_2) accounts for all irreversibilities occuring along the path followed by the coolant, i.e.:

- friction
- heat addition
- non-isentropic pumping
- non-isentropic acceleration to $v_{cl,is}$

Therefore, the value of P_1-P_2 is fictitious, always somewhat larger than the actual pressure drop along the cooling channels. Independently of the "type" of bleed pressure (see next Paragraph), points 1 to 4 of Fig. 3.6 are determined by assuming that:

- P_4 equals the current gas pressure (i.e. pressure of point 2i of Fig. 3.3)
- The peripheral speed is the same for all steps
- The pressure drop P_1-P_2 equals the expansion drop P_3-P_4

3.7.1 Coolant stream "type"

Each coolant stream can be of two "types":

1. "fixed-pressure", i.e. bleed pressure P_1 is constant.
2. "floating-pressure", i.e. bleed pressure P_1 can "float" according to the requirements imposed by the local gas pressure and the cooling system pressure loss.

For fixed-pressure streams P_1 of Fig. 3.6 is constant, while the overall pressure drop:

$$\Delta P_{c1}/P_{c1}=[(P_1-P_2)+(P_3-P_4)]/P_1 \tag{3.7}$$

is an output, and varies from step to step according to $P_4=P_g$. This option is the only one available for steam cooling.

Floating-pressure simulates the multiple-bleed cooling schemes adopted in modern engines; in this case $\Delta P_{c1}/P_{c1}$ is an input datum, and P_1 must be re-calculated at each step so that $P_4=P_g$. Compression 0−1 is performed with the same polytropic efficiency of the gas turbine compressor. This is equivalent to imagining that the turbine incorporates a small, variable-β compressor to compress its coolant flow (see Fig. 7.5).

The decrease (or rise) of coolant temperature due to heat transfer from the bleed point to the blade root is neglected*.

---

* However, it is possible to account for cooling air pre-cooling (i.e. before using it to cool the blades) by inserting a heat exchanger between the bleed point and the turbine, a practice adopted in several Westinghouse and ABB turbines.

3.7.2 Pumping losses

Conservation of energy for an adiabatic* flow entering at the rotor axis and exiting at the blade tip gives:

$$h_{cl,in} + w^2_{cl,in}/2 = h_{cl,out} + w^2_{cl,out} - u^2/2 \qquad (3.8)$$

where velocities $w_{cl,in}$ and $w_{cl,out}$ are taken in a coordinate system moving with the rotor. The difference $(w^2_{cl,in}-w^2_{cl,out})$ is always much smaller than $u^2/2$, thus giving:

$$h_{cl,out}-h_{cl,in} \simeq u^2/2$$

The work $w_{pum}=\Delta m_{clb}\cdot(u^2/2)$ absorbed by the coolant must be supplied by the rotor and is therefore a net loss. Since friction is charged totally to ΔP_{cl}, the pressure increase ΔP_{pum} ensuing from Δw_{pum} corresponds to the isentropic compression depicted in Fig. 3.6 (from Point 2 to Point 3). If $c_{p,cl}$ is constant:

$$\Delta P_{pum} = P_{cl,in}\cdot\left\{ \left[1+(u^2/2)/(c_{p,cl}\cdot T_{cl,in})\right]^{\gamma/(\gamma-1)}-1\right\} \qquad (3.9)$$

In the cooled turbine the model does not distinguish between stationary and rotating cascades; the coolant pumping work and the ensuing ΔP_{pum} are evaluated by averaging w_{pum} over the number $(2\cdot n^{cs}-1)$ of cooled turbine rows:

$$w_{pum} = [n^{cs}/(2\cdot n^{cs}-1)]\cdot\Delta m_{clb}\cdot(u^2/2) \qquad (3.10)$$

$$\Delta P_{pum} = P_{cl,in}\cdot\left\{ \left[1+w_{pum}/(c_{p,cl}\cdot T_{cl,in}\cdot\Delta m_{clb})\right]^{\gamma/(\gamma-1)}-1\right\} \qquad (3.9a)$$

* The cooling flow is obviously non-adiabatic. However, as already mentioned the pressure drop due to heat addition is "charged" to ΔP_{cl}.

3.8 Coolant acceleration and mixing

In addition to losses due to non-isentropic expansion, the nozzle and the cooled turbine suffer additional losses due to:

- acceleration of injected coolant up to mainstream velocity
- gas-coolant mixing

The calculation of gas conditions after coolant acceleration and mixing can be performed according to the method of influence coefficients developed by Shapiro (1953, p. 219). However, in our case such a method is inconvenient because one of the independent variables chosen by Shapiro is the cross-section variation dA/A, which in our scheme is unknown. More convenient expressions can be derived by writing the continuity, momentum and energy equations for the assumed hypothesis of constant mainstream velocity* v_g. Indicating with "D.." the total derivative with respect to changes in composition, pressure and temperature, the equations describing the injection of an infinitesimal $dm_{clt}=dm_{clb}+dm_{dsk}$ into the frictionless, adiabatic, 1-D flow depicted in Fig. 3.7 are:

Continuity:
$$dA/A + D\rho_g/\rho_g = 0 \tag{3.11}$$

Momentum:
$$dm_{clt}\cdot(v_g-v'_{cl}) = -A\cdot dP_{g,st}$$
$$(dP/P)_{g,st} = -\gamma_g\cdot Ma_g^2\cdot(1-v'_{cl}/v_g)\cdot dm_{clt}/m_g \tag{3.12}$$

Energy:
$$(m_g+dm_{clt})\cdot(h_{g,tot}+Dh_{g,tot}) = m_g\cdot h_{g,tot}+dm_{clt}\cdot h_{cl,tot}$$
$$Dh_{g,tot}= Dh_{g,st}= Dh_g = -(h_{g,tot}-h_{cl,tot})\cdot dm_{clt}/m_g \tag{3.13}$$

Molecular weight:
$$(m_g/W_g)+(dm_{clt}/W_{cl}) = (m_g+dm_{clt})/(W_g+dW_g) \tag{3.14}$$

---

* In the first nozzle, the gas velocity increases at each expansion (see Par. 3.4.1). However, it is always assumed that v_g before and after coolant acceleration and mixing is the same.

where v'_{cl} is the coolant velocity component along the direction of v_g and $Dh_{g,st}=Dh_{g,tot}$ comes from the assumption of constant v_g. The gas pressure and enthalpy after mixing are determined from Eqs.(3.12) and (3.13) by assuming that (recall Fig. 3.6):

$$v'_{cl} = r_{vcl} \cdot v_{cl,is} \tag{3.15}$$

The coolant enthalpy to be used in Eq.(3.13) is the one corresponding to the inlet conditions (Point 3 of Fig. 3.6), before exchanging heat. Therefore, the fact that dm_{clb} and dm_{dsk} are discharged at different temperatures is irrelevant. Once the new h_g and P_g are known, all other properties can be determined after calculating the new molecular weight (W_g+dW_g) from Eq.(3.14) and then resetting the composition by:

$$x_{i,g} + dx_{i,g} = \left[(x_{i,g} \cdot m_g/W_g)+(x_{i,cl} \cdot dm_{clt}/W_{cl})\right] \cdot (W_g+dW_g)/(m_g+dm_{clt}) \tag{3.16}$$

Notice that $Dh_g \neq dh_{g,st}=c_{p,g} \cdot dT_g$, because the variation of h_{cl} is <u>not</u> infinitesimal. In fact, the variations $dh_{g,st}$ and $\Delta h_{cl,st}$ of mainstream and coolant supposed unmixed are related to Dh_g by:

$$Dh_g = dh_{g,st}+(dm_{clt}/m_g) \cdot [(h_{cl,tot}-h_{g,tot})+\Delta h_{cl,st}+(v_g^2-v_{cl}^2)/2] \tag{3.17}$$

<u>3.8.1 Finite Δm_{cl}</u>

If dm_{clt}/m_g is not infinitesimal, the equations above must retain higher-order terms. Indicating with 1 and 2 the conditions before and after mixing, from continuity $(\rho_{g,1}/\rho_{g,2})=(A_{g,2}/A_{g,1})$ and thus:

$$\Delta A/A_1 + 1/(1+\rho_1/\Delta\rho) = 0 \tag{3.11a}$$

If we approximate $\int_{A_1}^{A_2} P \cdot dA$ as $(P_{g,1}+\Delta P/2) \cdot (A_2-A_1)$, the integral of the momentum equation gives:

$$-\gamma_{g,1}\cdot Ma^2_{g1}\cdot(1-v_d/v_g)\cdot\Delta m_{clt}/m_g = -\Delta P/P-0.5\cdot(\Delta P/P\cdot\Delta A/A)$$

and substituting Eq.(3.11a):

$$\Delta P_{g,st}/P_{g,st,1} = \left[-\gamma_{g,1}\cdot Ma^2_{g1}\cdot(1-v_d/v_g)\cdot\Delta m_{clt}/m_g\right]\cdot(\rho_{g,2}/\rho_{g,av}) \quad (3.12a)$$

where $\rho_{g,av}=(\rho_{g,1}+\rho_{g,2})/2$. Since $\rho_{g,2}$ is unknown, the calculation of ΔP_g requires an iteration over the conditions at 2. Finally, the energy equation becomes:

$$\Delta h_g = -(h_{g,tot}-h_{cl,tot})\cdot[1/(1+m_g/\Delta m_{clt})] \quad (3.13a)$$

Since the steps depicted in Fig. 3.3 are not necessarily infinitesimal, the conditions after mixing should always be calculated from Eqs.(3.12a) and (3.13a). However, in all practical cases $(\Delta P/P)_g$ due to mixing is always small (rarely larger than 1%); thus, the computer code resorts to Eqs.(3.12) and (3.13), which allow eliminating the iteration on $\rho_{g,2}$. The sensitivity analysis presented at Par. 7.4.3 shows that for a typical state-of-the-art turbine this procedure gives negligible errors as long as $n_{step} > 20-25$.

3.9 Cooling flow for disks, casings, struts

Besides blades and shrouds, which will be extensively analyzed in the next chapter, there are other turbine components which need to be cooled. The rotating disks sustaining the blades, the casings, the struts connecting the inner and outer casings and the shaft itself need some form of cooling either because they are exposed to the hot gas, or to prevent creep, excessive thermal expansion and/or thermal stresses. Given the trend toward higher compression ratios (to take advantage of higher TIT), future high-compression ratio engines, if not intercooled, will also need some form of HP compressor cooling, a practice already adopted in some aircraft engines (convective cooling of HP compressor disks – Koff, 1989).

3.9.1 Literature

While very little is published about casings and struts (see Rice, 1983a and 1983b for a qualitative description), the flow field and the heat transfer of rotating disks have received considerable attention. Most studies refer to the unshrouded or shrouded configurations depicted in Fig. 3.8: experimental data can be found in Bayley and Owen (1970), Metzger (1970) and Sparrow and Goldstein (1976), while Haynes and Owen (1975) present a boundary layer model. Owen (1977) also considers a rotating cavity with a central axial throughflow of coolant, a configuration similar to the one adopted to cool HP compressor disks. Metzger, Mathis and Grochowsky (1979) analyzed the disk rim impingement cooling scheme illustrated in Fig. 3.9. Compared to convection, this arrangement does not seem to yield cooling flow reductions. Finally, Farthing and Owen (1988) recently compared experimental results with the predictions of a theoretical model based on the momentum- and energy-integral equations for turbulent flow.

3.9.2 Fluidynamic aspects

A basic feature of the flow around rotating disks is the tendency of the rotor to pump fluid radially outward, through the action of viscous and centrifugal forces. Unless steps are taken to prevent it, a corresponding radially inward flow of hot gas will be established to replenish the pumped flow. Consequently, rotor disk cooling implies not only carrying away the heat conducted from the blade, but also eliminating hot gas inflow. Both goals can be achieved by introducing the coolant at the rotor hub and having it flow radially outward. The coolant flow, usually referred to as "purge" flow, picks up heat from the disks and, at the same time, prevents the hot gas from entering the disk gap.

The calculation of disk cooling flow could proceed from evaluating the minimum flow necessary to prevent hot gas inflow, and then verify whether it gives an acceptable temperature distribution. While evaluting the flow necessary to prevent gas inflow is relatively simple (see Bayley and Owen, 1970), determining the temperature distribution is quite involved, because temperature depends on disk shape and the pattern of local heat transfer coefficients. For the constant-thickness disk considered by Haynes and Owen (1975) the temperature distribution was approximately parabolic, i.e. $T(r)-T(0) \approx \kappa \cdot r^2$.

Although an attempt could be made to evaluate disk cooling flows, determining the overall m_{dsk} required by disks, casings and struts would still be subject to a number of major incertainties:

- Heat transfer areas depend very much on the "design style" adopted by each manufacturer and cannot be reasonably predicted by similarity laws as is done for blades and shrouds (Appendix A). For example, all ABB turbines have constant hub diameter with the blades "emerging" directly from the shaft and therefore no disk to be cooled (Fig. 3.10); the shaft constitutes the inner shroud and is protected from the hot gas by a continuous layer of coolant covering its whole surface.

- To meet their different design criteria, disks, casings and struts are made with materials different from the ones used for blades. Their maximum allowable temperature is much lower than the one afforded by state-of-the-art super-alloys and it is hard to predict because it is set by a number of economic, reliability and durability considerations.

- More than their maximum temperature, it is important that these components undergo thermal expansions compatible with safe and reliable operation (avoid undue thermal stresses, maintain tip clearances, limit leakages etc.). This applies both to steady state and, even more, to transients at start-up and shut-down. Determining the cooling flow necessary to warrant such safe operation obviously requires extremely detailed information about geometry, flow and materials.

For these reasons, attempting to calculate m_{dsk} is beyond the scope of this model, and it is assumed that for each stage m_{dsk} is simply a constant fraction of the gas flow, i.e.:

$$(m_{dsk}/m_g)^{stg} = \hat{m}_{dsk} = \text{constant} \qquad (3.18)$$

Since disks and casings are generally not exposed to the gas, most of the thermal power is transmitted by conduction from the shrouds, thus depending on the shroud temperature rather than the gas temperature. Assuming that the temperature of the metal exposed to the gas is always close to T_{bmx}, then m_{dsk} should be proportional to:

$$(T_{bmx}-T_{mx,dsk})/(T_{mx,dsk}-T_{cl})$$

where $T_{mx,dsk}$ is the maximum temperature tolerable by disks. The assumption of constant $\hat{m}_{dsk}$ neglects this dependence; it is like saying that the influence of geometry and materials is much larger than the influence of the coolant temperature.

3.9.3 Inclusion into calculation model

The flow of disk coolant for each step is calculated by assuming that $\Delta m_{dsk}/m_g$ stays constant:

$$\Delta m_{dsk} = (n^{cs} \cdot \hat{m}_{dsk} \cdot m_g)/n_{step} \tag{3.19}$$

i.e. $\hat{m}_{dsk}$ is taken as the ratio between $(m_{dsk}/m_g)^{sts}$ averaged over the number of steps per stage. $\hat{m}_{dsk}$ has been set to 1% for all calculations. The total coolant flow Δm_{clt} to be mixed with the gas at each step is simply given by:

$$\Delta m_{clt} = \Delta m_{clb} + \Delta m_{dsk} \tag{3.20}$$

REFERENCES

Ainley D.G. (1957), "Internal Cooling for Turbine Blades. A General Design Survey", Aeronautical Research Council R.&M. 3013, Ministry of Supply, London.

Bayley F.J. and Owen J.M. (1970), "The Fluid Dynamics of a Shrouded Disk System with Radial Outflow of Coolant", J. of Eng. for Power, Vol. 92, pp. 335-341.

Cohn A., Project Manager (1983), "Gas Turbine Evaluation (GATE) Computer Program", EPRI Report AP-2871-CCM, Palo Alto, CA.

Cohn A. and Waters M. (1982), "The Effect of Alternative Turbine Cooling Schemes on the Performance of Utility Gas Turbine Power-plants", ASME Paper 82-JPGC-GT-19.

Consonni S. and Macchi E. (1988), "Gas Turbine Cycles Performance Evaluation", Proc. *1988 ASME COGEN-TURBO* (Montreaux, Switzerland), pp. 67-77. Published by ASME, New York.

El-Masri M.A. (1986), "On Thermodynamics of Gas-Turbine Cycles: Part 2 - A Model for Expansion in Cooled Turbines", J. of Eng. for Gas Turbines and Power, Vol. 108, pp. 151-159.

El-Masri M.A. (1988a), "GASCAN - An Interactive Code for Thermal Analysis of Gas Turbine Systems", J. of Eng. for Gas Turbines and Power, Vol. 110, pp. 201-209.

El-Masri M.A. (1988b), "GT-PRO - A Flexible, Interactive Computer Program for the Design and Optimization of Gas Turbine Power Systems", ASME Paper 88-JPGC/GT-3.

Erbes M. (1991), Enter Software Inc. (Menlo Park, California), Personal Communication.

Farthing P.R. and Owen J.M. (1988), "The Effect of Disk Geometry on Heat Transfer in a Rotating Cavity with Radial Outflow of Fluid", J. of Eng. for Gas Turbines and Power, Vol. 110, pp. 70-77.

Koff B.L. (1989), "F100-PW-229 Higher Trust in Same Frame Size", J. of Eng. For Gas Turbines and Power, Vol. 111, pp. 187-192.

Hawthorne W.R. (1956), "The Thermodynamics of Cooled Turbines", Transactions of the ASME, Nov. 1956, pp. 1765-1786.

Haynes C.M. and Owen J.M. (1975), "Heat Transfer from a Shrouded Disk System with Radial Outflow of Coolant", J. of Eng. for Power, Vol. 97, pp. 28-36.

Liess C. (1969), "Introduction to Cooling of Gas Turbine Blades", Lecture Series 15, vonKarman Institute for Fluid Dynamics, Brussels.

Louis J.F. (1977), "Systematic Studies of Heat Transfer and Film Cooling Effectiveness", in *AGARD CP-229*, Neuilly sur Seine, France.

Louis J.F., Hiraoka K. and El-Masri M.A. (1983), "A Comparative Study of the Influence of Different Means of Turbine Cooling on Gas Turbine Performance", International J. of Turbo and Jet Engines, Vol. 1, pp. 123-137.

Metzger D.E. (1970), "Heat Transfer and Pumping on a Rotating Disk with Freely Induced and Forced Cooling", J. of Eng. for Power, Vol. 92, pp. 342-348.

Metzger D.E., Mathis W.J. and Grochowsky L.D. (1979), "Jet Cooling at the Rim of a Rotating Disk", J. of Eng. for Power, Vol. 101, pp. 68-72.

Owen J.M. (1977), "Heat Transfer from Turbine and Compressor Discs", in *AGARD CP-229*, op.cit.

Rice I.G. (1983a), "Steam-Cooled Gas Turbine Casings, Struts and Disks in a Reheat Gas Turbine Combined Cycle: Part I - Compressor and Combustor", J. of Eng. for Power, Vol. 105, pp. 844-850.

Rice I.G. (1983b), "Steam-Cooled Gas Turbine Casings, Struts and Disks in a Reheat Gas Turbine Combined Cycle: Part II - Gas Generator Turbine and Power Turbine", J. of Eng. for Power, Vol. 105, pp. 851-858.

Rufli P. (1987), "A Systematic Parametric Analysis of Combined Cycles", Proc. *1987 ASME COGEN-TURBO*, op.cit. pp. 135-146.

Shapiro A.H. (1953), The Dynamics and Thermodynamics of Compressible Fluid Flow, Vol. 1, Ronald Press, New York.

Sparrow E.M. and Goldstein L.Jr. (1976), "Effect of Rotation and Coolant Throughflow on the Heat Transfer and Temperature Field in an Enclosure", J. of Heat Transfer, Vol. 98, pp. 387-394.

Stecco S.S. and Facchini B. (1988), "A Simplified Thermodynamic Analysis of Blade Cooling Effects in Combined Gas-Steam Power Plants", Proc. *1988 ASME COGEN-TURBO*, op.cit., pp. 299-304.

Traupel W. (1977), Thermische Turbomaschinen, 3rd ed., Vol. 1, pp. 496-499, Springer-Verlag, Berlin.

Wilson, D.G. (1984), The Design of High-Efficiency Turbomachinery and Gas Turbines, The MIT Press, Cambridge, Massachusetts.

NOMENCLATURE

a_t	(Blades+shrouds surface)/(blade surface), see Eq.(A.1)	
A	Cross-sectional area	[m^2]
Bi_{bw}	Blade wall Biot number (see Par. 5.2.4.7)	
c	Blade chord	[m]
c_p	Constant pressure specific heat	[J/kg-K]
D_m	Mean diameter	[m]
h	Specific enthalpy or heat transfer coefficient	[J/Kg, W/m^2-K]
H	Blade height	[m]
$\tilde{m}$	Nondimensional mass flow, specific to M_a	[kg/kg_a]
$\hat{m}_{clb}$	Blades+shrouds non-D coolant flow per cascade	[kg/kg_a-cascade]
$\hat{m}_{dsk}$	Disk non-D coolant flow per stage	[kg/kg_a-stage]
M	Mass flow	[kg/s]
Ma	Mach number	
n	Number (stages, steps)	
P	Pressure	[Pa]
r_{vcl}	Ratio v'_{cl}/v_{cl}, see Eq.(3.15)	
S	Heat transfer area	[m^2]
SP	Turbomachinery size parameter (see Par. 2.1.1.4)	
St_g	Gas-side Stanton number $h_g/(c_{p,g}\cdot m_g/A_g)$	
T	Temperature	[K]
T_{bmx}	Maximum allowed blade temperature	[K]
T^*_{gr}	"Effective" gas recovery temperature (see Par. 5.2.2)	[K]
u	Blade peripheral speed	[m/s]
v	Velocity	[m/s]
w	Work specific to M_a; relative velocity	[J/kg_a, m/s]
$\mathcal{W}$	Molecular weight	[kg/kmol]
x	Mol fraction in gas	[gaseous mols/mixture gaseous mols]

Greek

β	Pressure ratio (compressor, >1); expansion ratio (turbine, <1)	
γ	Ratio c_p/c_v	
Δh	Enthalpy drop	[J/kg]
Δm_{clb}	Blades+shrouds nondim. coolant flow <u>per step</u>*	[kg/kg_a-step]
Δm_{clt}	Total non-D coolant flow <u>per step</u> ($\Delta m_{clb}+\Delta m_{dsk}$)	[kg/kg_a-step]
Δm_{dsk}	Disk&casings non-D coolant flow <u>per step</u>	[kg/kg_a-step]
ΔP	Pressure loss (or rise)	[Pa]
η	Efficiency	
φ	Cooling effectiveness (see Eq. 3.1)	
Φ	Ratio between blade perimeter and blade chord, see App. A	
η_p	Polytropic efficiency	
ε_1	Heat transfer effectiveness defined by Eq.(5.26)	
ρ	Density	[kg/m^3]
σ	Solidity, chord/pitch	

Subscripts

a	Air
b	Blade
bcl	Blade surface, coolant side
bg	Blade surface, gas side
c	Compressor

* When applicable, Δm_{clb}, Δm_{clt} and Δm_{dsk} are also indicated with the infinitesimal notation dm_{clb}, dm_{clt} and dm_{dsk}.

cl	Coolant
ct	Cooled turbine
dif	Diffuser
dsk	Refers to disks, casings, struts, etc.
g	Hot gas
in	Inlet
is	Isentropic
lk	Leakage
mx	Maximum
nz	Nozzle
org	Organic
out	Outlet
p	Polytropic
pum	Rotor pumping
sh	Shaft
st	Static conditions
step	Steps to calculate cooled expansion
t	Turbine
tot	Total conditions
ut	Uncooled turbine section
0	Inlet of first turbine nozzle; compressor inlet
1	Exit of first stage; before mixing; coolant bleed
1n	Exit of first nozzle
1t	Inlet of first gas turbine rotor
2	After mixing; coolant at turbine axis
3	Coolant at blade tip
4	Coolant at ejection holes
1i,2i,3i	Points defining ith expansion step (Fig. 3.3)

Superscripts

cs	Cooled stages
i	ith expansion step
stg	Stage

FIGURES

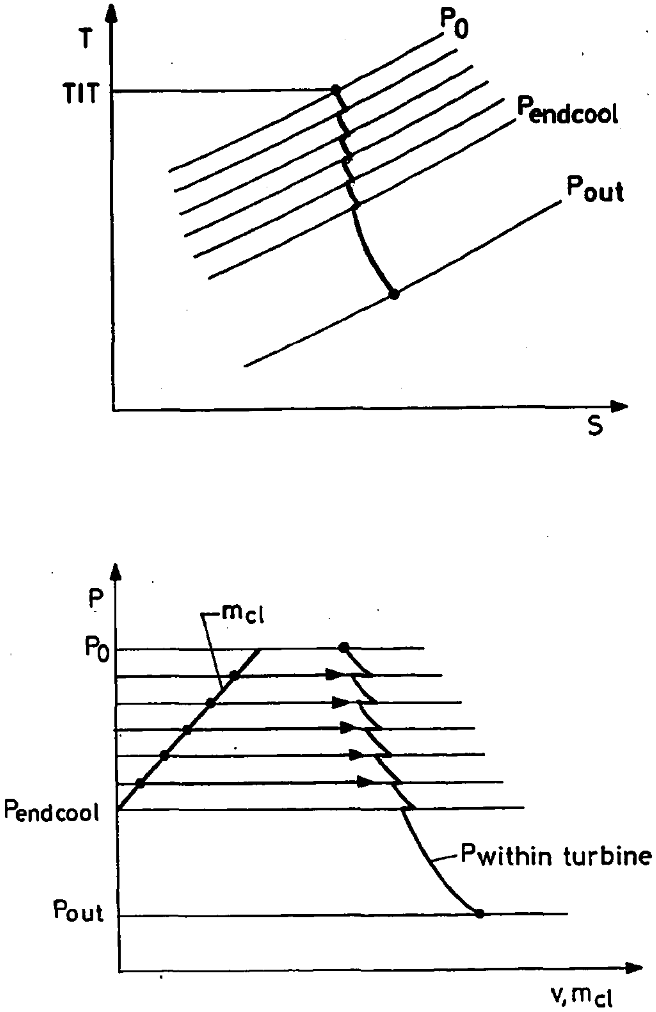

3.1 Schematic of cooled expansion model proposed by Traupel. The coolant flow to be injected at each infinitesimal expansion step is proportional to the difference $P-P_{endcool}$.

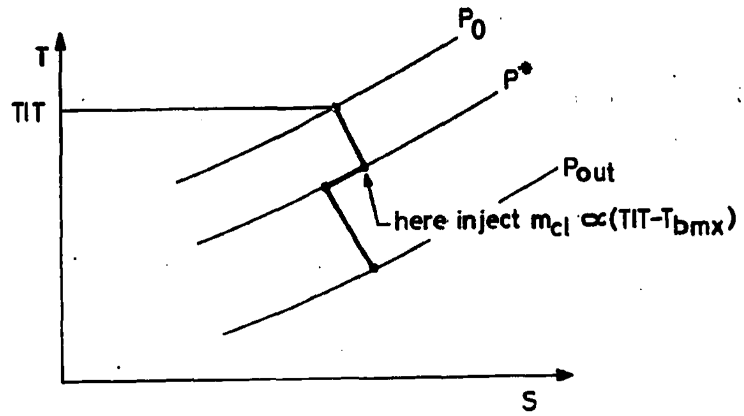

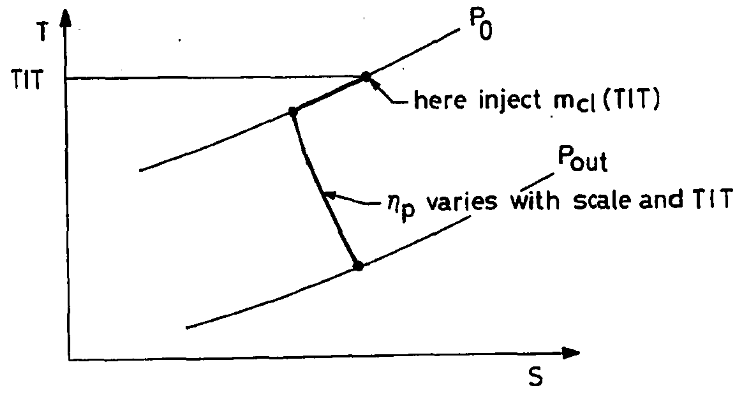

3.2 Schematic of simplified expansion models proposed by Stecco and Facchini (upper diagram) and Consonni and Macchi (lower diagram).

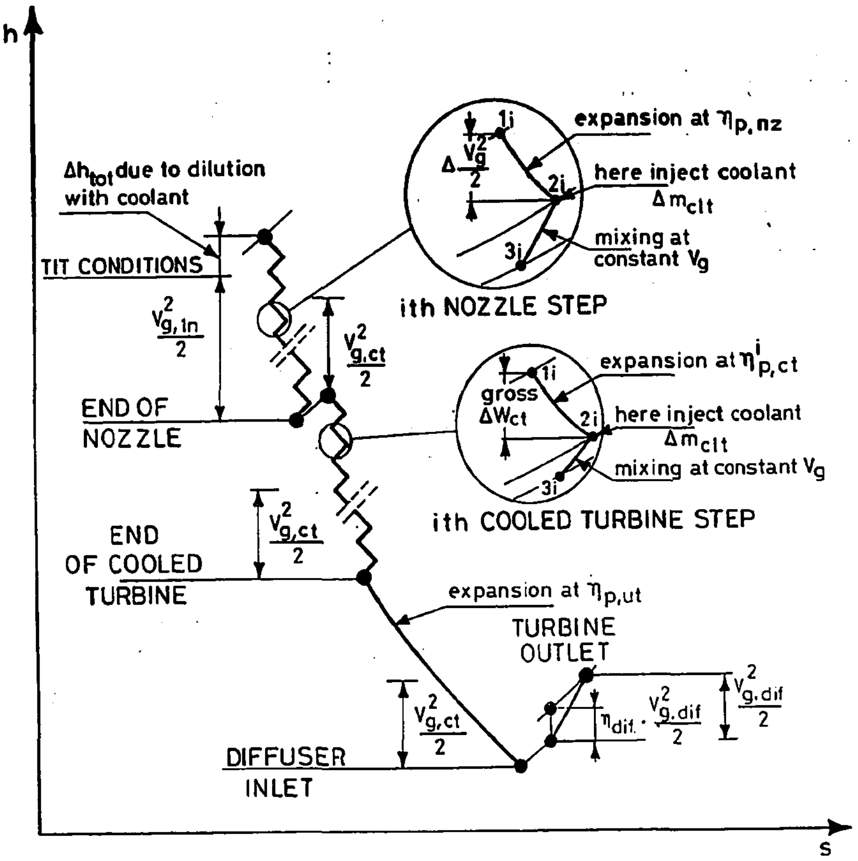

3.3 Schematic of gas turbine expansion. $v_{g,in}$, $v_{g,ct}$ and $v_{g,dif}$ are determined from the corresponding input Mach numbers (see Tab. 6.1). $\eta_{p,ct}$ changes from step to step according to the curve in Fig. 4.5. The expansion ratio $(P_{1i}-P_{2i})/P_{1i}$ is the same for all steps. The static pressure drop (P_{2i}-P_{3i}) is necessary to accelerate the coolant to the main-stream velocity. Discontinuities at nozzle outlet and at diffuser inlet are due to losses of kinetic energy: in fact, $(v^2_{g,in}-v^2_{g,ct})/2$ is recovered with efficiency $\eta^1_{p,ct}$, while $(v^2_{g,ct}-v^2_{g,dif})/2$ is recovered with efficiency $\eta_{p,ut}$.

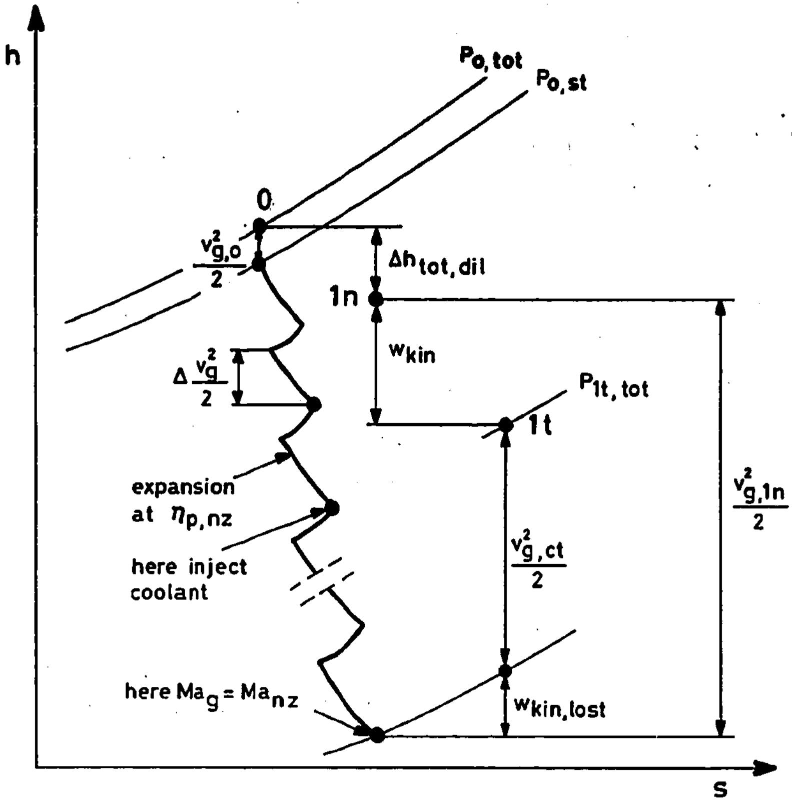

3.4a Schematic of cooled nozzle expansion. Notice that:

- $\Delta h_{tot,dil}$ is due to dilution with coolant
- Δh of each step is completely converted into kinetic energy
- the exit velocity $v_{g,1n}$ is the one that realizes the input Ma_{nz}
- m_g increases after each coolant injection
- the kinetic energy difference $(v^2_{g,1n}-v^2_{g,ct})/2$ is converted into work with efficiency $\eta^1_{p,ct}$ (i.e. η_p of first cooled turbine step). In other words:

$$w_{kin}=\eta^1_{p,ct}\cdot(v^2_{g,1n}-v^2_{g,ct})/2$$

Point 0 indicates total conditions at nozzle inlet; 1n total conditions at nozzle exit; 1t total conditions at turbine inlet.

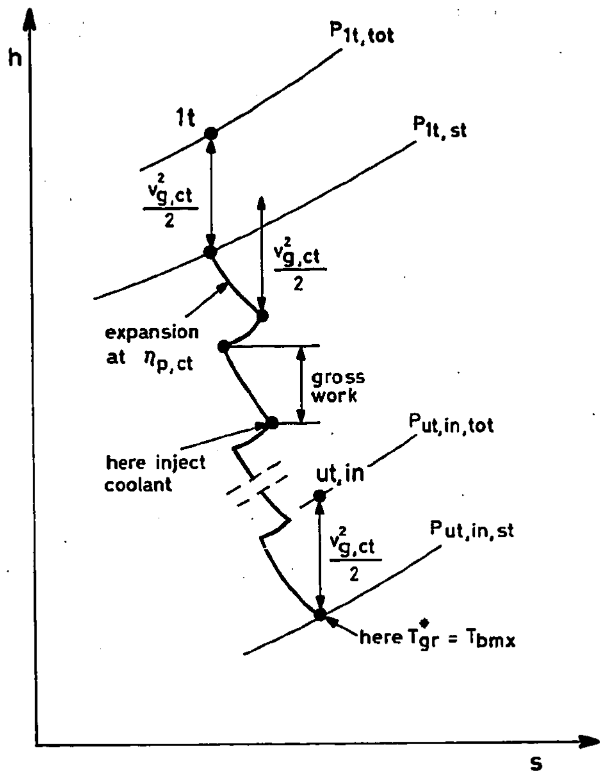

3.4b Schematic of cooled turbine. The net work per step is given by the difference between gross work ($m_g \cdot \Delta h_{step}$) and pumping work (Eq. 3.10). Notice that both $\eta_{p,ct}$ and m_g change throughout the expansion. Point ut,in indicates total conditions at the uncooled turbine inlet. The cooled expansion ends when $T_{gr}^* = T_{bmx}$.

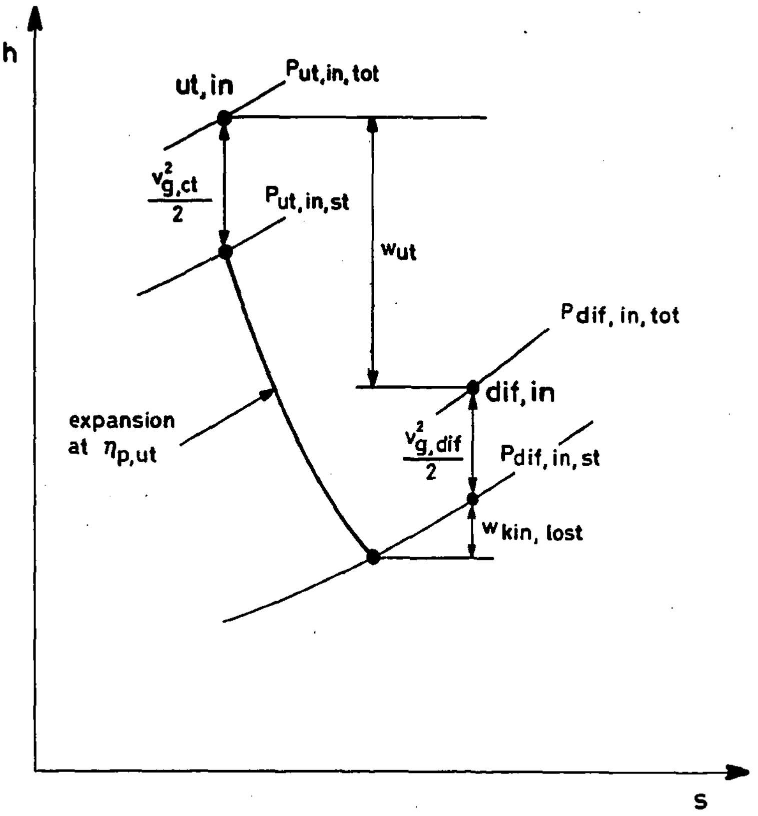

3.4c Schematic of uncooled turbine. $v_{g,dif}$ corresponds to Ma_{dif} assigned in input, while Point dif,in indicates total conditions at diffuser inlet. The difference between inlet and outlet kinetic energies is converted into work with he same efficiency $\eta_{p,ut}$ assumed for the static-to-static process, i.e.:

$$w_{kin,lost}=(1-\eta_{p,ut})\cdot(v_{g,ct}^2-v_{g,dif}^2)/2$$

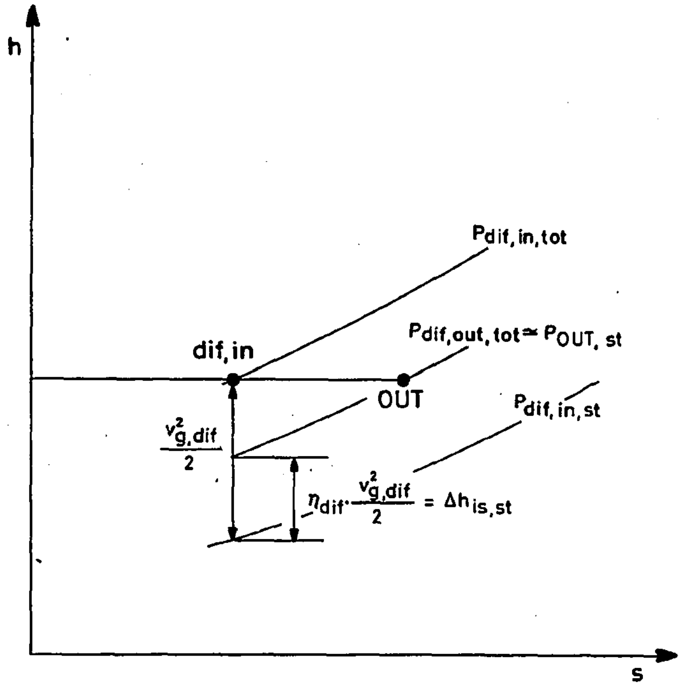

3.4d Schematic of turbine diffuser. Point dif,in indicates total inlet conditions, while OUT refers to total conditions far downstream (exhaust flange). Thus, η_{dif} actually embodies all losses occuring downstream the diffuser inlet.

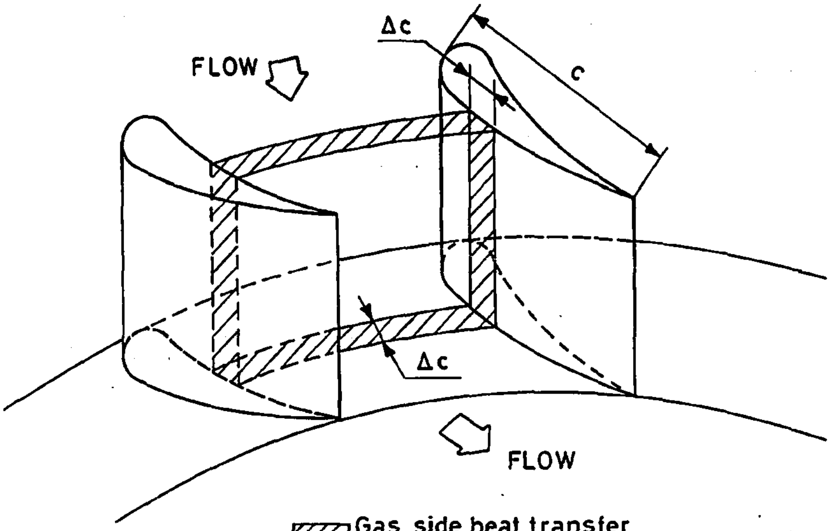

3.5 Schematic of the turbine section spanned at each step of the cooled expansion. The gas-side heat transfer area is computed by referring to a cascade with the average characteristics discussed in Appendix A.

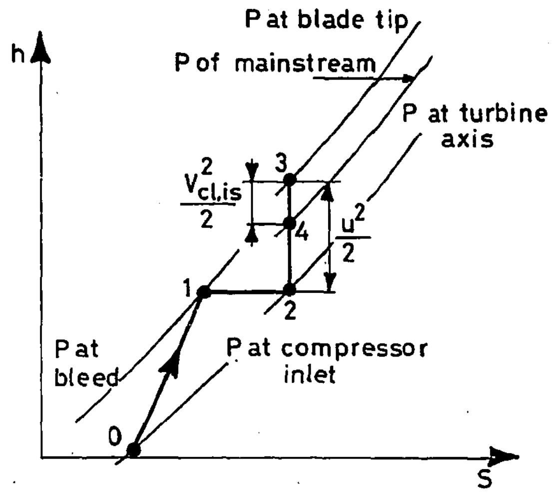

3.6 Rotor coolant enthalpy-entropy diagram. The pressure increase due to rotor centrifugal acceleration corresponds to an isentropic compression with $\Delta h = u^2/2$. Point 3 represents the conditions used to evaluate cooling flows. The coolant pumping work $m_{cl} \cdot (u^2/2)$ must be supplied by the rotor and is therefore a net loss. The figure is based on the assumption that the coolant is always bled at stationary points.

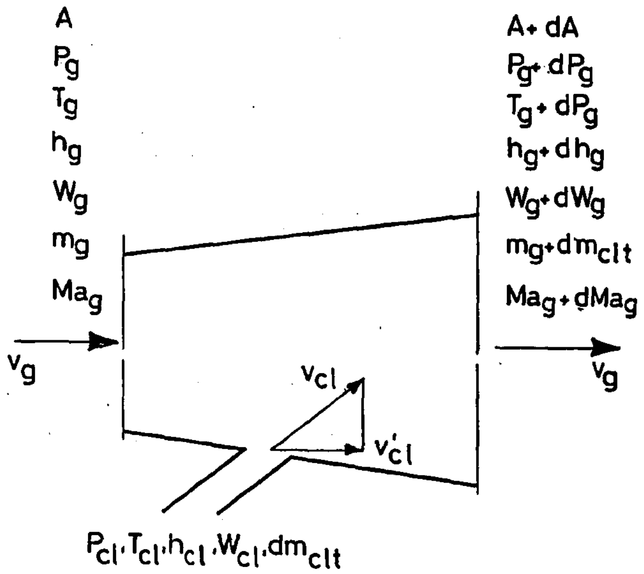

3.7 Schematics of coolant acceleration and mixing. Inlet and outlet gas velocities are the same. v_{cl} is the coolant inlet velocity; v'_{cl} is its component along the direction of v_g. At exit, coolant and gas are completely and uniformly mixed. dm_{clt} is the sum of dm_{clb} and dm_{dsk}.

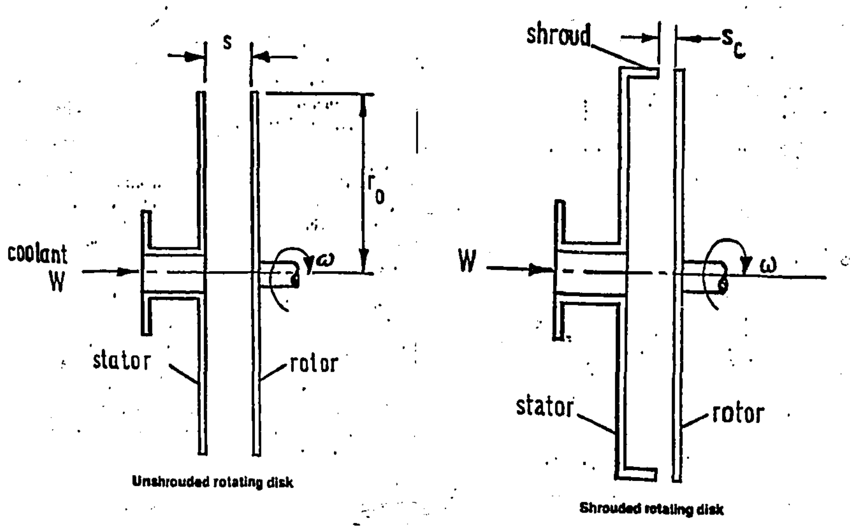

3.8 Unshrouded and shrouded rotating disk models considered by Haynes and Owen (1975).

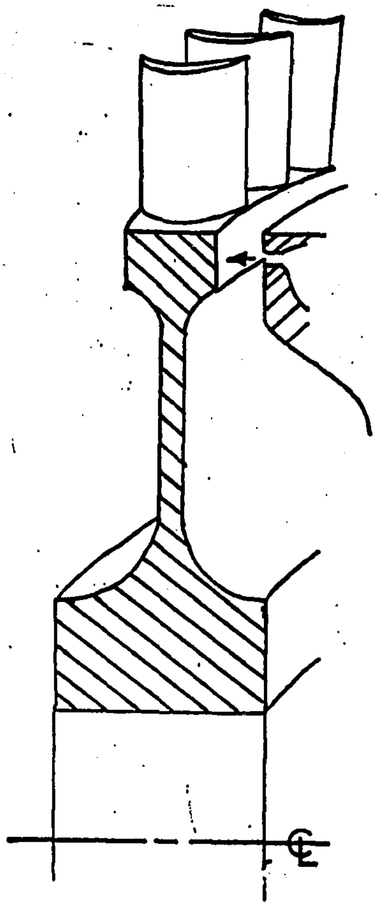

3.9 Disk rim impingement cooling considered by Metzger, Mathis and Grochowsky (1979).

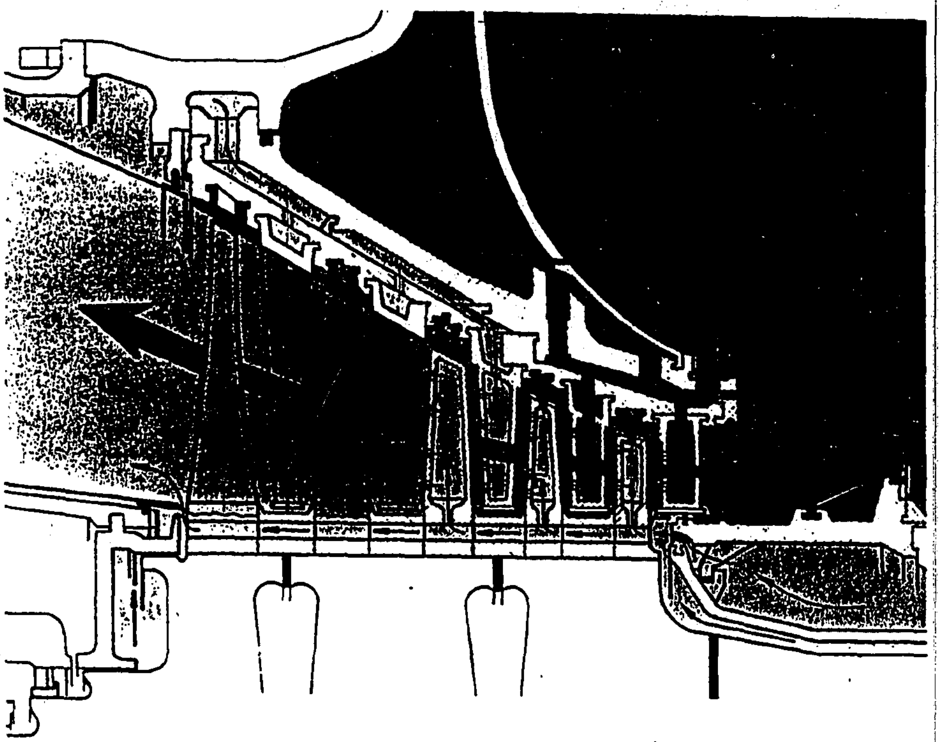

3.10 Cross-section of ABB 13E heavy-duty turbine. Notice the constant-hub diameter design and the absence of disks exposed to the hot gas.

4. TURBOMACHINERY EFFICIENCY

This Chapter addresses the evaluation of turbomachinery efficiencies. After assessing the relevance of the terms appearing in the gas turbine model and expanding some concept previously recalled in Par. 2.2, the functional form assumed for $\eta_{p,t}$ is justified with the support of theoretical results for optimized turbine stages and of data regarding commercial gas turbines.

Finally, based on similarity and fluidynamic arguments, these considerations are extended to the gas turbine compressor. The results for optimized turbine stages have been produced by a computer code due to Lozza, Macchi and Perdichizzi (1982).

4.1 Definitions

Fluidynamic losses occurring in turbomachines are evaluated by means of the following efficiencies (see Par. 2.2.3 for a discussion on their significance):

$$\eta_{p,nz} = (dh/dh_{is})_{st} = d(v^2/2)/dh_{is,st} \tag{4.1}$$

$$\eta_{p,t} = (dh/dh_{is})_{st} = \rho\cdot(dh/dP)_{st} \tag{4.2}$$

$$\eta_{dif} = \Delta h_{is,st}/(v^2_{g,dif}/2) \tag{4.3}$$

$$\eta_{p,c} = (dh_{is}/dh)_{tot} = (dP/dh)_{tot}/\rho \tag{4.4}$$

where all quantities refer to the mainstream. For the diffuser, $\Delta h_{is,st}$ is the isoentropic Δh corresponding to a compression *from* $P_{dif,in,st}$ to $P_{dif,out,st}$ (see Fig. 3.4d). Notice that $\eta_{p,t}$ is static-to-static, while $\eta_{p,c}$ is total-to-total. For the turbine, this has been done to be consistent with $\eta_{p,nz}$ which – given that in the nozzle h_{tot} is constant* – can be defined only as static-to-static; for the compressor there was no other choice because kinetic terms are not calculated. In the cooled turbine $(dh/dh_{is})_{st}=(dh/dh_{is})_{tot}$ because $v_{g,ct}$ is constant. $v_{g,dif}$ is the diffuser inlet velocity, based on the input value of Ma_{dif}.

* In the nozzle h_{tot} decreases due to dilution with cooling air. However, this decrease has nothing to do with work production nor flow acceleration.

4.2 Features and limits of approach adopted

While $\eta_{p,nz}$ and η_{dif} affect only a small portion of the cycle and thus have a relatively minor effect on overall performances, the correct evaluation of $\eta_{p,c}$ and $\eta_{p,t}$ is of the utmost importance: besides logical reasoning, this statement is demonstrated by the sensistivity analysis presented in Par. 7.4.

Given the rationale illustrated in Par. 3.3 – whereby it is crucial to limit the number of unknown parameters and the computational effort – in the present model it is assumed that:

- $\eta_{p,nz}$ and η_{dif} do not depend on the characteristics of the cycle: their values are assigned in input and kept constant.
- $\eta_{p,t}$ and $\eta_{p,c}$ depend only on the size parameter SP.

The functions $\eta_{p,t}(SP)$ and $\eta_{p,c}(SP)$ are determined by calibrating the performance prediction of 32 commercial gas turbines (see Ch. 7). Although their functional form is based on calculations developed only for turbines (Par. 4.5), the extension to compressors is justified by the analogy of many of the loss mechanisms (profile and annulus losses, finite trailing edge thickness, clearances, secondary flows).

Given their importance and the latitude evidenced in the following paragraphs, the method for the determination of $\eta_{p,t}$ and $\eta_{p,c}$ deserves further work; in particular the introduction of a dependence from specific speed could account for differences between single- and multi-shaft designs. On the other hand, the improvement of the correlations for η_p is strongly hampered by lack of data for actual turbomachines. Based on the results of numerous, unsuccessful attempts to identify alternative functional forms, the form presented here is the best result made possible by the data available.

4.3 Turbine nozzle and diffuser

$\eta_{p,nz}$ and η_{dif} are assumed to be independent of the turbine operating conditions; in particular, all results presented in the Thesis refer to $\eta_{p,nz}$=0.95 and η_{dif}=0.50.

Aside from engine size, in reality $\eta_{p,nz}$ and η_{dif} depend on a number of fluid dynamic and geometric parameters; for example (Adenubi, 1976; Wilson, 1984, Ch. 4), η_{dif} is a strong function of Ma_{dif}, diffuser shape (radial, axial, presence of splitters), inlet velocity profile (swirl, circumferential and/or radial variations), divergence angle, lenght-diameter ratio. However, accounting for such effects requires the full design of the turbine – which would defeat the rationale illustrated in Par. 3.3 – or further functional relationships – which would add to the already high number of parameters to be calibrated.

Since $\eta_{p,nz}$ and η_{dif} affect only a relatively small portion of the expansion, neglecting their variations seems compatible with the accuracy of the model and, most of all, with the data available for calibration. The sensitivity of results to this assumption is illustrated in Par. 7.4.

4.4 Similarity considerations

If turbines could be realized in perfect geometrical similarity, size would affect performance only indirectly, through variations of the Reynolds number. Aside from compressibility effects, in such case the efficiency of a stage would be a function of only two parameters: the specific speed n_s and the specific diameter D_s. Balje (1981) has presented a series of charts giving the maximum efficiency and the optimum geometrical parameters corresponding to each combination of n_s and D_s: Fig. 4.1 reports the one for axial turbines. According to the Balje charts, if the choice of n_s and D_s were unconstrained, it would always be possible to design turbine stages having an efficiency in excess of 90%. Such optimum stages would all be geometrically similar, and would have n_s between 0.6 and 1.3, D_s between 2.5 and 5.

4.4.1 Compressibility and scale effects

Balje charts work reasonably well for nearly-incompressible flows and "large" engines, where "large" means that the minimum dimension is well above the one allowed by manufacturing capabilities. Macchi and Perdichizzi (1981) have shown that if these conditions are not met, the efficiency of an optimized stage, i.e. a stage with D_s and all geometrical parameters optimized for maximum efficiency, depends not only on n_s, but also on:

- the size parameter $SP = V_{out}^{0.5}/\Delta h_{is}^{0.25}$, which accounts for scale effects
- the volumetric flow ratio V_{out}/V_{in}, which accounts for compressibility effects

As pointed out in Par. 2.2.2.10, in gas turbine stages the effects of compressibility on maximum attainable efficiencies are negligible because the volumetric flow ratio V_{out}/V_{in} is small – typically 1.5-2; besides Fig. 2.12, this is apparent from Fig. 4.2, which shows that for $V_{out}/V_{in} \leq 2$ the optimum n_s and the maximum attainable efficiency essentially depend only on SP. This does not mean that the flow is incompressible. It means that the variations of volumetric flow and Mach numbers between the stage inlet and outlet do not produce significant efficiency variations with respect to machines handling incompressible flow.

On the contrary, scale effects cause relevant efficiency variations. Small turbines have poorer performances because – due to manufacturing constraints – blade dimensions, trailing edge thicknesses and tip clearances cannot go below certain limits, thus preventing from maintaining geometrical similarity. In cooled engines this effect is much stronger because of: (i) bigger and thicker blades necessary to house the cooling channels; (ii) larger trailing edge thicknesses to allow for coolant ejection holes*; (iii) larger tip clearances to allow for greater thermal expansions**.

Problems related to the design of small, cooled, axial-flow turbines are the subject of a number of experimental programs carried out by NASA, Pratt&Whitney and others (see Due, Easterling and Haas, 1977 for an overview).

---

* The loss due to higher trailing edge thickness is partially compensated by the kinetic energy of the ejected coolant.

** Liess (1969) reports that discharge of cooling air from the blade tip reduces the "effective" tip clearance and can have beneficial effects on efficiency. Still, tip clearance losses of cooled engines are likely to be larger than for uncooled engines.

4.4.2 Other factors

Turbine efficiency is limited not only by manufacturing capabilities. Mechanical constraints pose limits on the maximum peripheral velocity – to limit centrifugal stresses – and on the blade shape – to ease vibration and fatigue problems. Economic considerations push toward reducing the number of stages and the number of blades of each cascade. Again, all these constraints are more compelling in highly cooled engines.

4.4.3 Actual determinants of efficiency

Due to the considerations above, the ideal situation predicted by the Balje charts is far from reality. Even assuming that the geometry of real gas turbine stages is actually optimized for maximum efficiency*, such efficiency still is a function of:

- rotational speed
- size parameter SP
- manufacturing, mechanical, economic constraints

Moreover, it must be noticed that: (i) the choice of ω has to account for compressor requirements; (ii) in a multi-stage turbine, efficiency also depends on the distribution of Δh_{is} among stages and the number of shafts**.

---

* Although efficiency maximization is certainly a sensible choice, other relevant optimization criteria could be the minimization of specific cost ($/kW) or specific weight (kg/kW). Moreover, it must be noticed that there is a substantial difference between maximizing the efficiency of a single stage and maximizing the efficiency of a whole multi-stage engine.

** Shafts constrain the variation of rotational speed from HP to LP stages.

4.5 Detailed estimates for turbine stages

The objective of this paragraph is to prove that for operating conditions typical of commercial gas turbines the influence of SP on η_t is larger than that of n_s. Then, as long as we want to represent η_t as a function of only one variable, the best choice is η_t=f(SP). The introduction of a two-variable function η=f(SP,n_s) would certainly be better, but would add to the already high number of parameters to be calibrated (see Ch. 7).

4.5.1 n_s vs. SP for commercial engines

Fig. 4.3 reports the specific speed and the size parameter SP for the first and last stages of the "current generation" of turbines listed in Tab. C.1 (the ones marked with an asterisk in the first leftward column of the table). While for both first and last stages SP varies of almost an order of magnitude, the corresponding variation of n_s is less than a factor of two. This suggests that, after all, scale effects and constraints do not influence much the choice of n_s, and that it is generally possible to choose a nearly-optimal distribution of specific speeds among turbine stages. According to Macchi and Perdichizzi (1981) the optimum specific speed of a single-stage turbine is in the range 0.75-0.95 (the higher values corresponding to lower SP). However, when more than one stage is mounted on the same shaft, a compromise must be realized among the optimum speed of each stage. High-pressure stages are typically designed for n_s lower than optimum, while the opposite is true for low-pressure stages. In view of this consideration, the data in Fig. 4.3, strongly support the presumption that the specific speed of commercial turbines is generally fairly close to the optimum for maximum efficiency.

4.5.2 Optimization

In order to show the relevance of n_s, SP and geometric constraints, calculations have been performed with an efficiency-maximization procedure developed by Lozza, Macchi and Perdichizzi (1982). The program searches for the maximum turbine efficiency by repeating at each iteration the mean-line design and then calculating losses according to the set of correlations proposed by Craig and Cox (1971), possibly the most accredited method now available for turbine efficiency predictions. The design of each stage depends on 9 independent variables (load factor, degree of reaction, stator and rotor discharge angles, etc.) and is subject to the constraints listed in Tab. 4.1. Although the code does not handle blade cooling, the resulting qualitative behaviour of η_t is also representative of cooled stages. Notice that several of the constraints listed in Tab. 4.1 never bind the optimal solution: they are used to "guide" the optimization process along a path of plausible solutions, thus reducing computing time.

For the sake of simplicity, it is assumed that the enthalpy drop of each stage has already been determined and refer to one single stage; consequently, the absolute values appearing in Fig. 4.4 and 4.5 cannot be translated directly to multi-stage turbines. The calculations have been performed for conditions typical of the first high-pressure and the last low-pressure stage of advanced, heavily-cooled engines. In the former case we have analyzed the influence of SP for n_s=0.35, 0.4 and 0.5; in the latter n_s=0.9, 1.0 and 1.6. As shown in Fig. 4.3, such values of n_s approximately correspond to the minimum, median and maximum values encountered in commercial engines. As illustrated in Tab. 4.1, calculations have been perfomed for two sets of constraints: the first (constraints A) is meant to represent uncooled "unconstrained", stages; the second (constraints B) suffers the consequences of high temperature and blade cooling, i.e.:

- Larger chord and trailing-edge thickness to accomodate the cooling system.
- Larger minimum radial clearance to account for larger thermal expansions.
- Smaller degree of reaction, to achieve higher gas ΔT within fewer stages.

For LP stages, which are likely to be uncooled anyway, the constraint on the degree of reaction has been neglected, while the one on the minimum trailing-edge thickness has been relaxed (see notes in Tab. 4.1). The constraints on the maximum number of blades reflects economic considerations; the ones on c_a/D_m are based on typical values adopted in actual turbines.

4.5.3 n_s vs. SP for optimized stages

Fig. 4.4 shows that for the range of n_s adopted in commercial engines scale effects are likely to be much more relevant than the ones of rotational speed. For HP stages (curves with n_s=0.35, 0.4, 0.5), if the effect of n_s is neglected – assuming, say, an average n_s=0.4 – the maximum error on η_t is around 1 percentage point; instead, if we neglect the effect of size – assuming, say, an average SP=0.35 – the error on η_t can be as high as 5 percentage points. Similar conclusions can be drawn for low-pressure stages, although in that case the relevance of SP vs. n_s appears lower.

For the range of SP and typical constraints encountered in practical applications η_t is an ever-increasing function of SP; however, at

<u>Assumptions maintained for all calculations:</u>

$W = 29$ kg/kmol, $\gamma = 1.33$
rotor unshrouded, with disk[a]
stator inlet angle = 90°
$D_{m,stator} = D_{m,rotor}$
$H_{rotor\ in} = 1.1 \cdot H_{stator\ out}$
suction-side curvature (downstream the throat)[b] = $1 \cdot 10^5$
surface roughness = $2 \cdot 10^{-6}$
(stator-rotor clearance)/(axial chord) = 0.02
(tip clearance)/D_m = $5 \cdot 10^{-4}$

(trailing-edge thickness)/throat		= 0.05		
peripheral velocity		≤ 420 m/s		
relative Mach rotor inlet		≤ 0.8		
relative Mach rotor outlet		≤ 1.4		
H/D_m		≤ 0.25		
$H_{rotor\ out}/H_{rotor\ in}$		≤ 1.5		
1.5	≤ $\Delta h_{is}/(u^2/2)$	≤ 6		
10	≤ number of blades	≤ 300	(both stator and rotor)	
0.225	≤ throat/(blade spacing)[c]	≤ 0.866	(")	
0.1	≤ throat/(axial chord)	≤ 1.0	(")	
10 mm	≤ throat	≤ 100 mm	(")	
0°	≤ flaring angle	≤ 15°	(")	

<u>Assumptions for:</u>	<u>n_s=0.35,0.4,0.5</u>	<u>n_s=0.9,1.0,1.6</u>
T_0	1200°C	700°C
P_0	25 bar	2.0 bar
P_0/P_1	2.25	2.0
Δh_{is}	310 kJ/kg	178 kJ/kg
Re	10^6	$0.5 \cdot 10^6$

<u>Assumptions for:</u>	<u>constraints A</u>		<u>constraints B</u>	
	min	max	min	max
degree of reaction	0.0	0.8	0.0	0.2[d] or 0.8[e]
(stator axial chord)/D_m	0.03	0.20	0.05	0.20
(rotor axial chord)/D_m	0.03	0.20	0.04	0.20
axial chord, mm	20.0	200.	40.0	200.
min trailing-edge thickness, mm	0.5		2.0[d] or 1.0[e]	
min tip clearance, mm	0.5		1.0	

[a] disks might be absent, with blades mounted directly on the shaft
[b] blade curvature affects supersonic expansion losses
[c] i.e. discharge angle between 13° and 60°
[d] for n_s=0.35, 0.4, 0.5
[e] for n_s=0.9, 1.0, 1.6

Table 4.1 Assumptions adopted for the evaluation of the influence of n_s and SP on η_t.

constant n_s the function $\eta_t(SP)$ will always have a maximum because:

- at low SP, η_t is low due to the greater relative importance of finite thicknesses and clearances;
- at high SP, some constraint will eventually intervene to limit the growth of η_t, most likely the one on the maximum absolute axial chord.

The constraint on H/D_m has been introduced because the calculation procedure does not account for radial variations, and its applicability beyond H/D_m=0.25 would be unrealistic*; for very high H/D_m efficiency tends to decrease due to the difficulty of optimizing radial blade profile variations. In actual gas turbines H/D_m is rarely greater than 0.25. Values up to 0.35 can be found in the last LP stages of steam turbines for large nuclear plants.

4.5.3.1 Comparison with calibration results

If we want to describe the behaviour of the turbine efficiency as a function of SP only, such function should be somewhere in between the two dashed lines of Fig. 4.5, approaching the one for n_s=0.4 at low SP, and the one for n_s=1 at high SP. Qualitatively, this situation is confirmed by the line resulting from the calibration discussed in Ch. 7, although such line is not as steep as we would expect from the results for fully optimized stages**. Fig. 4.5 suggests that the correlation resulting from the model calibration tends to overestimate the efficiency of HP stages and to underestimate that of LP stages.

---

* For high H/D_m it is necessary to resort to "through-flow", quasi-3D procedures, whereby the flow is solved in the meridional plane containing the turbine axis (see Par. 2.2.2.8).

** Notice that the efficiency represented by the thick dash-dot line is static-to-static, while the other lines represent total-to-total efficiencies. However, for one stage $\eta_{tot-tot} \simeq \eta_{st-st}$, because the difference between inlet and outlet absolute velocity is generally small.

Although more experimental data are needed to verify this conjecture, this situation appears totally coherent with the exclusion of n_s from the correlation for η_p. In fact, stages with the same SP will exhibit different efficiencies depending on their n_s: HP stages (lower n_s) will have lower efficiency than LP stages (higher n_s).

4.5.4 Influence of geometric constraints

Fig. 4.5 depicts the influence of constraints, and shows that the penalties imposed by the presence of the cooling system – particularly at small scale – can be quite substantial. At large scale and high n_s such effects obviously tend to disappear because in those conditions none of them can be binding. For example, at n_s=1.0, SP=1.5 and constraints B, the optimization procedure gives (in meters) D_m=2.09, c=0.235, H=0.432, a situation for which the constraints on the minimum trailing-edge thickness and tip clerance are clearly irrelevant. It must be noticed that besides lower efficiencies cooled stages also suffer mixing losses, which are accounted for separately as illustrated in Par. 3.8.

4.5.4.1 Comparison with commercial engines

Fig. 4.6 and 4.7 depict the trends of some of the geometric parameters utilized to determine heat transfer areas (see Appendix A). Comparing the data in the figures with the ones in Tab. A1 it can be observed that:

- The specific diameter adopted in the first stage of actual engines appears to be 10-15% lower than optimum. The reason might be due to compressor requirements or to weight, compactness, and economic considerations.

- As a consequence of lower-than-optimum specific diameters, actual engines exhibit higher-than-optimum blade heights. This statement applies particularly to large single-shaft heavy-duties, while multi-shaft aero-derivatives have H/D_m closer to the optimum predicted by Fig. 4.6.

- Solidities adopted in cooled engines are lower than the ones for optimum aerodynamic performance. The trade-off between efficiency and heat transfer area is evident.

- Probably due to mechanical and/or structural considerations, the ratios c_a/D_m adopted in practice are higher than optimum.

Overall, the assumptions of D_s=3.25, $(H/D_m)_0$=0.08, σ=1.25 and c_a/D_m=0.055 agree reasonably well with the prediction of the optimization code.

4.6 Turbine efficiency functional dependence

Provided that the influence of SP on the efficiency of actual gas turbines stages is much larger than the one of n_s, $\eta_{p,t}$ can be represented as a function of SP only. We emphasize that this does not mean that the rotational speed is of minor importance, but that since for actual engines the specific speed of corresponding stages* is approximately the same, size becomes the major factor. Based on the qualitative behaviour shown in Fig. 4.4 and 4.5, it is assumed that turbine efficiency is a parabolic function of $\log_{10}(SP)$, i.e.:

$$\begin{aligned} \eta_{p,t} &= \eta_{p,t\infty}\cdot(1-a_t\cdot[b_t-\log_{10}(SP)]^2) && \text{for } SP \le 10^{b_t} \\ \eta_{p,t} &= \eta_{p,t\infty} && \text{for } SP \ge 10^{b_t} \end{aligned} \qquad (4.5)$$

where $\eta_{p,t\infty}$ is the value of $\eta_{p,t}$ reached for "large" $SP \ge 10^{b_t}$. Since the constraints and the detailed design criteria used for actual gas turbines are unknown, $\eta_{p,t,\infty}$, a_t and b_t cannot be determined theoretically: average values giving good agreement with the performance of commercial engines have been determined through the calibration discussed in Ch. 7.

4.6.1 Definition of local SP

The efficiency given by Eq.(4.5) and the size parameter SP are properly defined only for one stage. Their definition is extended to a continuous expansion by assuming that the local $\eta_{p,t}$ of each step is still given by Eq.(4.5) provided that:

$$SP = V^{0.5}/\Delta h_{is}^{0.25}$$

---

* "Corresponding" refers to high-, intermediate-, low-pressure stages.

where V is the local volumetric flow and Δh_{is} is the current stage enthalpy drop, calculated as described in Par. 3.6. Using this local SP corresponds to smoothing the variations of $\eta_{p,t}$ from one stage to another as depicted in Fig. 4.8.

4.7 Extension to compressors

Similarly to turbines, Fig. 4.9 shows that also for compressors the variations of SP encountered in commercial gas turbines are much larger than the variations of n_s, suggesting that scale effects and constraints do not dramatically influence the choice of the rotational speed.

The values of n_s in Fig. 4.9 compare well with the Balje chart in Fig. 4.10. The chart appears* to confirm that also for compressors HP stages run at speeds lower than optimum, while the specific speed of low-pressure stages approximately falls in the region of maximum efficiency. The figure also shows that the sensitivity of η_c to n_s does not appear to be larger than it is for turbines, so that neglecting the effect of n_s on η_c appears coherent with the same assumption already made for the turbine. Again, it does not mean that n_s is irrelevant, but that since correspondent (low-, high-pressure) compressor stages operate in a relatively narrow range of n_s, size becomes the major factor in determining $\eta_{p,c}$. Further work is needed to confirm the correspondence between turbine and compressor scale effects.

Based on these considerations it is assumed that also for compressors efficiency is only a function of the size parameter $SP=V_{in}^{0.5}/\Delta h_{is}^{0.25}$ and that the functional dependence is the same:

$$\begin{aligned} \eta_{p,c} &= \eta_{p,c,\infty}\cdot(1-a_c\cdot[b_c-\log_{10}(SP)]^2) && \text{for } SP \le 10^{b_c} \\ \eta_{p,c} &= \eta_{p,c,\infty} && \text{for } SP \ge 10^{b_c} \end{aligned} \qquad (4.6)$$

As for the turbine, the determination of average values of $\eta_{p,c,\infty}$, a_c and b_c capable of predicting the performance of actual gas turbine compres-

---

* Caution must be exercised in interpreting the chart, because several underlying hypotheses may not be actually verified.

sors is addressed in Ch. 6. Similarly to Eq.(3.2), the average compressor efficiency is determined as:

$$\eta_{p,c}=\int_{in}^{out}\eta_{p,c}(SP)\cdot dSP/(SP_{c,in}-SP_{c,out}) \tag{4.7}$$

4.7.1 Distribution of compressor enthalpy drops

The enthalpy drop used for the evaluation of SP_{in} and SP_{out} can be calculated according to the same four options described in Par. 3.6 for the turbine:

1) Constant β^{stg} and given number of stages
2) Constant β^{stg} and given $\Delta h^{stg}_{is,max}$
3) Constant Δh^{stg}_{is} and given number of stages
4) Constant Δh^{stg}_{is} and given $\Delta h^{stg}_{is,max}$

The last stage V_{in} needed to calculate SP_{out} and the reheat factor η_p/η_{is} needed when using options 3) or 4) are based on the efficiencies calculated at the previous iteration.

Unlike for the turbine, the choice of the compressor design option has essentially no effect on cooling flows*; thus, such choice affects only $\eta_{p,c}$, with minor effects on performance predictions.

4.7.2 Number of compressor stages

In the HP turbine, the need for cooling drives toward higher Δh in order to reduce T_g faster, thus making constant-β^{stg} designs attractive. On the other hand, constant-Δh_{is} designs give a better distribution of stage aerodynamic loads and are more likely for the compressor. For

* A very small second-order effect is the variation of coolant temperature – and thus cooling flow – due to variations of compressor efficiency.

this reason, the calibration of Ch. 7 and the test cases presented in Ch. 10 have been performed using option 3) – when the number of stages was known – or otherwise option 4) with Δh_{is}=30 kJ/kg (aero-derivatives) or 20 kJ/kg (heavy-duties).

REFERENCES

Adenubi S.O. (1976), "Performance and Flow Regime of Annular Diffusers with Axial Turbomachine Discharge Inlet Conditions", J. of Fluids Eng., June 1976, pp. 236-243.

Balje O.E. (1981), Turbomachines. A Guide to Design, Selection and Theory, John Wiley, New York.

Binsley R. and Balje O.E. (1968), "Axial Turbine Performance Evaluation", J. of Eng. for Power, Vol. 90, pp. 341-360.

Craig H.R.M. and Cox H.J.A. (1971), "Performance Estimation of Axial Flow Turbines", Proc. Institute of Mechanical Engineers, London, Vol. 185, pp. 407-424.

Due H.F., Easterling A.E. and Haas J.E. (1977), "The Status of Small, Cooled, Axial-Flow Turbines", in *AGARD CP-229*, Neuilly sur Seine, France.

Liess C. (1969), "Introduction to Cooling of Gas Turbine Blades", Lecture Series 15, vonKarman Institute for Fluid Dynamics, Brussels.

Lozza G., Macchi E. and Perdichizzi A. (1982), "On the Influence of the Number of Stages on the Efficiency of Axial-Flow Turbines", ASME Paper 82-GT-43.

Macchi E. and Perdichizzi A. (1981), "Efficiency Prediction for Axial-Flow Turbines Operating with Nonconventional Fluids", J. of Eng. for Power, Vol. 103, pp.718-724.

Wilson, D.G. (1984), The Design of High-Efficiency Turbomachinery and Gas Turbines, The MIT Press, Cambridge, Massachusetts.

NOMENCLATURE

a,b	Coefficients of functions η_p(SP) (see Eqs.4.5 and 4.6)	
c	Blade chord	[m]
c_a	Blade axial chord	[m]
D_m	Stage mean diameter	[m]
D_s	Specific diameter	
h	Specific enthalpy	[J/kg]
H	Blade height	[m]
n_s	Specific speed	
P	Pressure	[Pa]
Re	Reynolds number	
SP	Turbomachinery size parameter	[m]
T	Temperature	[K]
u	Blade peripheral speed	[m/s]
v	Velocity	[m/s]
V	Volumetric flow rate	[m^3/s]
$\mathcal{W}$	Molecular weight	[kg/kmol]

Greek

β	Pressure ratio (compressors, >1); expansion ratio (turbines, <1)	
γ	Ratio c_p/c_v	
Δh	Enthalpy drop (or rise)	[J/kg]
η	Efficiency	
ρ	Density	[kg/m^3]
σ	Solidity, chord/pitch	

Subscripts

c	Compressor
dif	Diffuser
g	Hot gas
in	Inlet
is	Isoentropic
nz	Nozzle
opt	Optimum
out	Outlet
p	Polytropic
st	Static conditions
t	Turbine
tot	Total conditions
0	Stage inlet
∞	Refers to large SP, i.e. no more scale effects (Eqs. 4.5 and 4.6)

Superscripts

stg	Stage

FIGURES

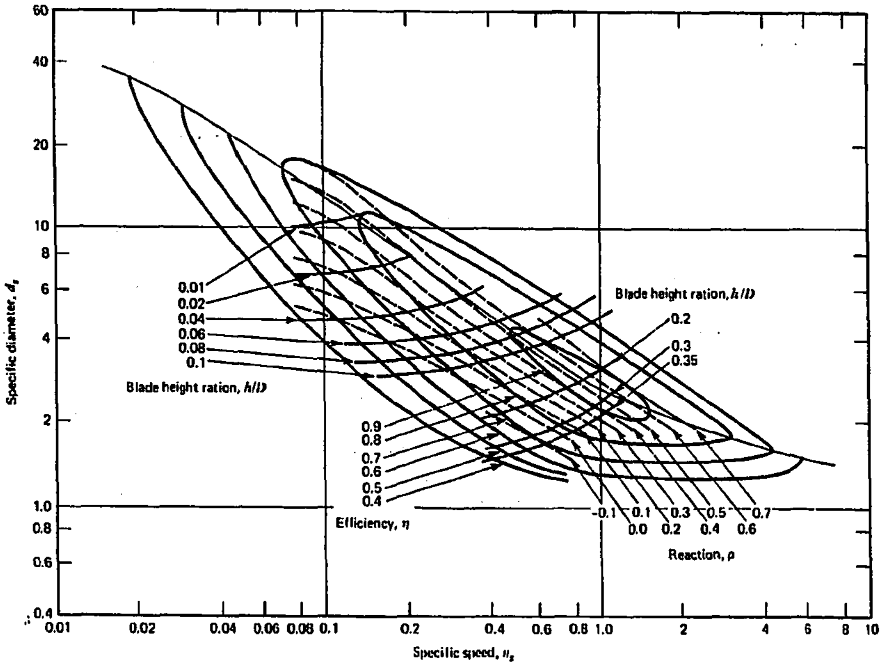

$n_s d_s$ diagram for turbines calculated for minimum loss coefficients

4.1 n_s-D_s diagrams for turbines calculated for minimum loss coefficients (after Binsley and Balje, 1968).

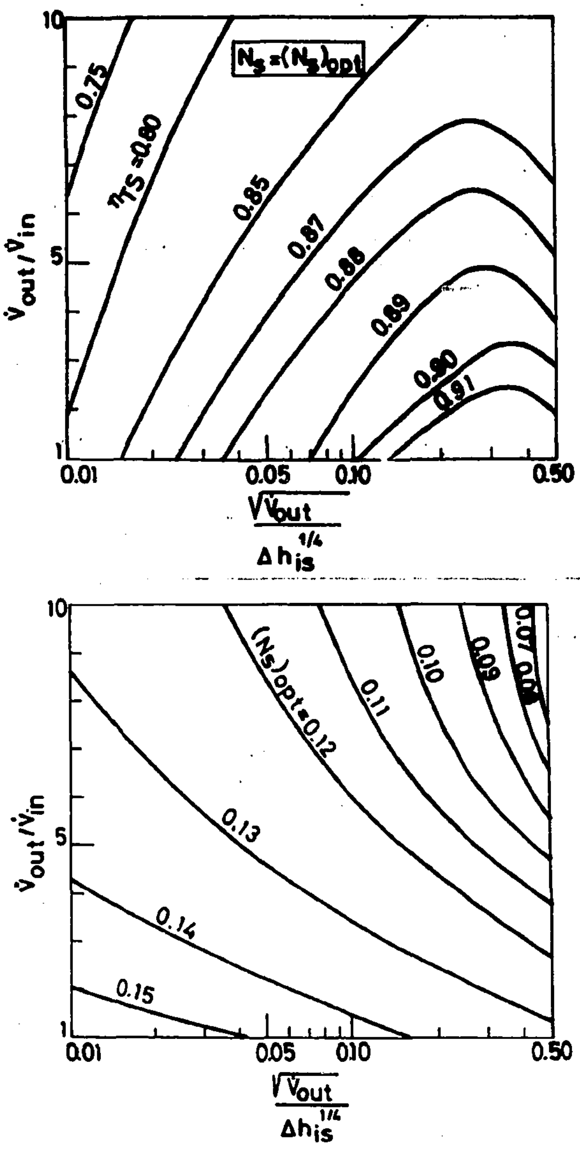

4.2 Efficiency predictions for a turbine stage at optimum specific speed (upper diagram) and optimum specific speed vs. $V_{out}^{0.5}/\Delta h_{is}^{0.25}$=SP and V_{out}/V_{in} (lower diagram, after Macchi and Perdichizzi, 1981). η_{TS}=total-to-static efficiency and $N_s = n_s/2\pi$. As long as $V_{out}/V_{in} \leq 2$, both $n_{s,opt}$ and η_{opt} essentially depend only on SP.

Similarity Parameters

Turbine ns vs. SP

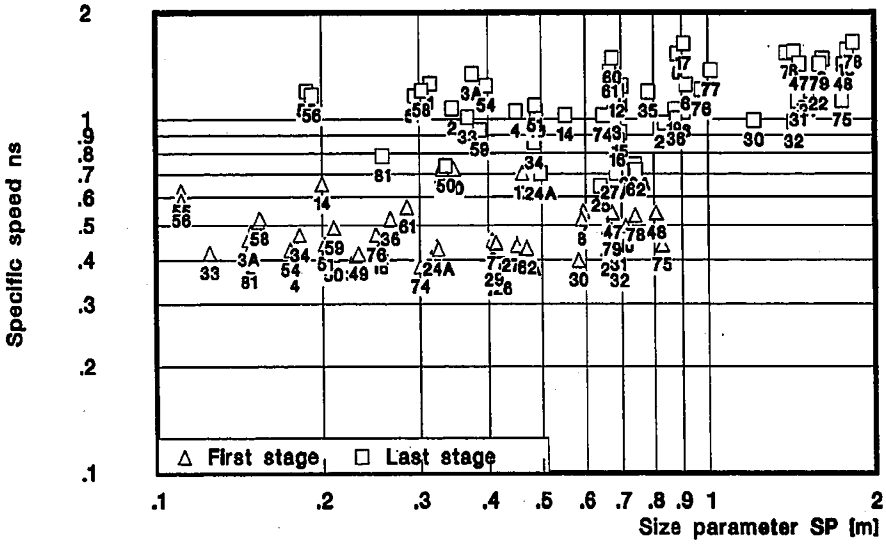

4.3 Specific speed n_s and size parameter SP of the first and last stage of axial (both compressor and turbine) engines. The numbers at each point identify the turbines listed in Table C.1; some have been excluded due to lack of information about the HP-shaft RPM. The pressure at the first stage exit and at the last stage inlet have been calculated by assuming that:

a) all cooled stages mounted on the same shaft have the same expansion ratio
b) all uncooled stages mounted on the same shaft have the same isoentropic enthalpy drop
c) the HP turbine power of multi-shaft engines equals the HP compressor power

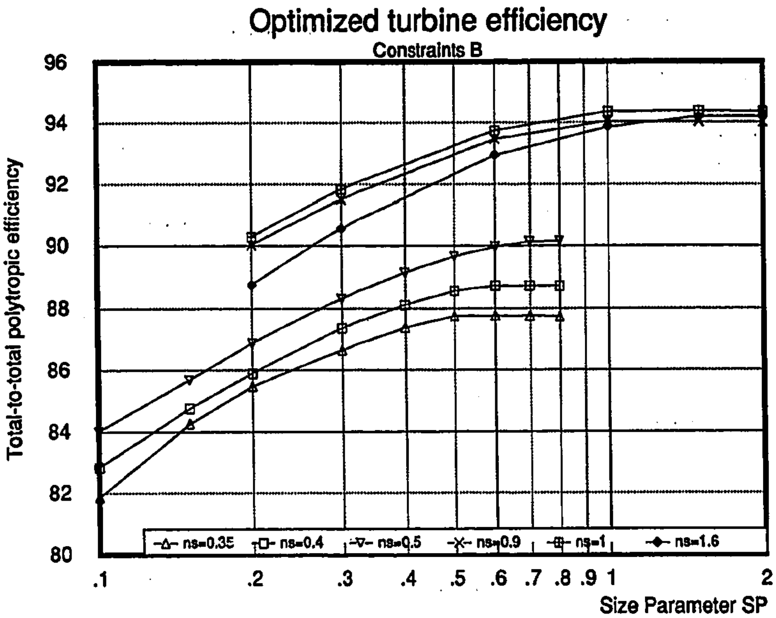

4.4 Optimized stage total-to-total efficiency as predicted by the model of Lozza, Macchi and Perdichizzi (1982) under the assumptions listed in Tab. 4.1 (constraints B).

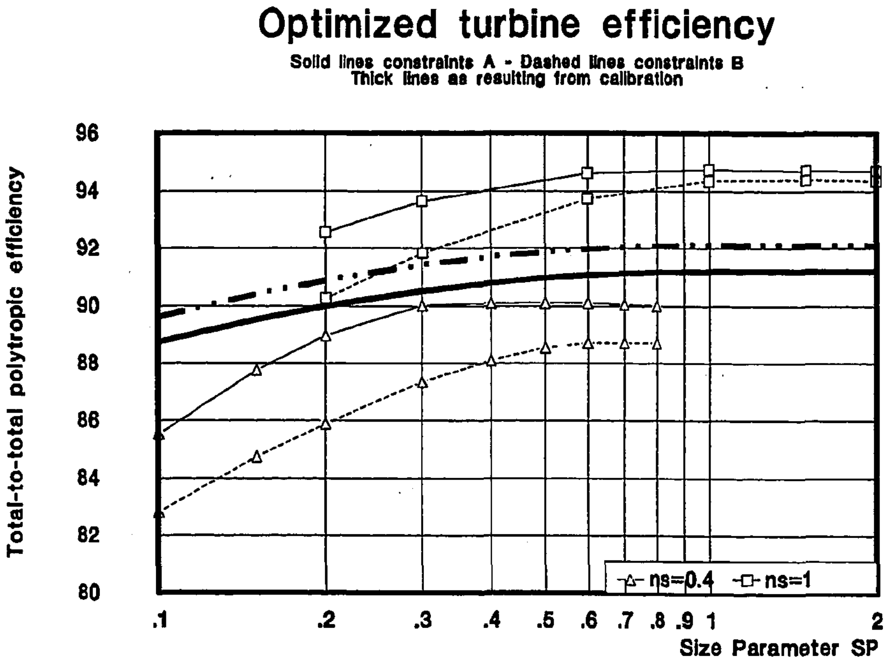

4.5 Influence of constraints on optimized stage total-to-total efficiency. The thick lines represent the static-to-static efficiency of "current" (solid line) and state-of-the-art (dash-dot line) turbines as resulting from the calibration carried out in Ch. 7.

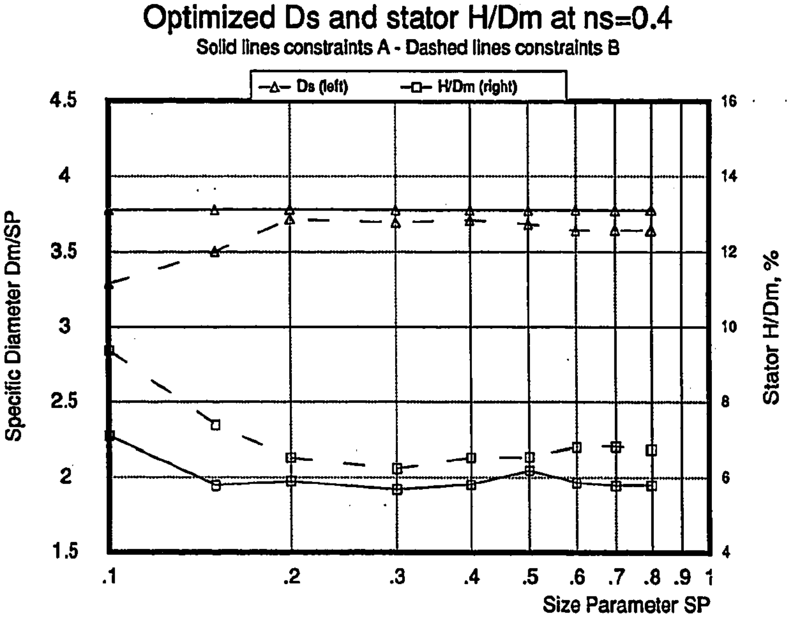

4.6 Optimized specific diameter and H/D_m for conditions typical of high-pressure turbine stages.

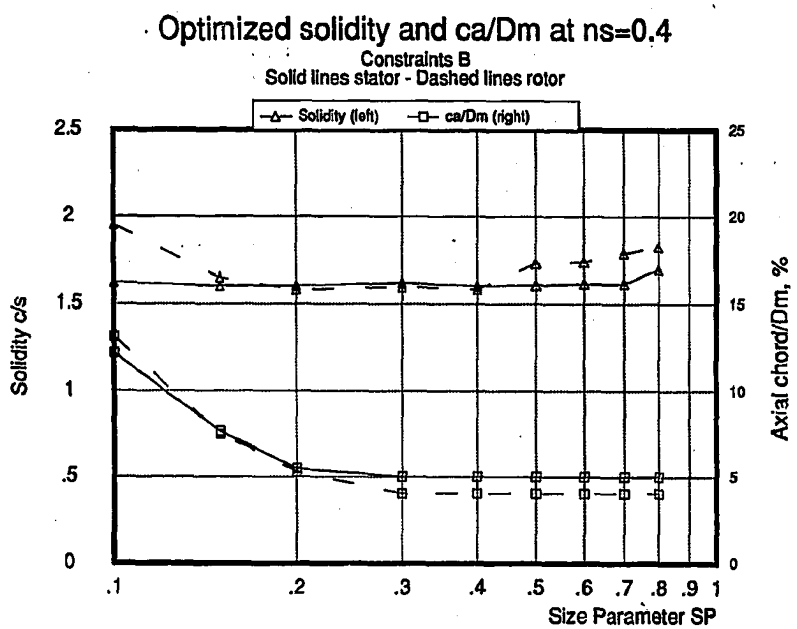

4.7 Optimized solidity and c_a/D_m for conditions typical of high-pressure turbine stages. For SP>0.3 the optimum solution is binded by the constraints on the minimum c_a/D_m.

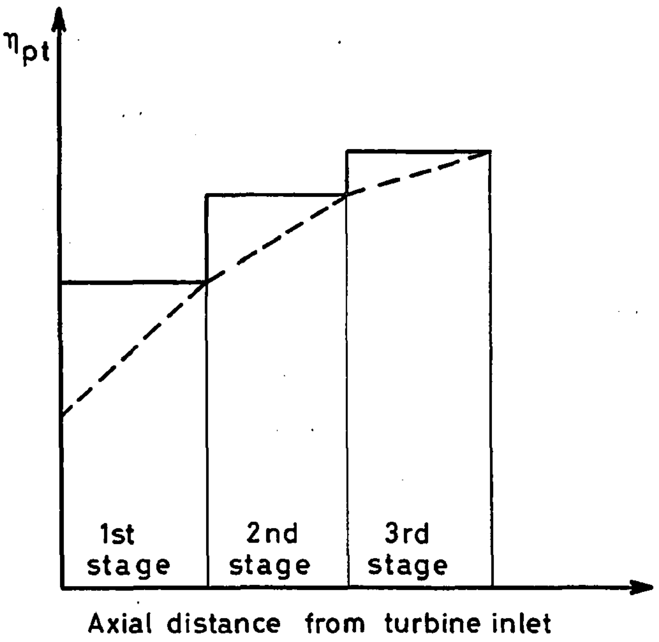

4.8 Variations of $\eta_{p,ct}$. The solid discontinuous line represents the efficiencies calculated from the function $\eta_{p,t}(SP)$ using the definition of "stage" SP, i.e. $V_{out}^{0.5}/\Delta h_{is}^{0.25}$. The dashed continuous line represents the efficiencies calculated from the same function $\eta_{p,t}(SP)$ using the definition of "local" SP, i.e. $V^{0.5}/\Delta h_{is}^{0.25}$. The two lines must obviously meet at the stage exit, where $V=V_{out}$.

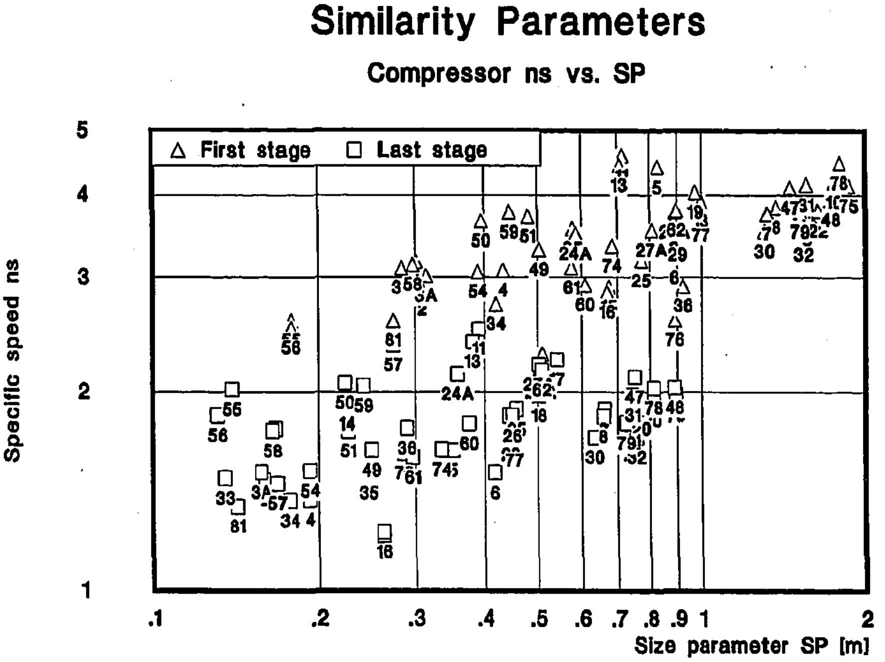

4.9 n_s vs. SP of first and last compressor stages of axial gas turbines (the same already considered for Fig. 4.3). The numbers at each point identify the turbines listed in Table C.1. SP and the volumetric flow at last stage inlet have been calculated by assuming that all stages mounted on the same shaft have the same Δh_{is}.

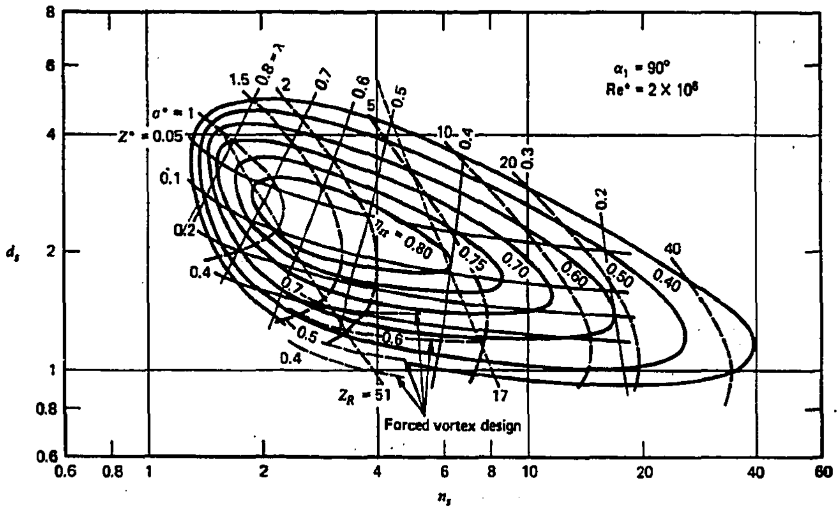

Calculated $n_s d_s$ diagram for single-stage axial machines.

4.10 Single-stage axial compressor n_s-D_s diagram as given by Baljé (1981).

5. BLADE COOLING

This Chapter deals with the evaluation of gas turbine blade cooling flows. After a review of cooling technologies in Par. 5.1, Pars. 5.2 and 5.3 illustrate the scheme for the calculation of convection and film cooling flows to be used in conjunction with the model of Ch. 3. The two basic features of this blade cooling model are:

- The characteristics of blade cooling technology are specified by means of two parameters: one to describe the "quality" of convection heat transfer inside the blade and another to describe the "quality" of film cooling. These two parameters need to be calibrated with experimental data.
- It is possible to account for variations of: (i) gas and coolant thermo-physical properties (c_p, Pr, μ, W); (ii) gas and coolant thermodynamic conditions (T, P); (iii) engine size and architecture (Re_g, meridional geometry).

The Chapter closes by presenting a scheme for the calculation of impingement cooling flows (Par. 5.4); this scheme is used to perform comparisons with the other two technologies, but it is not integrated with the expansion model of Ch. 3. Full-coverage film cooling and transpiration cooling are not analyzed.

Pars. 5.2 to 5.4 open with a summary of the strategy followed to model each cooling technology and close with results showing the influence of the most significant variables. Due to space limitations, the systematic investigation of the merits of the cooling model is not performed here; results are meant primarily to illustrate the capabilities of the model and – if applicable – to support the outcome of the calibration of Ch. 7. Notice that the results for convection and film cooling (Pars. 5.2.8 and 5.3.7) have been produced by the same subroutine used to calculate the turbine expansion described in Ch. 3.

5.1 Overview of blade cooling technology

Since the appearance of the first gas turbine engines in the late 40s, blade cooling has undergone tremendous developments. Although the maximum operating temperature of super-alloys has also improved remarkably (Fig. 5.1), most of the increases in turbine inlet temperature must be ascribed to improved cooling capabilities (Fig. 5.2). This paragraph briefly reviews the status of blade cooling technology.

5.1.1 Cooling methods

To satisfy the demand for increasing operating temperatures, blade cooling has evolved through a variety of different techniques: examples are illustrated in Fig. 5.3, while Fig. 5.4 illustrates the evolution of the schemes adopted in Rolls-Royce turbines. The design concept of a modern cooled blade includes an elaborate combination of enhanced convection, impingement and film cooling (Fig. 5.5). Together with improved performances, this sophisticated technology has brought about increased complexity and cost: design and testing of state-of-the-art blades might require years, at a cost which can be higher than US$ 2,500 per blade (Mom and Boogers, 1986). In the following I will briefly describe the features of the techniques already in use and the ones under study.

5.1.1.1 Convection cooling

Convection cooling is the simplest and still the most widely used technique, whereby the blade acts as a conventional heat exchanger. The coolant flowing inside the blade picks up heat conducted by the wall and is eventally discharged into the hot gas through orifices at the blade tip or at the trailing edge (in closed-loop systems like the ones examined by Stambler, 1989, the coolant would remain segregated from the gas). Although other methods are now used in many applications, they always coexist with some form of convection cooling.

5.1.1.2 Film cooling

In film cooling the coolant is ejected through slots or holes in the blade wall so as to establish a film of relatively cool air on the outer surface of the blade. The distinctive feature of film cooling is a reduction of thermal power exchanged to maintain a given blade metal temperature*. The cool film on the outer blade surface creates a shield "protecting" the blade from the hot gas, thus reducing the ΔT driving the gas-side heat transfer. As shown in Par. 5.3.7, coolant flow requirements can be reduced by a factor of 10 or more over convection cooling. Film cooling is now adopted in almost all commercial gas turbines: in heavy-duty units it is always limited to the first nozzle, while in aero-derivatives it is used also downstream.

Aside from thermal and fluidynamic aspects, the construction of film cooled blades is particularly demanding because holes and slots (i) enhance oxidation and are subject to vibration and fatigue failures; (ii) should not impair the blade mechanical integrity nor create strong fluidynamic disturbances. The latter drives toward a very high number of miniature holes, which are difficult and costly to manufacture (laser drilling is now helping to alleviate the problem).

5.1.1.3 Impingement cooling

Impingement cooling, a variation of convection cooling, is used to achieve high local heat transfer and more uniform temperature distribu-

* The thermal power transferred to the blade can actually be reduced also by TBC coatings (see 5.2.7).

tions by directing jets of coolant against the inner surface of the blade wall. As in convection cooling, the thermal power to be exchanged is fixed by the gas-side conditions and the temperature difference ($T_{gr}-T_{bmx}$). The results presented in Par. 5.4 show that coolant flow requirements are comparable, if not higher, than in convection systems.

5.1.1.4 Full-coverage film cooling

Full-coverage film cooling is an extreme form of film cooling whereby a film covering the whole blade surface is created by injecting the coolant through a very high number of small closely-spaced holes. Due to strong interaction among the film cooling jets, the thermo-fluidynamics of this configuration are substantially different from those where only a few coolant injection sites are used (Hempel and Friedrich, 1978). Its performances are somewhere in between film cooling and transpiration cooling.

5.1.1.5 Transpiration cooling

Transpiration cooling is accomplished by manufacturing the blade wall as a porous matrix. The coolant transpires uniformly across the porous wall, cooling it as well as reducing the gas-side heat transfer coefficient. For a given cooling flow, transpiration cooling yields the maximum reduction of thermal power transferred to the blade. Its heat transfer perfomances set an upper bound on all blade cooling technologies. According to Livinghood, Ellerbrock and Kaufman (1971), the main problem preventing actual implementation is the susceptibility of the porous materials to flow restriction due to oxidation. Once significant oxidation starts, the metal temperature rises and further accelerates the oxidation and flow restriction processes. The coolant flow can be completely obstructed in a few hundreds of hours of operation. Increasing the pore size would alleviate the problem but involves departure from ideal transpiration and a possible reduction in cooling effectiveness. Although it is still the subject of research, in the short to medium term the actual implementation of transpiration cooling appears unlikely.

5.1.2 Alternative cooling fluids

In recent years many papers have analyzed the use of steam and water as alternative cooling fluids. Obviously, this is feasible only for stationary turbines, where the added weight and complication of the water supply system and the boiler are not major drawbacks. They appear most interesting for application in Gas/Steam Cycles, where water and steam would be present anyway. Analyses of the impact of steam cooling on the performances of Combined Cycles have been presented by Rice (1982, 1983a and 1983b) and Wu and Louis (1984), while Takeya and Yasui (1987) have considered steam cooling for a steam-injected reheat turbine. Stambler (1989) discusses the potential benefits of closed-loop steam cooling. Compared to air cooling, the appeal of water and steam cooling comes from a number of factors:

- Due to much higher specific heat of water or steam, the flow rates necessary to exchange a given thermal power are much smaller. The reduction of cooling flow becomes dramatic when water evaporates inside the blade (two-phase cooling).
- The coolant can be compressed as liquid, thereby reducing the necessary pumping power by orders of magnitude. However, it must be noticed that, after evaporation, the reversible work losses due to pressure drops in the cooling circuit are comparable to those with any other compressible coolant.
- It is easier to have low coolant temperatures at high pressure ratios. In air-cooled engines this can be realized by cooling the air bled from the compressor (as is the case of several heavy-duty models produced by ABB, Fiat and Westinghouse) but it involves the use of additional heat exchangers. With water or steam the coolant

temperature can be kept low, even at very high pressures, without resorting to additional components.

- As pointed out by Han and Jenkins (1982), the film cooling effectiveness of steam (see definitions at Par. 5.3.2) is considerably higher than for air.
- In a closed-loop scheme, whereby the coolant is not discharged into the gas, acceleration and mixing losses are eliminated (see Ch. 8), and the heat absorbed by the steam can be utilized in a steam turbine. The closed-loop option is particularly interesting in a Combined Cycle, where the steam turbine would be present anyway.

Although very appealing and considerably studied (e.g. El-Masri and Louis, 1978; El-Masri, Kobayashi and Louis, 1982; El-Masri, 1983; Schilke and DeGeorge, 1982 and 1983), water cooling presents a series of major handicaps: erosion and scaling of cooling channels, instabilities of the liquid-vapour mixture, strong temperature gradients within the blade wall, high thermal stresses.

Steam cooling appears much closer to practical implementation. The major problems with steam are: (i) need for very high purity steam; (ii) corrosion and erosion of cooling passages; (iii) formation of deposits and plugging of film cooling channels and orifices. Due to its higher corrosion potential, steam cooling will almost certainly require the adoption of internal protective coatings, a technique already being introduced in air-cooled aircraft engines (Mom and Boogers, 1986).

5.1.3 Materials

The increase in operating temperature of both the compressor and the turbine (the former brought about by higher compression ratios) has resulted in increasing use of super-alloys (Tab. 5.1). According to Bradley (1988), in 1985 super-alloys constituted about 50% of jet engines weight, a figure expected to reach 60% by 1993. A super-alloy is an alloy developed for elevated temperature service, severe mechanical stress and resistance to hot corrosion and erosion. It generally consists of an austenitic face-centered cubic matrix phase plus a variety of secondary phases. The basic elements are iron, nickel, cobalt, and chromium, as well as lesser amounts of tungsten, molybdenum, tantalum, niobium, titanium and aluminum. Chromium is the basic element for hot corrosion resistance, and is present in significant amounts in all super-alloys: however, as shown Fig. 5.6 there is a trade-off between chromium-related corrosion resistance and temperature capability. The potential of high-strength, low-chromium alloys can be greatly enhanced by oxidation-resistant coatings, although reliability and expected life of such coatings can constitute a major concern. Recent major advances in superalloy technology have been the introduction of directional and single-crystal solidification – whereby mechanical properties are greatly improved by eliminating grain boundaries – and Powder Metallurgy – which gives higher property uniformity and manufacturing flexibility.

	1950	1970
Aluminum alloys	24	6
Composite materials	-	4
Nickel super-alloys	10	28
Steels	66	40
Titanium alloys	-	22

Table 5.1 Percent weight material usage in jet engines (from Meetham, 1981).

The three basic issues to be remarked about the choice of gas turbine materials are that:

- In the past 40 years, material temperature capability has steadily improved, but not as fast as cooling technology.
- Blade operating temperatures are the result of a very complex design process which is much beyond the scope of a thermodynamic analysis.
- There is a trade-off between operating temperature and life.

5.1.3.1 Requirements

Given the variety of engine components and their operating conditions, the requirements to be met by materials vary on a very broad spectrum. A basic factor is the interaction with the operating environment: since there is generally a trade-off between high-temperature strength and hot corrosion resistance (Fig. 5.6), mechanical properties alone are insufficient to identify the potential of a superalloy. Besides tensile strength and corrosion/oxidation resistance, other properties playing a critical role are:

- Creep/stress rupture resistance. In most instances the relationship between stress, temperature and life can be expressed in terms of the Larson-Miller parameter $P=T\cdot(C+\log_{10}t)$, where T is the temperature (Kelvin), t the time (hours) for creep/stress rupture and C a constant depending on the material (Larson and Miller, 1952). Experiments indicate that P is a reasonably well defined, decreasing function of stress, with the typical behaviour depicted in Fig. 5.7. In their original paper Larson and Miller proposed $C=20$, a value which gives good accuracy for a very wide variety of materials. This implies that, for the same stress, increasing T by 4-5% decreases life by one order of magnitude.
- Fatigue strength. Its importance can be appreciated when considering that, as quoted by Bradley (1988, p. 61), about 90% of all engineering structures fail because of fatigue.
- Ease and cost of manufacture. Fewer processing steps and lower cost are the main reasons for the remarkable increase in castings and powders usage shown in Tab. 5.2.

	1980	1984	1989
Sheet	7.0	6.0	3.5
Forging	45.3	43.1	21.4
Ring	17.2	16.7	8.2
Bar	10.3	11.8	12.2
Casting	19.0	20.2	43.6
Powder	1.2	2.2	11.0

Table 5.2 Evolution of percent weight superalloy usage in jet engines (Gorham International Studies, 1989).

The most arduous requirements are almost always faced by rotor blades, which are subject to high temperature, high stress, rapid temperature transients and highly oxidizing atmospheres. For stationary applications, state-of-the-art operating temperatures are in the range 750-850°C (Grünling, 1979; Erbes, 1990; Sabella, 1990; a slightly higher range can be drawn from the upper diagram in Fig. 5.2, taken from Meetham, 1986). Aircraft and military engine components operate in temperature ranges substantially higher: about 50-100°C in civil applications, 150°C and even more in military engines; on the other hand, component life is decreased by at least an order of magnitude.

The critical temperature-stress condition is generally encounterd around midspan because the root, although more stressed, is generally cooler, while at the tip centrifugal stresses go to zero*. However, it must be emphasized that stress-temperature is only one of the trade-offs to be considered: Fig. 5.8 shows relevant criteria for rotor blades of military jet engines. First stage vanes peak temperatures can reach 900°C, although stresses (predominantly bending) are about 50% lower than in rotors (Grünling, 1979). Combustion liner walls experience peak temperatures of 1000°C and mean temperatures around 800°C

* The centrifugal tensile stress at the root of a constant-cross-section blade is $2\cdot\rho_b\cdot u_m^2\cdot(H/D_m)$. For ρ_b=8900 kg/m^3 (Nickel density), u_m=400 m/s and H/D_m=0.10, this gives a value of about 285 MPa. From hub to tip, centrifugal stresses decrease parabolically to zero, so at mid-span they are likely to be in the range 50-90 MPa. Bending and shear stresses depend on blade aerodynamic loads. According to Grünling (1979), cooled stage vanes bending stresses are in the range 100-200 Mpa.

(Meetham, 1981). High mechanical and thermal stresses are endured by disks, where however the highest stresses occur in the region at the lowest temperature (the bore). Fig. 5.9 depicts the operating ranges of heavy-duty turbine blades reported by Grünling (1979): due to continuing metallurgical progress, the situation in the figure is now probably outdated.

5.1.3.2 Difficulty of appraising operating temperatures

Translating the data in Figs. 5.1, 5.2 and 5.6–5.9 to calculations of gas turbine cycles is extremely difficult because in order to quantify the maximum allowable operating temperature it is necessary to know:

a) Stress tensor under normal operating conditions.
b) Larson-Miller parameter.
c) Variation of the Larson-Miller parameter with the stress tensor.
d) Influence of corrosion.
e) Influence of fatigue.
f) Influence of non-uniform temperature distributions.
g) Influence of thermal cycling.
h) Off-design temperature and stress distributions.

Since each one of these items can be the responsible for temperature limitations, determining the operating temperature is very involved.

5.1.3.3 Implications for cycle analyses

The brief notes above make clear that the choice of materials and their operating temperature is extremely complex and it is much beyond the purpose of a thermodynamic analysis. For civil applications, the choice is ultimately based on economic, reliability and durability considerations. The calibration performed in Ch. 7 is based on:

- For "average" engines, maximum nozzle and cooled turbine temperatures of 800°C and 770°C, respectively.

- For state-of-the-art engines, maximum nozzle and cooled turbine temperatures of 830°C and 800°C.

Since these values have the meaning of average surface temperatures, and since temperature nonuniformities can be higher than 100°C, these assumptions imply that peak metal temperatures can be as high as 850-880°C.

5.2 Convection cooling

Convection cooling is modeled by assuming that the turbine portion spanned at each calculation step (Fig. 3.5) behaves like a heat exchanger subject to the heat flux:

$$\dot{q} = h_g \cdot (T^*_{gr} - T_{bg}) \qquad (5.1)$$

where T^*_{gr} is the gas recovery temperature corrected by the pattern factor (see Par. 5.2.2.1). At each expansion step (Fig. 3.3), h_g and T^*_{gr} are assumed constant, while the external (gas-side) blade temperature T_{bg} varies according to the coolant temperature inside the blade (and the shroud). The dependence of T_{bg} on coolant flow couples the gas-side and coolant-side heat transfer, thus requiring a simultaneous solution of the equations for both sides of the blade. The gas conditions (T, P, composition) used to calculate the cooling flow to be injected at each step are the ones corresponding to Point 2i of Fig. 3.3 (end of step-wise expansion).

The next three paragraphs discuss the evaluation of the quantities appearing in Eq.(5.1), while Pars. 5.2.4 to 5.2.6 show how to calculate the coolant flow per step (Δm_{clb}) and the corresponding coolant-side pressure loss. Aside from modifications of the geometrical arrangement (number of coolant channels, their diameter, number of passes), improvements in convection cooling can be achieved by three means:

1) Enhance coolant-side heat transfer
2) Reduce blade wall thickness
3) Apply Thermal Barrier Coatings (TBC) onto the external blade surface

The implications of these options are addressed in Pars. 5.2.4.4, 5.2.4.7 and 5.2.7. Finally, Par. 5.2.8 presents results obtained with the same subroutine used by program GS (see Ch. 9) to calculate the turbine expansion.

5.2.1 Gas-side heat transfer coefficient

Although h_g undergoes strong spanwise and chordwise variations (Fig. 5.10), determining its local variations is much beyond the scope of our analysis. It appears more appropriate to resort to correlations giving the average St_g as a function of Re_g. Fig. 5.11a reports a summary of the correlations developed by various investigators for the cascade mean Nusselt number (Nu_m) vs. the Reynolds number at the cascade exit (Re_e). The shaded area comprising these correlations and represented in the figure corresponds to:

$$Nu_m = K \cdot Re_e^{0.63} \qquad 0.135 \le K \le 0.285 \qquad (5.2a)$$

Pr does not appear because all the lines in Fig. 5.11a are based on tests performed with air. Assuming that the Prandtl number dependence is the same as for a flat plate* and that Pr_a=0.7 gives:

$$Nu_m = 1.126 \cdot K \cdot Re_e^{0.63} \cdot Pr_g^{1/3} \qquad (5.2b)$$

which can also be written as:

$$St_{me} = 1.126 \cdot K \cdot Re_e^{-0.37} \cdot Pr_g^{-2/3} \qquad (5.3)$$

where $St_{me}=h_g/(\rho_g \cdot c_{p,g} \cdot v_{ge})$ is the mean Stanton number referenced to the cascade exit velocity v_{ge}. Recasting Eq.(5.3) in terms of St_g and Re_g by

* Although it requires experimental verification, this is a fairly common assumption in many heat transfer studies.

noting that $(U_g/v_{ge}) = \sin\alpha_{ge}$ (where α_{ge} is the angle formed by the cascade exit velocity with the tangential direction, see Fig.2.10a):

$$St_g = (1.126/\sin^{0.63}\alpha_{ge}) \cdot K \cdot Re_g^{-0.37} \cdot Pr_g^{-2/3} \tag{5.4}$$

α_{ge} is typically in the range 20-45°. Assuming an average value of 30° gives:

$$St_g = 1.743 \cdot K \cdot Re_g^{-0.37} \cdot Pr_g^{-2/3} \tag{5.5a}$$

For $Pr_g = 0.7$ this equation gives the shaded area depicted in Fig. 5.11b. Considering that:

- typical HP turbine values of Re_g are in the range $0.2\text{-}1.5 \cdot 10^6$;
- both Louis, Hiraoka and El-Masri (1983) and El-Masri (1986a) assumed St_g=constant=0.005 (independent of Re_g);
- Measurements performed by Dunn (1985) give for St_g referenced to the stage inlet velocity the range 0.004-0.010;
- The high turbulence encountered in actual turbines should enhance gas-side heat transfer (Louis, 1977)

it was decided to use for K a value close to the upper bound of its range of variation, i.e. <u>K=0.258</u>. Consequently:

$$St_g = 0.45 \cdot Re_g^{-0.37} \cdot Pr_g^{-2/3} \tag{5.5b}$$

which for $Re_g = 0.2-2 \cdot 10^6$ gives St_g=0.0026-0.0062. The derivation of Eq.(5.5b) makes clear that the coefficient 0.45 is rather uncertain, and that its more precise definition definitely deserves further work.

For the HP stages of modern gas turbines, the quantities appearing in St_g are typically within the following ranges:

$\rho_g \cdot U_g \approx 500-1200$ kg/m²-s (corresponds to $\rho_g \approx 3\text{-}6$ kg/m³, $U_g \approx 150\text{-}250$ m/s)

$c_{p,g} \approx 1.2\text{-}1.3$ kJ/kg-K

Considering that higher $\rho_g \cdot U_g$ (i.e. high Re_g) correspond to lower St_g, Eq.(5.5b) suggests that $h_g = St_g \cdot c_{p,g} \cdot \rho_g \cdot U_g \approx$ 3-5 kW/m²-K, a range confirmed by many experimental and theoretical investigations: see for example Figs. 5.10 and 5.12.

5.2.2 Gas recovery temperature

An accurate evaluation of T_{gr}, accounting for the effects of blade curvature and pressure gradients, would require the solution of the boundary-layer equations and a detailed specification of blade geometry*; since this is beyond the scope of the present analysis, T_{gr} is estimated by (Holman, 1986, p. 254):

$$(T_{gr}-T_{g,st})/(\tilde{T}_{g,tot}-T_{g,st}) = Pr_g^{1/3} \tag{5.6}$$

which applies to turbulent flow (Prandtl number exponent would be 1/2 for laminar flow) and where $\tilde{T}_{g,tot}$ represents the average $T_{g,tot}$ of stationary and rotating cascades. Due to discontinuities of the velocity relative to the blade, in an actual engine $T_{g,tot}$ varies discontinuously as illustrated in Fig. 5.13; in the cooled turbine section such discontinuities are "smoothed" by using in Eq. (5.6):

$$\tilde{T}_{g,tot} = T_{g,st} + [(T_{g,tot}-T_{g,st})_{nz}+(T_{g,tot}-T_{g,st})_{ct}]/2 \tag{5.7}$$

where $T_{g,st}$ is the static temperature before mixing (point 2i of Fig. 3.3); $(T_{g,tot}-T_{g,st})_{nz}$ is the static-to-total ΔT corresponding to the

---

* At low-Mach numbers ($M < 0.2$-0.3) the difference between $T_{g,st}$, $T_{g,tot}$ and T_{gr} is negligible. However, at higher speeds the conversion of kinetic into thermal energy taking place within the boundary layer causes significant temperature increases. If the gas deceleration were adiabatic, T_{gr} would equal $T_{g,tot}$; however, such temperature can never be reached because the temperature gradient within the boundary layer generates a heat flux from the boundary layer itself toward the mainstream flow.

velocity $v_{g,in}$ at the first nozzle exit; $(T_{g,tot}-T_{g,st})_{ct}$ is the static-to-total ΔT corresponding to velocity $v_{g,ct}$ (see Figs. 3.3 and 3.4). Notice that the temperature used in nozzle is the actual $T_{g,tot}$, and that in the cooled turbine $(T_{g,tot}-T_{g,st})$ is constant. This procedure produces for $T_{g,tot}$ the profile shown in Fig. 5.13; the line indicated as "Model $T_{g,st}$" is the outcome of the step-by-step process portrayed in Fig. 3.3.

5.2.2.1 Pattern factor

Due to incomplete mixing, the temperature of the hot gases exiting the combustor is far from being uniform. The difference between peak and average gas temperatures can be accounted for by a pattern factor defined as (Lefebvre, 1983, p. 142; El-Masri, 1988):

$$\lambda = (T_{g,peak}-T_{g,avg})/\Delta T_{cmb} \tag{5.8}$$

where ΔT_{cmb} is the combustor temperature rise based on the hypothesis of complete mixing. λ depends on the combustor design (it is generally lower for annular combustors) and, due to mixing inside the turbine, it decreases rapidly after the nozzle. In order to insure an adequate safety margin, the design of the cooling system is likely to be based on the peak recovery temperature T^*_{gr} rather than its average:

$$T^*_{gr} = T_{gr} + \lambda\cdot\Delta T_{cmb} \tag{5.9}$$

where T_{gr} is given by Eq.(5.6) and, similarly to El-Masri (1988), λ is set to:

$\lambda = 0.10$ in the first nozzle
$\lambda = 0.03$ in the cooled turbine

All calculations of Ch. 7 and 10 have been performed by substituting T^*_{gr} for T_{gr} (and $\tau^*_{gr}=T^*_{gr}/T_{bmx}$ for τ_{gr}); in other words, cooling flows are estimated as if the gas temperature were T^*_{gr} rather than T_{gr}. It must be emphasized that – especially for the nozzle where λ=0.10 – this assumption has a rather important effect on cooling flow (see also sensitivity analysis of Par. 7.4).

5.2.3 Blade temperature

The gas-side blade temperature is a very complex function of geometry and flow conditions. To reduce thermal stresses it would be desirable to maintain constant T_{bg} over the whole blade surface; however, this can never be achieved because:

- There are always very strong chordwise variations of h_g. The typical behaviour depicted in Fig. 5.10 shows the much higher values obtained at the leading edge and at the transition from laminar to turbulent boundary layer.
- In correspondence of the coolant channels inlet, where the coolant is at its lowest temperature, T_{bg} is inevitably lower than at the channels outlet. This behavior is confirmed by Figs. 5.14, 5.15, and 5.16, showing that in the region close to the coolant entrance (blade hub in Figs. 5.14 and 5.15, vane tip in Fig. 5.16) T_{bg} can be 100-150°C lower than at the coolant exit.

A detailed description of the temperature field at the blade surface can be obtained only through elaborate 2-D or 3-D computations. On the other hand, while assuming that at each calculation step T_{gr} and h_g are constant appears reasonable, assuming that T_{bg} is also constant would completely uncouple gas-side and coolant-side heat transfer, concealing the fact that achieving $T_{bg} \leq T_{bmax}$ depends on both internal and external heat transfer. The situation is illustrated in Fig. 5.17: although the blade geometry is much more complex than the single tube considered in the figure, the behaviour of the wall temperature is similar. For a given geometry, the maximum wall temperature reached at the coolant exit will depend on m_{clb}, T_{gr} and $T_{cl,in}$, h_g and h_{cl}, where h_{cl} is a function of m_{clb}. I will deal with the variations of T_{bg} by proceeding as follows:

1) Stipulate the cooling channels geometry.
2) Assume that along the cooling channel T_{bg} is variable.
3) Calculate the value of m_{clb} giving $T_{bg}=T_{bmx}$ at the end of the cooling channel.
4) Calculate the coolant-side pressure drop ΔP_{cl} required by m_{clb}.

The limit on T_{bg} should be verified where the stress-temperature relation is most critical, which for rotor blades typically occurs at mid-span. Assumption 3) guarantees that $T_{bg} \leq T_{bmx}$ everywhere, and is therefore conservative. If ΔP_{cl} exceeds the maximum allowed value, then there is no solution, because if we reduced m_{clb} in order to meet the constraint on ΔP_{cl} we would increase ΔT_{cl} and therefore the maximum T_{bg}.

5.2.4 The blade as a heat exchanger

I will now show that, aside from the gas and coolant conditions, the cooling flow required to achieve $T_{bg} \leq T_{bmx}$ depends on a single parameter representative of convection cooling technology. This is accomplished by assuming that the blade behaves like a crossflow heat exchanger constituted of a tube bundle, with the thermal capacity of the hot fluid much larger than the one of the cold fluid (Fig. 5.18). The schematization is essentially an extension of the one presented by Ainley (1957), who however did not consider: (i) heat resistance of blade wall; (ii) multi-pass cooling channels; (iii) coolant-side heat transfer augmentation. On the other hand, unlike Ainley I will not calculate the spanwise temperature distribution.

5.2.4.1 Assumptions

The parallel between blades and heat exchangers is established by means of five assumptions:

1) Within each blade there are n_{ch} cooling channels with hydraulic diameter d, shape factor ψ_d, each consisting of n_p passes. $d=(4\cdot A)/(\text{periphery})$ and $\psi_d=(\text{periphery})/(\pi\cdot d)$, thus giving $A=\psi_d\cdot\pi\cdot d^2/4$. $\psi_d=1$ for circular channels, greater for all other shapes. Each pass goes from hub to tip and has a length equal to the blade height H. The cross-section of each blade will have $n_{ch}\cdot n_p$ "holes" (Fig. 5.18).

2) The total cross-section of the "holes" inside the blade is a constant fraction of the chord squared, i.e.:

$$n_{ch}\cdot n_p\cdot(\psi_d\cdot\pi\cdot d^2/4) = \alpha_h\cdot c^2 \tag{5.10}$$

where α_h is a constant. Since the average blade thickness* is typically around $[0.10\text{-}0.15]\cdot c$, a reasonable range for α_h will be 0.04-0.10. This assumption implies that there can be either few large or many small cooling channels.

3) Due to interference among adjacent cooling channels, the "effective" heat transfer area of each channel is reduced by a factor ψ_i. In practice, interference will be different for each channel, but its proper evaluation would require a full 3-D analysis. ψ_i is somewhat similar to the fin efficiency defined for extended-surface heat exchangers: both parameters testify to the impossibility of effectively utilizing the whole heat transfer surface.

4) The ratio between the blades+shrouds coolant flow ($\tilde{m}_{clb}$) and the coolant flow for the blades equals the ratio a_t between the area wet by the gas and the blade surface. This is like saying that cooling the blades and the shrouds is totally equivalent and that blade and shroud cooling flows follow separate, equivalent paths. $\tilde{m}_{clb}$ is calculated based only on what takes place into the blades, disregarding the shrouds. Notice that a_t (see Eq. A.1) is rarely larger than 1.3-1.4: thus, the shroud surface (and cooling flow) is always much smaller than the one of the blade.

5) The ratio between the coolant flow Δm_{clb} of the portion spanned at each step (Fig. 3.5) and the flow $\tilde{m}_{clb}$ for the whole cascade equals the ratio between the length of such portion and the blade chord, i.e.:

$$\Delta m_{clb}/\tilde{m}_{clb} = \Delta c/c \tag{5.11}$$

This is like saying that the coolant flow is uniformly distributed along the blade chord.

---

* By average blade thickness (denoted by t_b) I mean here the ratio between the blade cross-section and the blade chord.

Assumptions 2) and 3) allow calculating the ratio a_c between the effective heat transfer area of the cooling channels and the blade surface:

$$a_c = \psi_i \cdot (n_{ch} \cdot n_p \cdot \psi_d \cdot \pi \cdot d \cdot H)/(\Phi \cdot c \cdot H) = \psi_i \cdot (4 \cdot \alpha_h/\Phi) \cdot (c/d) \qquad (5.12)$$

where Φ is the ratio (blade periphery)/c. Before calculating the coolant flow (Par. 5.2.5), let's first express Re_{cl} and St_{cl} as functions of $\bar{m}_{clb}$.

5.2.4.2 Coolant Reynolds number

Denoting with z the number of blades and recalling Eq.(5.10), the flow within one blade can be expressed as:

$$\bar{m}_{clb}/(a_t \cdot z) = n_{ch} \cdot \rho_{cl} \cdot U_{cl} \cdot \psi_d \cdot \pi \cdot d^2/4 = \rho_{cl} \cdot U_{cl} \cdot \alpha_h \cdot c^2/n_p \qquad (5.13)$$

and after observing that $z \cdot c = \pi \cdot \sigma \cdot D_m$:

$$\rho_{cl} \cdot U_{cl} = [1/(\pi \cdot a_t \cdot \sigma)] \cdot (n_p/\alpha_h) \cdot \bar{m}_{clb}/(c \cdot D_m) \qquad (5.14)$$

$$Re_{cl} = \rho_{cl} \cdot U_{cl} \cdot d/\mu_{cl} = [1/(\pi \cdot a_t \cdot \sigma)] \cdot (n_p/\alpha_h) \cdot (d/c) \cdot [\bar{m}_{clb}/(D_m \cdot \mu_{cl})] \qquad (5.15)$$

It is now convenient to introduce m_g and to rearrange the last term of Eq.(5.15). Recalling that the gas cross-sectional area A_g equals $\pi \cdot \psi_g \cdot H \cdot D_m$ (see Eq. A.1):

$$\begin{aligned} \bar{m}_{clb}/(D_m \cdot \mu_{cl}) &= [m_g/(D_m \cdot \mu_g)] \cdot (\mu_g/\mu_{cl}) \cdot (\bar{m}_{clb}/m_g) \\ &= \pi \cdot \psi_g \cdot (H/c) \cdot Re_g \cdot (\mu_g/\mu_{cl}) \cdot (\bar{m}_{clb}/m_g) \qquad (5.16) \end{aligned}$$

which gives:

$$Re_{cl} = [\psi_g \cdot (H/c)/(a_t \cdot \sigma)] \cdot [Re_g \cdot (\mu_g/\mu_{cl})] \cdot [(n_p/\alpha_h)/(c/d)] \cdot (\bar{m}_{clb}/m_g) \qquad (5.17)$$

The three terms within square brackets express the influence of stage geometry, flow conditions and cooling channels geometry, respectively. Before proceeding further, let's determine whether the coolant flow is likely to be laminar or turbulent. Typical values of the parameters appearing in Eq.(5.17) are:

- $\psi_g \simeq 0.85$; $H/c = 0.7\text{-}2$ (lower in HP section); $a_t = 1.1\text{-}1.3$ (higher in HP section); $\sigma = 1\text{-}1.8$ (lower in HP section). These values give for the first term in Eq.(5.17) the range 0.5-0.9, with lower values corresponding to the HP section.

- Based on elementary kinetic theory considerations viscosity varies approximately with $T^{0.5}$. Since for air cooling the gas and coolant composition are similar, in this case $\mu_g/\mu_{cl} \simeq (T_g/T_{cl})^{0.5} \simeq 1.1\text{-}1.5$ At 1 bar and 400°C the viscosity of air is $33 \cdot 10^{-6}$ Pa·s, while for steam it is $24.5 \cdot 10^{-6}$ Pa·s. Assuming that the ratio of the two viscosities does not vary with T, we can say that for steam cooling $\mu_g/\mu_{cl} \simeq 1.5\text{-}2$.
  Finally, since Re_g is typically in the range $0.2\text{-}2 \cdot 10^6$, the second square-bracketed term of Eq.(5.17) will be $\simeq 0.2\text{-}4 \cdot 10^6$. The lowest values correspond to low-pressure ratio, low-power output turbines (low ρ_g and small c).

- $n_p = 1\text{-}3$; $\alpha_h = 0.04\text{-}0.10$; $c/d = 5\text{-}40$. Since cooling is most critical in the HP section, there we should expect the higher values of all these parameters. Therefore a reasonable range for $[(n_p/\alpha_h)/(c/d)]$ is $0.75\text{-}5$.

These estimates show that a lower bound for Re_{cl} is $\simeq 75 \cdot 10^3 \cdot (\bar{m}_{clb}/m_g)$. The lowest values are likely to be reached in the HP section, where although $(\bar{m}_{clb}/m_g)$ is large, the first and third terms of Eq.(5.17) are small. But in the HP section $\bar{m}_{clb}/m_g$ is generally a few percent, so that $Re_{cl} > \simeq 10{,}000$ and the occurence of laminar flow is very unlikely. In the following I will always use correlations for turbulent flow.

5.2.4.3 Coolant Stanton number

The Stanton number is estimated by the well-known Colburn equation:

$$St_{cl} = E_h \cdot 0.023 \cdot Re_{cl}^{-0.2} \cdot Pr_{cl}^{-2/3} \qquad (5.18)$$

where the enhancement factor E_h is introduced to account for the presence of turbolators and fins for heat transfer enhancement. Defined as the ratio of the heat transfer coefficient with and without heat transfer augmentation – referred to the smooth tube surface* – E_h will be a function of position, Re, geometry and, for rotor blades, of the rotational speed (Morris and Harasgama, 1985). However, for the sake of simplicity I will assume that it is constant; the range of its typical values is discussed in 5.2.4.4.

In view of further formulations, it is useful to substitute Eq.(5.17) into (5.18):

$$St_{cl} = [0.023\cdot/(C_{g1}^{0.2}\cdot C_{f1})]\cdot\{E_h\cdot[(c/d)\cdot\alpha_h/n_p]^{0.2}\}\cdot(m_g/\bar{m}_{clb})^{0.2} \qquad (5.19)$$

where C_{g1} depends on the stage geometry and C_{f1} depends on the gas and coolant flow characteristics:

$$C_{g1} = \psi_g\cdot(H/c)/(a_t\cdot\sigma) \qquad (5.20)$$

$$C_{f1} = Pr_{cl}^{2/3}\cdot[Re_g\cdot(\mu_g/\mu_{cl})]^{0.2} \qquad (5.21)$$

5.2.4.4 Heat transfer enhancement

Heat transfer enhancement is achieved either by inserting pin fins into the cooling channel (typically in the trailing-edge region), or by roughening the channel walls. Indicative experimental values of E_h are:

- ≃ 3.5-3.9 for the staggered pin fin array depicted in Fig. 5.19 (Metzger, Berry and Bronson, 1982)

---

* By referring to the surface of the smooth tube, E_h embodies the effects of increased heat transfer areas. As discussed further, E_h also includes the effects of increased heat transfer in the 180° bends of multi-pass channels.

- ≃ 3-3.3 for the in-line array shown in Fig. 5.20 (Arora and Abdel Messeh, 1985)
- ≃ 1.5-2.3 for the square duct with two opposite rib-roughened walls depicted in Fig. 5.21 (Han, 1984; Han, Park and Lei, 1984 and 1985)

El-Masri and Pourkey (1986) quote for E_h the range 2-6, although the results mentioned above suggest that obtaining values above 5 appears extremely difficult*.

5.2.4.5 Influence of 180° bends

Aside from the presence of heat transfer augmentation devices, in the 180° bends of a multi-pass channel heat transfer increases due to increased turbulence. Although this phenomenon is unrelated to heat transfer enhancement devices, I will include its effects in E_h: its proper definition is therefore the "ratio between the average h_{cl} of the actual cooling channel and the one of a smooth straight channel having the same cross-section, same length and same mass flow rate". According to this definition, for a multi-pass channel $E_h>1$ even for a smooth tube. Kakaç, Shah and Aung (1987, p. 10-13) report the following correlation for the local Nusselt number in a 180° bend of a circular tube:

$$Nu_x = 0.0285 \cdot Re_{cl}^{0.81} \cdot Pr^{0.4} \cdot (x/D_{bn})^{0.046} \cdot (D_{bn}/d)^{-0.133} \cdot (\mu_{bulk}/\mu_{wall})^{0.14} \quad (5.22)$$

where x is the axial distance along the bend axis measured from the bend inlet and D_{bn} is the bend diameter. The correlation is valid for

* Going toward high values of E_h will require a substantial augmentation of the effective heat transfer area of the coolant channels. However, at the low diameters required to have an efficient utilization of the coolant flow (no more than a few millimeters), such area augmentation poses formidable manufacturing problems.

$4.8 < D_{bn}/d < 26$ and $10^4 \le Re_{cl} \le 3\cdot 10^4$. Neglecting viscosity variations and integrating over the whole bend*:

$$Nu_m = [0.0437/(D_{bn}/d)^{0.133}]\cdot Re_{cl}^{0.81}\cdot Pr^{0.4} \qquad (5.23)$$

Due to space limitations, the bends of multi-pass channels are likely to have D_{bn}/d around 1.2-1.5. Extrapolating (5.22) to such range gives for $D_{bn}/d = 1.5$ an average Nu about 80% higher than the one of a straight tube. The bend will also cause variations of the heat transfer coefficient in the downstream pipe; however, according to other correlations given by Kakaç, Shah and Aung (1987, p. 10-15) the departure from undisturbed straight tube behaviour is very small.

The impact on E_h will depend on the ratio between the bend surface and the total channel surface, which is approximately given by:

$$[(n_p-1)\cdot\pi\cdot D_{bn}/2]/[n_p\cdot H] = (\pi/2)\cdot(1-1/n_p)\cdot(c/H)\cdot(D_{bn}/d)/(c/d)$$

Since $(c/H)\simeq 1$, for $(D_{bn}/d)=1.5$, $n_p=2\text{-}3$, $(c/d)=10\text{-}40$ this ratio ranges 0.03-0.15; this means that an 80% higher bend heat transfer translates to $E_h \simeq 1.02\text{-}1.12$.

For the non-circular cross-sections often adopted in gas turbines this estimate must be revised. Experimental data obtained from Metzger and Sahm (1986) for rectangular ducts (Fig. 5.22) indicate that the increase of Nu_{cl} is analogous to the one estimated above (about 30-90%). Therefore, it can be concluded that except for very low c/d (which are unlikely, because they yield poor heat transfer performances) the presence of 180° turns increases the overall coolant-side heat transfer by no more than 5-10%. As shown in Par. 5.2.6.2, the conclusion is dramatically different for pressure drops.

---

* Nu_m is simply calculated as $(2/\pi)\cdot\int_0^{\pi/2} Nu_x\cdot d(x/D_{bn})$.

5.2.4.6 Heat transfer effectiveness

Since at each step $\Delta T_g \ll \Delta T_{cl}$, the heat transfer effectiveness of one cooling channel can be calculated by assuming that the hot fluid thermal capacity is infinite. Following Kays and London (1964):

$$\varepsilon = 1 - \exp(-NTU) \tag{5.24}$$

where the effectiveness ε and the number of thermal units NTU are given by:

$$\varepsilon = (T_{cl,out} - T_{cl,in})/(T_{gr} - T_{cl,in}) \tag{5.25a}$$

$$NTU = U_h \cdot S/C_{cl} \tag{5.25b}$$

Since the external blade temperature can never exceed T_{bmx}, it is useful to introduce an effectiveness ε_1 defined by:

$$\varepsilon_1 = (T_{cl,out} - T_{cl,in})/(T_{bmx} - T_{cl,in}) = \varepsilon \cdot (T_{gr} - T_{cl,in})/(T_{bmx} - T_{cl,in}) \tag{5.26}$$

The above definition compares the actual ΔT_{cl} not to the maximum "thermodynamic" ΔT which would be realized with infinite heat transfer area, but to the maximum "technological" ΔT allowed by material limitations. For this reason I will present results in terms of ε_1 rather than ε.

5.2.4.7 NTU and blade wall Biot number

Observing that the area of each channel that effectively "participates" in heat transfer is*: $\psi_i \cdot n_p \cdot \psi_d \cdot \pi \cdot d \cdot H$:

$$NTU = [a_c \cdot (1/h_g + t_{bw}/k_b) + 1/h_{cl}]^{-1} \cdot (\psi_i \cdot n_p \cdot \psi_d \cdot \pi \cdot d \cdot H)/[\bar{c}_{p,cl} \cdot \tilde{m}_{clb}/(a_t \cdot z \cdot n_{ch})] \tag{5.27}$$

---

* I have assumed that the area of multi-pass channels is simply n_p times the area of one straight channel with length equal to the blade height.

But the mass flow of each channel is $\bar{m}_{clb}/(a_t \cdot z \cdot n_{ch}) = \rho_{cl} \cdot U_{cl} \cdot \psi_d \cdot \pi \cdot d^2/4$ and collecting h_{cl} in the first term:

$$NTU = 4 \cdot St_{cl} \cdot \psi_i \cdot n_p \cdot (c/d) \cdot (H/c)/[1+(a_c \cdot h_{cl}/h_g) \cdot (1+Bi_{bw})] \tag{5.28}$$

where the Biot number:

$$Bi_{bw} = h_g \cdot t_{bw}/k_b$$

accounts for the heat resistance of the blade wall. Based on typical values of 3-5 kW/m^2-K for h_g (HP stages), 1.5-2.5 mm for t_{bw}, 15-20 W/m-K for k_b (Inconel 718, Udimet 700), Bi_{bw} will range $\approx$ 0.3-0.8. These relatively high values reflect the non-trivial heat resistance of the blade wall, and call for a ΔT between the outer and inner blade surface which can be as high as 150°C (see Fig. 5.23).

5.2.4.8 Convection cooling parameter Z

Substituting Eq.(5.19) into (5.28):

$$NTU = 0.092 \cdot [(H/c)/(C_{gl}^{0.2} \cdot C_{fl})] \cdot Z \cdot (m_g/\bar{m}_{clb})^{0.2}/[1+(a_c \cdot h_{cl}/h_g) \cdot (1+Bi_{bw})] \tag{5.29}$$

where the parameter Z summarizes the heat transfer characteristics of the convection cooling technology:

$$Z = \psi_i \cdot \alpha_h^{0.2} \cdot n_p^{0.8} \cdot E_h \cdot (c/d)^{1.2} \tag{5.30}$$

Ainley (1957), who neglects interference and does not consider multi-pass channels and heat transfer enhancement, obtains $Z = \alpha_h^{0.2} \cdot (c/d)^{1.2}$. The definition of Eq.(5.30) embodies all relevant features of convection cooling technology. It is clear that the higher the value of Z, the more sophisticated the cooling system; consequently, cooling flow should always be a monotonic, decreasing function of Z, an expectation confirmed by the results of Pars. 5.2.8 and 5.3.7.

For the large engines likely to be used in central stations the probable range of Z can be estimated considering that:

- c is typically 50-80 mm for aeroderivatives and 100-200 mm for heavy-duties, while in order to reduce the risk of clogging it is very unlikely that d be smaller than 2-3 mm. As a consequence, upper bounds for c/d should be ≈ 40 for aeroderivatives and ≈ 100 for heavy duties. Based on cross-sections shown in company publications, actual engines appear to have c/d≈10-20.
- The smaller the value of d, the more difficult is the realization of heat transfer augmentation inside the cooling channels. Therefore, at the highest (c/d) E_h cannot be much greater than one. Since the bends of multi-pass channels increase the heat transfer coefficient (see 5.2.4.2), $n_p>1$ gives slightly higher E_h.
- The more "holes" inside the blade the lower the interference coefficient ψ_i, because for the channels deep inside the blade it becomes difficult to exchange heat effectively. From Eq.(5.10) the number of holes is:

  $$n_{ch} \cdot n_p = (4/\pi) \cdot \psi_d \cdot \alpha_h \cdot (c/d)^2$$

  showing that at high α_h and (c/d) we should expect lower ψ_i.
- In order to limit pressure losses (see Par. 5.2.6.1) n_p will rarely be greater than 3.

These considerations, together with α_h≈0.04-0.10 already mentioned in 5.2.4.1, give for Z a probable "technological" upper bound of 250, a value which could be obtained, for example, with:

ψ_i = 0.7
α_h = 0.10
n_p = 3
E_h = 2.5
c/d = 45

In actual engines Z is likely to be different for each cascade. To reduce costs, the intermediate-pressure stages, where cooling flow requirements are limited, will probably be designed with Z lower than in the HP stages.

Due to their smaller size, achieving high c/d and therefore superior heat transfer performances should be more difficult for aero-derivative engines. In fact, the implications of adopting small blade chords and its adverse effect on blade cooling has already been quoted by Liess (1969) and Livinghood, Ellerbrock and Kaufman (1971).

5.2.4.9 Ratio of heat resistances

Eq.(5.29) still contains one unknown, the ratio between gas-side and coolant-side heat resistance:

$$a_c \cdot h_{cl}/h_g = a_c \cdot (St_{cl}/St_g) \cdot (\bar{c}_{p,cl}/c_{p,g}) \cdot (\rho_{cl} \cdot U_{cl})/(\rho_g \cdot U_g) \qquad (5.31)$$

From Eqs.(5.5) and (5.19) the ratio of Stanton numbers becomes:

$$St_{cl}/St_g =$$
$$(0.046/C_{g1}{}^{0.2}) \cdot (Re_g{}^{0.37} \cdot Pr_g{}^{2/3}/C_{f1}) \cdot \{E_h \cdot [(c/d) \cdot \alpha_h/n_p]^{0.2}\} \cdot (m_g/\bar{m}_{clb})^{0.2} \qquad (5.32)$$

while recalling Eq.(5.14) and that $A_g = \psi_g \cdot \pi \cdot H \cdot D_m$:

$$(\rho_{cl} \cdot U_{cl})/(\rho_g \cdot U_g) = C_{g1} \cdot (n_p/\alpha_h) \cdot (\bar{m}_{clb}/m_g) \qquad (5.33)$$

Putting together Eqs.(5.12) and (5.31 to 5.33) gives:

$$a_c \cdot h_{cl}/h_g = 0.184 \cdot (C_{g1}{}^{0.8}/\Phi) \cdot C_{f2} \cdot Z \cdot (\bar{m}_{clb}/m_g)^{0.8} \qquad (5.34)$$

where C_{f2} depends on the characteristics of the fluid:

$$C_{f2} = Re_g{}^{0.17} \cdot (\bar{c}_{p,cl}/c_{p,g}) \cdot (\mu_{cl}/\mu_g)^{0.2} \cdot (Pr_g/Pr_{cl})^{2/3} \qquad (5.35)$$

Notice that while $\bar{c}_{p,cl}$ is averaged between $T_{cl,in}$ and $T_{cl,out}$, $c_{p,g}$ is evaluated at T_g, because ΔT_g of each calculation step is very small.

5.2.4.10 Blade temperature

The equations expressing the heat flux balance across the blade wall are*:

$$(h_g/a_c)\cdot(T_{gr}-T_{bg}) = [k_b/(a_c\cdot t_{bw})]\cdot(T_{bg}-T_{bcl}) = h_{cl}\cdot(T_{bcl}-T_{cl}) \qquad (5.36)$$

Dividing by h_{cl} and non-dimensionalizing the temperatures by T_{bmx}:

$$[h_g/(a_c\cdot h_{cl})]\cdot(\tau_{gr}-\tau_{bg}) = [h_g/(a_c\cdot h_{cl})]\cdot(1/Bi_{bw})\cdot(\tau_{bg}-\tau_{bcl}) = (\tau_{bcl}-\tau_{cl})$$

and solving for τ_{bg}:

$$\tau_{bg} = \{\tau_{cl}+[Bi_{bw}+h_g/(a_c\cdot h_{cl})]\cdot\tau_{gr}\}/[1+Bi_{bw}+h_g/(a_c\cdot h_{cl})] \qquad (5.37)$$

Together with Eqs.(5.24), (5.29) and (5.34), this equation allows determining τ_{bg}. For a "pure" counter-current situation with no heat conduction this could be done locally to give the temperature distribution along the channel. However, in our case all quantitites given by Eqs.(5.24), (5.29) and (5.34) – i.e. ε, NTU, ratio of heat resistances – are properly defined only for the whole blade; thus, using those equations to determine the terms appearing in Eq.(5.37) is legitimate only for the final temperature $T_{bg,out}$ at the end of the cooling channel. But from Eq.(5.25a):

$$\tau_{cl,out} = (1-\varepsilon)\cdot\tau_{cl,in}+\varepsilon\cdot\tau_{gr}$$

which gives for $\tau_{bg,out}$:

$$\tau_{bg,out} = \{(1-\varepsilon)\cdot\tau_{cl,in}+[\varepsilon+Bi_{bw}+h_g/(a_c\cdot h_{cl})]\cdot\tau_{gr}\}/[1+Bi_{bw}+h_g/(a_c\cdot h_{cl})] \qquad (5.38)$$

* As pointed out in 5.2.2.1, in order to include the effects of the pattern factor λ, in the calculations of Chs. 7 and 10 I have substituted T^*_{gr} for T_{gr} and and $\tau^*_{gr}=T^*_{gr}/T_{bmx}$ for τ_{gr}.

5.2.5 Calculation of coolant flow

Eqs.(5.24), (5.29), (5.34) and (5.38) allow expressing $\tau_{bg,out}$ as a function of:

- Stage geometry (H/c, Φ, C_{g1})
- Fluid and material properties (Re_g, C_{f1}, C_{f2}, Bi_{bw}, τ_{gr}, $\tau_{cl,in}$)
- Cooling technology parameter Z
- Nondimensional cooling flow $\tilde{m}_{clb}/m_g$

Since stage geometry and fluid properties are given*, the convection cooling problem consist of determining – for each value of Z – the cooling flow that gives an acceptable blade temperature distribution. Given that the highest T_{bg} is reached at the end of the cooling channel, we can assure that $T_{bg} \leq T_{bmx}$ by imposing:

$$\tau_{bg,out} = 1$$

This assumption is conservative because, as mentioned in Par. 5.1.3.1, the limit on T_{bg} should be verified where the stress-temperature-fatigue-corrosion conditions are most critical. Notice that since $T_{bg,out}$ is a monotonic decreasing function of $\tilde{m}_{clb}$ (see Par. 5.2.8.1 and Fig. 5.27), the flow giving $\tau_{bg,out}=1$ is the minimum among all those which warrant $T_{bg} \leq T_{bmx}$.

5.2.5.1 Scale effects

The list of paramters affecting $\tau_{bg,out}$ does not include the stage diameter nor any other absolute dimension. Size can influence the

---

* In practice there is always interaction between the design of the stage and the cooling system. For example, cooled stages tend to have lower σ (to reduce heat transfer areas) and higher Δh_{is} (to "bring down" the gas temperature in fewer stages). However, the effects of this interaction on the parameters appearing in our analysis is very small.

solution of the heat transfer problem only through variations of Re_g. However, since the exponents of Re_g in Eqs.(5.21) and (5.35) are small – 0.2 and 0.17, respectively – scale effects will be very small, a situation substantially different from the one encountered in Par. 4.5 for turbomachines.

It is also worth noting that ψ_d has dropped out, signifying that what matters is the coolant channel cross-section (α_h) and not the channel shape.

5.2.5.2 Iterative procedure

The system formed by Eqs.(5.24), (5.29), (5.34) and (5.38) establishes a relationship $f(\tau_{bg,out},\tilde{m}_{clb}/m_g)=0$ which, due to its non-linearity, cannot be solved explicitly for $\tau_{bg,out}$. Therefore, the cooling flow must be found iteratively, adjusting $\tilde{m}_{clb}/m_g$ until $\tau_{bg,out}=1$; given the variations of gas (and possibly coolant) conditions, this iterative procedure must be repeated for each expansion step of Fig. 3.3.

5.2.5.3 Significance of $\tilde{m}_{clb}$

Once $\tilde{m}_{clb}$ is known, the coolant flow Δm_{clb} required by the portion of blade represented in Fig. 3.5 is given by Eq.(5.11):

$$\Delta m_{clb}/\tilde{m}_{clb} = \Delta c/c$$

Since gas conditions change from one step to another, for the same blade row the calculation will give more than one value of $\tilde{m}_{clb}$, none of which will necessarily coincide with $\Sigma(\Delta m_{clb})$. This makes clear that $\tilde{m}_{clb}$ is just a fictitious variable, which would correspond to the cascade cooling flow only if gas conditions were constant along the whole chord.

5.2.6 Pressure Drops

The cooling flow must be verified against pressure drop requirements. For 1-D flow in a constant cross-section channel with friction, heat addition and centrifugal acceleration, the pressure change along an infinitesimal length dx in the outward radial direction is:

$$dP/P = [-\gamma \cdot Ma^2/(1-Ma^2)] \cdot d\dot{Q}/(\dot{m} \cdot c_p \cdot T) - (\gamma \cdot Ma^2/2) \cdot F \cdot 4 \cdot f \cdot dx/d + F \cdot [\omega^2 \cdot D/(2 \cdot R \cdot T)] \cdot dx$$

where $\dot{Q}$ is the thermal power transferred to the fluid, f the friction factor, D/2 the radius of rotation and $F=[1+(\gamma-1) \cdot Ma^2]/(1-Ma^2)$. The first term accounts for heat transfer, the second for friction, the third for centrifugal forces. The last term is present only in rotor blades (pumping effect) and in multi-pass channels it changes sign with the radial direction of the flow. In the following, this term will be dropped, thus obtaining conservative estimates for $\Delta P/P$. Since the coolant Mach number is typically low, $Ma^2 \ll 1$, and after eliminating the centrifugal term:

$$dP/P \simeq -\gamma \cdot Ma^2 \cdot d\dot{Q}/(\dot{m} \cdot c_p \cdot T) - (\gamma \cdot Ma^2/2) \cdot 4 \cdot f \cdot dx/d$$

Observing that in our case:

$$d\dot{Q}/(\dot{m} \cdot c_p \cdot T) = [h_{cl} \cdot \psi_d \cdot \pi \cdot d \cdot dx \cdot (T_{bcl}-T_{cl})]/(c_{p,cl} \cdot \rho_{cl} \cdot U_{cl} \cdot \psi_d \cdot \pi \cdot d^2/4)$$
$$= 4 \cdot St_{cl} \cdot (T_{bcl}/T_{cl}-1) \cdot dx/d$$

the first term can be related to the friction coefficient by means of the Reynolds analogy $St \cdot Pr^{2/3}=f/2$. Substituting into the expression for dP/P, the coolant pressure loss becomes:

$$dP_{cl}/P_{cl} = \gamma_{cl} \cdot Ma_{cl}^2 \cdot [Pr_{cl}^{-2/3} \cdot (T_{bcl}/T_{cl}-1) + E_f] \cdot 2 \cdot f \cdot dx/d \qquad (5.39)$$

where E_f is a multiplier of the ΔP due to friction that accounts for the presence of heat transfer augmentation devices and, for multi-pass channels, the extra-losses caused by curves. Its average value, discussed in the next paragraph, ranges from a minimum of 1 for single-pass, smooth channels to 10-40 and even higher for multi-pass channels with heat transfer enhancement. The term $Pr_{cl}^{-2/3}\cdot(T_{bcl}/T_{cl}-1)$ is due to heat transfer and ranges 0.2-0.6. Neglecting compressibility effects, the integration of Eq.(5.39) gives:

$$\Delta P_{cl}/P_{cl} = \gamma_{cl}\cdot Ma_{cl}^2\cdot E_P\cdot 2\cdot f\cdot n_p\cdot(H/c)\cdot(c/d) \tag{5.40}$$

where the two terms in square brackets of Eq.(5.39) have been lumped into:

$$E_P = \left[Pr_{cl}^{-2/3}\cdot(T_{bcl}/T_{cl}-1) + E_f\right]_{av} \tag{5.41}$$

The subscript 'av' indicates the average over the whole cooling channel. An expression for $Ma_{cl}^2 = U_{cl}^2/a_{cl}^2$ can be found by observing that, according to Eq.(5.16):

$$\begin{aligned}\bar{m}_{clb}/(\rho_{cl}\cdot c\cdot D_m) &= \left[\bar{m}_{clb}/(D_m\cdot\mu_{cl})\right]\cdot(\nu_{cl}/c) = \\ &= \pi\cdot\psi_g\cdot(H/c)\cdot(Re_g\cdot\mu_g/\mu_{cl})\cdot(\nu_{cl}/c)\cdot(\bar{m}_{clb}/m_g)\end{aligned}$$

and then substituting this expression into Eq.(5.14):

$$U_{cl} = C_{g1}\cdot(n_p/\alpha_h)\cdot(Re_g\cdot\mu_g/\mu_{cl})\cdot(\bar{m}_{clb}/m_g)\cdot(\nu_{cl}/c) \tag{5.42}$$

Now inserting into Eq.(5.40) and collecting the non-dimensional groups:

$$\begin{aligned}\Delta P_{cl}/P_{cl} = -2\cdot f\cdot[(H/c)\cdot C_{g1}^2]\cdot[Re_g\cdot\mu_g/\mu_{cl}]^2\cdot(\gamma_{cl}\cdot[(\nu_{cl}/c)/a_{cl}]^2)\cdot \\ [E_P\cdot(n_p^3/\alpha_h^2)\cdot(c/d)]\cdot(\bar{m}_{clb}/m_g)^2\end{aligned}$$

For $2\cdot10^4<Re_{cl}<10^6$ the smooth-tube friction factor can be expressed as*:

$$f = 0.046\cdot Re_{cl}^{-0.2} \qquad (5.43)$$

and using Eq.(5.17) to express Re_{cl} finally gives:

$$\Delta P_{cl}/P_{cl} = 0.092\cdot\left[(H/c)\cdot C_{gl}^{1.8}\right]\cdot\left[Re_g\cdot\mu_g/\mu_{cl}\right]^{1.8}\cdot(\gamma_{cl}\cdot\left[(\nu_{cl}/c)/a_{cl}\right]^2)\cdot Z_P\cdot(\bar{m}_{clb}/m_g)^{1.8} \qquad (5.44)$$

where Z_P summarizes the pressure loss characteristics of the cooling technology:

$$Z_P = \alpha_h^{-0.8}\cdot n_p^{2.8}\cdot E_P\cdot(c/d)^{1.2} = \left[(E_P/E_h)\cdot n_p^2/(\alpha_h\cdot\psi_1)\right]\cdot Z \qquad (5.45)$$

Eq.(5.45) reveals that for the same heat transfer performances (i.e. same Z), a multi-pass geometry yields much higher ΔP_{cl}. Should pressure losses become a binding constraint, single-pass channels with high c/d are preferable to multi-pass channels with lower c/d.

5.2.6.1 Pressure loss augmentation factor

According to Eq.(5.40), E_P is defined as the "ratio between ΔP_{cl} of the actual channel and the one of an incompressible flow through a straight smooth duct with the same cross-section, same length and same mass flow rate"**. E_P is the friction—analog of E_h, and it expresses how much it is necessary to "spend" in terms of pressure loss to increase the heat transfer coefficient by a factor E_h. For incompress-

* For a rough tube the friction factor is independent of the Reynolds number. A constant f would complicate the relationship between Z_P and Z, but wouldn't alter the considerations above. The same holds if Re_{cl} were lower than 20,000: in such case the smooth-tube friction factor is better approximated by $0.079\cdot Re_{cl}^{-0.25}$.

** Being referred to the same cross-section and mass flow rate, E_P embodies the effects of increased velocity due to reduced cross-sectional area.

ible flow $E_P=E_f$ – i.e. ΔP_{cl} is due only to friction. Fig. 5.24 depicts the relationship between E_h and E_f for transverse rib-roughened tubes, showing that there is a "ceiling" to heat transfer increase. Although the value of such ceiling can vary with the heat transfer augmentation technique, the trend is quite general: E_f tends to be larger than E_h, and increasing ΔP "pays off" only up to a certain point. For the straight ducts already quoted when discussing E_h (5.2.4.4), $E_{f,str}$ is very high*:

- $\simeq$ 50 for the staggered pin fins arrays of Fig. 5.19
- $\simeq$ 25 for the in-line pin fins arrays of Fig. 5.20
- $\simeq$ 3-10 for the rib-roughened walls of Fig. 5.21

These very high values signify that pressure losses can pose very significant constraints on the design of the cooling system. The implications for the calculation of cooling flows are discussed at Par. 5.2.6.3.

5.2.6.2 Influence of 180° bends

For multi-pass channels E_f also includes the effect of 180° turns. According to correlations given in Kakaç, Shah and Aung (1987, p. 10-4), the pressure drop across a 180° bend of a circular tube with $Re_{cl}\cdot(D_{bn}/d)^{-2} > 91$, $2 \le (D_{bn}/d) \le 15$ and $2\cdot10^4 \le Re_{cl} \le 4\cdot10^5$ can be expressed as:

$$\Delta P_{bn} = \{0.4338\cdot\left[1+116/(D_{bn}/d)^{4.52}\right]\cdot(D_{bn}/d)^{0.84}\cdot Re_{cl}^{-0.17}\}\cdot(\rho\cdot U^2/2) \qquad (5.46)$$

---

* Besides increased friction, the increase of E_f with pin fins is due to higher velocities caused by reduced cross-sectional areas. If we eliminated such kinetic energy effect, E_f would become $\simeq$ 20 for staggered arrays and $\simeq$ 9 for in-line arrays.

For a straight tube having the same length $\pi \cdot D_{bn}/2$ and friction factor given by Eq.(5.43) the pressure loss is:

$$\Delta P_{str} = 0.289 \cdot (D_{bn}/d) \cdot Re_{cl}^{0.2} \cdot (\rho \cdot U^2/2)$$

thus giving:

$$\Delta P_{bn}/\Delta P_{str} \simeq 1.5 \cdot \left[1+116/(D_{bn}/d)^{4.52}\right] \cdot (D_{bn}/d)^{-0.16} \cdot Re_{cl}^{0.03} \qquad (5.47)$$

Extrapolating Eq.(5.46) to the value $(D_{bn}/d)=1.5$ already considered in 5.2.4.4 gives, for $Re_{cl}=10^4$, a ratio $(\Delta P_{bn}/\Delta P_{str}) \simeq 36$. This can be restated by saying that the bend is equivalent to a straight tube 36 times longer than the actual bend, or that the bend adds $(36-1) \cdot \pi/2 \simeq 55$ tube diameters to the effective tube length. For $(D_{bn}/d)=1.5$, the ratio between total effective tube length and actual length (i.e. E_f of a smooth tube), can therefore be approximated by*:

$$[n_p \cdot H + 55 \cdot d \cdot (n_p - 1)]/(n_p \cdot H) = 1 + 55 \cdot (1 - 1/n_p) \cdot (c/H)/(c/d)$$

Based on correlations for bends with rectangular cross-section again given by Kakaç, Shah and Aung (1987, p. 10-16), the friction augmentation factor of non-circular channels is substantially higher.

In a roughened tube, the pressure drop across the bends is essentially the same as for the bends of a smooth tube because: (i) to reduce manufacturing problems, turbolators are generally placed only along the straight sections; (ii) even if bends were roughened, their ΔP is already so high that its additional increase is small. If the ΔP of the straight sections increases by a factor $E_{f,str}$, the overall incompressible flow ΔP increases approximately by a factor:

---

* Given the very small exponent appearing in Eq.(5.47), variations of Re_{cl} have essentially no effect on $\Delta P_{bn}/\Delta P_{str}$.

$E_{f,str} + 55\cdot(1-1/n_p)\cdot(c/H)/(c/d)$

Recalling that: (i) $E_{f,str}$ ranges 2-50; (ii) c/H is typically around one; (iii) the term due to heat transfer appearing in Eq.(5.41) ranges 0.2-0.6 we can conclude that:

$E_p \simeq (1.2 \text{ to } 1.6) + 55\cdot(1-1/n_p)/(c/d)$ for smooth circular tubes
$E_p \simeq (2 \text{ to } 50) + 55\cdot(1-1/n_p)/(c/d)$ for roughened circular tubes

Finally, considering the values of E_h given in 5.2.4.4, $n_p \leq 3$ and typical $(c/d)=10\text{-}40$, the ratio E_P/E_h is likely to be:

≃ 1.2-1.6 for smooth single-pass channels
≃ 2-12 and even higher for single-pass channels with heat augmentation
≃ 1.5-4 for smooth multi-pass circular channels
≃ 3-13 and even higher for multi-pass channels with heat augmentation

5.2.6.3 Limitations on coolant-side pressure drop

In an actual turbine the value of ΔP_{cl} required by the passage of m_{clb} through the channels of the cooling circuit cannot be arbitrary because:

- There is an upper bound set by the difference between the pressure at the compressor bleed and that of the gas where the coolant is eventually discharged.
- If the cooling channel cross-section is constant, $\Delta P_{cl}/P_{cl}$ cannot be larger than the value producing sonic flow (*frictional/thermal choking*). As illustrated by Shapiro (1953, pp.242-247), this limiting value depends on the nature of the heat transfer process*. Higher pressure drops would require variable-cross-section ducts

* For a flow initially at rest, $\gamma=1.4$ and no heat transfer (Fanno line), the pressure drop giving Ma=1 is about 90%; instead, with heat transfer and no friction (Rayleigh line) Ma=1 is reached with $\Delta P/P \simeq 60\%$. With both friction and heat transfer the value of $\Delta P/P$ giving Ma=1 depends on the laws of heat addition and friction: constant wall temperature, constant heat flux, constant friction factor, etc.

with supersonic flow, a situation very difficult to realize and which would presumably entail very large throttling losses*.

Given the severe penalties imposed by pressure losses on cycle efficiency and that $\Delta P_{cl}/P_{cl} \propto U_{cl}^2$, there are strong incentives toward the adoption of low coolant velocities. On the other hand, the derivation of Par. 5.2.6 shows that U_{cl} – and thus ΔP_{cl} – are fully determined by the thermal problem; if ΔP_{cl} is unacceptably high it means that there is no solution which simultaneously satisfies thermal ($T_{bg} \leq T_{bmax}$) and pressure drop constraints.

In this case the only possibility is to reduce the ratio Z_P (Eq.5.45) by acting on α_h, n_p, E_P or c/d. Accomplishing this reduction implies:

- *Modifying the whole design of the cooling system.*
- Modify Z, which depends on α_h, n_p and c/d. This alters the thermal problem and thus the value of m_{clb} which allows obtaining $T_{bg} \leq T_{bmax}$. Except for the increase of α_h – which mildly increases Z while decreasing Z_P – any change which reduces Z_P also reduces Z.

Provided that a solution satisfying both $T_{bg} \leq T_{bmax}$ and $\Delta P_{cl} \leq \Delta P_{cl,max}$ does exist, in general it will correspond to lower Z_P, lower Z and higher cooling flow.

To summarize, limitations on $\Delta P_{cl}/P_{cl}$ may require higher cooling flows and a complete re-design of the cooling system. Verifing the acceptability of $\Delta P_{cl}/P_{cl}$ given by the solution of the thermal problem would

---

* In theory, accelerating the coolant to high Mach numbers could be beneficial because it would decrease its temperature. However, the losses incurred in the expansion and in the subsequent high velocity flow through the cooling channels would totally offset the benefits brought about by lower temperatures.

More interesting possibilities might exists for the discharge through film cooling holes. In this case, realizing a transonic or supersonic expansion would decrease the boundary layer temperature – i.e. T_{aw} – while the coolant kinetic energy would be transferred to the mainstream gas (reduction of acceleration losses, see Par. 3.8). In addition, this practice would also "energize" the boundary layer, thus possibly contributing to a decrease of profile losses.

be desirable, but would require to define the laws of heat addition and friction along the cooling channels and to determine a value for Z_P. In particular, due to its dependence from $n_p^{2.8}$, Z_P is likely to undergo strong variations from one cascade to another, thus requiring the definition of its variation along the expansion. However, given the lack of experimental data even an approximate evaluation of these quantities would be very uncertain, strongly undermining the significance of pressure drop estimates.

For these reasons the estimate of $\Delta P_{cl}/P_{cl}$ has been neglected in all calculations of Chs. 7 and 10, assuming that the constant pressure loss discussed at Par. 3.7 (P_1-P_2 of Fig. 3.6) is always sufficient to let Δm_{clb} through the whole cooling circuit.

5.2.7 Thermal Barrier Coatings

For given gas and coolant conditions, the cooling flow requirements can be substantially reduced by applying on the blade and shroud surface a layer of ceramic material. Due to their low thermal conductivity, such layers create a barrier to the transfer of heat, and for this reason are referred to as Thermal Barrier Coating (TBC): as shown in Fig. 5.25, they act by decreasing the temperature difference driving the transfer of heat to the blade, thus reducing heat flux and cooling requirements.

Mainly based on zirconia, which has a thermal conductivity an order of magnitude lower than nickel superalloys, TBC coatings have been successfully used in combustors for more than 15 years; two-layer coatings* have recently been introduced in stator shrouds of the Rolls-Royce RB211-535E4, where they avoid the need for film cooling (Meetham, 1986). Despite their large pay-off potential, the incorporation of TBC coatings into commercial engines has been hampered by several problems recently overviewed by Sheffler and Gupta (1988):

- Thermally-driven spallation of the brittle coating resulting from accumulation of fatigue cracking damage in the ceramic adjacent to the metal interface. The phenomenon is basically due to the significant difference between the metal and ceramic coefficients of thermal expansion. Tolokan, Nablo and Brady (1982) have proposed to improve ceramic attachment by interposing an intermediate, expansivity-compensating layer between the ceramic and the metal.

- The lack of reliable methodologies to predict the life of these components. A tentative life-prediction model has recently been proposed by Miller (1988), although the author remarks that there are still many unanswered questions about the oxidation mechanism, the effects of creep and inelasticity, the role of shearing stresses, etc.

- Substantial sensitivity to fuel impurities, particularly Vanadium (Bratton et. al., 1982). This is particularly relevant to stationary applications, which might not rely on the high-grade fuels used for aircrafts.

- A number of fluidynamic problems: alteration of film cooling hole geometry as a result of ceramic deposition, increased surface roughness, variation of airfoil aerodynamics, etc. The trade-off between reduction of cooling flows and decrease of aerodynamic efficiency due to higher leading-edge and trailing-edge thicknesses (particularly important for small engines), is pointed out by Jaeger (1979).

5.2.7.1 Inclusion into cooling model

The inclusion of TBC coatings into the cooling model is straightforward. As already done by El-Masri (1986b), it simply requires adding one more heat resistance to the gas-coolant thermal model (Fig. 5.26). The heat flux balance (Eq. 5.36) becomes:

---

* The outer layer – consisting of partially yttria stabilized zirconia – is the actual TBC coat. The inner layer – a thinner Chromium-Aluminum-Yttria bond coat – is used to strengthen the attachment to the base superalloy.

$$(h_g/a_c)\cdot(T_{gr}-T_{TBCg}) = [k_{TBC}/(a_c\cdot t_{TBC})]\cdot(T_{TBCg}-T_{bg}) = $$
$$= [k_b/(a_c\cdot t_{bw})]\cdot(T_{bg}-T_{bcl}) = h_{cl}\cdot(T_{bcl}-T_{cl}) \qquad (5.48)$$

After dividing by h_{cl} and non-dimensionalizing the temperatures by T_{bmx}:

$$[h_g/(a_c\cdot h_{cl})]\cdot(\tau_{gr}-\tau_{TBCg}) = [h_g/(a_c\cdot h_{cl})]\cdot(1/Bi_{TBC})\cdot(\tau_{TBCg}-\tau_{bg})$$
$$= [h_g/(a_c\cdot h_{cl})]\cdot(1/Bi_{bw})\cdot(\tau_{bg}-\tau_{bcl})$$
$$= (\tau_{bcl}-\tau_{cl})$$

Solving for τ_{bg}:

$$\tau_{bg} = \{(1+Bi_{TBC})\cdot\tau_{cl}+[Bi_{bw}+h_g/(a_c\cdot h_{cl})]\cdot\tau_{gr}\}/[1+Bi_{TBC}+Bi_g+h_g/(a_c\cdot h_{cl})] \qquad (5.49)$$

As already discussed in Par. 5.2.5, the minimum coolant flow compatible with $T_b \leq T_{bmx}$ can be found by imposing $\tau_{bg,out}=1$. Recalling Eq.(5.25a), $\tau_{bg,out}$ is found by substituting $\tau_{cl}=(1-\varepsilon)\cdot\tau_{cl,in}+\varepsilon\cdot\tau_{gr}$ into Eq.(5.49). The effectiveness ε is found by observing that Eq.(5.27) for NTU becomes:

$$NTU = [a_c\cdot(1/h_g+t_{bw}/k_b+t_{TBC}/k_{TBC})+1/h_{cl}]^{-1}\cdot(\psi_i\cdot n_p\cdot\psi_d\cdot\pi\cdot d\cdot H)/[\bar{c}_{p,cl}\cdot\tilde{m}_{clb}/(a_t\cdot z\cdot n_{ch})] \qquad (5.50)$$

and similarly to Eq.(5.29):

$$NTU = 0.092\cdot[(H/c)/(C_{g1}{}^{0.2}\cdot C_{f1})]\cdot Z\cdot(m_g/\tilde{m}_{clb})^{0.2}/[1+(a_c\cdot h_{cl}/h_g)\cdot(1+Bi_{bw}+Bi_{TBC})] \qquad (5.51)$$

Typical values of blade and TBC thickness adopted in actual turbines are $t_{TBC}\simeq 0.2-0.3$ mm and $t_{bw}\simeq 2-3$ mm; since $k_{TBC}\simeq 10\cdot k_b$ (Brink, 1989)*, this implies $Bi_{TBC}\simeq Bi_{bw}$.

* The thermal conductivity of ceramics depends on temperature, density and method of manufacture. Thus, k_{TBC}/k_b is subject to considerable variations.

5.2.8 Results

The results presented in this section illustrate the role played by the most significant parameters of the convection cooling model. All calculations have been referenced to the operating conditions typical of the first nozzle of current heavy-duty engines (GE 9001E, ABB GT13E or similar) and to $\Delta c/c=0.25$ (see Fig. 3.5). $\Delta c/c=0.25$ means that Figs. 5.27 to 5.32 report the flow necessary to cool only one quarter of the nozzle; this is done because, by representing the situation for only one of the many steps comprising the expansion depicted in Fig. 3.3, it is possible to identify unequivocally h_g/h_{cl}, ε_1, $\Delta P_{cl}/P_{cl}$, etc. Recalling that $\Delta m_{clb}/\bar{m}_{clb}=\Delta c/c$ (Eq.5.11) and considering what was pointed out in Par. 5.2.5.3, the cooling flow $\bar{m}_{clb}$ for the whole cascade will be around 4 times the values in the figures. For the sake of clarity, in this illustration I have assumed $\lambda=0$, i.e. $T^*_{gr}=T_{gr}$ (see Par. 5.2.2.1).

Since they are not compared with experimental data (which are not available), the value of the results below is somewhat limited and, given the reference to only one operating condition, any generalization must be done with great care. Despite these limits, these results help in understanding the physics of convection cooling, as well as verifying whether the model can justify the evolution followed (and expected) by convection cooling. In addition, there is fairly good agreement with the outcome of the calibration of Ch. 7.

5.2.8.1 Parameter Z

Fig. 5.27 depicts the influence of Δm_{clb} and Z on coolant and blade temperature at the cooling channel outlet. As expected, $T_{bg,out}$ is a monotonic, decreasing function of Δm_{clb} and, given all things equal, it also decreases with Z. The reduction of $T_{bg,out}$ achieved with higher cooling flow increases the heat flux (see Eq.5.1), thus increasing the temperature drop ($T_{bg}-T_{bcl}$) across the blade. On the coolant-side, the higher heat flux is accommodated by a strong increase of the heat transfer coefficient, while the temperature difference $T_{bcl}-T_{cl}$ is substantially reduced.

Fig. 5.28 shows the influence of Z on cooling flow, ε_1, h_{cl}/h_g and $a_c \cdot h_{cl}/h_g$ necessary to achieve $\tau_{bg,out}=1$. Increasing the sophistication of the cooling technology "pays" until $Z \leq 100$-150; higher Z yield only marginal reductions of cooling flow. Given the value $Z=100$ resulting from the calibration of state-of-the-art engines (see Ch. 7), it can be inferred that gas turbine technology has already accomplished most of the gains achievable with convection cooling. Further gains will be achieved only by other means: TBC coatings, film cooling, impingement, etc.

Fig. 5.28 also shows that at high Z the internal heat transfer coefficient is only about 50% of the one on the gas-side. This unbalance is more than compensated by the area ratio a_c, so that the ratio $a_c \cdot h_{cl}/h_g$ of the gas-side and coolant-side heat resistances keeps on increasing with Z. Even at very high Z, the effectiveness ε_1 remains below 50%, testifying to the difficulty of utilizing the temperature difference ($T_{bmx}-T_{cl,in}$) without intervening on the gas-side ΔT_g. Variations with T_g are discussed later in conjuction with film cooling (Par. 5.3.7).

5.2.8.2 Pressure losses

Fig. 5.29 reports the pressure losses given by Eq.(5.44) and the corresponding coolant velocity U_{cl} for three different values of n_p. In order to account for the strong pressure drop caused by the 180° turns of multi-pass channels (see Par. 5.2.6.2), it is assumed that E_P/E_h increases with n_p. Since it is also assumed that α_h=0.08 and ψ_i=0.7, the curves in the figure correspond to (see Eq.5.45) Z_P/Z = 71, 426 and 1278, respectively.

At low Z, ΔP_{cl} decreases with Z because the reduction of cooling flow caused by higher Z more than compensates for higher c/d (see Eq.5.40). At large Z the situation is reversed, and ΔP_{cl} becomes an increasing function of Z. These opposing tendencies establish an optimum region in the range $50 \leq Z \leq 150$ where pressure losses are at a minimum. It is interesting to notice that the value Z=100 predicted by the calibration of state-of-the-art engines (see Ch.7) falls very close to the optimum; instead, the value Z=36 predicted for "current" engines suggests that the past generation of cooling systems was subject to some pressure loss penalty.

About coolant velocities, notice that values higher than 100-150 m/s obtained for Z<20-30 are probably unrealistic, and require a revision of the incompressible flow assumption.

5.2.8.3 Blade wall heat resistance

Effectiveness could be considerably improved by decreasing blade thickness. Fig. 5.30 shows the variations of cooling flow and effectiveness when going from Bi_{bw}=0.1 to Bi_{bw}=1. The improvements can be dramatic: for example, for Z=100 the cooling flow required with Bi_{bw}=0.1 is less than 1/4th of the one required with Bi_{bw}=1.

Achieving high effectiveness by adopting very thin blade walls is the basis of the "shell-spar" concept pursued by some manufacturer (Allison, Westinghouse, Fig. 5.31). It consists of an hollow investment cast structural spar with chordwise cooling channels cast in the outer surface and a 0.5 mm thick formed sheet shell of corrosion resistant superalloy diffusion bonded to the spar (Butt and North, 1985). The purpose of the spar is to bear axial and tangential loads* and possibly thermal stresses, while the shell has just to separate the coolant, flowing between the spar and the shell, from the gas. In this way the shell can be very thin, while at the same time the load-bearing spar operates at much lower temperatures and can be made with cheaper materials.

5.2.8.4 TBC coatings

Fig. 5.32 shows that also TBC coatings afford remarkable reductions of cooling flow: a layer just a few tenths of a millimeter thick can reduce m_{c1b} by as much as 50%, a gain which is fairly independent of Z and, as discussed in Par. 5.3.7, is fully comparable with the ones afforded by film cooling. The substantial increase of heat transfer effectiveness ε_1 shows how the thermal barrier created by the TBC coat allows fuller exploitation of the available coolant ΔT.

* Centrifugal loads, if present, act on all components.

5.3 Film cooling

The convection cooling model of the previous paragraph is now extended to the case where the coolant, instead of being discharged at the blade tip (or trailing edge), film-cools the blade surface. In this way the task accomplished by the coolant is twofold: 1) it picks up heat by convection while flowing inside the blade; 2) it lowers the temperature of the boundary layer at the blade surface and shields it from the hot mainstream gas.

The extension to film cooling is done by substituting the recovery temperature T^*_{gr} used in Eq.(5.1) with the adiabatic wall temperature T_{aw} now driving the gas-side heat transfer, where T_{aw} is the temperature reached by the wall for zero heat flux. Since the correlation giving T_{aw} involves both $\tilde{m}_{clb}$ and $T_{cl,out}$, the film-cooling and convection cooling problems are coupled and must be solved simultaneously.

The results presented in Par. 5.3.7 exemplify the model capabilities and the options available for technological improvements.

5.3.1 Strategy adopted to solve the problem

Predicting the heat transfer characteristics of film cooled blades is extremely demanding because the flow is generally compressible, turbulent, with strong pressure gradients and curvature effects and difficult to reproduce in laboratory-scale experiments. In particular, modeling coolant injection through holes presents formidable challenges because: (i) the flow is highly 3-D and (ii) at high blowing rates the coolant jet penetrates into the mainstream flow, generating a very complex velocity and temperature field.

Aside from being theoretically unresolved, an accurate calculation of the heat transfer problem would require a detailed specification of blade geometry and flow conditions. These data are very difficult to produce and, most of all, they are irrelevant to the analysis of the whole thermodynamic cycle.

For this reason the present model resorts to simple, algebraic correlations developed for flows over flat plates. Although the resulting film cooling predictions are locally inaccurate, they do provide a satisfying framework for the calculation of overall turbine performances.

5.3.2 Variables relevant to heat transfer

The "shielding effect" of film cooling can be quantified by means of several different effectiveness and/or variations of gas-side heat transfer. In this paragraph I review and discuss the definitions most commonly used.

5.3.2.1 Adiabatic wall temperature

The adiabatic wall temperature is the temperature reached by the wall for zero heat flux (i.e. adiabatic wall). Without film cooling such temperature is obviously the recovery temperature T_{gr}. With film cooling $T_{aw} < T_{gr}$ because the reduced boundary-layer temperature allows "blocking" the heat flux at lower wall temperatures. T_{aw} is a function of the distance from the injection point: at the injection point it equals the coolant total temperature, while at large distance it reaches T_{gr}.

5.3.2.2 Isothermal effectiveness

Isothermal effectiveness is defined in terms of the ratio between the heat flux with film cooling ($\dot{q}_{fc}$) and the purely convective heat flux ($\dot{q}_{cv}$):

$$\eta_{iso} = 1 - (\dot{q}_{fc}/\dot{q}_{cv}) \tag{5.52}$$

where the heat fluxes are given by:

$$\dot{q}_{cv} = h_{g,cv} \cdot (T_{gr} - T_{bg}) \tag{5.53}$$

$$\dot{q}_{fc} = h_{g,fc} \cdot (T_{aw} - T_{bg}) \tag{5.54}$$

5.3.2.3 Heat transfer coefficient

Eq.(5.54) emphasizes that the variation of heat flux accomplished through film cooling is due to changes in both h and the ΔT driving the heat transfer*. In most instances the latter is the predominant effect, because the variations of the average blade h_g are small. Among the many experimental investigations on the subject, Hartnett, Birkebak and Eckert (1961), Liess (1975) and Kruse (1985) show that immediately after the injection point there is a tendency toward higher h, but shortly downstream h reduces to the value expected with no blowing (Figs. 5.33, 5.34). Metzger, Carper and Swank (1968) and Metzger and Fletcher (1971) found that for injection through slots with $\alpha = 60°$ (see Fig. 5.36) and $M > 0.5$, over the first 50-70 slot widths h_{fc} can be 20-50% higher than h_{cv}; however, such difference totally disappears at injection angles of 20°. Fig. 5.35 shows the effect of the blowing rate for injection from a single row of holes (Eriksen and Goldstein, 1974): as long as $M<1$ also in this case $h_{fc} \approx h_{cv}$. Following the recommendation of Hartnett (1985), in my analysis I will always assume $h_{g,fc} = h_{g,cv}$, which gives:

* Some authors (Metzger, Carper and Swank, 1968; Metzger and Fletcher, 1971; Arts, 1991) prefer not to introduce T_{aw} and refer to a heat transfer coefficient defined as the ratio $q_{fc}/(T_{gr}-T_{bg})$. Even if this can be convenient to present experimental results, the use of T_{aw} more correctly breaks down the two effects of film cooling, i.e. variation of h and variation of "effective" ΔT.

$$\eta_{iso} = (T_{gr}-T_{aw})/(T_{gr}-T_{bg}) \tag{5.55}$$

5.3.2.4 Adiabatic effectiveness

Although η_{iso} gives a straightforward quantification of film cooling, its correlation to experimental data is generally poor. For film cooling over a flat plate and low-speed flows, a better correlation can be found by introducing the adiabatic effectiveness η_{ad}:

$$\eta_{ad} = (T_g-T_{aw})/(T_g-T_{cl,out})$$

For high-speed flows, a definition which is found to correlate experimental results better than the one above is:

$$\eta_{ad,i} = (T_{aw,i}-T_{aw})/(T_{wcl,i}-T_{wcl}) \tag{5.56}$$

where T_{wcl} is the wall temperature at the injection point and the subscript "i" refers to a situation with the same mainstream conditions, same flow rates, but coolant total temperature equal to the one of the mainstream flow ("isoenergetic" injection). Since $\eta_{ad,i}$ compares two situations with identical velocity fields, in the hypothesis of constant fluid properties it has the theoretical advantage of eliminating the effects of viscous dissipation. Therefore if the values of the pertinent dimensionless variables remain the same, $\eta_{ad,i}$ will be the same for both high and low-speed flows. Notice that $T_{aw,i}$ is a function of position (distance from injection location).

The use of $\eta_{ad,i}$ is rather complex since not only the effectiveness but also the adiabatic temperature distribution for isoenergetic injection ($T_{aw,i}$) is unknown. However, in many applications the difference between T_{gr} and $T_{aw,i}$ is much smaller than $(T_{wcl,i}-T_{wcl})$, so that T_{gr} can be used in place of $T_{aw,i}$ (Goldstein, Eckert and Wilson, 1968);

morever, in blade cooling applications the velocity of the injected coolant is small, so $T_{wcl} \approx T_{cl,out}$. This allows using a simpler expression for η_{ad} (Liess, 1975; Ito, Goldstein and Eckert, 1978):

$$\eta_{ad} = (T_{gr}-T_{aw})/(T_{gr}-T_{cl,out}) \tag{5.57}$$

where T_{gr} can be considered approximately constant also with film cooling. From now on I will refer to the definition above, which is by far the most commonly used; in the calculations of Chs. 7 and 10 the pattern factor λ is accounted for by substituting the fictitious T^*_{gr} to T_{gr} (see Par. 5.2.2.1).

5.3.3 Literature survey

The determination of η_{ad}, both analytical and experimental, is the subject of an extensive literature. After early studies on injection through slots, in the past two decades the attention has focused on injection through rows of circular holes, an arrangement much more common in gas turbine blades. Excellent overviews of the theoretical models and experimental data produced to predict η_{ad}, as well as h_{fc}, have been given by Goldstein (1971) and more recently by Hartnett (1985). Let's summarize here the findings which are particularly relevant to gas turbine applications:

- The correlations developed for incompressible flow can be used also for supersonic flows if the fluid properties are evaluated at a reference temperature $T_{ref} = T_{g,st} + 0.72 \cdot (T_{gr} - T_{g,st})$ (Goldstein, Eckert and Wilson, 1968).
- For moderate blowing rates (M<0.5) the correlations developed for injection through slots predict reasonably well the centerline effectiveness of single row of holes provided that the slot width w is replaced with the equivalent width w_e=(Area hole)/(hole pitch) (Goldstein, Eckert and Burggraf, 1974).
- As shown in Fig. 5.37, close to injection the effectiveness of a row of holes exhibits strong lateral variations.

- For injection through holes there is generally an optimum blowing rate. This is because at high M the momentum of the coolant carries it farther out into the mainstream, thus causing more rapid mixing and lower effectiveness.

- For similar reasons higher injection angles (relative to the wall) give lower effectiveness. This holds for both slots and holes.

- In general, convex curvatures results in effectiveness higher than the flat-plate value, while the opposite is true for concave curvatures. This holds for both slots (Mayle et al., 1977) and row of holes (Ito, Goldstein and Eckert, 1978)

- A favorable pressure gradient results in a slight decrease in effectiveness while adverse pressure gradients cause a slight increase, the latter being more pronounced for row of holes (Hartnett, 1985).

- The effect of rotation appears negligible, while swirl tend to decrease effectiveness (Hartnett, 1985).

- For injection from a row of holes and $Ma_g < 0.9$ the mainstream velocity has no measurable effect on the film cooling parameters (Liess, 1975).

- The mainstream Reynolds number has a relatively small influence (Goldstein, Eckert and Ramsey, 1968).

- There is a strong influence of the density ratio ρ_{cl}/ρ_g. For the same blowing rate higher density gases have lower momentum and remain closer to the surface, thus yielding higher effectiveness (Pedersen, Eckert and Goldstein, 1977; Goldstein, Eckert and Burggraf, 1974; Paradis, 1977).

- Staggered row of holes give performances superior to inline configurations (Hartnett, 1985).

- For moderate blowing rates and large row spacings the effectiveness of multiple hole rows can be predicted by a superposition principle. Once more, the heat transfer coefficient is approximately equal to the value with no film cooling (Hartnett, 1985).

Since in our model the geometry and actual mainstream conditions are unknown, I will resort to correlations developed for injection from slots over flat plates, with no pressure gradients and subsonic flow. As already mentioned, this approach is completely inadequate for predicting local flow variables; nonetheless, it should give a reasonable approximation of the effects of film cooling on overall turbine performances.

5.3.4 Correlations for slots over flat plates

Theoretical 2-D analyses are all based on heat sink models in which the added coolant is considered as a sink of heat at the point of injection, reducing the temperature in the downstream boundary layer and thus the temperature of the wall. Following the first study of Klein and Tribus (1953), which was mainly interested in the heat transfer along non-isothermal surfaces, Kutateladze and Leont'ev (1963), Librizzi and Cresci (1964), Stollery and El-Ehwany (1965, 1967), developed models which all proceed from an energy balance of the boundary layer and assume that the velocity profiles* are not affected by injection. The basic difference among the three analyses is the assumed location where the total mass flow in the boundary-layer starts. The resulting expressions for η_{ad} have been rearranged by Han and Jenkins (1982) to explicitly show the influence of cooling gas physical properties:

Kutateladze and Leont'ev:

$$\eta_{ad} = 1/\{1+(c_{p,g}/c_{p,cl})\cdot[0.329\cdot(4.01+(\mu_g/\mu_{cl})^{0.2}\cdot\xi)^{0.8}-1]\} \qquad (5.58)$$

Librizzi and Cresci:

$$\eta_{ad} = 1/\{1+0.329\cdot(c_{p,g}/c_{p,cl})\cdot(\mu_g/\mu_{cl})^{0.2}\cdot\xi^{0.8}\} \qquad (5.59)$$

Stollery and El-Ehwany:

$$\eta_{ad} = 3.03\cdot(c_{p,cl}/c_{p,g})\cdot(\mu_{cl}/\mu_g)^{0.2}\cdot\xi^{-0.8})/$$
$$\{1+[(c_{p,cl}/c_{p,g})-1]\cdot[3.09\cdot(\mu_{cl}/\mu_g)^{0.2}\cdot\xi^{-0.8}]\} \qquad (5.60)$$

where ξ is defined by:

---

* They all assume for the mainstream flow a (1/7)th power turbulent velocity profile. For further details see Goldstein (1971).

$$\xi = [x/(w\cdot M)]\cdot Re_w^{-0.25} \tag{5.61}$$

x is the distance from the injection location, M is the blowing rate $(\rho_{cl}\cdot U_{cl})/(\rho_g\cdot U_g)$, w is the injection slot width and $Re_w = U_{cl}\cdot w/\nu_{cl}$. For injection through hole rows, the centerline effectiveness can be found by substituting w with the equivalent slot width w_e (area holes per unit length).

Goldstein and Haji-Sheikh (1967) go one step further. Rather than making assumptions on the temperature and velocity boundary layer they resort to experimental data and include the effect of the injection angle and the mainstream Prandtl number. In the form rearranged by Han and Jenkins (1982) their correlation for η_{ad} is:

$$\eta_{ad} = 1.9\cdot Pr_g^{2/3}/[1+0.329\cdot(c_{p,g}/c_{p,cl})\cdot(\mu_g/\mu_{cl})^{0.2}\cdot\xi^{0.8}\cdot\beta] \tag{5.62}$$

β accounts for injection angles different from zero (see Fig. 5.36, $\alpha=0$ means injection parallel to the wall) and is calculated according to the following experimental relationship:

$$\beta = 1 + 1.5\cdot 10^{-4}\cdot Re_w\cdot(\mu_{cl}/\mu_g)\cdot(W_g/W_{cl})\cdot\sin\alpha \tag{5.63}$$

The coolant properties are calculated at the injection conditions. For high-speed flows, the gas properties should be calculated at the reference temperature $T_{ref}=T_g+0.72\cdot(T_{gr}-T_g)$ already mentioned*.

Figs. 5.38, 5.39, 5.40 depict the effectiveness given by some of the expressions above and show comparisons with experimental data. Fig. 5.41, taken from Abuaf and Cohn (1988), shows that the correlation of Goldstein and Haji-Sheikh gives best results for air-into-air

---

* As already discussed, the iso-energetic effectiveness $\eta_{ad,i}$ should also replace η_{ad}. All calculations of this Thesis always use η_{ad} and evaluate gas properties at its static temperature.

injection, while the ones by Librizzi and Cresci and Kutateladze and Leont'ev are more accurate for injection of helium and CO_2.

5.3.4.1 Region close to injection point

Since Eqs.(5.58) to (5.63) assume complete coolant mixing in the mainstream boundary layer, they are not valid close to the point of injection and are a solution for η_{ad} only at some distance downstream. In fact, Stollery and El-Ehwany (1965) point out that the heat sink model is strictly an asymptotically correct solution of the film cooling problem, whose accuracy improves as x/w increases. A proof of this situation is that at x=0 Eqs.(5.60) and (5.62) predict effectiveness greater than one, which is clearly impossible.

To avoid this inconsistency, Mukherjee (1976) proposes to use three different equations: for the region close to injection, characterized by $\xi<1$, he suggests $\eta_{ad}=1$; for the turbulent boundary layer region, defined by $\xi>4$, he recommends Eq.(5.62), while for the intermediate region with $1<\xi<4$ the correlation:

$$\eta_{ad} = 1.9\cdot Pr_g^{2/3}/\left[1+0.525\cdot(c_{p,g}/c_{p,cl})\cdot(\mu_g/\mu_{cl})^{0.1175}\cdot\xi^{0.47}\right] \qquad (5.64)$$

He also notices that for non-tangential injection with $\alpha \leq 30°$, better results are obtained by correcting η_{ad} by the factor $\cos(0.8\cdot\alpha)$ proposed by Papell (1960) rather than by the factor β given by Eq.(5.63).

5.3.4.2 Correlation adopted in the model

All calculations performed to discuss the effect of film cooling and to obtain the results of Chs. 7 and 10 are based on the correlation of Goldstein and Haji-Sheikh (Eq.5.62). Adapting the analysis and the computer program to other correlations is quite straightforward. Following the suggestion of Mukherjee (1976), the applicability of

Eq.(5.62) is verified by testing whether $\xi<4$: in practice, the values of ξ used for the evaluation of the average film cooling effectiveness are considerably higher, typically in the range 20-500.

5.3.5 Integration with convection cooling model

Extending the model of Par. 5.2 to film cooling calls for a revision of the equation expressing the gas-side heat flux (Eq.5.1). The recovery temperature T^*_{gr} appearing in this equation must be substituted with T_{aw}, whose value is determined from η_{ad}. Also in this case the system is closed by the heat balance across the blade (Eq.5.36), and coolant flow is found by imposing $r_{bg,out}=1$ (Par. 5.2.5). Even more than for convection, non-linearities prevent obtaining explicit expressions and dictate an iterative solution procedure.

5.3.5.1 Assumptions

In order to evaluate cooling flows we need to stipulate where and how the coolant is injected and then integrate the local η_{ad} given by Eq.(5.62) over the blade (or shroud) surface. This is done on the basis of the following assumptions:

1) As already stipulated for convection cooling, the coolant is uniformly distributed along the chord, i.e. $\Delta m_{clb}/\bar{m}_{clb}=\Delta c/c$. Moreover, the ratio between the coolant flow per step (Δm_{clb}) and the coolant flow for the blades equals the ratio a_t between the area wet by the gas and the blade surface (see Eq. A.1) This is like saying that film cooling the blades and the shrouds is equivalent and it approximately corresponds to a continuous slot extending along the whole perimeter of the gas cross-section* (Fig. 5.42).

2) After exchanging heat by convection, a fraction r_{fc} of the total blade coolant is injected through slots (or hole rows) running from the root to the tip of the blade (Fig. 5.42). The remaining coolant

* The correspondence is not exact because a_t is slightly different from the ratio between the gas cross-section perimeter and the lenght of the blade slots (2·H).

is ejected at the blade tip (or at the trailing edge) without contributing to film cooling.

3) The distance between two adjacent slots equals the chord segment spanned at each step, i.e. Δc.

4) Similarly to Louis, Hiraoka and El-Masri (1983), the average effectiveness $\bar{\eta}_{ad}$ over the surface wet at each step equals the value given by Eq.(5.62) for $\bar{x}=\Delta c$. Since η_{ad} is a monotonic decreasing function of x, this might seem a rather conservative assumption because: (i) it uses the minimum η_{ad} in place of its average value and (ii) it neglects all superposition effects. However, it must be remembered that the average spanwise* effectiveness of hole rows, much likely to be used in gas turbines, is substantially lower than the one of a slot. The ratio $\bar{x}/\Delta c$ could be used as a non-dimensional parameter to describe the "quality" of film cooling as an alternative to r_{fc}.

Based on assumption 2) and the continuity equation, coolant flow must satisfy:

$$r_{fc}\cdot\Delta m_{clb} = a_t\cdot\rho_{cl}\cdot U_{cl}\cdot(2\cdot z\cdot w\cdot H) = [2\cdot\pi\cdot a_t\cdot\sigma\cdot(H/c)\cdot w\cdot D_m]\cdot\rho_{cl}\cdot U_{cl} \qquad (5.65)$$

where U_{cl} now indicates the velocity at the injection slot.

5.3.5.2 Film cooling mass ratio r_{fc}

The ratio r_{fc} between the flow used for film cooling and the total cooling flow is essentially an indicator of the "quality" of film cooling technology. It correctly accounts for the fact that only part of the cooling flow is used for film cooling, but it can also be used to "tune" the value of η_{ad} given by Eq.(5.62) to the one corresponding to the actual geometry. It could also be defined as a "correction factor" of Δm_{clb} accounting for the performance of the actual geometry vs. the slot over a flat plate. r_{fc} should be close to one in the first nozzle and decreases in the cascades downstream, where film cooling is used mainly at the leading and trailing edge but not in the midchord region.

* "spanwise" refers to the direction perpendicular to the mainstream.

The reason why in actual blades only a fraction of $\tilde{m}_{clb}$ is used for film cooling is related to a number of drawbacks pointed out by Livinghood, Ellerbrock and Kaufman (1971):

- holes and slots result in weaker blade structures
- openings in the blade walls are susceptible to vibration and fatigue failures
- foreign object damage and clogging by surface oxidation or dirty cooling air pose serious problems
- injecting the coolant into the mainstream flow affects aerodynamic performance
- fabrication techniques are more complicated and expensive

We might also add that the coolant discharged at the trailing edge, which is generally a relevant fraction of $\tilde{m}_{clb}$, can effectively be utilized for film cooling only for a small fraction of the blade surface.

5.3.5.3 Number of film cooling slots

The number of steps of the film-cooled section is generally higher than the number of injection slots of an actual gas turbine. Therefore our model substitutes few, largely-spaced slots with several, closely-spaced slots, each having a lower coolant flow rate. Let's assess the impact of this assumption on the average effectiveness $\bar{\eta}_{ad}=\eta_{ad}(\bar{x})$. Based on Eq.(5.65) and recalling that $\rho_g \cdot U_g = m_g/A_g = m_g/(\pi \cdot \psi_g \cdot H \cdot D_m)$ (see Eq. A.1):

$$\bar{x}/(w \cdot M) = (2 \cdot a_t \cdot \sigma/\psi_g) \cdot (\bar{x}/c) \cdot (m_g/\Delta m_{clb}) \cdot (1/r_{fc}) \qquad (5.66)$$

The slot Reynolds number appearing in Eq.(5.61) can be rearranged as:

$$Re_w = M \cdot w \cdot \rho_g \cdot U_g/\mu_{cl} = \left[(w \cdot M)/x\right] \cdot (x/c) \cdot Re_g \cdot (\mu_g/\mu_{cl}) \qquad (5.67)$$

thus giving:

$$\xi = [x/(w\cdot M)]^{1.25}/[Re_g\cdot(\mu_g/\mu_{cl})\cdot(x/c)]^{0.25} \tag{5.68}$$

Now putting together (5.63), (5.61) and (5.67):

$$(\mu_g/\mu_{cl})^{0.2}\cdot\xi^{0.8}\cdot\beta = (x/c)^{0.8}\cdot Re_g^{-0.2}\cdot$$
$$[(2\cdot a_t\cdot\sigma/\psi_g)\cdot(m_g/\Delta m_{clb})/r_{fc}+0.00015\cdot\sin\alpha\cdot Re_g\cdot W_g/W_{cl}] \tag{5.69}$$

where since $(m_g/\Delta m_{clb})/r_{fc} >> 1$ the first term within square brackets dominates the second*. Eq.(5.69) shows that if we substitute one slot with n_{sl} slots each having:

$$\Delta m_{cl,k} = \Delta m_{clb}/n_{sl} \qquad \bar{x}_k = \bar{x}/n_{sl}$$

then the product $\xi^{0.8}\cdot\beta$ used to calculate $\bar{\eta}_{ad,k}$ of the small slots approximately increases by a factor $n_{sl}^{0.2}$. The ratio between $\bar{\eta}_{ad,k}$ and the effectiveness $\bar{\eta}_{ad}$ of the single-slot case is:

$$\bar{\eta}_{ad,k}/\bar{\eta}_{ad} =$$
$$[1+0.329\cdot(c_{p,g}/c_{p,cl})\cdot\xi^{0.8}\cdot\beta]/[1+0.329\cdot(c_{p,g}/c_{p,cl})\cdot n_{sl}^{0.2}\cdot\xi^{0.8}\cdot\beta] \tag{5.70}$$

which can be rearranged as:

$$\bar{\eta}_{ad,k}/\bar{\eta}_{ad} = 1.9\cdot Pr_g^{2/3}/[n_{sl}^{0.2}\cdot 1.9\cdot Pr_g^{2/3}-(n_{sl}^{0.2}-1)\cdot\bar{\eta}_{ad}] \tag{5.71}$$

This equation is plotted in Fig. 5.43, showing that at high n_{sl} and low $\bar{\eta}_{ad}$ the predicted film cooling effectiveness of the n_{sl}-slot case can be substantially lower. The calculations performed to calculate the results of Chs. 7 and 10 typically involve 4-7 expansion steps per cooled cascade. Since a film cooled blade has always at least 2-3 hole rows, it follows that in our calculations $n_{sl}\simeq 2$-3. In this range we can

* The second term disappears for tangential injection (α=0).

say that the effectiveness penalty given by Eq.(5.71) is simply one more conservative assumption*; however, if the number of expansion steps per cascade is very high the model tends to underestimate $\bar{\eta}_{ad}$.

5.3.5.4 Slots vs. hole rows

The correlations presented in 5.3.4 for 2-D film cooling do not capture two important features of film cooling through hole rows:

- The major effect of the coolant-to-freestream density ratio** ρ_{cl}/ρ_g. Together with the blowing rate M, the density ratio determines whether the coolant jet exiting the hole penetrates into the mainstream, and influences how much and how soon the jet spreads laterally.
- The fact that the average spanwise effectiveness might have a peak at some distance from the hole row. Before the peak, the average spanwise effectiveness is low due to poor lateral spreading of the jets; after the peak, it decreases due to mixing with the mainstream.

A set of correlations to predict the film cooling effectiveness of rows of circular holes has recently been presented by L'Ecuyer and Soechting (1985). Its application to our calculation scheme would certainly be interesting, although it would not eliminate the need for a parameter describing the "quality" of film cooling (similar to r_{fc}). As long as the blade and hole row geometry, as well as the mainstream conditions, are not specified precisely, such parameter is needed to match predictions with the cooling flow required by actual cascades.

5.3.5.5 Variation of r_{fc} along cooled turbine

---

* Since Δm_{clb} varies at each step, the assumption that each "small" slot injects the same flow rate is inaccurate. Adding that the real blade geometry and n_{sl} are unknown makes clear that attempting to quantify $\bar{\eta}_{ad,k}/\bar{\eta}_{ad}$ is rather useless.

** For a given blowing rate M, varying ρ_{cl}/ρ_g is equivalent to varying the coolant-to-freestream momentum ratio.

If there is film cooling, the mass ratio r_{fc} is varied along the turbine according to Fig. 5.43a:

- In the nozzle, r_{fc} is constant.
- In the cooled turbine r_{fc} can either be zero (i.e. no film cooling) or vary linearly with T_{gr} until it reaches zero at the end of the cooled turbine.

$r_{fc,ct}$=0 corresponds to current heavy-duty gas turbines, where film cooling is used only in the first nozzle. Instead, the linear variation of $r_{fc,ct}$ corresponds to current aero-derivatives; after the nozzle, film cooling becomes less relevant because (i) to improve mechanical strength, rotor blades are not as heavily film-cooled as stator blades; (ii) to reduce manufacturing costs, film cooling is rarely utilized in the last cooled cascades.

5.3.6 Calculation of cooling flow

As for convection cooling, the cooling flow is determined by imposing that the blade external temperature at the coolant channel exit be equal to T_{bmx}, i.e. $\tau_{bg,out}$=1. However, with film cooling the driving gas-side ΔT is $T_{aw}-T_{bg}$ rather than $T_{gr}-T_{bg}$, and Eq.(5.38) becomes:

$$\tau_{bg,out} = \{(1-\varepsilon)\cdot\tau_{cl,in}+[\varepsilon+Bi_{bw}+h_g/(a_c\cdot h_{cl})]\cdot\tau_{aw}\}/[1+Bi_{bw}+h_g/(a_c\cdot h_{cl})] \tag{5.72}$$

The adiabatic wall temperature can be found by observing that in this case (adapt Eq.25a):

$$T_{cl,out} = T_{cl,in} + \varepsilon\cdot(T_{aw}-T_{cl,in}) \tag{5.73}$$

Substituting this expression into the definition of η_{ad} (Eq.5.57), expliciting T_{aw} and dividing by T_{bmx}:

$$\tau_{aw} = [(1-\eta_{ad})\cdot\tau_{gr}+(1-\varepsilon)\cdot\eta_{ad}\cdot\tau_{cl,in}]/(1-\varepsilon\cdot\eta_{ad}) \tag{5.74}$$

The cooling flow corresponding to $\tau_{bg,out}=1$ is found by iterating on $\tilde{m}_{clb}$. Given $\tilde{m}_{clb}$, the heat transfer effectiveness ε is determined according to the relationships derived in 5.2.4.6, 5.2.4.7 and 5.2.4.9; the film cooling effectiveness comes from substituting Eq.(5.69) into (5.62):

$$\bar{\eta}_{ad} = 1.9\cdot Pr_g^{2/3}/(1+0.329\cdot(c_{p,g}/c_{p,cl})\cdot Re_g^{-0.2}\cdot(\bar{x}/c)^{0.8}\cdot$$
$$[(2\cdot a_t\cdot\sigma/\psi_g)\cdot(m_g/\Delta m_{clb})/r_{fc}+0.00015\cdot\sin\alpha\cdot Re_g\cdot W_g/W_{cl}]) \tag{5.75}$$

and from hyptheses 1) and 4) of Par. 5.3.5.1:

$$\Delta m_{clb}/\tilde{m}_{clb} = \Delta c/c$$
$$\bar{x}/c = \Delta c/c$$

5.3.7 Results

Similarly to Par. 5.2.8, this section presents results referring to the operating conditions typical of the nozzle of current heavy-duty engines and to $\Delta c/c=0.25$. Given the same hypotheses, Figs. 5.44 to 5.49 are directly comparable with Figs. 5.27 to 5.32.

5.3.7.1 Influence of Z and r_{fc}

Fig. 5.44 depicts the influence of Z and r_{fc} on the cooling flow required by the nozzle typical of heavy-duty engines already considered in Figs. 5.27 and 5.28. As usual, the cooling flow is for (1/4)th of the cascade, i.e. $\Delta c/c = \Delta m_{clb}/\tilde{m}_{clb} = 0.25$. Notice that the gains achievable with film cooling are comparable to the ones achievable with more sophisticated convection cooling. For example, starting from $Z=20$ and $r_{fc}=0$, approximately the same reduction of Δm_{clb} can be obtained by going to $r_{fc}=1$ or to $Z\approx250$; however, the latter option is likely to entail higher costs. The benefits of film cooling decrease at high Z:

going from r_{fc}=0 to r_{fc}=1 decreases Δm_{c1b} by a factor of about 8 at Z=10, and by a factor of about 2 at Z=300.

To summarize, the figure proves that it is the synergic combination of convection and film cooling that gives best results, a consideration already pointed out by Colladay (1972).

The effectiveness and the heat transfer characteristics depicted in Figs. 5.44 and 5.45 show that:

- By reducing the gas-side heat flux, film cooling allows reducing $(T_{bcl}-T_{cl})$ at the end of the cooling channel, thus increasing ε_1. Therefore, film cooling "pays twice", because besides reducing the heat flux it also affords higher heat transfer effectiveness.
- When going from no film cooling to r_{fc}=1 the internal heat transfer coefficient decreases by a factor between 2 and 8. Therefore, in film cooled blades we would expect more widespread use of impingement cooling as a way to achieve high local h_{cl} (see Par. 5.4).

5.3.7.2 Variations of gas temperature

Figs. 5.46, 5.47, and 5.48 shows the variations of $\Delta m_{c1b}/m_g$, h_{cl}/h_g, η_{ad}, ε_1 and dP_{cl}/P_{cl} with T_g. The value of 75 chosen for Z is close to the result of the calibration of Ch. 7 and could be achieved, for example, with ψ_i=0.7, α_h=0.08, n_p=3, E_h=1.6, c/d=24. It is clear that for T_g>1300°C some form of film cooling must necessarily be adopted*. Due to gas-coolant mixing before the first rotor – and leaving aside the pattern factor λ – T_g=1300°C at the nozzle inlet corresponds to TIT=1200-1230°C. Convection cooling performs so poorly at high T_g because in order to transmit the high heat fluxes imposed on the gas-side, $T_{cl,out}$ must become very low and ε_1 practically goes to zero.

* Considering that $\Delta c/c$=0.25, the value $\Delta m_{c1b}/m_g$=3.5% given by the figure for no film cooling and T_g=1300°C implies that in those conditions the cooling flow for the whole nozzle must be 11-14% of m_g, a fraction already very high, not to mention the effect of the pattern factor.

Besides, Fig. 5.48 shows that without film cooling the pressure drop of multi-pass cooling channels is likely to pose major constraints.

5.3.7.3 TBC coatings

The combined effect of film cooling and TBC coatings can be obtained by correcting Eq.(5.72) according to Eq.(5.49) and calculating NTU by Eq.(5.51). Fig. 5.49 shows that the relative gains afforded by TBC coatings decrease with the level of film cooling technology. For example, for T_g=1300°C and no film cooling, TBC coatings with Bi_{TBC}=Bi_{bw}=0.5 give a 60% reduction of cooling flow; however, if r_{fc}=0.5 the reduction of m_{clb} is only 30%. Conversely, with TBC coatings there is less incentive to go toward film cooling. This is to be expected because both TBC coatings and film cooling act by decreasing the heat flux to the blade, thus "competing" for the same task. If one of the two techniques is already in use, adding the other yields lower marginal gains. From the point of view of reliability, stable, corrosion-resistant TBC coatings should be preferable to film cooling because they eliminate the risk of plugging*.

* The obstruction of film-cooling holes, which is generally fatal to the integrity of the engine, is a problem often encountered in aircrafts operating in desert areas, where sand ingested into the compressor melts during combustion and then forms a glass-like cover on the turbine blades. With TBC coatings, such occurrence would actually increase the resistance opposed by the thermal barrier.

5.4 Impingement cooling

This paragraph reviews the basic features of impingement cooling, and presents a model for the calculation of the flow required by fully-impingement cooled blades.

Since the schematization is radically different from the one of convection and film, the model illustrated here is not one further extension of the model of Par. 5.3: it is an alternative method which cannot be used in conjunction with the others. The geometrical arrangement is particularly simple, different from the ones adopted in practice; nonetheless, the analysis allows appreciating the merits of this technique and the differences with convection and film.

The model of this paragraph has not been included into the computer code implementing the algorithms of Ch. 3 for two reasons:

- Generally, impingement is used only locally (e.g. leading edge region); thus, its effects on overall gas turbine performance are limited.
- A model handling convection+film+impingement cooling would require too much information on blade geometry.

Thus, the results discussed at Par. 5.4.4 have been obtained by a program different from the one used to calculate cooled gas turbines (see Ch.9), and the results of Ch. 7 and 10 do not include impingement cooling calculations.

5.4.1 Generalities

Impingement heat transfer consists in directing high velocity gas jets against the surface to be cooled (or heated). Besides gas turbines, it has considerable applications in drying of textile and paper, tempering of glass, spot cooling of electrical apparatus. Its distinctive features are the possibility of achieving:

- High heat transfer coefficients in localized regions
- Good heat transfer in regions where it is impractical to realize channels for convection cooling
- More uniform blade temperature distributions.

These capabilities are particularly relevant to cooling of the leading edge, a region which needs intense heat removal and where it is technologically difficult to realize cooling channels with good heat transfer performances. Impingement may also be used in the midchord region in order to obtain a more uniform temperature distribution.

The various flow regions formed by a jet impinging on a solid surface are shown in Fig. 5.50. The theoretical prediction of the heat transfer characteristics is extremely difficult because, in addition to the complexity of the flow field created by a single jet, the cooling schemes adopted in practice always consist of arrays of jets which strongly interfere with each other. Both local and average heat transfer are strongly influenced by a number of geometrical and fluidynamic parameters, such as jet type (slot or circular), jet spacing, arrangement of the jet array (inline or staggered), distance from the surface to be cooled, fluid properties and velocities, presence of crossflow perpendicular to the jets etc. Given the impossibility of solving the fluidynamic problem theoretically, investigators have aimed at determining empirical correlations of the relevant non-dimensional parameters. All such correlations express the Nusselt number as a function of Reynolds and Prandtl number*, the system geometry and the characteristic crossflow parameters. Nu and Re are generally, but not always, based on jet diameter and jet mass velocity.

5.4.2 Literature survey

Most of the research has focused on arrays of jets impinging against a flat surface, an arrangement which approximates reasonably well the one adopted in the mid-chord region of turbine blades (Fig. 5.51). Correlations for heat transfer from a single circular jet were first obtained by Perry (1954) and later by Gordon and Cobonque (1961) and Huang (1963), who also discussed and gave experimental data for jet arrays. In these papers it is recognized that the crossflow of spent gas, which after being impinged flows perpendicularly to the jets toward a discharge orifice, can substantially reduce heat transfer. Schuh and Pettersson (1966) developed a correlation for injection through a single row of slots and found that a crossflow with velocity up to 60% of jet velocity (v_j) does not reduce the heat transfer coefficient; instead, some reduction is observed with injection through a row of circular holes. After discussing the characteristics of the crossflow originated by the spent flow, Kercher and Tabakoff (1970) obtained a general heat transfer correlation for the square array of circular jets depicted in Fig. 5.52. The correlation requires the use of three graphical presentations and expresses Nu, averaged over one

---

* Since all the experimentation has been conducted with air, the Prandtl number dependence is simply assumed equal to the one for flow parallel to a flat plate ($Nu \propto Pr^{1/3}$) and, to our knowledge, has not been verified.

streamwise* hole spacing, as a function of:

- Re and Pr
- Hole spacing
- Distance between jet plate and heat transfer surface
- A parameter expressing crossflow intensity

Due to crossflow, it is not possible to find an expression for the average plate Nu; the heat transfer problem can be solved only after determining the crossflow and jet flow variations from one hole row to another.

More sophisticated analyses of crossflow and other effects have been performed in a series of recent papers:

- Hollworth and Berry (1978) pointed out that although small hole spacings increase the heat transfer coefficient, the average heat transfer per unit of coolant flow decreases. The strong reduction of cooling flow requirements afforded by large hole spacings is supported by the analysis developed in the next paragraph.

- Metzger et al. (1979) and Florschuetz, Berry and Metzger (1980) uncovered periodic streamwise variations of the heat transfer coefficient. This can produce significant temperature non-uniformities of the heat transfer surface and defeat one of the primary goals of impingement, i.e. the achievement of more uniform blade temperatures to reduce thermal stresses. Temperature variations can be smoothed by reducing the jet diameter; however, smaller holes yield higher pressure drops and increase the probability of plugging.

- Florschuetz, Truman and Metzger (1981) developed a theoretical model of the spent crossflow for the geometry of Fig. 5.52. They also present a correlation for Nu (averaged over one streamwise hole spacing) which does not require the use of charts and can account for both streamwise and spanwise hole spacing (non-square arrays).

- Florschuetz, Metzger and Su (1984) analyze the effect of an initial external crossflow at a temperature different from the one of the jets. This scheme correctly models the midchord region of a gas turbine blade (Fig. 5.51), where the jets are crossed by spent flow coming from the leading edge. Because of heat pickup at the leading edge, the temperature of such initial crossflow is substantially

* In this paragraph "streamwise" and "spanwise" refer to the direction of the crossflow.

> above the midchord jets. The situation can be viewed as a three-temperature problem, where the heat transfer is to a fluid in the process of mixing from two sources at different temperatures. This is very similar to film cooling, and can be modeled by introducing an effectiveness analogous to the one defined in Eq.(5.57).

Finally, Chupp et al. (1969) and Jusionis (1970) developed correlations for the impingement of a single row of jets over a concave circular heat transfer surface, a situation encountered at the blade leading edge (Fig. 5.53). In both papers it is assumed that there is only one row of jets, i.e. no crossflow effects.

5.4.3 Calculation of cooling flow

The heat transfer and the pressure loss of convection and impingement systems have been compared by Schuh and Pettersson (1966), who however did not discuss cooling flow requirements. Hollworth and Berry (1978) mention the importance of reducing the cooling flow but do not attempt any comparison with convection systems. Performing a rational comparison is intricate because in both systems there are a number of geometrical parameters which need to be optimized under the constraints imposed by manufacturing capabilities, blade thermal load, maximum allowable temperature. The optimum blade design is likely to include, as it is actually done in practice, a combination of convection and impingement. In the following I will determine the cooling flow requirements of the fully impingement cooled blade depicted in Fig. 5.54. Although approximate and referring to a design which is not adopted in actual blades, the analysis clarifies the relative merits of convection and impingement.

5.4.2.1 Assumptions

The cooling flow required by the blade in Fig. 5.54 has been estimated according to the following assumptions:

1) The ratio between the cascade and the blade cooling flow is again equal to the area ratio a_t (Eq. A.1).

2) Within each blade, the cooling flow is equally divided between pressure and suction side.

3) Blade curvature and compressibility effects are negligible. This allows using the correlations developed for flat plates.

4) The jet array is square, staggered, with length equal to the blade chord.

5) There are no flow and temperature variations along the radial direction

From hypothesis 5), and indicating with x_n the jet spacing, the number of jet rows for each blade side is:

$$n_{jr} = c/x_n = (c/d)/(x_n/d) \tag{5.76}$$

while the total number of holes is $2\cdot(H/x_n)\cdot(c/x_n)$. The "open area ratio" a_j between the total jet cross section and the blade surface is:

$$a_j = 2\cdot(H/x_n)\cdot(c/x_n)\cdot(\pi\cdot d^2/4)/(\Phi\cdot c\cdot H) = (\pi/2)/[\Phi\cdot(x_n/d)^2] \tag{5.77}$$

Based on assumptions 1) and 2), the average jet mass velocity $\bar{G}_j$ is:

$$\bar{G}_j = [\bar{m}_{clb}/(a_t\cdot z)]/[a_j\cdot\Phi\cdot c\cdot H] = [1/(\pi\cdot a_j\cdot a_t\cdot\Phi\cdot\sigma)]\cdot[m_g/(H\cdot D_m)]\cdot(\bar{m}_{clb}/m_g) \tag{5.78}$$

5.4.2.2 Flow distribution and Reynolds number

Due to the need to discharge the spent coolant, in the hiatus between the jet plate and the blade wall there will be a pressure gradient between the leading and trailing edge. Such pressure gradient cannot be ignored because it seriously affects the mass velocity G_j at each jet row, as well as the chordwise heat transfer and temperature distribution. Florschuetz, Truman and Metzger (1981) imagine to replace the discrete hole array by a surface over which injection is continuosly distributed; assuming that the streamwise pressure gradient is due only to crossflow acceleration (i.e. no wall shear), the integration of the force-momentum balance gives:

$$G(x)/\bar{G}_j = [\beta \cdot n_{jr}/\sinh(\beta \cdot n_{jr})] \cdot \cosh(\beta \cdot x/x_n) \qquad (5.79)$$

where x is the distance from the edge of the jet plate (in our case the leading edge, see Fig. 5.54) and, indicating with C_D the jet discharge coefficient $m_j/(\rho_j \cdot U_j \cdot A_j)$:

$$\beta = C_D \cdot 2^{0.5} \cdot (\pi/4)/[(x_n/d) \cdot (z_n/d)]$$

Assuming that in the discrete hole case the mass velocity of the ith row corresponds to G(x) calculated at the row centerline, where $x/x_n = (i-1/2)$:

$$G_{j,i}/\bar{G}_j = r_{j,i} = [\beta \cdot n_{jr}/\sinh(\beta \cdot n_{jr})] \cdot \cosh[\beta \cdot (i-1/2)] \qquad i=1,2,\ ..\ n_{jr} \qquad (5.80)$$

By the same argument, the crossflow G_c can be expressed by:

$$(G_c/G_j)_i = [1/(2^{0.5} \cdot C_D)] \cdot \sinh[\beta \cdot (i-1)]/\cosh[\beta \cdot (i-1/2)] \qquad (5.81)$$

As shown in Fig. 5.55, the variations of G_j and G_c with the jet row are quite substantial and are more pronounced for high n_{jr}. Although Kercher and Tabakoff (1970) have shown that the jet discharge coefficient C_D varies with Re_j and d within the range 0.75≃0.90, for the sake of the argument we'll assume constant C_D=0.8. Recalling Eq.(5.78) and observing that:

$$m_g \cdot d/[H \cdot D_m \cdot \mu_{cl}] = Re_g \cdot (\mu_g/\mu_{cl}) \cdot [\pi \cdot \psi_g/(c/d)] \tag{5.82}$$

the Reynolds number $G_{j,i} \cdot d/\mu_{cl}$ of the ith jet row can be expressed as:

$$Re_{j,i} = C_{g2} \cdot [(r_{j,i}/a_j)/(c/d)] \cdot [Re_g \cdot (\mu_g/\mu_{cl})] \cdot (\tilde{m}_{clb}/m_g) \tag{5.83}$$

$$C_{g2} = \psi_g/(a_t \cdot \Phi \cdot \sigma) \tag{5.84}$$

5.4.2.3 Heat transfer

The most complete correlation for the evaluation of wall-to-jet heat transfer has been proposed by Florschuetz, Truman and Metzger (1981). Correlations proposed by other investigators give similar dependencies of Nu vs. Re_j (Hollworth and Berry, 1978 give $Re_j^{0.8}$; Behbahani and Goldstein, 1983 give $Re_j^{0.78}$) but do not explicit the separate influence of x_n/d, y_n/d, z_n/d and G_c/G_j. For staggered arrays, the expression proposed by Florschuetz, Truman and Metzger (1981) is (in our case must set x_n=y_n):

$$Nu_i = Nu_1 \cdot [1-1.07 \cdot (x_n/d)^{-0.604} \cdot (z_n/d)^{0.788} \cdot (G_c/G_j)_i^{0.66}] \tag{5.85}$$

where Nu_1, the Nusselt number of the first row (where G_c=0), is:

$$Nu_1 = 0.363 \cdot (x_n/d)^{-0.976} \cdot (z_n/d)^{0.068} \cdot Re_{j,1}{}^{0.727} \cdot Pr_{cl}{}^{1/3} \tag{5.86}$$

and z_n is the wall-to-jet spacing. These expressions hold for:

$2.5 \cdot 10^3 < Re_j < 7 \cdot 10^4$
$4 < x_n/d < 10$
$1 < z_n/d < 3$
$0 < G_c/G_j < 0.8$

and refer to a heat transfer coefficient which in our case would be defined as (Metzger et al., 1979):

$$h_{cl,i} = \dot{q}_i/(T_{bcl,i}-T_{cl,in})$$

q_i is the heat flux averaged over the ith streamwise hole spacing and the subscript ",i" emphasizes that h_{cl} and T_{bcl} vary with the jet row*. This definition implies that the coolant-side ΔT to be used to determine the thermal power exchanged at each jet row is the whole $(T_{bcl,i}-T_{cl,in})$ rather than a suitable averaged ΔT.

5.4.2.4 Blade temperature

Neglecting conduction, the heat flux balance for the section of blade wall facing the ith jet row is therefore:

$$h_g\cdot(T_{gr}-T_{bg,i}) = (k_b/t_{bw})\cdot(T_{bg,i}-T_{bcl,i}) = h_{cl,i}\cdot(T_{bcl,i}-T_{cl,in})$$

Explicing $T_{bg,i}$ and non-dimensionalizing the temperatures this gives, similarly to Eq.(5.37):

$$\tau_{bg,i} = \left[\tau_{cl,in}+(Bi_{bw}+h_g/h_{cl,i})\cdot\tau_{gr}\right]/(1+Bi_{bw}+h_g/h_{cl,i}) \qquad i=1,2,\ ..\ n_{jr} \tag{5.87}$$

The ratio $h_g/h_{cl,i}$ can be found by observing that:

$$h_{cl,i}/h_g = (St_{cl,i}/St_g)\cdot(c_{p,cl}/c_{p,g})\cdot G_{j,i}/(\rho_g\cdot U_g) \tag{5.88}$$

where, consistently with the definition of $Re_{j,i}$, the ith row Stanton number is defined as $h_{cl,i}/(c_{p,cl}\cdot G_{j,i})$. Once Nu_i is known, $St_{cl,i}$ can be

* Rather than $T_{cl,in}$, Metzger et al. (1979) actually use a reference temperature which may be identified as the adiabatic wall temperature. However, they suggest that in applications like blade cooling the use of $T_{cl,in}$ adequately predicts the heat fluxes. Behbahani and Goldstein (1983) refer only to the adiabatic wall temperature, although for their experiments $T_{aw} \simeq T_{cl,in}$.

found from $St = Nu/(Re \cdot Pr)$; as for the ratio of mass velocities we have:

$$G_{j,i}/(\rho_g \cdot U_g) = G_{j,i} \cdot A_g/m_g = C_{g2} \cdot (r_{j,i}/a_j) \cdot (\bar{m}_{clb}/m_g) \qquad (5.89)$$

which allows determining $h_{cl,i}/h_g$ as a function of $(\bar{m}_{clb}/m_g)$. Similarly to what already done for convection cooling, we can now determine $\bar{m}_{clb}/m_g$ by imposing that $\tau_{bg,i} \leq 1 \ \forall \ i=1,2, \ldots n_{jr}$. Given the geometric parameters $(x_n/d,\ z_n/d,\ c/d,\ C)$, the gas Reynolds Re_g and the fluid conditions (T,P,μ), the temperature distribution resulting from each $\bar{m}_{clb}/m_g$ can be found by calculating:

(i) $r_{j,i}$ at each row from Eq.(5.80)
(ii) $Re_{j,i}$ from Eq.(5.83)
(iii) Nu_i from Eq.(5.85)
(iv) $h_{cl,i}/h_g$ from Eq.(5.88)
(v) $\tau_{bg,i}$ from Eq.(5.87)

Notice that no reference is made to the actual physical size of the system nor to absolute mass flows. Absolute quantities can be found after specifying the gas flow rate per unit cross-sectional area $m_g/(\pi \cdot H \cdot D_m)$ appearing* in Eq.(5.78).

5.4.3 Pressure drops

Assuming that the flow through the impingement holes is 1-D, adiabatic and frictionless, the pressure drop can be expressed as:

$$\Delta P = (\rho \cdot U^2/2) \cdot \left[1 + Ma^2/4 + (2-\gamma) \cdot Ma^4/24 + \ldots\right]$$

* Introducing the stage specific diameter $D_s = D_m \cdot \Delta h_{is}^{0.25}/V_{out}^{0.5}$ (Par. 2.1.1.3) gives:

$$m_g/(H \cdot D_m) = \rho_g \cdot \Delta h_{is}^{0.5}/\left[\pi \cdot D_s^2 \cdot (H/D_m)\right]$$

Since Δh_{is}, D_s and H/D_m typically fall within a narrow range (see Par. 2.1), the gas specific flow rate depends mainly on gas density.

Although the jet Mach number can be high (Metzger et al., 1979 report that for some of their experiments $Ma_j = 1$), I will neglect compressibility effects and assume $\Delta P_{cl} = (\rho \cdot U_{cl}^2/2)$. Besides its convenience, this is done to maintain compatibility with Eqs.(5.79) and (5.80), which are based on the hypothesis of incompressible flow; the resulting ΔP is therefore an optimistic estimate. The pressure drop at each hole row is:

$$\Delta P_i = \rho_{cl} \cdot U_{j,i}^2/2 = (G_{j,i}/C_D)^2/(2 \cdot \rho_{cl}) \tag{5.90}$$

Since $G_{j,i}$ is maximum at the last hole row (spent coolant discharge), the required coolant-side pressure drop corresponds to $i = n_{jr}$:

$$\Delta P_{cl} = \left[r_{j,n_{jr}}^2/(2 \cdot C_D^2 \cdot \rho_{cl})\right] \cdot G_j^2 \tag{5.91}$$

Recalling Eq.(5.78) and that $P_{cl} = \rho_{cl} \cdot a_{cl}^2/\gamma_{cl}$ we can obtain an expression similar to Eq.(5.44):

$$\Delta P_{cl}/P_{cl} = C_{g2}^2 \cdot \left[Re_g \cdot \mu_g/\mu_{cl}\right]^2 \cdot \{\gamma_{cl} \cdot \left[(\nu_{cl}/c)/a_{cl}\right]^2\} \cdot \left[r_{j,n_{jr}}^2/(2 \cdot C_D^2 \cdot a_j^2)\right] \cdot (\bar{m}_{clb}/m_g)^2 \tag{5.92}$$

Since the open area ratio a_j given by Eq.(1) varies with $(x_n/d)^{-2}$, the pressure loss is proportional to $(x_n/d)^4$.

5.4.4 Results

The impingement cooling model has been used to calculate the cooling flow required by a nozzle operating under the same conditions considered in Pars. 5.2.8 and 5.3.7. However, unlike the results presented for convection and film – which referred to 25% of the blade ($\Delta c/c = 0.25$) – in this paragraph all calculations refer to the whole blade and assume that T_{gr} is constant along the chord. This is done to exemplify an unequivocal chord-wise coolant distribution.

The calculation of impingement flows could be made compatible with the step-by-step model of Ch. 3 by assuming that if Δm_{clb} is the flow required to cool Δc, then $\Delta m_{clb}/\bar{m}_{clb}=\Delta c/c$ (Par. 5.2.4.1). In such case the distributions in Fig. 5.56 would become a fictitious representation corresponding to T_{gr}=constant.

5.4.4.1 Chord-wise distributions

Fig. 5.56 depicts the chord-wise heat transfer and blade temperature profiles corresponding to the situation with $\tau_{bg,i}\leq 1\ \forall i$. Disuniformities tend to disappear at high x_n/d, for which the highest temperature is reached at the last jet row (in our case the trailing edge). Since h_g is assumed constant, the solid curves represent the variations of h_{cl}.

In the leading edge region (low x/c) heat transfer benefits from the absence of cross-flow, but suffers from low coolant velocities. Moving toward the trailing edge (higher x/c), h_{cl} is subject to the antagonistic effects of increased crossflow and higher jet velocities. For $x_n/d=10$, crossflow effects prevail because, as illustrated in Fig. 5.55, jet velocity is almost constant. For $x_n/d=4$, crossflow prevails only in the leading edge region; past the mid-chord, h_{cl} starts increasing due to much higher jet velocities. For $x_n/d=10$, h_{cl} is about 2-3.5 times higher than for convection (compare with Fig. 5.28); local values up to 100% higher are obtained with $x_n/d=4$, which however gives strong chordwise variations.

5.4.4.2 Influence of geometry and gas temperature

The influence of geometry and T_g on the overall cooling flow is illustrated in Figs. 5.57 to 5.59. Points with $\Delta P_{cl}/P_{cl}$>55-60% have been removed because they would imply nearly supersonic flow and require a different analytic treatment. The figures show that:

- The adoption of large hole spacings allows dramatic reductions of the cooling flow. Low x_n/d require large cooling flows because, although h_{cl} is high, the heat transfer area corresponding to each jet row is very small and the coolant has no "room" nor "time" to exchange heat.

- The wall-to-jet spacing z_n/d has minor effects on cooling flows, but substantial effects on pressure losses. Although high z_n/d decrease h_{cl} (see Eq. 5.85), they also yield lower crossflow intensities (smaller β in Eq. 5.81). The relative insensitivity of $\bar{m}_{clb}/m_g$ is due to these two antagonistic effects. Instead, $\Delta P_{cl}/P_{cl}$ is affected only by crossflow and coolant flow variations, thus increasing at low z_n/d.

- Similarly to z_n/d, the ratio c/d mainly affects pressure losses. For each hole spacing there is an optimum c/d that minimizes the cooling flow and another, typically lower, that minimizes pressure losses.

- In order to obtain cooling flows comparable with convection cooling systems it is necessary to adopt $x_n/d \geq 6$. The most interesting solution ($x_n/d=10$, $z_n/d=2$, $c/d>100$) gives cooling flows corresponding to approximately the lower bound of convection systems.

- The values of $G_j \cdot a_j$ depicted in Fig. 5.57 (corresponding to $m_g/(\pi \cdot H \cdot D_m) = 300$ kg/s-m^2, a value typical of large heavy-duty engines) are substantially higher than the range 0.5-1 kg/s-m^2 quoted by Abdul Husain et al. (1988). This could perhaps be explained by considering that in actual blades impingement is only part of a complex scheme including also convection and film cooling.

- All configurations require a pressure loss of at least 8-10%. In practice, pressure losses are likely to be lower because, as already mentioned, actual blades utilize cooling schemes different from the one considered in the present study.

- At gas temperatures above 1200°C, $x_n/d=10$ appears the only viable solution.

The above results make clear that, compared to convection, impingement does not offer significant cooling flow reductions. The major advantage is therefore an increase of the local h_{cl} by a factor between 1.5 and 5. However, as illustrated by Andrews et al. (1988), the presence of film cooling on the external blade surface may substantially alter the situation.

The reason why ΔP is much higher than for convection is mainly due to the difference in coolant flow cross-sectional area and therefore its velocity. Recalling Eqs.(5.10) and (5.77), the total cross-sectional areas are:

for convection: $\alpha_h \cdot c^2/n_p$
for impingement: $C_D \cdot 2 \cdot (H/x_n) \cdot (c/x_n) \cdot \pi \cdot d^2/4$

For the same mass flow, the ratio of average coolant velocities is therefore:

$$U_{cl,i}/U_{cl,cv} = (2/\pi) \cdot \left[\alpha_h/(C_D \cdot n_p)\right] \cdot (c/H) \cdot (x_n/d)^2$$

For the values adopted in Figs. 5.29 and 5.58 (α_h=0.08, C_D=0.8, n_p=1, c/H=1.37) $U_{cl,i}$ can be, depending on x_n/d, 1.5 to more than 8 times higher than $U_{cl,cv}$.

5.5 Issues deserving further work

The schematization presented in this chapter allows predicting cooling flow requirements for all the three techniques now used in gas turbine: convection, film and impingement.

Although the detail and the accuracy of the present formulation are satisfactory for the purposes of this Thesis, there are areas where it would be desirable to perform further work:

- More precise definition of the average gas-side heat transfer coefficient.
- Calculation of pressure losses for each step of the cooled expansion.
- Development of an integrated scheme for convection, film and impingement
- For film cooling, differentiation between continuous slots and rows of holes.

In most cases these improvements will involve the collection of substantial amount of experimental data.

REFERENCES

Abuaf N. and Cohn A. (1988), "Gas Turbine Heat Transfer with Alternate Cooling Fluids", ASME Paper 88-GT-16.

Abdul Husain R.A.A., Andrews G.E., Asere A.A. and Ndiema C.K.W. (1988), "Full Coverage Impingement Heat Transfer: Cooling Effectiveness", ASME Paper 88-GT-220.

Ainley D.G. (1957), "Internal Cooling for Turbine Blades. A General Design Survey", Aeronautical Research Council R.&M. 3013, Ministry of Supply, London.

Anderson R.H. (1979), "Material Properties and Their Relationships to Critical Jet Engine Components", Proc. of the Workshop on *High-Temperature Materials for Advanced Military Engines (Arlington, VA, May 1979)*, Vol. 1, pp. 87-109, Institute for Defense Analyses, Alexandria, Virginia.

Andrews G.E. et al. (1988), "Impingement/Effusion Cooling: Overall Wall Heat Transfer", ASME Paper 88-GT-290.

Arora S.C. and Abdel Messeh W. (1985), "Pressure Drop and Heat Transfer Characteristics of Circular and Oblong Low Aspect Ratio Pin Fins", in *AGARD CP-390*, Neuilly sur Seine, France.

Arts T. (1991), "Convective Heat Transfer with Film Cooling Around a Rotor Blade", in *Modern Research Topics in Aerospace Propulsion*, pp. 253-274, Angelino G., De Luca L. and Sirignano W.A. editors, Springer-Verlag, New York.

Behbahani A.I. and Goldstein R.J. (1983), "Local Heat Transfer to Staggered Arrays of Impinging Circular Air Jets", Journal of Eng. for Power, Vol. 105, pp. 354–360.

Bradley E.F. (1988), Superalloys, A Technical Guide, ASM International, Metals Park, Ohio.

Bratton R.J., Lau S.K., Andersson C.A. and Lee S.Y. (1982), "Ceramic Thermal Barrier Coatings for Gas Turbine Engines", ASME Paper 82-GT-265.

Brink R.C. (1989), "Material Property Evaluation of Thick Thermal Barrier Coating Systems", J. of Eng. for Gas Turbines and Power, Vol. 111, pp. 570-577.

Butt G.P. and North E.W. (1985), "Heat Transfer Test Evaluation of the Shell-Spar Blade Cooling Concept Applied to Industrial Gas TUrbines", in *AGARD CP-390*, op.cit.

Chupp R.E., Helms H.E., McFadden P.W. and Brown T.R. (1969), "Evaluation of Internal Heat Transfer Coefficients for Impingement-Cooled Turbine Airfoils", J. of Aircraft, Vol. 6, pp. 203-208.

Colladay R.S. (1972), "Importance of Combining Convection with Film Cooling", AIAA Paper 72-8.

Dunn M.G. (1985), "Heat Flux Measurements and Analysis for a Rotating Turbine Stage", in *AGARD CP-390*, op.cit.

El-Masri M.A. (1983), "Two Phase Transpiration Cooling", J. of Eng. for Power, Vol. 105, pp. 106-113.

El-Masri M.A. (1986a), "On Thermodynamics of Gas-Turbine Cycles: Part 2 - A Model for Expansion in Cooled Turbines", J. of Eng. for Gas Turbines and Power, Vol. 108, pp. 151-159.

El-Masri M.A. (1986b), "Prediction of Cooling Flow Requirements for Advanced Utility Gas Turbines. Part 2: Influence of Ceramic Thermal Barrier Coatings", ASME Paper 86-WA/HT-44.

El-Masri M.A. (1988), "A Modified, High-Efficiency, Recuperated Gas Turbine Cycle", J. of Eng. for Gas Turbines and Power, Vol. 110, pp. 233-242.

El-Masri M.A., Kobayashi Y. and Louis J.F. (1982), "A General Performance Model for the Open-Loop Water-Cooled Gas Turbine", ASME Paper 82-GT-212.

El-Masri M.A. and Louis J.F. (1978), "On the Design of High Temperature Gas Turbine Blade Water-Cooling Channels", J. of Eng. for Power, Vol. 100, pp. 586-591.

El-Masri M.A. and Pourkey F. (1986), "Prediction of Cooling Flow Requirements for Advanced Utility Gas Turbines. Part 1: Analysis and Scaling of the Effectiveness Curve", ASME Paper 86-WA/HT-43.

Erbes M. (1990), Enter Software Inc., Menlo Park, CA, Personal Communication.

Eriksen V.L. and Goldstein R.J. (1974) "Heat Transfer and Film Cooling Following Normal Injection through Inclined Circular Tubes", J. of Heat Transfer, Vol. 96, pp. 235-246.

Florschuetz L.W., Berry R.A. and Metzger D.E. (1980), "Periodic Streamwise Variations of the Heat Transfer Coefficients for Inline and Staggered Arrays of Circular Jets with Crossflow of Spent Air", J. of Heat Transfer, Vol. 102, pp. 132-137.

Florschuetz L.W., Metzger D.E. and Su C.C. (1984), "Heat Transfer Characteristics for Jet Array Impingement with Initial Crossflow", J. of Heat Transfer, Vol. 106, pp. 34-41.

Florschuetz L.W., Truman C.R. and Metzger D.E. (1981), "Streamwise Flow Heat Transfer Distributions for Jet Array Impingement with Crossflow", J. of Heat Transfer, Vol. 103, pp. 337-342.

Goldstein R.J. (1971), "Film Cooling", in Advances in Heat Transfer, Vol. 7, pp. 321-379, Academic Press, New York.

Goldstein R.J., Eckert E.R.G. and Burggraf F. (1974), "Effects of Hole Geometry and Density on Three-Dimensional Film Cooling", Int. J. of Heat and Mass Transfer, Vol. 17, pp. 595-606.

Goldstein R.J., Eckert E.R.G. and Ramsey J.W. (1968), "Film Cooling Injection through Holes: Adiabatic Wall Temperatures Downstream of a Circular Hole", J. of Eng. for Power, Vol. 90, pp. 384-395.

Goldstein R.J., Eckert E.R.G. and Wilson D.J. (1968), "Film Cooling with Normal Injection into a Supersonic Flow", J. of Eng. for Industry, Vol. 90, pp. 584-588.

Goldstein R.J. and Haji-Sheikh A. (1967), "Prediction of Film Cooling Effectiveness", Proc. *1967 Semi-International Symposium* (Tokio), pp. 213-218. Published by Japan Society of Mechanical Engineers, Tokio.

Goldstein R.J., Rask R.B. and Eckert E.R.G. (1966), "Film Cooling with Helium Injected over an Incompressible Air Flow", Int. Journal of Heat and Mass Transfer, Vol. 9, pp. 1341-1349.

Gordon R. and Cobonque J. (1961), "Heat Transfer between a Flat Plate and Jets of Air Impinging on It", Proc. *2nd International Heat Transfer Conference* (Boulder, Colorado), Part II, pp. 454-460. Published by ASME, New York.

Graf H.J. (1985), "Engine Tests on a Cooled Gas Turbine Stage", in *AGARD CP-390*, op.cit.

Grünling H.W. (1979), "High Temperature Alloys In Power Plant Systems: Current Status and Future Demands", Proc. *Behaviour of High Temperature Alloys in Aggressive Environments* (Petten, The Netherlands, 15-18 Oct. 1979), pp. 137-168. Published by The Metal Society, London.

Hempel H. and Friedrich R. (1978), "Profile Loss Characteristics and Heat Transfer of Full Coverage Film-Cooled Blading", ASME Paper 78-GT-98.

Han J.C. (1984), "Heat Transfer and Friction in Channels with Two Opposite Rib-Roughened Walls", J. of Heat Transfer, Vol. 106, pp. 774-781.

Han J.C. and Jenkins P.E. (1982), "Prediction of Film Cooling Effectiveness of Steam", ASME Paper 82-GT-100.

Han J.C., Park J.S. and Lei C.K. (1984), "Heat Transfer and Pressure Drop in Blade Cooling Channels with Turbulence Promoters", NASA Contractor Report 3837, NASA Lewis Research Center, Cleveland, Ohio.

Han J.C., Park J.S. and Lei C.K. (1985), "Heat Transfer Enhancement in Channnels with Turbulence Promoters", J. of Eng. for Gas Turbines and Power, Vol. 107, pp. 628-635.

Hartnett J.P. (1985), "Mass Transfer Cooling", in <u>Handbook of Heat Transfer Applications</u>, Rohsenow W.M., Hartnett J.P. and Ganić E.N. editors, McGraw-Hill, New York.

Hartnett J.P., Birkebak R.C. and Eckert E.R.G. (1961), "Velocity Distributions, Temperature Distributions, Effectiveness and Heat Transfer for Air Injected Through a Tangential Slot Into a Turbulent Boundary Layer", J. of Heat Transfer, Vol. 83, pp. 293-306.

Hollworth B.R. and Berry R.D. (1978), "Heat Transfer from Arrays of Impinging Jets with Large Jet-to-Jet Spacing", J. of Heat Transfer, Vol. 100, pp. 352-357.

Holman J.P. (1986), Heat Transfer, 6th ed., McGraw-Hill, New York.

Huang G.C. (1963), "Investigations of Heat Transfer Coefficients for Air Flow through Round Jets Impinging Normal to a Heat Transfer Surface", J. of Heat Transfer, Vol. 85, pp. 237-245.

Ito S., Goldstein R.J. and Eckert E.R.G. (1978), "Film Cooling of a Gas Turbine Blade", J. of Eng. For Power, Vol. 100, pp. 476-481.

Jaeger A. (1979), "Turbine Technology", Workshop on *High-Temperature Materials for Advanced Military Engines*, op.cit., pp. 403-421.

Jusionis V.J. (1970), "Heat Transfer from Impinging Gas Jets on an Enclosed Concave Surface", J. of Aircraft, Vol. 7, pp. 87-88.

Kaminski D.A. editor (1979), "Forced Convection Surface-Roughness Effects in Ducts", Section 503,7 of *Heat Transfer Data Book*, General Electric Corporate Research and Development, Schenectady, New York.

Kakaç S., Shah R.K. and Aung W. (1987), Handbook of Single-Phase Convective Heat Transfer, John Wiley, New York.

Kays W.M. and London A.L. (1964), Compact Heat Exchangers, 2nd ed., McGraw-Hill, New York.

Kercher D.M. and Tabakoff W. (1970), "Heat Transfer by a Square Array of Round Air Jets Impinging Perpendicular to a Flat Surface Including the Effect of Spent Air", J. of Eng. for Power, Vol. 92, pp. 73-82.

Klein J. and Tribus M. (1953), "Forced Convection from Non-Isothermal Surfaces", in Heat Transfer, a Symposium, University of Michigan Press, Ann Arbor, Michigan.

Köhler H., Hennecke D.K., Pfaff K. and Eggebrecht R. (1977), "Hot Cascade Test Results of Cooled Turbine Blades and their Application to Actual Engine Conditions",in *AGARD CP-229*, op.cit.

Kruse H. (1985), "Effects of Hole Geometry, Wall Curvature and Pressure Gradient on Film Cooling Downstream of a Single Row", in *AGARD CP-390*, op.cit.

Kühl W. (1977), "Investigations on the Local Heat Transfer Coefficient of a Convection Cooled Rotor Blade", in *AGARD CP-229*, Neuilly sur Seine, France.

Kutateladze S.S. and Leont'ev A.I. (1963), "Film Cooling with a Turbulent Gaseous Boundary Layer", Thermal Physics of High Temperature, Vol. 1, pp. 281-290.

Larson F.R. and Miller J. (1952), "A Time-Temperature Relationship for Rupture and Creep Stress", Transactions of the ASME, Vol. 74, pp. 765-775.

L'Ecuyer M.R. and Soechting F.O. (1985), "A Model for Correlating Flat Plate Film Cooling Effectiveness for Rows of Round Holes", in *AGARD CP-390*, op.cit.

Lefebvre A.H. (1983), Gas Turbine Combustion, McGraw-Hill, New York.

Librizzi J. and Cresci R.J. (1964), "Transpiration Coolin of a Turbulent Boundary Layer in an Axisymmetric Nozzle", AIAA J., Vol. 2, pp. 617-624.

Livinghood J.N.B., Ellerbrock H.H. and Kaufman A. (1971), "1971 NASA Turbine Cooling Research Status Report", NASA TM X-2384, NASA Lewis Research Center, Cleveland, Ohio.

Liess C. (1969), "Introduction to Cooling of Gas Turbine Blades", Lecture Series 15, vonKarman Institute for Fluid Dynamics, Brussels.

Liess C. (1975), "Experimental Investigation of Film Cooling with Ejection from a Row of Holes for the Application to Gas Turbine Blades", J. of Eng. for Power, Vol. 97, pp. 21-27.

Louis J.F. (1977), "Systematic Studies of Heat Transfer and Film Cooling Effectiveness", in *AGARD CP-229*, op.cit.

Louis J.F., Hiraoka K. and El-Masri M.A. (1983), "A Comparative Study of the Influence of Different Means of Turbine Cooling on Gas Turbine Performance", International J. of Turbo and Jet Engines, Vol. 1, pp. 123-137.

Mayle R.E., Kopper F.C., Blair M.F. and Bailey D.A. (1977), "Effect of Streamline Curvature on Film Cooling", J. of Eng. for Power, Vol. 99, pp.77-82.

Meetham G.W. (1981), The Development of Gas Turbine Materials, Applied Science Publishers, London.

Meetham G.W. (1986), "Keynote Lecture - Materials for Advanced Gas Turbines", Proc. *High Temperature Alloys for Gas Turbines and Other Applications 1986* (Liege, Belgium, 6-9 Oct. 1986), Part 1, pp. 1-18. Published by D. Reidel Publishing Co., Boston.

Metzger D.E. et al. (1979), "Heat Transfer Characteristics for Inline and Staggered Arrays of Circular Jets", J. of Heat Transfer, Vol. 101, pp. 526-531.

Metzger D.E., Berry R.A. and Bronson J.P. (1982), "Developing Heat Transfer in Rectangular Ducts with Staggered Arrays of Short Pin Fins", J. of Heat Transfer, Vol. 104, pp. 700-706.

Metzger D.E., Carper H.J. and Swank L.R. (1968), "Heat Transfer with Film Cooling near Nontangential Injection Slots", J. of Eng. for Power, Vol. 90, pp. 157-163.

Metzger D.E. and Fletcher D.D. (1971), "Evaluation of Heat Transfer for Film-Cooled Turbine Components", J. of Aircraft, Vol. 8, pp. 33-38.

Metzger D.E., Mathis W.J. and Grochowsky L.D. (1979), "Jet Cooling at the Rim of a Rotating DIsk", J. of Eng. for Power, Vol. 101, pp. 68-72.

Metzger D.E. and Sahm M.K., (1986) "Heat Transfer around Sharp 180 Degree Turns in Smooth Rectangular Channels", J. of Heat Transfer, Vol. 108, pp. 500-506.

Miller R.A. (1988), "Life Modeling of Thermal Barrier Coatings for Aircraft Gas Turbine Engines", J. of Eng. for Gas Turbines and Power, Vol. 110, pp. 301-305.

Mom A.J.A. and Boogers J.A.M. (1986), "Simulated Service Test Behaviour of Various Internal and External Coatings Applied on CF6-50 First Stage Turbine Blades", Proc. *High Temperature Alloys for Gas Turbines and Other Applications 1986*, op.cit., Part 2, pp. 1245-1264.

Morris W.D. and Harasgama S.P. (1985), "Local and Mean Heat Transfer on the Leading Edge and Trailing Surfaces of a Square-Sectioned Duct Rotating in the Orthogonal Mode", in *AGARD CP-390*, op.cit.

Mukherjee D.K. (1976), "Film Cooling with Injection through Slots", J. of Eng. for Power, Vol. 98, pp. 556-559.

Papell S.S. (1960), "Effect of Gaseous Film Cooling of Coolant Injection through Angled Slots and Normal Holes", NASA TN D-299, NASA Lewis Research Center, Cleveland, Ohio.

Paradis M.A. (1977), "Film Cooling of Gas Turbine Blades: a Study of the Effect of Large Temperature Differences on Film Cooling Effectiveness", Journal of Eng. for Power, Vol. 99, pp. 11-20.

Pedersen D.R., Eckert E.R.G. and Goldstein R.J. (1977), "Film Cooling with Large Density Differences between the Mainstream and the Secondary Coolant Measured by the Heat, Mass Transfer Analogy", J. of Heat Transfer, Vol. 99, pp. 620-627.

Perry K.P. (1954), "Heat Transfer by Convection form a Hot Gas Jet to a Plane Surface", Proc. Institute of Mechanical Engineers, London, Vol. 168, pp. 775-780.

Rice I.G. (1982), "The Reheat Gas Turbine with Steam-Blade Cooling - A Means of Increasing Reheat Pressure, Output and Combined Cycle Efficiency", J. of Eng. for Power, Vol. 104, pp. 9-22.

Rice I.G. (1983a), "Steam-Cooled Gas Turbine Casings, Struts and Disks in a Reheat Gas Turbine Combined Cycle: Part I - Compressor and Combustor", J. of Eng. for Power, Vol. 105, pp. 844-850.

Rice I.G. (1983b), "Steam-Cooled Gas Turbine Casings, Struts and Disks in a Reheat Gas Turbine Combined Cycle: Part II - Gas Generator Turbine and Power Turbine", J. of Eng. for Power, Vol. 105, pp. 851-858.

Sabella D. (1990), Gas Turbine Design and Development, Nuovo Pignone, Firenze, Italy, Personal Communication.

Schilke P.W. and DeGeorge C.L. (1982), "Water-Cooled Gas Turbine Monometallic Nozzle Fabrication and Testing", J. of Eng. for Power, Vol. 104, pp. 607-616.

Schilke P.W. and DeGeorge C.L. (1983), "Testing and Evaluation of a Water-Cooled Gas Turbine Nozzle", ASME Paper 83-GT-240.

Schuh H. and Pettersson R. (1966), "Heat Transfer by Arrays of Two-Dimensional Jets Directed Normal to Surfaces Including the Effects of a Superposed Wall-Parallel Flow", Proc. *3rd International Heat Transfer Conference* (Chicago), Vol. II, pp. 280-291. Published by ASME, New York.

Seban R.A. (1960), "Heat Transfer and Effectiveness for a Turbulent Boundary Layer with Tangential Fluid Injection", Journal of Heat Transfer, Vol. 82, pp. 303-312.

Seban R.A. and Back L.H. (1962), "Velocity and Temperature Profiles in Turbulent Boundary Layers with Tangential Injection", Journal of Eng. for Power, Vol. 84, pp. 45-53.

Shapiro A.H. (1953), The Dynamics and Thermodynamics of Compressible Fluid Flow, Vol. 1, Ronald Press, New York.

Sheffler K.D. and Gupta D.K. (1988), "Current Status and Future Trends in Turbine Application of Thermal Barrier Coatings", J. of Eng. for Gas Turbines and Power, Vol. 110, pp. 605-609.

Stambler I. (1989), "EPRI sees near-term potential for closed circuit steam cooling", Gas Turbine World, Feb. 1989, pp. 28-30.

Stollery J.L. and El-Ehwany A.A.M. (1965), "A Note on the Use of a Boundary Layer Model for Correlating Film-Cooling Data", International J. of Heat and Mass Tranfer, Vol. 8, pp. 55-65.

Stollery J.L. and El-Ehwany A.A.M. (1967), "On the Use of a Boundary-Layer Model for Correlating Film Cooling Data", International J. of Heat and Mass Tranfer, Vol. 10, pp. 101-105.

Strang A. (1979), "High Temperature Properties of Coated Superalloys" Proc. *Behaviour of High Temperature Alloys in Aggressive Environments*, op.cit., pp. 595-611.

Takeya K. and Yasui H. (1988), "Performance of the Integrated Gas and Steam Cycle (IGSC) for Reheat Gas Turbines", J. of Eng. for Gas Turbines and Power, Vol. 110, pp. 220-224.

Tolokan R.P., Nablo J.C. and Brady J.B. (1982), "Ceramic to Metal Attachment Using Low Modulus BRUNSBOND Pad", J. of Eng. for Power, Vol. 104, pp. 594-600.

Wilson, D.G. (1984), The Design of High-Efficiency Turbomachinery and Gas Turbines, The MIT Press, Cambridge, Massachusetts.

Wu C. and Louis J.F. (1984), "A Comparative Study of the Influence of Different Means of Cooling on the Performance of a Combined (Gas and Steam Turbines) Cycle", J. of Eng. for Gas Turbines and Power, Vol. 106, pp. 750-755.

NOMENCLATURE

a	Speed of sound	[m/s]
a_j	Ratio between impingement jet cross-section and blade surface	
a_c	Ratio inner/outer blade heat transfer area (Eq. 5.12)	
a_t	Ratio between blades+shrouds surface and blade surface (Eq. A.1)	
A	Cross-sectional area	[m^2]
Bi_{bw}	Blade wall Biot number $h_g \cdot t_{bw}/k_b$ (Par. 5.2.4.7)	
Bi_{TBC}	Thermal Barrier Coating Biot number $h_g \cdot t_{TBC}/k_{TBC}$	
c	Blade chord	[m]
c_p	Constant pressure specific heat	[J/kg-K]
C	Thermal capacity $m \cdot c_p$	[W/K]
C_D	Impingement jet discharge coefficient $m_j/(\rho_j \cdot U_j \cdot A_j)$	
C_{f1}	Fluid properties coefficient defined by Eq.(5.21)	
C_{f2}	Fluid properties coefficient defined by Eq.(5.35)	
C_{g1}	Stage geometry coefficient defined by Eq.(5.20)	
C_{g2}	Stage geometry coefficient defined by Eq.(5.84)	
d	Cooling channel or impingement hole hydraulic diameter: $4 \cdot A/(\text{periphery})$	[m]
Δm_{clb}	Blades+shrouds coolant flow per step	[kg/kg_a-step]
D	Diameter	[m]
E_h	Heat transfer augmentation factor	
E_f	Friction augmentation factor	
E_P	ΔP augmentation factor (friction+heat transfer)	
f	Friction factor, see Eq.(5.43)	
G_j	Impingement jet mass velocity based on hole area m_j/A_j	[kg/s-m^2]
k	Thermal conductivity	[W/m-K]
K	Coefficient introduced by Eq.(5.2a)	
h	Specific enthalpy or heat transfer coefficient	[J/Kg or W/m^2-K]
H	Blade height	[m]
m	Mass flow rate, specific to compressor inlet air flow	[kg/kg_a]
$\bar{m}_{clb}$	Blades+shrouds coolant flow per cascade	[kg/kg_a-cascade]
M	Blowing rate parameter $(\rho_{cl} \cdot U_{cl})/(\rho_g \cdot U_g)$	
Ma	Mach number	
n_{ch}	Number of coolant channels per blade	
n_{jr}	Number of impingement jet rows per blade side (pressure, suction)	
n_p	Number of passes of each coolant channel	
n_{sl}	Number of small closely-spaced film cooling slots (see Par. 5.3.5.3)	
Nu	Nusselt number $h \cdot c/k$	
Nu_m	Mean Nu over one cascade or over a 180° bend	
P	Pressure	[Pa]
Pr	Prandtl number	
r_{fc}	Ratio between flow used for film cooling and total cooling flow	
r_j	Ratio actual/average impingement jet mass velocity	
R	Gas constant	[J/kg-K]
Re_{cl}	Coolant Reynolds number based on channel diameter $\rho_{cl} \cdot U_{cl} \cdot d/\mu_{cl}$	
Re_g	Gas Reynolds number based on chord and mass velocity $(m_g \cdot c)/(A_g \cdot \mu_g)$	
Re_e	Gas Reynolds number based on chord and stage exit velocity $\rho_g \cdot v_{ge} \cdot c/\mu_g$	
Re_j	Impingement jet Reynolds number $G_j \cdot d/\mu_{cl}$	
Re_w	Coolant Reynolds number based on slot width $\rho_{cl} \cdot U_{cl} \cdot w_e/\mu_{cl}$	
$\dot{q}$	Heat flux	[W/m^2]
$\dot{Q}$	Thermal power	[W]
S	Heat transfer area	[m^2 or J/K]

St_{cl}	Coolant Stanton number $h_g/(c_{p,g}\cdot\rho_{cl}\cdot U_{cl})$	
St_g	Gas Stanton number $h_g/(c_{p,g}\cdot m_g/A_g)$	
St_{me}	Mean cascade St based on cascade exit velocity, see Eq.(5.3)	
t_b	Average blade thickness: (blade cross-section)/c	[m]
t_{bw}	Blade wall thickness	[m]
t_{TBC}	Thermal Barrier Coating thickness	[m]
T	Temperature	[K]
$\hat{T}$	Average T used used in the cooled turbine, see Eq.(5.6)	[K]
T_{bmx}	Maximum allowed blade temperature	[K]
u	Blade peripheral speed	[m/s]
U	Average mass velocity: $m/(\rho\cdot A)$; average axial velocity	[m/s]
U_h	Overall heat transfer coefficient	[W/m^2-K]
w	Injection slot width	[m]
w_e	Equivalent injection slot width (area holes)/(hole pitch)	[m]
W	Molecular weight	[kg/kmol]
x	Distance from film cooling slot or edge of impingement jet plate	[m]
x_n	Streamwise spacing between impingement jets	[m]
y_n	Spanwise spacing between impingement jets	[m]
z	Number of blades	
z_n	Gap between heat transfer plate and impingement jet plate	[m]
Z	Cooling technology heat transfer parameter $\psi_i\cdot\alpha_h^{0.2}\cdot n_p^{0.8}\cdot E_h\cdot(c/d)^{1.2}$	
Z_P	Cooling technology ΔP parameter $[(E_P/E_h)\cdot n_p^2/(\alpha_h\cdot\psi_i)]\cdot Z$	

Greek

α	Film cooling injection angle or cascade exit angle	
α_h	Coolant passages cross-section/c^2, see Eq.(5.10)	
β	Coefficient defined by Eq.(5.63) or appearing in Eq.(5.79)	
γ	Ratio c_p/c_v	
Φ	Ratio between blade perimeter and blade chord	
Δh	Enthalpy drop	[J/kg]
ΔP	Pressure loss	[Pa]
η_{ad}	Film cooling adiabatic effectiveness, see Eq.(5.57)	
η_{iso}	Film cooling isothermal effectiveness, see Eq.(5.52)	
ε	Heat transfer effectiveness defined by Eq.(5.25a)	
ε_1	Heat transfer effectiveness defined by Eq.(5.26)	
λ	Pattern factor	
μ	Viscosity	[Pa·s]
ν	Kinematic viscosity	[m^2/s]
ξ	Film cooling parameter, see Eq.(5.61)	
ρ	Density	[kg/m^3]
τ	Ratio T/T_{bmx}	
σ	Solidity, i.e. chord/pitch	
ψ_a	Axial cross-section coefficient $1-\sigma\cdot t/c_a$, see Eq.(A.14)	
ψ_d	Cooling channel shape factor, (periphery of one channel)/$(\pi\cdot d)$	
ψ_g	Gas cross-section coefficient $1-\sigma\cdot t/c$, see Eq.(A.1)	
ψ_i	Coolant channels interference coefficient (Par. 5.2.4.1)	

Subscripts

a	Air
av	Average
aw	Adiabatic wall
b	Blade
bcl	Blade, coolant side
bg	Blade, gas side
bn	180° bend of multi-pass cooling channels

bw	Blade wall
c	Compressor
cl	Coolant
clb	Blades+shrouds cooling flow
cmb	Combustor
cv	Convection
fc	Film cooling
g	Hot gas
ge	Hot gas at cascade exit
gr	Hot gas at recovery temperature
i	Isoenergetic or ith impingement jet row
in	Inlet
j	Impingement jet
k	kth injection slot (Par. 5.3.7.3)
m	Mean
max	Maximum
out	Outlet
st	Static conditions
str	Straight tube
tot	Total conditions
wcl	Wall, at the point of coolant injection

Superscripts

-	average
*	corrected by pattern factor

FIGURES

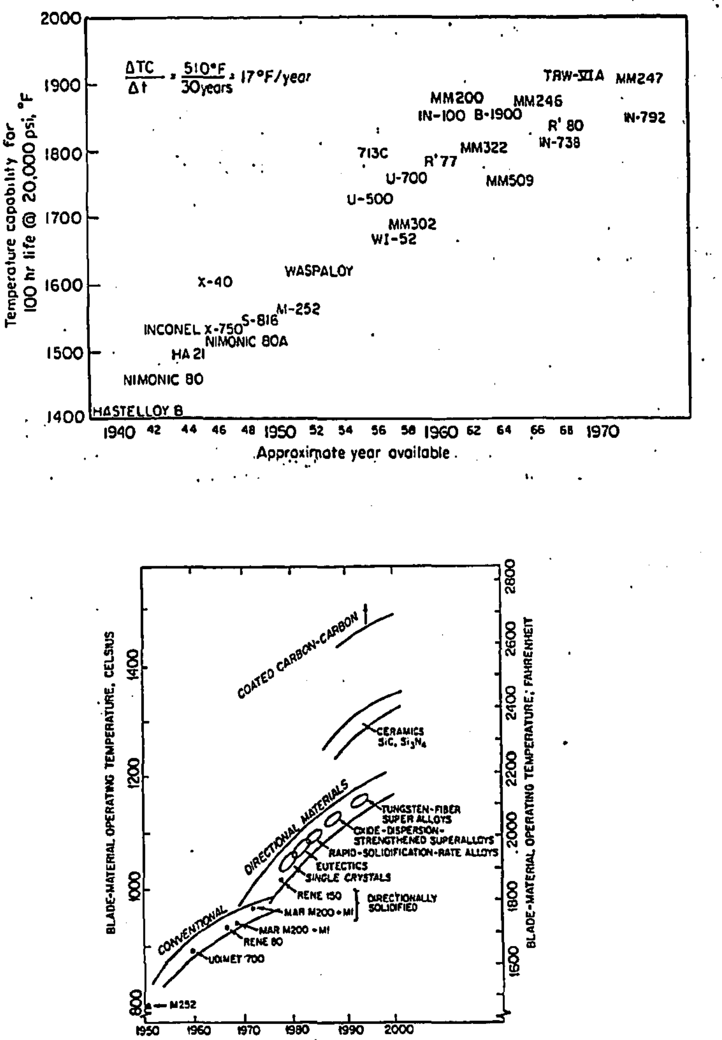

5.1 Historical development and typical temperature capability of superalloys. Upper diagram is from Bradley (1988). Lower diagram is from Wilson (1984), and refers to 1000 hrs life under a stress of 150 MPa.

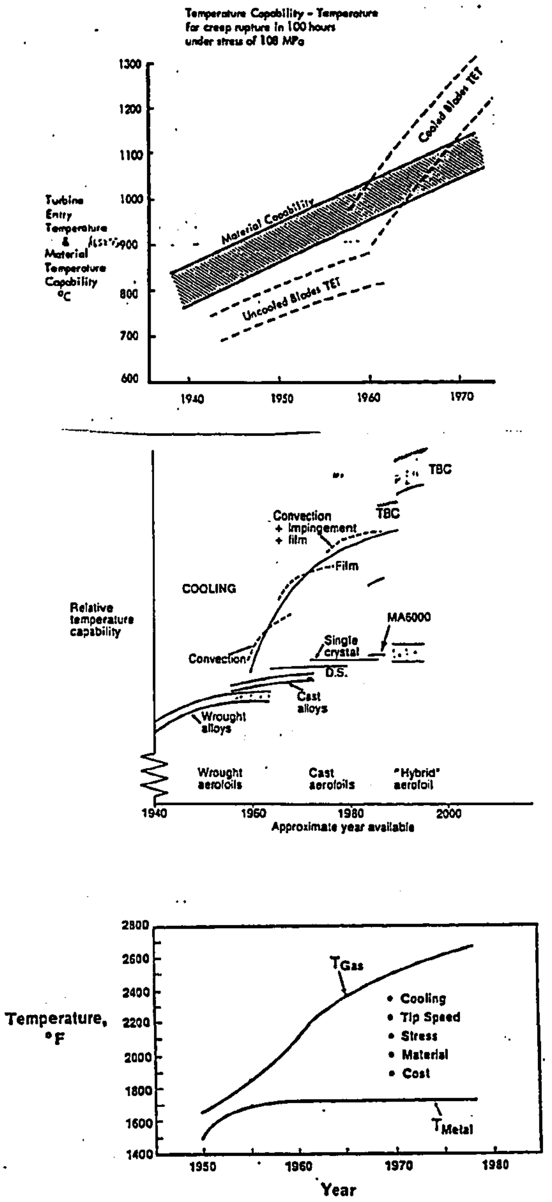

5.2 Relative evolution of turbine blade cooling and material capabilities. Upper diagram is from Meetham, 1986. Lower diagram is from Anderson (1979) and refers to military jet engines.

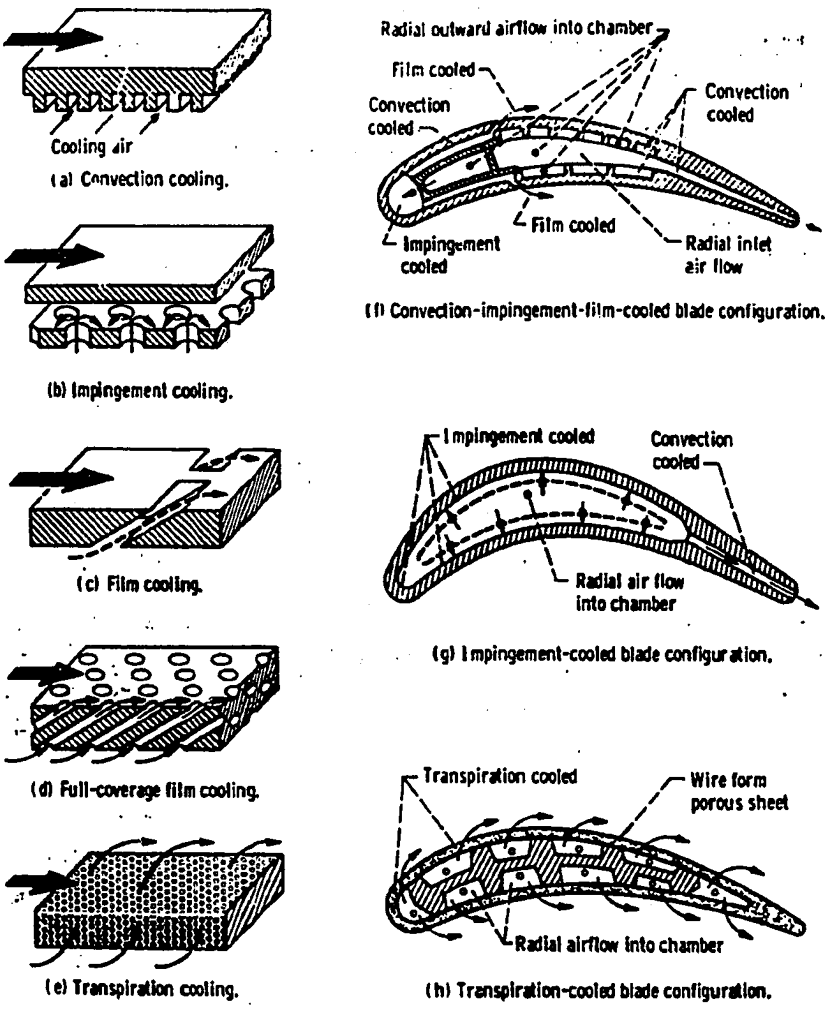

5.3 Methods for turbine blade cooling (from Livinghood, Ellerbrock and Kaufman, 1971).

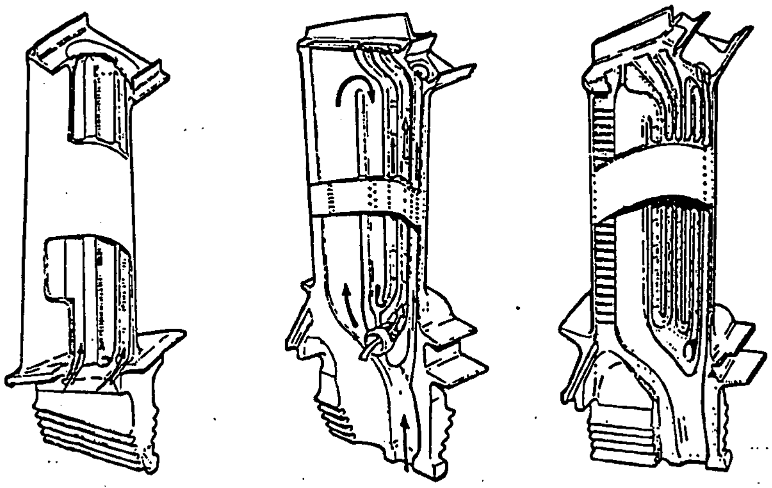

a) Conway b) RB211-22B c) RB211-535E4

5.4 Evolution of cooling schemes adopted in Rolls-Royce engines (from Meetham, 1986). Notice the two separate coolant circuits (black and white arrows) of the RB211-22B and the trend toward multi-pass channels with smaller diameters (implying higher values of the cooling technology parameter Z).

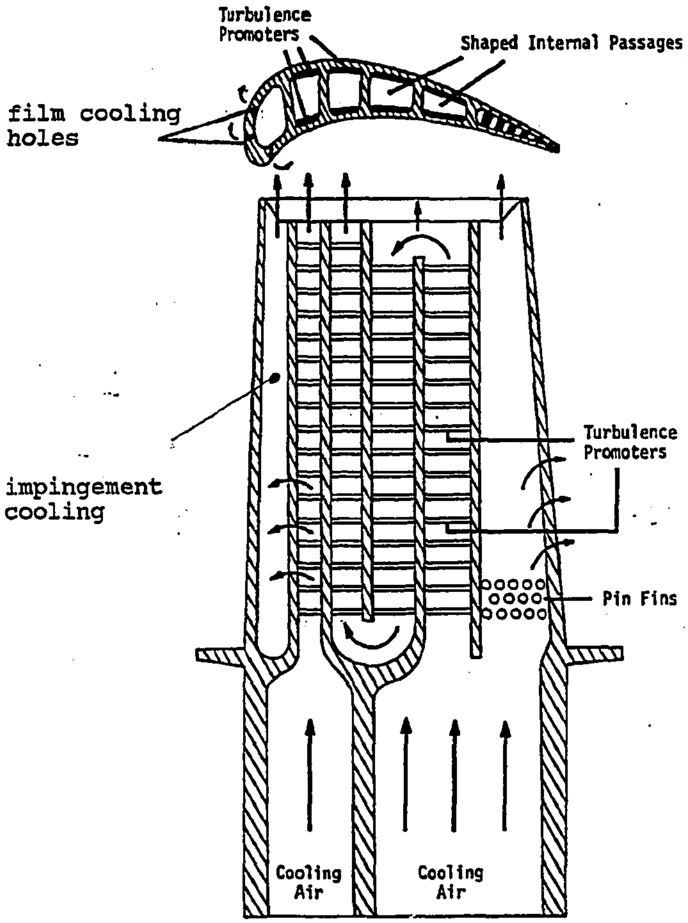

5.5 Design concept of a modern cooled blade.

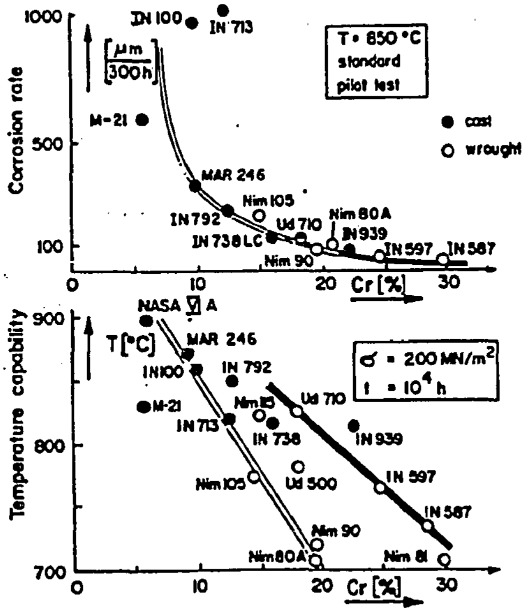

5.6 Corrosion resistance and temperature capability vs. chromium content of selected super-alloys (from Grünling, 1979). The former is quantitavely expressed by the penetration rate of the corrosion attack; the latter by the temperature producing rupture after 10,000 hrs under a stress of 200 MPa (≈ 20 Kg/mm²).

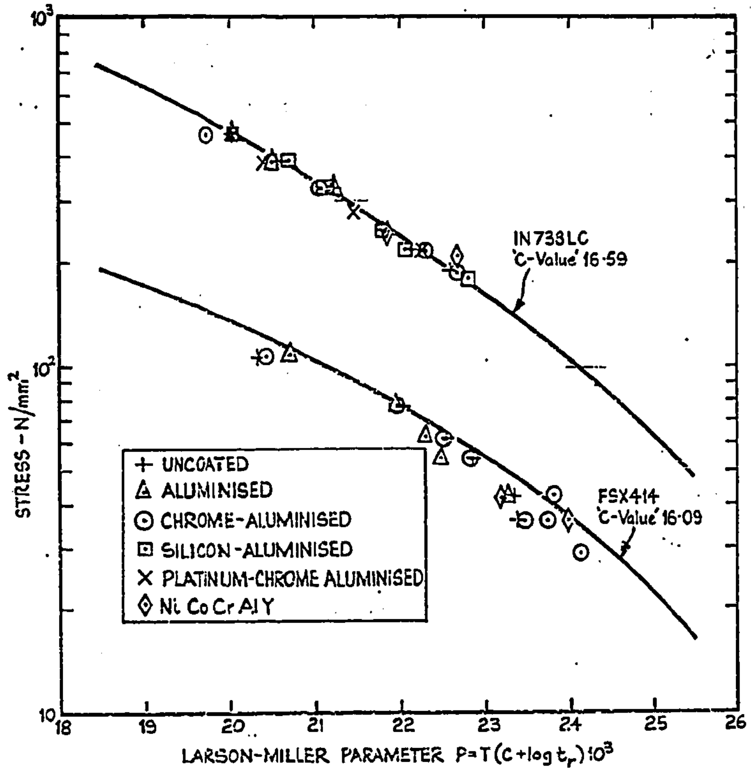

5.7 Creep/stress rupture properties of IN738LC and FSX414 in coated and uncoated conditions. (from Strang, 1979). The figure gives a feeling of the trade-off between operating temperature, stress and life. For IN738LC – an alloy widely used in gas turbines – under a stress of 100 Mpa – probably close to the one experienced at midspan of rotor blades – the maximum temperature compatible with a life of 100,000 hrs is approximately 830°C. At 300 Mpa – typical of rotor blade root conditions – such maximum temperature drops to ≈725°C.

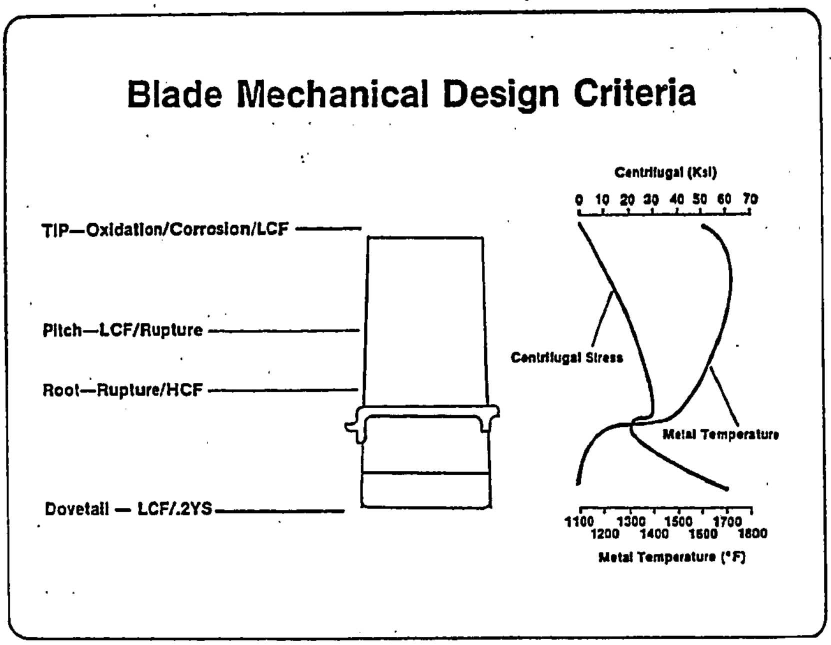

5.8 Relevant design criteria for rotor blades of military engines. The figure is taken from Anderson (1979), whose comments give an idea of the complexities of turbine blade design: "The tip of the blade is subjected to oxidation/corrosion since tip rubs occur removing protective coatings. LCF (Low Cycle Fatigue) and Thermal Fatigue is also a problem. The blade pitch is sized for rupture and LCF capability. Since complex cooling configurations can produce high thermal gradients and low life, the designer needs all the LCF margin he can get in this area. The root of the airfoil is another critical area and a good balance of rupture strength and LCF margin is essential. The dovetail area is LCF limited, but at a much lower temperature than the remainder of the airfoil".

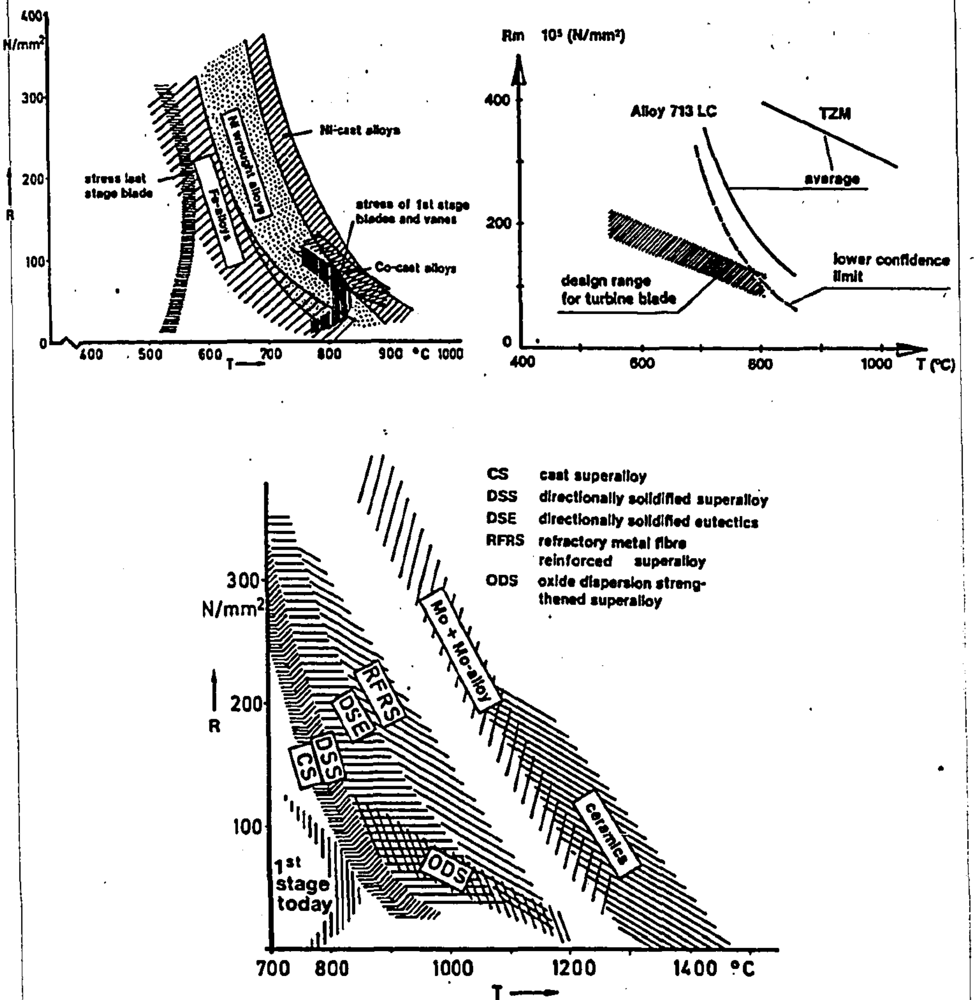

5.9 Temperature capabilities and design range of heavy-duty turbines as reported by Grünling (1979). The bottom figure shows the probable operating ranges of advanced materials. Directionally-solidified alloys are now being introduced in commercial stationary turbines.

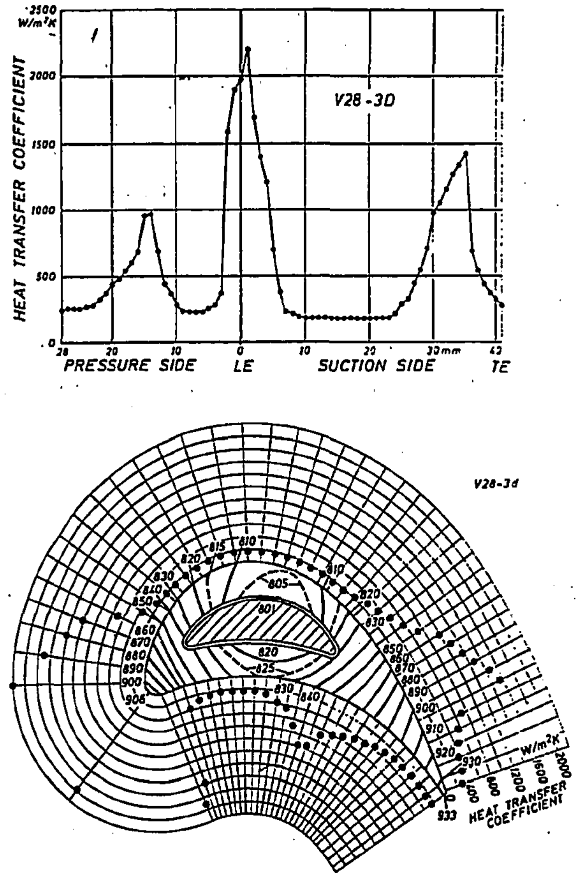

5.10 Heat transfer coefficient and temperature distribution (in Kelvin) of a convection cooled rotor blade (from Kühl, 1977). The figures refer to a single-stage turbine under the following test conditions:

Turbine inlet temperature: 1073 K
Turbine inlet pressure: 1.17 bar
Gas flow rate: 0.878 kg/s
Cooling air flow rate: 0.0469 kg/s
Rotational speed: 9480 rpm
Rotor blade inlet Re: 40,000

Assuming that St_g varies with $Re_g^{-0.37}$ (as stipulated in Eq. 5.4), the heat transfer coefficient of actual blades operating at 10-15 bar ($Re \approx 4\text{-}6 \cdot 10^5$) will be in the range 1-8 kW/m²-K.

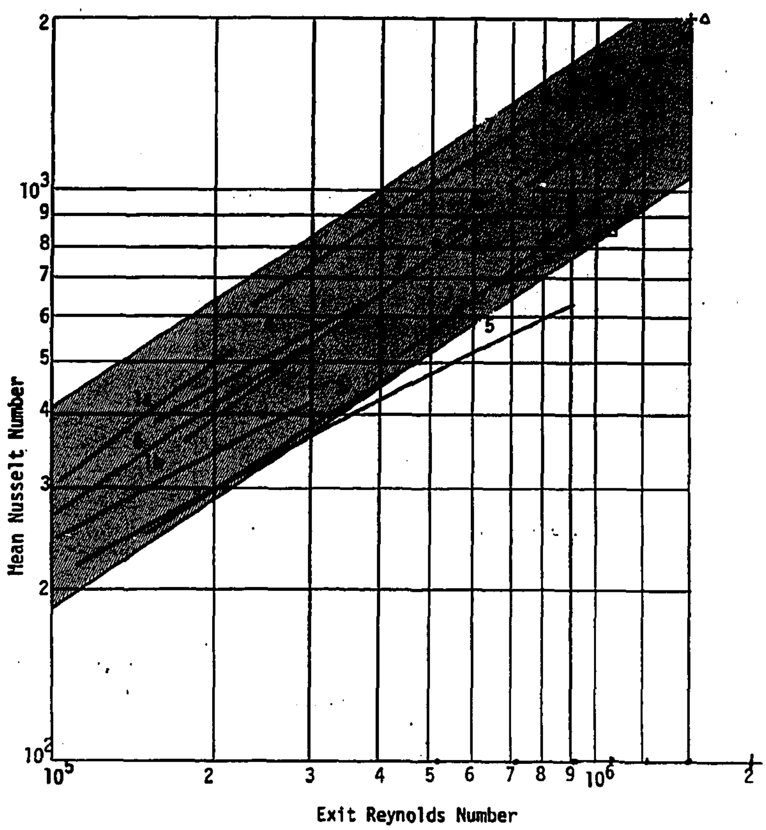

5.11a Summary given by Louis (1977) of the correlations for the average cascade Nu developed by various investigators.
1 - Ainley (1953, 1a-turbine, 1b-cascade)
2 - Wilson and Pope (1954)
3 - Hodge (1960)
4 - Bammert and Hahnemann (1951)
5 - Andrews and Bradley (1957)
6 - Fray and Barnes (1965)
7 - Halls (1967)
8 - Turner (1971)
9 - Louis (1977)

The source of each correlation can be found in Louis (1977). The shaded area represents the range spanned by Eq.(5.2a):

$$Nu = K \cdot Re^{0.63} \qquad 0.135 \leq K \leq 0.285$$

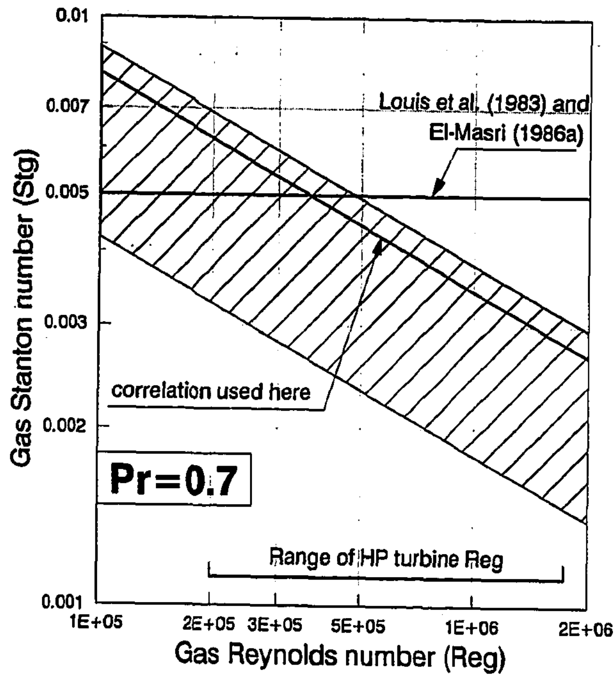

5.11b Correlation between St_g and Re_g given by Eq.(5.5a) (shaded area) and by Eq.(5.5b) (line corresponding to K=0.258) for Pr_g=0.7.

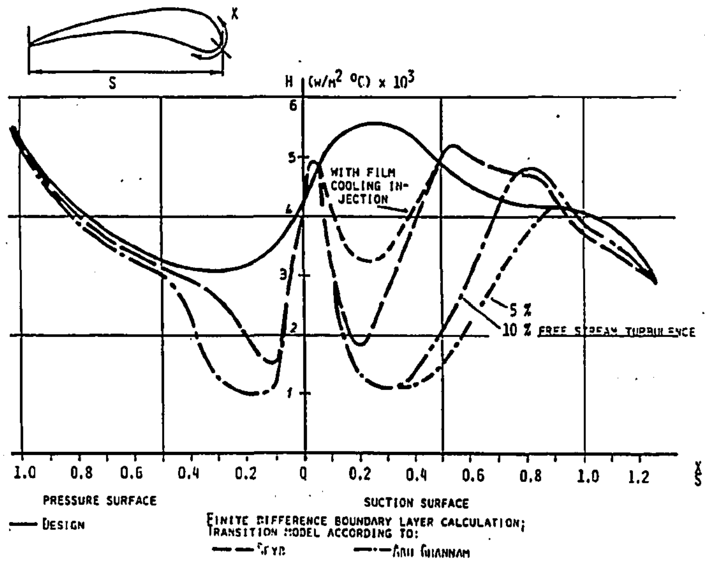

5.12 Calculated gas-side heat transfer coefficient for the vane of an actual ABB GT8 turbine (from Graf, 1985). The turbine pressure ratio is 16.3 and TIT≈1180°C.

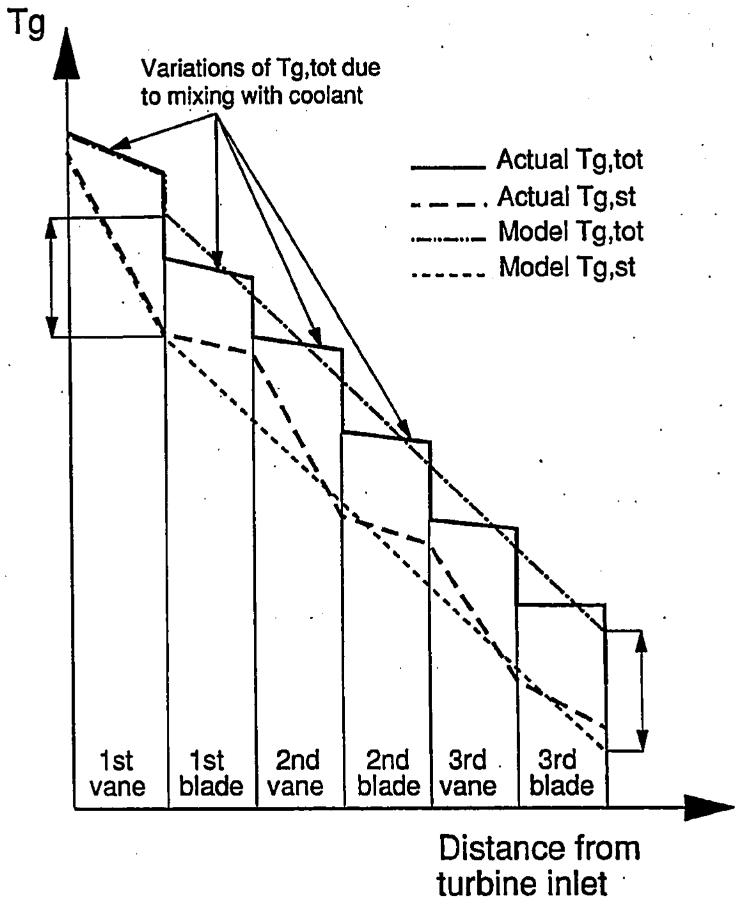

5.13 Actual and calculated temperature profiles. Within each row, the actual $T_{g,tot}$ varies only due to heat transfer and mixing, and in an uncooled turbine it would be constant. In the model, $T_{g,st}$ is the outcome of the step-by-step process shown in Fig. 3.3, while $T_{g,tot}$ is calculated by adding the constant term $[(T_{g,tot}-T_{g,st})_{nz}+(T_{g,tot}-T_{g,st})_{ct}]/2$appearing in Eq.(5.7).

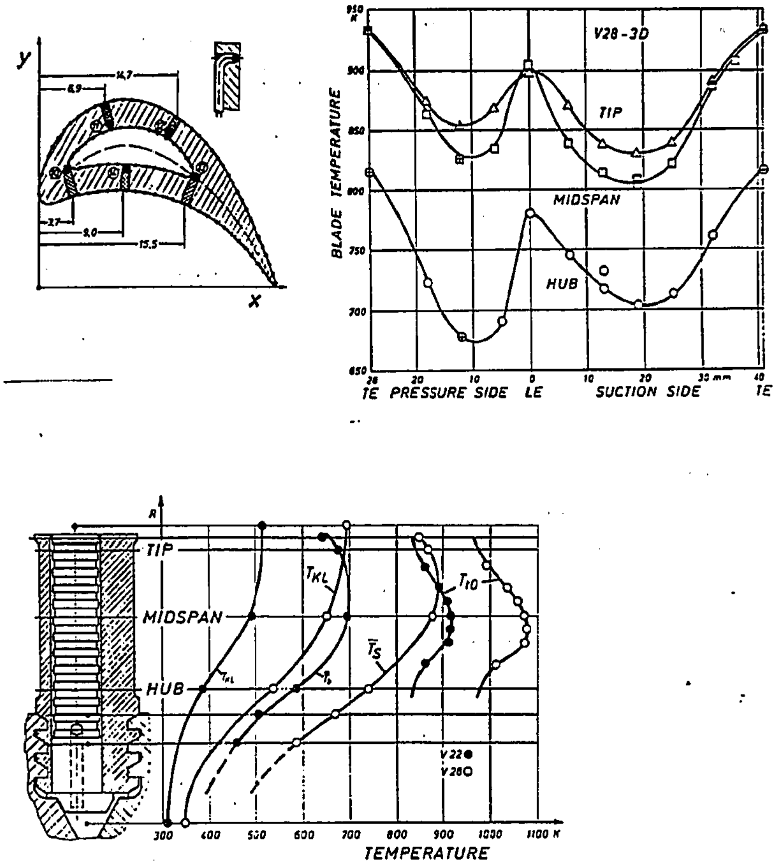

5.14 Spanwise variations of coolant temperature (T_{KL}), blade temperature (T_S) and gas total temperature (T_{t0}) in a rotor blade with one single-pass cooling channel (from Kuhl, 1977). V28 refers to the same test conditions listed for Fig. 5.10. The coolant flows from the hub to the blade tip.

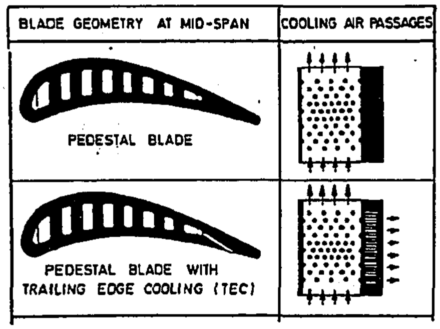

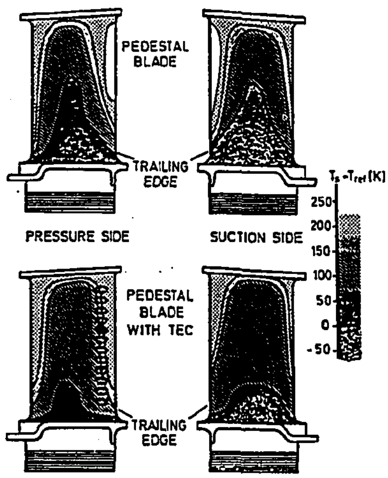

5.15 Measured surface temperatures – based on actual engine test runs – of two rotor blades with single-pass cooling channels (from Köhler et al., 1977). The pressure and suction side are connected by "pedestals" (pins) to enhance internal heat transfer; trailing edge cooling (TEC) is accomplished by a row of holes (spacing 2 diameters) discharging cooling air on the pressure side. In both cases the coolant flows from hub to tip.

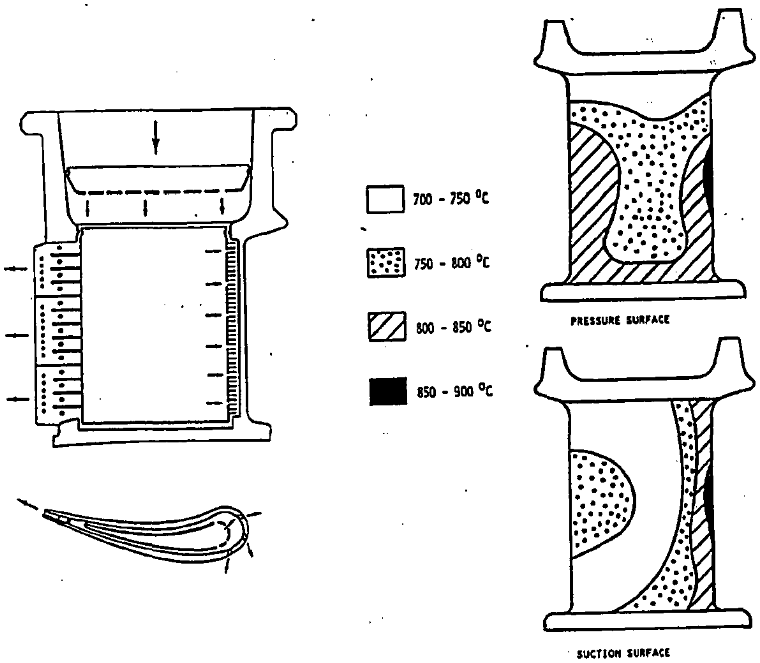

5.16 Temperature distribution at the surface of the vane tested by Graf (1985) under the following conditions:
Gas/coolant temperature ratio ($T_g/T_{cl,in}$): 2.1
Gas inlet pressure: 14.3 bar
Gas exit pressure: 9.0 bar
Gas exit Mach number: 0.84
Gas exit Re based on chord length (Re_{ge}): 2.6 106
Coolant inlet pressure: 15.4 bar
Coolant/gas mass flow ratio (m_{clb}/m_g): 0.045
The lower suction side temperatures can be explained in terms of the three film-cooling slots at the leading edge.

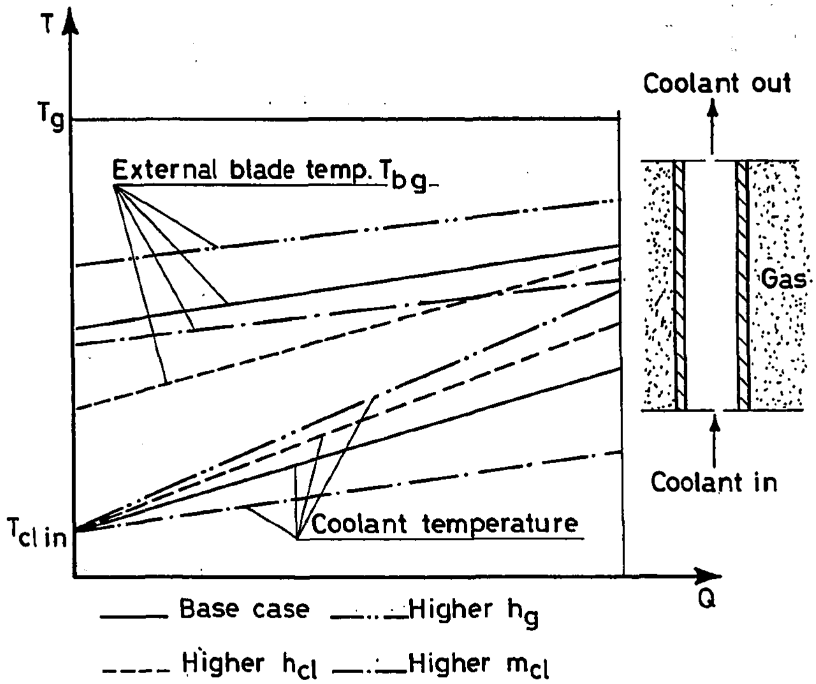

5.17 Qualitative temperature diagrams of a heat exchanger with constant hot fluid temperature.
Solid lines - base situation
Dashed lines - higher cold-side heat transfer coefficient
Dotted lines - higher hot-side heat transfer coefficient
Dash-dot lines - higher coolant flow rate
For a given geometry, the coolant flow rate necessary to maintain the wall temperature below a certain limit T_{bmx} depends on the internal and external heat transfer, as well as on the inlet hot and cold fluid temperatures.

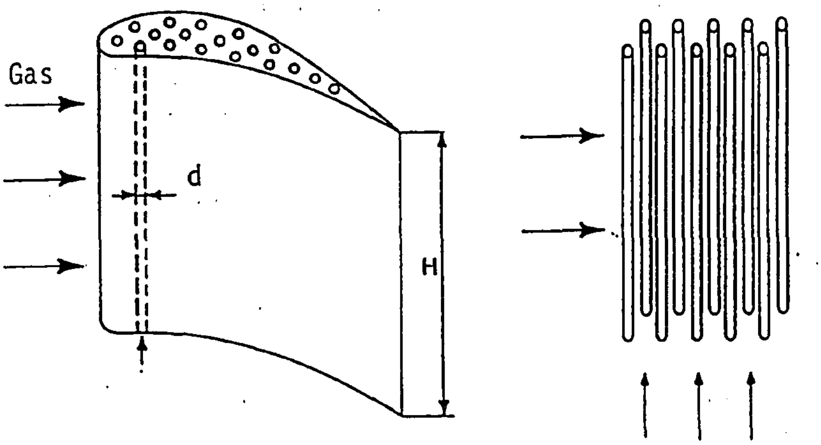

5.18 Geometry of the cooling channels considered in the analysis of convection cooling. Within each blade there are n_{ch} circular cooling channels with hydraulic diameter d and shape factor ψ_d, each consisting of n_p passes. Each pass goes from hub to tip and has a length equal to the blade height H. The cross-section of each blade will have $n_{ch} \cdot n_p$ "holes", with a total cross-section which is a constant fraction of the chord squared, i.e.:

$$n_{ch} \cdot n_p \cdot \psi_d \cdot (\pi \cdot d^2/4) = \alpha_h \cdot c^2$$

where α_h is a constant. The surface of each channel is n_p times the area of one straight channel with length equal to the blade height, i.e. $n_p \cdot \psi_d \cdot \pi \cdot d \cdot H$.

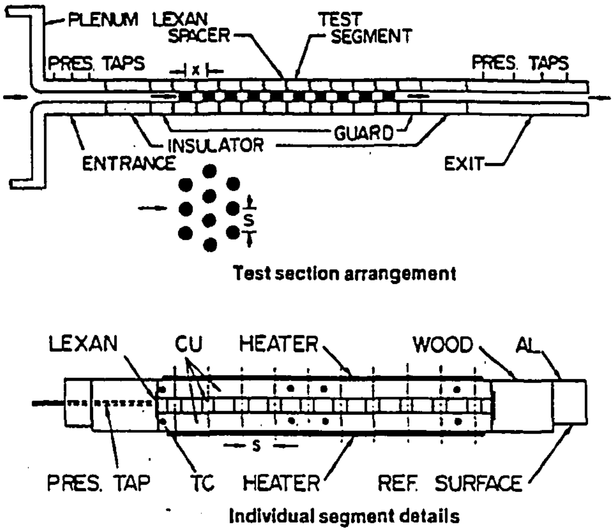

5.19 Geometry of the rectangular duct with staggered arrays of pin fins tested by Metzger, Berry and Bronson (1982). This configuration is close to the one often adopted in the trailing edge region of turbine blades (Fig. 5.5). Experiments show that compared to an identical rectangular duct with no pins the internal heat transfer coefficient increases 3.5-3.9 times, while the overall pressure drop is more than 50 times higher. Heat transfer tends to increase at lower ratios of pin row spacing to pin diameter (X/D).

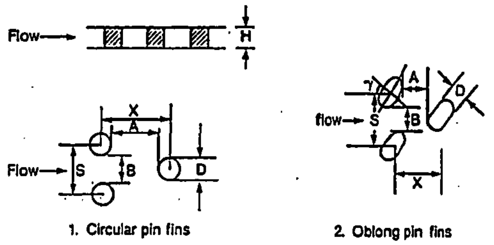

PIN FIN ARRAY NOMENCLATURE

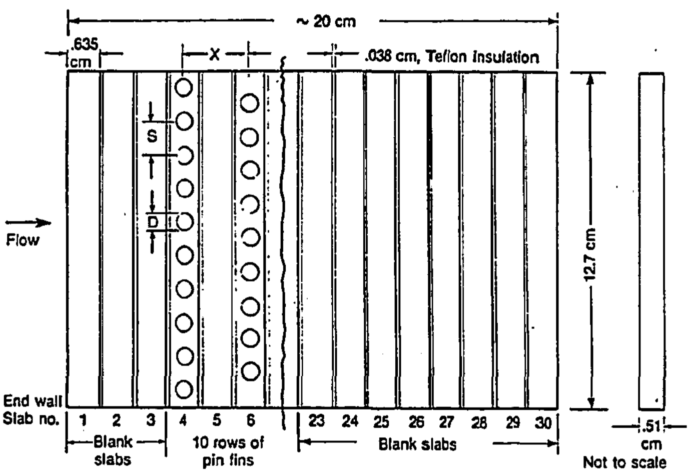

TEST SECTION GEOMETRIC SET UP

5.20 Geometry of the rectangular duct with in-line arrays of pin fins tested by Arora and Abdel Messeh (1985). Experiments show that compared to an identical rectangular duct with no pins the internal heat transfer coefficient increases 3-3.3 times, while the overall pressure drop is about 25 times higher. Oblong pins with the major axis aligned with the direction of the flow result in higher heat transfer coefficients and lower friction factors. For different orientations, oblong pins do not provide any significant advantage over the circular ones.

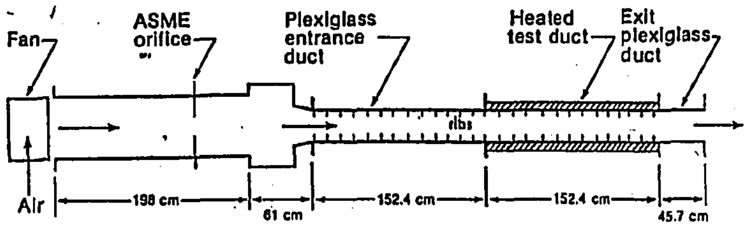

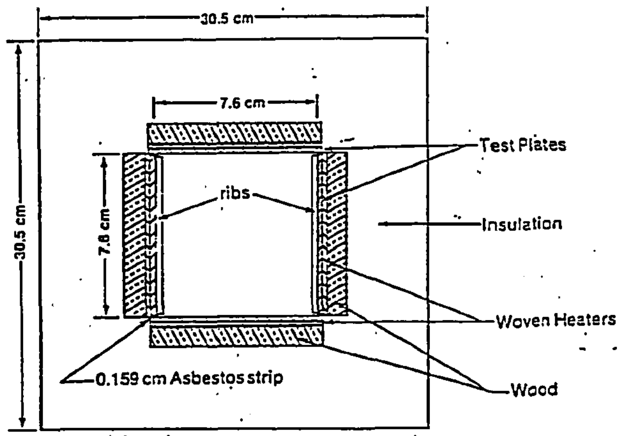

Cross-section of test duct

5.21 Geometry of the square duct with two opposite rib-roughened walls tested by Han (1984) and Han, Park and Lei (1984 and 1985). The duct closely approximates the ones adopted in the midchord region of modern gas turbine blades (Fig. 5.5), where it is beneficial to increase the heat transfer coefficient only on two sides of the duct. Experiments reveal that - depending upon rib spacing, angle of attack and Reynolds number - the heat transfer coefficient of the ribbed-side wall is about 1.5-3 times that of the four sided smooth duct. The heat transfer coefficient of the smooth side wall was also enhanced by 30-80% due to the presence of the ribs on the adjacent walls. The average friction factor was increased about 3 to 10 times. Best performances are obtained with rib angles of attack of 30° and 45°.

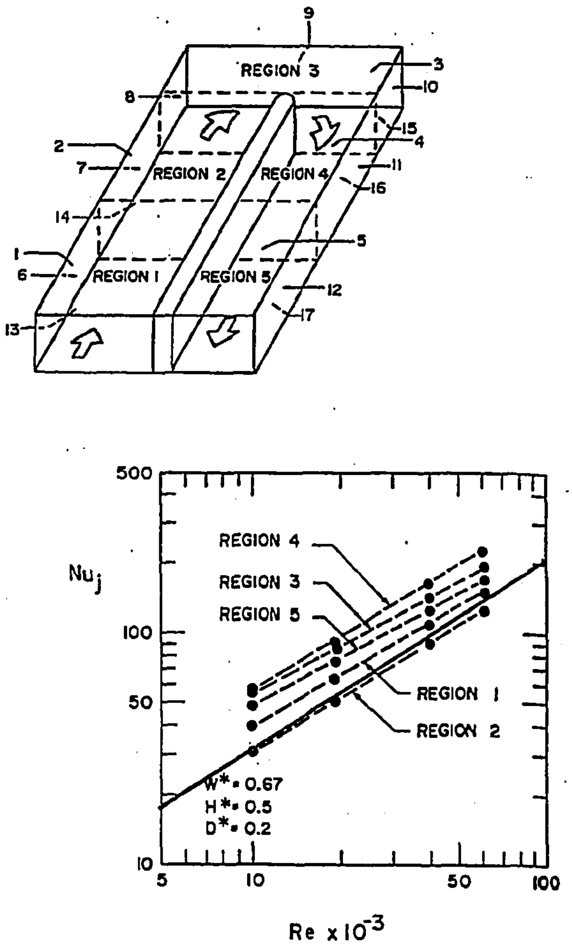

5.22 Schematic geometry and average Nusselt number for the sharp 180° turn tested by Metzger and Sahm (1985). All walls, except the dividing center wall, are heated and maintained at the same temperature. The authors have correlated their results with air heating for $10^4 \le Re \le 6 \cdot 10^4$ as:
$Nu_{m,j} = B1 \cdot Re^{B2}$
where subscript j indicates the region shown above and Re is defined on the basis of the hydraulic diameter of the inlet channel. The constants B1 and B2 depend upon the flow region, wall spacing and end clearance. For comparison, the Re-Nu diagram also includes the values predicted by the Colburn equation for Pr=0.7, showing that the heat transfer in the 180° turn is about 30-90% higher than in a straight duct.

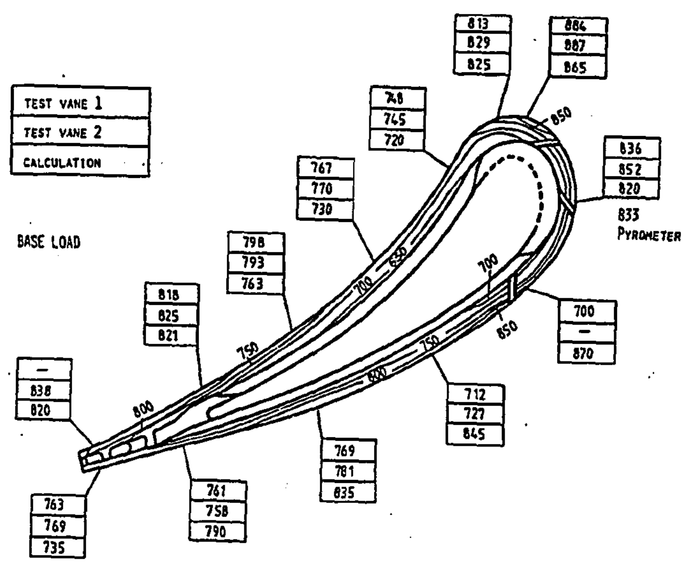

5.23 Calculated and measured wall temperatures of the first stage vane of a ABB GT8 turbine (from Graf, 1985).

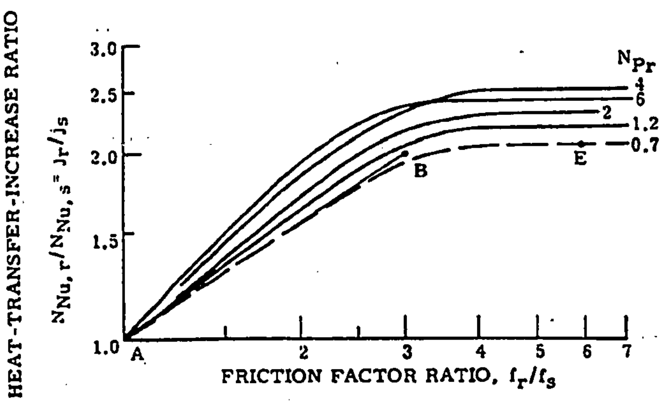

HEAT-TRANSFER EFFECT OF SAND-GRAIN ROUGHNESS AS AFFECTED BY PRANDTL NUMBER, FOR REYNOLDS NUMBERS FROM 10,000 TO 200,000 (AND PERHAPS MORE)

5.24 Heat transfer and friction augmentation in channels with sand-grain roughness and gases with Pr=0.7 as reported in Kaminski (1979). The heat transfer increase ratio and the friction factor ratio correspond to E_h and E_f, respectively. The figure shows that there is a "ceiling" to the heat transfer increase, which typically lies in the range 2-2.6.

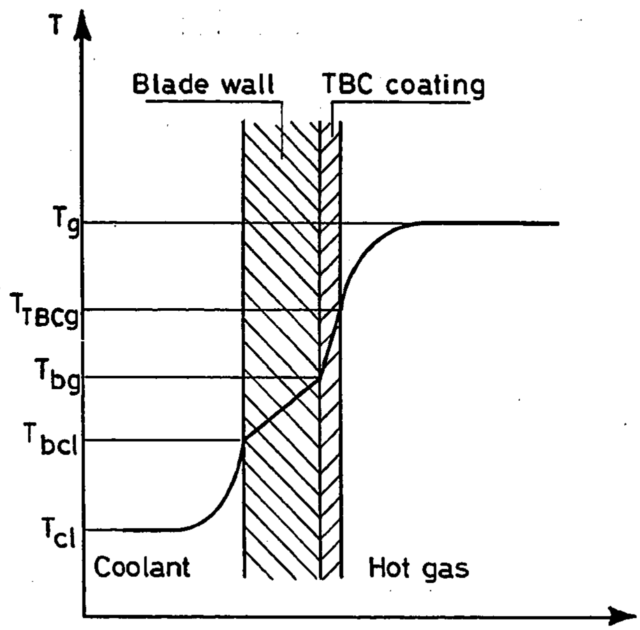

5.25 Temperature profile with Thermal Barrier Coatings (TBC). For the same T_{bg}, TBC coatings reduce the temperature difference driving the heat transfer to the blade ($T_g - T_{TBCg}$), thus reducing the heat flux and the required cooling flow.

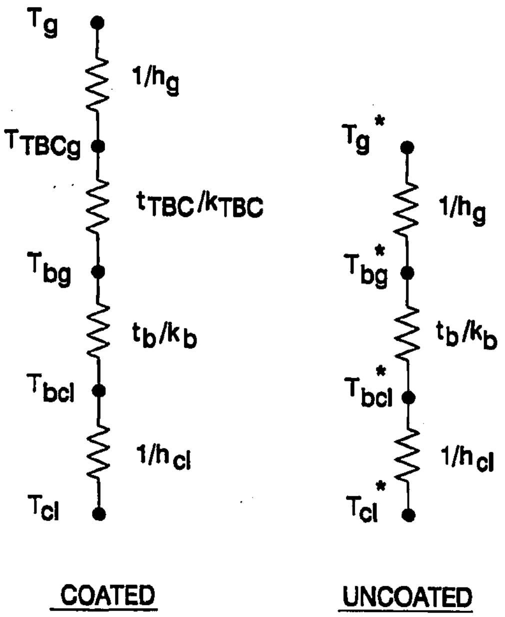

5.26 Electric analogue of coated and uncoated cooled surfaces.

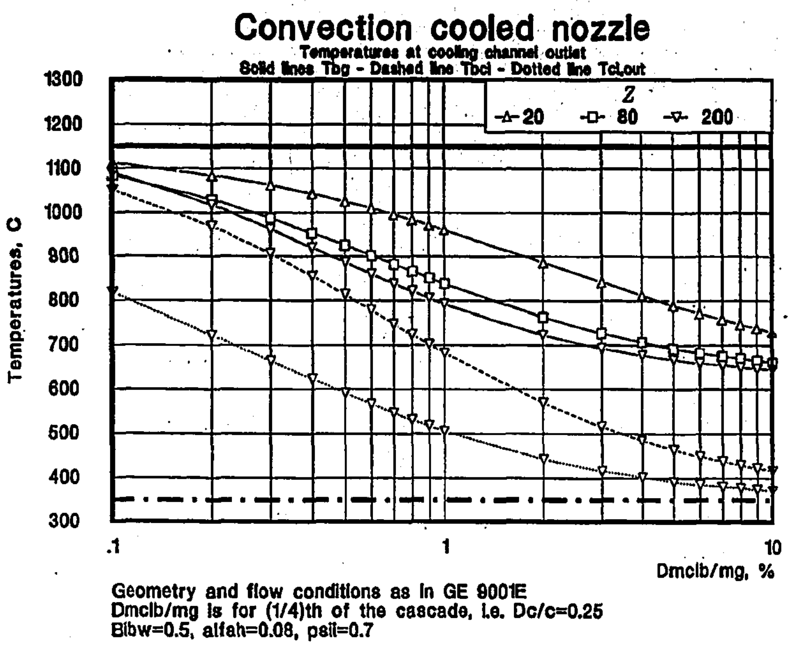

5.27 T_{bg} at the cooling channel outlet vs. $\Delta m_{clb}/m_g$ for a convection cooled nozzle subject to the following operating conditions:

T_{gr}=1150°C (with λ=0), P_g=11.5 bar

$T_{cl,in}$=350°C, Bi_{bw}=0.5

Re_g=1.8·10^6, Pr_g=Pr_{cl}=0.7 (air cooling)

$\bar{c}_{p,cl}/c_{p,g}$=0.85, μ_{cl}/μ_g=0.58

$\Delta m_{clb}/m_g$ is for (1/4)th of the cascade: $\Delta c/c$=$\Delta m_{clb}/\bar{m}_{clb}$=0.25.

Stage geometry is characterized by (see App.A for details):

a_t=1.3, σ=1.25, ψ_g=0.85, H/c=0.73, Φ=2.6

These conditions are representative of current heavy-duty engines like the GE 9001E. The figure also reports $T_{bcl,out}$ and $T_{cl,out}$ corresponding to Z=50. At very low $\Delta m_{clb}/m_g$, T_{bg} may increase with Z (lines for Z=50 and Z=200 cross around $\Delta m_{clb}/m_g$=0.15%) because the higher coolant-side heat transfer increases $T_{cl,out}$ so much that the heat flux balance can be satisfied only by higher T_{bg}.

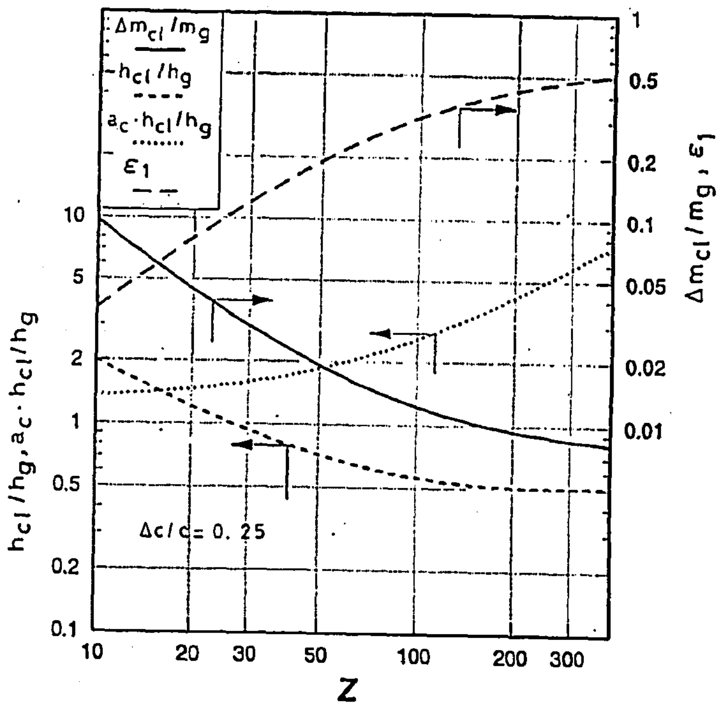

5.28 $\Delta m_{c1b}/m_g$, ε_1, h_{cl}/h_g and $a_c \cdot h_{cl}/h_g$ for a convection cooled nozzle typical of heavy-duty turbines. Δm_{c1b} refers to (1/4)th of the cascade, i.e. $\Delta m_{c1b}/\tilde{m}_{c1b} = \Delta c/c = 0.25$. All quantities refer to a situation with $\tau_{bg,out} = 1$, and to the same operating conditions and geometry of Fig. 5.27.

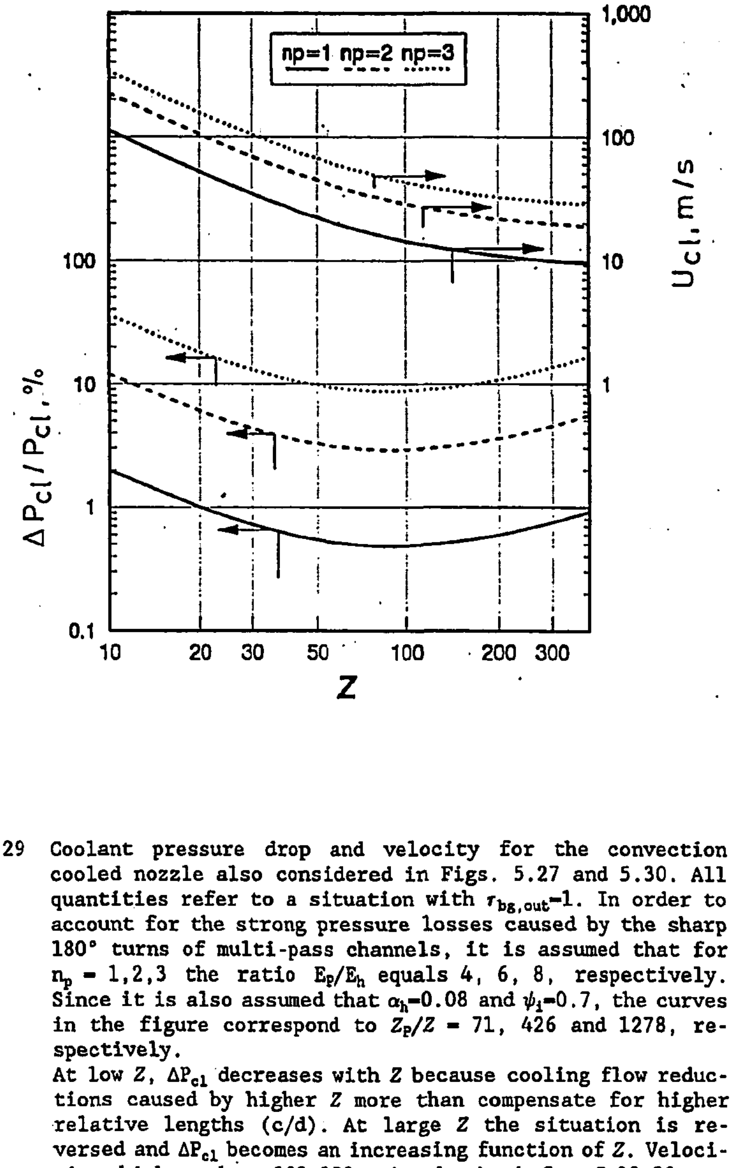

5.29 Coolant pressure drop and velocity for the convection cooled nozzle also considered in Figs. 5.27 and 5.30. All quantities refer to a situation with $r_{bg,out}$=1. In order to account for the strong pressure losses caused by the sharp 180° turns of multi-pass channels, it is assumed that for n_p = 1,2,3 the ratio E_p/E_h equals 4, 6, 8, respectively. Since it is also assumed that α_h=0.08 and ψ_i=0.7, the curves in the figure correspond to Z_p/Z = 71, 426 and 1278, respectively.
At low Z, ΔP_{cl} decreases with Z because cooling flow reductions caused by higher Z more than compensate for higher relative lengths (c/d). At large Z the situation is reversed and ΔP_{cl} becomes an increasing function of Z. Velocities higher than 100-150 m/s obtained for Z<20-30 are probably unrealistic and require a revision of the incompressible flow assumption.

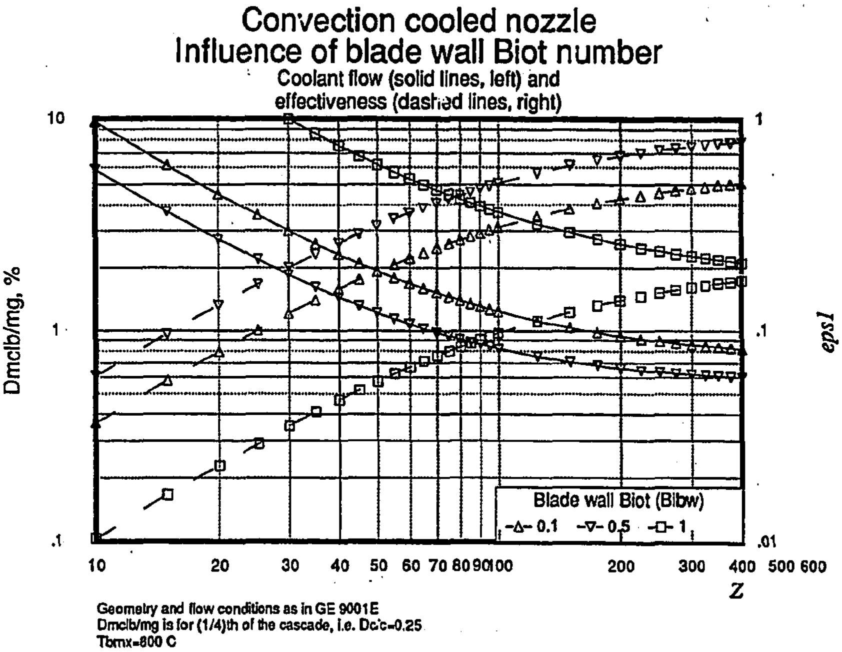

5.30 Influence of the Biot number $h_g \cdot t_{bw}/k_b$ on the coolant flow rate and the effectiveness ε_1 of the nozzle considered in Fig. 5.27. Δm_{c1b} refers to (1/4)th of the cascade, i.e. $\Delta m_{c1b}/\bar{m}_{c1b}=\Delta c/c=0.25$.

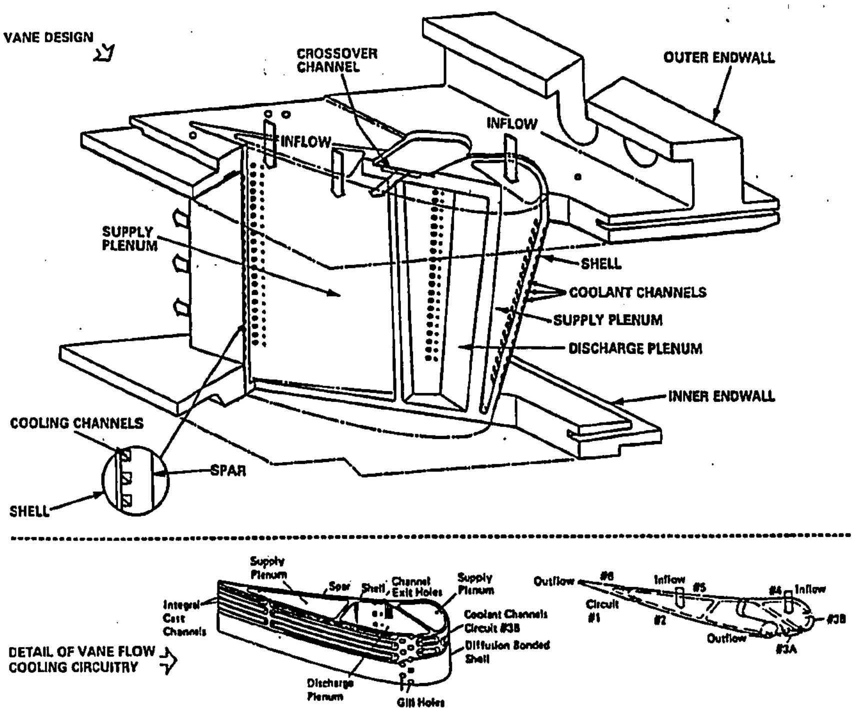

CONCEPTUAL DESIGN OF THE SHELL-SPAR ADVANCED COOLED VANE

5.31 Conceptual design of the shell-spar advanced cooled vane described by Butt and North (1985). The basic idea behind this concept is to transfer the load-bearing structure away from the external airfoil, thus allowing thinner walls and lower temperature differences across the material separating gas and coolant.

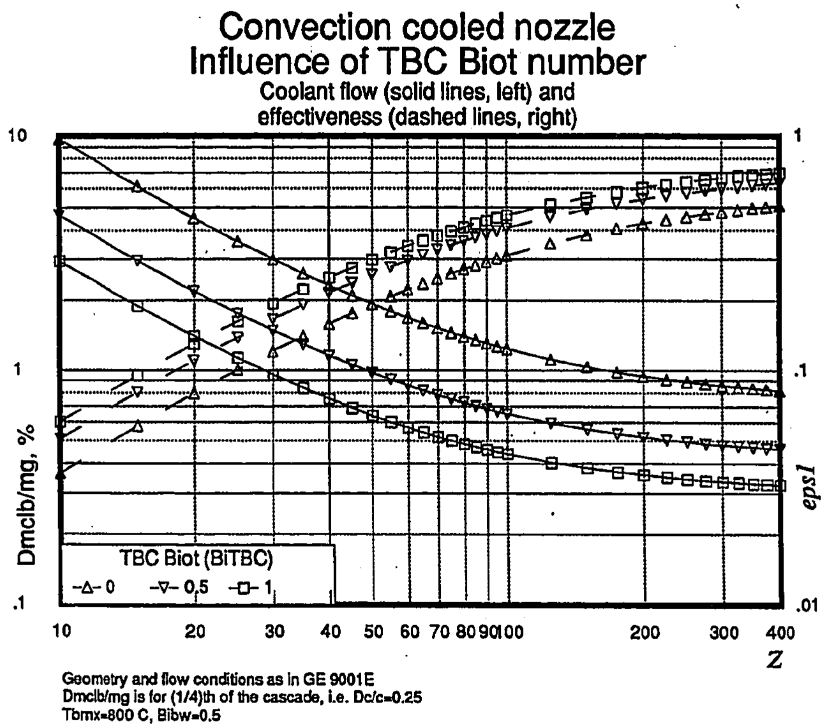

5.32 Influence of TBC Biot number $h_g \cdot t_{TBC}/k_{TBC}$ on the coolant flow rate and the effectiveness ε_1 of the nozzle considered in Fig. 5.27. As usual, Δm_{c1b} refers to (1/4)th of the cascade, i.e. $\Delta m_{c1b}/\bar{m}_{c1b}=\Delta c/c=0.25$.

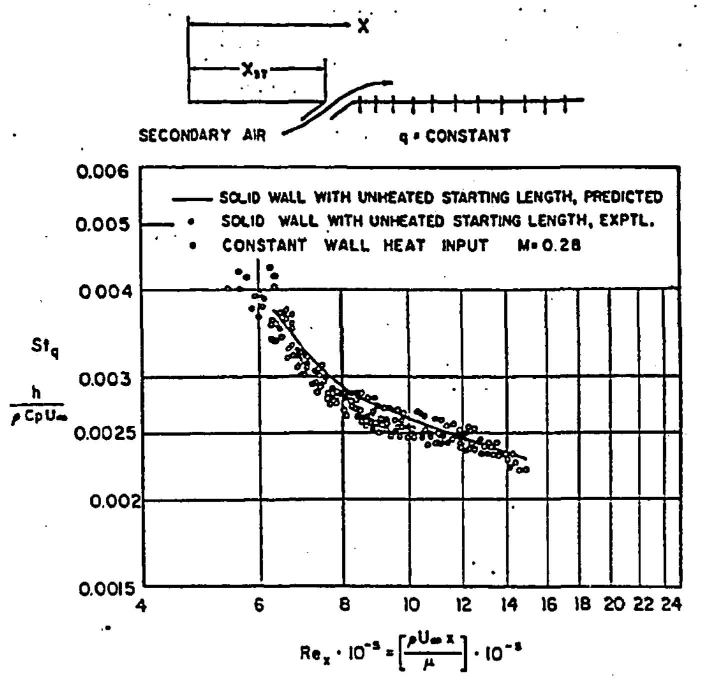

5.33 Heat transfer coefficient downstream a film cooling slot as given by Hartnett, Birkebak and Eckert (1961). "Solid wall with unheated starting length" stands for slot closed, i.e. no injection. The figure makes clear that at the conditions tested (flat plate, incompressible flow, no pressure gradients, tangential injection, M=0.28), film cooling does not alter the heat transfer coefficient.

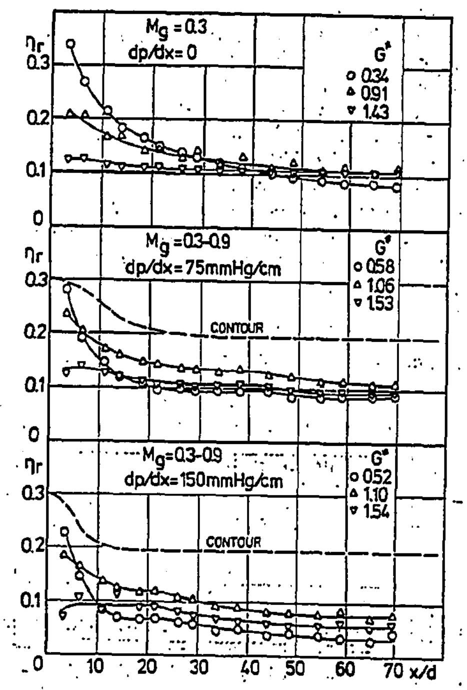

5.34 Ratio η_r between the heat transfer coefficient with and without film cooling for the flat plate with a row of circular ejection holes tested by Liess (1975). The three diagrams show the influence of the mainstream pressure gradient dp/dx. G^* is the blowing rate and M_g the mainstream Mach number. The "contour" dashed lines indicate the shape of the converging channel used to generate the pressure gradients; on the ordinate axis of h^* they have no meaning. The figure confirms that the influence of film cooling on h is fairly limited.

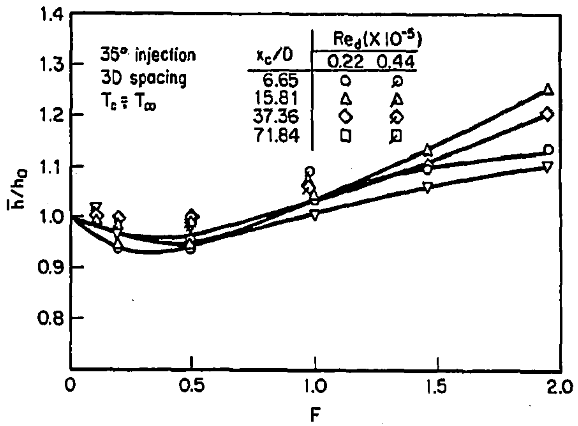

5.35 Influence of the blowing rate on the heat transfer coefficient for the single row of holes tested by Eriksen and Goldstein (1974).

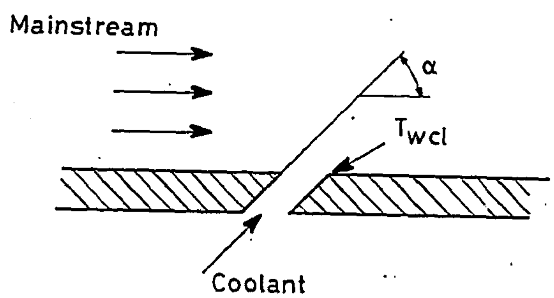

5.36 **Film cooling geometry.**

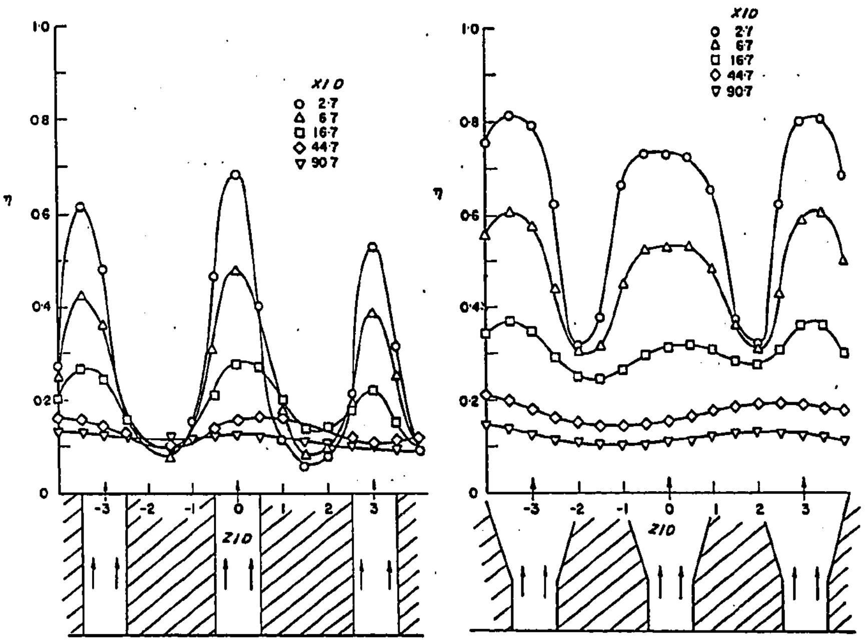

5.37 Lateral variation of film cooling effectiveness for air injection through a row of cyclindrical (left) and shaped (right) holes. (from Goldstein, Eckert and Burggraf, 1974).

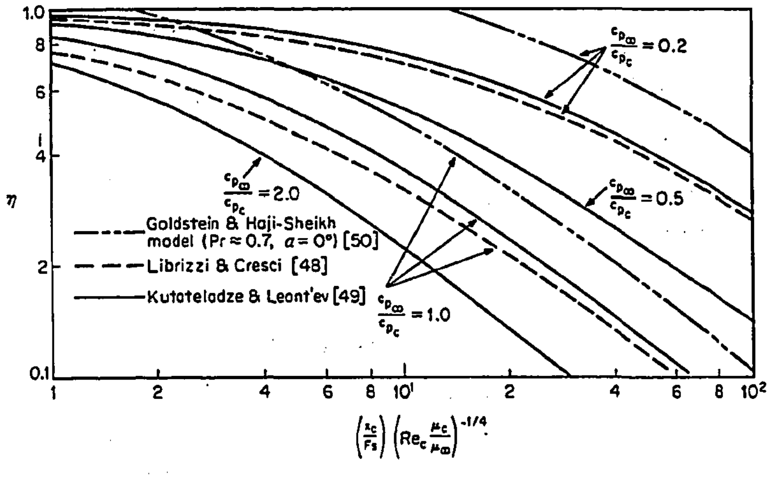

5.38 Prediction of film cooling effectiveness vs. ξ with $c_{p,g}/c_{p,cl}$ as a parameter (from Hartnett, 1985).

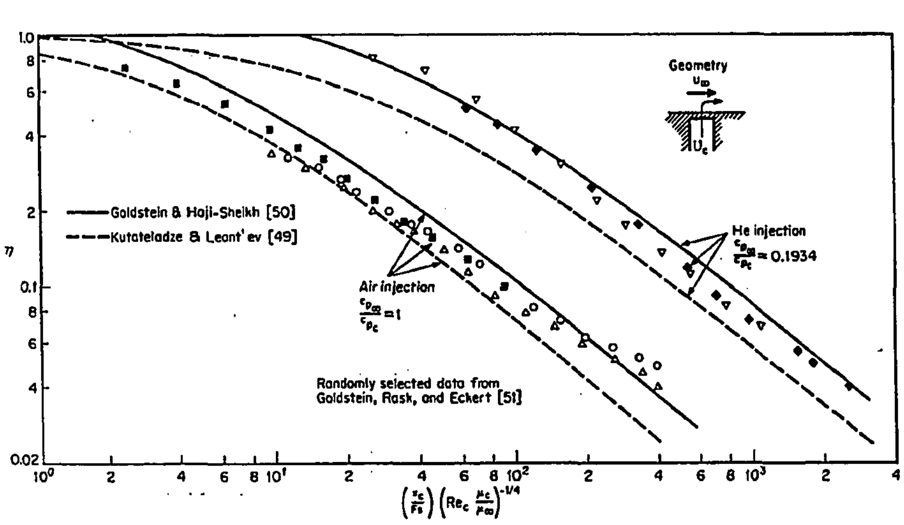

5.39 Comparison of predictions and experimental results for injection through porous slots into a subsonic flow over a flat plate (from Hartnett, 1985). Experimental data are from Goldstein, Rask and Eckert (1966).

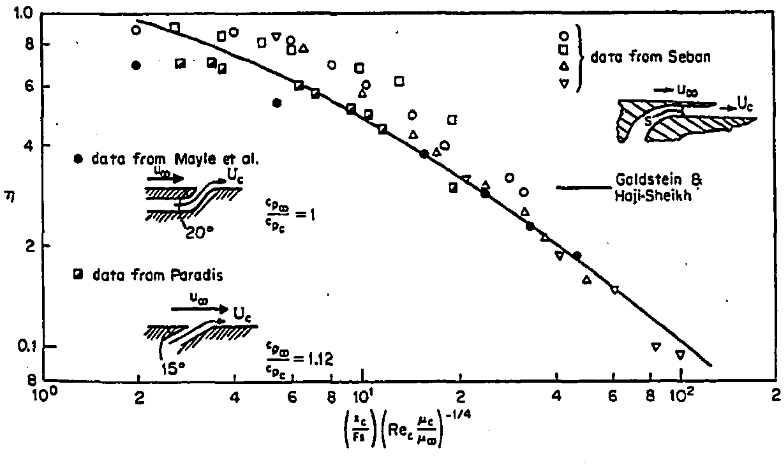

5.40 Comparison of Goldstein-Haji-Sheikh prediction with experimental results for nearly tangential injection through a slot on a flat plate in subsonic flow (from Hartnett, 1985). Experimental data are from Mayle et al. (1977), Seban (1960), Seban and Back (1962), Paradis M.A. (1977).

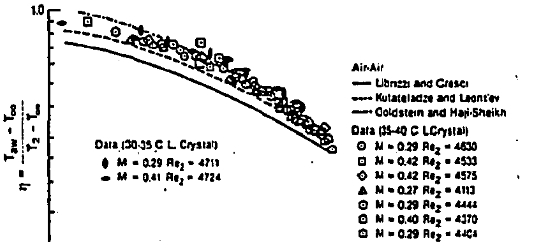

Film cooling effectiveness for air-air.

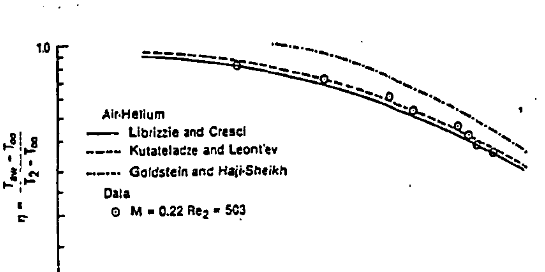

Film cooling effectiveness for air-helium.

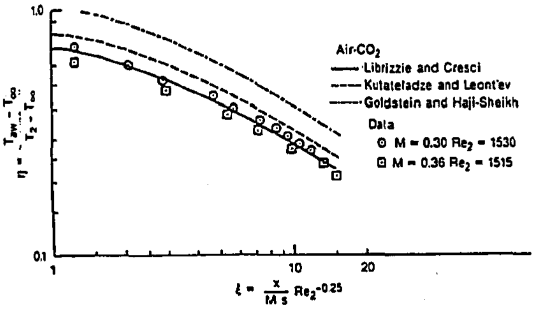

Film cooling effectiveness for air-carbon dioxide (CO_2).

5.41 Comparison between experimental data and film cooling effectiveness predictions (from Abuaf and Cohn, 1988).

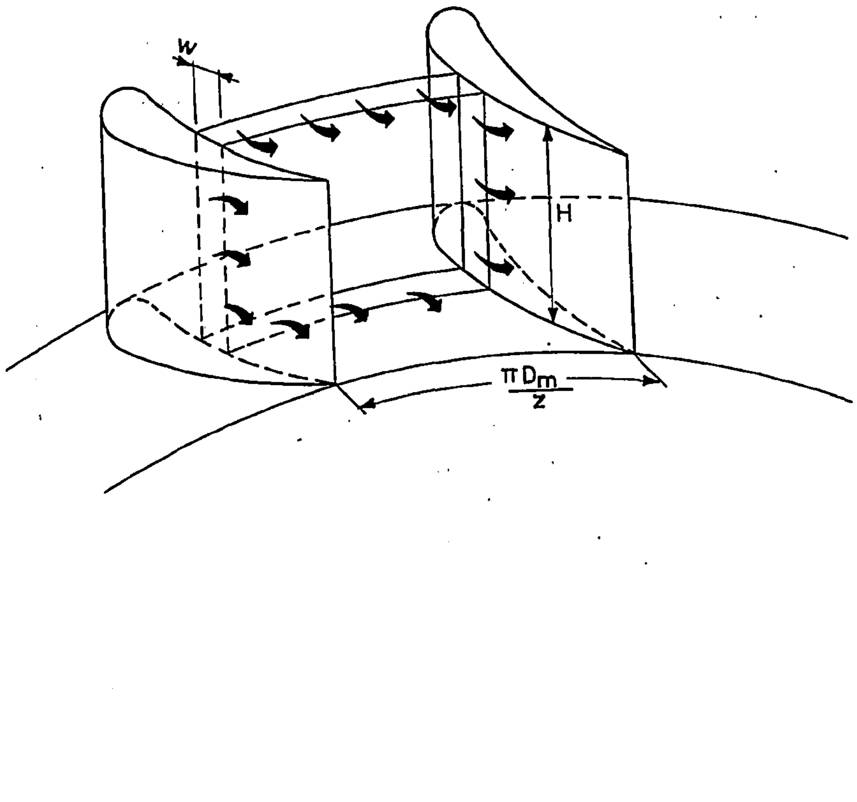

5.42 Constant-width film cooling slots considered in the present model. The cooling flow approximately corresponds to a continuous slot extending along the whole perimeter of the gas cross-section.

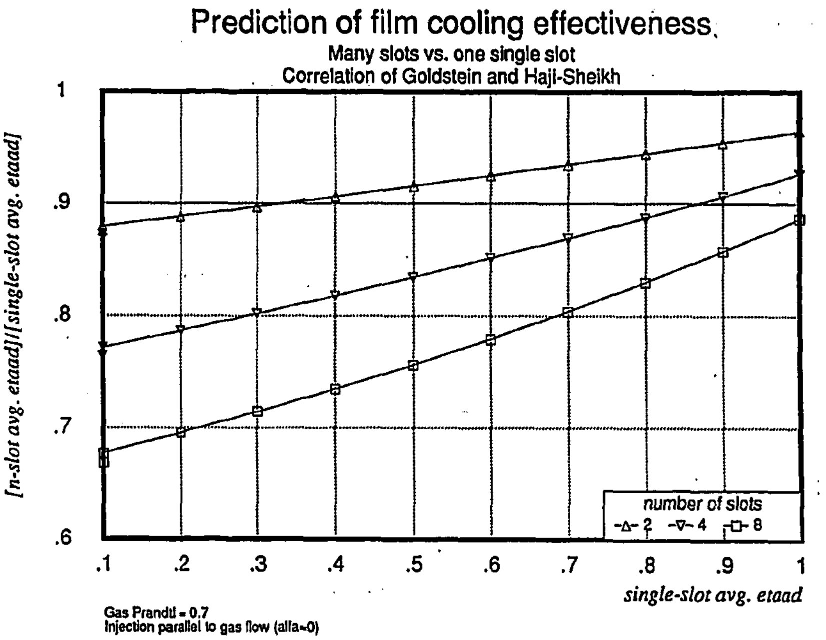

5.43 Ratio $\bar{\eta}_{ad,k}/\bar{\eta}_{ad}$ between the average film cooling effectiveness of n_{sl} closely-spaced slots and one single slot injecting the whole coolant flow. It is assumed that each one of the "small" slots injects $\Delta m_{clb,k} = \Delta m_{clb}/n_{sl}$. The single-slot effectiveness $\bar{\eta}_{ad}$ is evaluated from (5.79) at $x=\bar{x}$; the effectiveness $\bar{\eta}_{ad,k}$ of each of the small slots is evaluated at $\bar{x}_k = \bar{x}/n_{sl}$. Substituting one slot with n_{sl} smaller slots gives lower effectiveness.

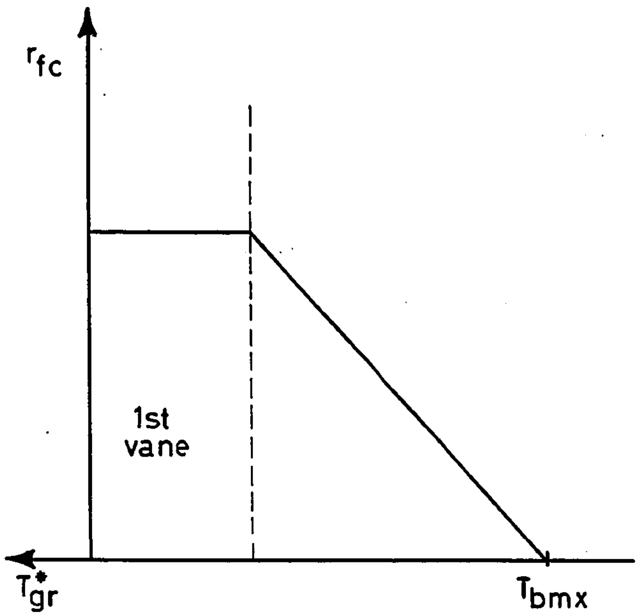

5.43a Variation of film-cooling parameter r_{fc} as a function of effective gas recovery temperature T^*_{gr}.

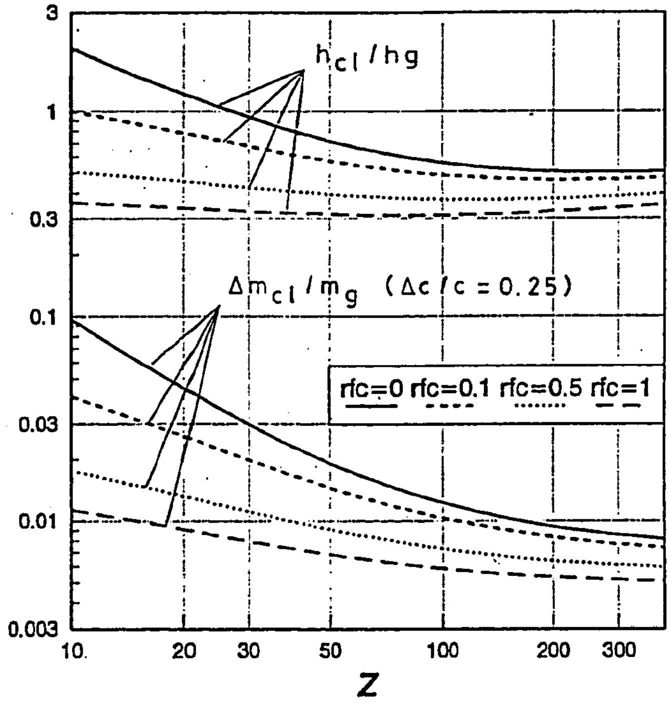

5.44 Influence of Z and r_{fc} on the cooling flow and h_{cl}/h_g of the nozzle already considered for Fig. 5.27. $\Delta m_{clb}/m_g$ is for (1/4)th of the cascade, i.e. $\Delta m_{clb}/\tilde{m}_{clb}=\Delta c/c=0.25$.

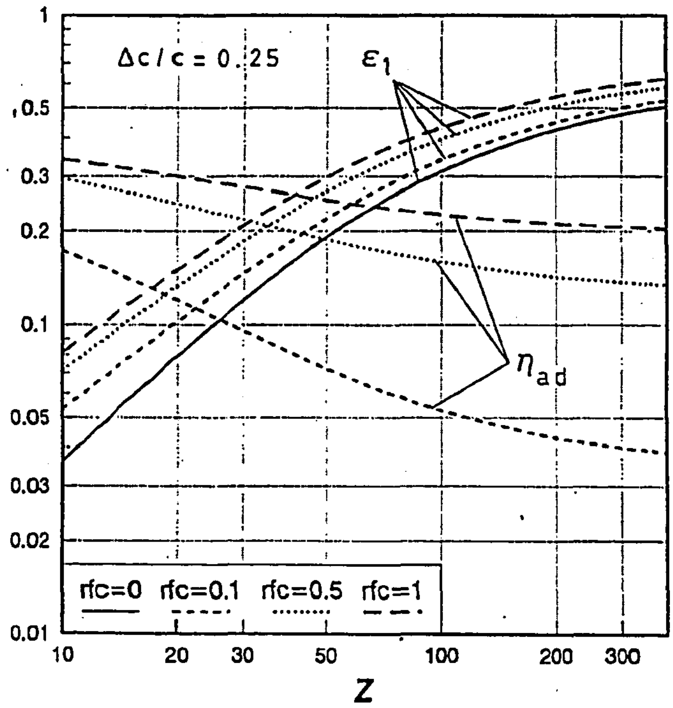

5.45 Average film cooling effectiveness $\bar{\eta}_{ad}$ and heat transfer effectiveness ε_1 for the nozzle already condidered in Fig. 5.27. Calculations refer to (1/4)th of the cascade, i.e. $\Delta m_{clb}/\bar{m}_{clb}=\Delta c/c=0.25$.

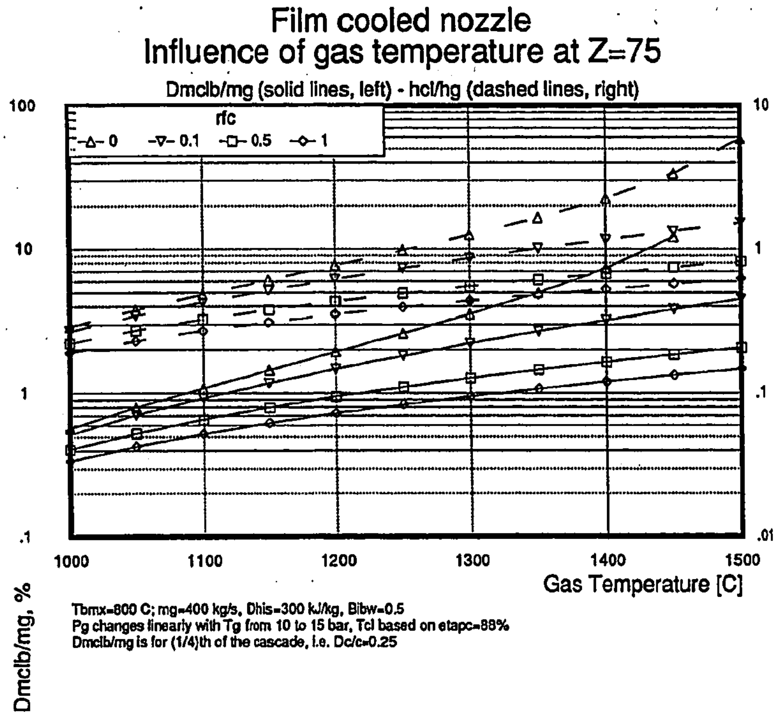

5.46 Influence of T_g and r_{fc} on $\Delta m_{clb}/m_g$ for a typical convection cooled nozzle of an heavy-duty turbine with T_{bmx}=800°C, m_g=400 m/s and first stage Δh_{is}=300 kJ/kg (Δh_{is} is used to compute SP and then D_m). In order to account for variations of the optimum pressure ratio, it is assumed that (i) P_g changes linearly from 10 to 15 bar when T_g goes from 1000 to 1500°C; (ii) P_{cl}=P_g; (iii) T_{cl} is the one resulting from a compression with η_{pc}=88%. All quantities refer to a situation with $r_{bg,out}$=1 and Z=75, a value probably correspondent to the state-of-the-art. Like in previous figures, λ=0 and Δm_{clb} is for (1/4)th of the cascade, i.e. $\Delta m_{clb}/\bar{m}_{clb}$=$\Delta c/c$=0.25.

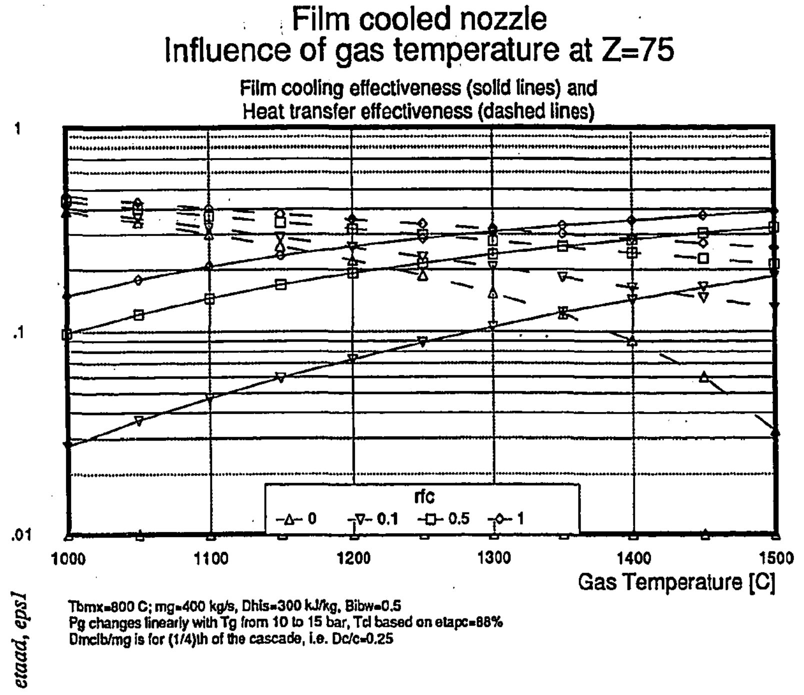

5.47 η_{ad} and ε_1 for the cooling flows depicted in Fig. 5.46.

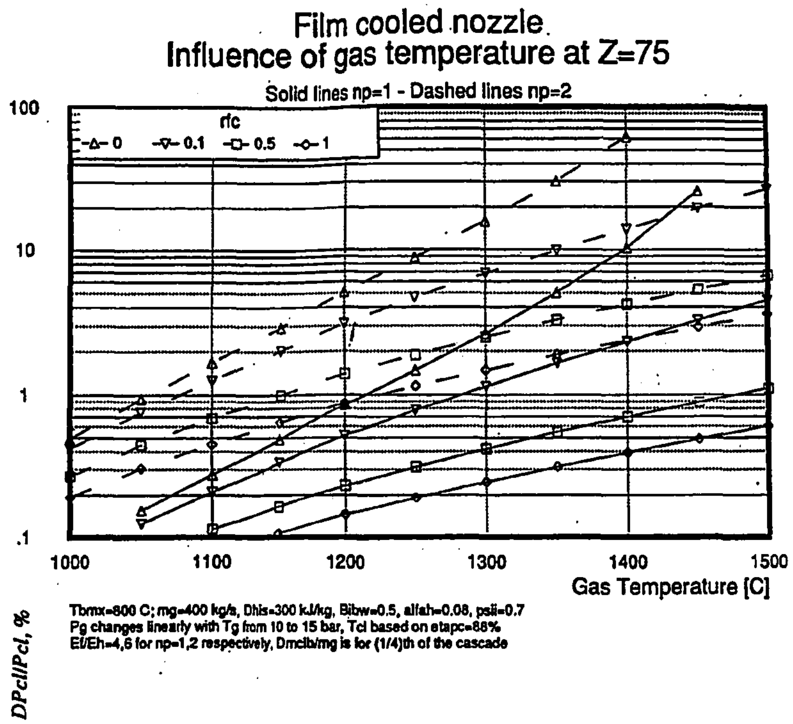

5.48 $\Delta P_{cl}/P_{cl}$ vs. T_g for the cooling flows depicted in Fig. 5.46. As already assumed in Fig. 5.29, for n_p=1,2, E_P/E_h=4,6, respectively.

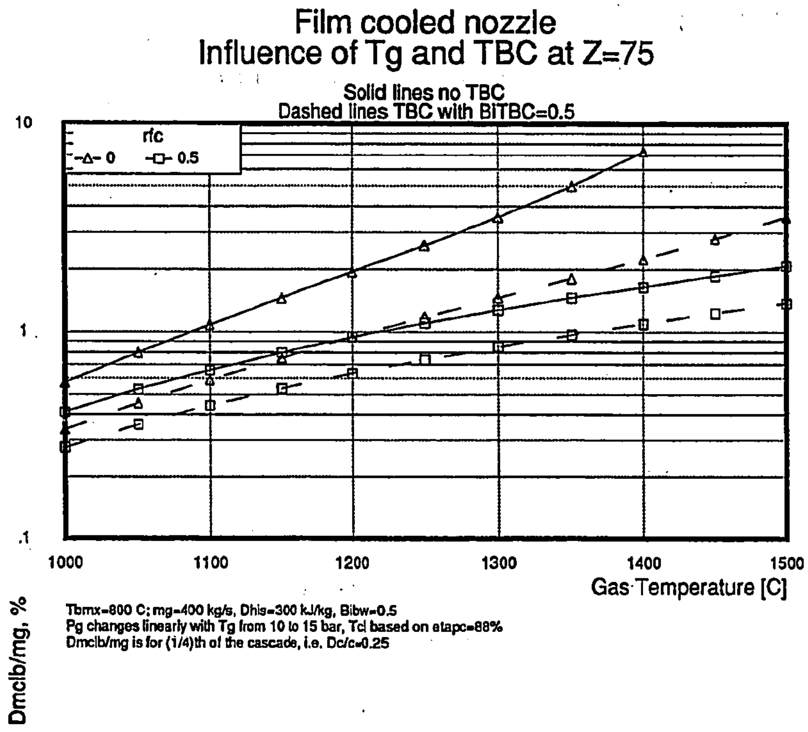

5.49 Effect of combining film cooling and TBC coatings for a nozzle operating under the same conditions used for Fig. 5.46.

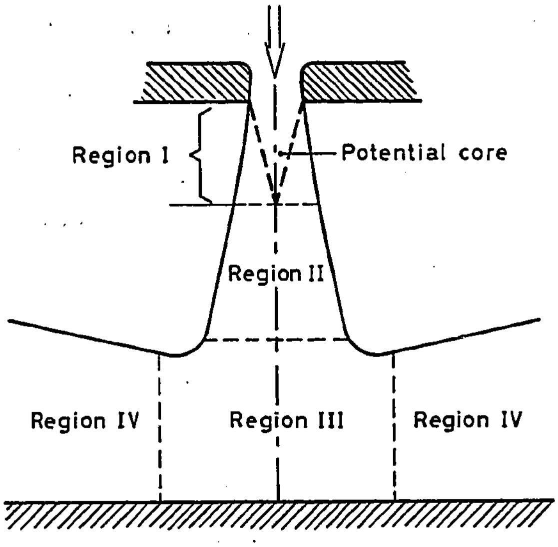

5.50 Flow regions for a jet impinging on a flat plate (Livinghood, Ellerbrock and Kaufman, 1971). Region I extends to the apex of the potential core, a central portion of the flow where the velocity remains constant and equal to the one at the nozzle exit; Region II is characterized by dissipation of the centerline velocity and by spreading of the jet in the transverse direction; Region III is the one where the jet deflects from the axial direction, while in Region IV the flow increases in thickness due the boundary layer build up along the solid surface.

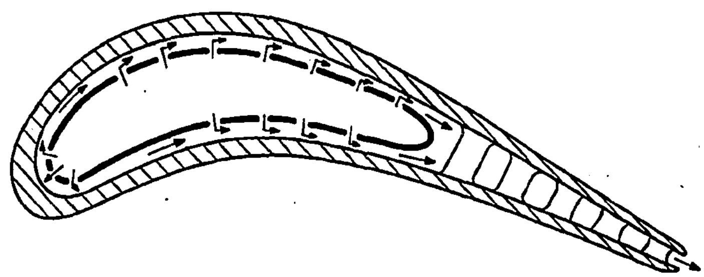

5.51 Cross-section of an impingement-cooled blade. In the mid-chord region the flow can be modeled as an array of jets impinging on a flat plate (Florschuetz et al. 1984).

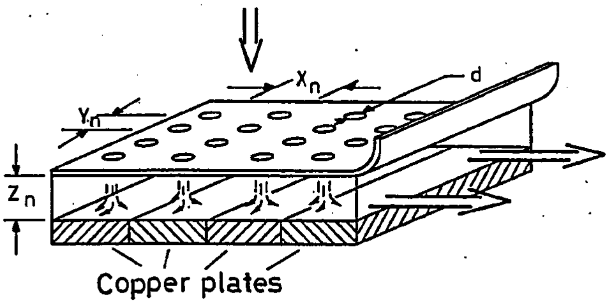

5.52 Schematics of the impingement cooling facility tested by Kercher and Tabakoff (1970). Notice the discharge of the spent flow along only one side of the plate, which creates a static pressure gradient within the enclosure at close space clearance z_n. Due to lower pressures near the exhaust end, more flow impinges on the plate to the right.

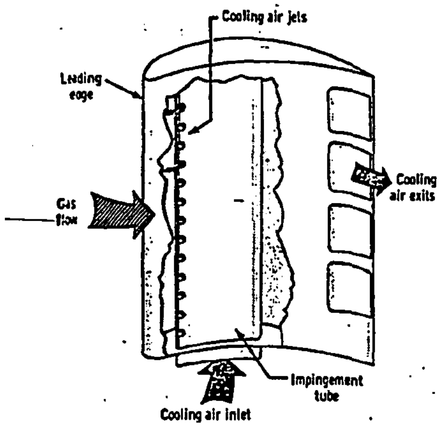

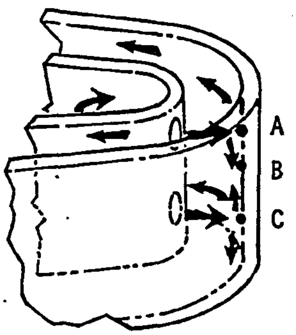

5.53 Schematic of the impingement cooled airfoil and airfoil leading edge considered by Chupp et al. (1969).

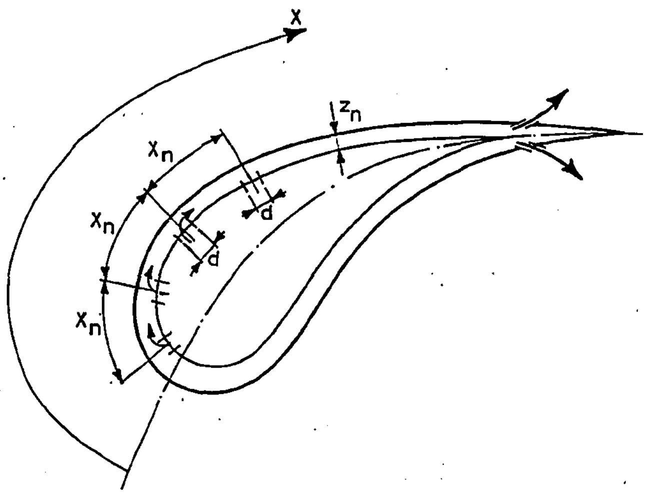

5.54 Schematic considered for the analysis of fully impingement cooled blades. It is assumed that the distribution of the cooling flow for the pressure and suction side is identical. The spent coolant flows chordwise and is all discharged at the trailing edge. Crossflow is zero at the leading edge and maximum at the trailing edge, with mass velocity $m_c(x)/(H \cdot z_n)$. The jet array is square (i.e. $x_n = y_n$), staggered, with length equal to the blade chord.

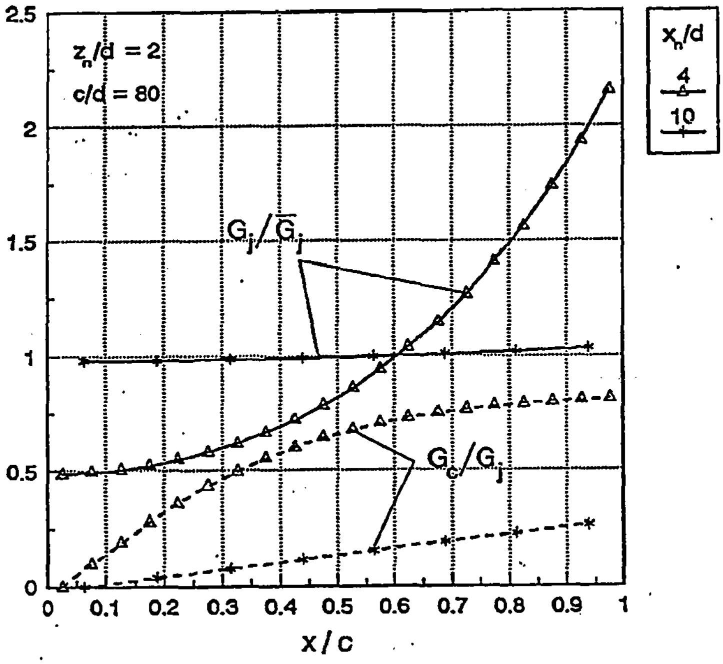

5.55 Variations of G_j and G_c as given by Eqs.(5.56) and (5.57) for C_D=0.8, c/d=100, z_n/d=2, x_n/d=4,10.

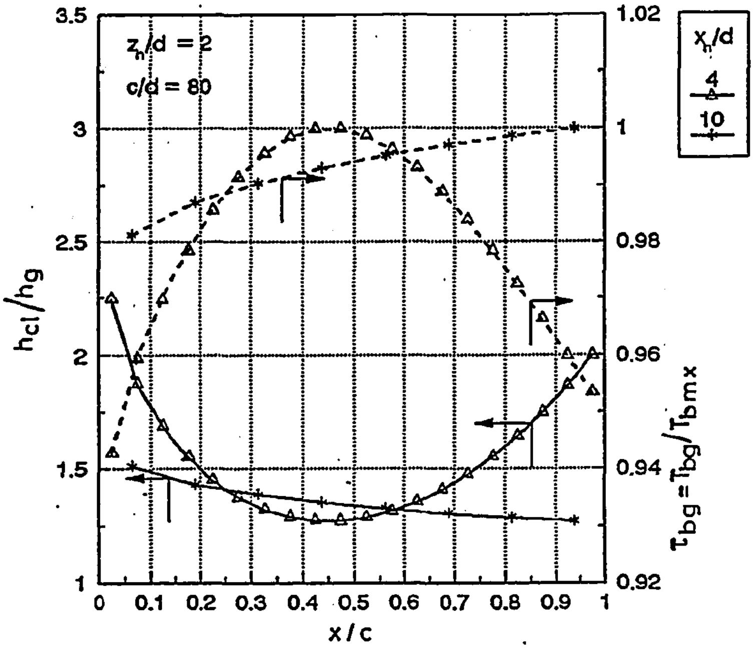

5.56 Chordwise heat transfer and temperature distribution for a fully impingement cooled nozzle operating under the same conditions assumed for Fig. 5.27. The cooling flow is the minimum value that gives $\tau_{bg} \leq 1$ at each jet row.

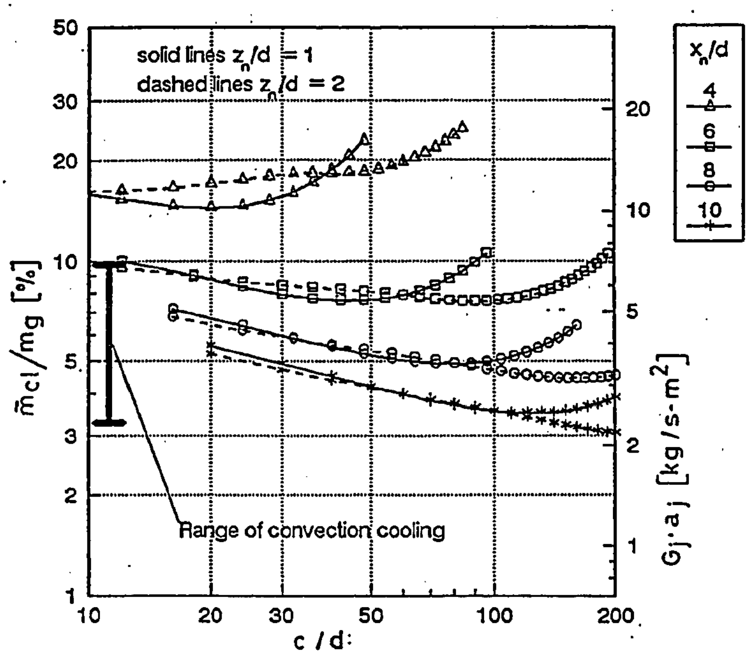

5.57 Cooling flow vs. c/d required by a fully impingement cooled nozzle operating under the same conditions assumed for Fig. 5.27. The right scale reports the flow $G_j \cdot a_j$ [kg/s-m^2] specific to the impingement cooled surface based on $m_g/(\pi \cdot H \cdot D_m)$ = 300 kg/s-m^2, a value typical of large heavy-duty engines. The range of cooling flows indicated for convection systems corresponds to the results presented in Par. 5.2.

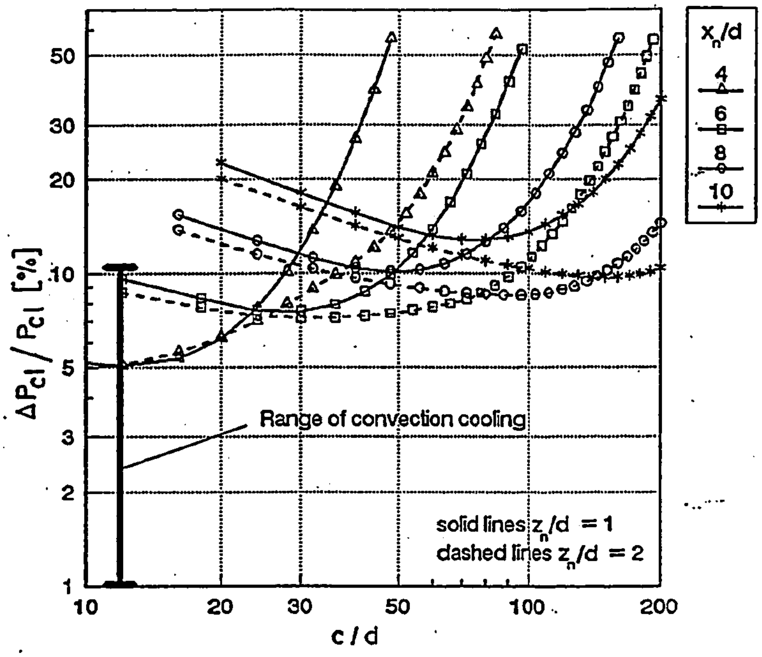

5.58 $\Delta P_{c1}/P_{c1}$ vs. c/d for the impingement cooling flows depicted in Fig. 5.57. Points with $\Delta P/P > 25$-30% are approximate, because the assumption of incompressible flow is inaccurate. $\Delta P/P > 50\%$ is unrealistic because it would imply supersonic flow.

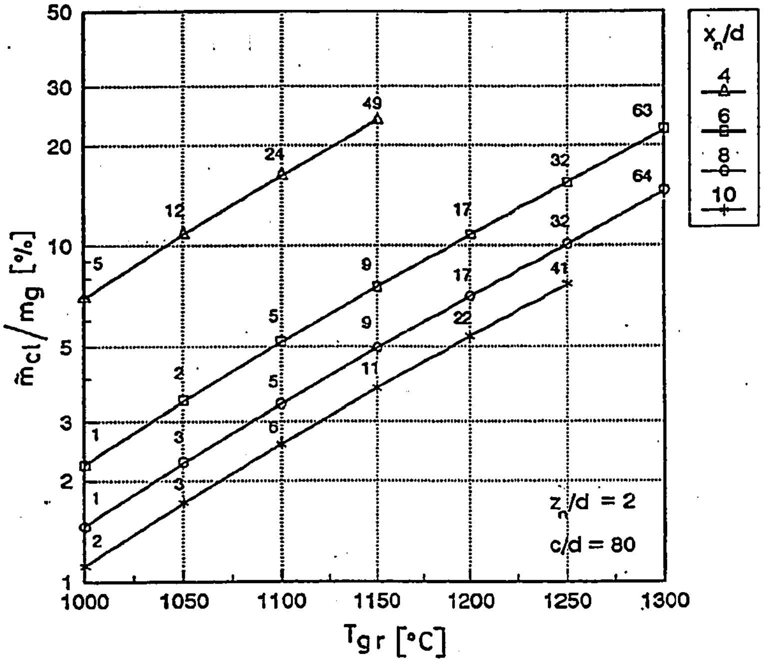

5.59 Cooling flow as a function of the gas temperature required by a fully impingement cooled nozzle. The numbers on top of each point indicate the corresponding $\Delta P_{cl}/P_{cl}$ [%]. In order to account for variations of the optimum pressure ratio, it is assumed that (i) P_g changes linearly from 10 to 13 bar when T_g goes from 1000 to 1300°C; (ii) $P_{cl}=P_g$; (iii) T_{cl} is the one resulting from a compression with $\eta_{p,c}=88\%$. Other assumtpions are: $T_{bmx}=800°C$; m_g = 400 m/s; first stage $\Delta h_{is}=300$ kJ/kg (Δh_{is} is used to compute SP and then D_m, see Par. 6.1). All quantities refer to a situation with $\tau_{bg}\leq 1$ for all jet rows and c/d=80.

PERFORMANCE PREDICTION OF GAS/STEAM CYCLES FOR POWER GENERATION

by

Stefano Consonni

VOLUME 2

A Dissertation

Presented to the Faculty

of Princeton University

in Candidacy for the Degree

of Doctor of Philosophy

Recommended for Acceptance

by the Department of

Mechanical and Aerospace Engineering

June, 1992

PLEASE NOTE

Page(s) missing in number only; text follows.
Filmed as received.

ii

University Microfilms International

TABLE OF CONTENTS

VOLUME 1

(.. cont. table of contents Vol.1)

(.. cont. table of contents Vol.1)

(.. cont. table of contents Vol.1)

VOLUME 2

(.. cont. table of contents Vol.2)

(.. cont. table of contents Vol.2)

(.. cont. table of contents Vol.2)

6. SUMMARY OF COOLED TURBINE CALCULATION

This Chapter reviews the actual implementation of the cooled turbine model described at Chs. 3 through 5. The description follows closely the procedure carried out by subroutine GSTUR which, in the framework of program GS, calculates gas turbine expansions. Given the adherence to the computer code, the Chapter constitutes a guide to the FORTRAN subprogram.

Notice that GSTUR is only one of the many subroutines composing program GS; the others calculate the cycle components listed in Par. 9.2.1.

The last paragraph (6.4) reviews the merits and the major limitations of the model, indicating the field of application and its relevance for research on power generation systems.

6.1 Data required to start the calculation

Tab. 6.1 lists the input data required to calculate the cooled turbine expansion. In addition, before calling subroutine GSTUR it is also necessary to calculate – or define* – the following quantities:

- T, P and composition of inlet gas. In general, these conditions coincide with the ones at combustor outlet.
- P at turbine outlet.
- Number, type and conditions (T, P, composition) of cooling flows. For floating-pressure flows, it is also necessary to indicate η_p and β of the corresponding compressor (see Par. 3.7.1).
- ΔT across the combustor preceeding the turbine, which is used to weigh the pattern factor λ (see Par. 5.2.2.1).

$\Delta h^{stg}_{is,mx}$ $\Delta h^{stg}_{is,ut}$, n^{stg}, Ma_{nz}, Ma_{ct}, Ma_{dif}, r_{vcl}, $\Delta P_{cl}/P_{cl}$, u, $m_{lk,t}$, $\eta_{p,nz}$, η_{dif}, η_{org}, $\eta_{p,\infty}$, a_t, b_t, $T_{bmx,nz}$, $T_{bmx,ct}$, Z, $r_{fc,nz}$, α, Bi_{bw}, Bi_{TBC}, $\hat{m}_{dsk}$, λ_{nz}, λ_{ct}, I_{geo}, I^{stg}, $I^{stg}_{i/r}$, $n_{step,mx}$, vector with coolant stream types
Notes: • $\eta_{p,\infty}$, a_t, b_t are the coefficients of Eq.(4.5) • I_{geo} determines the type of meridional geometry (constant D_m, constant D_{hub} or constant D_{tip}, see App. A). • I^{stg} determines the design option among those listed in Par. 3.6; the number of stages n^{stg} can be an input or an output depending on the value of I^{stg}. • $I^{stg}_{i/r}$ specifies whether n^{stg} is integer or real. • $m_{lk,t}$ is always extracted before the nozzle inlet. • The coolant stream vector specifies whether each stream is fixed-pressure or floating-pressure.

Table 6.1 Input data required by subroutine GSTUR.

---

* In most practical cases the data required by GSTUR are calculated by other GS subroutines (see Ch. 9). However, the flexibility of GS also allows specifying all data in an input file.

With these data GSTUR first calculates:

- Diffuser inlet conditions, proceeding backward from turbine outlet conditions (i.e. from point OUT of Fig. 3.2d).
- Δh_{is} and exit pressures of each stage, according to an input design option chosen among those listed in Par. 3.6.
- SP and mean diameter D_m at turbine inlet (the latter from the assumption of $D_{s,0}$=3.25, see App. A).

Since diffuser conditions and stage Δh_{is} converge very quickly, they are calculated only for few iterations. After the "freeze" described in Par. 9.2.3.3, GSTUR simply uses the values calculated at the previous iteration.

Before starting the calculation of the step-wise expansion, the program also evaluates:

- Coefficient used to adjust the ratio $n_{step,nz}/n_{step,ct}$ (see Par. 6.2.1).
- $(\Delta c/c)_{nz}$ and $(\Delta c/c)_{ct}$, based on the values of $n_{step,nz}$, $n_{step,ct}$ and n^{cs} found at the previous iteration (see Eq.3.5).
- $\Delta m_{dsk}/m_g$, as given by Eq.(3.19)

6.2 Step-by-step expansion

The calculation of the step-by-step expansion depicted in Fig. 3.3 is performed within a do-loop structured as follows:

- Check T^*_{gr} (see Par. 5.2.2.1). If $T^*_{gr} \leq T_{bmx}$ exit the loop
- Calculate P at end of expansion (P_{2i} of Fig. 3.3) and, if necessary, update stage number
- Choose coolant stream
- Calculate coolant conditions
- Calculate end of expansion (Point 2i of Fig. 3.3) and gross step work
- Calculate step cooling flow
- Calculate net step work; update total net work and total cooling flow
- Calculate conditions after mixing
- Update entropy productions; if necessary, print intermediate conditions
- If still within the nozzle, check if $Ma \leq Ma_{nz}$; when Ma reaches Ma_{nz} store nozzle outlet conditions.

The following paragraphs illustrate the details of some of these calculations. Points 1i, 2i and 3i define the boundaries among the transformations of the ith step as indicated in Fig. 3.3.

6.2.1 Pressure at end of step-expansion

A first tentative value of pressure P_{2i} can be evaluated from Eq.(3.2). However, since the nozzle expansion ratio (typically ≈2) is much larger than the one of the other cooled turbine rows, Eq.(3.2) would "assign" too many steps to the nozzle, thus giving $(\Delta c/c)_{nz} \ll (\Delta c/c)_{ct}$. In order to maintain approximately the same $\Delta c/c$, Eq.(3.2) is applied separately in the nozzle and the cooled turbine:

$$P_{2i} = P_{1i} \cdot [1 + \ln(\beta_{nz})/n_{step,nz}] \quad \text{in the nozzle} \tag{6.1a}$$

$$P_{2i} = P_{1i} \cdot [1 + \ln(\beta_{ct})/n_{step,ct}] \quad \text{in the cooled turbine} \tag{6.1b}$$

where $n_{step,nz}+n_{step,ct} \leq n_{step,mx}$ (see Par. 3.4.1), and their ratio is adjusted in order to obtain $(\Delta c/c)_{nz} \simeq (\Delta c/c)_{ct}$.

The tentative value given by Eq.(6.1) must be verified in order to guarantee that: (ii) the nozzle actually ends when $Ma_g = Ma_{nz}$; (ii) the cooled expansion actually ends when $T^*_{gr} = T_{bmx}$.

An approximate estimate of the static pressure $P_{1n,st}$ (see Fig. 3.4a) which should give Ma_{nz} is obtained from:

$$P_{1n,st} = (P_{2i-1}/P_{3i-1}) \cdot P_{g,tot}/\{[1+(\gamma_g-1)/2] \cdot Ma^2_{nz}\}^{[\gamma_g/(\gamma_g-1)] \cdot (1/\eta_p)} \qquad (6.2)$$

where (P_{3i-1}/P_{2i-1}) is the expansion ratio due to mixing of the previous, (i−1)th step and $P_{g,tot}$ is the current total gas pressure. If the ith mixing expansion ratio were still the same and γ=constant, $P_{1n,st}$ given by Eq.(6.2) would give exactly Ma_{nz}. In practice this doesn't happen because both γ and the cooling flow – and thus the mixing expansion ratio – change from step to step. The pressure $P_{ut,in,st}$ (see Fig. 3.4b) which should give $T^*_{gr} = T_{bmx}$ is found from:

$$T_{1i}/T_{bmx} = [(P_{1i}/P_{ut,in,st}) \cdot (P_{2i-1}/P_{3i-1})]^{\eta_p \cdot (\gamma_g-1)/\gamma_g} \qquad (6.3)$$

where P_{1i} is the current static pressure. Similarly to $P_{1n,st}$, also this estimate of $P_{ut,in,st}$ does not give exactly $T^*_{gr} = T_{bmx}$, because the "true" γ and (P_{2i}/P_{3i}) which should be used are unknown. It follows that the nozzle and the cooled turbine are terminated at values of Ma_g and T^*_{gr} slightly different from the input Ma_{nz} and T_{bmx}: however, this situation has no consequence on convergence because what matters is that – from one iteration to unother – the end of the nozzle and the cooled expansion remain the same.

Given $P_{1n,st}$, $P_{ut,in,st}$ and the tentative value given by Eq.(6.1), the actual P_{2i} is set equal to their maximum. With this procedure, the expansion ratio of the last step of the nozzle and the cooled turbine is typically smaller than the others. Given the final P_{2i} it is possible to update – if necessary – the stage number; this is done by comparing P_{2i} with the stage exit pressures defined at the beginning of the calculation (Par. 6.1).

6.2.2 Choose coolant stream

The coolant streams – ordered according to decreasing pressures – are scanned starting from the one at the highest pressure. The first stream of the list must always be at a pressure sufficient to allow cooling, i.e. (recall Par. 3.7.1 for fixed- and floating-pressure definitions):

- If "fixed-pressure", it must be higher than the current static gas pressure.
- If "floating-pressure", the compressor providing the coolant must be capable of compressing it up to P_1 of Fig. 3.6.

The selection criterion depends on the section being calculated. For the nozzle:

- If available, choose the stream at pressure immediately above nozzle inlet gas pressure.
- Otherwise, choose the "floating-pressure" stream at the highest pressure, and require that it be compressed up to nozzle inlet gas pressure.

In the cooled turbine the selection is accomplished as illustrated in Fig. 6.1; the procedure selects always the stream at the lowest pressure compatible with the constraints, disregarding its temperature. In some situation this may not be the best choice, because a cool, high-pressure stream may be preferable to a hot, low-pressure stream*. The optimum alternative will be determined by the trade-off between: (i) throttling losses incured by the HP stream; (ii) losses caused by the additional cooling flow required with the hot LP stream. The "lowest pressure" criterion behind the scheme of Fig. 6.1 has proved superior (i.e. higher cycle efficiency) in all cases tested so far, an occurence which emphasizes the importance of limiting coolant throttling losses.

6.2.3 Coolant conditions

The calculation procedure varies depending on the section being calculated (nozzle or cooled turbine) and the type of coolant stream.

A) Nozzle, fixed-pressure coolant. Coolant conditions are found simply by throttling it down to the gas static pressure, disregarding any pumping phenomena. The ideal outlet velocity $v_{cl,is}$ is determined by assuming that only half of the total pressure drop is lost by friction (last assumption of Par. 3.7); in other words, referring to symbols of Fig. 3.4:

$$P_3 = P_4 + (P_1 - P_4)/2$$

To avoid supersonic (unrealistic) ejection velocities P_3/P_4 cannot exceed 5/3. Notice that in this case $\Delta P_{cl}/P_{cl}$ expressed by Eq.(3.7) is an output, and may be lower than the value indicated in the input file.

* In a simple gas turbine cycle this situation cannot occur, because air at higher pressure is also at higher temperature. However, in an intercooled cycle it may possible to have the choice between: (i) cool, medium pressure air exiting the intercooler and (ii) warmer, low pressure air bled from the LP compressor.

B) Nozzle, floating-pressure coolant. The only difference with case A) is that – rather than being available at an arbitrary pressure P_1 set independently from gas inlet conditions – the coolant is compressed to P_1=nozzle inlet gas pressure ($P_{0,tot}$ of Fig. 3.4a). Such bleed pressure P_1 is kept constant, because it is assumed that throughout the nozzle the coolant is bled from one location only.

C) Cooled turbine, fixed-pressure coolant. Similar to case A), with the addition of the enthalpy rise due to pumping given by Eq.(3.9a). In this case the pressure rise ΔP_{pum} of Eq.(3.9a) is totally lost; the effect of pumping is only to increase coolant temperature.

D) Cooled Turbine, floating-pressure coolant. Bleed conditions must be determined by proceeding backward from the gas static pressure, adjusting the bleed pressure to meet the input $\Delta P_{c1}/P_{c1}$ and ΔP_{pum} given by Eq. (3.9). In this case the bleed pressure P_1 actually "floats", following the step-wise decrease of P_{2i}. Even if P_3-P_4 is constant (Par. 3.7), $v_{c1,is}$ varies from step to step due to variations of T and the expansion ratio P_4/P_3.

6.2.4 End of step-expansion

The conditions at the end of the expansion are fully determined from pressure P_{2i} (see Par. 6.2.1) and the entropy given by Eq.(D.6):

$$s_{2i} = s_{1i}+(1-\eta_p)\cdot R\cdot \ln(P_{1i}/P_{2i}) \qquad (6.4)$$

In the nozzle η_p is constant and equals the input $\eta_{p,nz}$; in the cooled turbine it changes from step to step according to Eq.(4.5). SP is calculated according to the specific volume at point 1i and Δh_{is} of the current stage (distribution of Δh_{is} and stage exit pressures are set at the beginning of the calculation, see Par. 6.1).

Given P_{2i} and s_{2i}, all other thermodynamic properties are found by the subroutines illustrated in App. B. In the nozzle, the new gas velocity is given by:

$$v_g = [2\cdot(h_{2i,tot}-h_{2i,st})]^{0.5}$$

where $h_{2i,tot}=h_{1i,tot}$. In the turbine, total enthalpy changes due to work extraction; gross work (specific to one kg of air) is simply given by $m_g\cdot(h_{1i,tot}-h_{2i,tot})$.

6.2.5 Cooling flow

Cooling flow is calculated according to the gas conditions at Point 2i of Fig. 3.3 and the coolant conditions at Point 3 of Fig. 3.6. The value of Δm_{clb} that gives $r_{bg,out}=1$ (Par. 5.2.5) is determined by a modified bisection algorithm. For the first step of the nozzle and of the cooled turbine the search interval is 0-2; at all other steps it is $0\text{-}1.5\cdot\Delta m_{clb,i-1}$, where $\Delta m_{clb,i-1}$ is the value found at the previous step. At the cooled turbine inlet the interval is reset because, due to discontinuities of T_{bmx} ($T_{bmx,nz}\neq T_{bmx,ct}$) and r_{fc} (see Par. 5.3.4.5), the cooling flow of the first cooled turbine step may be larger than the one for the last nozzle step.

The gas cross-sectional area and other geometric parameters necessary to calculate Re_g and cooling flows are evaluated according to the hypotheses discussed in App. A.

In the cooled turbine, the local value of r_{fc} corresponding to the linear variation depicted in Fig. 5.43a is calculated from:

$$r_{fc} = r_{fc,nz}\cdot(T^*_{gr}-T_{bmx,ct})/(T^*_{gr,1t}-T_{bmx,ct}) \qquad (6.5)$$

where $T^*_{gr,1t}$ is the effective gas recovery temperature of the first cooled turbine step.

Once Δm_{c1b} is known, Δm_{c1t} is found by adding Δm_{dsk} (see Eq. 3.20) and total cooling flow is updated by adding Δm_{c1t}.

As discussed in Par. 5.2.6.3 – no verification is performed on pressure drops, because it is assumed that $\Delta P_{c1}/P_{c1}$ is always sufficient to let Δm_{c1b} through the cooling circuit.

6.2.6 Net work

Net work is given by:

$$w_{net} = m_g \cdot (h_{1i,tot} - h_{2i,tot}) - \Delta m_{c1t} \cdot w_{pum} \tag{6.6}$$

where w_{pum} is given by Eq.(3.10); obviously, for the nozzle w_{net}=0. Total net turbine work is simply the summation of all w_{net} calculated at each step.

6.2.6 Mixing

As indicated by Eq.(3.12) and (3.15), the calculation of pressure P_{3i} after mixing requires the knowledge of the coolant ideal ejection velocity $v_{cl,is}$:

$$v_{cl,is} = \left\{ c_{p,cl} \cdot T_{cl} \cdot [1 - (P_{2i}/P_{cl})^{(\gamma_{cl}-1)/\gamma_{cl}}] \right\}^{0.5} \tag{6.7}$$

where $c_{p,cl}$, γ_{cl}, T_{cl} and P_{cl} are the ones at Point 3 of Fig. 3.6. The conditions after mixing are found by: (i) adjusting the composition according to Eq.(3.16); (ii) calculating P_{3i} from Eq.(3.12); (iii) calculating h_{3i} from Eq.(3.13); (iv) evaluating all other properties by the subroutines of App. B.

6.2.7 Final updates and TIT conditions

Once point 3i is known, it is possible to adjourn total conditions ($P_{g,tot}$, $T_{g,tot}$), Ma_g, entropy losses etc. and, if requested, print a number of information about the current step.

In the nozzle, if $Ma_{3i} \geq Ma_{nz}$ the point just calculated becomes the nozzle outlet, i.e. the point used to define TIT (see Fig. 2.15). In this case must store $n_{step,nz}$, $T_{3i,tot}$=TIT and "shift" from point 1n to point 1t as depicted in Fig. 3.4a. The static conditions at point 1t are found by calling the routines for the calculation of thermodynamic properties (see App. B) with the following input pair (refer again to Fig. 3.4a):

- Same static pressure as point 1n
- Static enthalpy $h_{1t,st}=h_{1n,st}+(1-\eta^1_{p,ct})\cdot(v^2_{g,1n}-v^2_{g,ct})/2$

where $\eta^1_{p,ct}$ is the efficiency of the first cooled turbine step calculated at the previous iteration and $v_{g,ct}=Ma_{ct}\cdot(\gamma_g\cdot R_g\cdot T_{1n,st})^{0.5}$

6.3 Uncooled turbine, diffuser, total cooling flow

After exiting the step-wise expansion loop the program proceeds as follows:

- Update $n_{step,ct}$, n^{cs} (Eq.3.6) and entropy losses.
- Calculate uncooled turbine expansion according to the scheme in Fig. 3.4c. SP_{out} (which is used to determine $\eta_{p,ut}$, see Eq.3.3) is estimated from the diffuser inlet conditions already calculated (Par. 6.1). The "shift" due to $w_{kin,lost}$ illustrated in Fig. 3.4c is calculated analogously to the shift at nozzle outlet (Par. 6.2.7).
- Update diffuser outlet T, h, s and composition.
- Calculate organic losses and final net work

The mass flow required for each coolant stream results automatically from the updates performed at each step (Par. 6.2.5). GSTUR does not verify whether such flows can actually be produced: it is the responsability of the main program (Ch. 9) to insure that other elements of the system provide the necessary coolant flows.

6.4 Review and critical appraisal

The model illustrated in the last four Chapters provides a new tool for the calculation of cooled gas turbines. At the end of this lengthy description it is worth reviewing its merits as well as its limitations.

The model meets the requirements of parametric thermodynamic analyses of complex GSC because:

a) Turbine efficiency and cooling flows, the two quantities which directly affect cycle thermodynamics, are evaluated according to their major physical determinants.

b) The inclusion of similarity-adjusted scale effects (size parameter SP) allows analyzing the influence of plant size and – to a limited extent – of pressure ratio*.

c) The dependence of cooling flows from coolant and gas conditions, as well as their thermophysical properties, allows analyzing the impact of: (i) intercooling; (ii) reheat; (iii) compressor aftercooling; (iv) steam cooling; (v) all other means affecting the coolant and/or gas conditions.

d) The inclusion of material characteristics (maximum allowed temperature, TBC coatings), allows estimating the consequences of progress in material technology.

e) The presence of parameters interpreting the sophistication of the cooling technology (Z, r_{fc}) allows investigating the improvements to be expected from progress in cooling technology.

f) Computing time and memory requirements allow its use for systematic parametric investigations.

In addition, the model produces a thermodynamically correct description of the gas turbine expansion because:

g) The distinction between expansion, mixing and acceleration losses properly breaks down the irreversibilities occuring during the expansion.

h) The distiction between nozzle, turbine and diffuser gives a correct distribution of fluid-dynamic losses and properly breaks down

* Through variations of volumetric flow V and thus SP.

chargeable and non-chargeable cooling flows (see Par 2.3.1). In particular, this distiction allows the correct calculation of the reheat turbine, where the whole cooling flow is chargeable.

These qualities allow assessing the potential and critically appraising the vast majority of the configurations of interest; in particular, points a), b) and c) justify the applicability of the model to cycles involving radical modifications with respect to the simple cycle.

Beside its positive features, it is important to point out that the model has some drawback, as well as limitations about aspects not targeted by this work:

- As already remarked in Par. 4.2, correlating η_p to both SP and specific speed should improve the accuracy of its prediction. However, in order to be effective such improvement would require much more data on turbomachine performance.
- The current version does not verify whether the available coolant-side pressure drop ($\Delta P_{cl}/P_{cl}$) is adequate to drive the required coolant flow. As discussed in 5.2.6.3, adding a test on this pressure drop would require the specification of one more unknown parameter – Z_p defined by Eq.(5.45) – and of the laws of heat addition and friction along the cooling channel.
- The accuracy of the model relies on an appropriate calibration with data regarding actual engines. The calibration described in the Ch. 7 is the best accomplishment made possible by the data publicly available. Access to more specific data (cooling flows, pressure-temperature distributions, detailed geometric descriptions, etc.) would probably allow some improvement.
- The continuous expansion model is not suited for modelling accurately stage-by-stage pressure-temperature variations. Consequently, imposing the mechanical balance of turbines and compressors mounted on the same shaft – which requires setting the first or second stage outlet pressure – might give questionable results (see also Par. 10.1.2).
- As already mentioned in Pars. 2.5 and 3.3, the model can calculate only on-design conditions.

It is also important to emphasize that there is no provision for the calculation of pollutant emissions because:

- Although few reactions might proceed at significant rates within the HP turbine, pollutants are formed almost exclusively in the combustor. Thus, the prediction of emission levels must be addressed by proper modelling of the combustor, which is much beyond the scope of this work.

- The inclusion of a chemical kinetic model for the prediction of pollutant formation into a thermodynamic model would be totally inappropriate because: (i) there is no need to solve the two problems together* and (ii) the computational requirements of the chemical kinetic model would prevent from performing cycle parametric analyses.

- The pollutants of interest – CO, NO_x, unburned hydrocarbons and particulates – are produced in such small quantities that their effect on cycle thermodynamics is absolutely negligible.

For similar reasons, the model does not account for:

- Combustor "blowout" or flame flashback, both because they are chemical kinetic phenomena and because they are relevant only for off-design operation.

- Effect of combustor outlet disuniform temperature distribution other than that accounted for by the pattern factor λ.

To summarize, the model is capable of addressing all issues raised by thermodynamic analyses of complex GSC. Further improvement strictly depends on the availability of adequate data for model calibration. The prediction of emission levels and chemical kinetic effects is neglected both because they do not affect cycle thermodynamics and because it would require an effort definitely comparable to that for this whole work.

* Thermodynamic and emission predictions should be performed in series. In fact, running a combustion model for the estimation of pollutant formation makes sense only after thermodynamic conditions have been defined.

NOMENCLATURE

a_t, b_t	Coefficients of Eq.(4.5)	
Bi_{bw}	Blade wall Biot number	
Bi_{TBC}	Thermal Barrier Coatings Biot number	
c	Blade chord	[m]
c_p	Constant pressure specific heat	[J/kg-K]
D_m	Mean diameter	[m]
h	Specific enthalpy	[J/Kg]
m	Mass flow, specific to compressor inlet flow	[kg/kg_a]
$\hat{m}_{dsk}$	Disk coolant flow per stage	[kg/kg_a-stage]
Ma	Mach number	
n	Number (stages, steps)	
P	Pressure	[Pa]
r_{fc}	Film cooling parameter, see Par. 5.3.4.2	
r_{vcl}	Coefficient defined by Eq.(3.15)	
R	Gas constant	[J/kg-K]
Re	Reynolds number	
s	Specific entropy	[J/kg-K]
SP	Stage Size parameter (Eq.2.3)	[m]
T	Temperature	[K]
T_{bmx}	Maximum allowed blade temperature	[K]
u	Blade peripheral speed	[m/s]
V	Volumetric flow	[m^3/s]
Z	Convection cooling parameter, see Par. 5.2.4.8	

Greek

α	Film cooling injection angle, see Fig. 5.36	
β	Pressure ratio (compressor, >1); expansion ratio (turbine, <1)	
γ	Ratio c_p/c_v	
Δh	Enthalpy drop	[J/kg]
Δm_{clb}	Blades+shrouds nondimen. coolant flow per step*	[kg/kg_a-step]
Δm_{clt}	Total non-D coolant flow per step (Δm_{clb}+Δm_{dsk})	[kg/kg_a-step]
Δm_{dsk}	Disk&casings non-D coolant flow per step	[kg/kg_a-step]
ΔP	Pressure loss (or rise)	[Pa]
η	Efficiency	
$\eta_{p,\infty}$	"Large scale" efficiency, see Eq.(4.5)	
λ	Pattern factor	

Subscripts

a	Air
cl	Coolant
ct	Cooled turbine
dif	Diffuser
g	Gas
gr	Gas at recovery conditions
in	Inlet
is	Isoentropic
lk	Leakage
mx	Maximum
nz	Nozzle
org	Organic

* When applicable, Δm_{clb}, Δm_{clt} and Δm_{dsk} are also indicated with the infinitesimal notation dm_{clb}, dm_{clt} and dm_{dsk}.

out	Outlet
p	Polytropic
pum	Rotor pumping
st	Static conditions
step	Steps to calculate cooled expansion
t	Turbine
tot	Total conditions
ut	Uncooled turbine section
0	Inlet of first nozzle
1	Coolant bleed
1n	Exit of first nozzle
1t	Inlet of first gas turbine rotor
3	Coolant at blade tip
4	Coolant at ejection holes
1i,2i,3i	Points defining ith expansion step (Fig. 3.1)
i-1	(i-1)th expansion step

Superscripts

cs	Cooled stages
stg	Stage
*	Corrected by pattern factor

FIGURES

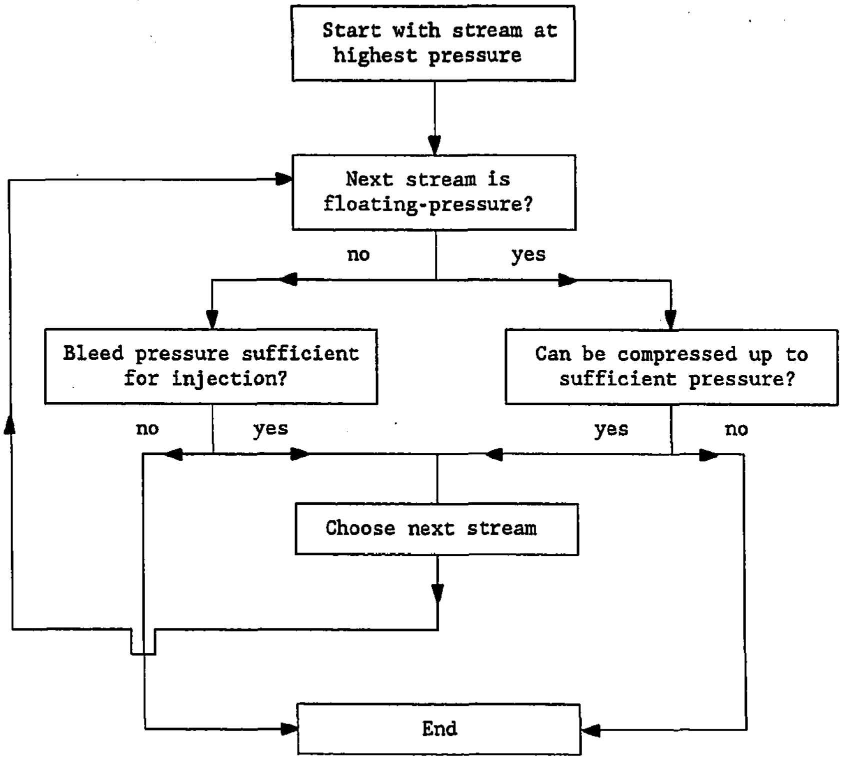

Fig. 6.1 Selection of coolant stream for the cooled turbine.

7. CALIBRATION OF GAS TURBINE MODEL

This Chapter describes the calibration of the turbine model described in Chs. 3 to 6. This was accomplished by reproducing the performance of commercial simple cycle gas turbines. The calibration has proceeded through three phases:

1. Selection of reference commercial engines and the data to be matched.
2. Selection of model parameters to be calibrated.
3. Minimization of discrepancies between the predictions of the present model and performance data to be matched.

Results indicate that the model can predict power output, efficiency and turbine outlet temperature of commercial engines with a maximum error of about 5%, 1 percentage point and 20°C, respectively.

Given the uncertainty (and in some case the incoherence) of the data used, these results are the best that can be achieved. Better agreement could perhaps be obtained by resorting to a more accurate and detailed data set. Nonetheless, the accuracy is satisfactory and, most of all, it is fully acceptable for GSC thermodynamic analyses.

7.1 Reference engines

The reference data used for the calibration are the characteristics of the 32 gas turbines marked by an asterisk ("*") or by a full dot ("•") in the leftmost column of Tab. C.1. These engines span the widest range of performance and operating parameters: power output from 1 to 215 MW, efficiency from 23 to 41%, pressure ratio from 7 to 30, turbine inlet temperature from 900 to 1260°C. Although the compressor and the turbine are always both axial, the engine architecture can vary substantially: single- and multi-shaft; annular, "cannular" and silo combustor; radial and axial turbine diffuser; cold-end (compressor inlet) and hot-end (turbine outlet) generator drive; constant-mean-diameter or constant-hub-diameter turbomachinery, etc.*

The 32 engines have been selected based on (i) year of commercialization and (ii) architecture. The ones commercialized before 1975 have been eliminated because they are too old to reflect even the "average" current technological level; the ones with radial components (compressor, turbine, or both) have been left out because the functional relationship between η_p and SP (see Eqs.4.5 and 4.6) is presumably different from that of axial machines.

The six turbines identified by an open dot ("o") have been discarded because – although they meet both criteria (i) and (ii) – they exhibit performances substantially below expectations. This situation – clearly demonstrated by the results in Figs. 7.12 to 7.14 – has no apparent justification; the high negative heat balance error (Par. 7.1.4) testifies to the poor reliability of manufacturers' data, but cannot be

---

* Due to space limitations, Tab. C.1 does not report all these data; however, they can easily be found in company publications on each specific model.

sole responsible for the deviations revealed by the present calculations*.

In any case, since the inclusion of these six engines (#2, 6, 15, 53, 59 and 74) could drive the minimization procedure of Par. 7.5 toward unacceptable values, they have been discarded.

7.1.1 Inhomogeneities of reference data

The group selected is the result of a compromise between the need to refer to as many engines as possible – to guarantee the generality of the model – and the need to use a congruous data set. The basic sources of inhomogeneities are:

- Aeroderivatives and heavy-duties are subject to very different design approaches.
- Due to the very high costs of developing a new model, manufacturer tend to improve their production lines simply by modifying existing models. Thus, their "design styles" remain considerably different, resulting in substantial discrepancies even among machines of the same generation.
- The last 2-3 years have witnessed the introduction of a new generation of engines with TIT and performances noticeably higher than those of pre-existing models. For this reason, it has been necessary to introduce a distinction between "average" and "state-of-the-art" engines (see Par. 7.1.8).

These observations point out that, aside from the inconsistencies evidenced in Par. 7.1.4, we should expect a substantial scatter of calibration results.

* Let's take for example the Allison 570KA (#2): although β, TIT, M_a, η_c^{stg} and η_t^{stg} are almost identical to those of the 571KA (#3), its efficiency is lower by almost 4 percentage points. Such large difference can be explained only by hypothesizing that its design is substantially different from that of the 571KA: it could be materials, cooling technology, compressor and turbine diffuser, combustor, etc.; most probably a combination of all of them.

The scatter could be reduced only be defining each model more specifically: compressor outlet temperature, combustor pressure drop, conditions at end of cooled expansion and at diffuser inlet, etc. Since this is impossible, either we accept a substantial tolerance on the predictions of the model or we must "fine tune" the input data listed in Tab. 6.1 to each single turbine. The latter approach has been adopted for the programs commercialized by Enter Software and El-Masri (see Par. 3.2).

7.1.2 Survey of commercial turbines

Performance data about commercial gas turbines can be found either in handbooks and catalogs issued yearly by specialized publishers (Diesel & Gas Turbine Worldwide Catalog; Gas Turbine World Handbook), or in the technical literature, or in company publications (see references of Appendix C). These data however are often incomplete or incoherent: TITs are often missing; the number of compressor and turbine stages are given only occasionally; cooling air flow rates are always considered proprietary information; it is often unclear whether the power output is at the turbine shaft or at the generator terminals, or whether inlet/outlet pressure losses are included.

In order to refer the calibration to a more reliable data set, several gas turbine manufacturers have been contacted directly, thus collecting the data reported in App. C. Without subtracting from the usefulness of such contacts, it must be said that the additional information gathered by this survey has clarified only part of the inconsistencies encountered. Such inconsistencies (see App. C for further details) could be partially explained in terms of company commercial policies, which may suggest to give slightly altered performance data to be in a better position for clients' acceptance tests.

7.1.3 Gear and generator efficiency

To avoid errors due to incorrect estimation of gear and generator efficiencies, the performances used for the calibration are — whenever possible — the ones of the mechanical drive version. In most cases the electric and mechanical drive versions have the same cycle parameters; however, in several cases the two versions exhibit slightly different M_a, RPM, β and TIT.

Fig. 7.1 depicts the values of η_g and η_{gg} reported in Table C.1. These data were either given explicitly by the manufacturer, or calculated as the ratio between the efficiency of the electric and mechanical drive versions. Such a ratio must be considered more reliable than the ratio of power outputs because power is much more sensitive than efficiency to even slight differences of operating parameters (e.g. RPM and air flow rate). The interpolating lines in Fig. 7.1 have been used to evaluate the shaft power of engines produced only as generator drives. Indicating with $\dot{W}_{el}$ the electric power (in Watts), their analytic expressions are:

$$\begin{aligned} \eta_{gg} &= 0.97-0.0065\cdot[8.5-\log_{10}(\dot{W}_{el})]^2 \\ \eta_g &= \eta_{gg}+0.015+0.002\cdot[8.5-\log_{10}(\dot{W}_{el})]^2 \end{aligned} \qquad 0.1\cdot10^6 \le \dot{W}_{el} \le 300\cdot10^6 \quad (7.1)$$

7.1.4 Overall energy balance

A first basic test of the coherence of manufacturers' data is the energy balance of the whole engine. Since JANAF tables enthalpies include the heat of formation (see App. B), for the whole gas turbine energy conservation can be written as (Fig. 7.2):

$$h_a + m_f \cdot h_f - m_g \cdot h_g - w_{sh} = \Sigma(m_{lk} \cdot h_{lk}) + \Sigma(q_{lost}) + \Sigma(w_{org}) \qquad (7.2)$$

where m_{lk} are the leakage flows escaping from seals, bolts, flanges, etc., q_{lost} is the heat lost by radiation, convection, incomplete combustion, lubricating oil and auxiliaries; w_{org} is the work dissipated by bearings and other mechanical components. The summation signs indicate that leakage, heat and organic losses occur at many locations. Notice that incorrect evaluation of processes internal to the system – blade cooling, pressure drops, turbomachine losses, etc. – would not affect the energy balance expressed by Eq.(7.2).

Except for very small uncertainties regarding fuel composition (which slightly affects the exhaust gas composition and thus h_g), manufacturers' data always allow for calculation of the LHS of Eq.(7.2). Fig. 7.3 shows that for the turbines listed in Tab. C.1 the LHS may vary between -2 and +4-6% of the heat input $q_{in}=m_f \cdot LHV$. The box-cross dots designate machines for which $\dot{W}_{sh}$ or η_{gg} were not directly available: for these machines $\dot{W}_{sh}$ was calculated from $\dot{W}_{el}$ and the correlations shown in Fig. 7.1, thus possibly introducing an error due to the incorrect estimation of η_{gg}.

For the turbines with LHS<0 the energy output is larger than the energy input! On the other hand, LHS=3-5% of fuel input implies dissipations much beyond the capabilities of the ventilation systems typically used in structures housing gas turbines (Foster-Pegg, 1988). These considerations prove that, even excluding the box-cross dots, the variations shown in Fig. 7.3 are much wider than can reasonably be expected, and set an upper bound to the accuracy achievable by using the data in Tab. C.1.

To appreciate the importance of Fig. 7.3, notice that for an engine with η=33%, a 3% difference between LHS and RHS of Eq.(7.2) could be due to: (i) a 9% error on W_{sh} or (ii) a 3% error on η or (iii) a 4.5% error on the exhaust gases sensible heat (for a TOT of 550°C, an error of about 24°C).

7.1.5 Leakage, organic and thermal losses

In the calculations performed here each of the three losses on the RHS of Eq.(7.2) is "concentrated" at one point as shown in Fig. 7.2, thus giving:

$$h_a + m_f \cdot h_f - m_g \cdot h_g - w_{sh} =$$
$$m_{lk,c} \cdot h_{lk} + \varepsilon_h \cdot m_f \cdot LHV + (1/\eta_{org} - 1) \cdot w_{c,grs} + (1 - \eta_{org}) \cdot w_{t,grs} \qquad (7.2a)$$

where ε_h is the combustor heat loss (as a fraction of total heat input $m_f \cdot LHV$), and subscript "grs" indicates gross work. The values of m_{lk}, ε_h and η_{org} to be used have been determined by minimizing the sum of squares of:

$$\Delta e = \text{LHS} - \text{RHS of Eq.(7.2a)}$$

for all the 32 engines considered for calibration. The final values are reported in Tab. 7.1, while Fig. 7.4 depicts the corresponding Δe. Engines with positive Δe indicate that w_{sh}, η_{sh} and TOT given by the manufacturer are probably very conserva-

m_{lk} :	0.8% of M_a – at HP compressor outlet
ε_h :	0.4% of $m_f \cdot LHV$ – at each combustor
η_{org}:	99.7% – both compressor and turbine

Table 7.1. Values assumed for the parameters affecting the energy balance (Eq.7.2a). Organic losses are considered for both turbines and compressors.

tive, i.e. some – or all – of them are actually higher; the opposite holds for engines with negative Δe.

The value of m_{lk} of Tab. 7.1 compares well with the estimate given by Hines (1990) who – besides suggesting that most of the leakage takes place in the compressor – has recommended 1% as a reasonable, average value for GE aero-derivative engines*. Based on data provided by Gelfand (1987), the leakage fraction of these engines appears to be about 0.4% for the LM500, 0.1% for the LM1600, 3% for the LM2500 and 1% for the LM5000.

With regard to organic losses let's remark that, since the sum of compression and turbine work is roughly $5 \cdot w_{sh}$, η_{org}=99.7% implies that organic losses are about 1.5% of net work output.

7.1.6 Data used to reproduce the actual gas turbine cycle

Calibration has consisted in reproducing the thermodynamic cycle of each reference engine and then verifying whether calculated performances match the ones given by manufacturers. The data used to reproduce the cycle realized by the actual reference engine are:

- Mass flow M_a at compressor inlet.
- Compression ratio β.
- Turbine Inlet Temperature TIT.
- Total number of compressor and turbine stages (n_c^{stg} and n_t^{stg})
- Number of turbine cooled stages (n^{cs}).
- If available, fuel LHV.

* Leakage flows depend very much on engine architecture, seal design, operating pressure, etc. Since theoretical predictions are subject to major uncertainties, all correlations used by manufacturers to predict leakage are experimental and specific to a given seal design (Horner, 1988).

The mass flow rate M_a is the basic determinant of size, while β and TIT define the "shape" and the "extension" of the thermodynamic cycle in the T,s plane. n_c^{sts} and n_t^{sts} are used to determine the distribution of Δh_{is} among stages, which in turn is necessary to calculate SP. The information on fuel LHV is helpful because, for the same cycle efficiency, the heating value affects m_f, m_g and thus turbine work. When the heating value is not specified, it is assumed that fuel is pure methane with LHV=50.01 MJ/kg; otherwise, it is assumed that the fuel is a mixture of methane and dry air with the specified LHV*.

7.1.7 Data to be matched by model predictions

The performances of the cycle defined by the parameters described at the previous paragraph are compared with the values given by manufacturers for:

- Specific power output [kJ/kg$_a$]
- Efficiency
- Turbine outlet temperature
- Compressor outlet temperature (whenever available)

The purpose of the calibration is to minimize the difference between calculated and manufacturers' estimates of the four quantities above. Since it uses only overall performance data, this procedure leaves considerable uncertainties about local variables. For example, since the temperature and the pressure at the end of the cooled expansion are unknown, it is impossible to establish whether the distribution of

* Since it maintains always the same fuel C:H ratio of 1:4, this procedure does not account for variations of combustion gas composition due to other hydrocarbons often found in natural gas (ethane, propane, buthane, etc.). However, the effects of such variations on cycle thermodynamics are definitely negligible.

turbine cooling flows is correct. A definitive verification of the merits of the model requires detailed knowledge of the pressure-temperature-mass flow histories of actual engines. One first substantial improvement could come from reliable data on compressor outlet temperatures (very few were available for the calculations performed here), because they allow isolating the turbine from the compressor*.

7.1.8 Current vs State-of-the-art technology

As already pointed out at Par. 7.1.1, the 32 engines chosen for the calibration do not constitute an homogeneous set. In fact, most of them represent what could be defined the "current generation" of engines, while the ones introduced in the past 2-3 years clearly show improved performance. On the other hand, since the number of "state-of-the-art" engines is very limited, it is not possible to accomplish a satisfactory calibration based on such a small data set. This contrast was settled by performing two separate calibrations:

- One for engines of the "current generation" (in Tab. C.1, the ones marked by an asterisk), using as independent variables all the parameters listed in Par. 7.2.1.
- Another for state-of-the-art engines (in Tab. C.1, the ones marked by a solid dot). This was done after increasing the maximum allowable metal temperature and "freezing" the scale coefficients a_c and a_t appearing in Eqs.(4.5) and (4.6) to the values found for "current" engines. Aside from reducing the number of independent variables, eliminating a_c and a_t was necessary because these engines fall in rather limited power range**

* Manufacturers are unwilling to provide such information because, since the compressor outlet temperature is generally one of the variables examined during customers' acceptance tests, they want to have the flexibility of changing such a temperature to meet performance guarantees (Merola, 1987).

** Since all state-of-the-art heavy-duties considered here have about the same power, it is clear that for them no scale effect could ever be derived.

	Type	#	β	TIT °C	TOT °C	η_{sh} %	$\dot{W}_{sh}$ [MW]	w_{sh} [kJ/kg]	$\Delta e/q_{in}$ %
"Current technology" engines									
Allison 501KB5	AD	1	9.3	1035	538	30.13	3.927	251.7	-.789
Asea-Stal Mars	HD	4	16	1057	465	33.04	9.396	259.0	2.514
BBC GT11N	HD	8	12.4	1065[1]	515	32.97	83.30	268.7	-2.15
BBC GT13E	HD	10	13.8	1137[1]	516	34.90	147.4	299.6	-.962
Coberra 3145	AD	14	19	988	404	34.40	12.55	223.0	-.943
Coberra 6462	AD	16	20	1164	465	37.30	26.10	294.6	-1.38
Fiat TG20 (b)	HD	19	14	1085	502	33.54	44.29	281.9	1.073
Fiat TG50D5	HD	22	14	1085	495	34.55	130.9	294.5	1.850
G.E. MS7001EA	HD	30	12.4	1104	530	33.06	84.77	291.6	.780
G.E. LM500	AD	33	14.3	1116	513	31.60	4.064	256.0	-.863
G.E. LM2500	AD	35	18.7	1212	513	37.00	22.00	330.0	-.420
G.E. LM5000	AD	36	25.3	1174	446	37.30	34.27	278.8	-1.96
KWU V94	HD	48	10.7	1100	545	34.00	152.6	305.3	-.991
Mitsub. MF111	HD	49	13	1160	547	31.90	13.28	278.7	-.949
N.P. PGT10	HD	51	14	1063	462	33.90	10.44	253.0	-.859
N.P. MS6001	HD	29A	11.5	1104	541	33.06	39.78	291.6	-.654
N.P. MS9001	HD	32A	11.6	1104	528	33.60	120.8	293.7	-.063
Ruston Typhoon	HD	81	12.8	1053	500	31.48	4.131	246.2	-1.11
Ruston Tornado	HD	54	12.1	1000	470	31.17	6.338	232.9	.771
Solar Sat 1500	HD	56	6.7	871	499	24.82	1.161	181.3	1.340
Solar Cent 4500	HD	57	9.6	904	451	27.96	3.274	192.0	1.585
Solar Cent H	HD	58	10.2	1010	516	29.39	4.101	233.7	-.192
Sulzer 10	HD	61	13.6	1145	517	33.80	22.60	292.8	.613
State-of-the-art engines									
G.E. MS7001F	HD	31	13.5	1260	583	35.07	152.3	365.7	2.211
G.E. MS9001F	HD	75	13.5	1260	583	34.66	215.4	359.0	2.160
Mitsub. 501F	HD	79	14	1260	578	35.72	155.1	362.7	.528
G.E. LM1600	AD	34	22	1210	482	37.20	13.99	311.6	-.278
TurboPower FT8	AD	73	20.3	1160	443	38.92	25.95	304.3	-.473
G.E. LM6000	AD	76	29.8	1240	448	41.23	42.99	342.2	-.259
Centrax CX571	AD	3A	12.7	1156	533	33.91	5.896	302.3	.106
KWU V64.3	HD	77	15.6	1221[1]	534	36.37	62.59	340.7	.474
KWU V94.3	HD	78	15.6	1201[1]	534	36.37	203.0	341.7	.647
Anomalous engines									
Allison 570KA	AD	2	12.1	1135	567	29.60	4.804	255.5	-2.12
BBC GT8	HD	6	16.3	1185	523	32.42	47.80	270.1	-1.41
Coberra 6456	AD	15	20	1162	475	35.60	24.79	279.7	-1.44
Sulzer 3	HD	59	9.5	970	478	28.15	6.280	197.9	-1.43
Ruston TB5000	HD	53	6.8	900	495	27.10	4.027	188.9	-3.60
Hitachi H25	HD	74	14.7	1260	530	33.60	24.44	277.7	-3.97

[1] Estimated from temperature obtained after full gas-coolant mixing

Table 7.2 Characteristics of all-axial gas turbines commercialized after 1975. The rightmost column reports the difference Δe=LHS−RHS of Eq.(7.2a) obtained with the assumptions of Tab. 7.1.

For convenience, the main characteristics of the two groups of engines have been repeated in Tab. 7.2. The table also reports the six "anomalous" engines left out from calibration (see Par. 7.1) and the heat balance error corresponding to the assumptions of Tab. 7.1.

Although their performances do not appear particularly anomalous, engines # 75 (GE MS9001F) and # 78 (KWU V94.3) have been excluded from error minimization due to inconsistencies with the 60Hz model (see comparison between 9001F and 7001F in App. C) and – for the KWU V94.3 – lack of reliable information on TIT.

7.2 Relevant model parameters

While the number of parameters appearing in the turbine model is relatively high, the information regarding actual turbines is limited to the four quantities listed at Par. 7.1.7: w, η, TOT and, if available, COT. Thus, it is unreasonable to pretend to calibrate *all* parameters, and attention must be restricted to the most significant ones. Fortunately, according to gas turbine design practice many parameters must fall in a rather narrow range, and can be assigned a fixed, constant value.

7.2.1 Parameters to be calibrated

The parameters to be considered "most relevant" — and thus to be used as the independent variables of the calibration — have been selected according to:

- The results of the sensitivity analysis of Par. 7.4.
- The acknowledgment that turbomachinery and cooling technology are the basic determinants of cycle performances. Consequently, their features must be among the quantities to be calibrated.

Both these criteria have led to the choice of the following parameters:

- Asymptotic turbine and compressor polytropic efficiencies ($\eta_{p,t\infty}$ and $\eta_{p,c\infty}$) appearing in Eqs.(4.5) and (4.6).
- Coefficients a_t and a_c giving the slope of functions $\eta_{p,t}(SP)$ and $\eta_{p,c}(SP)$ in Eqs.(4.5) and (4.6).
- Convection cooling technology parameter Z.
- Film cooling technology parameter r_{fc}.

This sums up to a total of six independent variables. However, the many numerical experiments performed have shown that results are substantially improved by differentiating between $\eta_{p,\infty}$ of heavy-duties and aero-derivatives, which brings the total to eight (see Tab. 7.5). This differentiation can be justified by considering that ADs are almost always multishaft; the additional degree freedom allows for better distribution of specific speeds among stages, with beneficial effects on efficiency.

It is clear that the larger the number of independent variables the lower the total error resulting after minimization; however, there is also the risk of obtaining unrealistic values of the parameters being calibrated. The choice of the eight parameters above has proved to be the best compromise between accuracy and adherence to gas turbine standards.

7.2.2 Parameters held constant

The values assumed for the other gas turbine parameters are listed in Tab. 7.3.

The choice of b_c=b_t=0 (see Eq.4.5 and 4.6) is based both on the behaviour of $\eta_{p,t}$ depicted in Fig. 4.4 and on results of tests performed with different values of b_c and b_t. These tests showed that, although the optimum values of a_c and a_t do depend on the values chosen for b_c and b_t, as long as $-0.05 \leq b_c$, $b_t \leq 0.3$ the accuracy achievable by optimizing $\eta_{p,c\infty}$, $\eta_{p,t\infty}$, a_c, a_t, Z and r_{fc} is essentially

Bi_{bw}	0.5
Bi_{TBC}	0.0
$\hat{m}_{dsk}$	0.01
Ma_{dif}	0.45
Ma_{ct}	0.7
Ma_{nz}	0.9
$n_{step,mx}$	30
$T_{bmx,ct}$	770°C
$T_{bmx,nz}$	800°C
r_{vcl}	0.5
u	400 m/s
α	30°
$\Delta h^{stg}_{is,ut}$	200 kJ/kg (HD) 100 kJ/kg (AD)
$\Delta P_{cl}/P_{cl}$	0.4
λ_{nz}	0.10
λ_{ct}	0.03
η_{dif}	0.5
$\eta_{p,nz}$	0.95
b_c	0.0
b_t	0.0
$\Delta h_{is,c}$	20 kJ/kg (HD) 30 kJ/kg (AD)

$\Delta h^{stg}_{is,mx}$ adjusted to match n^{cs}
Meridional section always with constant D_m. For state-of-the-art turbines $T_{bmx,ct}$=800°C and $T_{bmx,nz}$=830°C
$\Delta h_{is,c}$ used to evaluate SP_c

Table 7.3 Parameters maintained fixed during calibration. AD=aero-derivative; HD=heavy-duty.

constant. b_c, $b_t = 0$ means that $\eta_{p,c}$ and $\eta_{p,t}$ do not increase any further for $SP \gtrsim 1$, a behaviour physically correct for turbulent flows and no geometric constraints.

Although they correspond to typical values adopted in actual gas turbines, using the "base" values listed in Tab. 7.3 for all turbines is somewhat arbitrary and each one of the them could well be disputed. In reality, each turbine will have a unique combination of those parameters, a combination which however is known only by the manufacturer. On the other hand, any attempt to estimate the parameters in the Table would inevitably require exhaustive information on turbine geometry and aerodynamics (see discussion at Par. 4.3).

In summary, the decision to assign a fixed value to the parameters in Tab. 7.3 comes from the acknowledgement that: (i) reference data are scarce; (ii) any attempt to resort to correlations used in gas turbine practice would require at least a 1-D design, thus defeating the main purpose of the calculation model.

7.3 Calculation procedure

Since TIT and n^{cs} are outputs rather than inputs of the computer program, in order to reproduce the cycle corresponding to a given engine it is necessary to iterate on:

- Combustor outlet temperature, to match the given TIT
- Turbine $\Delta h^{stg}_{is,mx}$, which determines β of cooled stages and thus n^{cs}

Rather than referring to the TIT defined in Par. 2.3.1, some European manufacturer refers to an "effective mixing temperature" ideally obtained by mixing all coolant flow with the combustor outlet gas flow; in this case, instead of matching TIT the iteration on the combustor outlet temperature is targeted toward such a mixing temperature.

The configuration adopted for reproducing the performance of commercial engines is depicted in Fig. 7.5. The calculation proceeds as follows:

- Compressor outlet conditions are computed from overall compression ratio and Eq.(D.6). $\eta_{p,c}$ is calculated from Eqs.(4.6) and (4.7), using for $SP_{c,out}$ the value of the previous iteration ($SP_{c,in}$ is always the same). Then, $SP_{c,out}$ is updated on the basis of the new compressor outlet conditions.

- Combustor outlet temperature (point 6 in Fig. 7.5) is reset according to the error on TIT of the previous iteration.

- $\Delta h^{stg}_{is,mx}$ is reset according to the error on n^{cs} of the previous iteration. If, say, at the previous iteration n^{cs} was greater than the number of cooled stages of the turbine to be reproduced, the enthalpy drop $\Delta h^{stg}_{is,mx}$ is increased. Thus, the temperature drop across cooled stages increases, and the gas reaches $T_{bmx,ct}$ within fewer n^{cs}. Notice that n^{cs} is treated as a real number.

- The turbine is calculated on the basis of the new gas and coolant conditions, as well as the new distribution of stage expansion ratios.

Convergence is verified by testing the variations of TIT, n^{cs} and cooling flows (points 8 and 10 of Fig. 7.5) between successive iterations.

7.3.1 Assumptions

Besides the ones listed at Tabs. 7.1 and 7.3, the assumptions maintained throughout the calibration are:

- ISO conditions, i.e. ambient at 15°C, 1.0325 bar, 60% relative humidity, no compressor inlet nor turbine outlet ΔP.
- ΔP_{cmb}=3% (ADs) and 4% (HDs). This because the annular design adopted in aero-derivatives generally gives lower pressure losses.
- Unless otherwise specified, the fuel is natural gas with LHV=50.01 MJ/kg. When the heating value specified by the manufacturer was different, a mixture of CH_4 and air having the given LHV was assumed.
- HDs are film-cooled only in the first vane, i.e. $r_{fc,ct}$=0. In aero-derivatives film cooling is applied also downstream* as depicted in Fig. 3.9.
- Cooled turbine stages have the same expansion ratio (option 2 of Par. 3.6). Uncooled turbine stages and compressor stages have the same Δh_{is} (option 3 of Par. 3.6 and option 3 of Par. 4.7.1).

7.3.1.1 Pre-cooling of cooling air

One last assumption is that there is no heat transfer between the compressor bleed and the point where air is used for cooling. In some models produced by ABB, Fiat, Mitsubishi and Hitachi cooling air is pre-cooled by means of an air-to-air heat exchanger. Neglecting such heat transfer is a substantial drawback; however, no data were available to account for its effects.

---

* Except for the Allison 501-KA, where film cooling is utilized only for the first vane.

If manufacturer efficiency, air flow, power output and TOT were accurate and consistent, the presence of air pre-cooling could be revealed by a heat loss larger than expected. However, considering that such loss is likely to be 1-3% of the heat input and given the scatter of points in Fig. 7.3, there is little hope of detecting such loss through an energy balance. A clear confirmation of this argument comes from considering that, despite the substantial pre-cooling adopted in the Hitachi H25 (Urushidani et al, 1990), its heat balance shows a large negative error (Fig. 7.4)

7.3.2 Difference from procedure adopted in Ch. 10

It is important to notice that the procedure outlined above is slightly different from the one adopted to obtain the results of Pars. 10.2 and 10.3 because:

1. In the calibration, $\Delta h^{stg}_{is,max}$ is the result of an iteration whereby n^{cs} is matched to the value given by the manufacturer; the same procedure has been maintained for the calculations termed "same hypotheses" in Tabs. 10.3 to 10.8. On the contrary, all other calculations of Par. 10.2 and 10.3 refer to a constant value of $\Delta h^{stg}_{is,max}$.
2. In the calibration, HDs are film-cooled only in the first nozzle ($r_{fc,ct}$=0, as it actually is). Instead, except for the test reported in Par. 10.2.1.1 (Allison 501-KH), in Ch. 10 film cooling is always extended to the cooled turbine as depicted in Fig. 5.43a.

The reasons for these differences should be obvious: (i) the number of cooled stages n^{cs} is known only for actual, commercial engines; (ii) for systems designed to achieve outstanding efficiencies it is reasonable to expect a more widespread use of film cooling.

This differentiation between the two calculation procedures contributes to improve both the results of the calibration – using as much information as possible – and those of the parametric analysis – by neglecting fictitious constraints on n^{cs} and r_{fc}.

7.4 Sensitivity analysis

The choice of the calibration parameters described in Par. 7.2.1 has been verified by testing the sensitivity of the performances predicted for the GE LM6000. The choice of the GE LM6000 has no specific justification; similar results can be obtained by considering any other engine, except that for heavy-duties, where only the first vane is film cooled, the sensitivity to r_{fc} tends to be smaller.

7.4.1 Variation ranges

The variations considered for each parameter are summarized in Table 7.4 and are based on typical ranges adopted in gas turbine design practice.

The variation ranges do not span the same fraction of base value nor are they symmetric. This because the uncertainty on some parameter is much larger than on others, and assuming always the same variation - say ±5-10% - would be unrealistic. The concept can be appreciated by considering for example that:

- while there is almost no indication on the probable average value of Z and r_{fc}, the value of Ma_{ct} and Ma_{dif} cannot be too far from their base values of 0.7 and 0.45;
- the minimum and maximum values of r_{fc} (0.15 and 0.90) are used to span the whole feasible range, independently of the base value.

The base values of $\eta_{p,c\infty}$, $\eta_{p,t\infty}$, Z and r_{fc} are the ones resulting from error minimization (Par. 7.5). a_c, a_t are not listed because, since they are meant to represent scale effects, the sensitivity to their value can be appreciated only by considering a set of turbines with substantially different power outputs.

7.4.2 Results

Tab. 7.4 and Figs. 7.6 to 7.10 make clear that, although the sensitivity of w_{sh}, η_{sh}, m_{cl} and TOT to each parameter is different, $\eta_{p,c\infty}$, $\eta_{p,t\infty}$, Z and r_{fc} produce by far the overall strongest impact. Thus, in an error minimization procedure where only some of the parameters can be optimized, the bulk of the error can be reduced by chosing them as the independent variables. The figures also suggest that:

Parameter	Base value	Range	w_{sh}, kJ/kg	η_{sh}, %	TOT, °C	$m_{cl,nz}$, %	$m_{cl,ct}$, %
Bi_{bw}	0.5	.25-.75	343.6-329.8	41.58-40.62	448.0-447.8	08.62-15.19	7.49-9.11
$\hat{m}_{dsk}$	0.01	.005-.015	342.0-334.0	41.29-41.01	451.0-446.3	11.51-11.68	7.28-8.82
m_{lk}	0.01	.005-.015	340.8-334.5	41.37-40.89	448.5-448.5	11.57-11.48	8.08-8.03
Ma_{df}	0.45	.35-.45	343.0-332.1	41.77-40.44	444.2-453.8	11.53-11.53	8.06-8.06
$Ma_{g,ct}$	0.70	.55-.85	343.5-331.2	41.61-40.55	447.4-450.9	11.60-11.58	7.58-8.54
Ma_{nz}	0.90	.80-1.0	334.7-339.8	41.30-40.86	442.2-454.1	11.54-11.66	9.28-7.13
$T_{bmx,ct}$, °C	800	770-830	331.9-342.3	40.97-41.34	444.4-450.5	11.46-11.63	9.31-7.33
$T_{bmx,nz}$, °C	830	800-860	335.2-339.6	40.83-41.36	450.8-447.2	14.74-09.48	8.09-8.07
u, m/s	400	300-500	337.8-338.3	41.14-41.18	448.6-448.5	11.53-11.53	8.08-8.06
α	30°	0-60	338.8-337.3	41.25-41.07	447.9-449.2	10.62-12.47	8.06-8.06
$\Delta P_d/P_d$	0.4	0.25-0.55	341.8-326.2	41.36-40.47	449.4-445.9	11.60-11.44	7.52-9.76
ΔP_{amb}	0.03	0.02-0.04	339.8-336.3	41.38-40.84	446.9-450.2	11.53-11.53	8.07-8.06
c_h	.004	.001-.007	338.3-338.0	41.04-41.31	448.6-448.4	11.53-11.53	8.06-8.06
η_{dif}	0.5	.40-.60	335.5-340.7	40.86-41.49	450.8-446.2	11.53-11.53	8.06-8.06
η_{nz}	0.95	.92-.98	336.3-339.6	40.84-41.50	452.1-444.6	11.56-11.58	7.81-8.40
η_{org}	.997	.9955-.9885	336.0-340.2	40.92-41.43	448.5-448.5	11.53-11.53	8.06-8.06
$\eta_{p,c\infty}$	.902	.882-.922	315.7-358.7	39.53-42.57	448.7-448.6	12.50-10.96	8.26-7.89
$\eta_{p,t\infty}$	.921	.901-.941	323.3-352.6	39.42-42.93	460.5-435.9	11.59-11.53	8.21-8.05
Z	100.	15-200	304.9-340.9	39.21-41.35	440.6-448.7	21.50-10.04	12.94-7.69
r_{fc}	0.25	.075-.90	321.5-348.0	39.52-41.88	456.5-448.1	26.60-06.21	8.94-6.98
λ_{nz}	0.10	.05-.15	339.0-336.8	41.27-41.01	447.9-449.6	10.51-13.03	8.05-8.07
λ_{ct}	0.03	.015-.045	339.4-336.3	41.22-41.14	449.2-446.9	11.56-11.57	7.83-8.48
r_{vd}	0.5	.33-.66	335.2-340.7	40.80-41.49	451.3-446.0	11.53-11.53	8.04-8.10
D_{s0}	3.25	2.75-3.75	339.6-336.3	41.27-41.08	448.6-447.9	11.21-12.00	7.87-8.35
$(H/D_m)_0$	0.08	.05-.11	335.6-337.6	40.94-41.20	449.3-447.5	13.82-11.00	8.25-8.25
σ	1.25	.90-1.5	347.2-330.5	41.66-40.77	450.7-446.3	09.10-13.54	6.73-9.23
$(c_a/D_m)_{nz}$	.060	.045-.075	339.1-336.8	41.28-41.01	447.7-449.7	10.35-13.03	8.05-8.07
γ_{nz}	65°	55-75	338.2-337.7	41.19-41.12	448.4-448.9	11.44-12.03	8.06-8.07
Φ	2.6	2.2-3.0	341.6-334.4	41.31-41.01	450.2-446.8	11.10-11.95	7.43-8.72
t_b/c	.125	.10-.15	338.3-337.8	41.17-41.16	448.7-448.4	11.54-11.52	8.01-8.12
$(c_a/D_m)_{ct}$	.045	.03-.06	335.9-338.5	41.02-41.21	448.4-448.3	12.50-11.02	8.33-8.05
γ_{ct}	55°	45-65	335.9-340.7	41.05-41.28	447.8-449.6	11.98-11.08	8.41-7.62
With base values:			338.1	41.17	448.5	11.53	8.06
GE data:			342.2	41.23	448.0	-	-

Left and right values in w_{sh}, η_{sh}, TOT, $m_{cl,nz}$ and $m_{cl,ct}$ columns correspond to lower and upper values of each parameter. Parameters are varied one at a time, keeping all others at their base value.

Table 7.4 Results of sensitivity analysis.

- In all cases the influence of the geometric parameters discussed in App. A is modest, with the only exception of the solidity σ.

- Turbine diffuser losses have a substantial impact on efficiency (see influence of paramter #4-Ma_{dif} and #14-η_{dif} in Fig. 7.6a). Aside from materials and cooling technology, the improvement of diffuser performance is the subject of significant research efforts by manufacturers (Lüthi, 1989); it is interesting to notice that for its latest heavy-duty machine (7001F and 9001F), GE has abandoned the radial design (compact, but relatively inefficient) and has adopted an axial diffuser*, a design traditionally employed in ABB machines.

- As expected, cooling flows are basically determined by Z and r_{fc}, although Bi_w, m_{dsk} and T_{bmx} are also relevant. Decreasing the blade wall thickness by a factor of two (Bi_{bw} changes from 0.5 to 0.25) achieves approximately the same cooling flow reduction as increasing $T_{bmx,ct}$ by 30°C (Fig.7.7a) and even more than increasing $T_{bmx,nz}$ by the same amount (Fig.7.8a).

- r_{fc} has the strongest impact on $m_{cl,nz}$; instead, the influence on $m_{cl,ct}$ is small because in the cooled turbine film cooling is used with decreasing intensity (Fig. 5.43a).

- The very small sensitivity to the peripheral velocity u shows that pumping losses have negligible effects on overall performances and could be ignored.

- Fig. 7.9 shows that not only the diffuser, but also the nozzle characteristics have a substantial impact on TOT. While the reason of the influence of M_{dif} (#4) and η_{dif} (#14) are obvious, for the nozzle (#6-Ma_{nz} and #15-$\eta_{p,nz}$) it must be recalled that all calculations refer to the same TIT. Thus, varying Ma_{nz} or $\eta_{p,nz}$ changes: (i) combustor outlet temperature; (ii) nozzle outlet pressure; (iii) expansion ratio of section downstream the nozzle.

- For the same 2 percentage point variation of η_p, w_{wh} is more sensitive to $\eta_{p,c}$ than to $\eta_{p,t}$ because of: (i) the opposite roles played by turbine and compressor reheat factors; (ii) the presence of cooling flows, which increase with lower $\eta_{p,c}$ due to higher compressor outlet temperatures; (iii) turbine losses other than the ones

---

* Presumably, for the GE 7001F the choice of an axial diffuser is also the outcome of the low number of stages (three), implying large stage Δh_{is} and a high Ma_{dif} of about 0.55 (Scheper, 1989). With such a high inlet Mach number, the performance of a radial diffuser would be inevitably poor.

contributing to $\eta_{p,t}$ (nozzle, diffuser, acceleration, mixing): such losses are present anyway and "dilute" the effect of η_{pt}*.

7.4.3 Number of steps

One final important verification regards the sensitivity to the number of steps used to model the cooled expansion. As mentioned in Par. 3.4.1, the hypothesis of "continuous" expansion is legitimate as long as there are at least 3-4 steps per cooled row. Lower number of steps produce step-to-step discontinuities comparable to that between actual cascades, thus invalidating the assumption of smooth, continuous variations of thermodynamic and kinetic terms. On the other hand, Fig. 5.43 shows that if the number of steps is too high there might be an underestimation of film cooling effectiveness and thus an overestimation of cooling flows.

The variation of η, w, TOT and cooling flows predicted for the lm6000 for different values of the maximum number of steps are reported in Fig. 7.11, which confirms that:

- For low n_{step} the model is unreliable because results vary significantly with the number of steps.
- For $n_{step} > 20-25$ variations with n_{step} become much smaller. However, there is a persisting influence of n_{step} on cooling flows, causing an increase of $m_{cl,nz}$ and $m_{cl,ct}$ of the order of few percent**. Aside

---

* For example, taking an uncooled, constant-η_p turbine with the same characteristics considered here (β=29.8, TIT=1240°C, other parameters from Tab. 7.3 except that there is no cooling and $\eta_{p,t}$ is constant), when $\eta_{p,t}$ goes from 92 to 94% the overall isentropic efficiency goes from 92.2 to 93.7%. Thus, despite the reheat effect, nozzle and diffuser losses can make the overall η_{is} smaller than η_p. With cooling this is even more true due to mixing and acceleration losses, although the concept of isentropic efficiency becomes inappropriate because the expansion is no longer adiabatic.

** Notice that compared to the inlet air flow variations are much smaller, because the values in Fig. 7.11 are non-dimensionalozed by the base values $m_{cl,nz}$=0.1153 and $m_{cl,ct}$=0.0804. Thus, a 5% variation of $m_{cl,ct}$ means a 0.4% variation with respect to compressor inlet flow.

> from numerical inaccuracies, this increase is mostly due to the reduction of film cooling effectiveness shown in Fig. 5.43. In any case, the variations of η, w and TIT−TOT are within 0.3%, much less than the incertainty on the results of the calibration discussed in the next Paragraph.

It is important to emphasize that the sensitivity to n_{step} varies with the cycle parameters, in particular with the expansion ratio of the cooled section. For low TIT such expansion ratio is low, and thus the value of n_{step} below which model predictions become unreliable is low.

These considerations allow to conclude that, for state-of-the-art TIT and $n_{step} > 25\text{-}30$, the sensitivity of overall perfomance predictions to variations of n_{step} is much smaller than the accuracy to be expected by the results of the calibration, as well as of the tolerance of actual plant specifications. Nonetheless, in order to eliminate any fictitious influence of n_{step} on other variables it is appropriate to perfom all calculations with the same n_{step}.

7.5 Calibration

As already anticipated, the calibration of the 23 "current technology" engines of Tab. 7.2 is performed by determining the value of:

- $\eta_{p,c\infty}(AD)$, $\eta_{p,c\infty}(HD)$, $\eta_{p,t\infty}(AD)$, and $\eta_{p,t\infty}(HD)$
- a_c and a_t of Eqs. (4.5) and (4.6)
- Z and r_{fc}

which minimizes total error (sum of squares) on:

- power output
- efficiency
- turbine outlet temperature
- compressor outlet temperature (wherever available)

The error on η and w is non-dimensionalized by using the values given by the manufacturer. The errors on TOT and COT are non-dimensionalized by (TIT-TOT) and (COT-T_0), respectively: the resulting error approximately equals the error on turbine and compressor work. All four errors are weighted equally, i.e. total error is simply the sum of squares of all non-dimensional errors. The least-square minimization routine is based on a Levenberg-Marquardt finite difference algorithm (An., 1985).

7.5.1 State-of-the-art engines

State-of-the-art engines have been calibrated according to the same procedure described above. The only differences are that a_c and a_t have been left out from the set of independent variables (using the value already found for "current" engines) and the values assumed for $T_{bmx,nz}$ and $T_{bmx,ct}$ have been increased by 30°C (see Tab. 7.3).

It is worth mentioning that, rather than performing two separate calibrations, differences between average and state-of-the-art technology could be appraised by introducing a time-dependence (with the year of introduction into the market) of η_p, Z and r_{fc}. Despite its strong appeal, this idea is very difficult to realize because manufacturers frequently upgrade their engines by changing cycle parameters, materials, cooling technology, etc. Consequently, the current performance of a model introduced 10 years ago does not necessarily reflect ten-year-old technology.

7.5.2 Results

The optimized values of the eight independent variables are listed in Tab. 7.5; Fig. 7.12 depicts functions $\eta_{p,c}(SP)$ and $\eta_{p,t}(SP)$, while Figs. 7.13 to 7.16 compare calibration results with manufacturers' data. The error function to be minimized has proved much more sensitive to turbomachinery efficiencies than to cooling system parameters. Therefore, while the confidence interval on η_p is smaller than 0.1%, the confidence interval on Z, r_{fc}, a_c and a_t is of the order of 1%.

	Current technology	State-of-the-art
Z	36	100
r_{fc}	0.194	0.25
$\eta_{p,c\infty}$(HD)	0.896	0.896
$\eta_{p,c\infty}$(AD)	0.902	0.902
$\eta_{p,t\infty}$(HD)	0.912	0.921
$\eta_{p,t\infty}$(AD)	0.912	0.921
a_c	0.02688	0.02688[1]
a_t	0.07108	0.07108[1]

[1] a_c and a_t of state-of-the-art engines are not optimized

Table 7.5. Optimized values of cooling parameters, turbomachinery efficiencies and scale coefficients.

The first important comment on Tab. 7.5 is that the calibration confirms the expectation of higher η_p, Z and r_{fc} for state-of-the-art engines. The only exception is compressor efficiency, for which there appear to be no significant difference between the latest and the previous generation of engines.

Compared to the results obtained with a simplified model developed earlier (Consonni and Macchi, 1988), there is a strong improvement in the prediction of efficiency, which has been narrowed down to an uncertainty of about one percentage point. Power and TOT are also better predicted, although the improvement is smaller. The reason why predictions are still relatively poor is basically the lack and the uncertainty of data, a reality which is best illustrated by the scatter of points in Fig. 7.3. This does not sound very enthusiastic for the sophisticated model, through which it was not possible to obtain dramatic improvements. However, as already pointed out in Par. 3.3.1, the sophisticated model is the only one which can reasonably be extended to cycles very different from the simple cycle.

Fig. 7.14 shows that there is a tendency to overestimate TOT, which could be the symptom of an underestimation of either $\eta_{p,t}$ or the cooling flow, or both.

Overall, the ability to predict the performance of the current generation of engines appear satisfactory. The results shown in Ch. 10 show that the error bounds of 1 percentage point on efficiency and 5% on power output generally hold also for configurations very different from the simple cycle although in that case, rather than with experimental data, comparisons are made with figures given by other authors.

7.5.2.1 Heavy-duty vs. aeroderivative

Aside from the advantages coming from multi-shaft architecture and more widespread use of film cooling – which are both built into the model by assuming higher $\eta_{p,\infty}$ and $r_{fc,ct}>0$ – ADs do not show a systematic superiority over HDs. Yet, the optimized values of $\eta_{p,t\infty}$(AD) and $\eta_{p,t\infty}$(HD) are the same, suggesting that the advantage of going to multi-shaft architecture is mainly on the compressor side. The much higher simple cycle efficiency of ADs is mainly the result of a different choice of cycle parameters: in fact, while ADs have β near the optimum for efficiency, HDs are designed much closer to the point of maximum specific work. This can be explained by considering that:

- In aircrafts, reducing fuel consumption is very important not only to decrease operating costs, but also to decrease weight at take-off.
- In industrial applications gas turbines are used either as peaking units – where capital cost is more important than fuel consumption – or as part of Combined Cycles – for which efficiency generally peaks at relatively low compression ratios. In both cases economic optimization pushes toward low/medium compression ratios.

The apparent equality of ADs and HDs does not constrast with the fact that for the former cooling technology is generally more advanced: HDs can "make up" for this disadvantage by a better design of the LP section – LP turbine and diffuser, which for ADs must be designed from scratch anyway* – or by means like pre-cooling of cooling air with external heat exchangers. In order to fully capture all these effects it is necessary to broaden the set of variables being calibrated and – most of all – to use much more experimental data. The calibration performed here "lumps" all factors into the eight parameters listed in Tab. 7.5.

Given the important technological implications of the development of HDs vs. ADs (Williams and Larson, 1989), additional clarification about their specific performance potential is definitely desirable. However, the results of this calibration indicate that further differentiation between the two classes of engines would not significantly alter the

* An important recent innovation has been the introduction of the GE LM6000, which by utilizing the same LP turbine of the aircraft version (CF6-80C2) allows substantial reduction of development costs. In any case, some LP turbine redesign and the addition of the diffuser must still be done.

results. Since performance predictions are not biased toward either of the two classes, there are good reasons to believe that its predictions do not sistematically favor either of them.

7.5.3 Summary and critical appraisal

The calibration presented in this chapter constitutes a crucial point of this work. As already mentioned in Par. 3.2 a critical issue of all gas turbine models is their capability to reproduce the performances of actual engines. If the object of the study were a device which could be tested in a laboratory, the issue could be addressed by means of extensive experimentation. However, this is not possible for gas turbines because:

- Costs would be prohibitive.
- Most of the required information is highly proprietary.
- Given the important differences among the "design style" of different manufacturers, testing one single engine would not be enough. In fact, in order to gather significant information it would be necessary to test at least one engine for each manufacturer.

These considerations clarify once more that, although the calibration performed here leaves room for much improvement, there is actually no better means to adjust model predictions to the real world.

As suggested by Erbes (1991), closer agreement with actual engines could be obtained by "tweaking" the model parameters to reproduce the performances of each single engine. This is desirable in case it is necessary to simulate one single engine (e.g. the verifications of Par. 10.2), but not for a parametric analysis like the one presented in Par. 10.3. In any case, improvements could possibly be obtained by adding information which may be obtained without dramatic efforts:

- Type of diffuser (radial diffuser should be assigned lower efficiencies).
- Type of meridional section (constant hub, mean or tip diameter).
- Presence of cooling air pre-cooling.
- Pattern factor (should be lower for silo combustors).

REFERENCES

An. (1985), Subroutine ZXSSQ, IMSL User's manual, *International Mathematical and Statistical Library*, Houston, Texas.

Consonni S. and Macchi E. (1988), "Gas Turbine Cycles Performance Evaluation", Proc. *1988 ASME COGEN-TURBO* (Montreaux, Switzerland), pp. 67-77. Published by ASME, New York.

Foster-Pegg R.W. (1988), Consultant, Cape May, NJ, Personal Communication.

Gelfand L.E. (1987), General Electric Aircraft Engines, Advanced Programs & Ventures, Cincinnati, Ohio, Personal Communication to Eric D. Larson.

Hines W.R. (1990), General Electric Marine & Industrial Engines, Cincinnati, Ohio, Personal Communication.

Horner M. (1988), General Electric Marine & Industrial Engines, Cincinnati, Ohio, Personal Communication.

Lüthi H.K. (1989), New Products and Business Development, Power Generation Division, ABB, Baden, Switzerland, Personal Communication.

Scheper G. (1989), Personal Communication, Gas Turbine Aerothermo Division, General Electric, Schenectady, New York.

Urushidani H., Sasada T., Wada M. and Kawaike K. (1990), "Development of a New 25 MW High Efficiency Heavy Duty Gas Turbine", ASME Paper 90-GT-72.

Williams R.H. and Larson E.D. (1989), "Expanding Roles for Gas Turbines in Power Generation", in Electricity, Johansson T.B., Bodlund B. and Williams R.H. eds., pp. 503-553, Lund University Press, Lund, Sweden.

NOMENCLATURE

a,b	Coefficients of function η_p(SP) (Eqs.4.5 and 4.6)	
Bi_{bw}	Blade wall Biot number	
Bi_{TBC}	Thermal Barrier Coating Biot number	
D_m	Mean diameter	[m]
LHS	Left-end-side	
m	Mass flow rate, referred to compressor inlet flow rate	[kg/kg_a]
M	Mass flow	[kg/s]
$\hat{m}_{dsk}$	Disk coolant flow per stage	[kg/kg_a-stage]
Ma	Mach number	
n	Number (stages, steps)	
P	Pressure	[Pa]
q	Heat, specific to M_a	[J/kg_a]
r_{fc}	Film cooling parameter, see Par. 5.3.5.2	
r_{vcl}	Coefficient defined by Eq.(3.15)	
RHS	Right-end-side	
SP	Turbomachinery size parameter	[m]
T_{bmx}	Maximum allowed blade temperature	[K]
u	Blade peripheral speed	[m/s]
w	Specific work	[J/kg_a]
$\dot{W}$	Power	[kW]
Z	Convection cooling parameter, see Par. 5.2.4.8	

Greek

α	Film cooling injection angle	
β	Pressure ratio	
γ	Stagger angle, see Fig. A.1	
Δe	Difference between LHS and RHS of Eq.(7.2a)	
Δh_{is}	Isentropic enthalpy drop	[J/kg]
ΔP	Pressure loss	[Pa]
ε_h	Heat loss, as a fraction of heat input	
λ	Pattern factor	
η	Efficiency	
η_g	Generator efficiency	
η_{gg}	Gear+generator efficiency	
$\eta_{p,\infty}$	"Large scale" efficiency, see Eq.(4.5)	

Subscripts

a	Air
c	Compressor
cl	Coolant
clt	Blades+shrouds+disk cooling flow
cmb	Combustor
ct	Cooled turbine
dif	Diffuser
dsk	Refers to disks, casings, struts, etc.
f	Fuel
g	Gas
grs	Gross, i.e. including organic work losses
in	Input; inlet
is	Isentropic
lk	Leakage
mx	Maximum
nz	Nozzle
org	Organic

FIGURES

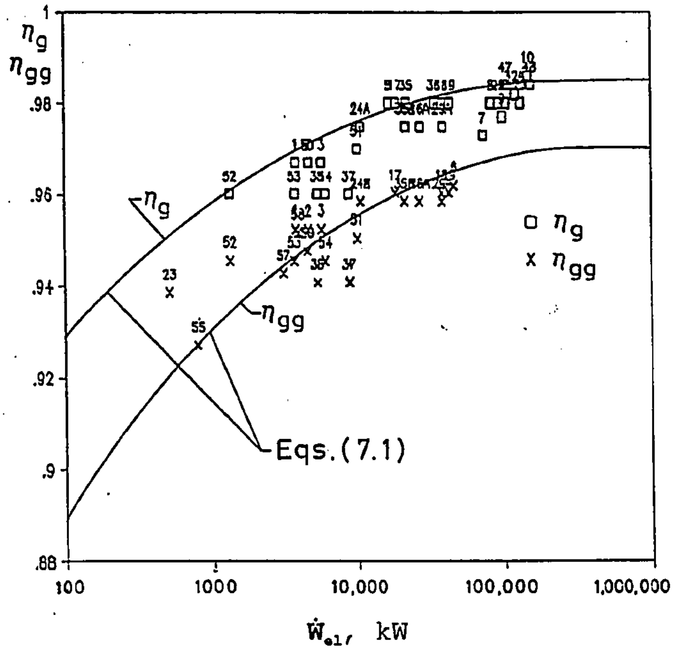

7.1 Gear and generator efficiencies. The number on top of each point refer to the gas turbines listed in Table C.1

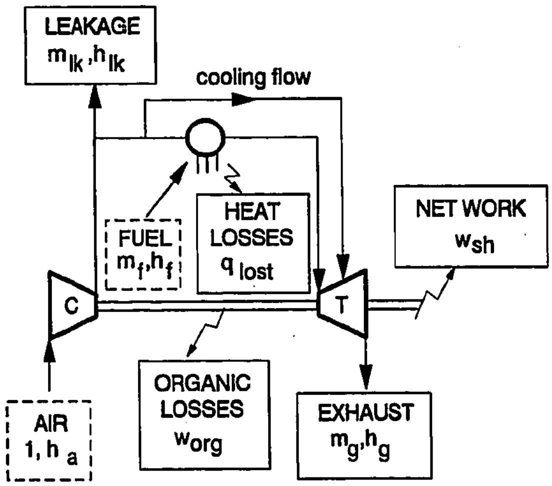

7.2 Overall energy balance of simple cycle turbine. Dashed-line boxes indicate inputs; solid-line boxes indicate outputs. In an actual machine, leakage, heat and organic losses occur at many locations.

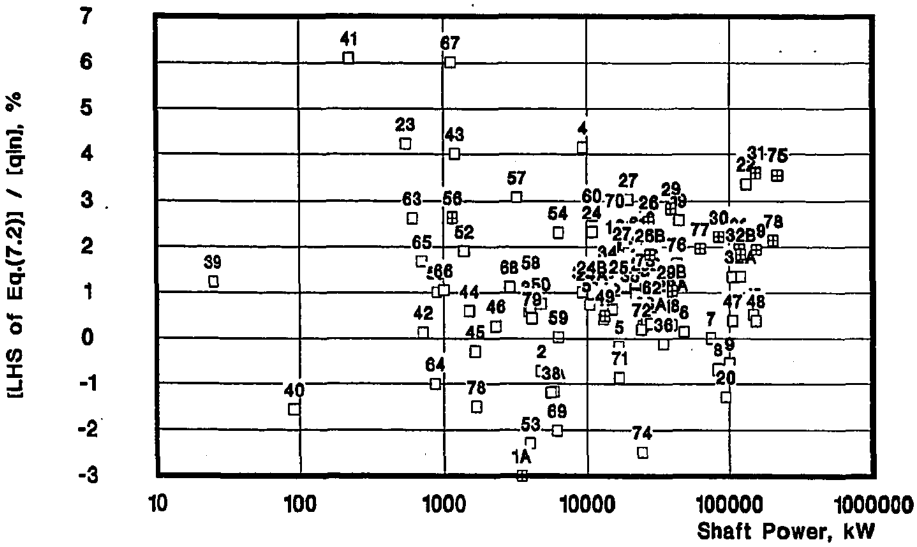

7.3 LHS of Eq.(7.1) for the turbines listed in Tab. C.1. Manufacturers' data used: M_a, m_f, TOT, $\dot{W}_{sh}$. The number on top of each point correspond to the numbers of the leftmost column of Tab. C.1. For the turbines identified by black dots, the correlations shown in Fig. 7.1 have also been used.

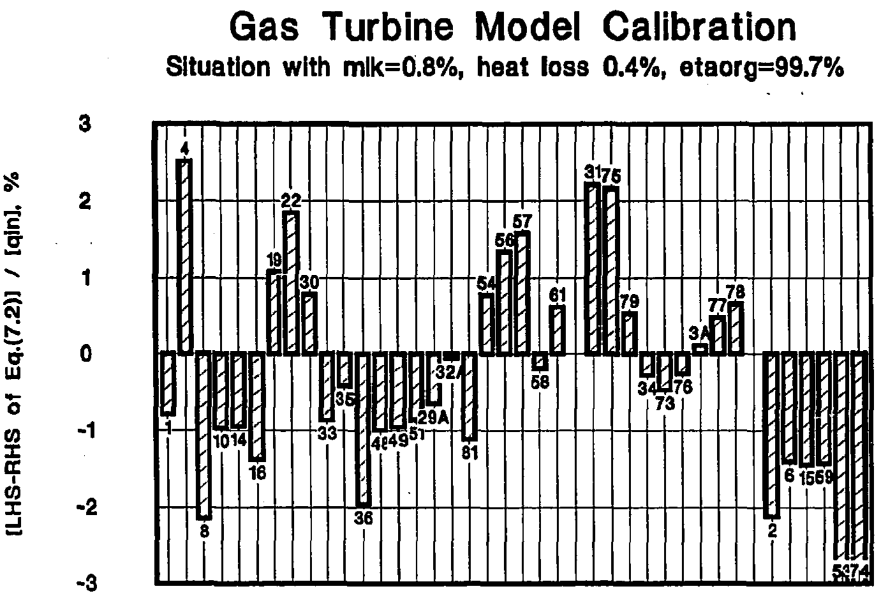

7.4 Error of heat balance equation (i.e. LHS-RHS of Eq.7.2a) for the turbines listed in Tab. 7.2. Notice that all "anomalous" engines exhibit strong negative Δe.

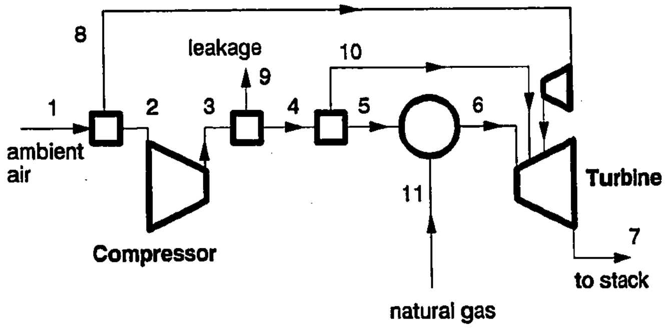

7.5 Scheme of simple cycle considered for the calibration of the turbine model. The small compressor depicted on top of the turbine (which doesn't actually exist) stands for the "floating-pressure" bleed from the compressor (see Par. 3.7.1); the efficiency of such fictitious compressor is the same as the one of the main compressor.

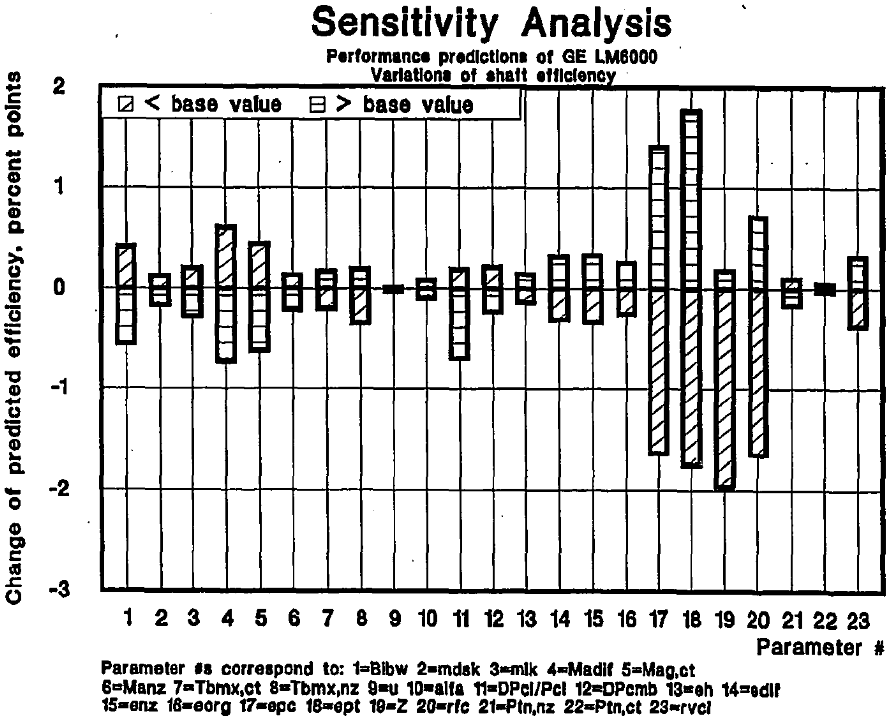

7.6a Variations of η_{sh} predicted for GE LM6000. Each parameter is varied one at a time, keeping all others at their base value. Parameters numbers on x-axis correspond to: 1=Bi_{bw}, 2=$\hat{m}_{dsk}$, 3=m_{lk}, 4=Ma_{dif}, 5=$Ma_{g,ct}$, 6=Ma_{nz}, 7=$T_{bmx,ct}$, 8=$T_{bmx,nz}$, 9=u, 10=α, 11=$\Delta P_{cl}/P_{cl}$, 12=ΔP_{cmb}, 13=ε_h, 14=η_{dif}, 15=η_{nz}, 16=η_{org}, 17=$\eta_{pc,\infty}$, 18=$\eta_{pt,\infty}$, 19=Z, 20=r_{fc}.

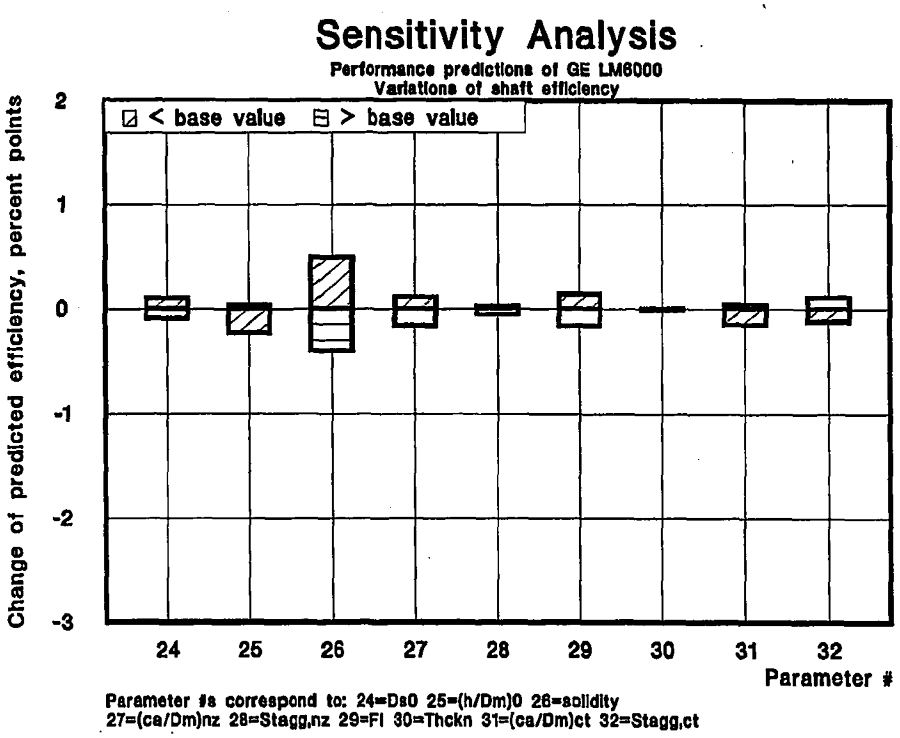

7.6b Influence of geometric characteristics on η_{sh} predicted for GE LM6000. Each parameter is varied one at a time, keeping all others at their base value. Parameters numbers on x-axis correspond to (for details see App. A): 24–D_{s0}, 25–$(H/D_m)_0$, 26–σ; 27–$(c_a/D_m)_{nz}$; 28–γ_{nz}, 29–Φ, 30–t_b/c, 31–$(c_a/D_m)_{ct}$, 32–γ_{ct}.

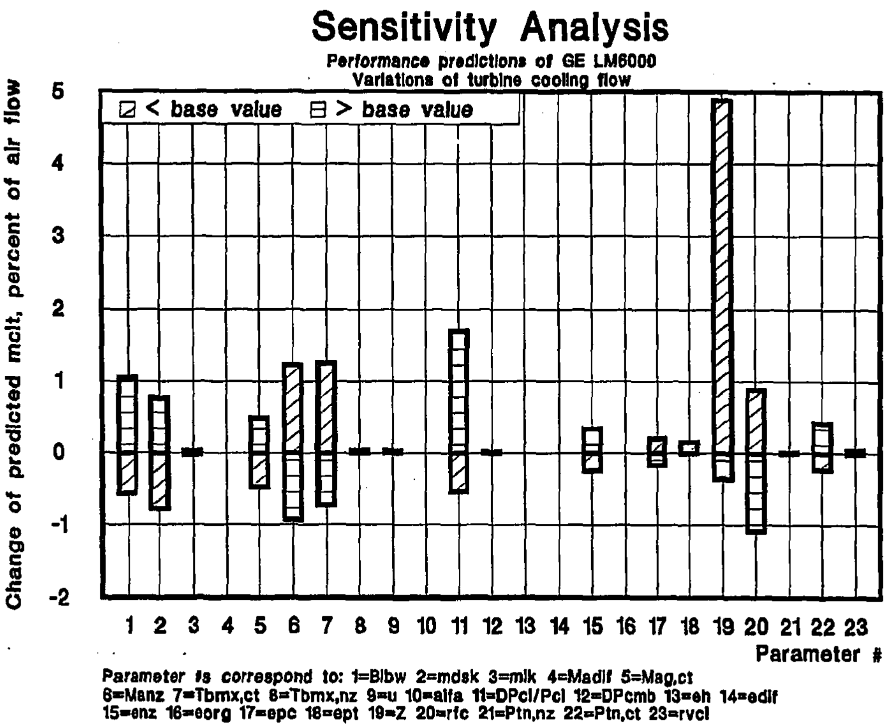

7.7a Variations of cooled turbine cooling flow predicted for GE LM6000. Nomenclature as in Fig. 7.6a.

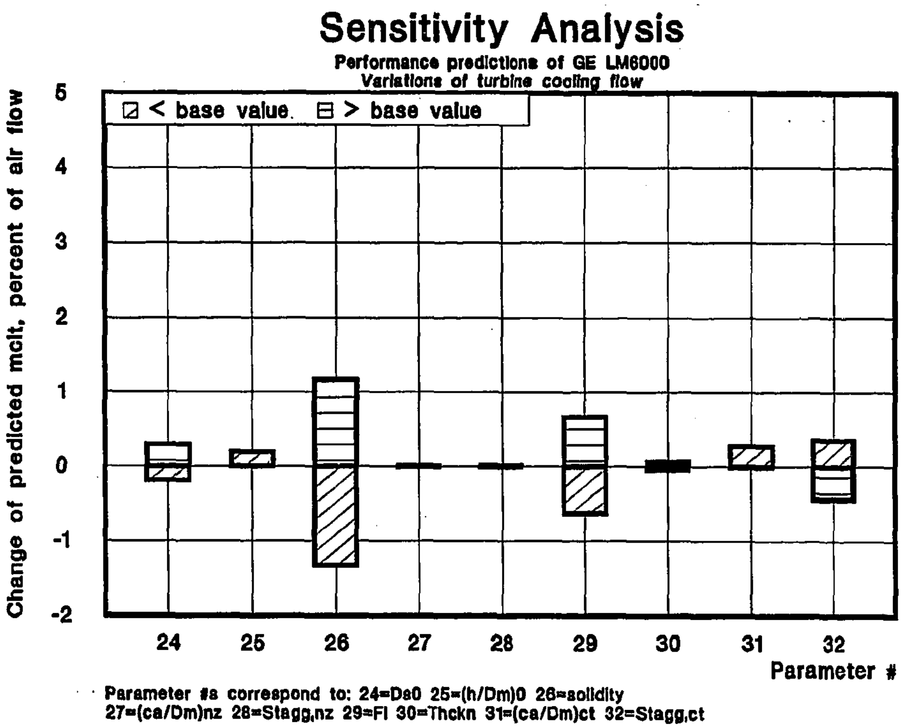

7.7b Influence of geometric characteristics on cooled turbine cooling flow predicted for GE LM6000. Nomenclature as in Fig. 7.6b.

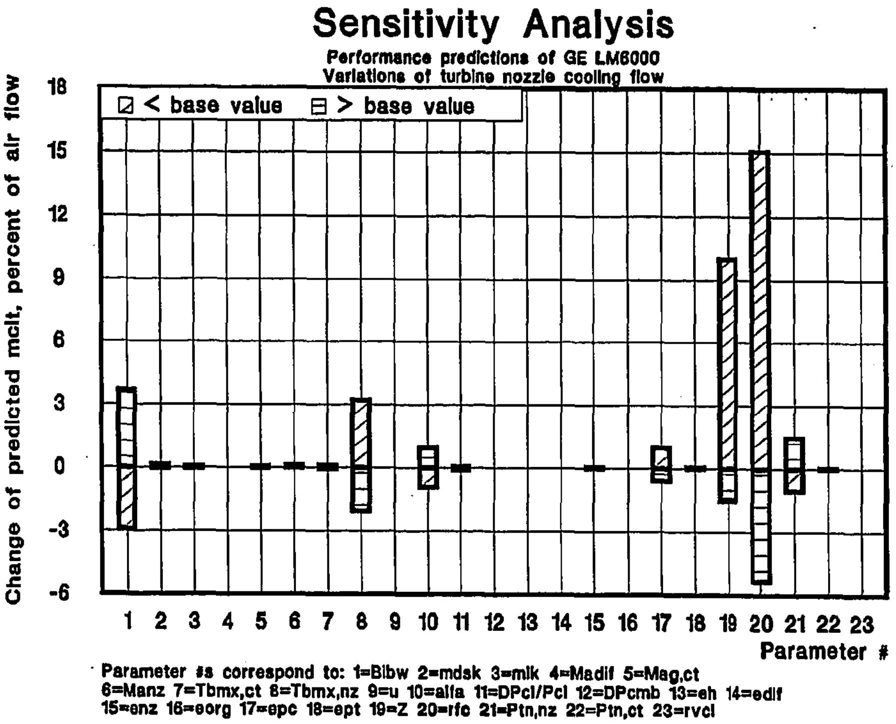

7.8a Variations of nozzle cooling flow predicted for GE LM6000. Nomenclature as in Fig. 7.6a.

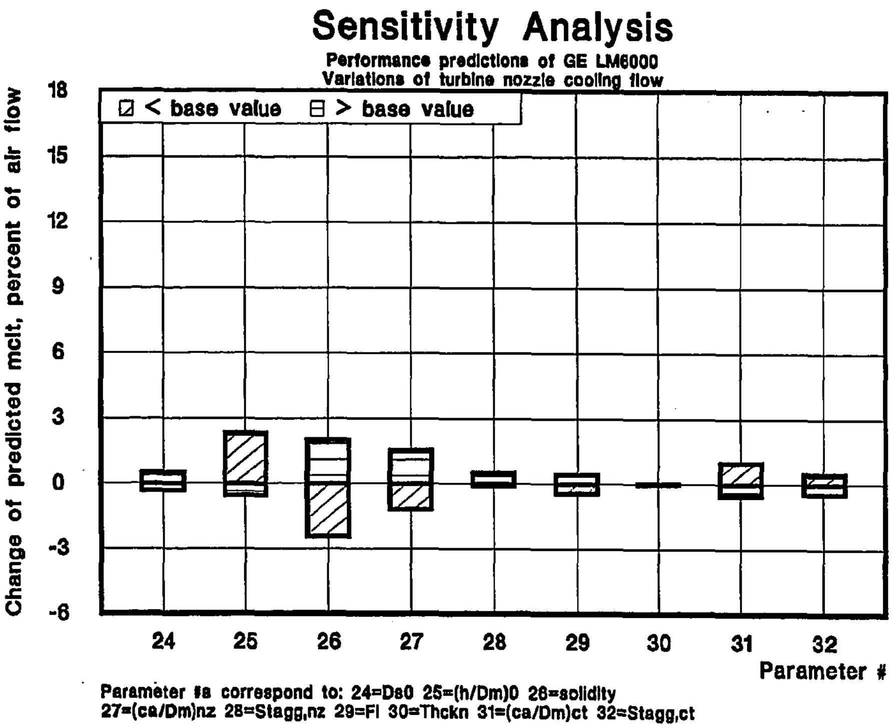

7.8b Influence of geometric characteristics on nozzle cooling flow predicted for GE LM6000. Nomenclature as in Fig. 7.6b.

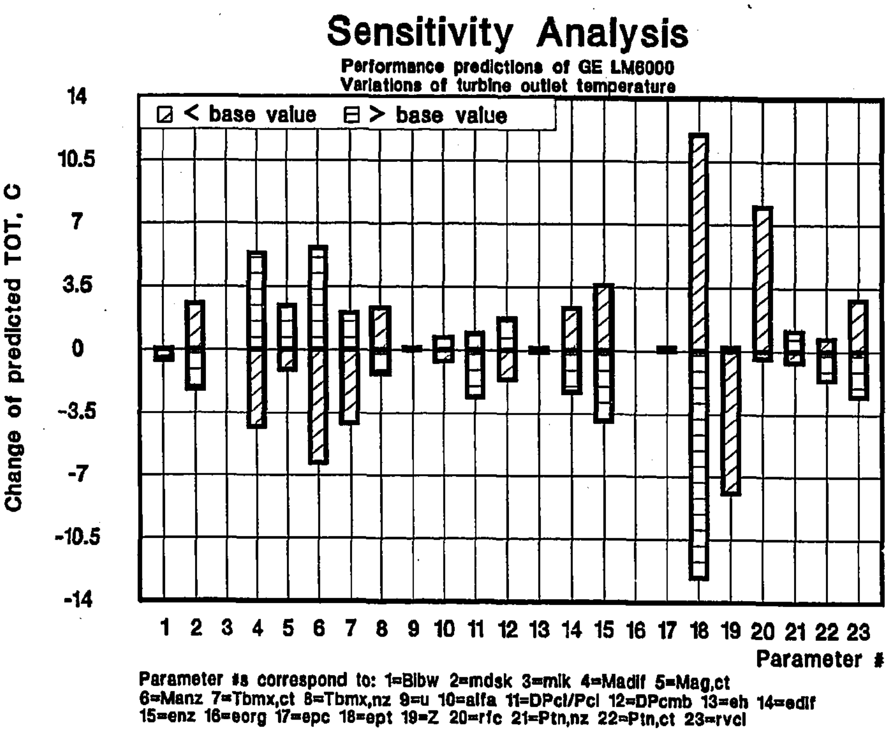

7.9a Variations of turbine outlet temperature predicted for GE LM6000. Nomenclature as in Fig. 7.6a.

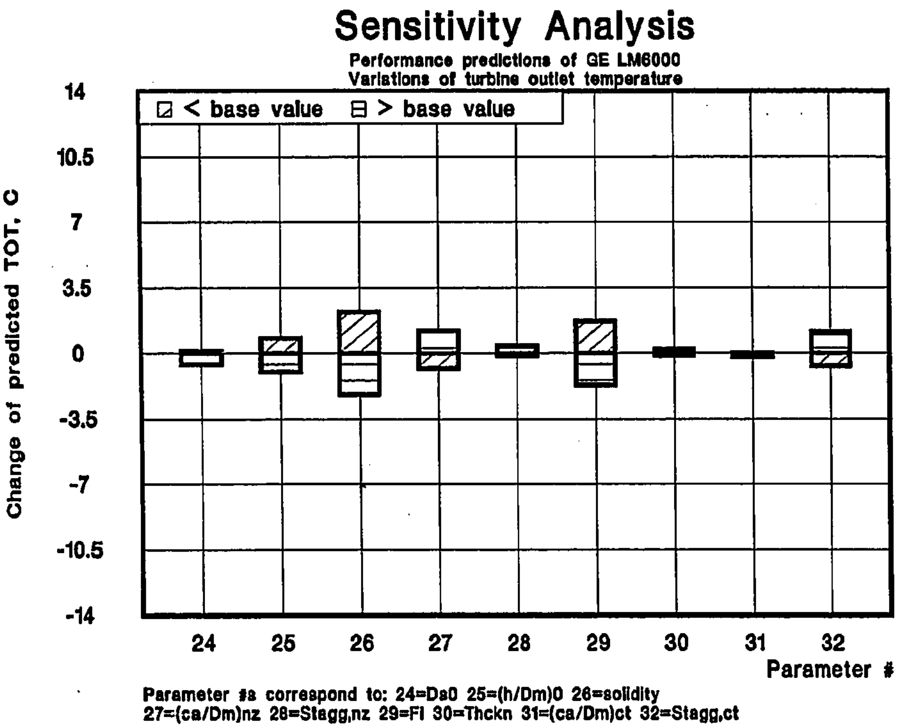

7.9b Influence of geometric characteristics on TOT predicted for GE LM6000. Nomenclature as in Fig. 7.6b.

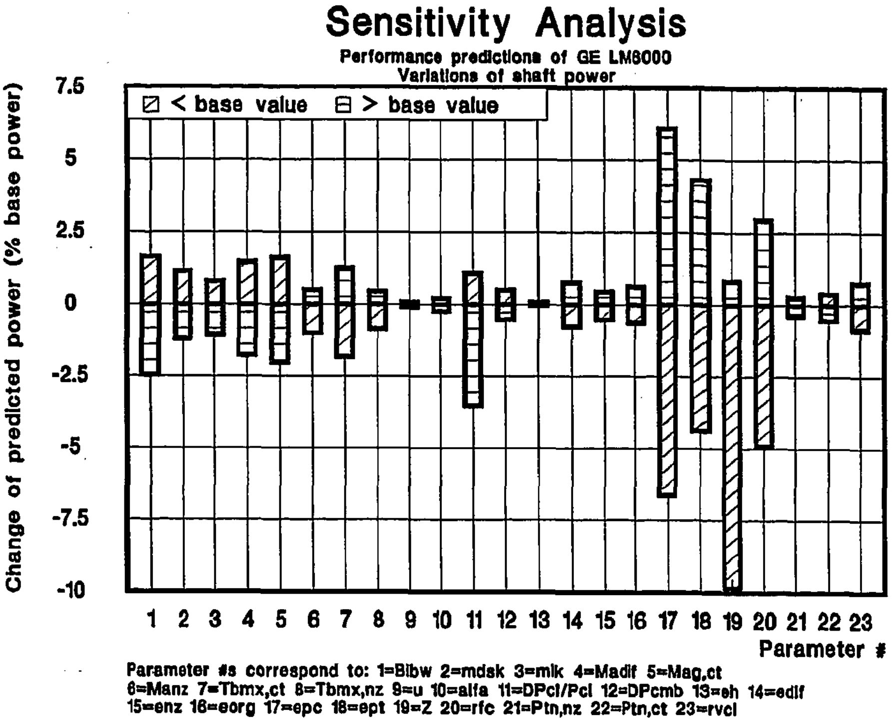

7.10a Variations of shaft power predicted for GE LM6000. Nomenclature as in Fig. 7.6a.

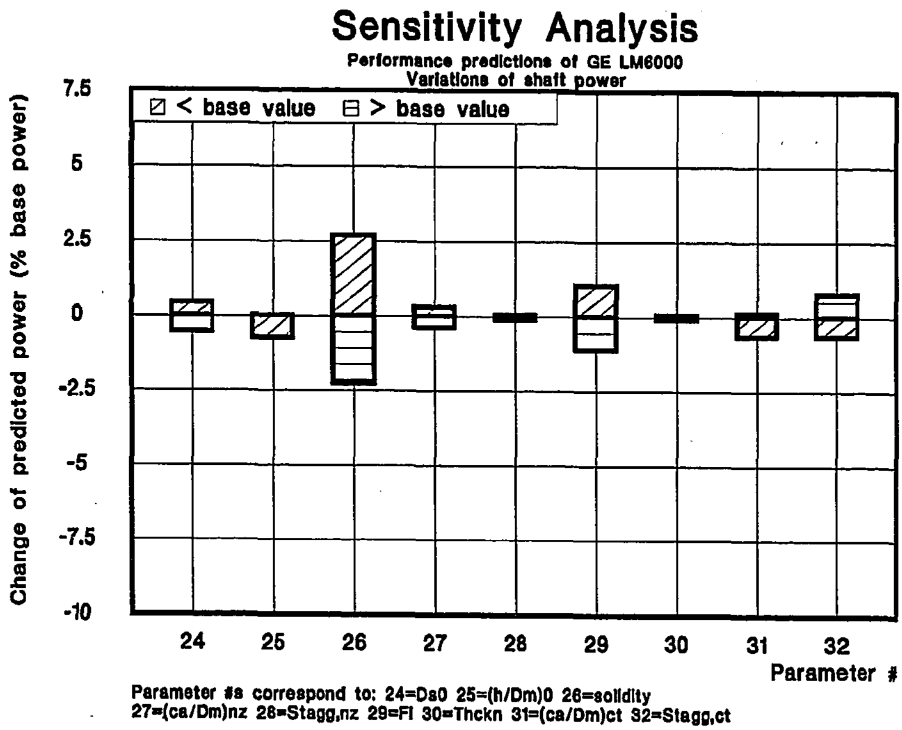

7.10b Influence of geometric characteristics on shaft power predicted for GE LM6000. Nomenclature as in Fig. 7.6b.

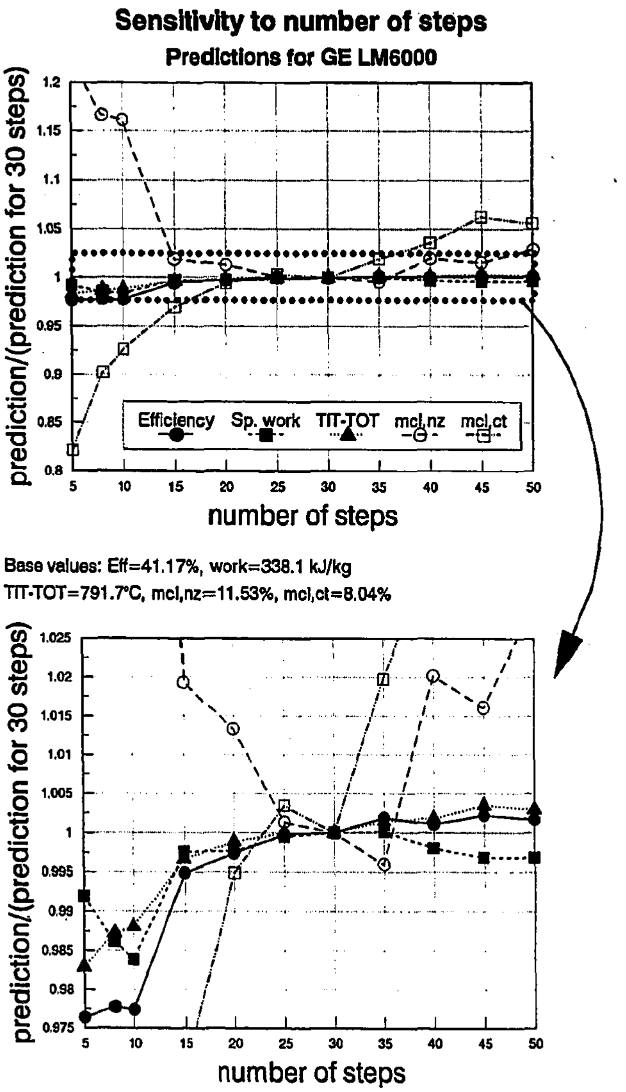

7.11 Sensitivity of the predictions for the GE LM6000 to the number of cooled expansion steps. Diagrams report results of calculations where, except for n_{step}, all inputs have been kept constant (values of Tab.7.3 and calibrated values of Tab.7.5).

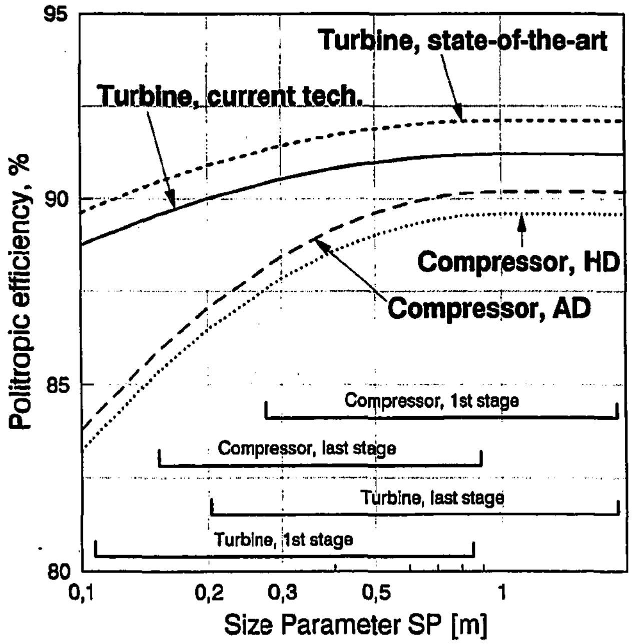

7.12 Functions $\eta_{p,c}$ and $\eta_{p,t}$ as resulting from calibration.

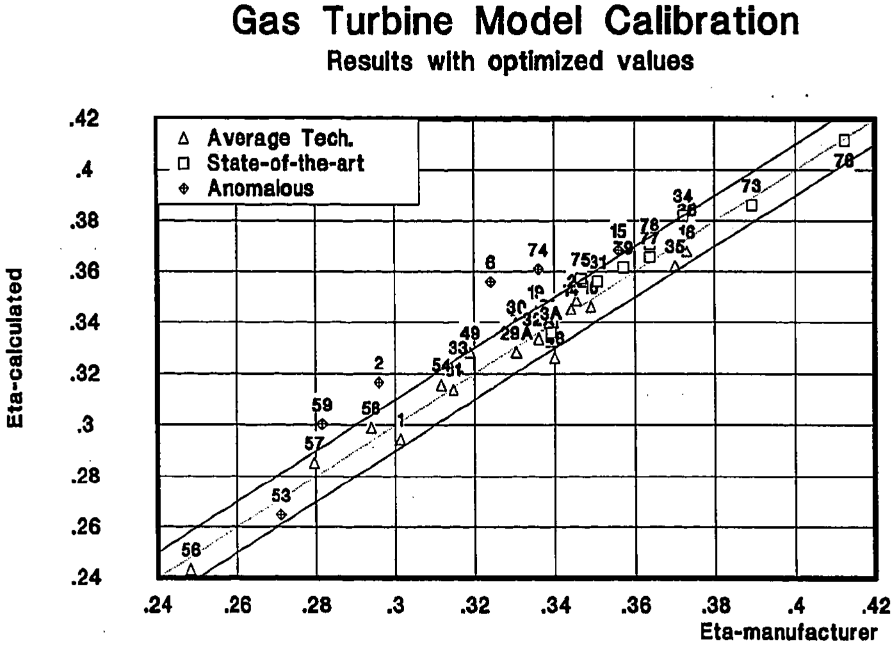

7.13 Comparison between efficiencies given by manufacturers and values predicted with the optimized set of model parameters. The two straight lines delimit the region where the discrepancy is less than one percentage point. The six turbines indicated by a crossed box (#2, 6, 15, 53, 59 and 74) are the ones excluded from the calibration; their poor performances could not be reproduced by the calculation model.

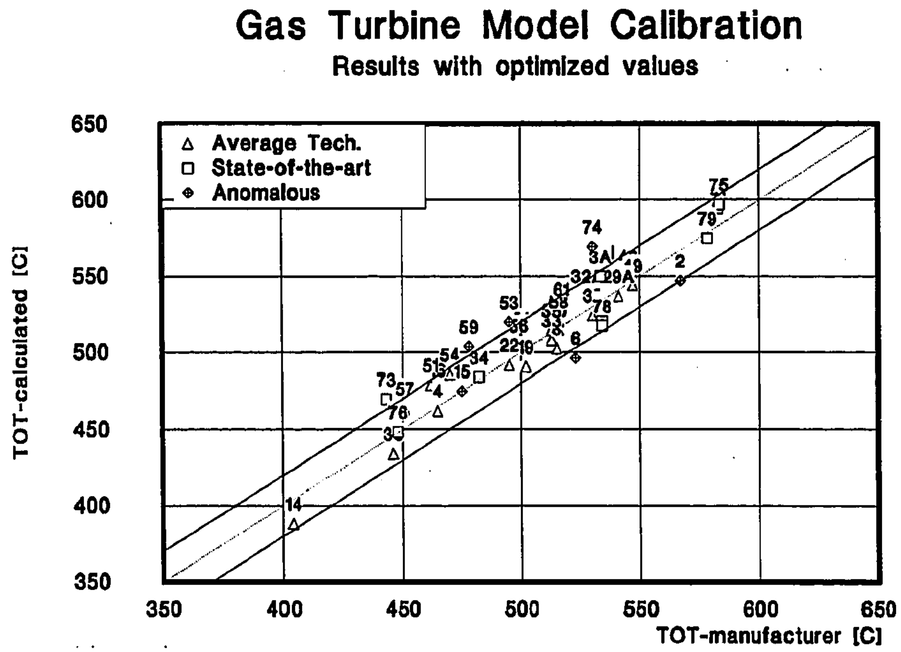

7.14 Comparison between turbine outlet temperatures given by manufacturers and values predicted with the optimized set of model parameters. The two straight lines delimit the region where the discrepancy is less than 20°C. The six turbines indicated by a crossed box (#2, 6, 15, 53, 59 and 74) are the ones excluded from the calibration.

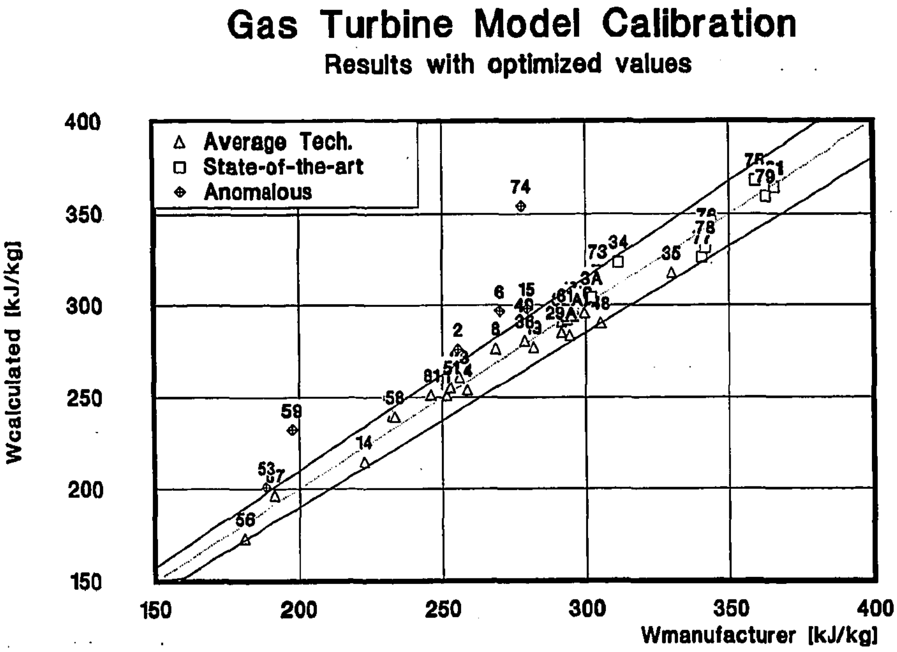

7.15 Comparison between specific work given by manufacturers and values predicted with the optimized set of model parameters. The two straight lines delimit the region where the discrepancy is less than 5%. The six turbines indicated by a crossed box (#2, 6, 15, 53, 59 and 74) are the ones excluded from the calibration.

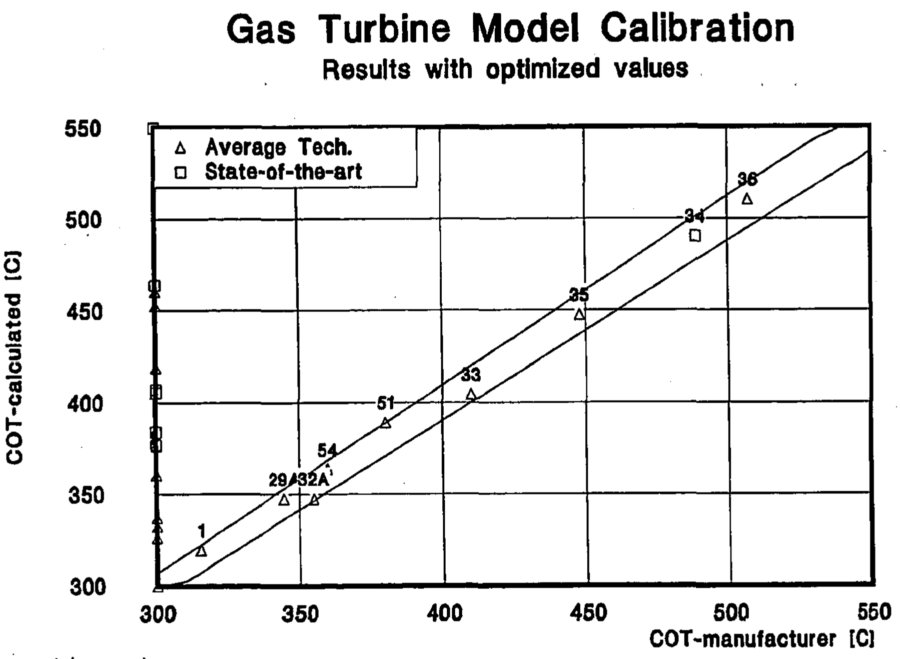

7.16 Comparison between compressor outlet temperatures given by manufacturers and values predicted with the optimized set of model parameters. The two straight lines delimit the region where the discrepancy is less than 10°C.

8. ENTROPY ANALYSIS

This Chapter illustrates the basic relationships to be used for the entropy analysis of GSC systems. Entropy analysis is not part of the procedure followed to evaluate cycle performance; it is a further calculation which – based on the thermodynamic conditions reached after convergence – quantifies the irreversibilities occuring in each component.

For most processes the evaluation of entropy production is rather elementary. Instead, mixing, combustion and discharge to ambient require a more elaborate schematization; in particular we will show that, differently from non-condensible gases, the entropy production due to mixing of condensible vapours may depend on the conditions at which mixing is performed, an occurrence overlooked by many thermodynamic textbooks.

The paragraph on combustion allows drawing important conclusions on the maximum efficiencies to be expected by any GSC operating with a given TIT. In particular, it is shown that for state-of-the-art TIT around 1250°C any claim of cycle efficiencies above 56-60% is highly questionable.

The Chapter closes with an example for a steam injected turbine, illustrating how losses are broken down among the different elementary thermodynamic processes which compose the cycle.

Due to space limitations, Ch. 10 reports only brief discussions of entropy losses breakdowns; however, their importance for the comprehension of power system thermodynamics cannot be overemphasized.

8.1 Background

The purpose of "2nd-law" or "entropy" analyses is to identify the sources of irreversibilities. Entropy analyses are more general than "1st-law" or "energy balance" analyses, because they account for both the 1st and 2nd law of thermodynamics. The performances of actual systems are compared to the ones obtainable through ideal, reversible processes; rather than correlating losses to how much energy is lost, losses are related to how irreversible are the processes taking place in each component. In recent years, entropy analyses have been the subject of a vast body of literature (Liu and Wepfer, 1983), while some software package for the evaluation of power plant performance now include the detailed calculation of all entropy productions (El-Masri, 1988).

Although a number of different treatments have been presented in the literature (e.g. Borel, 1979; Ahern, 1980; Kotas, 1985; Bejan, 1988) the basis of all entropy analyses is the recognition that if ΔS_{irr} is the entropy rise originated by a given process*, the same final conditions could be reached, reversibly, after producing the extra-work:

$$\Delta W_{rev} = T_0 \cdot \Delta S_{irr} \tag{8.1}$$

where T_0 is the ambient temperature. The importance of this relation was already recognized by Stodola (1922)**; later, Tolman and Fine (1948)

* ΔS includes the entropy variation of both the system being studied and the ambient. By including the ambient, every process is adiabatic and becomes reversible if $\Delta S=0$. The ambient intensive properties (T_0, P_0, composition) remain always constant.

** Much before, Gouy (1889) had introduced the concept of "énergie utilizable", which corresponds to what is now called availability and from which it is possible to derive Eq.(8.1).

presented a systematic evaluation of ΔS_{irr} of a number of processes encountered in nature.

Eq.(8.1) holds as long as the 1st and 2nd law are applicable, and can be used for any thermodynamic process: heat transfer, throttling, compression, combustion, radiative heat transfer, magneto-hydrodynamics, chemical reactions, etc. If $W_{rev,in}$ is the input of reversible work to a power system, the reduction of efficiency caused by the loss given by Eq.(8.1) is:

$$\Delta\eta = T_0 \cdot \Delta S_{irr} / W_{rev,in} \tag{8.2}$$

where the input of reversible work can be in the form of fuel chemical energy (plants operating on fossil fuels, fuel cells), heat (heat recovery systems), electro-magnetic radiation (photo-voltaic systems), gravitational potential (hydro-electric plants), etc. As shown in Par. 8.4, W_{rev} of a fuel differs from both its LHV and HHV; to emphasize the reference to 2nd-law considerations, the efficiency appearing in Eq.(8.2) is often indicated by η_{II}.

8.2 Thermo-mechanical processes

For an open, steady-state system not subject to gravitational or electro-magnetic actions, the reversible specific work [J/kg] obtainable by bringing a flow with total* enthalpy h and entropy s into mechanical and thermal equilibrium with the environment (i.e. $P=P_0$, $T=T_0$) is given by:

$$w_{rev} = (h-T_0\cdot s)-(h_0-T_0\cdot s_0) = b-b_0 = ex_{ph} \tag{8.3}$$

Following Bejan (1988), the quantity $b=(h-T_0\cdot s)$ is named the flow "availability", while $ex_{ph}=(b-b_0)$ is the flow "physical exergy". Physical exergy constitutes the maximum work obtainable by bringing the flow to the "dead" state of thermo-mechanical equilibrium with the environment.

Eqs.(8.1) and (8.3) allow determining the reversible work losses of processes relevant to cycle analyses (1 and 2 indicate initial and final conditions, respectively):

Compression of a perfect gas at constant η_p:

$$w_{lost} = (1/\eta_p-1)\cdot R\cdot T_0\cdot \ln(P_2/P_1)$$

Liquid compression**:

$$w_{lost} = v\cdot(P_2-P_1)\cdot[(1-\eta)/\eta]\cdot(T_0/T)$$

where T is the average temperature at which the heat generated by friction is introduced into the liquid. For constant v and η, $T=(P_2-P_1)/\int(dP/T)$; if c_p is constant, $T=T_1+[(P_2-P_1)/(\rho\cdot c_p)]\cdot[(1-\eta)/\eta]$. Since

---

* Unless otherwise indicated, in this Chapter we will always refer to total quantities.

** For a liquid the distinction between polytropic and isoentropic efficiency is meaningless because v is constant.

for liquids the thermal capacity $\rho \cdot c_p$ is large, the temperature increase $(P_2-P_1)\cdot[(1-\eta)/\eta]/(\rho\cdot c_p)$ caused by friction is generally small, and it can often be assumed that $T_1 \simeq T_2 \simeq T$

<u>Expansion of a perfect gas at constant η_p</u> (for throttling set $\eta_p=0$):

$$w_{lost} = (1-\eta_p)\cdot R\cdot T_0\cdot \ln(P_1/P_2)$$

<u>Liquid expansion</u> (for throttling set $\eta=0$):

$$w_{lost} = v\cdot(P_1-P_2)\cdot(1-\eta)\cdot(T_0/T)$$

<u>Heat exchangers</u>:

$$\dot{W}_{lost} = T_0\cdot(\dot{M}_{hot}\cdot\Delta s_{hot}+\dot{M}_{cold}\cdot\Delta s_{cold})$$

and if specific heats are constant:

$$\dot{W}_{lost} = T_0\cdot\{[\dot{M}\cdot c_p\cdot(\ln(T_2/T_1)]_{hot}+[\dot{M}\cdot c_p\cdot(\ln(T_2/T_1)]_{cold}\}$$

<u>Heat Q discharged at constant temperature T</u>:

$$W_{lost} = Q\cdot(1-T_0/T)$$

<u>Heat flux q across a wall</u> with cross-section A, thermal conductivity k, thickness t and hot-side temperature T_h:

$$\dot{W}_{lost} = (q^2/T_h)\cdot(t/k)\cdot A$$

8.2.1 Flow acceleration

One further process relevant to gas cycle analyses is the acceleration of a mass dm_{clt} of coolant injected into a mainstream flow m_g with velocity v_g. If acceleration is performed at constant v_g (i.e. the component of v_{cl} along v_g is increased up to v_g at the expense of mainstream total pressure losses), the enthalpy variation of the mainstream can be found by combining Eqs.(3.13) and (3.17):

$$dh_g = -(dm_{clt}/m_g)\cdot[\Delta h_{cl,st}+(\vec{v}_g^2-\vec{v}_{cl}^2)/2] \qquad (8.4)$$

This equation shows that the enthalpy variation of the mainstrem goes partly to increase coolant temperature – to bring T_{cl} up to T_g – and partly to coolant acceleration – to bring v_{cl} up to v_g. The variation to be "charged" to acceleration is:

$$dh_{g,acc} = -(dm_{clt}/m_g)\cdot(v_g^2-v_{cl}^2)/2 \tag{8.4a}$$

As long as $dm_{clt} \ll m_g$, the coolant entropy change $dm_{clt}\cdot ds_{cl,acc}$ is negligible* compared to $m_g\cdot ds_{g,acc}$; thus:

$$ds_{acc} = ds_{g,acc} = dh_{g,acc}/T_g - v_g\cdot dP_g/T_g \tag{8.5}$$

Substituting Eqs.(8.4a), (3.12) and the equation of state:

$$ds_{acc} = (dm_{clt}/m_g)\cdot\left\{\gamma_g\cdot Ma_g^2\cdot R_g\cdot(1-v_{cl}/v_g)-\gamma_g/2\cdot Ma_g^2\cdot R_g\cdot[1-(v_{cl}/v_g)^2]\right\} \tag{8.6}$$

If $v_{cl} \ll v_g$ – but only in this case – this expression simplifies to the one frequently given in fluid dynamic textbooks:

$$ds_{acc} = \gamma_g/2\cdot Ma_g^2\cdot R_g\cdot(dm_{clt}/m_g) \tag{8.6a}$$

If dm_{clt} is not infinitesimal, the governing equations must be modified as indicated in Par. 3.8.1, thus using Eqs.(3.12a) and (3.13a) rather that Eqs.(3.12) and (3.13). The computer program does not actually refer to the system formed by Eqs.(3.12a), (3.13a), (3.17) and (8.5); after calculating the conditions after mixing, the whole entropy variation due to coolant discharge – i.e. acceleration <u>and</u> heat transfer to bring T_{cl} up to T_g – is found as:

$$\Delta s_{cldis} = (m_g+\Delta m_{clt})\cdot s_{g,2}-m_g\cdot s_{g,1}-\Delta m_{clt}\cdot s_{cl,1} \tag{8.7}$$

---

* This holds for the entropy change due to coolant acceleration; it is not true for the entropy change due to coolant temperature variations.

8.3 Mixing

As long as composition doesn't change, and provided that h and s indicate the mass-weighted averages:

$$h_{mix} = \Sigma(y_i \cdot h_i) = \Sigma(x_i \cdot \mathcal{W}_i \cdot h_i)/\mathcal{W}_{mix} \qquad \text{(the same for } s_{mix}\text{)}$$

then Eqs.(8.3) to (8.7) also hold for mixtures. However, mixtures bring about another type of irreversibility – the mixing loss – which is particularly relevant to Gas/Steam Cycles.

8.3.1 Perfect gas mixing

For a perfect gas, mixing losses can simply be explained in terms of partial pressures, i.e. the work which could be produced by reversibly expanding the unmixed gases from their initial pressure to their final partial pressures $P_{mix} \cdot x$, where x is the molal concentration into the final mixture. Adiabatic, irreversible mixing of perfect gases is always isothermal, because internal energy and enthalpy do not depend on partial pressure. Since the entropy rise due to throttling from P_1 to P_2 is $M \cdot R \cdot \ln(P_1/P_2) = n \cdot \mathfrak{R} \cdot \ln(P_1/P_2)$, ΔS_{mix} and the corresponding reversible work are:

$$\begin{aligned} \Delta S_{mix} &= \mathfrak{R} \cdot \Sigma[n_i \cdot \ln(1/x_i)] = M_{mix} \cdot R_{mix} \cdot \Sigma[x_i \cdot \ln(1/x_i)] \\ W_{rev,mix} &= T_0 \cdot \Delta S_{mix}/M_{mix} = R_{mix} \cdot T_0 \cdot \Sigma[x_i \cdot \ln(1/x_i)] \end{aligned} \qquad (8.8)$$

This holds within the limits of Dalton's law, and excludes any type of interaction between the molecules of the two species.

8.3.1.1 Reversible process

An ideal process which could actually produce $W_{rev,mix}$ is depicted in Fig. 8.1. In order to meet the same initial and final conditions, transformations are no longer adiabatic. Reversibility is achieved by means of ideal, semi-permeable mebranes and, if mixing takes place at $T_{mix} \neq T_0$, of an ideal engine exchanging heat between T_{mix} and T_0. Ideal, semi-permeable membranes can be crossed only by molecules of one single chemical species and are impervious to all others. In Fig. 8.1 membrane MA can be crossed by gas A but is impervious to gas B, while the opposite is true for membrane MB. Starting from a situation with the gases totally unmixed and the two membranes overlapping at the position which gives $P_A = P_B = P_{mix}$, let's move membrane MA leftward so as to expand isothermally gas B: if $T_{mix} \neq T_0$, the heat Q necessary to maintain constant T is provided (or rejected) by a reversible engine absorbing the work $W = Q \cdot (1 - T_0/T_{mix})$. During this process nothing happens to gas A, since membrane MA is "transparent" to its molecules. When membrane MA reaches the left wall of the box, gas B reaches its final specific volume and hence its final partial pressure $P_{mix} \cdot x_B$. The net work produced during this phase is:

$$W_{MA} = n_B \cdot \mathfrak{R} \cdot T_{mix} \cdot \ln(1/x_B) - n_B \cdot \mathfrak{R} \cdot T_{mix} \cdot \ln(1/x_B) \cdot (1 - T_0/T_{mix}) = n_B \cdot \mathfrak{R} \cdot T_0 \cdot \ln(1/x_B) \tag{8.9}$$

The first term is the isothermal expansion work, i.e. $(\int P \cdot dv)_T = Q$; the second is the reversible work necessary to maintain constant T. At this point the pressure in the left section of the box – which is occupied by both gases – is $P_{mix} \cdot (1 + x_B)$; the pressure in the right section of the box – which is occupied only by gas B – is $P_{mix} \cdot x_B$. The condition of gases fully mixed can now be reached by moving membrane MB rightward: in this case nothing happens to gas B, since its molecules do not "see" membrane MB, while gas A expands isothermally. By the time membrane MB reaches the right wall, the additional net work production is

$W_{MB}=n_A\cdot\Re\cdot T_0\cdot\ln(1/x_A)$; the pressure in the whole box is $P_{mix}\cdot(x_A+x_B)=P_{mix}$ and the total net work produced is:

$$\begin{aligned} W_{rev,mix} &= \Re\cdot T_0\cdot[n_A\cdot\ln(1/x_A)+n_B\cdot\ln(1/x_B)] \\ &= M_{mix}\cdot R_{mix}\cdot T_0\cdot[x_A\cdot\ln(1/x_A)+x_B\cdot\ln(1/x_B)] \end{aligned}$$

which coincides with the expression in Eq.(8.8). $w_{rev,mix}$ (and thus Δs_{mix}) does not depend on T_{mix} nor P_{mix}: it is only a function of mixture composition.

8.3.1.2 Multi-component mixtures

Repeated application of Eq.(8.8) gives the entropy rise ensuing from mixing n^{m1} kmols of a mixture with composition x_i^{m1} with n^{m2} kmols of another mixture with composition x_i^{m2}, thus obtaining $(n^{m1}+n^{m2})$ kmols of a third mixture with composition x_i^{mix}:

$$\begin{aligned} \Delta S_{mix} &= \Re\cdot\Sigma[n_i^{m1}\cdot\ln(x_i^{m1}/x_i^{mix})+n_i^{m2}\cdot\ln(x_i^{m2}/x_i^{mix})] \qquad (8.10) \\ &= M_{mix}\cdot R_{mix}\cdot[1/(1+n^{m2}/n^{m1})]\cdot\Sigma[x_i^{m1}\cdot\ln(x_i^{m1}/x_i^{mix})+(n^{m2}/n^{m1})\cdot x_i^{m2}\cdot\ln(x_i^{m2}/x_i^{mix})] \end{aligned}$$

where some of the x_i^{m1} or x_i^{m2} may be zero*. This equation allows the determination of the loss of any mixing process involving perfect gases.

8.3.2 Mixing of real gases

For real gases Δs_{mix} is not only a function of mixture composition, but also of the conditions at which mixing is performed. This is apparent when considering that, referring to the ideal process illustrated in Fig. 8.1, the work produced during the isothermal expansion of component i is:

---

* The corresponding term becomes zero because $\lim_{x\to 0} x\cdot\ln(1/x) = 0$

$$(\int P\cdot dv)_{T,i}\cdot(T_0/T_{mix}) = R_i\cdot T_0\cdot\int[(\partial z_i/\partial P)_T-1/P]\cdot dP$$

where the compressibility factor $z=P\cdot v/(R\cdot T)$ and the integral (extending from P_{mix} to $x_i\cdot P_{mix}$) of its derivative are function of P_{mix} and T_{mix}. Adiabatic mixing of real gases is non-isothermal because, since internal energy and enthalpy do depend on pressure, when each component expands to its partial pressure it also exchanges heat. This means that real-gas mixing inherently implies transfer of heat, a situation particularly evident when involving a change of phase: for example, adiabatic, isobaric mixing of water and dry air at $P_{mix}>P_{sat}(T_w)$, where P_{sat} is the saturation pressure at the water initial temperature T_w, causes all or part of the water to evaporate. If mixing is adiabatic, the heat required by the evaporation must be provided either by the gas or by the liquid water itself.

<u>8.3.3 Vapours behaving like perfect gases</u>

For mixtures encountered in practical applications the partial pressure of all gaseous components is generally much lower than their critical pressure, thus allowing neglecting the pressure/temperature dependence introduced by z(P,T). If we assume that all gaseous components behave like perfect gases, the only case when ΔS_{mix} cannot be evaluated by Eq.(8.10) is when mixing implies a change of phase. An ideal process whereby a liquid A at P_{mix},T_{mix} is mixed with a perfect gas B at P_{mix}, T_B to give a mixture at P_{mix},T_{mix} is illustrated in Fig. 8.2. We will assume that in the liquid phase species A is perfectly incompressible, and that its vapour behaves like a perfect gas. The initial temperature of the gas B must be higher than T_{mix} because the gas has to provide the heat necessary to evaporate the liquid. The liquid enters an ideal hydraulic turbine where it expands to $P_{sat}(T_{mix})$ producing the work*:

$$M_A \cdot v_{A\ell} \cdot [P_{mix} \cdot (1-r_{sat})] \tag{8.11}$$

$v_{A\ell}$ is the liquid specific volume and $r_{sat}=P_{sat}(T_{mix})/P_{mix}$; since liquid compressibility is negligible, $v_{A\ell}\simeq$constant and the temperature at the exit of the hydraulic turbine $\simeq T_{mix}$. The saturated liquid then enters a heat exchanger where it evaporates at the expense of a work W_A provided to an ideal heat pump. Gas B is cooled down to T_{mix} by providing heat to an ideal engine producing the work W_B. The difference W_B-W_A – always positive – is the reversible work associated with heat transfer; the corresponding entropy rise is:

$$\Delta S_{HT} = (W_B-W_A)/T_0 \tag{8.12}$$

Vapour A and gas B, now both at T_{mix}, finally enter a device utilizing ideal semi-permeable membranes like the one depicted in Fig. 8.1, where they produce the work:

$$n_A \cdot \mathfrak{R} \cdot T_0 \cdot \ln\left[P_{sat}(T_{mix})/(x_A \cdot P_{mix})\right] + n_B \cdot \mathfrak{R} \cdot T_0 \cdot \ln(1/x_B) \tag{8.13}$$

Aside from W_B-W_A, the reversible work obtained through mixing is the sum of expressions (8.11) and (8.13). The correspondent entropy rise is:

$$\Delta s_{mix} =$$

$$(M_A/M_{mix}) \cdot v_{A\ell} \cdot P_{mix} \cdot (1-r_{sat})/T_0 + R_{mix} \cdot \left[x_A \cdot \ln(r_{sat}/x_A) + x_B \cdot \ln(1/x_B)\right] \tag{8.14}$$

where the first term (liquid expansion work) is generally negligible and applies only to open systems. Eq.(8.14) holds for:

---

* The liquid expansion work must be considered only for open systems. For a closed system, the expansion work of an incompressible liquid is always zero.

$x_A < r_{sat} < 1$

If $r_{sat} \geq 1$ it means that also species A is initially gaseous, and we must use the expressions derived for perfect gases. If $r_{sat}=x_A$ it means that the final mixture is saturated; in this case $w_{rev,mix}$ of species A is only the liquid expansion work.

8.3.3.1 Variations with mixture temperature

Given P_{mix} and M_A/M_{mix}, the heat transfer and mixing entropy given by Eqs.(8.12) and (8.14) vary with T_{mix} as qualitatively illustrated in Fig. 8.3, while Fig. 8.4 illustrates quantitative calculations performed for mixtures of water (species A) and dry air (species B). T^*_{sat} is the maximum temperature still giving a saturated mixture. We can identify three regions:

- For $T_{mix}<T^*_{sat}$ the mixture is saturated with $x_A=r_{sat}(T_{mix})$ and $x_B=1-r_{sat}$. The only contribution of species A to Δs_{mix} is due to liquid expansion (zero for closed systems). The contribution of species B decreases with decreasing T_{mix}, because the lower T_{mix} the lower the "effective" mixing. In proximity of the triple point temperature the vapour pressure of A becomes so low that the two species remain separated. Δs_{HT} and the initial perfect gas temperature T_B vary according to the fraction of A which actually evaporates. At $T_{mix}=T^*_{sat}$ the mixture is still saturated but there is no liquid.

- For $T^*_{sat}<T_{mix}<T_{sat}(P_{mix})$ species A is initially liquid, but it thoroughly evaporates into the final mixture, where x_A and x_B are constant. The contribution to Δs_{mix} of liquid expansion decreases with the difference $P_{mix}-P_{sat}(T_{mix})$, while the contribution of vapour A expansion increases with $\ln(r_{sat}/x_A)$. The contribution of species B is constant. When $T_{mix}=T_{sat}(P_{mix})$, Δs_{mix} reaches the value corresponding to perfect gas. Δs_{HT} decreases with T_{mix} because of reductions of the heat of evaporation and of the average heat transfer ΔT. Due to the former, the initial temperature of the perfect gas (T_B) increases more slowly than T_{mix} (Fig. 8.4).

- For $T_{mix}>T_{sat}(P_{mix})$ also species A is initially gaseous. Due to the assumption of perfect gas behaviour for all gaseous species, Δs_{mix} is constant, Δs_{HT} is zero and $T_B=T_{mix}$. If A did not behave as a perfect gas, Δs_{mix} and Δs_{HT} would approach their perfect-gas values at large T_{mix}.

Fig. 8.4 shows that at 1 atm and $M_w/M_{dry\ air}$=10%, steam mixing gives Δs_{mix}≈121 J/K-kg$_{air}$. For T_0=15°C, such Δs translates into a work loss of about 35 kJ/kg$_{mix}$ = 38.5 kJ/kg$_{air}$. Comparing this figure with typical work outputs of 350-450 kJ/kg$_{air}$ of steam injected gas cycles (see Par. 2.4 and Tab. 8.2) shows how mixing losses pose serious constraints to the efficiency attainable by such cycles.

8.3.3.2 Multi-component mixtures

If n_A kmols of liquid A are mixed with n^m kmols of a mixture with composition x_i^m to give $(n_A+n_i^m)$ kmols of a mixture with composition x_i^{mix}, Eq.(8.14) must be modified as follows:

$$\Delta s_{mix} = (M_A/M_{mix})\cdot v_{Al}\cdot P_{mix}\cdot(1-r_{sat})/T_0 +$$
$$R_{mix}\cdot[1/(1+n^m/n_A)]\cdot[\ln(r_{sat}/x_A^{mix})+(n^m/n_A)\cdot\Sigma x_i^m\cdot\ln(x_i^m/x_i^{mix})] \qquad (8.15)$$

where we remind that x_A^{mix} is the mol fraction in gas. The case of mixtures with more than one liquid species requires the knowledge of the mixture state diagram and is beyond the scope of this analysis.

8.3.3.3 Deviations from perfect gas behaviour

In order to close the entropy analysis performed to obtain Fig. 8.4 it is necessary to introduce an artificial term ΔS_{rg} accounting for inconsistencies in the evaluation of H_2O properties. In other words, the entropy of the mixture is:

$$S_{mix} = S_w+S_{air}+\Delta S_{mix}+\Delta S_{BT}+\Delta S_{rg}$$

Before mixing, steam properties are evaluated according to S.I. Tables (Schmidt, 1982), thus including real gas effects; instead, after mixing water vapour is treated as a perfect gas (see App. B). The fictitious "work loss" $T_0\cdot\Delta s_{rg}$ is the difference between the exergy of the incoming steam and the exergy of the corresponding "perfect-gas" steam flow (Fig. 8.5). In order to obtain the same mixture conditions, the corresponding perfect-gas flow must have the same P and h of the real-gas (open, adiabatic system); for a closed system, we should conserve internal energy.

8.3.4 Means for reducing mixing losses

Whilst perfect gas mixing losses can be eliminated (or reduced) only by using semi-permeable membranes, the mixing loss of a condensible vapour can be reduced by means of thermo-mechanical processes. The concept is illustrated in Fig. 8.6. In case 1, M_A kg of condensible vapour at P,T are mixed with M_B kg of perfect gas and then brought to thermo-mechanical equilibrium with the ambient; in case 2, the two steps are reversed. The extra-work produced in case 2 is:

$$\Delta W = T_0 \cdot [\Delta S_{mix}(P,T) - \Delta S_{mix}(P_0,T_0)] \quad (8.16)$$

As long as the initial temperature of A is above saturation and the mixture at P_0,T_0 does not contain liquid, ΔW is constant and equals:

$$M_A \cdot \left\{ R_A \cdot T_0 \cdot \ln[P_0/P_{sat}(T_0)] - v_A \cdot [P_0 - P_{sat}(T_0)] \right\} \quad (8.17)$$

The production of this extra-work can be accomplished by expanding A down to $P_{sat}(T_0)$ and, after condensation, by pumping it to P_0 at the expense of negligible work. For steam mixing and T_0=15°C, Eq.(8.17) gives $\Delta W \simeq 543$ kJ/kg_{steam}. While Eq.(8.16) is always applicable, Eq.(8.-17) over-estimates the work loss when:

1) A is initially liquid. In this case ΔW depends on P and T (see variations of Δs_{mix} with P in Fig. 8.4), while there will also be losses due to heat transfer ($\Delta S_{HT} \neq 0$).

2) The final mixture at P_0,T_0 contains some liquid. In such circumstance the reversible transformation from P,T to P_0,T_0 of Case 1 (Fig. 8.6) includes condensation: since the heat of evaporation is made available in a range of temperatures above T_0, it is possible to produce more work, thus reducing the gap with Case 2. This consideration explains why the loss of 35 $kJ/kg_{mix} \simeq 385$ kJ/kg_{steam} obtained from Fig. 8.4 is lower than predicted from Eq.(8.17). In fact, at ambient conditions a mixture with $M_w/M_{dry\ air}$=10% has a liquid mass fraction $[M_{liquid}/M_{mix}]$ of about 8%.

In most cases ΔW is positive, implying an actual loss; however, for liquid water at high P and low T the work loss can be negative, implying that mixing in those conditions entails a loss smaller than the one incurred at ambient conditions. Often, the dependence of Δs_{mix} on P and T is not adequately emphasized (e.g. Manfrida et al., 1989), a comprehensible posture only if: (i) mixing does not entail evaporation and (ii) the mixture at P_0,T_0 does not contain liquid. El-Masri (1988) evaluates the mixing loss by solving the differential equations governing air-steam mixing.

8.3.5 Discharge to ambient and reversible thermo-mechanical work

A particular type of mixing loss is the one originated by discharging a flow at T_0,P_0 to the environment. The reversible work produced through this process is made possible by the difference between the composition x_i of the flow being considered and the composition x_i^{amb} of the "dead state". Similarly to the physical exergy defined by Eq.(8.3) – which is due to mechanical and thermal disequilibria – such work is referred to as "chemical exergy". For a mixture of perfect gases the chemical exergy ex_{ch} is (from Eq.8.8):

$$ex_{ch} = T_0 \cdot \Delta s_{dis} = T_0 \cdot R \cdot \Sigma[\ln(x_i/x_i^{amb})] \qquad (8.18)$$

while for liquid water (from Eq.8.13):

$$ex_{ch} = T_0 \cdot \Delta s_{dis} = v_l \cdot P_0 \cdot (1-r_{sat,0}) + T_0 \cdot R \cdot \ln(1/\Phi_0) \qquad (8.19)$$

where $r_{sat,0}=P_{sat}(T_0)/P_0$ and $\Phi_0=x_w^{amb}/r_{sat,0}$ is the ambient relative humidity. If there is a species for which $x_i^{amb}=0$, then $ex_{ch}\rightarrow\infty$, because the environment would be permanently modified by the discharge process. In practice this is not true because, even if at very low concentrations, by definition the ambient must contain all species. The sum $ex_{ch}+ex_{ph}=ex_t$ gives the maximum reversible work which could be obtained by bringing a flow into chemical, mechanical and thermal equilibrium with the environment.

8.3.6 Mixing loss book-keeping

Since the only mixing loss recoverable through thermo-mechanical processes is the one incurred by mixing a condensible species at $T\neq T_0$ and/or $P\neq P_0$, the flows of physical exergy ex_{ph} must be evaluated considering that:

- chemical exergies (Eqs.8.18 and 8.19) are unrecoverable
- perfect gas mixing losses (Eq.8.10) are unrecoverable
- for water (or steam) it is possible to recover the work given by Eq.(8.16)

A 2nd-law analysis based on these assumptions detects the losses which could be avoided by means of better thermodynamic processes, while it is "transparent" to the losses which can be recovered only by resorting to semi-permeable membranes.

8.4 Combustion and fuel exergy

Provided that enthalpy and entropy of all species are referred to the same reference conditions and that enthalpies also include the heat of formation*, the overall reversible work obtainable through combustion is given by (Bejan, 1988, p. 380):

$$W_{rev,cmb} = \Sigma[M_r \cdot (h - T_0 \cdot s)_r] - \Sigma[M_p \cdot (h - T_0 \cdot s)_p] \tag{8.20}$$

where the subscripts "r" and "p" designate the reactants and the products, respectively. $W_{rev,cmb}$ is the sum of two terms:

1) Thermo-mechanical work produced by the reaction in which each reactant and product participates as a single component at the pressure P_{mix}.

2) Difference $T_0 \cdot [(\Delta S_{mix})_r - (\Delta S_{mix})_p]$ between $W_{rev,mix}$ of the reactants and the products. Ideally, this work could be recovered by:
   a) starting with unmixed reactants
   b) mixing the reactants reversibly, thus obtaining work $T_0 \cdot (\Delta S_{mix})_r$
   c) performing the combustion process
   d) separating the products reversibly, thus adsorbing work $T_0 \cdot (\Delta S_{mix})_p$

	LHV	HHV	ex_{ph}	ex_t
H_2	119.954	141.781	117.653	118.047
C(solid)	32.763	32.763	32.837	34.193
CH_4	50.010	55.495	50.986	52.100
C_2H_4	47.158	50.295	47.455	48.673
C_2H_2	48.222	49.912	47.437	48.719

Table 8.1 Heating values and exergies [MJ/kg] of selected fuels at 1 atm, 25°C.

If chemical exergies and perfect gas mixing losses are considered unrecoverable, the second term must be neglected. If not, the entropy analysis cannot be closed because the mixing loss introduced during combustion is not compensated by a corresponding chemical exergy loss at the discharge of the combustion products to the environment. If

---

* As outlined in Appendix B, h and s are evaluated according to the conventions adopted in the JANNAF tables (Stull and Prophet, 1971): (i) at 25°C h = heat of formation (zero for elementary substances); (ii) s → 0 for T → 0 K.

both reactants and products are at P_0, T_0 and the fuel/oxidizer ratio is stoichiometric, Eq.(8.20) gives the fuel total exergy; the thermo-mechanical work ex_{ph} can be obtained after subtracting the contribution of $W_{rev,mix}$. Tab. 8.1 reports heating values and exergies of selected fuels. Notice that:

- Like the heating value, also fuel exergy varies with the reference temperature (Tab. 8.2).
- Unlike the heating value, fuel exergy also depends on the pressure at which the fuel is made available (Tab. 8.3).

T_0 [°C]	ex_{ph} [MJ/kg]	ex_t [MJ/kg]
10	51.208	51.988
15	51.135	52.027
20	51.061	52.064
25	50.986	52.100
30	50.910	52.135

Table 8.2 Variation of the exergy of methane with reference ambient temperature for $T_{CH4}=T_0$, $P_{CH4}=P_0=1$ atm.

P_{CH4} [bar]	ex_{ph} [MJ/kg]	ex_t [MJ/kg]
1.01	51.135	52.027
10	51.477	52.369
20	51.580	52.472
50	51.717	52.609
100	51.821	52.713

Table 8.3 Variation of the exergy of methane with pressure for $T_{CH4}=T_0=15$°C, $P_0=1$ atm.

8.4.1 Appraisal of combustion losses

In a GSC the losses due to combustion are by far larger than the losses of any other transformation. These losses can be quantified by introducing the second-law efficiency of combustion, defined as the ratio between the augmentation of exergy $(Ex_p-Ex_a-\Delta Ex_f)$ conferred by the fuel to the working fluid, and the fuel exergy $Ex_{f,0}$ (to avoid confusion, subscript "0" explicitly indicates that Ex_f is referred to ambient conditions):

$$\eta_{II,cmb} = (Ex_p-Ex_a-\Delta Ex_f)/Ex_{f,0} \tag{8.21}$$

where Ex_p is the exergy of combustion products at combustor outlet; ΔEx_f is the difference between fuel exergy at combustor inlet conditions and $Ex_{f,0}$; Ex_a is the exergy of air at combustor inlet. Tab. 8.4 reports the variations of $\eta_{II,cmb}$ with the air/fuel ratio for the isobaric combustion of methane and air at 15°C and 1 atm. The efficiency defined by

Eq.(8.21) is indicated as $\eta_{II,cmb,ph}$ or $\eta_{II,cmb,t}$ depending on whether exergies are physical or total. Calculations have been performed with the subroutines described at App. B under the hypothesis of complete combustion, i.e. only CO_2 and H_2O as combustion products; due to dissociation, the predictions for T_p>1700-2000°C are approximate. The table shows that even at stoichiometric conditions η_{II} is rather low: combustion inevitably "dissipates" at least 28-29% of the exergy initially "contained" in the fuel.

T_p, °C	M_a/M_f	$\eta_{II,cmb,ph}$	$\eta_{II,cmb,t}$
2028*	17.35*	71.33	72.35
2000	17.68	71.07	72.05
1800	20.39	69.10	69.93
1600	23.81	66.82	67.55
1400	28.25	64.13	64.79
1200	34.25	60.90	61.51
1000	42.76	56.93	57.51
800	55.71	51.92	52.47
600	77.63	45.34	45.88
400	122.3	36.22	36.76
200	262.4	22.39	22.92
100	577.1	12.28	12.71
50	1404.	6.140	6.412
25	4914.	2.566	2.676

* stoichiometric conditions

Table 8.4 $\eta_{II,cmb}$ for the isobaric combustion of air and methane at 15°C and 1 atm (T_0=15°C, P_0=1 atm, Φ_0=60%).

Tab. 8.5 shows that pre-heating combustion air yield substantial increases of $\eta_{II,cmb}$. In addition, in this case the limit of η_{II} for $M_f/M_a \to 0$ is greater than zero because the heat generated by combustion is introduced into the working fluid at a temperature above ambient. Thus, $\eta_{II,cmb}$ approaches the efficiency of a Carnot cycle operating between ambient and the initial air temperature, which in our case would be 57.19%. In practice this limit cannot be

T_p, °C	M_a/M_f	$\eta_{II,cmb,ph}$	$\eta_{II,cmb,t}$
2276*	17.35*	78.27	79.17
2200	18.32	77.87	78.67
2000	21.34	76.73	77.37
1800	25.25	75.43	75.97
1600	30.49	73.94	74.39
1400	37.87	72.21	72.58
1200	49.01	70.16	70.45
1000	67.68	67.68	67.89
800	105.3	64.61	64.72
600	218.5	60.67	60.60
500	445.2	58.26	57.99
450	898.6	56.95	56.47
410	4525.	55.84	55.04

* stoichimetric conditions

Table 8.5 $\eta_{II,cmb}$ for the combustion of methane at 15°C, 1 atm and air at 400°C, 1 atm (T_0=15°C, P_0=1 atm, Φ_0=60%).

reached because: (i) since methane is initially at 15°C, part of the heat is used (irreversibly) to bring its temperature to 400°C; (ii) except for exceptional circumstances, the entropy terms appearing in the definition of exergy are such that $\Delta h \approx \Delta ex$.

8.4.2 Limit η_{II}

In a gas turbine, TIT is constrained by material capabilities. The maximum combustion efficiency achievable at a given TIT can be evaluated by imagining to pre-heat both fuel and air at a temperature TIT-dT, then reaching TIT through the combustion of an infinitesimal amount of fuel. The schematic of this ideal combustion is depicted in Fig. 8.7, while Fig. 8.8 reports the corresponding $\eta_{II,cmb}$. As a first approximation, the limit $\eta_{II,cmb}$ equals the efficiency of a Carnot cycle operating between TIT and T_0; in other words, combustion "derates" fuel exergy to the exergy of a heat source available at TIT.

The information in Fig. 8.8 is very important, since it sets the limit to the efficiency of any GSC operating with a given TIT. For example, it says that a fully reversible (except combustion, of course) system with TIT=1250°C can achieve at most $\eta_{II,ph} \approx 80\%$. Considering that actual systems reach only exceptionally 70-75% of the reversible efficiency, it can be concluded that <u>for TIT=1250°C any claim of cycle efficiencies above 56-60% is highly questionable</u>.

One way to circumvent this limitation would be to substitute the combustor with a high pressure fuel cell, whereby the production of a hot mixture of oxidized species would take place simultaneously to the production of electricity. This possibility, which would open even more promising prospects to gas turbines, is seriously considered by one major turbine manufacturer (Lüthi, 1989).

8.5 Example of losses breakdown

As an example of entropy analysis, Tab. 8.6 reports the losses breakdown of the one-pressure level STIG cycle represented in Fig. 8.9. The cycle corresponds to the system based on the Allison 501 turbine also discussed at Par. 10.2.1.1. The first two columns on the left report the flows of thermo-mechanical work ex_{ph}; the other two columns on the right describe the flows of total exergy $ex_{ch}+ex_{ph}$. By definition, the perfect gas mixing loss appearing in the first left column (ex_{ph}) is always zero; for both ex_{ph} and ex_t calculations, the loss at the stack (Point 9) includes the work obtainable by steam condensation (at P_0,T_0 exhaust gases are saturated). Based on the Table, it can be observed that:

- the loss due to steam-air mixing is almost 5% of total work input
- ex_{ph} of make-up water is zero because such water is at P_0,T_0; on the contrary, its total exergy is positive (coincides with ex_{ch})
- the heat transfer loss due to H_2O mixing is zero because there is no evaporation (steam rather than liquid water)
- the real gas loss is negative, signifying that at the given P and h the exergy of the perfect gas is greater than the one of the real gas
- the chemical exergy lost at the stack (point 9) is about 2% of total input.

Although it is listed among turbine losses, the coolant compression loss actually takes place within the compressor. The 0.003% and 0.002% errors indicated in the 2nd and 4th column are due to numerical inaccuracies, as well as the 0.001% discrepancy in net work.

		ex_{ph} [%]	TOTAL	ex_t [%]	TOTAL
Input flows:	Point 1	00.000	00.000	.000	.000
	Point 12	00.000	00.000	1.059	1.059
	Point 14	100.000	100.000	98.941	100.000
Air filter:	Pressure losses	.088	.088	.085	.085
Compressor:	Friction	3.206	3.293	3.119	3.205
	Organic losses	.109	3.402	.106	3.310
Steam injectn:	Pressure losses	.520	3.922	.506	3.816
	Heat transfer	.134	4.055	.130	3.946
	H2O mixing	4.890	8.945	4.758	8.704
	H2O mix heat transfer	.000	8.945	.000	8.704
	Mixing (perfect gas)	00.000	8.945	.011	8.715
	Real gas effects	-.014	8.931	-.013	8.701
Combustor:	Thermal losses	.568	9.500	.553	9.255
	Pressure losses	.499	9.998	.485	9.740
	Combustion	30.218	40.216	29.405	39.144
	Mixing (perfect gas)	00.000	40.216	.132	39.277
Cooled turbine:	Coolant compression	.090	40.306	.088	39.364
	Coolant throttling	.217	40.524	.212	39.576
	Friction	1.025	41.549	.998	40.574
	Heat transfer	.313	41.862	.305	40.878
	Coolant discharge	1.205	43.067	1.172	42.051
	Mixing (perfect gas)	00.000	43.067	.060	42.110
	Organic losses	.075	43.142	.073	42.183
Uncooled turb.:	Friction	1.878	45.019	1.827	44.010
	Diffuser	.707	45.726	.688	44.698
	Organic losses	.155	45.881	.151	44.849
HRSG:	Gas-side DP	.284	46.165	.276	45.125
	Thermal losses	.198	46.363	.192	45.317
	El. Org. losses	.012	46.374	.011	45.328
	Makeup water mix	.002	46.376	.001	45.330
	Pumps and DP	.022	46.398	.022	45.352
	Mix and friction	.113	46.511	.110	45.462
	Deaerator heat tr.	.544	47.055	.529	45.991
	1st level heat tr.	5.744	52.799	5.589	51.580
Output flows:	Point 8	7.745	60.544	10.025	61.605
	Point 10	.273	60.817	.266	61.871
NET WORK		39.183	100.001	38.129	100.000
TOTAL INPUT [kJ/kg_{air}]		950.289		976.580	
ABSOLUTE WORK [kJ/kg_{air}]		372.352		372.359	

Table 8.2 Entropy analysis of the STIG cycle represented in Fig. 8.9. Coolant discharge losses are due to heat transfer and to total pressure losses necessary to accelerate the spent coolant. Main assumptions are: η_{pc}=86.4%; η_{pt}=89.5%; turbine has 4 stages, cooling is applied to 1st stage; ΔP of rotor cooling flow = 40%; turbine diffuser efficiency 50%; air filter ΔP = 1%; combustor ΔP = 3.5% (includes ΔP due to steam injection); combustor heat loss 0.4% of fuel LHV; leakage 0.8% of inlet air flow; organic losses 0.3%. For the HRSG: T_{ev}=199°C; Pinch=5°C; ΔP_{gas}=2.5%; heat losses 0.7%; η_{pump}=65%

REFERENCES

Ahern J.E. (1980), The Exergy Method of Energy System Analysis, John Wiley, New York.

Borel L. (1979), "Théorie Générale de l'Exergie et Applications Pratiques", Entropie, n. 85, pp. 3-14 (Part 1); n. 86, pp. 3-12 (Part 2); n. 87, pp. 4-16 (Part 3).

Bejan A. (1988), Advanced Engineering Thermodynamics, John Wiley, New York.

El-Masri M.A. (1988), "A Modified, High-Efficiency, Recuperated Gas Turbine Cycle", J. of Eng. for Gas Turbines and Power, Vol. 110, pp. 233-242.

Gouy G. (1889), "Sur l'énergie utilisable", Journal de Physique, Vol. 8, pp. 501-518.

Kotas T.J. (1985), The Exergy Method of Thermal Plant Analysis, Butterworths, London.

Liu Y.A. and Wepfer W.J. (1983), "Theory and Applications of Second Law Analysis: A Bibliography", in *Thermodynamics: Second Law Analysis*, Vol. II, R. Gaggioli ed., American Chemical Society Symposium Series, Washington D.C.

Lüthi H.K. (1989), New Products and Business Development, Power Generation Division, ABB, Baden, Switzerland, Personal Communication.

Manfrida G., Bidini G. and Alessandrello P.P. (1989), "Exergy Analysis of Viable Options for Steam/Water Injection in Gas Turbines", ASME Paper 89-GT-148.

Schmidt E. (1982), Properties of Water and Steam in S.I. Units, Springer-Verlag, Berlin.

Stodola A. (1922), Dampf- und Gas-Turbinen, 5th ed., p. 1057, Springer-Verlag, Berlin.

Stull D.R. and Prophet H. (1971), Project Directors, JANAF Thermochemical Tables, 2nd Edition, U.S. National Bureau of Standards, Washington D.C.

Tolman R.C. and Fine P.C. (1948), "On the Irreversible Production of Entropy", Reviews of Modern Physics, Vol. 20, pp. 51-77.

NOMENCLATURE

b	Flow availability, $h-T_0 \cdot s$	[J/kg]
c_p	Specific heat	[J/kg-K]
dm_{clt}	Non-dimensional blades+shroud+disk coolant flow	[kg/kg_a]
ex	Specific exergy	[J/kg]
Ex	Exergy	[J]
h	Specific enthalpy	[J/Kg]
m	Non-dimensional gas flow rate	[kg/kg_a]
M	Mass	[kg]
$\dot{M}$	Mass flow rate	[kg/s]
n	Number of kmoles	
P	Pressure	[Pa]
q	Heat flux	[W/m^2]
Q	Heat	[J]
r_{sat}	Ratio P_{sat}/P	
R	Gas constant	[J/kg-K]
$\mathfrak{R}$	Universal gas costant	[J/kmol-K]
s	Specific entropy	[J/Kg-K]
S	Absolute entropy	[J/K]
T	Temperature	[K]
v	Velocity	[m/s]
v	Specific volume	[m^3/kg]
w	Specific work	[J/kg]
W	Work	[J]
W	Molecular weight	[kg/kmol]
x	Mol fraction in gas	[gaseous mols/mixture gaseous mols]
y	Mass fraction	[kg/kg of mixture]
z	Compressibility factor	

Greek

η_p	Polytropic efficiency	
η_{II}	2nd-law efficiency	
Φ	Relative humidity	
ρ	Density	[kg/m^3]

Subscripts

a	Air
acc	Acceleration
A,B	Species A, B
ch	Chemical, refers to diffusion and mixing processes
cl	Coolant
cldis	Coolant discharge into mainstream gas
cmb	Combustion
dis	Discharge into ambient
f	Fuel
g	Gas
HT	Heat transfer
i	ith species
in	Input
ℓ	Liquid
mix	Mixing or mixture
p	Products
ph	Physical, refers to thermo-mechanical processes
r	Reactants
rev	Reversible

rg	Real gas
st	Static conditions
sat	Saturation conditions
t	Total (thermo-mechanical + chemical)
w	Water
0	Ambient conditions
1	Initial conditions
2	Final conditions

FIGURES

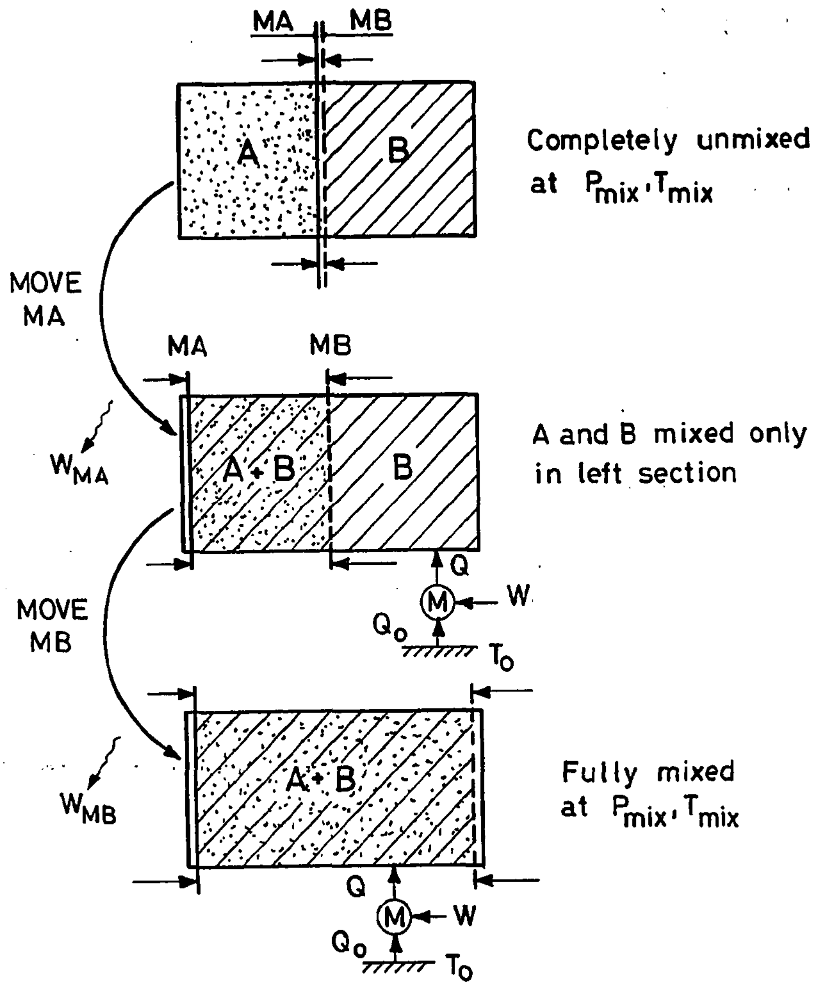

8.1 Sequence of ideal reversible processes allowing the production of $W_{rev,mix}$ of perfect gases. The ideal engine M provides the heat necessary to maintain constant temperature.

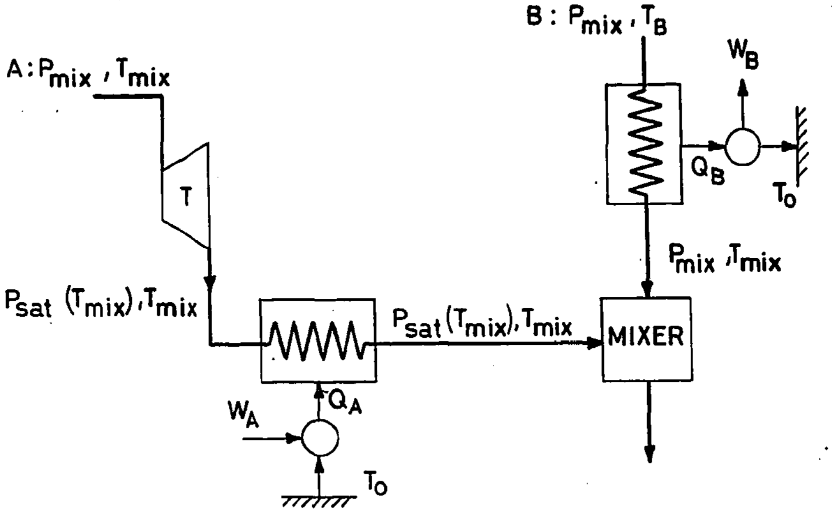

8.2 Sequence of ideal processes allowing reversible mixing between a liquid A and a perfect gas B. The heat Q_B rejected by the gas equals the heat Q_A necessary to evaporate the liquid.

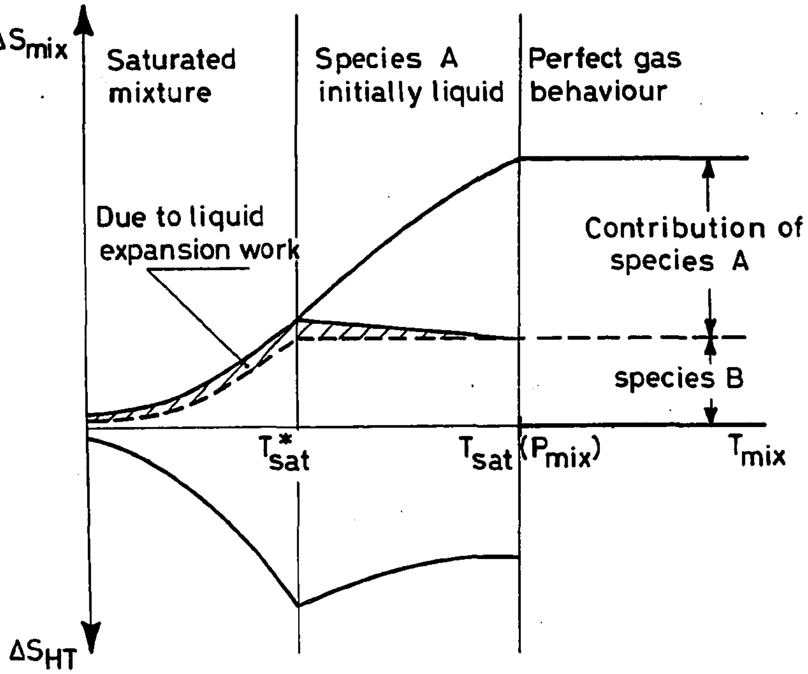

8.3 Qualitative behaviour of ΔS_{mix} and ΔS_{HT} of a mixture obtained from mixing a liquid with a perfect gas. The contribution due to liquid expansion has been exaggerated. If the vapour of species A behaves as a perfect gas, $\Delta S_{HT}=0$ as long as $T>T_{sat}(P_{mix})$.

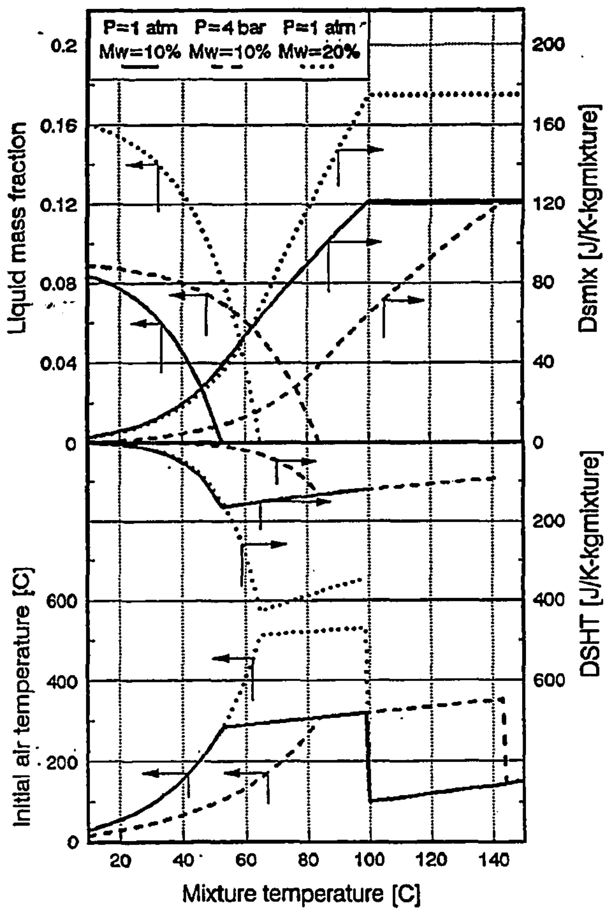

8.4 Variations of Δs_{mix}, Δs_{HT}, liquid fraction and initial air temperature (T_B of Fig. 8.2) of a mixture of water and dry air. The heat rejected by air (going from T_B to T_{mix}) is used to evaporate liquid water; M_w=$kg_w/kg_{dry\ air}$.

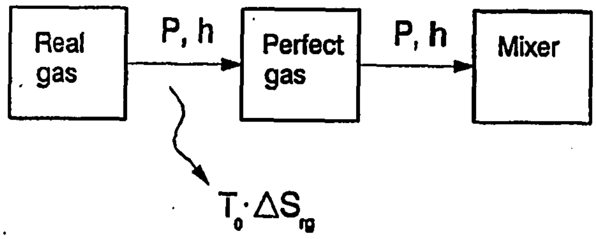

8.5 Artificial work loss due to water real gas behaviour.

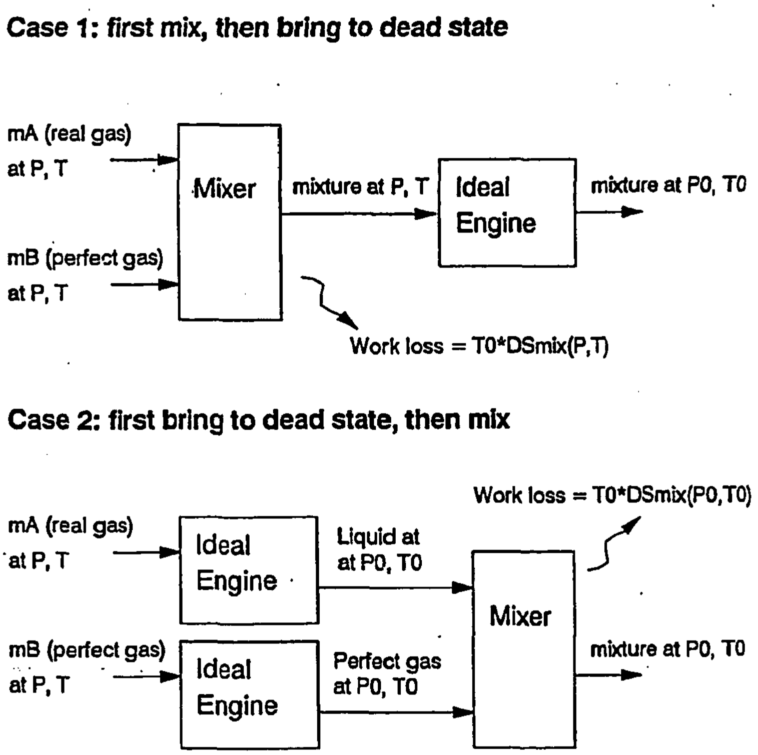

8.6 Reduction of mixing losses of a condensible vapour achieved by performing the mixing process at ambient conditions.

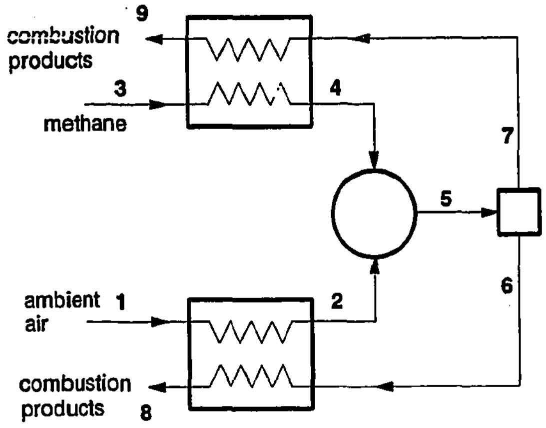

8.7 Schematic of system to be used to realize the maximum possible $\eta_{II,cmb}$. The two heat exchangers pre-heat fuel and air at the same temperature $T_2=T_4=T_5-dT$. The temperature increase across the combustor and the fuel flow rate dM_f are both infinitesimal. Due to higher specific heats, combustion gases are always capable of bringing air and fuel up to $T_2=T_4$.

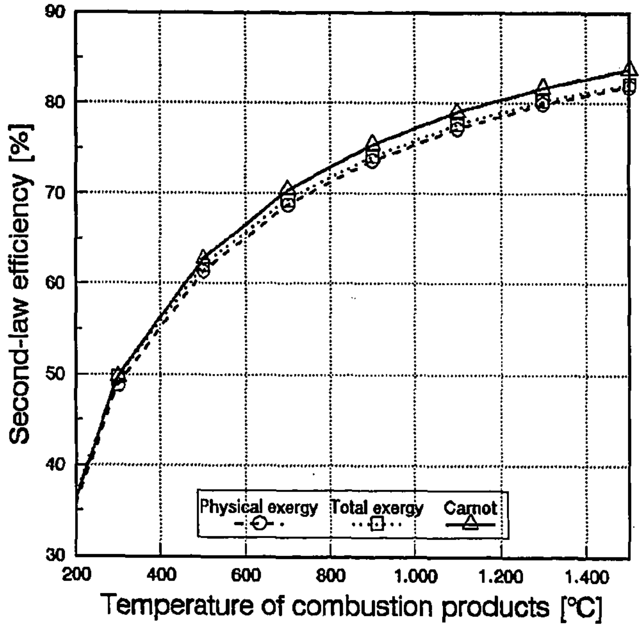

8.8 $\eta_{II,cmb}$ achievable by the system represented in Fig. 8.7. The region with T_p>1500°C has not been represented because in that case dissociation can be significant, thus requiring a different calculation procedure. Carnot efficiency is simply given by $1-T_0/T_p$.

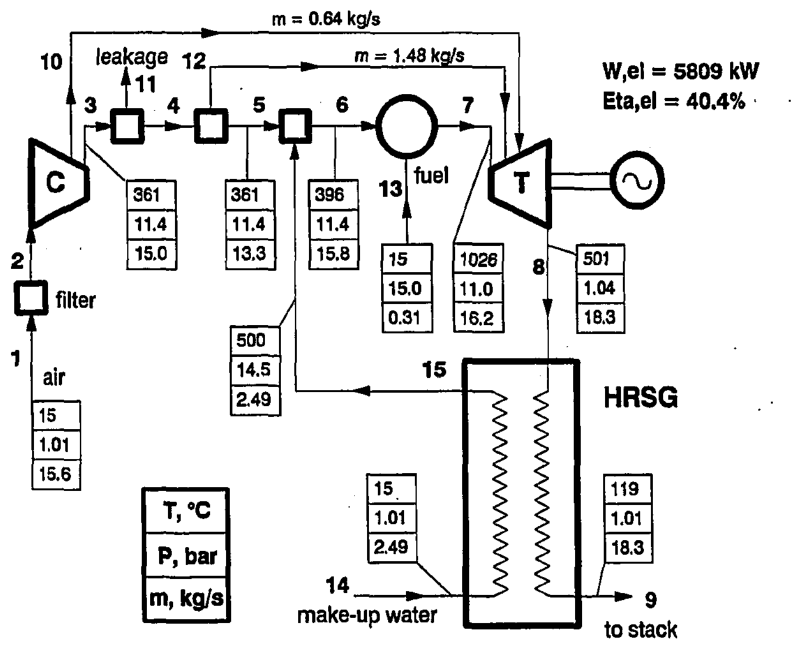

8.9 Steam injected gas cycle considered for the entropy analysis summarized in Table 8.6. Points 10 and 12 represent the first rotor and nozzle cooling flow, respectively.

9. DESCRIPTION OF COMPUTER CODE

The gas turbine model described at Chs. 3 to 6 has been implemented into a more general computer code for the calculation of Gas/Steam Cycles which is briefly illustrated in this Chapter.

The system to be calculated is defined modularly as an ensemble of interconnected components. The program poses no limitations on the complexity of the cycle configuration, although the size of the RAM memory sets a limit on the number of cycle components.

The current version of the program handles 10 different component types, whereby it is possible to reproduce the configuration of practically all systems proposed in the literature. Given the modular structure, it is relatively easy to extend the program to other systems; for example, the analysis of Integrated Gasification Combined Cycles (IGCC) requires only the addition of a subroutine for the gasifier.

Besides the author, the program has already been tested and used by P. Chiesa* and A. Lloyd**, who have introduced extensions, suggested helpful modifications and identified numerous bugs. In particular, the author acknowledges the valuable contribution of P. Chiesa in enhancing the flexibility, reliability and computing capabilities of the program.

Due to space limitations, this chapter summarizes only the basic features of the program and is by no means a manual for its use. Appendix E reports a sample of input and output files.

---

* Politecnico di Milano, Italy.

** As part of his M.S. Thesis in Mechanical Engineering at Princeton (Lloyd, 1990).

9.1 Existing codes

Aside from programs specifically developed by researchers for the analysis of particular configurations, there are three commercial codes currently available for the calculation of complex cycles (with intercooling, regeneration, reheat, etc.):

1) NNEP (Navy/NASA Engine Program)*, jointly developed by the US Navy and NASA for the calculation of aircraft engine cycles (Caddy and Shapiro, 1975; Fishbach and Gordon, 1988).

2) GATE/CYCLE, which combines the gas turbine model developed by EPRI (Cohn, 1983) with the steam cycle model developed by Enter Software (An., 1989). The package essentially consists of two separate programs – GATE for gas turbines and CYCLE for steam cycles – properly interfaced.

3) GT-PRO, developed by El-Masri on the basis of a gas turbine model illustrated in several papers (Louis, Hiraoka and El-Masri, 1983; El-Masri, 1987; El-Masri, 1988).

Without entering the details of each code, we summarize here the most relevant features:

- NNEP and GATE/CYCLE are based on a philosophy similar to our program, i.e. the definition of the cycle configuration as a collection of modules each calculated separately. Instead, in GT-PRO the system is defined by adding options to a base configuration: on one hand this limits the cycles which can be calculated but, on the other, allows solving simultaneously and more efficiently the equations governing the system.

- All programs can calculate the gas turbine off-design performance; however, the off-design behaviour of the other components (heat exchangers, boiler, steam turbines, etc.) is not always included.

- The current version of NNEP can calculate only cycles for propulsion applications, although an extension to stationary applications appears relatively simple.

- GATE/CYCLE and GT-PRO include a matrix of model parameters which allows reproducing the performances of actual engines.

---

* NNEP was not developed for commercial purposes and has no interactive interface; it is available free of charge to US Universities and research institutions.

9.1.1 Motivation for the development of a new program

With regard to parametric analyses of Gas/Steam Cycles, the main drawbacks of the existing programs are:

- The need to specify a large number of parameters which are generally unknown (compressor and turbine efficiency, cooling effectiveness curves, pressure and thermal losses, compressor bleed points, etc.).
- The detailed calculation of a number of component characteristics (velocity triangles, rotational speeds, turbine geometry, etc.) which are relevant only for specific applications.
- The inability to perform automated series of calculations spanning specified ranges of thermodynamic parameters (pressure ratios, temperatures, steam/air ratios etc.)
- The inability to handle some configurations relevant to our investigation. In fact, NNEP and GATE/CYCLE cannot handle steam cooling; GT-PRO is limited to two steam injections and cannot handle steam reheat before steam injection, etc.*

These caveats alone were sufficient to justify the development of a whole new program. In addition, it must also be noticed that:

- Developing a new program has a much higher pedagogical value.
- Except for special circumstances, the source code of a commercial program is not available.

* As already pointed out in Par. 3.3, commercial programs keep on being upgraded. Therefore, several of the present limitations may soon be removed.

9.2 Program GS

Program GS (Gas/Steam Cycles) is an interactive FORTRAN program running on Personal Computer capable of calculating the performances and the entropy analysis of almost all GSC configurations. The only exception is closed steam cooling (after cooling the gas turbine, steam returns to the Rankine cycle and expands through a steam turbine), which requires a tighter connection between the calculation of the gas turbine and the steam section.

9.2.1 Cycle components

Cycle configuration is specified by assigning the characteristics and the interconnections among cycle components, which can be of ten basic types (see Fig. 9.1):

0) Pump
1) Compressor
2) Combustor
3) Gas Turbine
4) Heat Exchanger
5) Mixer
6) Splitter
7) Steam section (HRSG with steam turbines and condenser)
8) Chemical reformer
9) Shaft

Cycle complexity is limited only by the size of the RAM memory (or by the capabilities of the Linker, see Par. 9.2.7), which constrain the maximum number of components and state points. The subroutines for the calculation of pumps and chemical reformers have been written by P. Chiesa and A. Lloyd, respectively; the subroutine for the calculation of the steam section has been written by G. Lozza* (see also Lozza, 1989; Lozza, 1990; Lozza and Bombarda, 1991) in close cooperation with the author. A brief description of each component is given in the following.

9.2.1.1 Pump

Pumps are calculated according to the incompressible flow hypothesis. There must be only one input flow and one output flow. Input data are: β, η_{ad}, η_{org}, η_{el} and $\Delta P/P$ at outlet (which might be due to valves and/or losses in outlet ducts).

9.2.1.2 Compressor

The compressor is calculated on the basis of Eqs.(4.6), (4.7) and (D.6). It can have one input flow and up to 10 output flows. The first output flow must be the compressor outlet; the second must be leakage, which is always assumed to be at the compressor outlet pressure; the other output flows are fixed-pressure bleeds (see Par. 3.7.1), ordered according to increasing pressure. Input data are: β, $\Delta h^{stg}_{is,dx}$ η_{org}, $m_{lk,c}$, $\eta_{p,c\infty}$, a_c, b_c.

9.2.1.3 Combustor

The combustor can be calculated according to one of the options implemented for CNSJ subroutines (App. B): A) calculate m_f based on a given $T_{cmb,out}$; B) calculate $T_{cmb,out}$ based on a given m_f; C) stoichiometric combustion. Must have two input flows (fuel and oxidizer) and one output flow. If required, it also calculates the fuel compressor. Input

---

* Research Engineer at the University of Pavia, Italy.

data are: η_{cmb}*, ΔP_{cmb}, m_f and, for the fuel compressor (if present) β, η_p, η_{org}, η_{el}.

9.2.1.4 Gas Turbine

The calculation procedure and the input data are described at Ch. 6. Can have up to 7 input flows and one or two output flows. The first input flow is the mainstream gas; the others are turbine cooling flows ordered according to increasing pressures. The first output flow is turbine outlet; the second is leakage, which is always assumed to be at the turbine inlet pressure.

Although the number of parameters to be specified is relatively high (see list of Tab. 6.1), the designation of the input data is relatively simple, because most of them can be given the "default" values discussed at Par. 7.2.

9.2.1.5 Heat Exchanger

The heat exchanger must always have two input flows and two output flows (one for the hot fluid and the other for the cold fluid). Given the inlet temperatures $T_{h,in}$ and $T_{c,in}$, the outlet temperatures $T_{h,out}$ and $T_{c,out}$ can be calculated by setting:

A) The hot-side $\Delta T = T_{h,in} - T_{c,out}$

B) The cold side $\Delta T = T_{h,out} - T_{c,in}$

C) The cold fluid outlet temperature $T_{c,out}$

D) The hot fluid outlet temperature $T_{h,out}$

E) The cold fluid temperature increase $T_{c,out} - T_{c,in}$

F) The hot fluid temperature drop $T_{h,in} - T_{h,out}$

---

* $\eta_{cmb} = 1 - \varepsilon_h$, where ε_h is the heat loss as a fraction of heat input $m_f \cdot LHV$

G) The heat exchanger effectiveness $\varepsilon = Q/Q_{S=\infty}$, where $Q_{S=\infty}$ indicates the heat which could be exchanged with infinite heat transfer area

H) ΔT_{min} to be maintained between T_h and T_c; ΔT_{min} cam be realized either at the hot end ($\Delta T_{min} = T_{h,in} - T_{c,out}$) or at the cold end ($\Delta T_{min} = T_{h,out} - T_{c,in}$)

Input data are: ε; $(\Delta P/P)_{hot\text{-}side}$, $(\Delta P/P)_{cold\text{-}side}$, ε_h, $\Delta T_{hot\text{-}side}$, $\Delta T_{cold\text{-}side}$, ΔT_{min}, Tolerance used for identifying flow with the highest thermal capacity C_{max}*.

9.2.1.6 Mixer

Can have up to 7 input flows and only one output flow. It is always assumed that at output all inputs are totally and uniformly mixed. Input data are $\Delta P/P$ and ΔT_h, where ΔT_h is the output flow temperature drop due to heat losses (adiabatic mixing would give an output temperature ΔT_h degrees higher). A mixer with only one input flow can be used as a pressure- and/or thermal-loss element (e.g. air filter at gas turbine compressor inlet).

9.2.1.7 Splitters

Splitters must always have one input flow and two output flows. The only input datum is an index specifying how to assign the output mass flows. It can also be used to separate the liquid phase from the gaseous phase.

9.2.1.8 Steam section

The steam section is calculated according to a model illustrated in Lozza (1990) and Lozza and Bombarda (1991). The subroutine that

* Thermal capacities must be distiguished in order to calculate ε; when C_{min}/C_{max} is very close to one instabilities might arise due to variation, from one iteration to the other, of the flow taken as the one with C_{max}.

calculates it constitutes an independent program successively integrated with GS subroutines. The HRSG can have up to four pressure levels; each level can be of three basic types:

- "full" level, i.e. economizer+boiler+superheater
- "saturated" level, i.e. only boiler+reheat
- "reheat" level, i.e. only superheat of steam coming from steam turbines at higher levels

The first HP level can be ipercritical. Steam for injection and/or blade cooling can be bled from:

- The exit of each superheater
- The steam turbine (up to four bleeds, at pressures to be given in input)
- The drum of each level (saturated steam for steam blade cooling)

It is also possible to extract saturated water from each drum and to inject water into the condenser and the deaerator. Such water import into the HRSG may be interesting in a cycle with intercooling, whereby the warm water used in the intercooler is "recycled" into the steam section.

The arrangement of economizers, boilers and superheaters is optimized to give maximum steam production: this is accomplished by splitting economizers and superheaters into two or more sections connected in series, and by arranging sections at different pressure levels in parallel (see Fig. 2.16). The steam turbine expansion is evaluated according to a model capable of accounting for both scale and specific speed effects, as well as the consequences of moisture formation in the last LP stages. For a full description see Lozza (1990).

The input data set is considerably complex. After indicating number and type of each pressure level and each steam (or water) bleed, the user must specify: condensation pressure (or temperature), maximum allowable steam temperature, heat losses, gas-side pressure drop, consumption of auxiliaries. For the steam turbine must give: number of LP cylinders, maximum blade height, maximum peripheral speed, vapour fraction below which η is reduced due to moisture; Finally, for each pressure level must give: evaporation pressure (or temperature), T and approach ΔT at superheater exit, ΔT at pinch, subcooling at economizer exit, speed of revolution of steam turbine, η_{pump}, economizer and superheater $\Delta P/P$.

9.2.1.9 Chemical Reformer

It calculates methane-steam reformers to be used in chemically recuperated cycles (Lloyd, 1990). Ideally, it is like a heat exchanger where the hot fluid is the gas turbine exhaust and the cold fluid is a mixture of steam and methane. The peculiarity is that steam and methane react to give a low-Btu fuel rich in hydrogen and CO. The fuel composition is calculated based on the hypothesis of equilibrium conditions (corrected by an approach ΔT, for details see Lloyd, 1990). The fuel-side can have up to two separate streams at different pressures. Input data are: number of fuel-side streams, gas-side and fuel-side $\Delta P/P$, heat losses, minimum ΔT to be maintained between hot gas and reacting mixture, minimum allowable HHV of outlet fuel.

9.2.1.10 Shaft

It is a fictitious element used to schematize organic and generator losses, particularly useful when it is necessary to balance the power of compressor(s) and turbine(s) mounted on the same shaft. In this case, the shaft balance is achieved by imposing that total shaft power output is zero. Input data are: speed of revolution, η_{org}, η_{el}; rotational speed is necessary to judge whether there must be a gearbox.

9.2.2 Input data file

The initial system specifications, most of which can be changed interactively during execution, must be contained in an input file which must indicate:

- Number, type, characteristics and interconnections among all cycle components. Component characteristics (see previous paragraph) can be changed interactively after reading the input file. Component interconnections cannot be changed interactively and remain in effect until a new input file is read.
- Initial conditions (P, T, m) of all state points.
- Definition of variables to be tested for convergence ("convergence variables"), which can be both thermodynamic conditions of state points (P, T, m) and component characteristics (e.g. work output, efficiency).
- Definition of relationships to be imposed among variables (e.g. fuel pressure greater than compressor discharge pressure, HP compressor power equal to HP turbine power, steam P_{ev} higher than steam injection pressure, etc.).
- Definition of which variables have to be adjusted in order to meet the constraints (see Par. 9.2.5).

Before starting the execution, the program checks the coherence of component interconnections (e.g. the same state point cannot represent the inlet or outlet of more than one component) and of several component characteristics (e.g. efficiencies cannot be greater than one, $\Delta P/P$ cannot exceed 100%, etc.)

9.2.3 Calculation procedure

The scheme of the calculation procedure is illustrated in Fig. 9.2. At each iteration, all components are calculated sequentially following the order in which they appear in the input file. Convergence is achieved when the variation of the "convergence variables" (see Par. 9.2.4) between the beginning and the end of one iteration is within a tolerance specified among input data. Although convergence should be tested on all variables, in practice when few properly chosen variables have converged, also all others do the same.

9.2.3.1 Phase I

The search for convergence is divided into two phases. In Phase I, each iteration simply starts from the values calculated at the previous iteration, without any attempt to derive information about "where" the calculation is directed. This method gives no guarantee of convergence, because convergence variables might oscillate without ever stabilizing toward a fixed value. Nonetheless, in most cases – yet, almost always – convergence is achieved within 5-8 iterations (0.1% error on convergence variables).

9.2.3.2 Phase II

If after a number of iterations to be specified in input the procedure followed in Phase I is unsuccessful, convergence is searched by linearizing the system around the point $\underline{\bar{x}}=(\bar{x}_1,\bar{x}_2, \ldots,\bar{x}_n)$ reached at the last iteration. To do this, the program builds the sensitivity matrix $\underline{A} = \partial x_i/\partial x_j$ of the convergence variables x around point $\underline{\bar{x}}$. Then, total error (sum of squares) is minimized by assuming that each convergence variables varies linearly with all others according to matrix $\underline{A}$, i.e.:

$$Dx_i = a_{i1} \cdot dx_1 + a_{i2} \cdot dx_2 + \ldots + a_{in} \cdot dx_n$$

If the system behaved linearly and if $\bar{\underline{x}}$ and $\bar{\underline{y}}$ are the convergence variable vectors at the beginning and at the end of the last iteration, respectively, re-performing the iteration with initial values $\underline{x}=\bar{\underline{x}}+\Delta\underline{x}$ should give at the end $\underline{y}=\bar{\underline{y}}+\Delta\underline{y}$, where:

$$\Delta\bar{\underline{y}} = \underline{y}-\bar{\underline{y}} = \underline{\underline{A}} \cdot \Delta\bar{\underline{x}}$$

The error vector $\underline{e}=\underline{y}-\underline{x}$ giving the difference between the convergence variables at the end and at the beginning of the iteration is therefore:

$$\underline{e} = \bar{\underline{y}}+\underline{\underline{A}} \cdot \Delta\bar{\underline{x}}-(\bar{\underline{x}}+\Delta\underline{x}) = (\bar{\underline{y}}-\bar{\underline{x}})+(\underline{\underline{A}}-\underline{\underline{I}}) \cdot \Delta\underline{x} \qquad (9.1)$$

where $\underline{\underline{I}}$ is the identity matrix. If the n×n matrix $(\underline{\underline{A}}-\underline{\underline{I}})$ is non-singular, the vector $\Delta\underline{x}$ giving $\underline{e}=0$ can be found from Eq.(9.1):

$$(\underline{\underline{A}}-\underline{\underline{I}}) \cdot \Delta\underline{x} = (\bar{\underline{x}}-\bar{\underline{y}}) \qquad (9.2)$$

Since the non-singularity of $(\underline{\underline{A}}-\underline{\underline{I}})$ cannot be guaranteed, the solution of Eq.(9.2) may be troublesome. Thus, the program minimizes the norm of $\underline{e}$ by means of a least-square minimization routine (IMSL, 1985); since the evaluation of $\underline{e}$ from Eq.(9.1) is very fast, this implies almost no computational penalties.

If the system were really linear, this procedure would give the best initial values of the convergence variables; in practice, this is not true because the system is highly non-linear, implying that higher order terms should appear in Eq.(9.1). Nonetheless, system linearization is an approximation aimed at reducing computing time which has always given positive results for all test cases performed.

9.2.3.3 Freeze of selected variables

During the search for convergence only relatively few variables undergo significant variations. For example, the distribution of enthalpy drops among gas turbine stages (see Par. 3.6 and 6.1), the nozzle expansion ratio, the diffuser inlet pressure stabilize very quickly.

Besides being useless, repeating all calculations at each iteration may cause numerical instabilities due to rounding errors. For these reasons, after a number of iterations to be given in input (typically 3-4), several calculations are skipped, and the value of numerous variables is frozen at the value reached at that point. Besides speeding up the calculation, this freeze also reduces the total number of iterations necessary to achieve convergence.

9.2.3.4 Critical appraisal

Since the main target of this Thesis was the study of GSC thermodynamics, the numerical implications of the calculation procedure just described have been given lower priority, and are perhaps one of the areas where future work should concentrate the most.

Essentially all the calculations performed to produce the results of Chs. 7 and 10 converged within Phase I. Therefore, the operating experience on Phase II is limited and the efficacy of local linearization should be verified by adequate numerical experimentation.

Another point deserving particular attention is the "freeze" of selected variables after few iterations: on one hand such freeze accelerates convergence but, on the other, it may alter the "true" final solution, especially if the freeze is performed too early. Probably the best way of proceeding would be to freeze only if there are oscillations of the solution, or if convergence is too slow.

9.2.4 Choice of convergence variables

Whether e can actually be brought down to zero depends on whether all relevant variables have been included into the convergence variables. In other words, if a variable which is crucial for convergence is not included into the set of convergence variables, convergence might never be achieved because x does not include all determinants of e. A "brute force" approach to this problem would be to include all variables (state point and component properties) into the convergence vector x. However, since this would be highly redundant and require large memory, it was decided to leave the proper choice of the convergence variables to the intuition and experience of the user.

Notice that in most cases the number of convergence variables is small; for example, for the steam injected cycle represented in Fig. 8.9 it is sufficient to check convergence on (see figure for state point numbers):

- $m_{cl,nz}$, i.e. mass flow at point 11
- $m_{cl,ct}$, i.e. mass flow at point 9
- Mass flow at turbine outlet (point 7)
- TOT, i.e. temperature at point 7

9.2.5 Implementation of constraints

In many circumstances there are cycle variables which must meet constraints interpreting particular interconnections among cycle components. Let's give few examples:

- The combustor (see Par. 9.2.1.3) is calculated by imposing the temperature at outlet. However, the most signifcant parameter defing the gas cycle is TIT, which can be found only after knowing the nozzle coolant flow. Thus, a given input TIT can be matched only by iterating over the combustor outlet temperature.

- In a steam injected cycle, the evaporation pressure of the steam injected into the gas turbine combustor must be higher than P_{cmb} augmented by superheater and fuel injector losses. If the gas cycle pressure ratio is being varied, the evaporation pressure cannot be set in advance.

- In an evaporative-regenerative cycle (see Par. 10.2.4 and 10.3.2) there must be a limit on the maximum relative humidity of the flow exiting the evaporative intercooler. Thus, the amount of water to be injected into the intercooler depends on intercooling pressure and water temperature, and cannot be set in advance.

- If a compressor and a turbine are mounted on a shaft which must be balanced, it is necessary to adjust β_c or β_t or both in order to equate compressor and turbine power.

The program allows specifying up to 15 constraints to be met by cycle variables. Each constraint – which can involve at most two variables – is assigned by indicating in the input file:

- Cycle variable(s) involved, which can be the condition at a state point (T, P or m) or the characteristic of a component (e.g. TIT, w_c, w_t, $m_{cl,nz}$, $m_{cl,ct}$, etc.). Let's indicate such variables V1 and V2.

- The value $\bar{V}$ to be met by V1 (e.g. impose value of TIT) or the ratio $\bar{R}$ to be realized for V1/V2 (e.g. to balance a shaft must be $w_{c,net}/w_{t,net}$=1)

- The variable V3 which must be varied in order to meet the constraint. For example, to meet a given TIT it is necessary to act on combustor outlet temperature.

- The type of correction to be used, which can be (i) linear, (ii) logarithmic; (iii) exponential.

- The relaxation factor λ.

When the target to be met is the ratio $\bar{R}$=V1/V2, at the end of each iteration variable V3 is reset according to:

linear correction:	$V3_{new} = V3_{old}\cdot[1+\lambda\cdot(\bar{R}-V1/V2)/\bar{R}]$	(9.3a)
logarithmic correction:	$V3_{new} = V3_{old}\cdot\left\{1+\lambda\cdot\ln[\bar{R}/(V1/V2)]\right\}$	(9.3b)
exponential correction:	$V3_{new} = V3_{old}\cdot\left\{1+\lambda\cdot[\exp(\bar{R}-V1/V2)-1]\right\}$	(9.3c)

When the target is the value $\overline{V}$ to be met by V1 the relationships are the same, provided that $\overline{R}$ is substituted with $\overline{V}$ and V1/V2 with V1.

9.2.6 Cycle optimization

In many complex configurations the values of some cycle parameter cannot be set a priori, but they must be optimized according to a relevant design criterion. This is the case, for example, of the intercooling pressure ratio, the reheat turbine expansion ratio, the amount of water to be injected into an evaporative-regenerative cycle (see Par. 10.2.4 and 10.3.2), etc.

The current version of the program can optimize selected parameters by means of a non-linear optimization subroutine developed at Politecnico di Milano (Buzzi-Ferraris, 1976). The optimization criterion is always efficiency maximization. The parameters to be optimized and the constraints (only linear) to be met must be provided in the input file.

With optimization the increase of computational time is dramatic: for each variable being optimized it is necessary to perform at least few hundreds of iterations, which means that on a 386 machine the calculation of an optimized cycle can require several hours. The acceleration of the optimization process is one of the points deserving further work.

9.2.7 Memory requirements

Due to limitations of the Microsoft 5.0 Fortran Linker, it is not possible to create a single executable program including both the subroutines for cycle optimization (see Par. 9.2.6) <u>and</u> the ones for the calculation of chemical reformers.

The current version including cycle optimization but excluding chemical reformers necessitates 415 kBytes to handle up to 25 components, 50 state points and 15 convergence variables; going to 50 components, 100 state points and 30 convergence variables brings size to about 436 kBytes. In order to handle 25 components, 50 state points and 15 convergence variables, the version including chemical reformers but excluding cycle optimization necessitates about 385 kBytes.

9.2.8 Computing time

On an IBM PS/2 Mod.80 running at 20 MHz with math co-processor, computing time is about 25 sec. for a simple cycle gas turbine and about 75 sec. for an intercooled cycle with reheat and two-pressure level boiler like the one discussed in Par. 10.2.2.1. This compares with approximately 30 sec. required by GATE/CYCLE to calculate a simple gas turbine cycle, and 60 sec. for a heat recovery steam cycle with two evaporation pressures. Therefore, as long as the gas and steam section can be calculated independently, the present model does not offer substantial computational advantages. However, unlike in GATE/CYCLE computing time is not affected by the need to iterate between the gas and the steam section: in fact, computing time is still around 75 sec. for the intercooled cycle with reheat, steam injection, steam cooling and two-pressure level boiler like the one discussed in Par. 10.2.2.2. With the 3.1 version of GATE/CYCLE the calculation of the same cycle can be performed only by iterating on the steam injection and steam cooling flows, i.e. by a sequence of runs, each providing inputs for the successive iteration and requiring about 90 sec. to execute*.

Computing time of the present model could be substantially reduced - possibly by a factor of 2 - by simplifying the calculation of the working fluid thermodynamic properties illustrated in Appendix B. The current scheme, derived from the STANJAN code developed at Stanford (Reynolds, 1986) affords the calculation of reacting mixtures at any point along the cycle, an option which can be vital for certain applications (Consonni and Lloyd, forthcoming), but that is computationally inefficient for applications where such capability is not needed.

* Erbes (1991) points out that the newer version of GATE/CYCLE is now considerably faster due to built-in memory management and disk-caching. Moreover, the iteration described above can be performed automatically, without the need for "manual" adjustments.

9.3 Relevance and potential of the program

Program GS realizes successfully the goal stated at Par. 1.6 of developing a tool for the analysis of possibly all GSC systems of interest.

The issues related to the integration and the optimization of complex energy systems are somewhat under-represented in the technical literature, perhaps because they do not involve exotic fundamental research and/or sophisticated mathematical treatment. On the other hand, the outcome of the competition between antagonistic power generation technologies will depend not only on the performances of single components, but also on their intelligent integration. The program developed here makes available a new, flexible tool to cope with the latter issue.

Due to its modular structure, the program can be used also for systems very different from those considered here, like heat exchanger networks or industrial processes.

The present version has operated satisfactorily for all the calculations presented at Ch. 10; nonetheless numerical aspects related to convergence and optimization deserve further work.

REFERENCES

An. (1985), Subroutine ZXSSQ, IMSL User's manual, *International Mathematical and Statistical Library*, Houston, Texas.

An. (1989), "GATE/CYCLE User's Guide, version 3.1", Enter Software Inc., Menlo Park, CA.

Buzzi-Ferraris M. (1976), "Subroutine OPTNOV", Technical Note of CILEA (Intra-University Consortium for Electronic Computing), Segrate, Milan, Italy.

Caddy M.J. and Shapiro S.R. (1975), "NEPCOMP - The Navy Engine Performance Computer Program", Report no. NADC-74045-30, Naval Air Development Center, Warminster, Pennsylvania.

Cohn A., Project Manager (1983), "Gas Turbine Evaluation (GATE) Computer Program", EPRI Report AP-2871-CCM, Palo Alto, CA.

Consonni S. and Lloyd A. (to be published), "Chemically Recuperated Gas Turbine Cycles".

El-Masri M.A. (1987), "Exergy Analysis of Combined Cycles: Part 1 - Air-Cooled Brayton-Cycle Gas Turbines", J. of Eng. for Gas Turbines and Power, Vol. 109, pp. 228-236.

El-Masri M.A. (1988), "GASCAN - An Interactive Code for Thermal Analysis of Gas Turbine Systems", J. of Eng. for Gas Turbines and Power, Vol. 110, pp. 201-209.

Erbes M. (1991), Enter Software Inc. (Menlo Park, California), Personal Communication.

Fishbach L.H. and Gordon S. (1988), "NNEPEQ - Chemical Equilibrium Version of the Navy/NASA Engine Program", NASA Technical Memorandum 100851, NASA Lewis Research Center, Cleveland, Ohio.

Lloyd A. (1990), "Chemically Recuperated Gas Turbine Cycles", PU/CEES report No. 256, Princeton University, Princeton, NJ.

Louis J.F., Hiraoka K. and El-Masri M.A. (1983), "A Comparative Study of the Influence of Different Means of Turbine Cooling on Gas Turbine Performance", International J. of Turbo and Jet Engines, Vol. 1, pp. 123-137.

Lozza G. (1988), "Ottimizzazione Termodinamica dei Cicli a Vapore per Recupero di Calore", Proc. 2nd Meeting on *Gruppi Combinati: Prospettive Tecniche ed Economiche* (Florence, May 1988), pp. 177-195. Published by Pitagora Editore, Bologna, Italy.

Lozza G. (1990), "Bottoming Steam Cycles for Combined Gas-steam Power Plants: a Theoretical Estimation of Steam Turbine Performance and Cycle Analysis", Proc. *1990 ASME Cogen-Turbo, (New Orleans, Lousiana)*, pp.83-92, 1990.

Lozza G. and Bombarda P. (1991), "Cicli a vapore avanzati per impianti combinati", Proc. 5th Meeting on *Gruppi Combinati: Prospettive Tecniche ed Economiche* (Bologna, June 1991), pp. 137-156. Published by Pitagora Editore, Bologna, Italy.

Reynolds W.C. (1986), "The Element Potential Method for Chemical Equilibrium Analysis: Implementation in the Interactive Program STANJAN - version 3", Dep. of Mechanical Engineering, Stanford University, Stanford, CA.

NOMENCLATURE

a,b	Coefficients of function η_p(SP) (Eqs.4.5 and 4.6)	
a_{ij}	Element of matrix $\underline{A}$	
$\underline{A}$	nxn sensitivity matrix of convergence variables	
C	Thermal capacity	[W/°C]
$\underline{e}$	Error vector	
m	Mass flow	[kg/kg_{air}]
n	Number of convergence variables	
P	Pressure	[Pa]
Q	Heat	[J]
$Q_{S=\infty}$	Heat exchanged with infinite heat transfer area	[J]
R	Target ratio between cycle variables (Eq.9.3)	
T	Temperature	[K, °C]
$\underline{V}i$	Value of cycle variable (Eq.9.3)	
V	Target value of cycle variable (Par. 9.2.5)	
w	Specific work	[J/kg_{air}]
x	Convergence variable	
$\underline{x}$, $\underline{y}$	Vectors of convergence variables	

Greek

β	Compression ratio	
$\Delta h^{stg}_{is,mx}$	Maximum stage enthalpy drop (or rise)	[J/kg]
ΔP	Pressure drop	[Pa]
ΔT_h	Temperature drop due to heat loss	[°C]
ε	Heat transfer effectiveness	
ε_h	Combustor heat loss as a fraction of fuel input (LHV)	
η	Efficiency	
λ	Relaxation factor, see Eqs.(9.3)	

Subscripts

ad	Adiabatic
c	Compressor or Cold
cl	Coolant
cmb	Combustor
ct	Cooled turbine
el	Electric generator (or motor drive)
ev	Evaporation
f	Fuel
h	Hot
lk	Leakage
nz	Nozzle
org	Organic
p	Politropic
t	Turbine

FIGURES

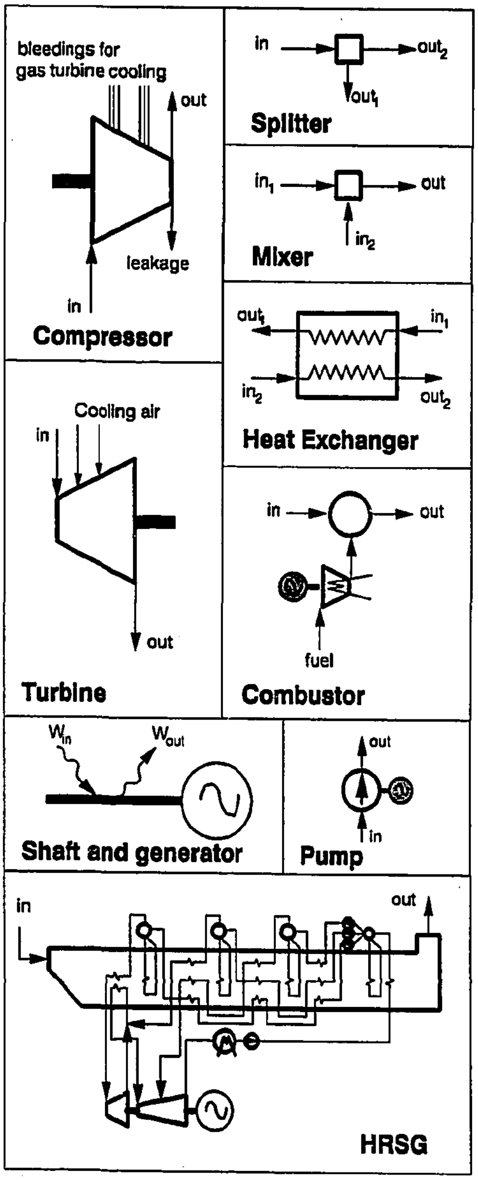

9.1 Schematic of cycle components.

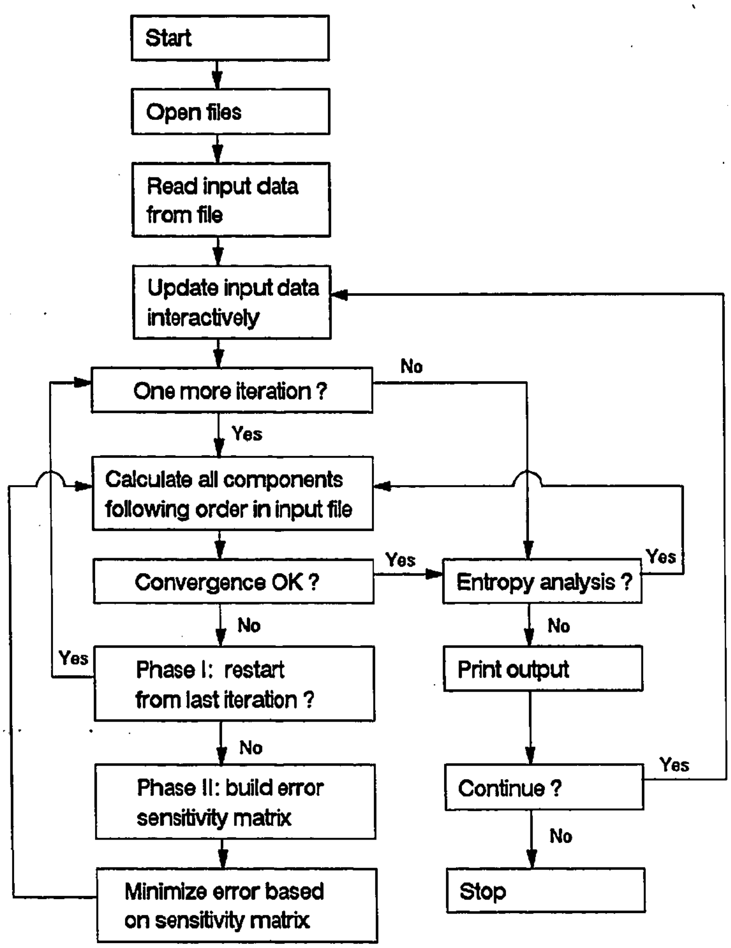

9.2 Schematic of calculation procedure

10. RESULTS FOR COMPLEX CYCLE CONFIGURATIONS

In this chapter the calculation model described in Chs. 3 to 6 is used to: (i) compare the results produced by the model with the ones of other authors (Par.10.2) and (ii) perform a parametric analysis aimed at identifying the potential of various GSC configurations (Par.10.3).

For two systems – Allison 501 and GE LM5000 STIG – the verification of model results has been done by referencing plants actually operating in the field; for the others, the data used for comparison are the outcome of other calculation models. Therefore, rather than validating our model with experimental values, the calculations of Pars. 10.2.2 to 10.2.4 verify the agreement with predictions given by other authors.

Except for the "Moonlight" IGSC and ISTIG systems described in Pars. 10.2.2.2 and 10.2.3, the agreement with data produced by other models is good. Although the usefulness of more experimental data cannot be overemphasized, this agreement gives substantial confidence in the capabilities of the model.

Par. 10.3 presents results of parametric analyses of complex cycle configurations already published in Consonni et al. (1991) and Macchi et al. (1991). These results indicate that "conventional" unmixed Combined Cycles give efficiencies 4-5 percentage points higher than mixed (steam- or water-injected) configurations, an advantage that decreases to about 3 percentage points when considering intercooling and reheat.

Despite this efficiency penalty, mixed cycles could still play an important role due to their higher specific work, which translates into lower investment costs. The competition between mixed and unmixed configurations is likely to be centered around the trade-off between the higher efficiency afforded by Combined Cycles and the lower investment costs of steam- (or water-) injected systems.

10.1 Assumptions

If not indicated otherwise in Tabs. 10.3 to 10.8*, the assumptions shared by all the calculations of this Chapter are the ones in Tabs. 10.1 and 10.2. The values in Tab. 10.1 are representative of state-of-the-art GSC technology, and many of them can easily be verified against data given in publications of Combined Cycle manufacturers. The justification of several of the assumptions in the table is the following:

- The inlet flow of 600 kg/s for heavy-duty units and the HP turbine inlet volumetric flow of 30 m^3/s for aero-derivatives are typical of state-of-the-art engines (e.g. GE 9001F and LM6000) and have been set to "freeze" the effect of scale. Given the curves in Fig. 7.12, the results of Par. 10.3 would not be different for flows higher than these values. However, at small scale – say, for $M_a \leq 100$ kg/s – there could be variations due lower turbomachinery efficiencies.

- The assumption of real n^{cs} and n_t^{stg}, which is obviously an idealization, is adopted to avoid discontinuities in the curves produced by the parametric analyses of Par. 10.3. For the verifications of Par. 10.2 (results under the heading "Same hypotheses" of Tab. 10.3 to 10.8) it is assumed that:
  - n_t^{stg} is integer
  - n^{cs} must be a multiple of 1/2 (e.g. n^{cs}=1.5 means that cooling is applied to the first two stators and the first rotor).

- The isothermal fuel compressor models the intercooled compressor typically adopted for high β_{gc} in order to: (i) reduce compression work; (ii) limit exit fuel temperature.

- Since fuel is assumed to be available at 15°C and 40 bar, for an ambient temperature of 15°C its exergy (see Par. 8.4) is 51684 kJ/kg, i.e. 3.35% higher than its LHV. Hence, given all things equal η_{II} is 3.35% lower than the more usual LHV efficiency.

- The limit of 620°C on compressor exit temperature avoids the use of cooling and/or superalloys also for the HP compressor.

- The limit on reheat combustor inlet temperature comes from considerations about reheat combustor cooling. Imposing a limit is a shortcut to avoid the calculation of the flow required to cool the liner

---

* For easier reference to the plant configurations reported in Figs. 10.1 to 10.6, all tables are placed at the end of the Chapter, immediately after the figure representing each system.

and the transition piece, an estimation which appears as difficult as the one for the turbine.

- Provided that there is a blowdown heat exchanger to recover its sensible heat, neglecting blowdown has almost no effect on the HRSG heat balance; In fact, the only effect is to increase the drum thermal load by:

  $$m_{blowdown} \cdot c_p \cdot (T_{sv} - T_{makeup})$$

  where the makeup temperature at the exit of the blowdown heat exchanger is at most 20-30°C lower than T_{sv}.

- For pumps, the curves giving η_{pump} as a function of volumetric flow and η_{org} and η_{el} as a function of power output are taken from Karassik (1989). For the calculations presented here, a typical value of the resulting overall efficiency is 65%.

The differences among cooling parameters and turbomachinery efficiencies summarized in Tab. 10.2 come from the recognition that the Allison 501-KH and the GE LM5000 are not state-of-the-art; thus, their calculation must be performed according to the values resulting from the calibration of "current" engines (see Tab. 7.5). Even if they are both aero-derivative, further distinctions between the Allison 501 and the GE LM5000 must be introduced to reflect their rather different technological level: therefore, the Allison is calculated based on parameters typical of heavy-duties (see Par. 10.2.1.1), an hypothesis fully justified by the results in Tab. 10.3*.

10.1.1 Calculation procedure

As discussed in Par. 7.3.2, the calculation according to the assumptions of Tab. 10.1 is slightly different from that used for the calibration. This is due to different assumptions on the number of stages n^{sts} and n^{cs} (in parametric analyses n^{sts} and n^{cs} are unknown and therefore are treated as real numbers) and the film cooling parameter

* This situation evidences once more that each engine is somehow unique and that accurate performance prediction of commercial engines inevitably requires to "tune" the model parameters (see also Pars. 7.5.3 and 3.2).

r_{fc} which – except for the verification of the Allison 501-KH – is non-zero also in the cooled turbine (see Fig. 5.43a).

Under the hypotheses of Tab. 10.1 the number of cooled (n^{cs}) and uncooled (n_{ut}^{stg}) turbine stages is calculated by assuming that (recall Par. 3.6):

- For the cooled section, all stages have the same expansion ratio and $\Delta h_{is}^{stg} \leq \Delta h_{is,mx}^{stg}$. $\Delta h_{is,mx}^{stg}$=425 kJ/kg for cycles involving aeroderivative units (verifications of Par.10.2 and mixed cycles of Par.10.3), and $\Delta h_{is,mx}^{stg}$=350 kJ/kg for cycles involving heavy-duty units (unmixed cycles of Par.10.3).
- For the uncooled section, Δh_{is}^{stg}=constant. Δh_{is}^{stg}=100 kJ/kg for ADs and Δh_{is}^{stg}=200 kJ/kg for HDs.

Since the assumption that n_{ut}^{stg} and n^{cs} are real is obviuosly and idealization, the corresponding results are slightly optimistic because, as long as $\Delta h_{is}^{stg} \leq \Delta h_{is,mx}^{stg}$, the actual n^{cs} – and thus cooling flow – will be slightly higher.

10.1.2 Shaft balance

All calculations for multi-shaft machines neglect the need to balance HP compressor and HP turbine power – as well as, if present, LP compressor and IP turbine power. Shaft balance would excessively constrain the calculation, so that even a small error on $\eta_{p,c}$, $\eta_{p,t}$ or cooling flows could give substantial discrepancies on the final solution.

Let's take for example the ISTIG cycle of Fig. 10.5: if we imposed $\dot{W}_{LPC}$=$\dot{W}_{IPT}$ the IPT outlet temperature (Point 14a in Tab. 10.7) would be much higher; as a consequence also the LP turbine should be cooled, resulting in a configuration substantially different from the one to be reproduced. To summarize, either we accept an imbalance of turbine and compressor power or must we accept a discrepancy of the cooling scheme.

Since this work focuses on thermodynamics, the adherence to the given configuration is more important than "mechanical" issues like shaft balance, which in most cases can be adjusted without altering cycle thermodynamics by:

- Varying the number of turbine and/or compressor stages mounted on the same shaft.
- Varying the enthalpy drop (or rise) of both turbine and compressor stages.

Moreover, since even a slight variation of $\eta_{p,c}$ and/or $\eta_{p,t}$ has dramatic consequences on shaft balance, mechanical equilibrium should be considered only on the basis of detailed, definite information on turbomachine efficiencies and engine architecture.

To summarize, the constraint imposed by shaft balance has been neglected because (i) HP and IP shafts can almost always be balanced a posteriori without changing cycle thermodynamics; (ii) imposing the shaft balance while calculating thermodynamic characteristics strongly amplifies the sensitivity to turbomachinery efficiency, cooling flows and the distribution of enthalpy drops among stages.

10.2 Model verification

Model verification has consisted in reproducing the thermodynamic cycle of systems for which enough information was available. The reference data listed in the three leftmost columns of Tabs. 10.3 to 10.8 are compared with the outcome of two calculations:

- One named "Same hypotheses", whereby we have tried to reproduce exactly the cycle used for the comparison.
- Another performed under the assumptions summarized in Tab. 10.1 and 10.2. These results are the ones which would be obtained if one knew "almost nothing" about the reference cycle, and calculated it according to average values representative of state-of-the-art technology.

Besides differences in gas turbine and HRSG specifications (especially pinch and approach ΔT), an important distinction between the two calculations is the number of cooled stages, which determines total heat transfer area and has important effects on cooling flows (see Par. 10.1.1).

The first option ("same hypotheses") is obviously more meaningful, because it uses all available information about the turbine being calculated. The second is helpful to evaluate the impact of the difference between the assumptions of Tab. 10.1 and those underlying the test case.

Although the results can be considered satisfactory, in some case there are susbstantial discrepancies with those of other authors (e.g. steam-cooled, steam injected Moonlight, Par. 10.2.2.2). However, these differences do not allow drawing any firm conclusion because the values used for comparison have been produced by models for which there is little (if any) experimental verification.

Since there is no assurance that the performance estimated by other models is really the one achievable by actual plants, there is no way of knowing who is more "correct". Nonetheless, comparisons are useful to verify the consistency with models developed by others.

10.2.1 Steam Injected systems

These systems constitute the rare instance in which predictions can be verified against the performances of plant actually operating. The computer model has been tested for the system commercialized by IPT – based on an Allison 501-KH (An., 1986; Sheperd, 1987) – and the one realized at Ripon – based on a GE LM5000 (Gelfand, 1987; Kolp and Moeller, 1989).

Since both engines were not originally designed for STIG operation, the actual systems operate off-design (see Par. 2.5), an effect not accounted for by the model. As discussed in Consonni, Lozza and Macchi (1988), off-design operation should have relatively small effects on cycle performance; in any case, Tab. 10.3 and 10.4 show that the agreement between calculated and experimental data is very good.

10.2.1.1 Allison 501-KH

The Allison 501-KH is the first successful commercial application of a steam injected cycle. The engine is a modified version of the aero-derivative 501-KA, originally designed for installation on helicopters. Despite its origin, the 501-KH does not exhibit the typical features of aero-derivatives: it is single-shaft, film cooling is used only in the first nozzle and TIT is definitely below average. Thus, besides assuming that the turbine is "current technology" (see Tab. 10.2), the calculations summarized in Tab. 10.3 are based on hypotheses typical of heavy-duties:

$\Delta h^{stg}_{is,mx}$ = 350 kJ/kg

$\Delta h^{stg}_{is,c}$ = 20 kJ/kg

$\eta_{p,c\infty}$ = 0.896

The results in Tab. 10.3 suggest the following observations:

- Due to underestimation of TOT, reproducing the same steam temperature requires the unrealistic assumption of HRSG approach=1°C because, if evaporation pressures and steam flows are fixed, any discrepancy on TOT must be compensated by pinch and approach variations. However, if we don't pretend the same cycle conditions and conform to the values in Tab. 10.1 (approach=25°C), the calculated values of $\dot{W}_{sh}$ and η_{sh} are still very close to those declared by IPT.
- The values of $m_{cl,nz}$ and $m_{cl,ct}$ are close to estimates given by Donolo (1988)
- The higher compressor outlet temperature reveals a slight underestimation of $\eta_{p,c}$. Since overall power ouput is still overestimated, it means that this pessimistic estimate is more than compensated by an optimistic estimate of $\eta_{p,t}$, which is confirmed by the underestimation of TOT.

10.2.1.2 General Electric LM5000

After approaching the issue from a purely thermodynamic standpoint (Brown and Cohn, 1981), in 1983 GE started evaluating the possibiity of realizing steam-injected cycles with its family of LM aero-derivative engines. The first steam-injected version to be launched was the LM5000, soon followed by the LM2500 (Oganowski, 1987) and the LM1600 (Thames and Coleman, 1989).

Fig. 10.2 reports the schematic of the cogeneration system realized at the Simpson Paper Mill in Ripon (California), the first utilizing a fully steam-injected LM5000. HP steam is injected into the compressor discharge plenum and also directly into the combustor, through the fuel injector itself; IP steam is injected in the space between the HP and IP turbine, while LP steam is used totally as a heat source for the Mill.

Tab. 10.4 compares calculated data with those given by Kolp and Moeller (1989), and suggests the following observations:

- The cooling flows $m_{cl,nz}$ and $m_{cl,ct}$ of 22.76% and 15.02% (Points 15 and 13, respectively) are much above the values of 6.3% and 7.5% given in An. (1984). Although it is most probably true that the flows predicted by the present model are too large, it is also true that the values given by An. (1984) are very optimistic: in fact, for a system with TIT=1180°C the same study quotes a cycle efficiency of 50.67%, much above the 43% reached at Ripon and still higher than the 50% which could be realized by an optimized plant with TIT=1250°C (see Fig. 10.14)..

- The strong unbalance of the HP shaft (see $\dot{W}_{HPC}-\dot{W}_{HPT}$, which for a balanced shaft should be zero) reveals that HP turbine power is underestimated, a situation most probably due to the overestimation of m_{cl}.

- Due to the very large $m_{cl,nz}$, the total temperature drop of 160°C across the nozzle is much above typical values of 60-100°C quoted by Merola (1991). This means that the values r_{fc}=0.194 and Z=36 assumed for the LM5000 are presumbly too low, i.e. the LM5000 falls somewhat in between "current" and state-of-the-art engines.

- Since the temperature drop between Points 9 and 11 is predicted very well, the calculated $\eta_{p,ut}\simeq91\%$ is very close to that of the actual engine.

- The steam flows given by Kolp and Moeller can be reproduced only by assuming that ΔT_{pp} are smaller than the values typically adopted in practice, for which 5°C is a lower bound very rarely violated*.

- The higher power output obtained under the hypotheses of Tab. 10.1 is mainly due to the reduction of $m_{cl,ct}$ from 15% to ≃12.5%; in turn, this is due to the reduction of n^{cs} from 2 to 1.7 (but in practice n^{cs} can be either 1.5 or 2.0).

- The HP shaft remains unbalanced also under the assumptions of Tab. 10.1.

To summarize, the very good agreement on $\dot{W}_{sh}$ and η_{sh} is achieved despite a presumably significant overestimation of turbine cooling flows. If cooling flows were lower there would an overestimation of $\dot{W}_{sh}$ and η_{sh},

* If ΔT_{pp} is too low, steam production becomes extremely sensitive to gas temperature disuniformities.

which could be partly reduced by introducing the very high leakage (3%) quoted by Gelfand (1987)*.

10.2.2 "Moonlight" Cycles

Within the framework of the national project for energy conservation called "Moonlight", in the early eighties a consortium of Japanese companies realized a pilot reheat gas turbine for large scale power generation (Hori and Takeya, 1981; Takeya, Oteki and Yasui, 1984; Arai et. al. 1988). The pilot plant reached all main targets and, from a technical point of view, can be considered successful; however, the project was abandoned because it did not appear economically competitive with configurations based on commercial simple cycle engines. In fact, the first version of the pilot plant (AGTJ-100A, 1984) had a target Combined Cycle efficiency of 50%, a value definitely lower than that now achievable by non-reheat Combined Cycles offered by major manufacturers.

The next two paragraphs compare calculated data with the detailed information given by Takeya and Yasui (1988) on the version designed to reach an efficiency close to 55% (which however was never realized). While for the Combined Cycle the agreement is good, for the steam-injected, steam-cooled version there are strong discrepancies.

10.2.2.1 Combined Cycle

Table 10.5 compares the estimates of Takeya and Yasui with the ones produced by the present model. The unbalance $\dot{W}_{HPC}-\dot{W}_{HPT}$ of the HP shaft is not indicated because the HP compressor is driven by the single-

* Aero-derivatives generally incorporate substantial bleeds of compressed air to power aircraft auxiliaries. The high leakage implied by Gelfand's data may be related to such air bleeds, although it is unclear why in the stationary version they cannot be eliminated.

stage HP turbine, which I have lumped together with the single-stage IP turbine. The Table suggests that:

- Estimated power and efficiency agree very well; apparently, the discrepancy is due only to the steam turbine, for which Takeya and Yasui give contradicting information (if its efficiency is really 85%, the exit temperature – Point 24 in Fig. 10.3 – cannot be 327°C)

- Despite the agreement of overall performances, there are substantial differences in the distribution of cooling flows. The present model under-estimates the HP and IP turbine flows, and over-estimates the ones of the reheat turbine. This discrepancy is difficult to reconcile because, even assuming that the turbine geometry considered by Takeya and Yasui is substantially different from the one defined in Appendix A (i.e. $D_s \neq 3.25$, inlet $H/D_m \neq 0.08$ etc.), the consequences on cooling flows are minor (see Par. 7.4). The most probable explanation could be that, unlike in the HP and IP turbine, reheat turbine blades are protected by TBC coatings, although this is not mentioned by the authors.

- In order to reproduce the same steam flows it is necessary to assume HRSG pinch and approach ΔTs different from the ones of Takeya and Yasui.

- The HP compressor efficiency is slightly underestimated.

- Under the assumptions of Tab. 10.1 the model predicts a strong increase of power output due to a substantial reduction of cooling flows; in turn, the lower m_{cl} is due to a reduction of n^{cs} from 4 to ≈3.

10.2.2.2 Integrated Gas/Steam Cycle (IGSC)

In addition to the reheat Combined Cycle considered in the previous paragraph, Takeya and Yasui (1988) also present estimates of the performances achievable by what they call "Integrated Gas and Steam Cycle" (IGSC), which consists of a steam-injected, steam-cooled reheat turbine with a two-pressure level HRSG. LP superheated steam is used to cool the LP reheat gas turbine; HP saturated steam is used to cool HP and IP turbines; HP superheated steam is injected into the HP combustor. According to the schematic given by Takeya and Yasui, some air is bled from the HP compressor and injected into the HP and IP turbine, presumably to cool discs bearings, casings and/or to act as purge flow. On the contrary, no air is supplied to the reheat turbine, for which it is assumed that all cooling is done with steam.

The comparison summarized in Tab. 10.6 evidences a strong under-estimation of power output ($\simeq -10\%$), basically due to an over-estimation of reheat turbine cooling flow: such higher cooling flow gives much lower TOT ($\simeq -25°C$), and thus much less HP steam available for injection ($\simeq 14\%$ against 18.5%). On the other hand, and similarly to the Moonlight Combined Cycle, the HP and IP turbine cooling flows are under-estimated. Within the framework of the present model, these differences can be explained only by assuming that the cooling technology adopted for the reheat turbine is more sophisticated than the one used for the others, a rather odd situation which is not mentioned nor implied by Takeya and Yasui.

With the hypotheses of Tab. 10.1 the situation is still the same, except that $\dot{W}_{sh}$ is larger mainly due to lower intercooler exit temperature (40 vs. 60°C). HP cooling flow is higher due to a slight increase of n^{cs}.

Aside from considerations about the calculation model, the discrepancies illustrated in Tab. 10.6 emphasize the "chain effect" associated to the prediction of steam-injected cycles performance: even a small error on cooling flows can have substantial impact on power output through variations of TOT and thus the steam flow available for injection. In a Combined Cycle the consequences of an error on turbine cooling flow are much less dramatic because there is no feedback between the steam and the gas section.

10.2.3 Intercooled Steam-Injected Cycle (ISTIG)

Since 1984, the addition of intercooling to a multi-evaporation pressure steam-injected cycle was suggested as a way to increase both power output and efficiency (An., 1984)*. The former is brought about by a decrease of compression work; the latter by the lower temperature of the coolant, which allows increasing TIT while still maintaining the same metal temperature**.

Calculations have been carried out for the system based on the LM6000 gas generator (Fig. 10.5), for which General Electric and PG&E have estimated a net electric efficiency of 52% with a power output of 114 MW (An., 1989b; Di Candia, 1989; Hines, 1990). The fuel pre-heater has been included under the suggestion of Hines (1990): although it increases gas compression work, it also increases heat recovery from the intercooler, thus producing a slight beneficial effect on efficiency. Notice that fuel pre-heating implies substantial modifications of the fuel feed system, which is typically designed for $T_f \leq 100$-120°C.

Reproducing the performances quoted by GE is problematic due to the uncertainty over two key parameters:

- It is unclear whether the temperature of 2500°F (1371°C) refers to the combustor outlet or to the first rotor inlet. In my calculations I have assumed the latter hypothesis, although an earlier study (An., 1984) explicitly indicates a combustor outlet temperature of 2470°F. The same study also quotes an efficiency of 54.9%, later downgraded to 52%. Independently from the agreement with my calcu-

---

* It is unclear whether the very promising estimates given in this work refer to the gas generator of the LM6000 or of the LM5000. Based on the results presented here, it seems that such estimates can be (partially) justified only by assuming the LM6000 technological level.

** However, since blade cooling heat transfer takes places under higher ΔT, there is an increase of the irreversibilities due to turbine cooling. The benefit on cycle efficiency is the result of the trade-off between such irreversibilities and the higher TIT.

lation model, this and other inconsistencies do not contribute to give confidence into the figures provided by GE.

- According to Hines (1990) the IP turbine should have two stages. However, such turbine operates with an expansion ratio of 0.76 and $\Delta h_{is} \simeq 105$ kJ/kg, which do not justify the use of two stages. In addition, with TIT=1371°C the IP turbine should be completely cooled and it is very unlikely that the penalty caused by the additional heat transfer area of the second stage can be compensated by the higher efficiency of the two-stage turbine. Notice that the IP turbine exit temperature of 951°C quoted by GE (Point 14a of Fig. 10.5) is too high to be accepted by an uncooled LP turbine. In my calculations Point 14a represents the end of the cooled expansion, a situation which is reached at a much lower pressure.

Due to the large cooling flows required by the two-stage IP turbine, calculated values of $\dot{W}_{sh}$ and η_{sh} are much below the ones quoted by GE. Given the agreement with the temperature history given in An. (1989b) – i.e. temperatures at Points 9, 13 and 17 – GE estimates are puzzling.

Much better agreement is achieved by conforming to the hypotheses of Tab. 10.1, whereby the reduction of m_{cl} due to lower n^{cs} give a much higher TOT; in turn, the higher TOT allows increasing steam production, with substantial beneficial effects on $\dot{W}_{sh}$ and η_{sh}. In practice this situation cannot be realized because $n^{stg}_{HPT}=1.3$ is obviously an idealization; the designer will have to compromise between $n^{stg}_{HPT}=1$ – implying lower m_{cl} but, presumably, also lower $\eta_{p,t}$ – and $n^{stg}_{HPT}=2$ – with higher m_{cl} but also higher $\eta_{p,t}$.

Finally, let's notice that, similarly to the IGSC of Par. 10.2.2.2, the results reported in Tabs. 10.7 emphasize once more how the power output of steam injected systems is very sensitive to the estimates of cooling flows.

10.2.4 Evaporative-Regenerative Cycle

The last system used to verify model predictions is the evaporative, water-injected, regenerative cycle proposed by El-Masri (1988). In this cycle, water-injection is used both for intercooling and to create the optimal conditions for regeneration by decreasing the temperature of the HP air exiting the compressor (Fig. 10.6). This cycle is very similar to the HAT (Humid Air Turbine) cycle under study by EPRI and Fluor Daniel, which appears a promising candidate for tight integration with coal gasification systems (Cook, McDaniel and Rao, 1991).

To appreciate the peculiarities of this cycle it is important to notice that:

- In order to balance the heat capacities of the two regenerator streams, the HP air exiting the HP water injector is over-saturated, i.e. it is a mixture of saturated air and liquid water.
- The calculation under the assumptions of Tab.10.1 has included the water pre-heater of Fig. 10.6, which however has been neglected in the study of El-Masri. Besides enhancing heat recovery from gas turbine exhaust, the pre-heater allows injecting more water due to higher water temperature at the injectors, thus increasing efficiency by about one percentage point and specific work by about 5%.
- The nozzle is cooled with the hot air exiting the HP compressor. The mixture exiting the HP water injector (Point 8 of Fig. 10.6) is at a lower temperature but its use, due to higher heat transfer irreversibilities, would be detrimental to efficiency. This clearly shows that lowering the coolant temperature is not always beneficial.
- For the calculation according to the assumptions of Tab. 10.1 the amount of water to be injected into the intercooler is the one that gives Φ=90% at outlet; instead, the amount of water injected into the HP aftercooler is the one that maximizes efficiency.

Tab. 10.8 shows that, despite the 2.5% difference in power output, the agreement with the estimates of El-Masri is very good. An important difference is that our model over-estimates nozzle cooling flow and under-estimates the remaining ("chargeable") flow, a situation exactly opposite to the one encountered for Moonlight cycles (Par. 10.2.2). Also, HP compressor efficiency is lower than that assumed by El-Masri.

The evaporative-regenerative cycle appears as the direct competitor of the ISTIG cycle, a situation clearly confirmed by the results of Par. 10.3. Economically, relative merits crucially depend on the costs of the regenerator vs. the multi-pressure HRSG required by ISTIG.

10.2.5 Conclusions

The results of Tab. 10.3 to 10.8 show that – except for the Moonlight IGSC and ISTIG systems – the predictions for complex cycle configurations are within the same boundaries obtained for the simple cycle (Par. 7.5), i.e. 5% for power output and 1 percentage point for efficiency.

The larger discrepancies obtained for the "Moonlight" IGSC and ISTIG are mainly due to different estimates of turbine cooling flows and can be resolved only by resorting to experimental data for the temperature and mass flow distributions along the turbine. However, since a systematic, publicly available collection of such data would be very difficult to produce, the discrepancies evidenced in Tabs. 10.6 to 10.7 are likely to remain unresolved until the realization of commercial systems. It must also be emphasized that the issue of cooling flows becomes more crucial for mixed cycles, due to the feedback between the steam and the gas section.

Regarding the prediction of thermodynamic conditions along the cycle, the model appears definitely satisfactory, except for a tendency to under-estimate HP compressor efficiency. Such deviations could perhaps be adjusted by introducing a dependence of $\eta_{p,c}$ from specific speed, which would account for the better operating speed of multi-spool engines (see discussion of Par. 4.2).

10.3 Parametric analyses

This last paragraph presents findings of parametric analyses of selected GSC configurations obtained with the computer program described in Ch. 9. These results have been produced in close collaboration with Prof. E. Macchi, Dr. G. Lozza, P. Chiesa and P. Bombarda, and have already been published in two companion papers: Consonni et al. (1991) and Macchi et al. (1991). Most of the material — including figures — is taken from the second paper and is repeated here both to illustrate the capabilities of the calculation model and to answer the questions posed in Par. 1.6. The assumption maintained throughout all calculations are the ones listed in Tab. 10.1. Except indicated otherwise, TIT of both HP and reheat turbine is 1250°C.

10.3.1 Entropy analysis of simple cycles

Before discussing parametric analyses, it is useful to elucidate the thermodynamic features of simple gas turbine cycles by means of the entropy analysis illustrated in Ch. 8. The 2nd-law efficiency η_{II} can be expressed as:

$$\eta_{II} = 1 - \Sigma_i(\Delta\eta)_i \tag{10.1}$$

where the terms $\Delta\eta_i$ are the efficiency losses related to the various irreversible processes occurring in the cycle and, recalling Eq.(8.2), are given by:

$$\Delta\eta_i = T_0 \cdot \Delta S_i/(M_f \cdot ex_f) \tag{10.2}$$

Equation (10.2) shows that there are two means to decrease the efficiency loss of a process: (i) acting on the term ΔS_i, i.e. trying to make the process as reversible as possible, and/or (ii) increasing the term ($M_f \cdot ex_f$), i.e trying to introduce as much exergy as possible into the power cycle.

For the sake of simplicity, the analysis developed in the next paragraphs refers to the following six groups of irreversibilities:

$\Delta\eta_{Q1}$ Losses related to irreversibilities in combustors (Par. 8.4), including thermal and pressure losses.

$\Delta\eta_c$ Losses related to inefficiencies in compression devices.

$\Delta\eta_e$ Losses related to inefficiencies in expansion devices; for gas turbines it includes losses due to cooling (see Par. 8.2.1 and 8.3).

$\Delta\eta_{Q2}$ Losses related to irreversibilities of heat rejection, either when releasing the working fluid to ambient or when discharging heat to a refrigerating medium.

$\Delta\eta_r$ Losses related to inefficiencies (heat transfer + pressure drops) in regenerators.

$\Delta\eta_v$ Losses not included in the previous terms (mechanical/electrical losses, leakages, etc).

10.3.1.1 Simple gas turbine cycle

Fig. 10.7 depicts the variation of $\Delta\eta_i$ vs cycle pressure ratio β for gas turbine cycles with the characteristics summarized in Tab. 10.1. The Figure shows that:

- The largest losses are by far the ones taking place into the combustor ($\Delta\eta_{Q1}$) and due to the release to ambient of hot combustion gases ($\Delta\eta_{Q2}$). At the low pressure ratios typical of heavy-duties, the two terms are almost equal, each close to 30%: this means that even by stipulating ideal turbomachines, absence of fluid-dynamic, thermal and cooling losses, etc., for such engines it would be impossible to obtain efficiencies larger than 40%.

- Turbomachinery losses are relatively small. Mainly due to irreversibilities associated to blade cooling, turbine losses are almost twice as large as those of the compressor.

It is important to emphasize that there is a fundamental difference between the thermodynamic significance of $\Delta\eta_{Q1}$ and Δn_{Q2}. $\Delta\eta_{Q2}$ is a real measure of poor cycle performance and can theoretically be decreased to very low values by configurations capable of discharging heat at temperatures close to ambient. Instead, a large portion (about 2/3) of $\Delta\eta_{Q1}$ is due to irreversibilities inherent to the combustion process (see Par. 8.4.2), which could be avoided only by radically changing the process itself (e.g. substitute the combustor with a fuel cell). The magnitude of this "unavoidable" loss is depicetd in Fig. 8.8: for TIT=1250 °C, it is 18.92% of the physical exergy of methane at 40 bar. Given this "physical" limit, all cycle improvements can only reduce the remaining portion of $\Delta\eta_{Q1}$, i.e. about 10%.

In order to improve the performance of low-pressure ratio cycles it is possible to act along two directions: (i) increase pressure ratio and (ii) adopt a regenerative cycle. The first path is followed successfully by aero-derivatives: in fact, increasing β from 12 to 30 decreases $\Delta\eta_{Q1}$ and $\Delta\eta_{Q2}$ of about 2.7 and 6 percentage points, respectively. However, further increases of β would be useless because losses in turbomachines become larger and larger, thus offsetting the positive influence of high β on heat exchanges.

10.3.1.2 Regeneration

The adoption of a regenerative cycle (Fig. 10.7b) is more effective than increasing β. For instance, at optimal pressure ratios (around 12), the sum of $\Delta\eta_{Q1}$ and $\Delta\eta_{Q2}$ decreases from about 59.6% down to 47.3%. However, the regenerator brings about a loss of 2.2% and there is a remarkable (30%) increase of losses in turbomachinery; consequently $\eta_{II,mx}$ is below 41.5%, corresponding to a LHV efficiency of $\approx$42.9% (the difference is due to the difference between ex_f and LHV, see Par. 10.1).

This somewhat disappointing performance of the regenerator is mostly due to the large difference of thermal capacities of the two fluids counter-flowing in the exchanger: owing to the large flow rates required to cool the turbine, the flow exiting the turbine is much larger than the one of compressed air flowing on the other side of the regenerator; moreover, turbine exhausts also have larger specific heat due their chemical composition and higher temperature. Independently of heat transfer effectiveness, this unbalance of thermal capacities causes a large temperature difference between air entering into the combustor and turbine exhaust gases. The situation can be drastically improved by the massive water injection at compressor exit realized in the cycle of Fig. 10.6.

10.3.1.3 Intercooling and reheat

Quite surprisingly, introducing an intercooler amidst the compression proves to be a more effective cycle variation than regeneration (Fig. 10.7c). The lower air temperature at compressor discharge allows the introduction of a larger amount of fuel into the engine, thus decreasing the magnitude of all other losses. The full exploitation of these advantages requires however very high pressure ratios, which are necessary to reduce drastically $\Delta\eta_{Q2}$.

Unlike intercooling, reheating the gas amidst the expansion gives poor thermodynamic performances (Fig. 10.7d): the benefits produced by the increase of the heat introduced into the cycle are more than offset by the large $\Delta\eta_{Q2}$ resulting from the release to ambient of high temperature turbine exhausts.

10.3.1.4 Intercooling, reheat and regeneration

Even the combination of all three cycle modifications discussed above (regeneration, intercooling and reheat), does not yield substantial advantages over intercooling alone, mostly because of the very high losses occurring in the regenerator (Fig. 10.7e). Notice that in this case the mismatch of thermal capacities discussed in Par. 10.3.1.2 is even higher, owing to the larger amount of cooling flow required by the two turbine sections.

10.3.1.5 Efficiency vs specific work

Fig. 10.8 summarizes in the efficiency-specific work diagram the performances of the five cycle options considered: it can be seen that η_{II}>40% can be obtained either by low-pressure ratios regenerative cycles or by high-pressure ratio cycles with intercooling, either with or without regeneration. The highest specific works are obtained by reheat cycles, which however can reach acceptable efficiencies only by resorting to regeneration and intercooling.

10.3.2 Mixed Cycles

The injection of steam or water alleviates two basic shortcomings of the Joule cycle: (i) the high losses related to the discharge of hot gases at turbine outlet and (ii) the impossibility of accomplishing an efficient regeneration due to the unbalance of thermal capacities in the heat exchanger. Two basic arrangements are possible:

A) Heat recovery + steam injection. The heat available from turbine exhausts is recovered to generate steam, which is then re-injected into the gas stream directly (STIG) or – if steam is generated at pressures larger than required for injection – is first expanded in an auxiliary back-pressure steam turbine and then injected (Fig. 10.9). When compared to a simple cycle, the main advantages of this scheme are: (i) the great reduction of $\Delta\eta_{Q2}$ and (ii) the increase of the heat introduced into the engine. However, as discussed in Par. 8.3 gas/steam mixing is highly irreversible.

Steam injection can be adopted not only for simple cycles but, as shown in Fig. 10.9, also for more complex configurations like ISTIG (intercooled steam injected turbine) and IR_hSTIG (intercooled/reheat steam injected turbine).

<u>B) regeneration + water injection (R_gWI)</u>. Water injection is used to: (i) increase the thermal capacity of the stream to be preheated ahead of the combustor in order to balance the thermal capacity of gas turbine exhausts; (ii) recover the heat of gas turbine exhausts to a larger extent than by regeneration. The latter is realized by first preheating a large quantity of water in a heat recovery exchanger and then, after mixing, by vaporizing it into the regenerator. Fig. 10.10 depicts the two cycle arrangements considered here: an intercooled cycle (R_gWI) and a cycle with both reheat and intercooling (R_gR_hWI).

<u>10.3.2.1 Entropy analysis</u>

The entropy analysis of the five configurations considered (STIG, ISTIG, IR $_{,\,Rg}$WI, R_gR_hWI) is summarized in Fig. 10.11. For each cycle three pressure ratios have been considered: the one giving maximum efficiency and two other values, respectively lower and higher. Besides the terms already introduced in Par. 10.3.1, it is necessary to consider three further $\Delta\eta_i$:

$\Delta\eta_{SG}$ Losses due to irreversibilities in the HRSG.

$\Delta\eta_{mix}$ Losses due to mixing irreversibilities (Par. 8.3)

$\Delta\eta_{SC}$ Losses due to irreversibilities in the steam cycle (auxiliary steam turbine, valves, pressure drops, pumps, etc.)

For a better understanding of the situation, the results of the entropy analysis shown in Fig. 10.11 should be examined together with the thermodynamic cycles illustrated in the temperature-specific entropy diagrams of Fig. 10.12 and 10.13, and with the curves in Fig. 10.14 giving the performances in the efficiency-specific work diagram.

One first observation which can be drawn from the figures is that both cycle modifications achieve efficiency and specific work much higher than the simple cycle. Most of the gains come from the drastic reduction of losses related to heat discharge, with both plants achieving stack temperatures around 100 °C. Nonetheless, the presence of large quantities of steam in the exhaust gases, which release their latent heat of condensation during the cooling process, maintains $\Delta\eta_{Q2}$ of mixed cycles at much higher values than in Combined Cycles.

10.3.2.2 STIG vs ISTIG

For steam injected cycles, intercooling increases efficiency of about one percentage point: penalties related to less efficient heat introduction (lower compressor discharge temperature) and to higher exhaust gas temperature* are more than counterbalanced by the decrease of losses occurring in all other components, which take advantage of the larger amount of heat introduced into the cycle.

It is important to emphasize that intercooling brings about one further potential efficiency gain: when an existing simple cycle engine is intercooled, the resulting lower temperature at compressor exit allows higher TIT for the same material temperature and cooling air flow rate. For instance, the GE ISTIG study used for the comparison in Tab. 10.7 assumes that TIT is 121°C higher than for the simple cycle.

---

* The temperature at the stack is lower in the regenerative cycle.

The present calculation model indicates that this TIT increase is obtained by maintaining approximately the same cooling flows and the same metal temperature of the original LM6000 simple cycle; the higher TIT increases efficiency by about one percentage point, thus bringing the overall efficiency gain of ISTIG vs STIG to about two percentage points.

10.3.2.3 ISTIG vs R_gWI

In spite of their different "thermodynamic shapes", the two cycles yield very similar overall results and loss distribution. Regenerator losses of R_gWI are slightly higher than the corresponding term of ISTIG ($\Delta\eta_{SG} + \Delta\eta_{SC}$); however, $\Delta\eta_{Q1}$ is lower, owing to the higher temperature at which heat is introduced.

10.3.2.4 Influence of reheat

For both cycle configurations, the adoption of reheat yields remarkable efficiency gains (over 3 percentage points) and practically doubles specific work. In both cases there is a substantial increase of turbine and heat discharge losses; nonetheless, the great increase of heat introduced into the cycle drastically reduces all other losses. Optimum pressure ratios are always very high; in particular, for β<60 the amount of steam generated is so large that almost all the oxygen of combustion air is used in the first combustor, and the reheat combustor cannot bring gases up to the desired value of TIT.

10.3.2.5 Auxiliary steam turbine

The adoption of a back-pressure steam turbine yields significant efficiency gains only at relatively low β, i.e. only when there are large differences between the evaporation pressure that optimizes steam generation and the maximum gas pressure. At optimmum β (see Fig. 10.14) these gains are negligible or even disappear for ISTIG.

10.3.2.7 Prospects of mixed cycles

Mixed cycles exhibit very interesting performances: without reheat, they can almost double specific work* and reach LHV efficiencies as high as 51%. The two options considered (steam or water injection) are thermodynamically equivalent; hence, the choice should be based upon technological/economical considerations rather than thermodynamics.

The addition of reheat can greatly enhance both η and w. However, the substantial R&D efforts required for its realization undermine the idea behind mixed cycles, namely the addition of "low-tech" components to an "high-tech", aero-derivative core.

Nonetheless, it should be noted that by adapting a simple-cycle 40 MW engine like the GE LM6000 (β=30) to an optimized IR_hSTIG cycle (β=96), the contemporary increase of mass flow rate (+179%) and specific work (+236%) would result in a power output of about 380 MW, with a LHV efficiency over 54%. The presumable reduction of specific cost ensuing from this huge power augmentation could be dramatic.

10.3.3 Combined Cycles

The main idea behind Combined Cycles is the attempt to reduce the efficiency loss occurring at gas turbine discharge by means of a heat recovery steam generator and a closed steam cycle. Heat recovery can be applied to all gas cycles considered in Fig. 10.8 by means of the arrangements indicated in Fig. 10.15. Provided that a certain degree of

---

* Even more for ISTIG cycles if, when adapting an existing engine to the ISTIG configuration, full advantage is taken of the possibility to increase TIT as a consequence of lower cooling air temperature.

plant complexity is accepted and the process is properly optimized, the efficiency of the heat recovery cycle can be very high: the results presented in this section refer to the three-pressure cycle with steam reheat shown in Fig. 10.15. This configuration has proved to be the most effective for gas temperatures ranging from 400 to 800°C (Lozza and Bombarda, 1991). The only parameter affecting the selection of the steam cycle is the HRSG inlet gas temperature; hence, the thermodynamic analysis of the recovery steam cycle can be performed independently of the characteristics of the gas cycle. This does not mean that multivariable optimization of combined cycles is unnecessary, since the presence of the bottoming cycle changes the optimum working parameters of the gas cycle.

10.3.3.1 Entropy analysis

The results of bottoming cycle calculations are summarized in Fig. 10.16; in the lower part efficiency losses are expressed as fractions of the exergy content of the exhaust gases — i.e as fraction of $\Delta\eta_{Q2}$. The abcissa is the HRSG inlet gas temperature; the range of variation and the optimum values corresponding to the various plant schemes are indicated at the bottom. Losses are grouped in the following items:

Condenser loss, accounting for losses due to condensing temperatures higher than ambient.

HRSG loss, accounting for irreversibilities related to heat transfer under finite temperature differences.

Exhaust discharge loss, accounting for losses related to stack temperatures higher than ambient.

Turbine efficiency losses, accounting for fluid-dynamic losses and losses related to liquid extraction.

Miscellaneous losses, accounting for various irreversibilities present in the steam cycle (pumps, valves, leakages, thermal, mechanical, electrical and auxiliary losses).

The upper part of Fig. 10.16 reports the optimized values of the most significant thermodynamic variables, showing that HP steam conditions increase continuosly with gas inlet temperature; over 550°C – i.e. for all cycles but R_{ε}CC and high pressure ratio CC – the highest steam pressure is supercritical. On the contrary, IP and LP pressures are optimized at their minimum value (20 and 3 bar respectively, see Tab. 10.1), increasing only for the very high gas temperatures produced by reheat gas turbines.

As shown in the lower part of Fig. 10.16, the fraction of available work achievable with the proposed bottoming cycle increases with gas temperature, reaching its maximum at a gas temperature as high as 700 °C. As clearly pointed out in the figure, this behaviour is mostly due to the increasing importance assumed at low gas temperatures by the exhaust discharge loss. The small decrease of the useful work fraction occurring at very high gas temperatures is due to the increasing weight of heat transfer irreversibilities, an increase due to the upper limit (565 °C) set for the steam temperature.

As a general comment to the results of Fig. 10.16, it can be stated that the thermodynamic performance of the proposed steam bottoming cycle is excellent over the entire span of gas temperatures, including the ones resulting from reheat cycles or expected as a result of future TIT increases. Considering that:

- about 70% of the reversible work available in the gas turbine exhausts is converted into useful work;
- a large portion of the remaining losses – the ones occurring in the condenser, the fraction of heat transfer loss due to finite pinch

point (dotted line in fig.10), or part of miscellaneous losses - would be present in any bottoming cycle

it follows that the practical possibility of finding better thermodynamic solutions by resorting to other working fluids (e.g. Kalina cycle) is doubtful.

10.3.3.2 Efficiency vs specific work

The overall performance of the combined cycle schemes of Fig. 10.15 are given in Fig. 10.17, which suggests the following comments:

- Combined cycles (CC), reach efficiencies as high as 55.5%: this result is in fair agreement with other theoretical calculations based on state-of-the-art gas turbines and advanced steam bottoming cycles (Bolland, 1990). The optimum pressure ratio of the gas cycle is about 15, close to values adopted in advanced heavy-duties. The efficiency drop at β higher than optimum is relatively small (1.15 points, for β=30), making CCs an interesting option also for aero-derivatives*.

- The introduction of reheat is not as effective as in mixed cycles: specific work increases of about 30%, while the efficiency gain is limited to about one percentage point. To maximize efficiency, it is necessary to adopt pressure ratios much higher than usual ($\approx$40), thus requiring a substantial re-design of the gas turbine.

- The presence of a regenerator ahead of the HRSG does not improve cycle performance in any plant arrangement: R_gCC, I_rR_gCC and R_hR_gCC. Three events produce this somewhat surprising result: (i) large heat transfer irreversibilities in the regenerator; (ii) decrease of bottoming cycle efficiency caused by lower temperatures at HRSG inlet and (iii) decrease of heat introduced into the cycle. The third circumstance is also responsible for lower specific work.

- The best plant configuration, both in terms of efficiency and specific work, is the intercooled/reheat combined cycle (I_cR_hCC), the same configuration selected for the Japanese "Moonlight" program (see Par. 10.2.3). According to the present calculations, at β=54 η_{sh} can reach 57.2%, with a specific work of about 770 kJ/kg. A direct comparison of these results with the ones in Tab. 10.5 is impossible, due to differences in cycle parameters (TIT, reheat TIT, β) and steam cycle arrangement.

---

* The results of Fig. 10.17 refer to HD machines; however, differences between AD and HD units are relatively small, since better AD turbomachinery efficiencies are counterbalanced by scale effects. For a CC based one a single AD unit, there would be however a severe scale effect on steam turbine performance.

In conclusion, it appears that increasing plant complexity does not dramatically improve CC performance (less than 2 percentage points at best), and that the development of new gas turbines specifically designed to meet the requirements of these cycles may be unjustified*.

10.3.4 Gains expected from future developments

Curve A in Fig. 10.18 reports the variation of simple gas cycle efficiency (for optimized β) vs TIT: the maximum efficiency is found for TIT close to the value of 1250 °C set as representative of the state-of-the-art: for higher TIT, the losses produced by larger cooling flows and higher TOT prevails upon the benefits of operating at higher temperatures. This result – which strongly depends on the assumptions about cooling technology and maximum allowable material temperature – indicates that current TITs are optimized to reach maximum simple cycle efficiency.

Curve A' – the analog of A for CCs – shows that for Combined Cycles the situation is different: efficiency increases with TIT up to values much larger than 1250 °C, indicating that in this case the gains achievable with higher TITs overcome the losses related to higher cooling flows. In other words, for CC applications it would be better to modify current gas turbine design and operate at higher TITs, even if this would require larger cooling flows to maintain the same material temperature.

The evident historic trend toward higher TITs at an average annual rate of about 15°C (Macchi, 1990) has been animated by two factors:

* The validity of this statement obviously depends on a number of economic factors: development cost, fuel cost, interest rates, maintenance costs, etc. It is not difficult to envisage an economic scenario where the development is worthwhile.

(i) improvements of cooling technology and (ii) adoption of higher material temperatures. Since there is no reason to doubt that this trend will continue, it is worth investigating the consequences of advances in these two key areas. In Fig.10.18 the two effects have been separated by:

- Constructing curves B and B′ corresponding to "infinitely good" cooling technology, i.e. $Z=\infty$, and $r_{fc}=1$. Such curves indicate that efforts addressed toward better cooling technology can produce (if associated at higher TITs) efficiency gains of about 2 percentage points for both simple cycles and CCs.
- Repeating the same process for $T_{bmx,nz}=930°C$ and $T_{bmx,ct}=900°C$, i.e. 100°C above current state-of-the-art material technology. This produces curves C and C′, showing that with today's cooling technology and tomorrow's materials it is possible to achieve efficiency gains higher than those afforded by "perfect" cooling technology (for TIT=1350°C efficiency increases by about 2.5 percentage points).

Future gas turbines will contemporarily benefit of both effects. Since it is reasonable to assume that by the end of this decade TIT will approach 1350°C, according to Fig. 10.18 the efficiency of CCs could rise to values close to 58%.

10.3.5 Configurations allowing higher TIT

The reader may have noticed that while the verification of the ISTIG system of Par. 10.2.3 has been referenced to the TIT of 1371°C assumed in An. (1989b), the results of the parametric analysis depicted in Fig. 10.14 have been obtained for TIT=1250°C.

The reason why TIT is kept constant also for intercooled systems - which could operate at higher TIT by taking advantage of the lower coolant temperature - is that the main objective of this parametric analysis is making comparisons given all things equal. The choice of the "things equal" to be maintained constant throughout the calculation is somewhat subjective. I've chosen to maintain the same TIT because TIT is definitely the most important parameter defining the thermodynamic cycle (the other is the pressure ratio, which is varied to obtain the curves in the figures).

Given that intercooling allows increasing TIT without improving the cooling technology, one could make a comparison between a non-intercooled and an intercooled cycle having – say – the same cooling flow. Such a comparison would be definitely worthwhile but – to avoid a bias toward intercooling – it should be part of a comprehensive analysis of all the means which allow increasing TIT without improving the cooling technology. In addition to intercooling, other possible techniques are (i) steam cooling and (ii) pre-cooling of air to be used for blade cooling.

Besides going beyond the scope of this work, an analysis of these techniques calls for an enhancement of the calculation model. Since pressure drops pose a limit on the amount of coolant which can flow inside a blade (see Par. 5.2.6.3), the comparison should be made after including such a limitation. Then, the TIT of each configuration should be allowed to increase up to either:

- the value maximizing cycle efficiency or
- the value corresponding to the maximum coolant-side pressure drop

According to these hypotheses, the rank of the antagonistic technologies analyzed here may result different, presumably more favorable to the cycles (both mixed and unmixed) with intercooling.

10.3.6 Conclusions

With state-of-the-art technology both mixed and unmixed cycles can reach conversion efficiencies around 55%, i.e close to 70% of the efficiency of an ideal engine working within the assumed TIT of 1250 °C. Even if they operate within a much larger temperature span, their thermodynamic "quality" is therefore as good as that of Rankine cycles.

The calculations presented here show a rather clear thermodynamic superiority (varying between 3 to 5 percentage points) of Combined Cycles vs mixed cycles, mostly related to the capability of the steam cycle of releasing heat at temperatures close to ambient.

Among the various alternatives considered, the combination of advanced heavy-duty gas turbines with a proper steam bottoming cycle appears to be the most appealing and non-risky* choice for base-load electricity generation from natural gas or other premium fuels.

However, although they require substantial R&D efforts, at least two other unconventional solutions should be mentioned as potential candidates for future power generation: (i) the intercooled/reheat combined cycle and (ii) the reheat version of ISTIG. The first calls for the development of a high-pressure-ratio gas turbine specifically designed for this application, but it exhibits efficiencies about 2 percentage points higher than those of conventional CCs and a specific work increase of about 40%. The second could be built around the high-tech core of an aero-engine by adding an LP compressor and an inter-cooler ahead of the existing compressor, and an after-burner followed

* Combined Cycles based on heavy-duty units are now offered by all major world manufacturers. Their implementation does not require any R&D effort nor development cost.

by a power turbine downstream of the existing HP turbine. Despite the difficulties of this development, the resulting very high specific work (above 1100 kJ/kg) and the absence of a bottoming steam cycle could give a plant with very low specific cost.

Finally, it is important to emphasize that the criterion of constant TIT used for this parametric analysis is not the only possible choice. An alternative could be to choose for each configuration the TIT which maximizes efficiency under a constraint on coolant-side pressure losses. The adoption of this criterion requires to enhance the calculation model by adding the step-by-step calculation of coolant-side pressure losses.

REFERENCES

An. (1984), "Scoping Study: LM5000 Steam-Injected Gas Turbine", Marine and Industrial Engine Projects Dept., General Electric, Evendale, Ohio. Research performed for P.G.& E., California.

An. (1986), "Cheng Cycle Series 7-Cogen. Summary Product Description", International Power Technology, Redwood City, CA.

An. (1989a), flow diagram of high pressure steam injection into the GE LM5000 combustor, part of a presentation given by the GE Marine and Industrial Engine Division (M. Horner organizer, Feb. 1989), Cincinnati, Ohio.

An. (1989b), *LM8000 ISTIG Power Plant*, handout distributed at a presentation given by the GE Marine and Industrial Engine Division (M. Horner organizer, Feb. 1989), Cincinnati, Ohio.

Arai M, Imai T, Teshima K. and Koga A. (1988), "Research and Development on the HPT of the AGTJ-100B", J. of Eng. for Gas Turbines and Power, Vol. 110, pp. 259-264.

Bolland O. (1990), "A Comparative Evaluation of Advanced Combined Cycle Alternatives", ASME Paper 90-GT-335.

Brown D.H. and Cohn A. (1981), "An Evaluation of Steam Injected Combustion Turbine Systems", J. of Eng. for Power, Vol. 103, pp. 13-19.

Consonni S., Lozza G. and Macchi E. (1988), "Turbomachinery and Off-Design Aspects in Steam-Injected Gas Cycles", Proc. 23rd IECEC (Denver, Colorado), pp. 99-108. Published by ASME, New York.

Consonni S., Lozza G., Macchi E., Chiesa P. and Bombarda P. (1991), "Gas-Turbine-Based Cycles for Power Generation. Part A: Calculation Model", presented at the *1991 Yokohama International Gas Turbine Congress*, Yokohama, Japan, Oct. 1991.

Cook D.T., McDaniel J.E. and Rao A.D. (1991), "Coal to Clean Power without Steam: Higher Efficiency at Lower Cost", Paper T403 presented to the 1st World Coal Institute Conference on *Coal in the Environment*, London, Apr. 1991.

Di Candia F., Project Manager (1989), "ISTIG Enhancement Evaluation — Vol. I", Advanced Energy Systems Report no. 007.4-89.1, Dept. of Research and Development, PG&E, San Ramon, CA.

Donolo J. (1988), Allison Gas Turbine Division, Gennevilliers Cedex, France, Personal Communication.

El-Masri M.A. (1988), "A Modified, High-Efficiency, Recuperated Gas Turbine Cycle", J. of Eng. for Gas Turbines and Power, Vol. 110, pp. 233-242.

Gelfand L.E. (1987), General Electric Aircraft Engines, Advanced Programs & Ventures, Cincinnati, Ohio, Personal Communication to Eric D. Larson.

Hines W.R. (1990), General Electric Marine and Industrial Engines, Cincinnati, Ohio, Personal Communication.

Hori A. and Takeya K. (1981), "Outline of Plan for Advanced Reheat Gas Turbine", J. of Eng. for Power, Vol. 103, pp. 772-775.

Jones J.L., Flynn B.R. and Strother J.R., (1982), "Operating Flexibility and Economic Benefits of a Dual-Fluid Cycle 501-KB Gas Turbine Engine in Cogeneration Applications", ASME Paper 82-GT-298.Sahm

Karassik I.J. (1989), Centrifugal Pump Clinic, Marcel Dekker, New York.

Kolp D.A. and Moeller D.J. (1989), "Wolrd's First Full STIG LM5000 Installed at Simpson Paper Company", J. of Eng. for Gas Turbines and Power, Vol. 111, pp. 200-210.

Lozza G. and Bombarda P. (1991), "Cicli a vapore avanzati per impianti combinati", Proc. 5th Meeting on *Gruppi Combinati: Prospettive Tecniche ed Economiche* (Bologna, June 1991), pp. 137-156. Published by Pitagora Editore, Bologna, Italy.

Macchi E. (1990), "Power Generation (Including Cogeneration)", invited lecture given at the IEA Conference on *Emerging Gas Technologies - Implications and Applications*, Oct. 8-11, 1990, Lisbon, Portugal.

Macchi E., Bombarda P., Chiesa P., Consonni S. and Lozza G. (1991), "Gas-Turbine-Based Cycles for Power Generation. Part B: Performance Analysis of Selected Configurations", presented at the *1991 Yokohama International Gas Turbine Congress*, Yokohama, Japan.

Merola A. (1991), Fiat Aviazione, Turin (Italy), Personal Communication.

Oganowski G. (1987), "LM5000 and LM2500 Steam Injection Gas Turbine, Proc. *1987 Tokio Int. Gas Turbine Congress*, Vol. III, pp. 393-397.

Sheperd S. (1987), International Power Technology, Redwood City, CA, Personal Communication.

Takeya K., Oteki Y. and Yasui H. (1984), "Current Status of Advanced Reheat Gas Turbine AGTJ-100A. Part 3: Experimental Results of Shop Tests", ASME Paper 84-GT-57.

Takeya K. and Yasui H. (1988), "Performance of the Integrated Gas and Steam Cycle (IGSC) for Reheat Gas Turbines", J. of Eng. for Gas Turbines and Power, Vol. 110, pp. 220-224.

Thames J.M. and Coleman R.P. (1989), "Preliminary Performance Estimates for a GE Steam Injected LM1600 Gas Turbine", ASME Paper 89-GT-97.

NOMENCLATURE

Bi_{bw}	Blade wall Biot number	
D_s	Specific diameter	[m]
ex	Specific exergy	[J/kg]
m	Nondimensional mass flow, specific to M_a	[kg/kg$_a$]
$\hat{m}_{dsk}$	Disk coolant flow per stage	[kg/kg$_a$-stage]
M	Mass flow	[kg/s]
Ma	Mach number	
n^{stg}	Number of stages	
P	Pressure	[Pa]
r_{vcl}	Ratio defining useful coolant ejection velocity, see Eq.(3.15)	
S	Entropy	[J/K]
T	Temperature	[K]
T_{bmx}	Maximum allowed blade temperature	[K]
u	Peripheral speed	[m/s]
V	Volumetric flow	[m^3/s]
$\dot{W}$	Power	[W]

Greek

β	Pressure ratio (compressors, >1); expansion ratio (turbines, <1)	
Δh	Enthalpy drop	[J/kg]
ΔP	Pressure loss	[Pa]
ΔT	Temperature difference	
ε_h	Heat loss fraction	
η	Efficiency	
η_{II}	Second-law efficiency	
Φ	Relative humidity	
λ	Pattern factor	

Subscripts

a	Air
ad	Adiabatic
ap	Approach
c	Compressor
cl	Coolant
cmb	Combustor
ct	Cooled turbine
dif	Diffuser
el	Electric
ev	Evaporation
f	Fuel
g	Hot gas
gc	Gas compressor
gg	Gear+Generator
in	Inlet
is	Isentropic
lk	Leakage
min	Minimum
mx	Maximum
nz	Nozzle
org	Organic
out	Outlet
p	Polytropic
pp	Pinch point
sc	Subcooling at economizer exit

sh	Shaft
st	Steam turbine
t	Turbine
ut	Uncooled turbine section
0	Ambient conditions
1n	Exit of first nozzle

Acronyms for Cycle Configurations

STIG	Steam injection
ISTIG	Intercooling and steam injection
R_hSTIG	Reheat and steam injection
IR_hSTIG	Intercooling, reheat and steam injection
R_gWI	Regeneration and water injection
R_gR_hWI	Regeneration, reheat and water injection
CC	Combined Cycle
ICC	Intercooling and Combined Cycle
R_hCC	Reheat and Combined Cycle
IR_hCC	Intercooling, reheat and Combined Cycle
R_gCC	Regeneration and Combined Cycle
R_hR_gCC	Reheat, regeneration and Combined Cycle
IR_hR_gCC	Intercooling, reheat, regeneration and Combined Cycle

FIGURES AND TABLES

<u>Compressors</u>
Δh_{is}^{stg}=20 (HD) or 30 (AD) kJ/kg; n_c^{stg} is integer
Inlet ΔP (filter): 1 kPa
Maximum outlet temperature: 620°C
Inlet flow: for HDs, 600 kg/s; for ADs, such that $V_{HPT,in}$=30 m^3/s
<u>Combustors</u>
ΔP_{cmb}=3%;
Fuel compressor: isothermal (η=55%) for β>3, otherwise adiabatic with η_p=75%; fuel must be injected at $P_f \geq 1.5 \cdot P_g$
Max T_g at inlet: 800°C
<u>Turbine</u>
$\eta_{p,nz}$=95%, η_{dif}=50%
$Ma_{g,in}$=0.9, $Ma_{g,ct}$=0.7, $Ma_{dif,in}$=0.45
$T_{bmx,nz}$=830°C, $T_{bmx,ct}$=800°C
λ_{nz}=0.10, λ_{ct}=0.03
$\dot{m}_{dsk}$=1% for air air cooling, 0.5% for steam cooling; Bi_{bw}=0.5
Cooled stages: β^{stg}=constant and $\Delta h_{is,mx}^{stg}$=350 (HD) or 425 (AD) kJ/kg
Uncooled stages: $\Delta h_{is,ut}^{stg}$=200 (HD) or 100 (AD) kJ/kg
n^{cs} and n_t^{stg} are both real, with $n_t^{stg} \geq 1$
Coolant circuit: r_{vcl}=0.5; u=400 m/s (determines pumping work); α=30°; HP nozzle coolant bled at HP compressor exit, all other bled continuously with $\Delta P_{cl}/P_{cl}$=40% (see Par. 3.7.1);
Meridional section: constant mean diameter
Maximum number of cooled expansion steps: 30
Exit ΔP: 1 kPa (simple cycle), 3 kPa (HRSG)
<u>Intercoolers</u>
Surface-type: air-side ΔP=3%, water exit T=40°C
Evaporative-type: air-side ΔP=2%, Φ_{out}=90%
<u>Regenerators</u>
ΔP (both sides): 4%, 2% for water pre-heater of Fig. 10.6
For evaporative-regenerative cycles (R_gWI and R_hR_gWI) ΔT_{min}=40°C
For all other cycles effectiveness=90%
<u>HRSG</u>
Condenser and deaerator P: 0.05 bar, 1.4 bar
Max steam P, T: 350 bar, 565°C
Reheat P $\geq$ 20 bar; $P_{ev,LP} \geq$ 3 bar
ΔT_{ap}=25°C, ΔT_{pp}=10°C, ΔT_{sc}=10°C
Heat losses: 0.7%; no blowdown
$\Delta P/P$: superheaters 8%, economizers 10%
Auxiliaries need 0.5% of condenser thermal power
Steam turbine: exit velocity=220 m/s; at condensing stage mean diameter u=450 m/s; topping turbine η_{ad}=75% (STIG cycles).
<u>Other</u>
Pumps: η_{pump}=f(V), η_{org} and η_{el} functions of $\dot{W}_{el}$
Ambient air: 15°C, 1.01325 bar, Φ=60%
Water: 15°C, 1.01325 bar
Fuel: Methane at 15°C, 40 bar, LHV=50.01 MJ/kg
Generator efficiency varies with $\dot{W}_{el}$ as in Fig. 7.1 (for $\dot{W}_{el} \geq$200 MW, η_{el}=constant=98.5%)
Steam must be injected at P $\geq 1.2 \cdot P_g$ (combustor) or P $\geq 1.1 \cdot P_g$ (turbine)

Table 10.1 Assumptions adopted for the calculations of Par. 10.3 and – if not indicated otherwise – also for the verifications of Par. 10.2.

	Allison 501-KH	GE LM 5000	All others
Z	36.0	36.0	100.0
r_{fc}	0.194	0.194	0.250
$\eta_{p,c\infty}$	0.896	0.902	0.902
$\eta_{p,t\infty}$	0.912	0.912	0.921
a_c	←-----	0.02688	-----→
a_t	←-----	0.07108	-----→

Table 10.2. Cooling parameters and turbomachinery efficiencies adopted for the calculations of this Chapter.

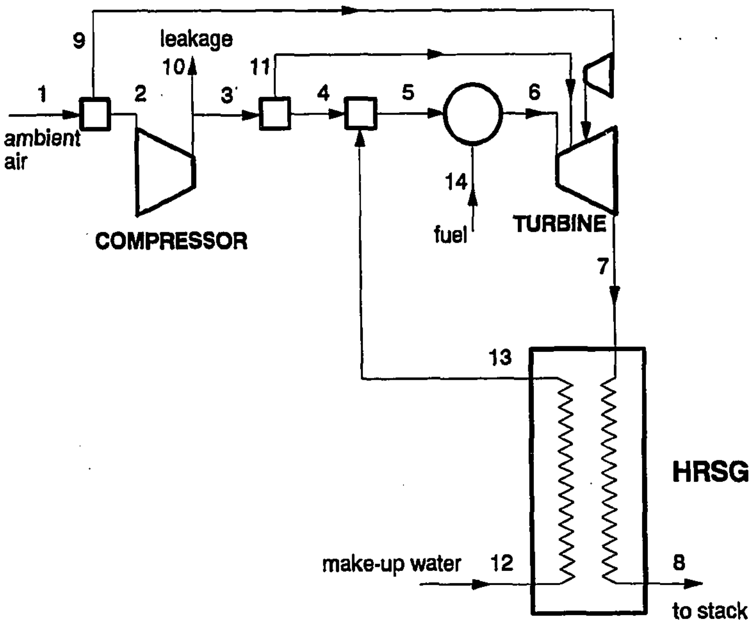

Fig. 10.1 Schematic used to reproduce the performances of the Allison 501 STIG plant commercialized by IPT.

Point	IPT data[a]			Calculated data: Same hypotheses			Calculated data: Tab. 10.1		
	T,°C	P,bar	m	T,°C	P,bar	m	T,°C	P,bar	m
1	15	1.013	15.6 kg/s	$\underline{15}$	$\underline{1.013}$	$\underline{15.6\ kg/s}$	$\underline{15}$	$\underline{1.013}$	$\underline{15.6\ kg/s}$
3	354[b]	11.44[b]	-	361	$\underline{11.44}$	0.9510	361	$\underline{11.44}$	0.9420
5	-	-	-	396	11.44	1.0160	389	11.44	1.0088
6	-	-	-	1026	11.04	1.0358	1026	11.09	1.0273
TIT	982	-	-	$\underline{982}$	10.47	1.1305	$\underline{982}$	10.50	1.1198
7	511	1.038	1.178[d]	501	1.038	1.1715	499	1.044	1.1698
8	123	1.013	1.178	119	1.013	1.1715	123	1.013	1.1698
9	-	-	-	15	1.001	0.0410	15	1.001	0.0500
10	-	-	-	361	11.44	$\underline{0.0080}$[c]	361	11.44	$\underline{0.0080}$
11	-	-	-	361	11.44	0.0947	361	11.44	0.0925
12	15	1.013	0.1644[d]	$\underline{15}$	$\underline{1.013}$	0.1597	$\underline{15}$	$\underline{1.013}$	0.1593
13	500	14.14	0.1595	$\underline{500}$	14.01[e]	0.1597	477	14.01[e]	0.1593
14	15	18.3	0.0186	$\underline{15}$	$\underline{18.3}$	0.0198	$\underline{15}$	$\underline{18.3}$	0.0185
n_c^{stg}					$\underline{14}$			16	
n_t^{stg}/n^{cs}					$\underline{4/1}$			3.4/1.4	
$\dot{W}_{sh}$, kW		5670[f]			5809			5750	
η_{sh}, %		39.8[f]			40.42			39.95	

Besides the underlined figures and the assumptions in Tab. 10.1, other data used to obtain the results under the heading "Same hypotheses" are: fuel LHV=46.26 MJ/kg[a]; ΔP_{cmb}=3.5%[a]. For the HRSG: T_{ev}=199°C[a]; water subcooling at economizer exit=5°C[a]; Pinch=8°C[g]; Approach=1°C[h].

- [a] From An. (1986) and Sheperd (1987)
- [b] From Jones, Flynn and Strother (1982), for β=11.4
- [c] According to Sheperd's data, leakage is apparently zero
- [d] Corresponds to 3% blowdown.
- [e] $P_{13}<P_{ev}$=15.23 bar due to superheater pressure drops ($\Delta P/P$=8%, see Tab. 10.1). Further downstream, steam is throttled to P_5=11.44 bar
- [f] Based on η_{gg}=95%
- [g] Sheperd (1987) gives Pinch=3°C, which is unusually low; the value of 8°C has been used to mach the steam flow m_{13}=0.1595
- [h] This unrealistically low value has been used to match the steam temperature T_{13}=500°C.

Table 10.3 Performance prediction of the IPT plant based on the Allison 501. State point numbers refer to the scheme in Fig. 10.1. Except for point 1, m is the mass flow relative to the compressor inlet flow. Underlined numbers indicate data used as inputs.

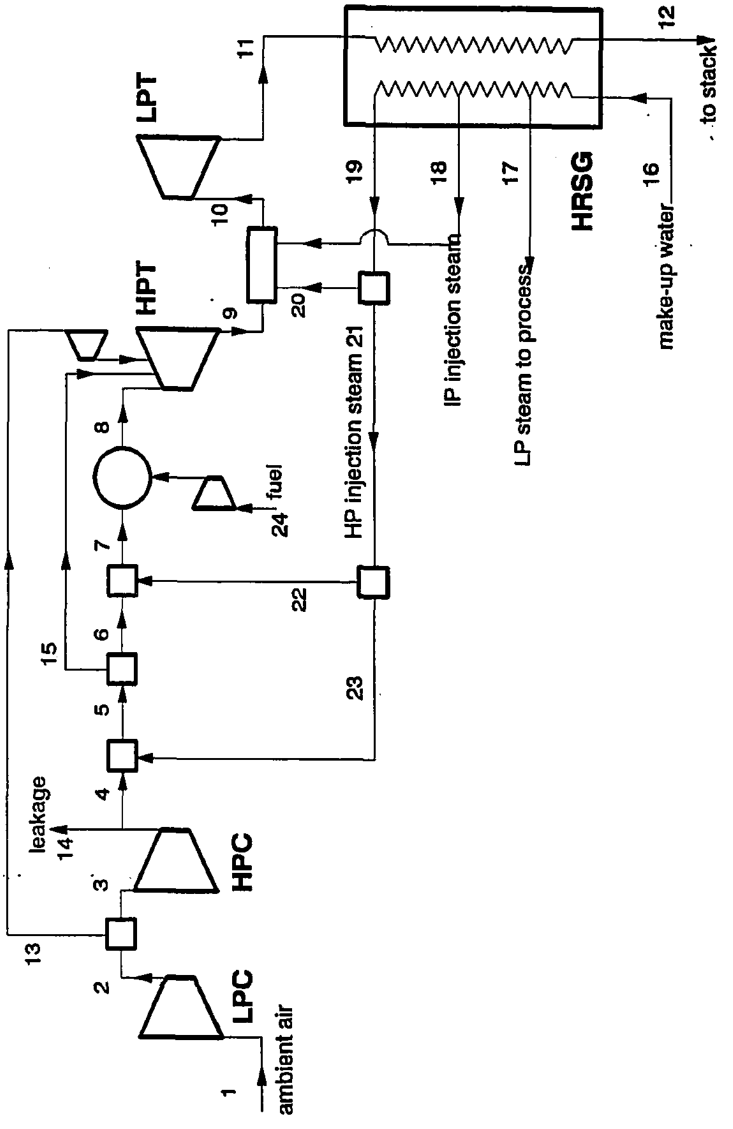

Fig. 10.2 Schematic used to reproduce the performances of the GE LM5000 STIG plant installed at Ripon.

Point	Ripon plant[a]			Calculated data					
				Same hypotheses			Tab. 10.1		
	T,°C	P,bar	m	T,°C	P,bar	m	T,°C	P,bar	m
1	15	1.013	*138.1 kg/s*	$\underline{15}$	$\underline{1.013}$	$\underline{138.1kg/s}$	$\underline{15}$	$\underline{1.013}$	$\underline{138.1kg/s}$
2	125[b]	2.757[b]	-	124	$\underline{2.757}$	1.0	123	$\underline{2.757}$	1.0
4	566[b]	32.35[b]	-	571	$\underline{32.35}$	0.8416	570	$\underline{32.35}$	0.8682
5	-	-	-	566	32.35	0.8496[c]	564	32.35	0.8762
7	-	-	-	514	32.35	0.6871	515	32.35	0.7123
8	-	-	-	1334	30.73	0.7036	1329	31.39	0.7293
TIT	1174[d]	-	-	$\underline{1174}$	27.28	0.9309	$\underline{1174}$	27.87	0.9568
9	788[b]	7.488[b]	-	785	$\underline{7.448}$	1.0812	789	$\underline{7.448}$	1.0807
11	403[d]	1.038	1.118	398	$\underline{1.038}$	1.1245	403	1.044	1.1232
12	134[e]	1.013	-	85	$\underline{1.013}$	1.1245	93	$\underline{1.013}$	1.1232
13	-	-	-	124	2.757	0.1503	123	2.757	0.1239
14	-	-	-	571	32.35	$\underline{0.0080}$[f]	570	32.35	$\underline{0.0080}$
15	-	-	-	566	32.35	0.2273	564	32.35	0.2275
16	21	2.752	-	$\underline{21}$	$\underline{2.752}$	0.1462	21	$\underline{2.752}$	0.1450
17	130	1.720	0.0300	130[g]	$\underline{2.70}$[g]	0.0299	130[g]	$\underline{2.70}$[g]	0.0306
18	235	20.70	0.0240	235[g]	$\underline{30.63}$[g]	0.0240	235[g]	$\underline{30.63}$[g]	0.0233
19	315	51.75	0.0922	$\underline{315}$[g]	$\underline{53.36}$[g]	0.0923	$\underline{315}$[g]	$\underline{53.36}$[g]	0.0910
20	315	-	0.0193	315	53.36	$\underline{0.0193}$	315	53.36	$\underline{0.0193}$
21	315	-	0.0730	315	53.36	0.0730[c]	315	53.36	0.0717
24	-	17.25	0.0164	$\underline{15}$	$\underline{17.25}$	0.0165	$\underline{15}$	$\underline{17.25}$	0.0169
n_c^{stg}						$\underline{5+14}$		4+15	
n_t^{stg}/n^{cs}						$\underline{2+1+3/2}$		1.7+3/1.7	
$\dot{W}_{HPC}-\dot{W}_{HPT}$, kW						3586		1841	
$\dot{W}_{sh}$, kW		49500[h]				49251		50993	
η_{sh}, %		43.00[h]				43.10		43.60	

Besides underlined figures and the assumptions in Tab. 10.1, other data used to obtain the results under the heading "Same hypotheses" are: compressor inlet ΔP=1.5 kPa[a]; ΔP_{cmb}=5%[i],; β_{gc}=2.8[a]; T_{ev}(LP-IP-LP)=130-216-268°C[a]; ΔT_{sc}(deaerator-LP-IP-HP)=5-9.5-5-9.5°C[a] ΔT_{pp}(LP-IP-HP)=3-4-3.5°C[j]; Kolp and Moeller (1989) also give blowdown (LP-IP-HP) = 1.2-1.1-0.5%.

[a] From Kolp and Moeller (1989).
[b] From Gelfand (1987).
[c] A steam flow equal to 0.8% of M_a mixes with the nozzle cooling flow (An., 1989a); thus m_{22}=0.0650, m_{23}=0.008.
[d] From Oganowski (1987), who also gives TOT (i.e. T_{12}) = 411°C.
[e] At Ripon the deaerator is fed with LP steam; instead, in our model there is an economizer+boiler which cool the gases below 90°C.
[f] According to Gelfand's data, for a simple cycle LM5000 m_{1k}=~3%.
[g] Evaporation conditions; all superheater pressure drops are charged to the steam injectors downstream.
[h] It is unclear whether $\dot{W}_{gc}$ is included.
[i] Includes ΔP due to steam injection.
[j] Adjusted to reproduce the same steam flows.

Table 10.4 Performance prediction of the Ripon plant based on a GE LM5000. State point numbers refer to the scheme in Fig. 10.2. Except for point 1, m is the mass flow relative to the compressor inlet flow. Underlined numbers indicate data used as inputs.

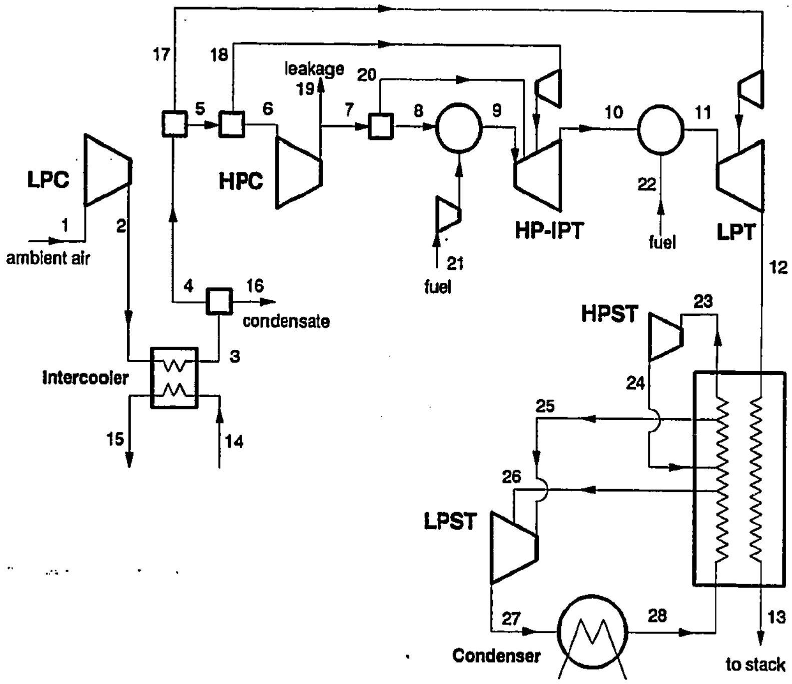

Fig. 10.3 Schematic used to reproduce the performances of the "Moonlight" Combined Cycle described by Takeya and Yasui (1988).

Point	Moonlight CC[a]			Calculated data					
				Same hypotheses			Tab. 10.1		
	T,°C	P,bar	m	T,°C	P,bar	m	T,°C	P,bar	m
1	15	1.013	*542 kg/s*	$\underline{15}$	$\underline{1.013}$	$\underline{542\ kg/s}$	$\underline{15}$	$\underline{1.013}$	$\underline{542\ kg/s}$
2	702	5.023	-	205	$\underline{5.023}$	1.00	205	$\underline{5.023}$	1.00
3	60	4.915	0.9850	$\underline{60}$	$\underline{4.915}$	1.00	$\underline{40}$	$\underline{5.023}$	1.00
7	438	58.86	0.7730	445	$\underline{58.86}$	0.8555	407	$\underline{58.86}$	0.8837
9	1300	56.80	0.7910	$\underline{1300}$	$\underline{56.80}$	0.8165	$\underline{1300}$	57.12	0.8448
10	800	11.77	0.9430	812	$\underline{11.77}$	0.9378	820	11.84	0.9502
11	1175	11.48	0.9540	$\underline{1175}$	$\underline{11.48}$	0.9472	$\underline{1175}$	$\underline{11.48}$	0.9595
12	587	1.053	1.0830	577	$\underline{1.053}$	1.0193	581	1.044	1.0208
13	-	1.013	-	100	$\underline{1.103}$	1.0193	89	1.013	1.0208
17	-	-	0.0480	60	4.925	0.0721	40	4.872	0.0612
18	-	-	[b]	60	4.925	0.0645	40	4.872	0.0472
19	-	-	-	445	58.86	$\underline{0.0080}$	407	58.86	$\underline{0.0080}$
20	-	-	[b]	445	58.86	0.0569	407	58.89	0.0581
21	-	-	0.0180	$\underline{15}$	$\underline{20.00}$	0.0179	$\underline{15}$	$\underline{20.00}$	0.0192
22	-	-	0.0100	$\underline{15}$	$\underline{20.00}$	0.0094	$\underline{15}$	$\underline{20.00}$	0.0094
23	552	143.3[c]	0.1199	$\underline{552}$	$\underline{143.3}$[c]	0.1200	556	$\underline{143.3}$[c]	0.1037
24	327	26.47	0.1199	$\underline{327}$[d]	$\underline{26.47}$	0.1200	347	$\underline{26.47}$	0.1037
25	479	-	0.1199	$\underline{479}$	25.67[e]	0.1200	556	24.35	0.1037
26	213	2.944[c]	0.0387	$\underline{213}$	$\underline{2.944}$[c]	0.0386	556	$\underline{2.944}$[c]	0.0496
27	32	0.049	0.1587	$\underline{32}$	0.049	0.1587	$\underline{32}$	0.049	0.1532
n_c^{stg}					- 6+13			6+12	
n_t^{stg}/n^{cs}					$\underline{2}+\underline{3}$[a]/$\underline{2}+\underline{2}$[a]			1.6+3.1/1.6+1.6	
$\dot{W}_{sh,st}$, kW		103000			98004			102257	
$\dot{W}_{sh,CC}$, kW		406090[f]			398663			423456	
$\dot{W}_{gc}$, kW		?			4557			4908	
η_{sh}, %		54.3[f]			53.85			54.56	

Besides underlined figures and the assumptions in Tab. 10.1, other data used to obtain the results under the heading "Same hypotheses" are: P_{ev}(deaerator-LP-HP)=1.177[a]-2.944[a]-143.32[a] bar; ΔT_{pp}(LP-HP)=23-10°C[g]; steam turbine η_{ad}(LP-HP)=85[a]-81[d]%; superheater $\Delta P/P$ (LP-reheat-HP)=2[a]-3-3.3[a]%; economizer $\Delta P/P$=10%; β_{gc}=5.

[a] From Takeya and Yasui (1988).
[b] Overall HP turbine cooling flow $m_{18}+m_{20}=0.1660$
[c] Evaporation conditions; outlet pressure is lower due to pressure losses in superheater.
[d] HP steam turbine η_{ad}=81% to match T_{24}=327°C given by Takeya and Yasui, although in the same paper they also quote η_{ad}=85%.
[e] Based on a 3% ΔP in the superheater.
[f] Assuming η_{gg}=98.5%. It is unclear whether the consumption of the gas compressor is included.
[g] Takeya and Yasui give a generic 20°C; the values above have been adjusted to reproduce the same steam flows.

Table 10.5 Performance prediction of the "Moonlight" reheat Combined Cycle plant. State point numbers refer to the scheme in Fig. 10.3. Except for point 1, m is the mass flow relative to the compressor inlet flow. Underlined numbers indicate data used as inputs.

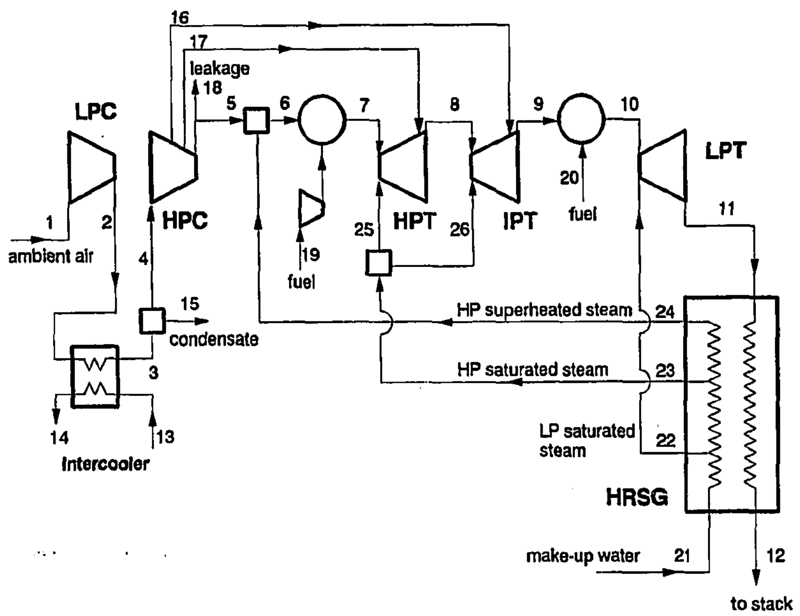

Fig. 10.4 Schematic used to reproduce the performances of the "Moonlight" Integrated Gas Steam Cycle (IGSC) described by Takeya and Yasui (1988).

Point	Moonlight IGSC[a]			Calculated data: Same hypotheses			Calculated data: Tab. 10.1		
	T, °C	P, bar	m	T, °C	P, bar	m	T, °C	P, bar	m
1	15	1.013	*335 kg/s*	15	1.013	*335 kg/s*	15	1.013	*335 kg/s*
2	202	5.023	-	205	5.023	1.00	205	5.023	1.00
3	60	4.915	0.9850	60	4.915	1.00	40	4.872	1.00
5	500	78.48	0.9730	512	78.48	0.9770	471	78.48	0.9770
7	1300	75.73	1.1880	1300	75.73	1.1410	1300	76.13	1.1367
8	986	28.84	1.2420	976	28.84	1.1970	964	28.84	1.2027
9	800	13.05	1.2630	791	13.05	1.2186	780	13.14	1.2245
10	1175	12.75	1.2780	1175	12.75	1.2338	1175	12.75	1.2402
11	608	1.053	1.3070	583	1.053	1.3098	583	1.044	1.3148
12	-	1.013	-	72	1.013	1.3098	86	1.013	1.3148
16	222	-	0.0100[b]	222	16.50[b]	0.0100	188	16.50	0.0100
17	356	-	0.0050[b]	356	37.40[b]	0.0050	322	37.50	0.0050
19	-	-	0.0287	15	20.00	0.0259	15	20.00	0.0269
20	-	-	0.0161	15	20.00	0.0152	15	20.00	0.0158
21	15	1.013	0.2790	15	1.013	0.2774	15	1.013	0.2788
22	311	15.70[c]	0.0286	311	15.70[c]	0.0760[d]	311	15.70[c]	0.0746
23	306	94.10[c]	0.0657	306	94.10[c]	0.0627	306	94.10[c]	0.0723
24	588	94.10[c]	0.1851	582	94.10[c]	0.1382	558	94.10[c]	0.1329
25	304	-	0.0549	306	94.10	0.0510[e]	306	94.10	0.0610
26	242	-	0.0106	242	40.00	0.0115[e]	242	40.00	0.0118

	Moonlight IGSC[a]	Same hypotheses	Tab. 10.1
n_c^{stg}		6+15	6+14
n_t^{stg}/n^{cs}		1+1+3[a]/1+1+2[a]	1.2+1+3.6/1.2+1+1.8
$\dot{W}_{HPC}-\dot{W}_{HPT}$, kW		11035	2690
$\dot{W}_{sh}$, kW	406090[f]	362540	374446
$\dot{W}_{gc}$, kW	?	4938	5119
η_{sh}, %	55.1[f]	52.60	52.42

Besides underlined figures and the assumptions in Tab. 10.1, other data used to obtain the results under the heading "Same hypotheses" are: P_{ev}(LP-HP)=15.7−94.1[a] bar; ΔT_{pp}(LP−HP)=1-55°C[g]; β_{gc}=7.

- [a] From Takeya and Yasui (1988)
- [b] Although Takeya and Yasui do not specify its use, air bled from the HP compressor is presumably used to cool discs and/or as purge flow. In our calculations such air is mixed with the turbine exit flow; its bleed pressure is determined by matching the bleed temperature.
- [c] Evaporation conditions.
- [d] Includes a flow of 0.0129 for discs, bearings, etc.
- [e] Due to the presence of m_{16} and m_{17}, does not include disc cooling flow; unlike LP cooling flow, HP cooling flow is saturated.
- [f] Assuming η_{gg}=98.5%. It is unclear whether $\dot{W}_{gc}$≈3.3 MW is included.
- [g] Adjusted to satisfy the demand of turbine cooling flow. All extra HP steam is superheated as much as possible and then injected.

Table 10.6 Performance prediction of the "Moonlight" Integrated Gas Steam Cycle (IGSC). State point numbers refer to Fig. 10.4. Except for point 1, m is the mass flow relative to the compressor inlet flow. Underlined numbers indicate data used as inputs.

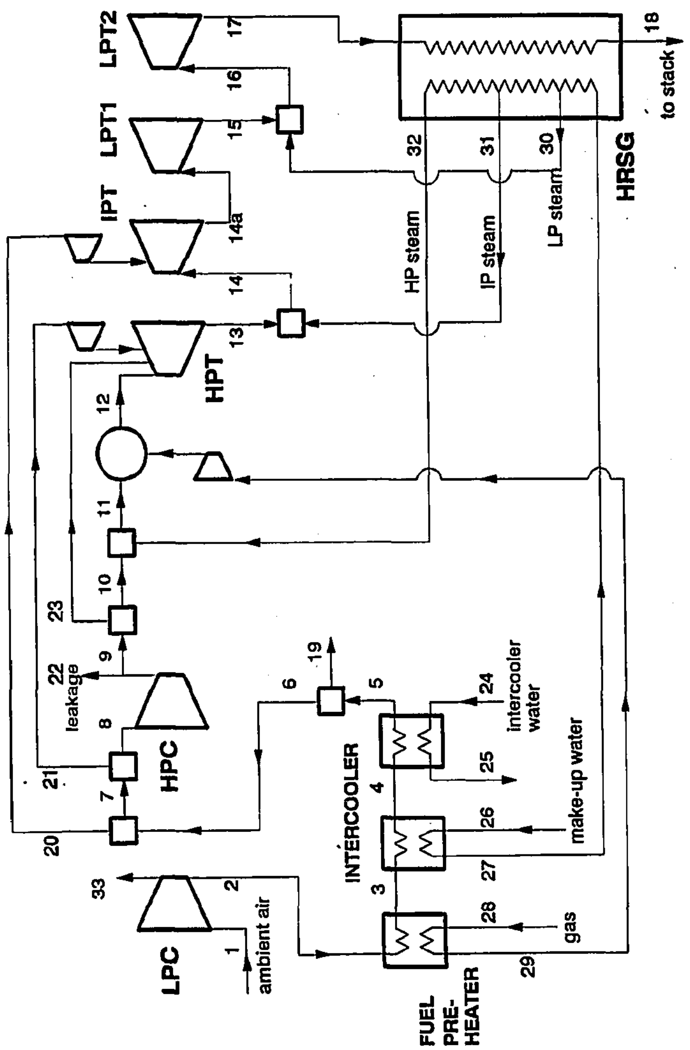

Fig. 10.5 Schematic used to reproduce the performances of the ISTIG system proposed by General Electric (An., 1984 and 1989b). The fuel pre-heater has been introduced upon suggestion of Hines (1990).

Point	GE data[a]			Calculated data: Same hypotheses			Calculated data: Tab. 10.1		
	T,°C	P,bar	m	T,°C	P,bar	m	T,°C	P,bar	m
1	15	1.013	*161.5 kg/s*	15	1.013	*161.5kg/s*	15	1.013	*161.5kg/s*
2	121	2.666	-	119	2.666	0.9920	119	2.666	1.00
5	23	2.590	0.9920	23	2.590	0.9920	40	2.590	1.00
9	385	34.44	-	395	34.44	0.7552	431	34.44	0.8345
12	-	32.81	-	1479	32.81	0.7877	1483	33.43	0.8705
TIT	1371[b]	-	-	1371	30.70	0.9064	1371	31.15	1.0133
13	1042	13.65	-	1044	13.65	1.0626	1079	13.65	1.1134
14a	951[c]	10.41	-	811[d]	6.467[d]	1.1578	811	5.342	1.1923
15	-	-	-	551	1.800	1.1578	588	1.800	1.1923
17	463	1.041	-	456	1.041	1.1831	500	1.044	1.2161
18	134	1.013	1.1780	127	1.013	1.1831	123	1.013	1.2161
20	-	-	-	23	2.590	0.0726	40	2.590	0.0575
21	-	-	-	23	2.590	0.1561	40	2.590	0.1001
22	-	-	-	23	2.590	0.0080	40	2.590	0.0080
23	-	-	-	395	34.44	0.1187	431	34.44	0.1428
27	97	-	0.1670	97	2.000	0.1704	97	2.000	0.1925
28	-	-	0.0300	15	20.00	0.0288	15	20.00	0.0315
30	121	2.070	0.0250[e]	121	2.070[f]	0.0254	475	2.070[f]	0.0238
31	370	14.50	0.0223	370	14.50[f]	0.0226	475	14.50[f]	0.0214
32	449	43.10	0.1226	449	43.10[f]	0.1225	475	43.10[f]	0.1473
n_c^{stg}					5+14			4+13	
n_t^{stg}/n^{cs}					2+2+7[g]/2+2[g]			1.3+1.2+4.6/1.3+1.2	
$\dot{W}_{HPC}-\dot{W}_{HPT}$, kW					4024			1587	
$\dot{W}_{sh}$, kW		116300[h]			104957			118939	
η_{sh}, %		53.1[h]			50.89			52.79	

Besides the underlined figures and the assumptions in Tab. 10.1, other data used to obtain the results under the heading "Same hypotheses" are: fuel LHV 44.5 MJ/kg[a]; P_{ev}(deaerator-LP-IP-HP)=1.01-2.07-14.5-43.1 bar; ΔT_{pp}(LP-IP-HP)=13-11-9.5°C[i]; economizer $\Delta P/P$=10%; $\eta_{p,gc}$=75% and β_{gc}=2.75.

[a] From An. (1989b)
[b] It is unclear whether it is TIT or it refers to combustor outlet.
[c] Exit of IP turbine.
[d] Total conditions at end of cooled expansion.
[e] LP steam injection before last turbine stage.
[f] Evaporation conditions; all superheater pressure drops are charged to the steam injectors downstream.
[g] From Hines (1990), although the assumption of a two-stage IP turbine contradicts current turbomachinery design practice.
[h] Based on η_g=98%. It is unclear whether $\dot{W}_{gc}\approx$1.5 MW is included.
[i] Adjusted to reproduce the same steam flows.

Table 10.7 Performance prediction of the ISTIG plant proposed by GE. State point numbers refer to Fig. 10.5. Except for point 1, m is non-dimensionalized by M_a=161.5 kg/s. Underlined numbers indicate data used as inputs.

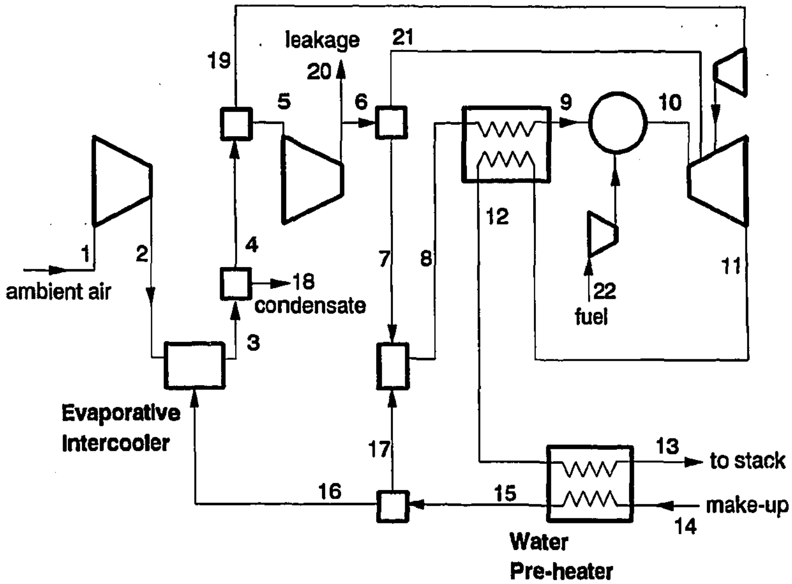

Fig. 10.6 Schematic used to reproduce the performances of the water-injected cycle proposed by El-Masri (1988), who however did not considered the water pre-heater.

Point	El-Masri[a]			Calculated data: Same hypotheses			Calculated data: Tab. 10.1		
	T,°C	P,bar	m	T,°C	P,bar	m	T,°C	P,bar	m
1	15	1.013	99.09 kg/s	15	1.013	99.09kg/s	15	1.013	99.09kg/s
2	103	2.375	1.00	105	2.375	1.00	105	2.375	1.00
3	47	2.304	1.0220	49	2.304	1.0223	52	2.327	1.0275
7	365	22.12	0.7889	381	22.12	0.8055	383	22.12	0.7704
8	138	21.68	0.9112	137	21.68	0.9278	147	21.68	0.9290
9	535	21.23	0.9112	526	21.23	0.9278	532	20.81	0.9290
10	1377	20.38	0.9354	1377	20.38	0.9524	1377	20.19	0.9542
11	577	1.054	1.1688	568	1.054	1.1689	572	1.077	1.2032
12	180	1.013	1.1688	186	1.013	1.1689	187	1.034	1.2036
13	180	1.013	1.1688	186	1.013	1.1689	114	1.013	1.2036
16	15	2.375	0.0223	15	2.375	0.0223	150	2.375	0.0275
17	15	22.12	0.1223	15	22.12	0.1223	150	22.12	0.1586
19	-	-	0.1559[b]	49	2.375	0.1167	52	2.375	0.1384
20	-	-	-	381	22.12	0.0003[c]	383	22.12	0.0080
21	365	22.12	0.0776[b]	381	22.12	0.0998	383	22.12	0.1106
22	15	20.7	0.0239	15	20.70	0.0246	15	20.00	0.0252
n_c^{stg}					3+11[d]			3+11	
n_t^{stg}/n^{cs}					3/2.5[e]			6[f]/2.7	
$\dot{W}_{sh}$, kW		60000			61539[g]			64258	
η_{sh}, %		50.4			50.53[g]			51.43	

Besides underlined figures and the assumptions in Tab. 10.1, other data used to obtain the results under the heading "Same hypotheses" are: ε_h=1%[e]; $T_{bmx,nz}$=847°C[a], $T_{bmx,ct}$=820°C[h].

[a] From El-Masri (1988)

[b] Assuming to bleed the coolant flow at three pressures: 22.12 (compressor discharge), 11.04 and 4.17 bar.

[c] m_{lk}=0.03% to conform to the indications of El-Masri's mass balances.

[d] El-Masri does not specify n_c^{stg}; he simply assumes $\eta_{p,LPC}$=92% and $\eta_{p,HPC}$=91%.

[e] For the turbine, El-Masri assumes an "uncooled" efficiency of 89.5, 91 and 92% (1st, 2nd and 3rd stage, respectively).

[f] The high value of n_t^{stg} comes from the assumption $\Delta h_{is,ut}^{stg}$=100 kJ/kg.

[g] Net of gas compressor power of ≈200 kW.

[h] El-Masri assumes different T_{bmx} for each blade row; proceeding from the turbine inlet T_{bmx} [°C] = 847 (stator 1), 827 (rotor 1) ,827 (stator 2), 797 (rotor 2), 827 (stator 3), 747 (rotor 3).

Table 10.8 Performance prediction of the water-injected cycle proposed by El-Masri. Point numbers refer to Fig. 10.6; the water pre-heater is considered only for the calculation based on Tab. 10.1. As usual, underlined numbers indicate inputs.

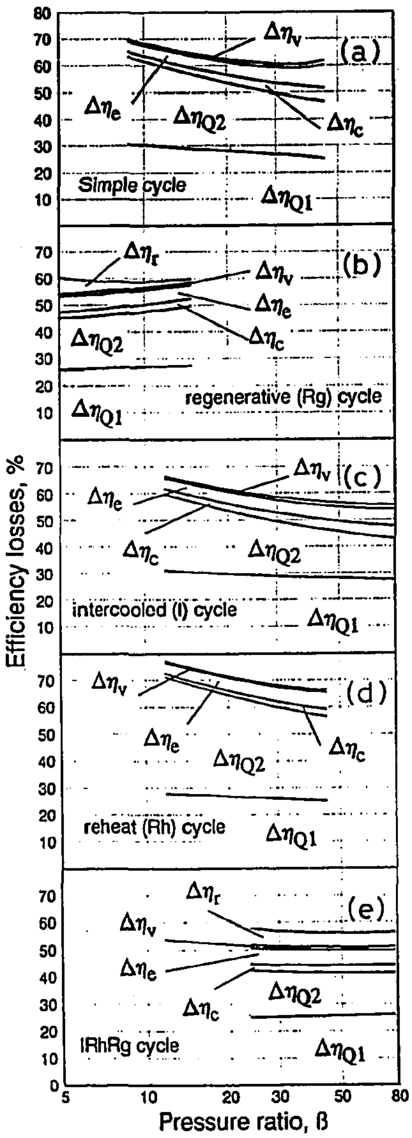

Fig. 10.7 Efficiency losses (as defined in Par. 10.3.1) of simple gas cycles with TIT=1250°C as a function of pressure ratio β. The difference between unity and the sum of all losses represents η_{II}. The upper value of β of non-regenerative cycles is set by the limit on maximum compressor outlet temperature (see Tab. 10.1); for regenerative cycles, the limit is set by the need to maintain a minimum ΔT across the regenerator.

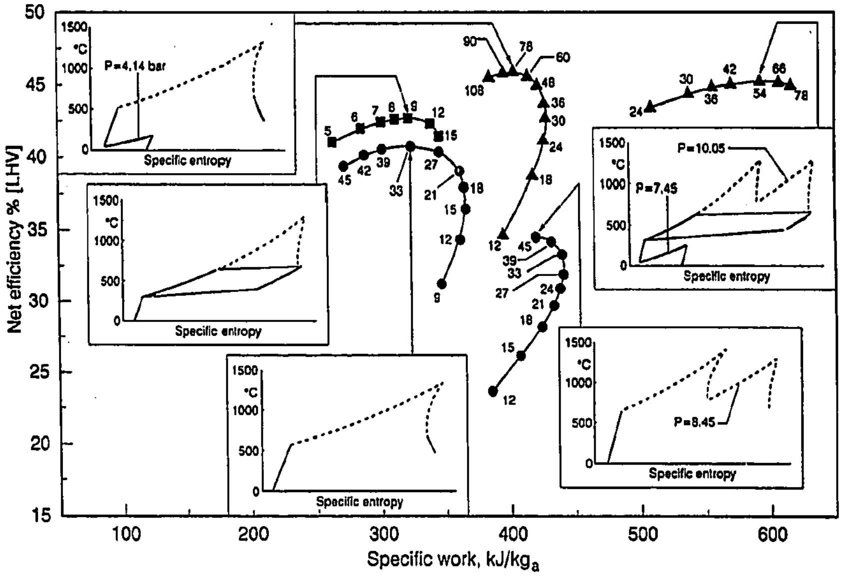

Fig. 10.8 Performance of simple gas turbine cycles with TIT=1250°C as a function of pressure ratio β; specific work is relative to the air flow at compressor inlet. Both η and w refer to the shaft output. The figure also shows the T-s diagram of each cycle at its optimum β. The small numbers on top of each point indicate the pressure ratio β.

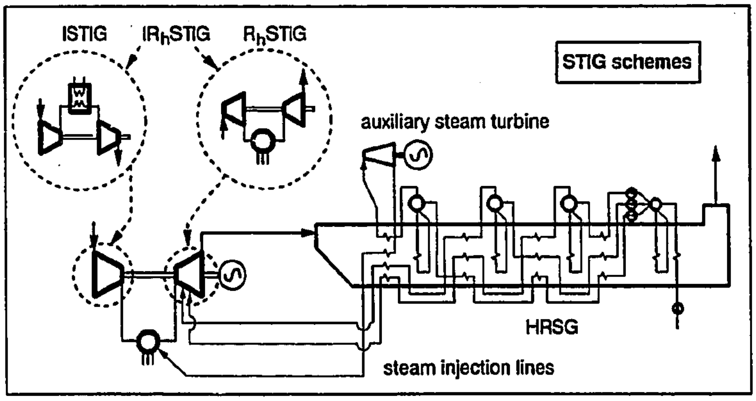

Fig. 10.9 Simplified plant schemes of steam-injected cycles. In the three-pressure-level HRSG steam is always superheated up to its maximum possible temperature, which is set either by ΔT_{ap}=25°C or by the limit of 565°C (see Tab. 10.1). When the auxiliary steam turbine is present (as in the figure), after expansion steam is sent back to the HRSG for further reheat before injection. With reheat gas turbines IP steam is injected into the reheat combustor.

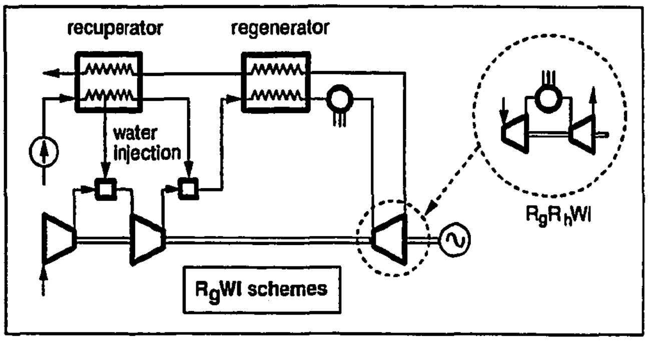

Fig. 10.10 Simplified plant scheme of R_gWI and R_gR_hWI cycles (blade cooling flows are not shown). Water is injected into the aftercooler at the maximum temperature allowed by the recuperator. The intercooling water temperature is limited in order to keep the heat capacity of gases higher (or equal) than the one of water.

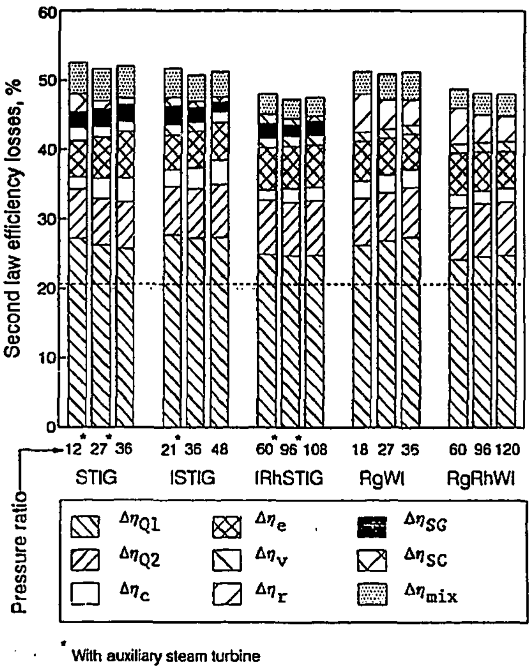

Fig. 10.11 Second-law efficiency losses of mixed cycles with TIT=1250°C. The dotted line at $\Delta\eta$=0.2064 represents the loss due to an isothermal combustion process producing heat at 1250°C (see Par. 8.4.2).

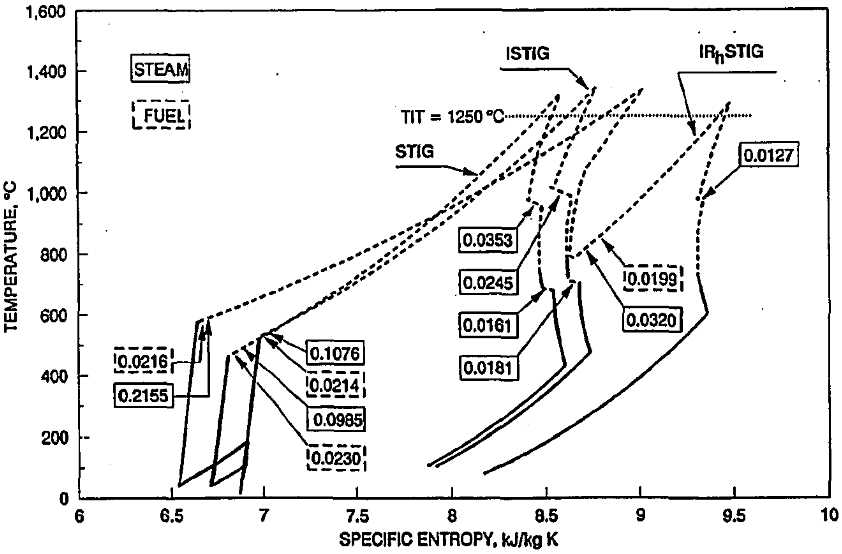

Fig. 10.12 Temperature-specific entropy diagram of STIG, ISTIG and IR_hSTIG cycles with TIT=1250°C (both HP and reheat turbine) at their optimum β. The specific entropy indicated in abscissa is relative to the actual working fluid unitary mass and chemical composition. Both vary due to water and/or steam injection and to combustion processes; the injected mass flows, specific to the air flow at compressor inlet, are shown in the figure. Dashed lines connecting points at different chemical composition have no physical meaning, and are represented for clarity.

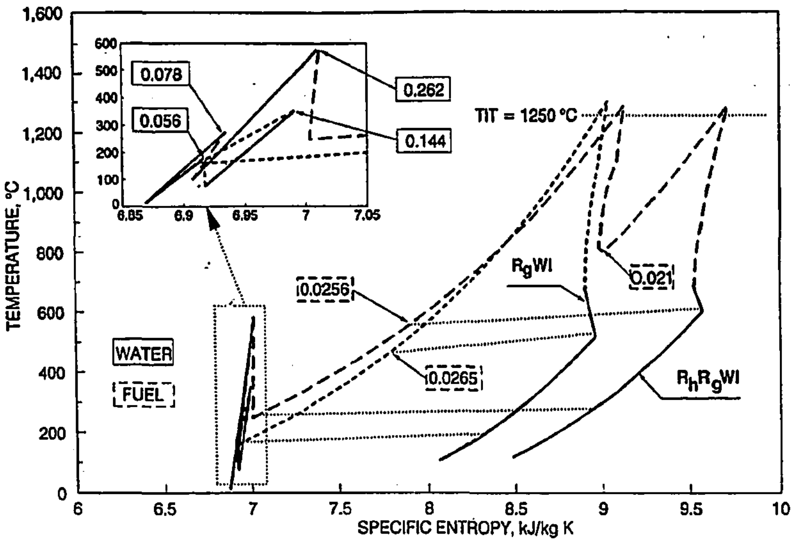

Fig. 10.13 Temperature-specific entropy diagram of R_gWI and R_hR_gWI cycles with TIT=1250°C (both HP and reheat turbine), at their optimum β (see caption of Fig. 10.12 for comments).

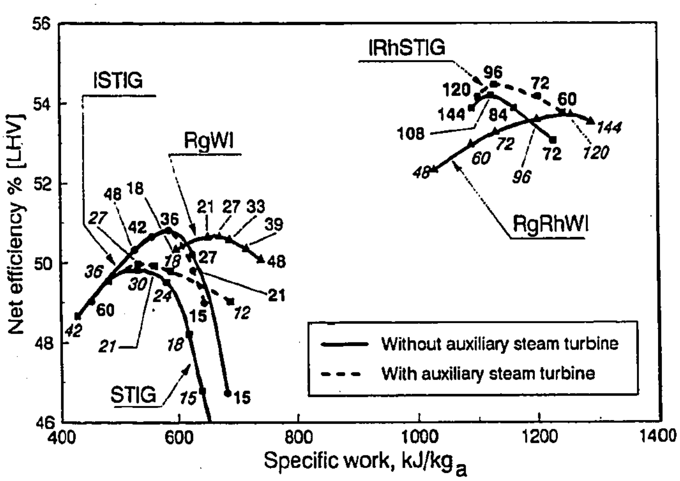

Fig. 10.14 η_{LHV}-specific work diagram for steam-injected and water-injected cycles with TIT=1250°C (both η and w refer to shaft output). The small numbers on top of each point indicate the pressure ratio β.

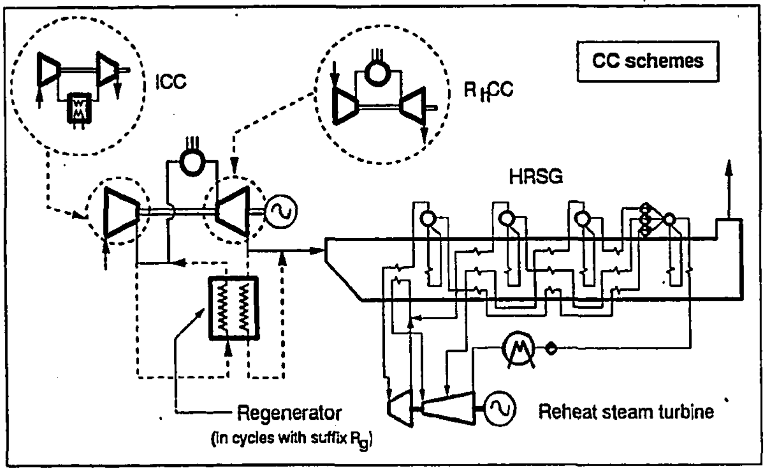

Fig. 10.15 Simplified plant schemes of Combined Cycles. The HRSG has three evaporation pressures and steam reheat. Steam pressures and superheat temperatures are optimized within the maximum limits set in Tab. 10.1.

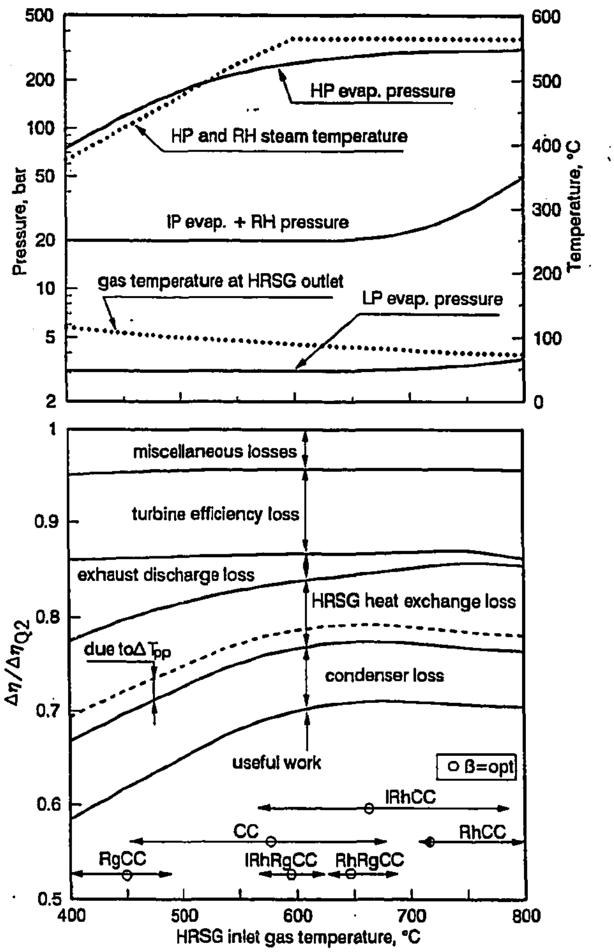

Fig. 10.16 Second-law efficiency losses ($\Delta\eta$) vs. HRSG inlet temperature of heat recovery from gas turbine exhaust as a fraction of the exergy content of the stream exiting the gas turbine ($\Delta\eta_{Q2}$). Results are relative to a three-pressure-level, reheat steam bottoming cycle subject to the assumptions of Tab. 10.1. The upper part of the figure shows the optimum steam pressures and HP/steam reheat temperatures, together with the resulting stack gas temperatures. the figure refers to a gas turbine exhaust composition typical of simple cycle heavy-duty gas turbines with β=15.

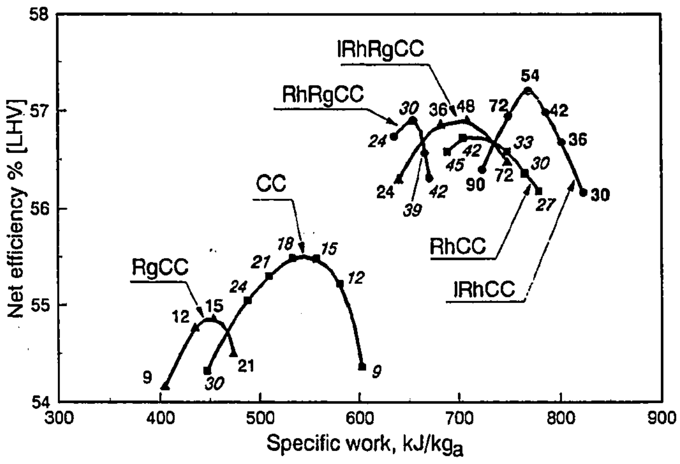

Fig. 10.17 η_{LHV}-specific work diagram for Combined (unmixed) Cycles with TIT=1250°C (both HP and reheat turbine). Both η and w refer to shaft output. The small numbers on top of each point indicate the pressure ratio β.

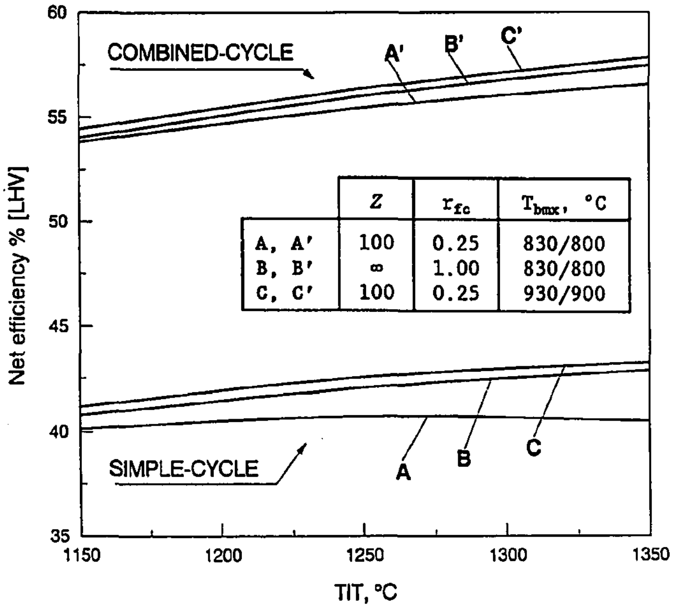

	Z	r_{fc}	T_{bmx}, °C
A, A'	100	0.25	830/800
B, B'	∞	1.00	830/800
C, C'	100	0.25	930/900

Fig.10.18 Influence of cooling technology, blade temperature and TIT on the performance of simple cycle turbines and Combined Cycles.

11. CONCLUSIONS

The work developed in the Thesis has satisfactorily accomplished all the objectives stated at its outset, i.e.:

- Development of a model for the prediction of complex GSC configurations.
- Calibration according to state-of-the-art gas turbine technology.
- Parametric analysis of the most interesting configurations.

Important aspects to be remarked about these three issues are:

- The computer program for the prediction of GSC performance can be applied to a vast class of energy systems and, due to its modularity, can be further extended with relatively modest efforts.
- The calibration with performance data of commercial engines has allowed to "anchor" the predictions of the model to those of actual, state-of-the-art gas turbines.
- The calculation of mixed cycles has proved very sensitive to the estimates of gas turbine cooling flows, due to a "chain effect" linking very closely the performance of the gas and steam section.
- For state-of-the-art turbine inlet temperatures of 1250°C, Combined (unmixed) Cycles have the potential to reach efficiencies above 55%, which could go beyond 57% by adding a reheat turbine.
- For the same turbine inlet temperatures of 1250°C mixed (steam- or water-injected) schemes promise lower efficiencies: about 51% without reheat, close to 55% with reheat. However, mixed cycles exhibit higher specific work (+10-20% without reheat, +50% with reheat), and simpler configuration due to the absence of steam turbine and condenser.

The last two observations suggest that the competition between unmixed and mixed solutions is likely to be centered around the trade-off between the higher efficiency afforded by the former and the presumable lower costs of the latter.

Aside from the specific results obtained here, one major achievement of the Thesis is the calculation model itself, which now allows assessing a number of issues relevant to the future of GSC technology:

- Potential of cycle configurations other than those already considered here, e.g. cycles with steam cooling, pre-cooling of cooling air, bottoming air cycles, etc.
- Gains achievable by progress in material technology (higher maximum blade temperature, TBC coatings) and/or cooling technology.
- Effect of scale on the full range of possible cycle configurations.
- Implications of the variation of any means affecting cooling flows and/or turbomachinery operating conditions.
- Verification of claims of GSC suppliers and/or those for new cycle configurations.

Important extensions and/or refinements which can constitute the subject for future work are:

- Inclusion of provisions for the calculation of coolant-side pressure drops, which would allow setting meaningful upper bounds on coolant flow rates. In particular, this could allow performing comparisons at constant maximum coolant-side pressure drop rather than at constant TIT, a criterion which is perhaps more appropriate for configurations with intercooling and/or steam cooling.
- Inclusion of specific speed effects on turbomachinery efficiency, which should improve the adherence of the model to actual turbomachine performances.
- Inclusion of provisions for the calculation of emissions levels, which may soon become the major determinant of technological development. This is perhaps the most challenging issue, because it would require a schematization of the combustion process which appears as demanding as that of the turbine.
- Clarification of differences between heavy-duty and aero-derivative technology and of the implications for GSC developments.
- Calculation of off-design performance.

Many of these extensions make sense only if additional data are available to calibrate an enhanced version of the model. The acquisition of reliable data on the performances of actual systems is therefore a crucial point to be addressed.

APPENDIX A: TURBINE CROSS-SECTIONAL AREA AND BLADE SURFACE

As shown in Chps. 3 and 5, evaluating cooling flows requires the knowledge of the gas cross-sectional area A_g and of a number of non-dimensional parameters describing turbine geometry. These parameters are evaluated according to the following hypotheses:

1) The specific diameter $D_{s,0}$ and the ratio $(H/D_m)_0$ of the first nozzle have the same value for all engines[a]
2) The solidity σ and the ratios c/D_m, t_b/c, c_a/c and Φ of each cascade are constant
3) Nozzle diameter and blade height are constant, while in the cooled turbine A_g varies so as to maintain constant U_g
4) The meridian section can be of three types: a) constant D_m; b) constant D_h; c) constant D_t

As discussed in Par. 4.4, according to similarity rules the specific diameter and the (H/D_m) ratio of a turbomachine designed for optimum efficiency should depend only on its specific speed. Besides the manufacturing and economic considerations mentioned in Par. 4.4, in actual applications this is not true also because the optimum design of the turbine and the compressor are often antagonistic; the compressor fluidynamic performances are typically more crucial, and its design is generally given higher priority.

Assuming that $D_{s,0}$ and $(H/D_m)_0$ are the same for all engines is equivalent to assume that: (i) first stages of all engines approximately run at the same specific speed and (ii) size has negligible effects on $D_{s,0}$ and $(H/D_m)_0$. As shown in Tab. A1, $n_{s,1}$ and $D_{s,0}$ indeed fall within a very narrow range. On the other hand, Tab. A2

[a] As emphasized in Par. 4.6.1, D_s is defined only for a whole stage. However, since in the first stage D_m is always approximately constant it is assumed that $D_{s,0} \simeq D_{s,1} \simeq D_{m,1} \cdot \Delta h_{is,1}^{0.25}/V_1^{0.5}$ and $D_{m,0} = D_{s,0} \cdot V_1^{0.5}/\Delta h_{is,1}^{0.25}$, where subscript "0" refers to nozzle inlet and "1" to the first rotor outlet.

Turbine	W_{sh} MW	β	TIT °C	$n_{s,1}$	SP_1	$D_{s,1}$	$(H/D_m)_0$	$(H/c)_0$	σ_0
Asea Brown Bovery									
GT8	47.800	16.3	1122	0.455	0.406	n.a.	0.068	0.91	1.14
GT11N	83.300	12.4	1054	0.520	0.590	n.a.	0.098	1.12	1.17
GT13E	147.400	13.8	1116	0.497	0.712	n.a.	0.097	1.06	1.16
General Electric									
LM500	4.064	14.3	1116	0.418	0.125	3.52	0.085	n.a.	n.a.
LM1600	13.420	22.2	1210	0.469	0.182	3.18	0.075	n.a.	n.a.
LM2500	22.000	18.7	1212	0.411	0.229	3.70	0.055	n.a.	n.a.
LM5000	34.270	25.3	1174	0.520	0.265	3.16	0.065	n.a.	n.a.
Nuovo Pignone									
MS1002	4.773	8.3	943	0.413	0.209	3.36	0.081	0.50	n.a.
PGT10	10.440	14.0	1063	0.487	0.202	3.59	0.058	0.53	n.a.
MS3002	10.890	7.1	943	0.429	0.324	3.45	0.081	0.64	n.a.
MS5001	27.960	10.2	957	0.385	0.431	3.25	0.068	0.79	n.a.
MS5002	26.100	8.2	927	0.429	0.466	3.34	0.080	0.64	n.a.
MS6001	39.770	11.5	1104	0.406	0.412	3.24	0.095	0.79	n.a.
MS9001	120.800	11.6	1104	0.412	0.711	3.18	0.095	0.77	n.a.
PGT25	22.000	18.0	1213	0.412	0.234	3.63	0.055	0.85	n.a.

Notes:
- ABB TIT are estimated from the values of 1085 (GT8), 1027 (GT11N) and 1070°C (GT13E) of the temperature corresponding to complete mixing of all the coolant flow.
- The first stage exit pressure necessary to evaluate $n_{s,1}$ and SP_1 has been calculated by assuming that: (i) all stages of single-shaft engines have the same expansion ratio; (ii) the HP turbine of multi-shaft engines has the same power of the HP compressor and all its stages have the same expansion ratio.
- Data are based on Company publications (GE) and on personal communications from R. Gusso (Nuovo Pignone, 1990), and H.K. Lüthi (ABB, 1990).

Table A.1 Geometric characteristics of the first stage of commercial gas turbines. Although power output and cycle parameters vary in a very wide range, $n_{s,1}$, $D_{s,1}$, $(H/D_m)_0$, $(H/c)_0$ and σ_0 fall within a rather small interval.

reveals that large machines tend to have higher $(H/D_m)_0$, while according to Fig. 4.6 the optimum H/D_m of HP stages with $SP \geq 0.2$ should be approximately constant and equal to $\simeq 0.07$.

Since attempting to reproduce the geometry of actual machines would be extremely difficult, assuming that $D_{s,0}$, $(H/D_m)_0$, c_a/D_m and σ are constant and half-way the range encountered in practice appears the only reasonable option. Notice that while hypotheses 1) and 2) above

	Allis. 501-KA	Allis. 571-KA	Sulzr 3	Sulzr 10	GE LM2500	GE LM5000	ABB GT11N	NuovoP. 9000
W_{sh} (MW):	3.95	5.92	6.50	22.6	22.0	34.3	83.	120.8
SP (m):								
stage 1:	.166	.144	.217	.278	.223	.253	.574	.686
stage 2:	.206	.203	.311	.387	.335	.358	.732	1.028
H/D_m (%):								
stator 1	6.4	6.7	7.2	7.7	6.8	6.4	9.5	8.4
rotor 1	7.6	7.6	9.4	9.1	8.1	6.9	9.5	10.7
stator 2	9.4	9.3	11.5	12.1	11.5	10.9	13.3	14.8
rotor 2	11.8	11.9	13.5	14.0	12.9	11.9	14.9	16.5
c_a/D_m (%):								
stator 1	4.9	5.3	8.4	6.6	5.8	6.9	6.7	5.3
rotor 1	3.6	4.6	7.1	5.1	3.8	5.5	4.5	4.9
stator 2	4.8	5.3	8.0	6.6	5.8	5.9	5.6	6.1
rotor 2	4.2	5.3	6.2	5.9	4.0	4.5	4.0	4.8

Table A.2 Geometrical characteristics of selected commercial gas turbines. Data are taken from cross-sections portrayed in Company publications. For all the turbines in the table, the variations of D_m in the first two stages are within 4%.

imply that the first stages of all machines are similar, 3) and 4) imply that the subsequent stages are not similar to the first one. The premise 3) of constant axial velocity has been suggested by Scheper (1989) and differs from the one of constant axial Mach number adopted for the GATE program (Cohn, 1983). The assumption of constant U_g gives, at the end of the cooled expansion, H/D_m between 0.15 and 0.25; since these values are slightly larger than those encountered in practice, a better schematization should assume increasing U_g along the expansion, rather than – as in GATE – U_g decreasing with the speed of sound.

A.1 Values assumed for the geometrical parameters

The values assumed for $D_{s,0}$ and the other geometrical parameters are based on empirical data for existing turbines (Tabs. A1 and A2):

- $D_{s,0}$=3.25. Based on data in Tab. A1, this value is about 15% lower than the optimum shown in Fig. 4.6. According to the Cordier diagram of Fig. 2.4, the optimum spefic speed corresponding to D_s=3.25 is about 0.9, which is substantially higher than the values of $n_{s,1}$ listed in Tab. A1. The mismatch between D_s and n_s can be explained by considering that in a multi-stage engine the first stage inevitably runs at n_s lower than optimum.

- $(H/D_m)_0$=0.08. Similarly to D_s, this value is about the median of the values in Tab. A1 and A2. The optimization discussed in Par. 4.5.2 predicts $H/D_m \simeq 0.07$ (Fig. 4.6).

- c_a/D_m=0.06 for first nozzles and 0.045 in the section downstream. As confirmed in Tab. A2, the chord of first nozzles is generally larger than for the other cascades. The values in Fig. 4.7 predicted by the code of Lozza, Macchi and Perdichizzi (1982) are substantially lower, and would be much lower without the constraint on the minimum c_a/D_m (see Tab. 4.1). The greater chords adopted in actual machines are probably due to economic and mechanical considerations: greater chords reduce the number of blades, while increasing their resistance to bending stresses.

- σ=1.25, an average between typical σ=1 for stators and σ=1.5 for rotors. In stators, low σ and low H/c imply fewer blades, thus reducing total surface and coolant flow requirements – as well as cost. Since the effects of cooling are not included into the optimization described in Par. 4.5.2, results in Fig. 4.7 show no tendency toward lower stator solidities.

- Stagger angle γ=65° for first nozzles and 55° downstream. As shown in Fig. A.1 the stagger angle is measured from the axial direction.

- t_b/c=0.125, Φ=2.6, values typical of high- and medium-pressure stages.

The sensitivity to these assumptions has already been discussed in Par. 7.4, showing that except for σ the impact on predicted performances is small.

A.2 Flow cross-sectional area

The gas cross-sectional area at a generic point is (see Fig. A.1):

$$A_g = (\pi \cdot D_m - z \cdot t_b) \cdot H = \pi \cdot (1 - \sigma \cdot t_b/c) \cdot H \cdot D_m = \pi \cdot \psi_g \cdot H \cdot D_m \qquad (A.1)$$

where $\psi_g=(1-\sigma\cdot t_b/c)$ accounts for the reduction of A_g due to the blade thickness. According to assumptions 3) of the previous paragraph the cross-sectional area of the first nozzle is constant, so:

$$A_{g,0} = A_{g,1n} = \pi\cdot\psi_g\cdot(H/D_m)_0\cdot D^2_{m,0} = \pi\cdot\psi_g\cdot(H/D_m)_0\cdot D^2_{s,0}\cdot SP^2_1 \qquad (A.2)$$

The variation of A_g after the first nozzle is found from continuity ($m_g=\rho_g\cdot U_g\cdot A_g$) which, after assuming constant U_g gives:

$$(A_{g,2}/A_{g,1n}) = (m_{g,2}/m_{g,1n})\cdot(W_{g,1n}/W_{g,2})\cdot(P_{1n}/P_2)\cdot(T_2/T_{1n}) \qquad (A.3)$$

A.3 Diameter and blade height

The variation of D_m and H/D_m depends on the type of meridian section.

Constant D_m. In this case H/D_m can be immediately derived from Eq.(A.1):

$$H/D_m = A_g/(\pi\cdot\psi_g\cdot D^2_m) \qquad (A.4)$$

Constant D_h. The first nozzle hub diameter is:

$$D_{h,0} = D_{m,0}\cdot[1-(H/D_m)_0] \qquad (A.5)$$

If such diameter is constant:

$$D_m = D_{h,0}\cdot(1+y)/2 \qquad (A.6)$$

$$H/D_m = (y-1)/(y+1) \qquad (A.7)$$

where y is:

$$y = [1+4\cdot A_g/(\pi\cdot\psi_g\cdot D^2_{h,0})]^{0.5} \qquad (A.8)$$

Constant D_t. The first nozzle tip diameter is:

$$D_{t,0} = D_{m,0}\cdot[1+(H/D_m)_0] \qquad (A.9)$$

If such diameter is constant:

$$D_m = D_{t,0}\cdot(1-y)/2 \qquad (A.10)$$

$$H/D_m = (1+y)/(1-y) \tag{A.11}$$

where y is:

$$y = \left[1-4\cdot A_g/(\pi\cdot\psi_g\cdot D_{t,0}^2)\right]^{0.5} \tag{A.12}$$

Obviously, in this case it must be $A_g < \pi\cdot\psi_g\cdot D_{t,0}^2$. Once the type of meridian section has been specified, the expressions above allow determining A_g and H/D_m as a function of m_g, W_g, P and T. Notice that there is no need to specify the stage number or whether the cascade is a stator or a rotor. Once H/D_m is known, the ratio H/c can simply be found from:

$$H/c = \left[\cos\gamma/(c_a/D_m)\right]\cdot(H/D_m) \tag{A.13}$$

A.4 Ratio a_t

For the cascade depicted in Fig. A.1, the surface wet by the gas is:

$$z\cdot\Phi\cdot c\cdot H + 2\cdot\pi\cdot\psi_a\cdot c_a\cdot D_m$$

where the first and second term are the surface of the blades and the shrouds, respectively. Φ is the ratio between the blade perimeter and the blade chord; ψ_a accounts for the area of the blade cross-section and is defined by[a]:

$$\psi_a = 1 - (z\cdot t_b\cdot c)/(\pi\cdot c_a\cdot D_m) = 1 - \sigma\cdot t_b/c_a \tag{A.14}$$

Recalling that $z\cdot c = \pi\cdot\sigma\cdot D_m$, the ratio between the total wet area and the blade surface is:

[a] It is assumed that t does not change from hub to tip. If t did change, the same expressions would still hold after redefining t as the weighted average along the blade.

$$a_t = 1 + 2\cdot\psi_a\cdot(c_a/D_m)/[\Phi\cdot\sigma\cdot(H/D_m)] \qquad \text{(A.15)}$$

Substituting the expressions previously found for H/D_m into (A.15) allows determining a_t as a function of m_g, W_g, P and T.

REFERENCES

Cohn A., Project Manager (1983), "Gas Turbine Evaluation (GATE) Computer Program", EPRI Report AP-2871-CCM, Palo Alto, CA.

Csanady G.T. (1964), Theory of Turbomachines, McGraw-Hill, New York.

Gusso R. (1990), Divisione Produzione Macchine, Nuovo Pignone, Firenze, Italy, Personal Communication.

Lozza G., Macchi E. and Perdichizzi A. (1982), "On the Influence of the Number of Stages on the Efficiency of Axial-Flow Turbines", ASME Paper 82-GT-43.

Lüthi H.K. (1989), New Products and Business Development, Power Generation Division, ABB, Baden, Switzerland, Personal Communication.

Scheper G. (1989), Gas Turbine Aerothermo Division, General Electric, Schenectady, New York, Personal Communication.

NOMENCLATURE

a_t	Ratio between blades+shrouds surface and blade surface	
A	Cross-sectional area	[m^2]
c	Blade chord	[m]
c_a	Blade axial chord	[m]
D	Diameter	[m]
D_m	Mean diameter	[m]
D_s	Specific diameter	
H	Blade height	[m]
m	Mass flow rate, referred to compressor inlet flow	[kg/kg_a]
n_s	Specific speed	
P	Pressure	[Pa]
s	Blade spacing	[m]
SP	Turbomachinery size parameter	
t_b	Average blade thickness, (blade cross-section)/c	[m]
T	Temperature	[K]
U	Average axial velocity, $m/(\rho \cdot A)$	[m/s]
$\dot{W}_{sh}$	Shaft power	[W]
$\mathcal{W}$	Molecular weight	[kg/kmol]
z	Number of blades	

Greek

β	Pressure ratio	
γ	Stagger angle	
Φ	Ratio between blade perimeter and blade chord	
Δh_{is}	Isoentropic enthalpy drop	[J/kg]
σ	Solidity, c/s	
ψ_a	Axial cross-section coefficient $1-\sigma \cdot t/c_a$ (Eq. A.1)	
ψ_g	Gas cross-section coefficient $1-\sigma \cdot t/c$ (Eq. A.1)	
ω	Rotational speed	[rad/s]

Subscripts

a	Air
b	Blade
g	Gas
h	Hub (blade root)
0	Turbine inlet (i.e. first nozzle inlet)
1	First stage exit
1n	First nozzle exit
2	Station downstream the first nozzle

FIGURES

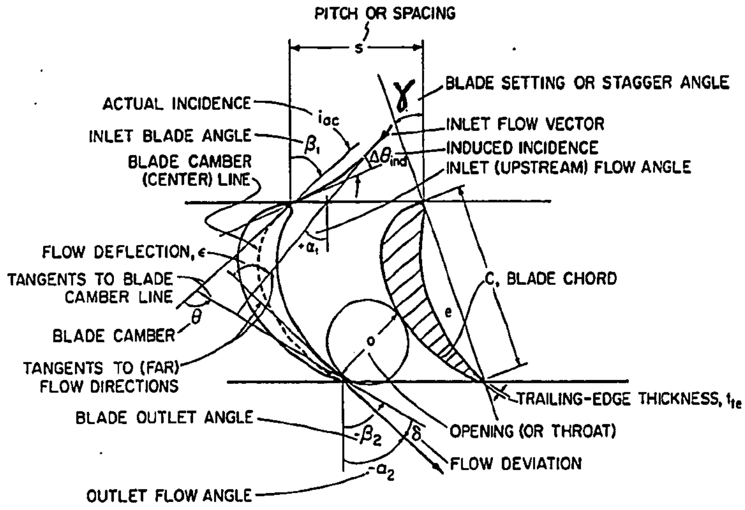

A.1 Schematic of cascade geometry.

APPENDIX B: CALCULATION OF FLUID THERMODYNAMIC PROPERTIES

Thermodynamic prorperties of working fluids (h, s, c_p, γ) are calculated by two sets of FORTRAN subroutines:

- Subroutines CNSJ (Consonni, 1987), based on a program for the calculation of chemical equilibria of multi-phase mixtures (STANJAN) developed by Reynolds (1986) at Stanford University. These subroutines are used whenever H_2O is not the only component of the working fluid.
- A set of subroutines reproducing the S.I. Steam Tables as in Schmidt (1982) developed at Politecnico di Milano. These subroutines are used whenever H_2O is the only component of the working fluid.

The reference point for the enthalpy and entropy of steam has been adjusted in order to be coherent with the one used in CNSJ, i.e. the one adopted in the JANAF Tables (Stull and Prophet, 1971): at 25°C h=enthalpy of formation (zero for pure substances), while $s \to 0$ for $T \to 0$. The set of equations covering each zone of the steam P,v diagram is listed in Schmidt (1982) and will not be repeated here; although substantially more complex, these equations give better accuracy and robustness than an alternative set proposed by Irvine and Liley (1984), which was used in an early work (Consonni, 1987) but later abandoned. It is also worth noting that an attempt to produce a unified calculation method by modifying CNSJ on the basis of the Principle of Corresponding States (Reynolds, 1987) gave for H_2O an unacceptably low accuracy.

As already discussed in Par. 8.3.3.3, some inconsistency arises when the two sets of calculation methods are interfaced. When part of a mixture, water vapour is always calculated as a perfect gas, while when it is the only component real gas effects are taken into account. This inconsistency is irrelevant for cycle performance prediction, but must be taken into account to close properly the entropy analysis (see Fig. 8.5).

In both sets of subroutines T, P, v, h, u, s, c_p and γ can be found after specifying any of the following pairs as inputs:

- T, P
- T, v
- T, s
- P, v
- P, h
- P, s
- v, u
- v, h
- v, s
- h, s

Since h always includes the heat of formation, for combustion calculations the concept of Fuel Heating Value is unnecessary; LHV and HHV are introduced only to define the cycle efficiency.

B.1 CNSJ subroutines

The set of CNSJ routines calculates thermodynamic properties of mixtures (either reacting or with fixed composition) composed of any of the following 20 species:

CH_4	Methane	S(L)	Liquid Sulfur
CO	Carbon Monoxide	C(S)	Solid Carbon
CO_2	Carbon Dioxide	Ar	Argon
H_2	Hydrogen	H	Hydrogen Atom
H_2O	Gaseous Water	NO	Nitrogen Monoxide
H_2S	Hydrogen Sulfide	NO_2	Nitrogen Dioxide
N_2	Nitrogen	O	Oxygen Atom
O_2	Oxygen	SO_2	Sulfur Dioxide
C_2H_2	Acetylene	OH	Hydroxyl Radical
C_2H_4	Ethylene	$H_2O(L)$	Liquid Water

These 20 CNSJ species allow representing the equilibrium combustion products of most fuels encountered in practical applications: also other species may be present, but even at very high flame temperatures

their concentration is generally order of magnitudes less than the one of the species above and, most of all, they are irrelevant for cycle performance predictions. Except for peculiar cycle configurations (e.g. Consonni and Lloyd, unp.), the capability to calculate chemical equilibria is unecessary, and calculations can be performed with fixed composition. Combustion product composition is simply found by oxidizing all C atoms to CO_2 and all H atoms to H_2O. The standard molal composition of dry air is set to:

78.09% N_2, 20.95% O_2, 0.93% Ar, 0.03% CO_2.

The JANAF tables give h and s at 1 ata at the reference temperature of 298.15 K and every 100 K from 200 K to 6000 K. At intermediate temperatures h and s are determined by a four-point interpolation using 3rd order Lagrange polynomials. Unlike in STANJAN (Reynolds, 1986), such 3rd order interpolation was applied over the whole range 200-6000 K*.

B.2 Viscosity and Prandtl number

The next three paragraph describe the procedure followed to calculate the values of μ and k necessary to evaluate Pr and then cooling flows.

B.2.1 Species other than water

For these species we have referred to formulas given by Danner and Daubert (1983). Although all relationships below should be applied only at low pressures (typically up to 1 bar), we have extended their use to

* In the intervals 200-298.15 K and 298.15-300 K, STANJAN interpolates the JANAF data linearly. This produces discontinities of $\partial c_p/\partial T$ and $\partial \gamma/\partial T$ at T=298.15 K and T=300 K.

all GSC operating conditions based on two reasons: (i) except for N_2, the partial pressure of all gas components is about an order of magnitude smaller than the gas pressure, rarely larger than 10 bar; (ii) several verifications with data given in Weast (1988) and Vargaftik (1983) have revealed good accuracy over the whole field covered by GSC applications.

The viscosity of polar species, i.e. NO and CO, is caluclated from:

$$\mu = a^{*} \cdot T_r/[1+0.36 \cdot (T_r-1)]^{1/6} \tag{B.1}$$

where:

$$a^{*} = 1.6104 \cdot 10^{-10} \cdot W^{1/2} \cdot P_c^{2/3}/T_c^{1/6} \tag{B.2}$$

and symbols and units are:

μ - viscosity [Pa·s]
P_c - critical pressure [Pa]
T - temperature [K]
T_c - critcal temperature [K]
T_r - reduced temperature T/T_c
W - molecular weight [kg/kmol]

For non-polar molecules, i.e. Ar, CO_2, SO_2, CH_4, O_2, N_2, NO_2 we have used:

$$\mu \cdot \xi \cdot 10^8 = 46.10 \cdot T_r^{0.618} - 20.40 \cdot \exp(-0.449 \cdot T_r) + 19.40 \cdot \exp(-4.058 \cdot T_r) + 1 \tag{B.3}$$

where in addition to the symbols already defined above:

$$\xi = 2173.424 \cdot T_c^{1/6} \cdot W^{-1/2} \cdot P_c^{-2/3} \tag{B.4}$$

Eq.(B.3) does not apply to molecular hydrogen (H_2), for which we have used:

$$\mu \cdot \xi \cdot 10^8 = 47.65 \cdot T_r^{0.657} - 20.00 \cdot \exp(-0.858 \cdot T_r) + 19.40 \cdot \exp(-3.995 \cdot T_r) + \quad (B.5)$$

Once μ is known, the calculation of thermal conductivity depends on the geometrical structure of the molecule. For monoatomic gases (Ar):

$$k = 2.5 \cdot \mu \cdot c_v / W \qquad (B.6)$$

For linear molecules (CO, CO_2, H_2, NO, N_2, O_2):

$$k = (\mu/W) \cdot (1.30 \cdot c_v + 14644.00 - 2928.80/T_r) \qquad (B.7)$$

and for non-linear molecules (CH_4, H_2S, NO_2, SO_2):

$$k = (\mu/W) \cdot (1.15 \cdot c_v + 16903.36) \qquad (B.8)$$

where:

k = thermal conductivity [W/m-K]
c_v = constant volume molar specific heat [J/kmol-K]

B.2.2 Water

For water it was decided to use more specific correlations because the ones given by Danner and Daubert did not prove adequately accurate. For T<800°C μ is calculated from a correlation given by Yaws (1987), while k is determined by a parabolic regression of data taken from Haar, Gallagher and Kell (1984):

$$\mu = -31.89 \cdot 10^{7} + 41.45 \cdot 10^{-9} \cdot T - 8.272 \cdot 10^{13} \cdot T^2 \qquad (B.9)$$

$$k = -4.865485 \cdot 10^{-3} + 6.185329 \cdot 10^{5} \cdot T + 4.0035892 \cdot 10^{-8} \cdot T^2 \qquad (B.10)$$

where, as usual, T is in Kelvin, μ in Pa·s and k in W/m-K. For T>1000°C the viscosity given by Eq.(B.9) is corrected by the factor:

$(T/1273.15)^{5/6}$

while for T>800°C thermal conductivity is calculated from Eq.(B.8), which for H_2O becomes:

$$k = \mu\cdot(c_v+787.75) \qquad (B.11)$$

B.2.3 Mixtures

Once the viscosity and the thermal conductivity of each component have been calculated, the mixture μ and k are calculated according to a semi-empirical formulas reported by Bird, Stewart and Lightfoot (1960):

$$\mu_{mix} = \Sigma_i\left\{(x_i\cdot\mu_i)/[\Sigma_j(x_j\cdot\Phi_{ij})]\right\} \qquad (B.12)$$

$$k_{mix} = \Sigma_i\left\{(x_i\cdot k_i)/[\Sigma_j(x_j\cdot\Phi_{ij})]\right\} \qquad (B.13)$$

where μ_{mix} and k_{mix} are the viscosity the thermal conductivity of the mixture, x_i, μ_i and k_i the mol fraction, the viscosity and the thermal conductivity of the ith component and:

$$\Phi_{ij} = (1/8^{1/2})\cdot(1+W_i/W_j)^{-1/2}\cdot[1+(\mu_i/\mu_j)^{1/2}\cdot(1+W_j/W_i)^{1/4}]^2 \qquad (B.14)$$

REFERENCES

Consonni S. (1987), "A Computer Program to Calculate Working Fluid Thermodynamic Properties of Steam-Injected Gas Turbine Cycles", CEES/Princeton University Working Paper No. 87.

Consonni S. and Lloyd A. (unpublished), "Chemically Recuperated Gas Turbine Cycles", to be presented at forthcoming ASME meeting.

Danner R.P. and Daubert T.E. editors (1983), Manual for Predicting Chemical Process Design Data, American Institute of Chemical Engineers, New York.

Haar L., Gallagher J.S. and Kell G.S. (1984), Steam Tables, Thermodynamic and Transport Properties and Computer Programs for Vapor and Liquid States of Water in SI Units, Hemisphere Publishing, New York.

Irvine T.F. and Liley P.E. (1984), Steam and Gas Tables with Computer Equations, Academic Press, New York.

Reynolds W.C. (1986), "The Element Potential Method for Chemical Equilibrium Analysis: Implementation in the Interactive Program STANJAN - version 3", Dep. of Mechanical Engineering, Stanford University, Stanford, CA.

Reynolds W.C. (1987), Thermodynamic Properties in S.I., Dept. of Mech. Eng., Stanford University, Stanford, CA.

Schmidt E. (1982), Properties of Water and Steam in S.I. Units, Springer-Verlag, Berlin.

Stull D.R. and Prophet H. (1971), Project Directors, JANAF Thermochemical Tables, 2nd Edition, U.S. National Bureau of Standards, Washington D.C.

Vargaftik N.B. (1983), Handbook of Physical Properties of Liquids and Gases, Hemisphere Publishing, New York.

Weast R.C. editor-in-chief (1988), CRC Handbook of Chemistry and Physics, CRC Press, Boca Raton, Florida.

Yaws C.L. (1977), A Guide to the Physical, Thermodynamic and Transport Property Data of Industrially Important Chemical Compounds, McGraw-Hill, New York.

NOMENCLATURE

c_p	Constant-pressure specific heat	[J/kg-K]
c_v	Constant-volume molar specific heat	[J/kmol-K]
h	Enthalpy	[J/kg]
k	Thermal conductivity	[W/m-K]
P	Pressure	[Pa]
Pr	Prandtl number	
s	Entropy	[J/kg-K]
T	Temperature	[°C or K]
u	Internal energy	[J/kg]
v	Specific volume	[m^3/kg]
W	Molecular weight	[kg/kmol]
x	Mol fraction	
γ	Ratio c_p/c_v	
Φ	Coefficient appearing in Eq.(B.12) and (B.13)	
μ	Viscosity	[Pa·s]

APPENDIX C: PERFORMANCES OF COMMERCIAL GAS TURBINES

Tables C.1, C.2 and C.3 report the information regarding commercial gas turbines gathered thorugh the survey mentioned at Par. 7.1.1. Due to upgrades frequently introduced by manufacturers, for some engines the perfomances in the table could be already outdated. In the text and in figures, each turbine is identified by the numbers in the first left column of Tab. C.1; numbers are not progressive to maintain compatibility with previous, earlier results reported in [32]. Identical models produced by different manufacturers are differentiated by a latin letter added to the identification number (e.g. 3 and 3A). The asterisk "*" identifies axial machines commercialized after 1975 considered for the calibration of "current technology" engines; the solid dot "•" identifies the ones considered representative of the state-of-the-art (see Par. 7.1.6). The open dot "o" indicates engines which - although conforming to the criterion adopted to define "current technology" engines (all-axial, introduced after 1975) —have revealed performances clearly below expectations; for this reason, they are included into the diagrams reporting calibration results, but they have not been used for the error minimization procedure described at Par. 7.5.

The table covers the widest range of engine type and architecture: first and second generation heavy-duty and aero-derivative; all-axial, all-radial and axial/radial; single and multiple shaft; cooled and uncooled. The power output ranges from 23 kW to 215 MW, the pressure ratio from 3.8 to 30.0, the TIT from 773°C to 1260°C. For electric generation versions (type "E") power, efficiency and specific work refer to the generator terminals, i.e. they include gear and generator losses; for mechanical drive versions (type "M") power, efficiency and specific work refer to the power turbine shaft and do not include transmission and generator losses.

Despite all the efforts bestowed into the collection of the data in the tables, there remain several uncertainties and inconsistences. The ones related to the overall heat balance are discussed in Par. 7.1.3; others can be noted simply by performing some comparison:

- Turbine 3 (Allison 571KA) and 3A (Centrax CX571) should be identical; yet, power outputs differ by ≈0.25% and – much more important – TOT by 15°C. Since the accuracy of the TOT predicted by our model is of the order of 10°C (see Par. 7.5), this discrepancy is clearly troublesome.

- Different sources may quote performances significantly different for the same model of the same manufacturer. The table reports for example two quotes for the GE LM1600 (34 and 34A) and the Mitsubishi 501F (79 and 79A); to avoid confusion, many others have been left out.

- In some case differences between 50Hz and 60Hz models are in the direction opposite to the one expected. Take for example the GE7001F and 9001F (31 and 75): since the thermodynamic cycle and the architecture are identical (same TIT, β, TOT, n_c, n_t, n_{CN}, n_{CR}), we would expect a slightly higher efficiency for the larger model, which benefits from smaller scale effects (see Par. 4.4.1); yet, the larger 50Hz model is quoted with a lower efficiency! This situation may be due to the particularly cautious commercial policy adopted by GE, which prefers to give conservative estimates before completaion of all tests on the 50Hz model (# 75).

Since ABB and KWU did not provide the actual TIT, the values in Tab. C.1 have been calculated by matching the given "fully mixed" temperature obtained after mixing the combustor outlet flow with the whole coolant flow; it follows that for these turbine the definition of the thermodynamic cycle is subject to some uncertainty.

Regarding Tab. C.2, it must be emphasized that the reliability of compressor outlet temperatures is questionable because the sources did not specify whether the given temperature: (i) is static or total; (ii) refers to the compressor diffuser inlet or outlet.

In summary, the "quality" of the data in the tables is rather unsatisfactory. On the other hand, the purpose of this Thesis is to produce predictions of GSCs performances which will be compared with data of the same quality (manufacturers' estimates, predictions of other authors).

#	Ref.	Name	Year 19..	Type	CT	TT	n_c	n_t	n_{CN}	n_{CR}	n_{sh}	RPM[1]	$\dot{W}_{sh}$ MW	$\dot{W}_{el}$ MW	β	TIT °C	TOT °C	η_{sh}	η_{el}	M_{air} kg/s	w_{sh} kJ/kg	η_g/η_{gg}[2]
Allison																						
* 1	4,5	501KB5	82	E	A	A	14	4	1	1	1	14250	3.927	3.740	9.3	1035	538	.301	.287	15.6	251.7	.952
1A	3,30	501KH	86	E	A	A	14	4	1	1	1	13820	3.465*	3.318	15.1	982	528	.301*	.287	15.1	230.8*	.952*
0 2	4,5	570KA	79	E	A	A	13	4	2	2	2	11437	4.804	4.576	12.1	1135	567	.296	.282	18.8	255.5	.952
3	4,5	571KA	86	E	A	A	13	5	2	2	2	11437	5.910	5.636	12.7	1156	539	.339	.323	19.8	298.5	.952
Allison/Centrax																						
• 3A	3	CX571	87	E	A	A	13	5	2	2	2	11437	5.886	5.620	12.7	1156	554	.339	.323	19.5	302.3	.952
ABB (former Asea-Stal)																						
* 4	1,11	Mars	77	M	A	A	15	2+2	2	1	2	9400	9.396	8.840	16.0	1057	465	.330	.311	36.3	259.0	.941
5	1,11	GT-35	68	M	A	A	10+8	1+2+3	None	None	3	3600	16.68	16.30	12.0	835	363	.330	.323	91.6	182.1	.980
ABB (former Brown Bovery)																						
0 6	10	GT8	84	E/M	A	A	12	3	n.a.	n.a.	1	6339	47.80	46.00	16.3	1145[3]	523	.324	.312	177	270.1	.952
7	10	GT11	71	E/M	A	A	17	5	n.a.	n.a.	1	3600	73.90	71.90	11.0	1022[3]	520	.320	.311	282	262.1	.973
* 8	10	GT11N	87	E/M	A	A	18	5	n.a.	n.a.	1	3600	83.30	81.60	12.4	1065[3]	515	.330	.323	310	268.7	.980
9	10	GT13	70	E/M	A	A	18	5	n.a.	n.a.	1	3000	100.0	97.70	12.5	1005[3]	490	.326	.319	399	250.6	.977
*10	10	GT13E	83	E/M	A	A	21	5	n.a.	n.a.	1	3000	147.4	145.3	13.8	1137[3]	516	.349	.344	492	299.6	.986
Cooper-Rolls (COBERRA)																						
11	1	2348	64	M	A	A	17	3+2	n.a.	n.a.	2	5200	13.01	-	8.9	818	404	.284	-	78.1	166.7	-
12	1	2648	71	M	A	A	17	3+2	n.a.	n.a.	2	5500	15.06	-	9.2	872	435	.299	-	77.0	195.6	-
13	1	2656	74	M	A	A	17	3+2	n.a.	n.a.	2	4950	15.55	-	9.2	872	430	.304	-	77.0	202.0	-
*14	1	3145	75	M	A	A	5+11	2+2+2	n.a.	n.a.	3	6350	12.55	-	19.0	988	404	.344	-	56.3	223.0	-
015	1	6456	83	M	A	A	7+6	1+1+2	n.a.	n.a.	3	4950	24.79	-	20.0	1162	475	.356	-	88.6	279.7	-
*16	1	6462	84	M	A	A	7+6	1+1+2	n.a.	n.a.	3	4800	26.10	-	20.0	1164	465	.373	-	88.6	294.6	-
Fiat Aviazione																						
17	12	TG16	68	E	A	A	15	5	None	None	1	4850	18.95	18.20	7.0	778	409	.270	.259	117.	161.3	.960
18	12	TG20(a)	71	E	A	A	18	3	2	1	1	4920	39.41	37.85	11.0	1044	520	.307	.294	159.	247.6	.960
*19	12	TG20(b)	84	E	A	A	19	3	2	2	1	5400	44.29	42.54	14.0	1085	502	.335	.322	157.	281.9	.960
20	12	TG50(c)	n.a.	E	A	A	20	4	2	2	1	3000	94.49	92.60	11.8	1065	510	.314	.308	386.	244.5	.980
21	12	TG50(d)	75	E	A	A	20	4	2	2	1	3000	105.1	103.0	12.5	1096	535	.317	.310	386.	272.5	.980
*22	12	TG50D5	85	E	A	A	19	4	2	2	1	3000	131.0	128.3	14.0	1085	495	.345	.339	445.	294.5	.980
Garrett																						
23	1,13	IM831-800	80	E/M	R	A	2	3	n.a.	None	1	41730	.5481	.5145	11.0	963	499	.217	.204	3.52	155.7	.939
General Electric																						
24	17	MS3002J	52	M	A	A	15	2	1	None	1	6500	10.89	-	7.1	943	526	.267	-	51.4	211.9	-
25	17	MS5001R	58	M	A	A	16	2	1	None	1	4860	18.64	-	7.5	957	524	.264	-	80.2	206.7	-
26	17	MS5001PA	58	E	A	A	17	2	1	None	1	5100	27.33	26.30*	10.2	957	483	.300*	.289	120.	227.9*	.962*
27	17	MS5002A	72	M	A	A	15	2	1	None	2	4670	19.57	-	6.7	921	520	.260	-	96.0	203.9	-
28	17	MS5002B	72	M	A	A	16	2	1	None	2	4670	26.10	-	8.6	927	491	.288	-	120.	217.9	-
29	17	MS6001B	78	E	A	A	17	3	2	2	1	5100	38.78	37.40*	11.7	1104	543	.326*	.314	134.	288.9*	.964*
*30	3	MS7001EA	76	E	A	A	17	3	2	2	1	3600	84.77	83.50*	12.4	1104	530	.331*	.326	291.	291.6*	.983*
•31	3	MS7001F	89	E	A	A	18	3	3	2	1	3600	152.2*	150.0	13.5	1260	583	.351*	.346	416.	365.7*	.985*
32	17	MS9001E	76	E	A	A	17	3	2	2	1	3000	118.8	116.9*	12.1	1104	529	.336*	.331	403.	294.9*	.984*
•75	17	MS9001F	92	E	A	A	18	3	3	2	1	3000	215.4*	212.3	13.5	1260	583	.347*	.342	600.	359.0*	.985*
*33	9	LM500	80	E/M	A	A	14	6	1	2	2	7000	4.064	n.a.	14.3	1116	513	.316	n.a.	15.9	256.0	-
•34	3,29	LM1600	88	E/M	A	A	3+7	1+1+2	2	2	3	7000	13.99	n.a.	22.0	1210	482	.372	n.a.	44.9	311.6	-
34A	9	LM1600	88	E/M	A	A	3+7	1+1+2	n.a.	n.a.	3	n.a.	13.42	n.a.	22.2	1210	478	.369	n.a.	45.3	296.0	-
*35	9	LM2500	79	E/M	A	A	16	2+6	2	2	2	3600	22.00	21.56	18.7	1212	513	.370	.363	66.7	330.0	.980
*36	9	LM5000	86	E/M	A	A	5+14	2+1+3	3	2	3	3600	34.27	33.58	25.3	1174	446	.373	.365	123.	278.8	.980
•76	3,23	LM6000	92	E	A	A	5+14	2+5	3	2	2	3600	42.99	41.50	29.8	1240	448	.412	.398	126.	342.2	.965
Hispano-Suiza																						
37	22	THM1304	83	E/M	A/R	A	10+1	2+2	1	1	2	8000	9.250	8.702	9.9	975	500	.280	.263	44.0	210.2	.941
38	22	THM1203	71	E/M	A/R	A	9+1	2+2	None	None	2	7800	5.600	5.268	7.6	905	498	.240	.226	34.1	164.2	.941
Hitachi																						
074	27	H25	89	E	A	A	17	3	3	2	1	7280	24.44	23.50	14.7	1260[4]	530	.336	.323	88.0	277.7	.961
Kawasaki																						
39	4	S5A-01	82	E/M	R	R	1	1	None	None	1	96000	0.025	n.a.	3.8	830	590	.133	n.a.	.222	112.6	-
40	4	S3A-01	82	E/M	R	n.a.	n.a.	n.a.	None	None	1	n.a.	.0924	n.a.	5.8	960	585	.157	n.a.	.800	115.5	-
41	4	S1A-02	78	E/M	R	A	2	2	None	None	1	53000	.2228	n.a.	9.0	910	520	.177	n.a.	1.73	128.5	-
42	4	S2A-01	79	E/M	R	A	2	3	None	None	1	31500	.7158	n.a.	9.0	940	500	.223	n.a.	4.70	152.2	-
43	4	M1A-01	78	E/M	R	A	2	3	None	None	1	22000	1.204	n.a.	8.0	920	515	.211	n.a.	7.78	154.7	-
44	4	M1A-03	82	E/M	R	A	2	3	1	1	1	22000	1.502	n.a.	9.2	980	545	.220	n.a.	9.04	166.2	-
Kongsberg																						
45	8	KG3-11	85	E/M	R	R	1	1	1	None	1	35115	1.654	n.a.	9.0	1050[5]	581	.290	n.a.	6.44	256.8	-
46	8	KG3-13	n.a.	E/M	R	R	1	1	n.a.	n.a.	1	35115	2.310	n.a.	9.0	1230[5]	718	.306	n.a.	6.44	358.7	-
KWU-Siemens																						
47	21	V84.2	85	E	A	A	17	4	3	2	1	3600	104.9	103.2	10.7	n.a.	540	.339	.334	349.	300.7	.984
*48	6,21	V94.2	74	E	A	A	16	4	2	2	1	3000	152.6	150.2	10.7	1100	545	.340	.335	500.	305.3	.984
•77	3,28	V64.3	90	E	A	A	17	4	4	3	1	3000	62.59*	60.50	15.6	1221[6]	534	.364*	.352	184.	340.7	.967*
•78	3,28	V94.3	92	E	A	A	17	4	4	3	1	3000	203.1*	200.0	15.6	1201[6]	534	.364*	.358	594.	341.7	.985*

Tab. C.1 Characteristics of commercial gas turbines (cont.)

#	Ref.	Name	Year 19..	Type	CT	TT	n_c	n_t	n_{CN}	n_{CR}	n_{sh}	RPM[1]	$\dot{W}_{sh}$ MW	$\dot{W}_{el}$ MW	β	TIT °C	TOT °C	η_{sh}	η_{el}	M_{air} kg/s	w_{sh} kJ/kg	η_g/η_{gg}[2]
Mitsubishi																						
*49	3,7	MF-111	85	E/M	A	A	15	3	2	2	1	9651	13.27*	12.61	13.0	1160	547	.318*	.303	47.6	278.7	.950*
•79	3	501F	90	E	A	A	16	4	3	3	1	3600	155.1*	152.8	14.0	1260	578	.357*	.352	428.	362.7	.985*
79A	26	501F	90	E	A	A	16	4	3	3	1	3600	147.2*	145.0	14.2	1260	572	.346*	.341	414.	356.0	.985*
Mitsui																						
67	2	SB5	87	E								26600	1.130	n.a.	9.1	1000	522	.271	n.a.	4.98	226.9	n.a.
68	2	SB15	86	E								13070	2.880	n.a.	11.5	1000	492	.286	n.a.	13.6	212.5	n.a.
69	2	SB30	73	E								9410	6.150	n.a.	11.5	1000	487	.304	n.a.	28.1	218.9	n.a.
70	2	SB60	81	E								5680	15.80	n.a.	12.4	1100	527	.312	n.a.	59.4	267.0	n.a.
71	2	SB90	68	E								5475	16.81	n.a.	6.8	927	514	.266	n.a.	85.7	196.1	n.a.
72	2	SB120	85	E								5070	24.17	n.a.	12.4	1000	483	.311	n.a.	104.	231.7	n.a.
Nuovo Pignone																						
50	19	MS1002	72	M	A	A	16	2	1	None	2	10290	4.773	4.520	8.3	943	525	.260	.246	24.0	199.2	.948
*51	19	PGT10	86	M	A	A	17	4	2	2	2	7800	10.44	9.920	14.0	1063	462	.339	.322	41.3	253.0	.951
24A	19	MS3002	52	M	A	A	15	2	1	None	2	6500	10.89	10.45	7.1	943	527	.267	.256	52.3	208.2	.958
26A	19	MS5001	58	E	A	A	16	2	1	None	1	5100	27.96	26.80	10.2	957	481	.305	.292	125.	224.2	.958
28A	19	MS5002	72	M	A	A	n.a.	n.a.	n.a.	n.a.	2	4670	26.10	-	8.2	927	490	.288	-	122.	214.5	-
*29A	19	MS6001	78	E	A	A	17	3	2	2	1	5100	39.77	38.12	11.5	1104	541	.330	.317	136.	291.6	.958
*32A	19	MS9001	76	E	A	A	17	3	2	2	1	3000	120.8	118.6	11.6	1104	528	.336	.330	411.	293.7	.982
35A	19	LM2500	79	M	A	A	16	8	2	2	2	3600	22.00	21.56	18.0	1213	513	.369	.360	66.9	328.8	.975
35B	19	PGT25	81	M	A	A	16	4	2	2	2	6500	22.00	21.10	18.0	1213	513	.370	.355	66.9	328.8	.958
Ruston																						
52	18	TA1750	69	M	A	A	13	2+2	None	None	2	6600	1.398	1.322	4.3	825	510	.183	.173	11.3	123.7	.946
80	2	RH	88	E	R	A	2	2	1	None	1	27245	1.683	1.575	9.2	1134	611	.272	.255	6.98	241.1	.936
*81	3,24	Typhoon	89	E	A	A	10	2	1	1	1	16570	4.131	3.915	12.8	1053	500	.315	.298	16.8	246.2	.948
053	18	TB5000	77	M	A	A	12	2+2	1	None	2	7950	3.878	3.667	7.0	900	480	.265	.251	21.3	181.9	.946
*54	18	TORNADO	81	M	A	A	15	2+2	1	1	1/2	10000	6.338	5.993	12.1	1000	470	.312	.295	27.2	232.9	.946
Solar																						
55	20	Sat.1200	60	M	A	A	8	3	None	None	1	22124	0.895	0.800	6.2	773	448	.233	.216	6.21	144.1	.927
*56	20	Sat.1500	n.a.	E	A	A	8	3	n.a.	None	1	22124	1.161	1.080*	6.7	871	499	.248*	.231	6.40	181.3*	.930*
*57	20	Cent.4500	85	M	A	A	8	3	1	None	1	15500	3.274	3.087	9.6	904	451	.280	.264	17.0	192.0	.943
*58	20	Cent.H	85	M	A	A	11	3	1	1	1	16520	4.101	3.903	10.2	1010	516	.294	.280	17.5	233.7	.952
Sulzer																						
059	15	3	76	M	A	A	17	3	1	1	1	10600	6.280	-	9.5	970	478	.281	-	31.7	197.9	-
60	15	7	70	M	A	A	13	6	1	None	1	6400	11.00	-	7.6	925	493	.248	-	64.1	171.7	-
*61	15	10	81	M	A	A	10	2+2	2	2	2	7700	22.60	-	13.6	1145	517	.338	-	77.2	292.8	-
Thomassen																						
24B	14	PG3142J	49	E/M	A	A	15	1+1	1	None	2	6500	10.89	10.44	7.1	943	526	.267	.256	52.3	208.3	.958
25A	14	PG5261R	72	M	A	A	16	2	1	None	1	4860	18.65	-	7.5	938	524	.264	-	91.4	204.0	-
27A	14	M5262A	72	M	A	A	15	1+1	1	None	2	4670	19.60	-	6.7	921	520	.261	-	97.3	201.4	-
62	14	M5382C	72	M	A	A	16	1+1	1	None	2	4670	28.35	-	8.2	963	516	.292	-	123.	230.1	-
28B	14	M5352B	72	M	A	A	16	1+1	1	None	2	4670	26.10	-	8.6	927	491	.288	-	122.	214.6	-
26B	14	PG5371PA	81	E	A	A	17	2	1	None	1	5105	27.86	26.82*	10.2	957	480	.303*	.292	123.	227.3*	.962*
29B	14	PG6531B	81	E	A	A	17	3	2	2	1	5105	39.51	38.11*	11.7	1104	540	.329*	.317	136.	289.7*	.964*
32B	14	PG9161	79	E	A	A	17	3	2	2	1	3000	120.6	118.7*	12.1	1104	526	.339*	.333	405.	298.1*	.984*
Turbomeca																						
63	16	BastanVI	68	E/M	A/R	A	2	3	n.a.	n.a.	1	32750	0.610	n.a.	5.5	n.a.	480	.207	n.a.	4.46	136.8	-
64	16	BastanVII	72	E/M	A/R	A	3	3	n.a.	n.a.	1	32750	0.870	n.a.	7.2	n.a.	460	.232	n.a.	6.04	144.0	-
65	16	TurmoIII	n.a.	E/M	A/R	A	2	2+2	n.a.	n.a.	2	19850	0.710	n.a.	4.9	n.a.	510	.192	n.a.	5.41	131.2	-
66	16	TurmoXII	n.a.	E/M	A/R	A	3	2+2	n.a.	n.a.	2	19850	1.000	n.a.	8.2	n.a.	450	.232	n.a.	6.94	144.1	-
Turbo Power (Pratt & Whitney)																						
•73	3,25	FT8	89	M	A	A	8+7	1+2+4	2[7]	2[7]	2	5000	25.95	-	20.3	1160	443	.389	-	85.3	304.3	-

Tab. C.1 Characteristics of commercial gas turbines.

Notes
1) Speed of power turbine shaft. The rotational speed of HP and MP shafts used to construct Figs. 4.3 and 4.9 is reported in Tab. C.3.
2) If RPM=3000 or RPM=3600, the figure in the last column gives the generator efficiency η_g; otherwise it gives the gear+generator efficiency η_{gg}. The values in this columns are the ones used to construct Fig. 7.1.

(cont.)

(... cont. notes Tab. C.1))

3) Estimated from the values of 1085 (GT8), 1002 (GT11), 1027 (GT11N), 990 (GT13), 1070 (GT13E) given for the temperature ideally obtained after mixing the combustor outlet flow with the whole cooling flow.
4) As indicated in [27], this value is achieved by pre-cooling the air bled from the compressor before using it for turbine cooling. Since the relevant operating conditions are unknown, the turbine has not been considered for calibration.
5) Estimated from the combustor outlet temperatures of 1108 (KG3-11) and 1315 (KG3-13).
6) Estimated from the temperature of 1120°C obtained after complete gas-coolant mixing (same as ABB turbines).
7) Prario and Voss [25] quote one "air-cooled high turbine" stage, but do not mention whether other stages are cooled. If cooling is actually carried out until the gas temperature goes below 800-830°C, the assumption of 2 cooled stages gives reasonable values for stage enthalpy drops and allows for balancing the HP shaft.

#	Ref.	Name	COT, °C	β
1	30[1]	Allison KB5	315	9.3
33	9	GE LM500	410	14.3
34	29	GE LM1600	489	22
35	9	GE LM2500	448	18.7
36	9	GE LM5000	507	25.3
50	19	N.P. MS1002	285	8.3
51	19	N.P. PGT10	380	14
24A	19	N.P. MS3002	260	7.1
26A	19	N.P. MS5001	320	10.2
28A	19	N.P. MS5002	285	8.2
29A	19	N.P. MS6001	345	11.5
32A	19	N.P. MS9001	355	11.6
35A	19	N.P. PGT25	450	18
54	31	Ruston Tornado	360	12.1

Tab. C.2 Compressor outlet temperatures.

[1] The value given in [30] has been corrected to account for the different pressure ratio.

#	Name	RPM of HP shaft	RPM of MP shaft
2	Allison 570KA	14281	-
3A	Centrax 571CX	14879	-
4	ABB Mars	10780	-
5	ABB GT-35	6965	5550
11	Coberra 2348	7650	-
12	Coberra 2648	7560	-
13	Coberra 2656	7560	-
14	Coberra 3145	12250	7580
15	Coberra 6456	9245	6555
16	Coberra 6462	9255	6560
33	GE LM500	17000	-
34	GE LM1600	16000	12960
35	GE LM2500	9500	-
36	GE LM5000	10080	3571
76	GE LM6000	10100	-
37	Hisp.-S. THM1304	11900	-
38	Hisp.-S. THM1203	11700	-
50	N.P. MS1002	11140	-
51	N.P. PGT10	10800	-
24A	N.P. MS3002	7100	-
28A	N.P. MS5002	5100	-
54	Ruston Tornado	11085	-
59	Sulzer 3	10600	-
60	Sulzer 7	6400	-
61	Sulzer 10	9770	-
24B	Thomass. PG3142J	7107	-

Tab. C.3 HP shaft and MP shaft speed of revolution used to construct Figs. 4.3 and 4.9.

ACRONYMS AND SYMBOLS

Ref.	Indicates reference listed at the end of this Appendix C
E	Electric generation
M	Mechanical drive
CT, TT	Compressor and turbine type (A=axial, R=radial)
n_c, n_t	Number of compressor and turbine stages
n_{CN}	Number of cooled nozzles
n_{CR}	Number of cooled rotors
n_{sh}	Number of shafts
RPM	Speed of revolution (rounds per minute)
$\dot{W}_{sh}$	Shaft power
$\dot{W}_{el}$	Electric power
β	Compression ratio
TIT	Turbine inlet temperature
TOT	Turbine outlet temperature
η_{sh}	Shaft efficiency
η_{el}	Efficiency at generator terminals
M_{air}	Air flow rate at the compressor inlet
w_{sh}	Specific work
η_g	Generator efficiency
η_{gg}	Gear+generator efficiency
COT	Compressor outlet temperature

Asterisk in column 1 of Tab. C.1 indicates engines considered representative of "current" technology; dot "•" indicates the ones considered representative of the state-of-the-art (see Par. 7.1.6).

An asterisk in W_{sh}, η_{sh}, w_{sh} and η_g/η_{gg} columns of Tab. C.1 indicates data obtained by the correlations for gear and generator efficiency shown in Fig. 7.1.

REFERENCES

1. Gas Turbine World 1987 Handbook, Vol.10, Pequot Publishing, Southport, Connecticut, 1987.
2. Gas Turbine World 1989 Handbook, Vol.12, Pequot Publishing, Southport, Connecticut, 1989.
3. Gas Turbine World 1990 Handbook, Vol.13, Pequot Publishing, Southport, Connecticut, Feb. 1990.
4. Pinoli M., Ergen S.p.A. (Lomagna, Como, Italy), Personal Communication, Apr. 1988.
5. Donolo J., Allison Gas Turbine Division (Gennevilliers Cedex, France), Personal Communication, Apr. 1988.
6. Maghon H. et al., "Development and application of highly efficient heavy-duty gas turbines in Europe", Proc. *1987 Tokio Int. Gas Turbine Congress*, Vol. I, pp. 19-26.
7. Akita E. et al., "Development and testing of the 13MW Class Heavy Duty Gas Turbine MF-111", ASME Paper 87-GT-37.
8. Mowill R.J. et al., "New Radial Engine Technology from Kongsberg", ASME Paper 83-GT-221.
9. Payzer R., General Electric Aircraft Engines (Evendale, Ohio), Personal Communication, Mar. 1988.
10. Kehlhofer R., Brown Bovery & C. (Baden, Switzerland), Personal Communication, Nov. 1987.
11. Svensson B., Asea-Stal Co. (Finspong, Sweden), Personal Communication, Nov. 1987.
12. Merola A., Fiat TTG (Torino, Italy), Personal Communication, Dec. 1987.
13. Rule J.G., Garrett Turbine Engine Company (Phoeniz, Arizona), Personal Communication, Nov. 1987.
14. Visser M.C.L., Thomassen International (Rheden, The Netherlands), Personal Communication, Nov. 1987.
15. Ryrie J., Sulzer-Escher Wyss (Winterthur, Switzerland), Personal Communication, Dec. 1987.
16. Turbines for petroleum industry applications, Turbomeca Company publication, Nov. 1984.
17. Brandt D.E., General Electric Co. (Schenectady, New York), Personal Communication, Nov. 1987.
18. Grocock J., Ruston Turbines (Lincoln, England), Personal Communication, Nov. 1987.
19. Gusso R., Nuovo Pignone (Firenze, Italy), Personal Communication, Dec. 1987.
20. Jones M.D., Solar Turbines, Personal Communication, Nov. 1987.
21. Joyce J.S., Siemens/KWU (Erlangen, West Germany), Personal Communication, Dec. 1987.
22. Knudsen H., Hispano-Suiza (Bois-Colombes, France), Personal Communication, Nov. 1987.
23. Oganowski G., "GE LM6000 Development of the first 40% Thermal Efficiency Gas Turbine", presented at the 1990 ASME Gas Turbine Congress and Exhibition (Brussels), GE Marine & Industrial Engine & Service Division (Evendale, Ohio), Jun. 1990.
24. King R., Ruston Turbines (Houston, Texas), Personal Communication, Mar. 1990.
25. Prario A. and Voss H., "FT8A, A New High Performance 25 MW Mechanical Drive Aero Derivative Gas Turbine", ASME PAper 90-GT-287.

26. Entenmann D.T., Fukue I., North W.E. and Muyama A. "Shop Test of the 501F, a 150 MW Combustion Turbine", ASME Paper 90-GT-362.
27. Urushidani H., Sasada T., Wada M. and Kawaike K., "Development of a New 25 MW High Efficiency Heavy Duty Gas Turbine", ASME Paper 90-GT-72.
28. Maffei E. et al., "Le turbine a gas Ansaldo/Siemens per repowering e topping" (in Italian), Proc. Meeting on *Repowering of power generation plants*", organized by the Italian Thermotechnical Association, Milan, Italy, March. 15th, 1991.
29. Gelfand L.E., General Electric Aircraft Engines, Advanced Programs & Ventures, Cincinnati, Ohio, Personal Communication to Eric D. Larson, 1987.
30. Jones J.L., Flynn B.R. and Strother J.R., "Operating Flexibility and Economic Benefits of a Dual-Fluid Cycle 501-KB Gas Turbine Engine in Cogeneration Applications", ASME Paper 82-GT-298, 1982.
31. "The Ruston Tornado", Company Publication, Ruston Gas Turbines Ltd., Lincoln, England, 1987.
32. Consonni S. and Macchi E., "Gas Turbine Cycles Performance Evaluation", Proc. *1988 ASME COGEN-TURBO* (Montreaux, Switzerland), pp. 67-77. Published by ASME, New York.

APPENDIX D: POLYTROPIC TRANSFORMATIONS

Polytropic transformations are generally defined in integral form by:

$$P \cdot v^n = \text{constant} \tag{D.1}$$

For perfect gases following the equation of state $P \cdot v = R \cdot T$, it can be shown that the exponent n is related to quantities having physical meaning by:

$$n = (c_x - c_p)/(c_x - c_v) \tag{D.2}$$

where c_x is the "apparent" specific heat $[dQ/(M \cdot dT)]$ of the reversible transformation described by Eq.(D.1). If the process is also adiabatic, Eq.(D.2) gives $n = c_p/c_v = \gamma$, which substituted in Eq.(D.1) gives the usual:

$$P \cdot v^\gamma = \text{constant} \tag{D.3}$$

used for perfect gas isoentropic processes. For pluri-atomic gases undergoing large ΔT – where variations of c_p and c_v with T may be significant – the use of Eqs.(D.1) and (D.3) is inconvenient because they require a weighted-average value of n and γ. In such cases it is better to introduce immediately the notion of polytropic efficiency, redefining polytropic transformations as processes characterized by:

$$\begin{array}{ll} dh_{is}/dh_{polytropic} = \text{constant} = \eta_p & \text{for compressions} \\ dh_{polytropic}/dh_{is} = \text{constant} = \eta_p & \text{for expansions} \end{array} \tag{D.4}$$

This definition does not require adjustments for temperature-dependent specific heats, nor does it rely on the concept of perfect gas. It is helpful when modeling a whole turbomachine, since it makes sense to assume that departures from ideal behaviour – quantitavely given by the ratio dh_{is}/dh_{actual} – are the same all along the machine. Recalling that $T\cdot ds = dh - v\cdot dP$, Eqs.(D.4) give:

$$
\begin{aligned}
{}_1\int^2 ds &= \left[(1-\eta_p)/\eta_p\right]\cdot {}_1\int^2 (v/T)\cdot dP && \text{for compressions} \\
{}_1\int^2 ds &= (\eta_p - 1)\cdot {}_1\int^2 (v/T)\cdot dP && \text{for expansions}
\end{aligned}
\tag{D.5}
$$

which, for perfect gases following $p\cdot v = R\cdot T$, yield:

$$
\begin{aligned}
s_2 - s_1 &= \left[(1-\eta_p)/\eta_p\right]\cdot R\cdot \ln(P_2/P_1) && \text{for compressions} \\
s_2 - s_1 &= (1-\eta_p)\cdot R\cdot \ln(P_1/P_2) && \text{for expansions}
\end{aligned}
\tag{D.6}
$$

These equations, which do not require c_p=constant, allow determining the final point of the transformation by setting P and s. For real gases following the equation of state $p\cdot v = z(P,T)\cdot R\cdot T$, where z is the compressibility factor, Eqs.(D.6) become:

$$
\begin{aligned}
s_2 - s_1 &= \left[(1-\eta_p)/\eta_p\right]\cdot \bar{z}\cdot R\cdot \ln(P_2/P_1) && \text{for compressions} \\
s_2 - s_1 &= (1-\eta_p)\cdot \bar{z}\cdot R\cdot \ln(P_1/P_2) && \text{for expansions}
\end{aligned}
\tag{D.7}
$$

where the average compressibility factor $\bar{z}$, to be determined iteratively, is a function of T, P and the path followed from 1 to 2.

NOMENCLATURE

c	Specific heat	[J/kg-K]
h	Enthalpy	[J/kg]
M	Mass	[kg]
n	Polytropic exponent	
P	Pressure	[Pa]
Q	Heat	[J]
R	Gas Constant	[J/kg-K]
s	Entropy	[J/kg-K]
T	Temperature	[K]
v	Specific volume	[m^3/kg]
z	Compressibility factor	

Greek

γ	Ratio c_p/c_v
η_p	Polytropic efficiency

Subscript

is	Isoentropic
1,2	Refer to initial and final point of trasformation

APPENDIX E: SAMPLE OF INPUT AND OUTPUT FILES

This Appendix reports the input and output files of the calculation of the ISTIG Cycle represented in Fig. 10.5.

The performances appearing in the output file coincide with those in the three, rightmost columns of Tab. 10.7.

SAMPLE OF INPUT FILE (cycle of Fig. 10.5)

```
$* COMPONENT DATA
A 5 Air filter   1 1  1 34
.01

B 1 LPC           1 2 34  2 33
2.659   .902    .902    3.e4    .9970   0.008   .07108
  3  5  1
C 4 Gas Heater   2 2  2 28  3 29
.90     .01     .02     0.0     10.     82.
  0  1  2  1  1
D 4 Interclr 1   2 2  3 26  4 27
.773    .01     .02     0.0     10.0    82.0
 -1  1  2  1  1
E 4 Interclr 2   2 2  4 24  5 25
.70     .01     .02     0.0     10.0    8.00
  2  1  2  1  1
F 6 Conds split  1 2  5  6 19
 -1
G 6 LPair split1 1 2  6  7 20
  2
H 6 LPair split2 1 2  7  8 21
  2
I 1 HPC          1 2  8  9 22
13.315  .902    .902    3.e4    .9970   0.008   .07108
  3 14  1
J 6 HP air split 1 2  9 10 23
  2
K 5 HP steam inj 2 1 10 32 11
.00

L 2 Combustor    2 1 11 29 12
.996    .048    .02     .75     .997    2.75    0.00
 -1  1  1  0
M 3 HP Turbine   3 1 12 21 23 13
4.25e5  800.    .250    .010    30.0    0.9     100.    .95     .921    400.
0.70    .40     .921    .45     .50     1.0     .997    0.      830.    0.0
2.0     .1      .03     .50     1.0e5   .026878 0.0
  1  1  0 25  L  I  0
N 5 IP steam inj 2 1 13 31 14
.01

O 3 IP/LP Turb.  2 1 14 20 15
2.20e5  800.    .250    .010    30.0    0.7     100.    1.0     .921    400.
0.70    .40     .921    .45     .50     1.0     .997    0.      830.    0.0
8.0     .1      .03     .50     0.70e5  .026878 0.0
  1  2  1 25     I  0
P 5 LP steam inj 2 1 15 30 16
.01

Q 3 Last trb stg 1 1 16 17
4.25e5  800.    .250    .010    30.0    0.7     100.    1.0     .921    400.
0.70    .40     .921    .45     .50     0.5     .997    0.      830.    0.0
1.0     .1      .03     .50     1.0e5   .026878 0.0
  1  1  0 25
R 7 HRSG          2 4 17 27 18 30 31 32
  1  1  3  4  0  0  1  0  0  0
  0  0  0  0  0
  3  2  2  2  2  0  0  0  0
32.     .993    .02     590.    0.0     0.0     .03     450.    0.00    220.
100.    10.     0.65    0.1     0.0
121.    121.5   1.      13.     10.     3000.   .80     .00     .65     .10
196.7   370.0   1.      11.     10.     3000.   .80     .00     .65     .10
254.8   449.0   1.      9.5     10.     3000.   .80     .00     .65     .10
$* END OF COMPONENT DATA
```

```
POINT DATA must be given as follows
 Line 1:      TO,PO,Mref,HumO           (fmt 3X,F7.1,3F10.1)
 Other lines: T,P,m,FluidType,Xmol(i)  (fmt 3X,F7.1,2F10.1,5X,A5,20F5.1)

NOTES: 1) The type of fluid must be written in SMALL CASE LETTERS, RIGHT-
          JUSTIFIED TO COLUMN 40. Composition is read only for type of
          fluid = 'fuel' or 'gas*', otherwise it is assumed equal to air
          or real-gas H2O
       2) All T are in Centigrades, all P in Bars

Note: use dry air to avoid condensation within intercooler

$* POINT DATA                                   xCH4  xCO xCO2  xH2 xH2O xH2S  xN2  xO2xC2H2xC2H4  xSL  xCS
Amb    15.0   1.01325      161.5       .0065
 1     15.0   1.01325         1.         air
 2    121.0      2.67         1.         air
 3    100.0      2.65         1.         air
 4     80.0      2.65         1.         air
 5     23.0      2.59         1.         air
 6     23.0      2.59        .99         air
 7     23.0      2.59        .99         air
 8     23.0      2.59        .98         air
 9    385.0      34.5        .93         air
10    385.0      34.5        .90         air
11    385.0      34.5        .85         air
12   1500.0      32.8        .97         gas
13   1000.0     13.64       1.05         gas
14    950.0     13.64       1.11         gas
15    500.0       1.8       1.15         air
16    450.0       1.8       1.15         air
17    400.0    1.0410       1.15         air
18    134.0   1.01325       1.15         air
19     23.0      2.59      .0010       water
20     23.0      2.59        .05         air
21     23.0      2.59        .05         air
22    385.0      34.5      .0100         air
23    385.0      34.5        .05         air
24     15.0       1.1       1.29       water
25     21.0       1.1       1.29       water
26     15.0       1.1      0.174       water
27     97.0       1.1      0.174       water
28     15.0      20.0        .02        fuel .932                          .053 .014
29    100.0      19.6        .02        fuel .932                          .053 .014
30    121.5      2.07       .025       steam
31    370.0      14.5       .022       steam
32    449.5      43.1       .123       steam
33    121.0      2.67       .008         air
34     15.0   1.00325         1.         air

$* CONVERGENCE VARIABLES (format 5I3,F10.1)
  6 20                                          m coolant for IP turbine
  6 21                                          m coolant HP turbine
  6 23                                          m coolant HP turbine nozzle
  6 12                                          m HP turbine inlet
  6 16                                          m LPT2 turbine inlet
  1 14                                          T IP turbine inlet
  1 16                                          T LPT2 turbine inlet
 23  M  2  0  0  1 12  0 1644.26    1.0         TIT HP turbine
  2  B  1                                       LPC Beta
  2  I  1                                       HPC Beta
 21  O  2  0  0  4  0  0  2.0     -0.75         IP turbine cooled stages
 56  O  2  0  0 58  0  0  8.0     -1.50         IP/LP turbine stages
```

SAMPLE OF OUTPUT FILE (cycle of Fig.10.5)

COMPONENT LIST

#	Type	Description	Input Pts	Output Pts
A	5	Air filter	1	34
B	1	LPC	34	2 33
C	4	Gas Heater	2 28	3 29
D	4	Interclr 1	3 26	4 27
E	4	Interclr 2	4 24	5 25
F	6	Conds split	5	6 19
G	6	LPair split1	6	7 20
H	6	LPair split2	7	8 21
I	1	HPC	8	9 22
J	6	HP air split	9	10 23
K	5	HP steam inj	10 32	11
L	2	Combustor	11 29	12
M	3	HP Turbine	12 21 23	13
N	5	IP steam inj	13 31	14
O	3	IP/LP Turb.	14 20	15
P	5	LP steam inj	15 30	16
Q	3	Last trb stg	16	17
R	7	HRSG	17 27	18 30 31 32

Convergence variables after entropy analysis

Convergence variable		Current value	Error [%]
M [kg/kg0]	at 20	.72625E-1	.080
M [kg/kg0]	at 21	.15614	.068
M [kg/kg0]	at 23	.11873	.068
M [kg/kg0]	at 12	.78771	.068
M [kg/kg0]	at 16	1.1831	.045
Temp [K]	at 14	1294.9	.002
Temp [K]	at 16	809.73	.004
TIT [K]	of M	1644.3	.000
Comp ratio	of B	2.6590	00.000
Comp ratio	of I	13.315	00.000
Coold stages	of O	2.0000	.000
Stages	of O	7.9994	.007

Final Thermodynamic properties

Point #	T	P	h	s	m	xCO2	xH2O	xN2	xO2	xAr	xH2OL	xCH4	HHV	LHV
	C	Bar	kJ/kg	kJ/K-kg	kg/kg0	%	%	%	%	%	%	%	MJ/kg	MJ/kg
amb	15.0	1.01	-100.8	6.866	161.50	.03	1.03	77.28	20.73	.92	00.00			
1 (g)	15.0	1.01	-100.8	6.866	1.0000	.03	1.03	77.28	20.73	.92	00.00			
2 (g)	119.2	2.67	4.9	6.900	.9920	.03	1.03	77.28	20.73	.92	00.00			
3 (g)	113.3	2.64	-1.1	6.887	.9920	.03	1.03	77.28	20.73	.92	00.00			
4 (g)	55.1	2.61	-60.1	6.725	.9920	.03	1.03	77.28	20.73	.92	00.00			
5 (g)	23.0	2.59	-92.7	6.624	.9920	.03	1.03	77.28	20.73	.92	00.00			
6 (g)	23.0	2.59	-92.7	6.624	.9920	.03	1.03	77.28	20.73	.92	00.00			
7 (g)	23.0	2.59	-92.7	6.624	.9194	.03	1.03	77.28	20.73	.92	00.00			
8 (g)	23.0	2.59	-92.7	6.624	.7632	.03	1.03	77.28	20.73	.92	00.00			
9 (g)	395.3	34.46	292.9	6.717	.7552	.03	1.03	77.28	20.73	.92	00.00			
10 (g)	395.3	34.46	292.9	6.717	.6364	.03	1.03	77.28	20.73	.92	00.00			
11 (g)	402.6	34.46	-1795.6	7.488	.7589	.02	24.35	59.07	15.85	.70	00.00			
12 (g)	1478.8	32.81	-1871.0	9.063	.7877	5.23	33.41	56.07	4.63	.66	00.00			
13 (g)	1044.0	13.64	-1623.1	8.636	1.0626	3.99	25.71	61.11	8.45	.73	00.00			
14 (g)	1021.7	13.50	-1855.2	8.704	1.0852	3.87	27.97	59.26	8.20	.70	00.00			
14a	811.4	6.47			1.1578									
15 (g)	551.0	1.80	-2321.7	8.667	1.1578	3.65	26.42	60.29	8.92	.72	00.00			
16 (g)	536.6	1.78	-2556.2	8.735	1.1831	3.54	28.71	58.42	8.64	.69	00.00			
17 (g)	455.5	1.04	-2662.0	8.769	1.1831	3.54	28.71	58.42	8.64	.69	00.00			
18 (g)	126.8	1.01	-3068.7	8.038	1.1831	3.54	28.71	58.42	8.64	.69	00.00			
19 (w)	23.0	2.59	-92.7	6.624	.0000	00.00	00.00	00.00	00.00	00.00	100.00			
20 (g)	23.0	2.59	-92.7	6.624	.0726	.03	1.03	77.28	20.73	.92	00.00			
21 (g)	23.0	2.59	-92.7	6.624	.1561	.03	1.03	77.28	20.73	.92	00.00			
22 (g)	395.3	34.46	292.9	6.717	.0080	.03	1.03	77.28	20.73	.92	00.00			
23 (g)	395.3	34.46	292.9	6.717	.1187	.03	1.03	77.28	20.73	.92	00.00			
24 (w)	15.0	1.10	-15907.1	3.740	1.2900	00.00	00.00	00.00	00.00	00.00	100.00			
25 (w)	21.0	1.08	-15882.1	3.826	1.2900	00.00	00.00	00.00	00.00	00.00	100.00			
26 (w)	15.0	1.10	-15907.1	3.740	.1704	00.00	00.00	00.00	00.00	00.00	100.00			
27 (w)	97.0	1.08	-15563.7	4.789	.1704	00.00	00.00	00.00	00.00	00.00	100.00			
28 (f)	15.0	20.00	-4153.8	9.646	.0288	00.00	00.00	5.30	1.40	00.00	00.00	93.20	49.143	44.285
29 (f)	108.7	19.60	-3949.6	10.267	.0288	00.00	00.00	5.31	1.40	00.00	00.00	93.29	49.143	44.285
30 (s)	121.5	2.05	-13261.7	10.637	.0254	00.00	100.00	00.00	00.00	00.00	00.00			
31 (s)	370.0	14.50	-12777.3	10.705	.0226	00.00	100.00	00.00	00.00	00.00	00.00			
32 (s)	449.0	43.10	-12645.5	10.412	.1225	00.00	100.00	00.00	00.00	00.00	00.00			
33 (g)	119.2	2.67	4.9	6.900	.0080	.03	1.03	77.28	20.73	.92	00.00			
34 (g)	15.0	1.00	-100.8	6.869	1.0000	.03	1.03	77.28	20.73	.92	00.00			

Final Component Characteristics
Compressors

	LPC	HPC
W [J/kg0]	-.10598E+6	-.29515E+6
Comp ratio	2.6590	13.315
VHin [m]	.98414	.58113
VHout [m]	.75262	.22455
Etap,VH=inf	.90200	.90200
Etapol	.90166	.88855
Eta ad.	.88777	.84461
Wclt [J/kg]	.00000	-48552.
Dhis [J/kg]	93802.	.32566E+6
Dhis,lastage	19054.	24471.
Organic eff.	.99700	.99700
Mbled kg/kg0	.00000	.22876
Reheat fctr	1.0156	1.0520
Dhis,stg,max	30000.	30000.
Leakage	.80000E-2	.80000E-2
Slope aC	.71080E-1	.71080E-1
Vertex bC	.00000	.00000
I-stages	3	3
Nstages	5	14
I-flow	1	1
I-beta	0	0

Final Component Characteristics
Combustors

	Combustor
W [J/kg0]	-9057.0
Etacomb	.99600
DP/Pin	.48000E-1
Tstoich [K]	2116.8
Fuel/Oxy	.37995E-1
xO2,exit	.46270E-1
Etapol comp.	.75000
Organic eff.	.99700
Press. ratio	2.7500
Dh [J/kg]	.29159E+6
Elec. effic.	.93120
Mode	-1
I-DP	1
I-Fuel comp.	1
I-el. effic.	0

Final Component Characteristics

Turbines

	HP Turbine	IP/LP Turb.	Last trb stg
W [J/kg0]	.27023E+6	.66615E+6	.12476E+6
Etap,1st exp	.91351	.91675	-1.0000
Dhis,lastage	.22955E+6	68454.	.15146E+6
Dhis,stg,max	.42500E+6	.21208E+6	.42500E+6
Machnzl,actl	.91969	.69953	.71591
Tbmx,rot [K]	1073.2	1073.2	1073.2
rfc,inlet	.25000	.25000	.25000
Mdsk,stg	.10000E-1	.10000E-1	.10000E-1
Mcltnzl	.11873	.23644E-1	.00000
Mcltdsc,tot	.18514E-1	.22556E-1	.00000
Mclt,tot	.27486	.72625E-1	.00000
dc/c,rotor	.33333	.15789	.00000
Alfa,film	30.000	30.000	30.000
Machnzl,trgt	.90000	.70000	.70000
Zeta	100.00	100.00	100.00
Etanzl	.95000	1.0000	1.0000
Etap,VH=inf	.92100	.92100	.92100
u [m/s]	400.00	400.00	400.00
Mach,rotor	.70000	.70000	.70000
DPbled	.40000	.40000	.40000
Coold stages	2.0000	2.0000	.00000
Etap,uncoold	.91558	.92084	.92100
TIT [K]	1644.3	1281.7	809.73
TIP [Pa]	.30702E+7	.13442E+7	.17820E+6
Mach,diff,in	.45000	.45000	.45000
Biot,blade	.50000	.50000	.50000
VHout [m]	.34603	1.0671	1.0635
TScool [K]	1275.1	997.39	747.92
PScool [Pa]	.11966E+7	.44952E+6	.12846E+6
Diff recvry	1.0000	1.0000	.50000
Tdiff,in K	1280.7	798.35	705.22
Pdiff,in Pa	.12004E+7	.15783E+6	97384.
Beta,cooled	.36591	.33288	.72087
Organic eff.	.99700	.99700	.99700
App. Etapol	1.5723	.97818	.80453
App. Etaad	1.4958	.98282	.81488
App. Dhis	.45422E+6	.66435E+6	.12979E+6
Biot,TBC	.00000	.00000	.00000
Tbmx,nzl [K]	1103.2	1103.2	1103.2
Leakage	.00000	.00000	.00000
Nzl pattern	.10000	.10000	.10000
Rot pattern	.30000E-1	.30000E-1	.30000E-1
Vclus/Vcl	.50000	.50000	.50000
Inlet Dm [m]	.84153	1.3698	4.1735
Dm endcool	.84153	1.3698	4.1735
H/Dm endcool	.11678	.15024	.00000
Inlet Ds	3.2500	3.2500	3.2500
Inlet H/Dm	.80000E-1	.80000E-1	.80000E-1
Solidity	1.2500	1.2500	1.2500
Nzl cax/Dm	.60000E-1	.60000E-1	.60000E-1
Nzl stgr ang	65.000	65.000	65.000
Perimtr/chrd	2.6000	2.6000	2.6000
Thickns/chrd	.12500	.12500	.12500
Rot cax/Dm	.45000E-1	.45000E-1	.45000E-1
Rot stgr ang	55.000	55.000	55.000
Stages	2.0000	7.9994	1.0000
Wunc [J/kg]	.00000	.40380E+6	.12476E+6
Dhis,unc	.10000E+6	68454.	.10000E+6
Slope aT	.26878E-1	.26878E-1	.26878E-1
Vertex bT	.00000	.00000	.00000
Flow [m^3/s]	41.129	61.706	298.77
DT comb. [K]	1076.3	.00000	.00000
I-geometry	1	1	1
I-stages	1	2	1
R/I stages	0	1	0
Nstep,max	25	25	25
Nstep,nzl	6	5	1
Nstep,actual	15	24	1

Final Component Characteristics
Heat Exchngs

	Gas Heater	Interclr 1	Interclr 2
W [J/kg0]	.00000	.00000	.00000
H.T. Effect.	.90000	.83415	.80038
Hot-side DP	.10000E-1	.10000E-1	.10000E-1
Cold-side DP	.20000E-1	.20000E-1	.20000E-1
Heat losses	.00000	.00000	.00000
DTlm [K]	39.153	26.432	17.997
UA [W/C-kg0]	150.42	2214.2	1796.2
NTU	.14948	2.2029	1.7823
DT hot [C]	5.8525	58.227	32.076
DT cold [C]	93.740	82.000	5.9908
DT h end [C]	10.416	16.303	34.086
DT c end [C]	98.303	40.076	8.0000
DTend [C]	.00000	.00000	.00000
I-mode	0	-1	2
I-flow hot	1	1	1
I-flow cold	2	2	2
I-DP hot	1	1	1
I-DP cold	1	1	1
I-RgIC	0	0	0

Final Component Characteristics
Mixers

	Air filter	HP steam inj	IP steam inj	LP steam inj
W [J/kg0]	.00000	.00000	.00000	.00000
Psat-Ph2o Pa	666.62	**********	**********	**********
DP/Plowst,in	.10000E-1	.00000	.10000E-1	.10000E-1
DThtloss [C]	.00000	.00000	.00000	.00000
Ph2o/Psat	.60877	**********	**********	**********
Xh2o/Xsat	.60468	**********	**********	**********
I-filter	0	0	0	0

Final Component Characteristics
Boiler

Heat to steam =	77166.870	Heat from gas =	77710.860
Turb.gross power=	.000	Heat exiting sys=	77316.870
Net power output=	-171.351	Condenser heat =	.000
1° law error =	.00000	2° law error =	.00000
Cycle efficiency=	-.00222	Recovery effic. =	-.00166
Mass error =	.00000		

INPUT DATA: Gas mass flow= 191.077 kg/s

no.	DT at pinch pt	DT at appr.pt	DT of subcool	water dp/p	steam dp/p	pumps effic.	turbines effic.
0	.00	.00	10.00	.1000	.0000	.6500	.0000
1	13.00	1.00	10.00	.1000	.0000	.7649	.8000
2	11.00	1.00	10.00	.1000	.0000	.7570	.8000
3	9.50	1.00	10.00	.1000	.0000	.7522	.8000

Other efficiencies: thermal= .9930 - mech.= .0000 - electric= .0000
Turbine eff. is stage(ncs) - steam vap.frct.corr: f= .87, x0= .0000

Steam data and mass flow

no.	T	p	hl	hv	sl	sv	Mass flow	Type
-1	32.03	.048	134.13	2560.0	.4643	8.4134	.0000	Condenser
0	99.98	1.013	419.00	2676.0	1.3067	7.3556	.5137	Deaerator
1	120.99	2.049	507.94	2707.4	1.5383	7.1188	4.0958	Boiler
2	196.72	14.504	837.59	2788.9	2.2996	6.4524	3.6466	Boiler
3	254.81	43.103	1109.30	2798.8	2.8374	6.0373	19.7814	Boiler
	97.00	1.078	406.43		1.2729		27.5238	Make-up

```
HRSG:             ----- GAS ----              ---- STEAM ---     thermal
                  T       h      s            T       h      s     power     NTU
ref.     :     15.00-3200.8 7.651
eco 0    : ex. 126.82-3068.7 8.038 - in.   97.00  406.4 1.273
eco 0    : in. 123.21-3073.0 8.027 - ex.   89.98  376.9 1.192   -813.54    .000
boi 0    : in. 128.35-3066.9 8.043 - ex.   99.98 2676.0 7.356   1159.43    .000
eco 1    : ex. 128.35-3066.9 8.043 - in.   99.98  419.2 1.307
eco 1    : in. 133.99-3060.1 8.059 - ex.  110.99  465.5 1.429   1275.78    .000
boi 1    :                         - ex.  120.99 2707.4 7.119  10175.94    .000
eco 2    : ex. 178.75-3006.5 8.185 - in.  120.99  509.9 1.540
eco 2    :                         - ex.  186.72  792.9 2.204   6630.14    .000
shtr1    : ex. 178.75-3006.5 8.185 - in.  120.99 2707.4 7.119
shtr1#1  : in. 207.72-2971.6 8.260 - ex.  121.50 2708.4 7.121      4.39    .000
boi 2    :                         - ex.  196.72 2788.9 6.452   8162.93    .000
eco 3    : ex. 243.10-2928.5 8.346 - in.  196.72  842.6 2.304
eco 3    :                         - ex.  244.81 1060.7 2.744   4313.11    .000
shtr2    : ex. 243.10-2928.5 8.346 - in.  196.72 2788.9 6.452
shtr2#2  : in. 264.31-2902.6 8.395 - ex.  263.31 2856.9 6.788    612.68    .000
boi 3    :                         - ex.  254.81 2798.8 6.037  34382.69    .000
shtr3    : ex. 409.19-2721.4 8.693 - in.  254.81 2798.8 6.037
shtr3#2  : in. 455.46-2662.0 8.777 - ex.  370.00 3192.9 7.189    860.46    .000
shtr3#3  : in. 455.46-2662.0 8.777 - ex.  449.00 3324.7 6.897  10402.87    .000
                                                               77166.87

STEAM TURBINES:
no.    Pin    Tin    hin    sin    xin     Pex    Tex    hex    sex    xex

no.      flow  in.v.flow     power   ad.eff.        rpm
number of LP parallel flows: 0 - steam speed at turbine outlet:  220.00

BLEEDINGS: steam conditions and mass flow
no.    T       h       p       s       x       flow
 3  449.0  3324.7  43.103  6.897  1.000   19.781
 2  370.0  3192.9  14.504  7.189  1.000    3.647
 1  121.5  2708.4   2.049  7.121  1.000    4.096

ENTROPY ANALYSIS:  Eff.decays            Reversible power          =  40958.3
Turbine leakage loss     =   .00000      Kinetic energy loss       =   .00000
Make-up exergy/mixing    =  -.02779      Moisture removal          =   .00000
Bleedings                =   .81252      Gas exhausts to stack     =   .09646
Cooling sys. mech.power  =   .00001      Condenser heat transfer   =   .00000
Mech./Electr. losses     =   .00052      HRSG thermal losses       =   .00632

         pumps   turbines   trb.inl.        ----heat transfer----
no.    eff/frct    effic.   mix/frct.       eco      boiler     shtr
 0      .00000     .00000    .00000      -.00119     .00163    .00000
 1      .00003     .00000    .00000       .00141     .01465    .00961
 2      .00027     .00000    .00000       .00000     .00727    .00401
 3      .00061     .00000    .00000       .00000     .06026    .01759

HEAT/WORK BALANCES                       OTHER RESULTS
Heat available from gas = 102950.4      Turbine gross power        =       .0
HRSG Thermal losses     =    544.0      Power required by pumps    =    171.4
Useful heat exiting HRSG=  77316.9      Heat rejected by HRSG      =  25239.5
Heat given to cycle     =  77166.9      HRSG global NTU            =     .000
Heat rejected by cond.  =       .0      Second law efficiency      = -.00418
Cycle power output      =   -150.0
Net power output        =   -171.4      Mass error                 =   .00000
Cycle efficiency        =  -.00222      First law error            =   .00000
Recovery efficiency     =  -.00166      Second law error           =   .00000
```

OVERALL CYCLE PERFORMANCES

Net sp. work, kJ/kg1	649.887	Net produced work	1061.134
Net absorbed work	-411.247	Coolant comp. work	-48.552
Total Power, kW	104956.800	Steam tur powr, kW	-171.351
HHV efficiency, %	45.860	LHV efficiency, %	50.890

Entropy Analysis

	Wrev [%]	TOT	Exergy [%]	TOT
TOTAL INPUT [kJ/kg1]		1317.982		1434.333
Input flows				
Point 1	00.000	00.000	.000	.000
Point 24	.001	.001	5.825	5.825
Point 26	.000	.001	.770	6.595
Point 28	99.999	100.000	93.405	100.000
Air filter				
9 Pressure losses	.063	.063	.058	.058
LPC				
3 Compression	.672	.735	.618	.676
10 Organic losses	.024	.759	.022	.698
Gas Heater				
5 Pressure losses	.069	.829	.063	.761
5 Heat transfer	.054	.883	.050	.811
Interclr 1				
5 Pressure losses	.088	.971	.081	.892
5 Heat transfer	.286	1.257	.263	1.155
Interclr 2				
5 Pressure losses	.276	1.533	.254	1.408
5 Heat transfer	-.038	1.494	-.035	1.373
HPC				
3 Compression	1.561	3.056	1.435	2.808
10 Organic losses	.067	3.123	.062	2.870
HP steam inj				
9 Pressure losses	.265	3.388	.244	3.113
9 Heat transfer	.003	3.391	.003	3.116
9 H2O mixing	2.675	6.066	2.458	5.574
9 H2O mix heat tr.	.000	6.066	.000	5.574
9 Mixing	00.000	6.066	.005	5.580
9 Real gas effects	-.044	6.022	-.040	5.539
Combustor				
1 Thermal losses	.541	6.564	.497	6.037
1 Pressure losses	.412	6.976	.379	6.415
1 Combustion	24.953	31.929	22.929	29.344
1 Mixing	00.000	31.929	-.191	29.153
3 Compression	.105	32.033	.096	29.249
10 El. Org. losses	.049	32.083	.045	29.294
HP Turbine				
3 Coolant compress	.228	32.310	.209	29.503
4 Throttling	.341	32.651	.313	29.817
4 Nzle & cld expns	.583	33.235	.536	30.353
4 Heat transfer	.674	33.909	.619	30.972
4 Coolant dischrge	2.450	36.359	2.252	33.224
4 Mixing	00.000	36.359	.188	33.412
10 Organic losses	.070	36.429	.065	33.477
IP steam inj				
9 Pressure losses	.089	36.519	.082	33.559
9 Heat transfer	.226	36.744	.207	33.766
9 H2O mixing	.300	37.044	.275	34.041
9 Mixing	00.000	37.044	.000	34.041
9 Real gas effects	-.004	37.039	-.004	34.037
IP/LP Turb.				
3 Coolant compress	.070	37.110	.065	34.102
4 Throttling	.086	37.196	.079	34.181
4 Nzle & cld expns	.493	37.689	.453	34.634
4 Heat transfer	.283	37.972	.260	34.894
4 Coolant dischrge	.506	38.478	.465	35.360
4 Mixing	00.000	38.478	.034	35.394
4 Uncooled expans	.876	39.355	.805	36.199
10 Organic losses	.155	39.509	.142	36.341
LP steam inj				
9 Pressure losses	.115	39.624	.106	36.447
9 Heat transfer	.245	39.869	.225	36.672
9 H2O mixing	.330	40.199	.303	36.975

9 Mixing	00.000	40.199	.000	36.975
9 Real gas effects	-.005	40.194	-.004	36.870
Last trb stg				
4 Nzle & cld expns	.010	40.204	.009	36.879
4 Uncooled expans	.317	40.521	.291	37.270
4 Diffuser	.538	41.059	.494	37.765
10 Organic losses	.028	41.087	.026	37.791
HRSG				
7 Gas-side DP	.222	41.310	.204	37.995
7 Thermal losses	.122	41.431	.112	38.107
10 El. Org. losses	.010	41.441	.009	38.116
8 Cooling system	.000	41.442	.000	38.116
8 Make up w. mix.	.000	41.442	.000	38.116
8 Pumps and DP	.018	41.459	.016	38.132
8 Mix and friction	.000	41.459	.000	38.132
7 Deaerator H.T.	.009	41.468	.008	38.140
7 1st level H.T.	.494	41.962	.454	38.594
7 2nd level H.T.	.217	42.179	.199	38.794
7 3rd level H.T.	1.498	43.677	1.376	40.170
Output flows				
2 Point 18	6.662	50.339	8.374	48.544
2 Point 19	00.000	50.339	00.000	48.544
3 Point 22	.265	50.604	.244	48.788
6 Point 25	.026	50.630	5.848	54.636
3 Point 33	.058	50.688	.054	54.690
NET WORK	49.309	99.997	45.309	99.999